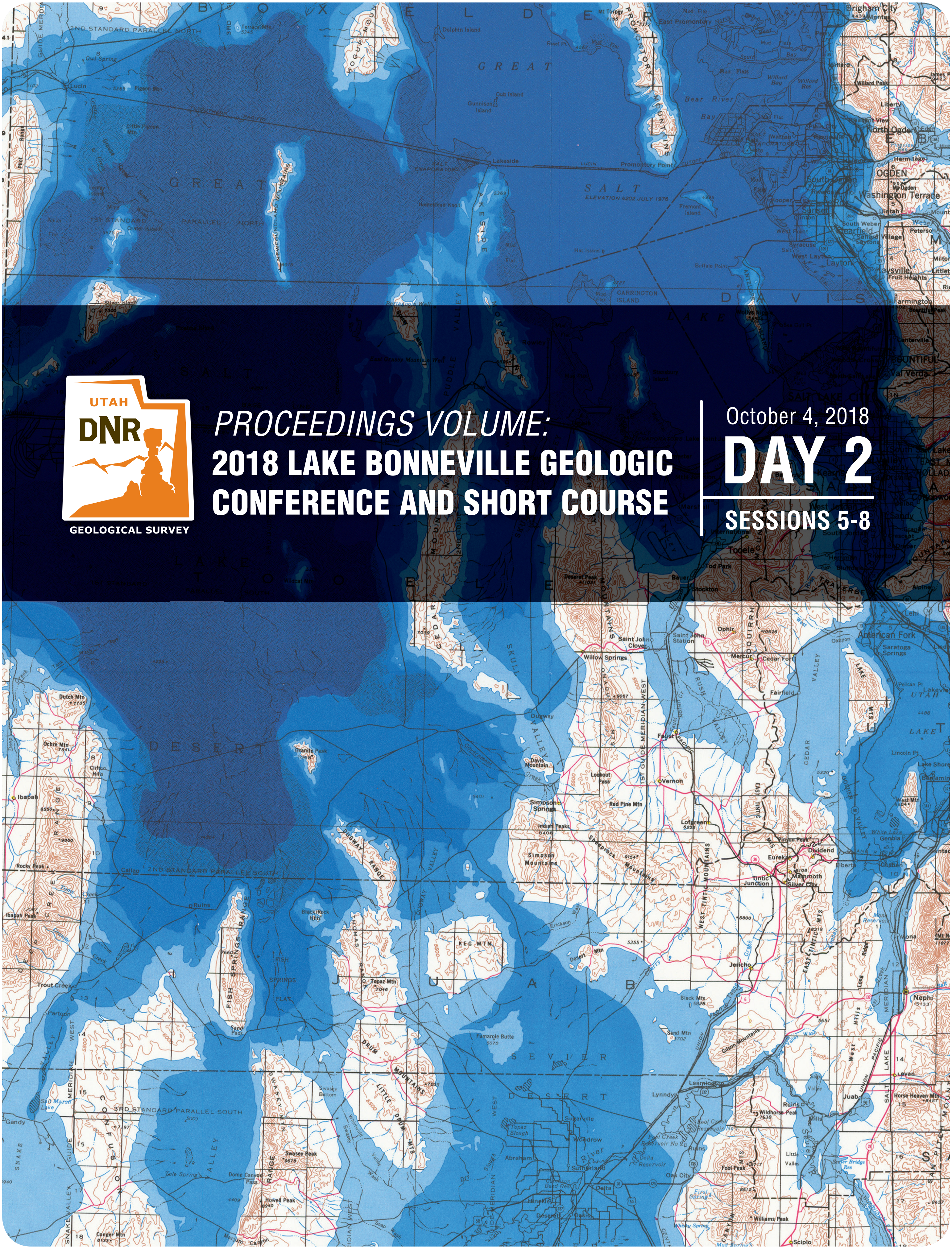

UTAH DNR GEOLOGICAL SURVEY

PROCEEDINGS VOLUME:

2018 LAKE BONNEVILLE GEOLOGIC CONFERENCE AND SHORT COURSE

October 4, 2018

DAY 2

SESSIONS 5-8

AN ELASTIC PLATE MODEL APPLIED TO NEW ESTIMATES OF THE VERTICAL DEFLECTION PATTERNS ON BONNEVILLE AND PROVO SHORELINES

Bruce G. Bills[1], Kenneth D. Adams[2], and Charles G. Oviatt[3]

[1]Jet Propulsion Laboratory, Pasadena, CA 91109;
[2]Desert Research Institute, Reno, NV 89512;
[3]Kansas State University (retired), Manhattan, KS 66506

Corresponding author (Bills): bruce.g.bills@nasa.gov

ABSTRACT

The water load associated with Lake Bonneville was large enough to produce 80 m of vertical deformation of the crust on the Bonneville shoreline, and 60 m of deformation on the Provo shoreline. This pattern was first noted by G.K. Gilbert, and has since been used to estimate the long-term strength of the crust and upper mantle in the eastern Great Basin.

We have recently compiled a new collection of surface-point-elevation measurements on the Bonneville and Provo shorelines. Compared to earlier work by Currey (1982), our compilation has many more points and much improved positional accuracy.

The objective of the present work is to use these elevations to constrain parameters in a simple model of crustal deformation. All past studies of the rebound pattern, which attempted to estimate effective viscosity in the upper mantle, concluded that the effective viscosity is very low compared to global mean estimates obtained from glacial rebound studies of marine shoreline elevation patterns.

We take an end-member case of such models, and approximate the subsurface structure as an elastic plate floating on a fluid substrate. The model has effectively three free parameters: plate thickness, substrate density, and water surface elevation. An advantage of this model is that the predicted deformation does not depend upon the loading history.

Over most of lake history, the water surface elevation was changing slowly enough that viscoelastic models suggest that the surface deformation was close to being in equilibrium with the applied load. The only obvious departure from that pattern is the Bonneville flood, during which the water level dropped more than 100 m is less than one year. If the lake stood at the post-flood Provo level long enough that the Provo shorelines also reflect equilibrium, then they should only represent response to the load at Provo time, with no memory of the larger load present at Bonneville shoreline time. That situation has been hypothesized by Miller and others (2014).

Our best-fitting elastic plate models for the Bonneville and Provo shoreline deformation patterns yield the parameters given in the table below.

Parameter	**Thickness (km)**	**Density (kg/m^3)**	**Elevation (m)**	**ResidualVariance (m^2)**
Bonneville	19.9	3825	1553.5	10.2
Provo	16.0	3730	1453.3	15.3

The best-fitting values are different, with higher thickness and density values for Bonneville. As a result, a given load produces more deflection response on Provo than it does on Bonneville. That suggests the observed Provo elevation pattern was produced by a larger load that was present at the Provo time.

Another feature of our model is that the residuals are not random. This could imply lateral variations in effective parameters, but certainly is mainly due to un-modeled sedimentary loads.

REFERENCES

Currey, D.R., 1982, Lake Bonneville—selected features of relevance to neotectonic analysis: U.S. Geological Survey, Open-File Report 82-1070, 31 p., doi 10.3133/ofr821070.

Gilbert, G.K., 1890, Lake Bonneville: United States Geological Survey Monograph 1, 438 p.

This content is a PDF version of the author's PowerPoint presentation.

An elastic plate deformation model for the Bonneville and Provo shoreline elevation patterns

Bruce G. Bills[1]
Kenneth D. Adams[2]
Charles G. Oviatt[3]

[1]Jet Propulsion Laboratory, Pasadena, CA
[2]Desert Research Institute, Reno, NV
[3]Kansas State University, Manhattan, KS

outline

- geodynamic background
- new data on shoreline elevations
- apply elastic plate model
- examine residuals
- discuss implications

geodynamic background

Geodynamics is the study of
mechanical properties of the Earth,
on a wide range of time scales.

On short time scales (year or less),
the Earth behaves as an elastic solid,
from the surface to the core-mantle boundary

On long time scales (10^6 years or more),
the behavior is that of rigid tectonic plates,
floating on a low viscosity fluid.

A key question is: how does this transition occur?

Lake Bonneville shoreline elevation geometry,
and lake level history have
played an important role in
the history of geodynamics research.

The shorelines are well preserved,
and the loading history is well resolved.

The picture which emerges is that
the geodynamic behavior of the Great Basin
is quite different than the global average.

The effective viscosity of the upper mantle can be estimated from spatio-temporal patterns of marine shoreline elevations associated with continental ice sheets, and similar studies of Bonneville shorelines.

The glacial rebound studies yield viscosity values of 10^{21} Pa s, which is a global average.

In contrast, Bonneville studies yield viscosity values of 10^{18} – 10^{19} Pa s, or roughly 100-1000 times lower.

Recent volcanism, high heat flow values, and active tectonic deformation are all consistent with the view of a hotter than average upper mantle beneath the Great Basin.

With low values of viscosity, the viscous flow is rapid enough that the vertical deformation is likely close to equilibrium, over most of the lake loading history.

An obvious exception would be right after the Bonneville flood, when lake level dropped by more than 100 m is less that one year.

new data

To aid in investigating various aspects
of the shoreline deformation problem,

we have recently compiled new
measurements of shoreline point positions

- 531 for Bonneville
- 208 for Provo

Typical measurement error is 10 cm.

The next several figures show slightly smoothed versions of the patterns of elevation on Bonneville and Provo shorelines.

The positions are in UTM (Universal Transverse Mercator) coordinates, and are shown relative to a ***reference point***, which is near the center of the basin.

It has UTM coordinates, in zone 12,

Easting = 340,270 m
Northing = 4,458,463 m

The corresponding latitude and longitude are

lat = 40.261389 deg N
lon = 112.848384 deg W

The location is a few km north and west of Dugway, UT.

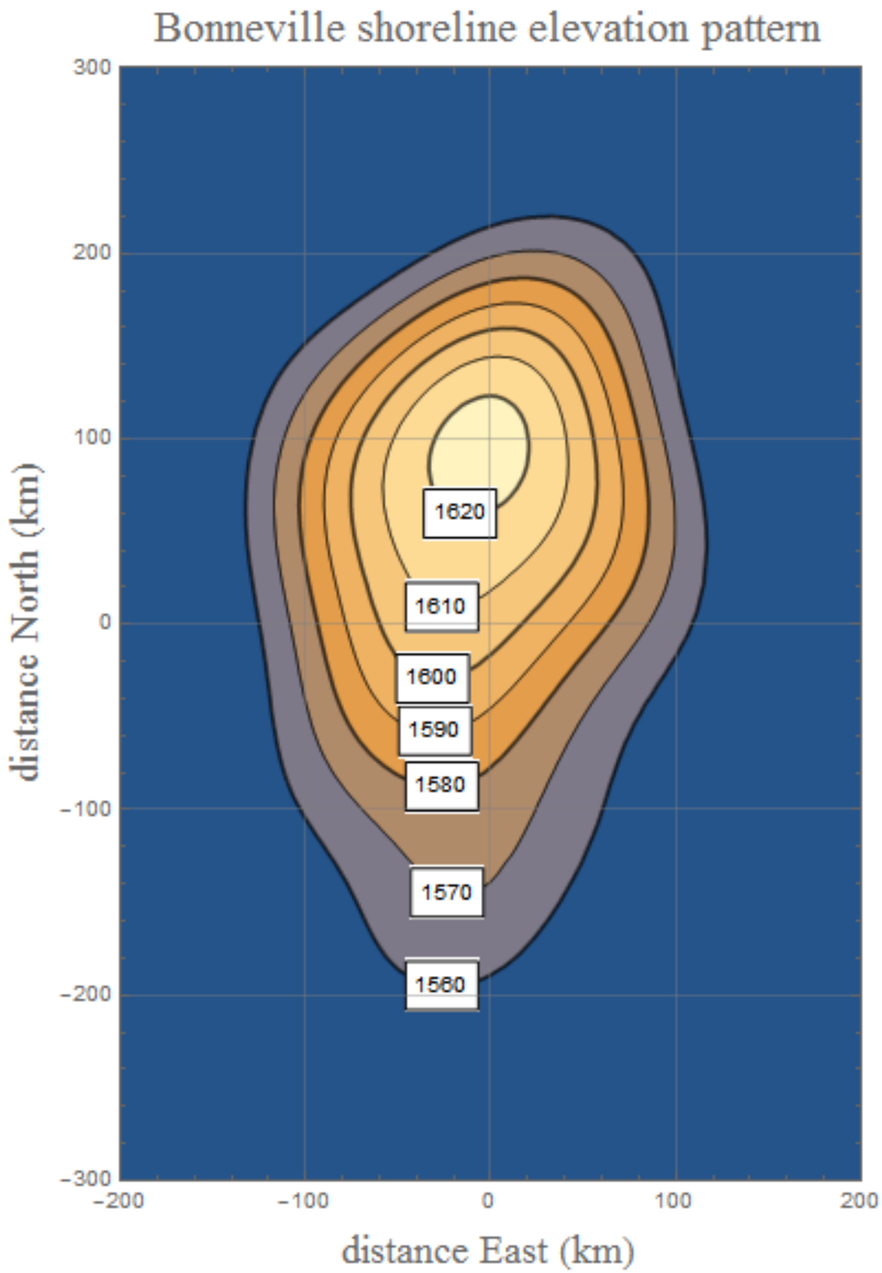
Bonneville shoreline elevation pattern
distance North (km)
distance East (km)
300
200
100
0
-100
-200
-300
-200
-100
0
100
200
1620
1610
1600
1590
1580
1570
1560

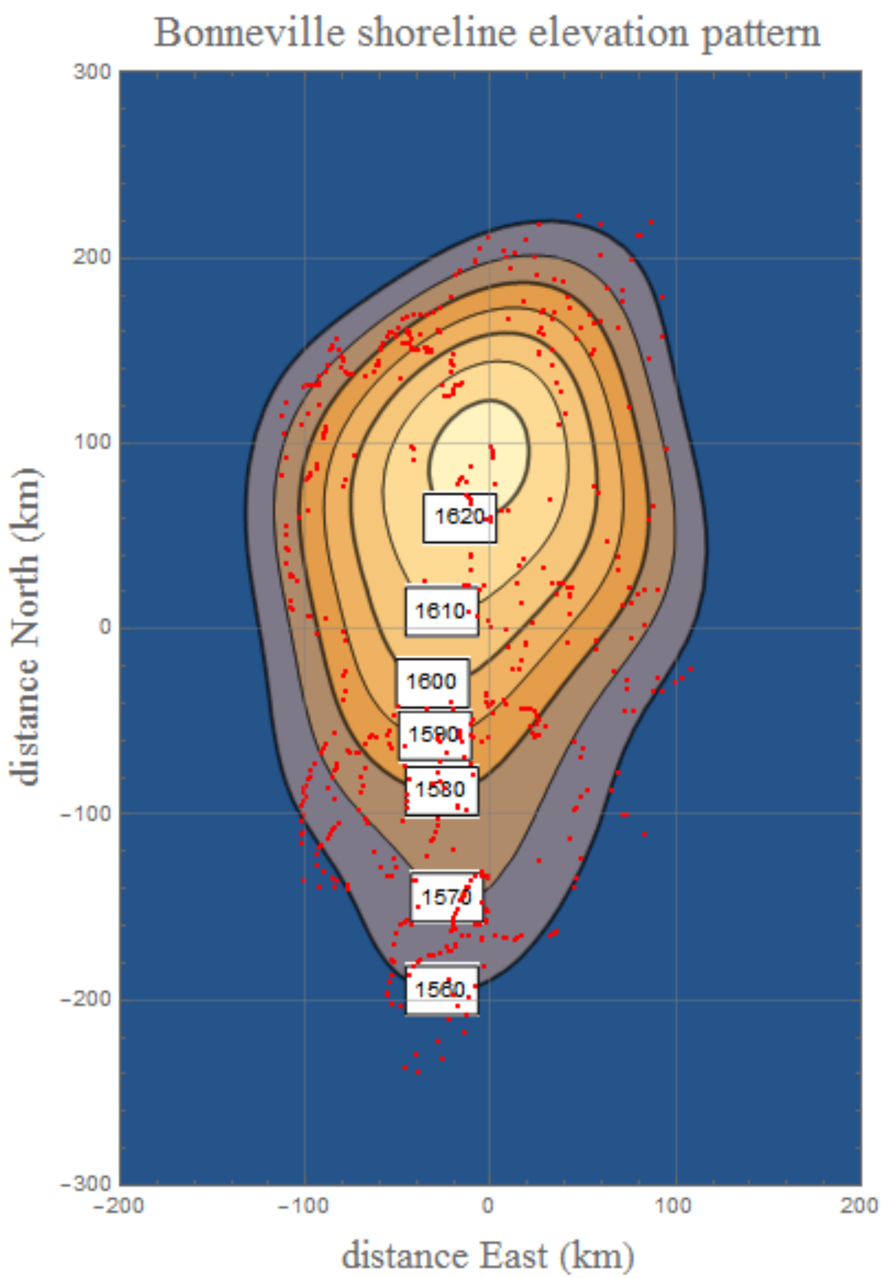
Bonneville shoreline elevation pattern
distance North (km)
distance East (km)
300
200
100
0
-100
-200
-300
-200
-100
0
100
200
1620
1610
1600
1590
1580
1570
1560

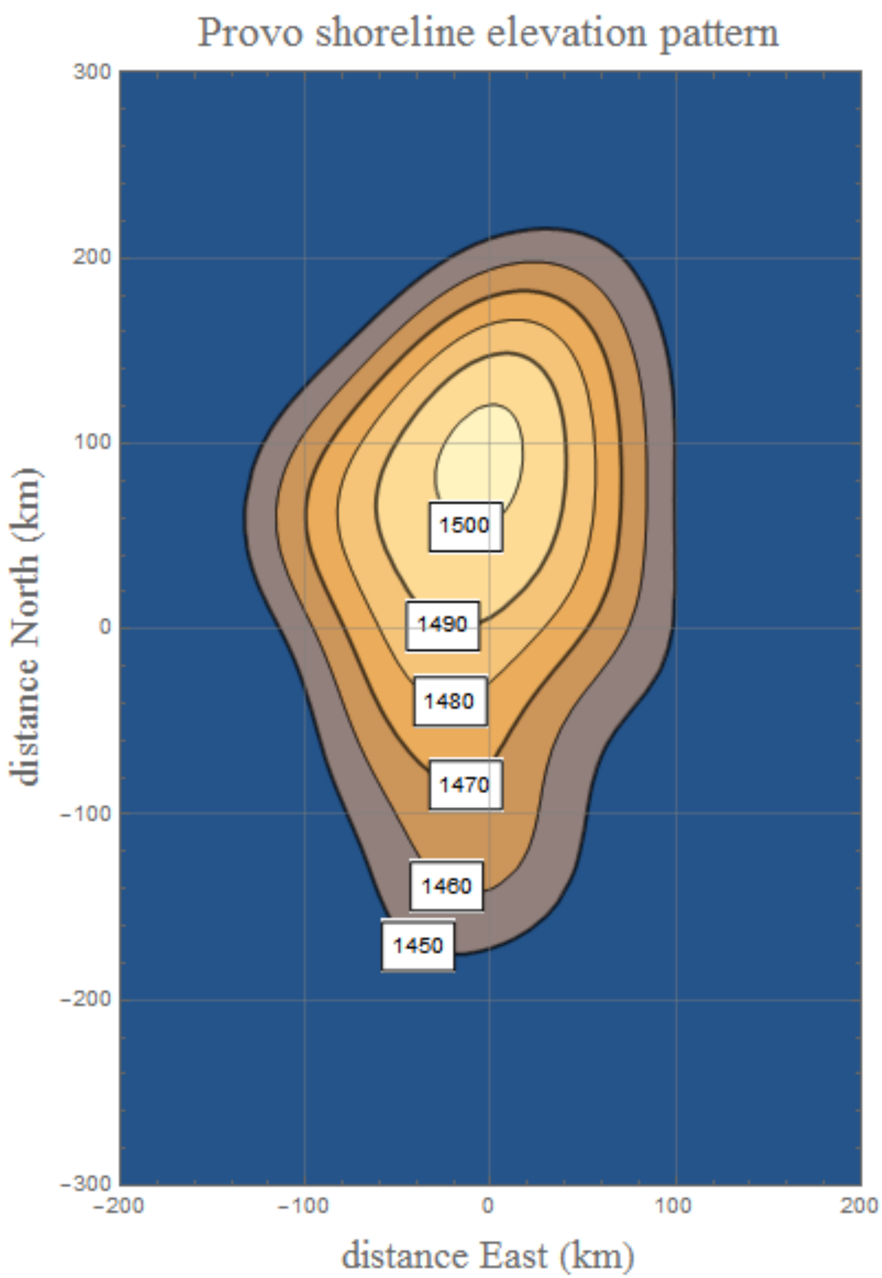

Provo shoreline elevation pattern
300
200
100
0
-100
-200
-300
-200
-100
0
100
200
distance North (km)
distance East (km)
1500
1490
1480
1470
1460
1450

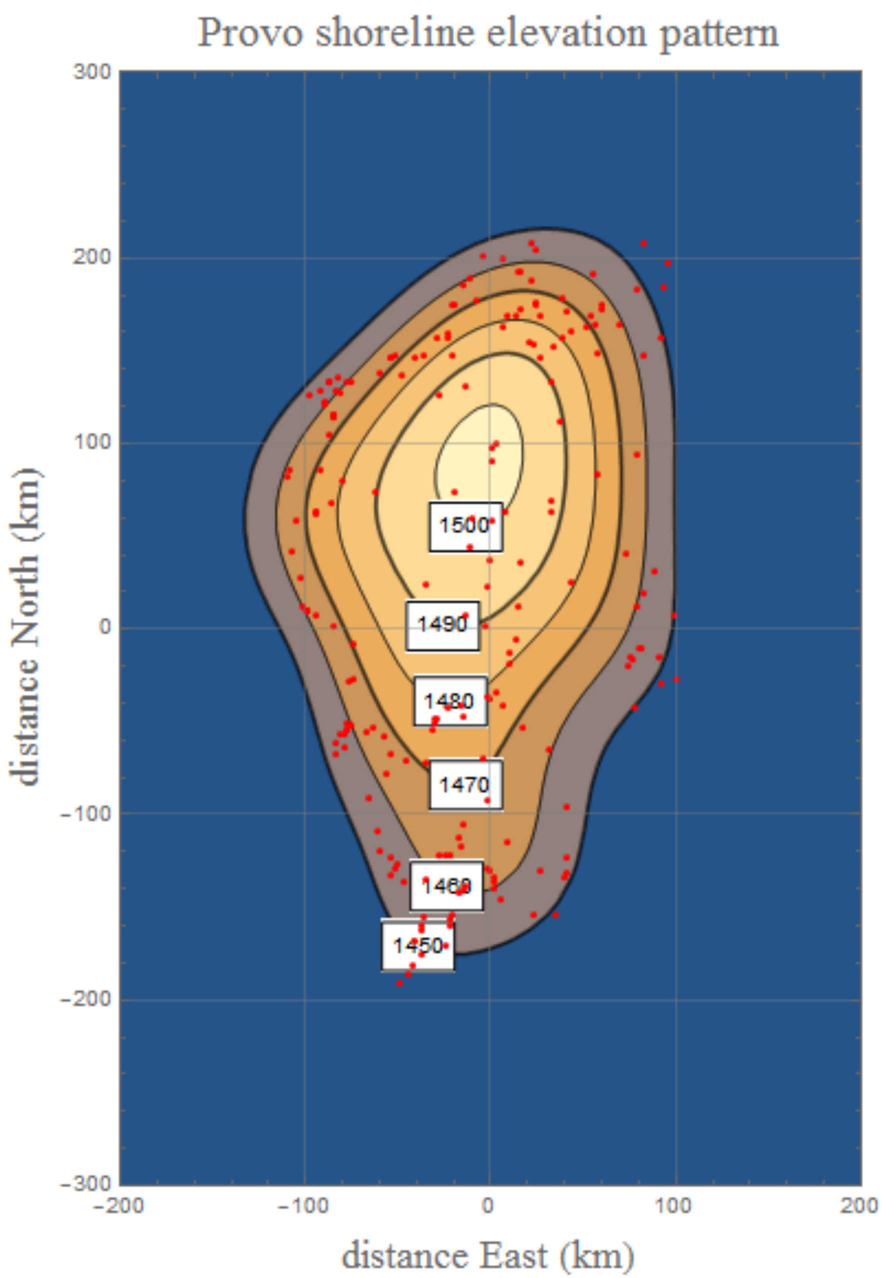
Provo shoreline elevation pattern
distance North (km)
distance East (km)
300
200
100
0
−100
−200
−300
−200
−100
0
100
200
1500
1490
1480
1470
1460
1450

The next 4 figures show the Bonneville and Provo shoreline elevation patterns,
projected onto N-S profiles and E-W profiles.

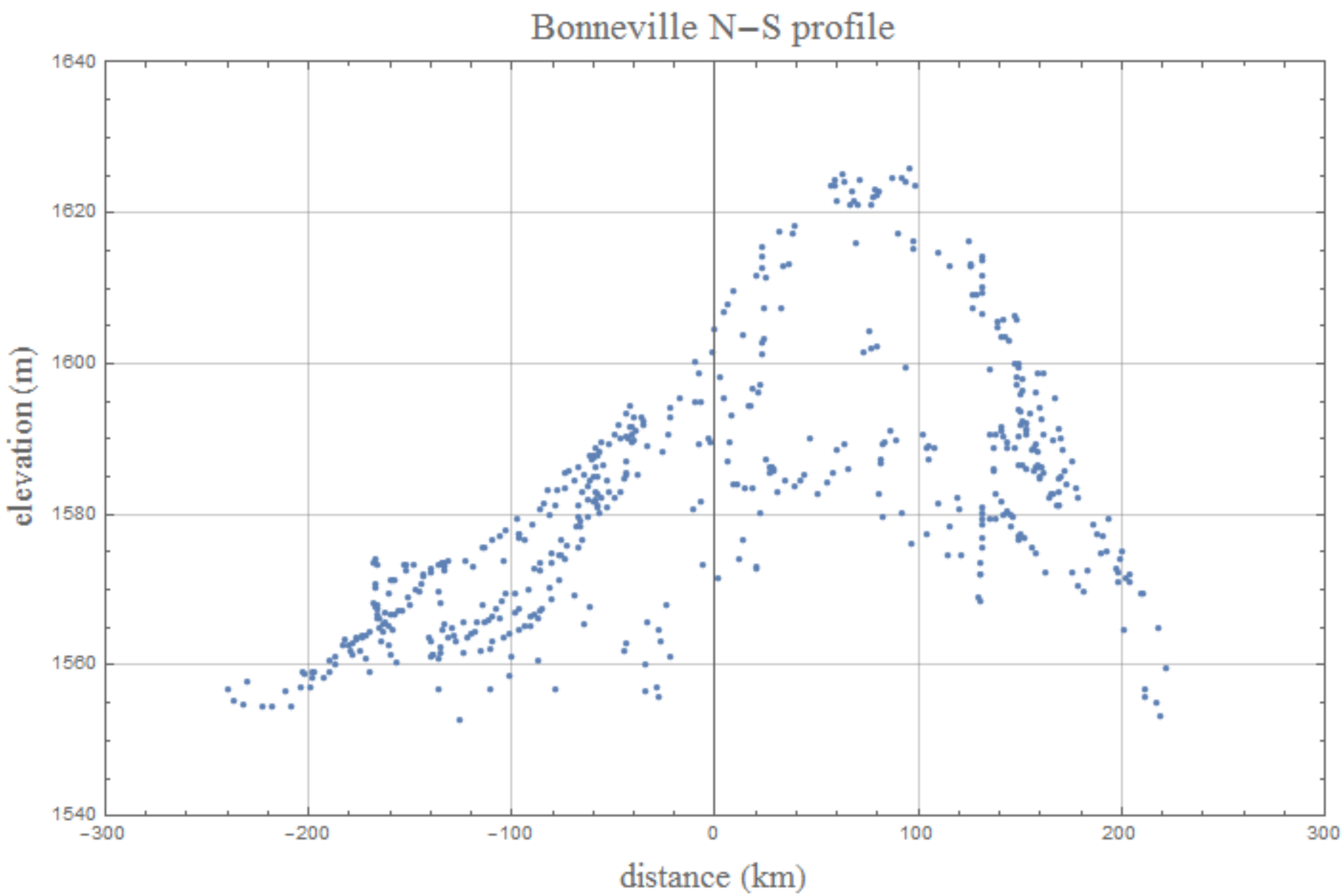
Bonneville N–S profile
elevation (m)
distance (km)
1640
1620
1600
1580
1560
1540
−300
−200
−100
0
100
200
300

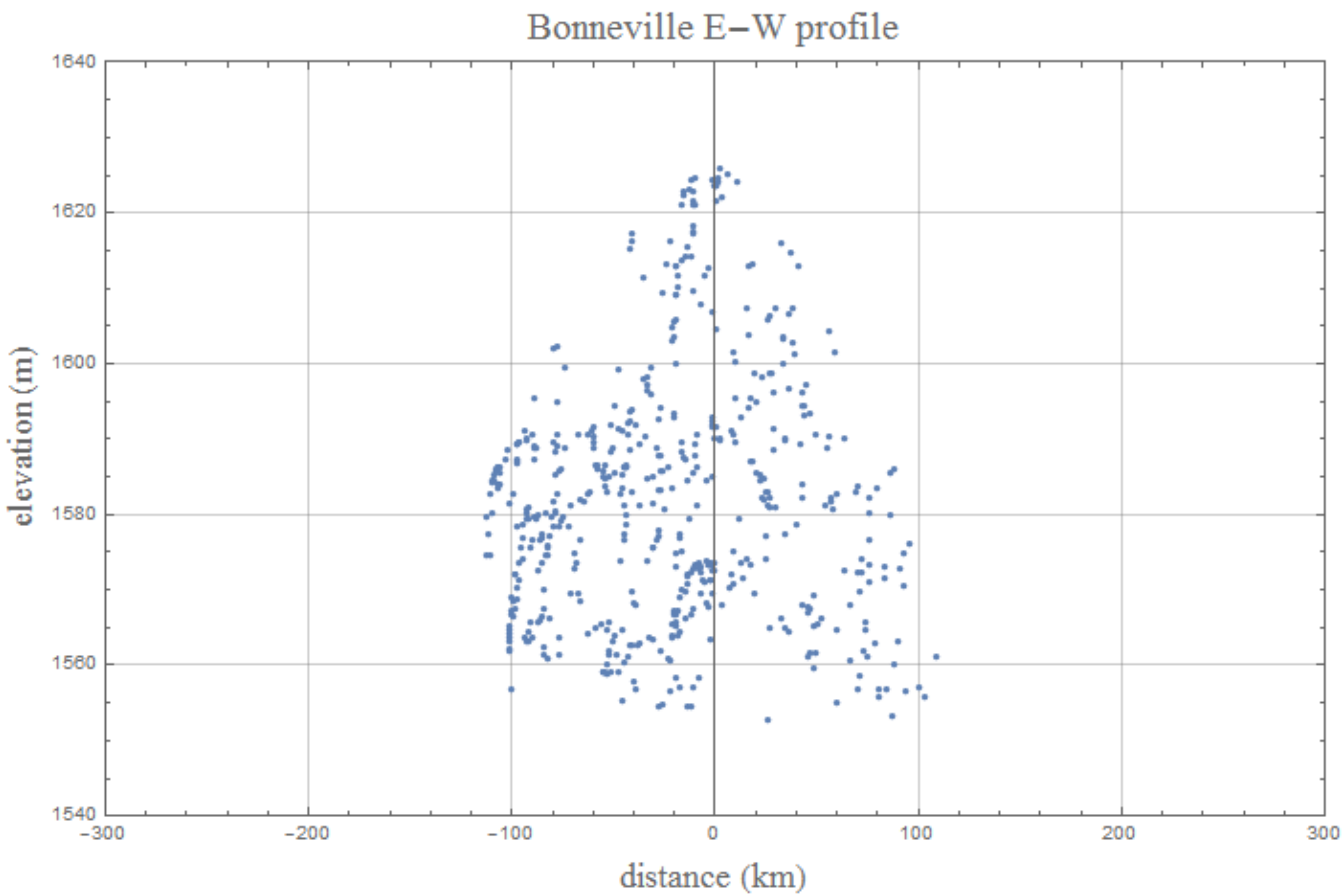
Bonneville E–W profile
elevation (m)
distance (km)
1640
1620
1600
1580
1560
1540
−300
−200
−100
0
100
200
300

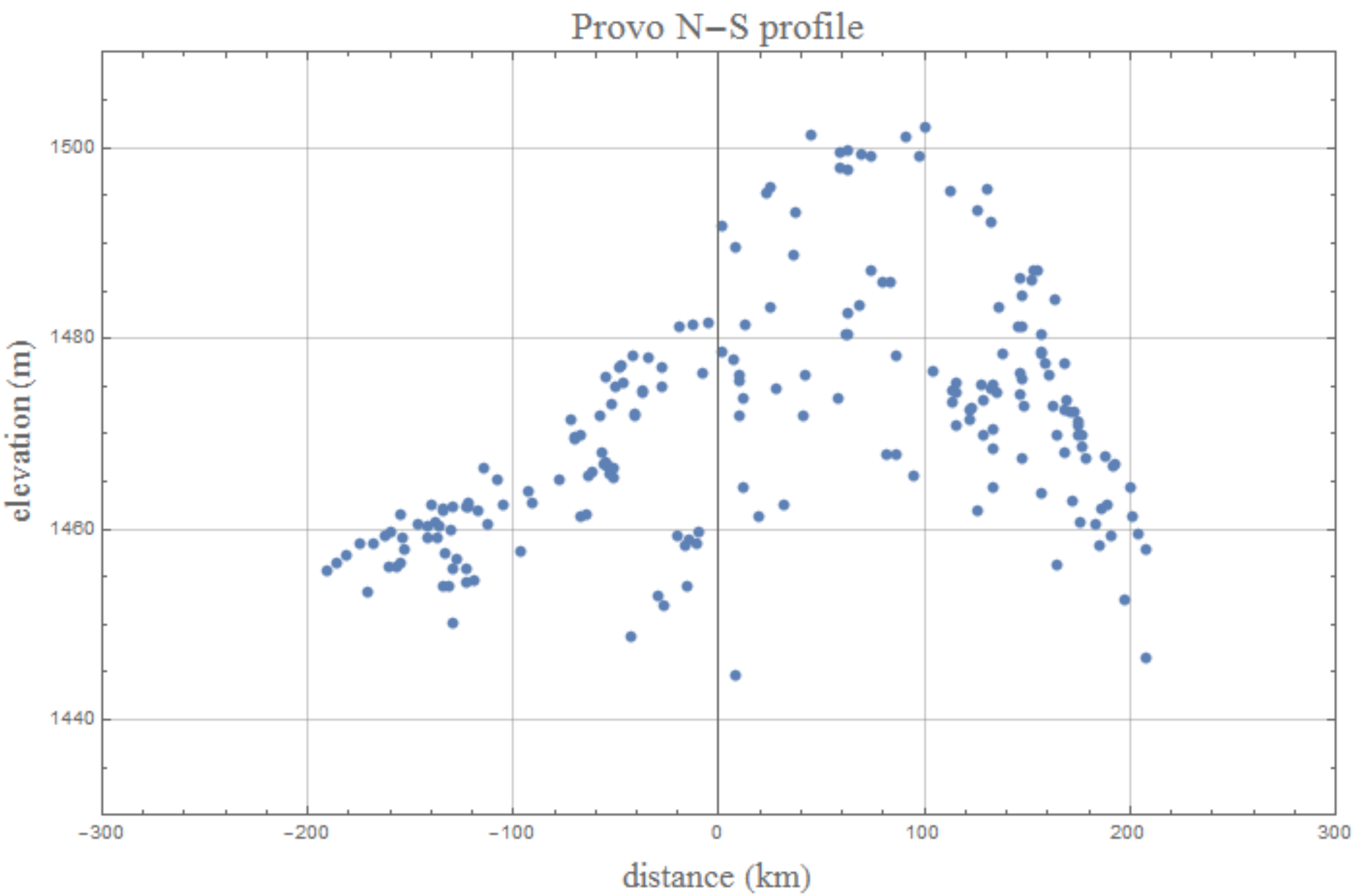
Provo N–S profile
elevation (m)
1500
1480
1460
1440
-300
-200
-100
0
100
200
300
distance (km)

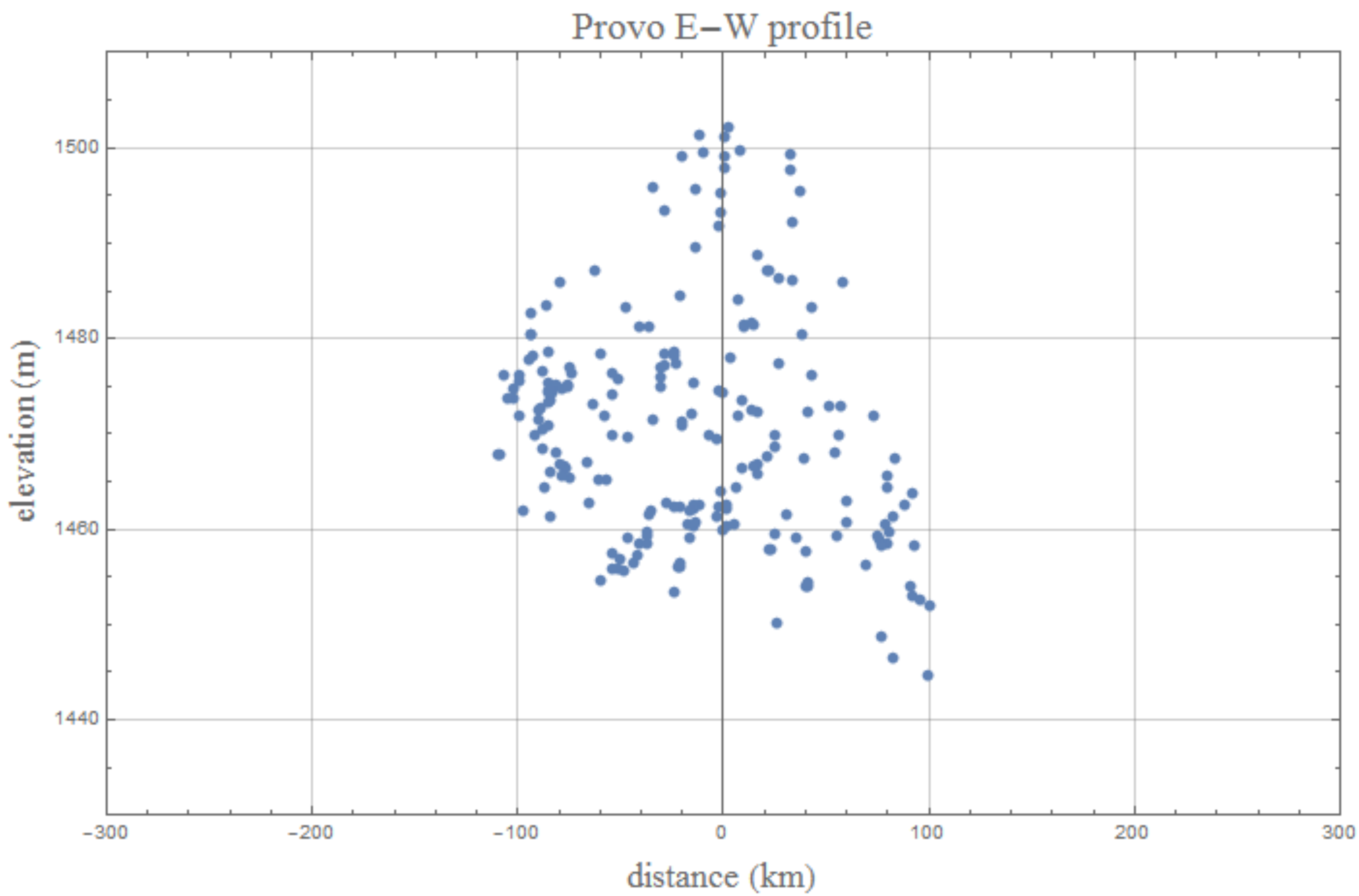
Provo E–W profile
elevation (m)
distance (km)
1500
1480
1460
1440
−300
−200
−100
0
100
200
300

elastic plate model

We examine the response
to applied loads (force/unit area)
of an elastic plate floating on a fluid substrate.

The load is resisted by two different processes:

- buoyant response of the substrate
- bending of the plate

Archimedes' principle states that the upward buoyant force is equal to the weight (mass times gravity) of the displaced material.

Bending of an elastic plate requires a force proportional to the curvature of the plate.

We can write the vertical force balance as

$$\underbrace{k_{wat}}_{\text{load}}\, d = \underbrace{k_{sub}}_{\text{buoyancy}}\, w + D\, \underbrace{\nabla^4}_{\text{bending}} w$$

where:

d is water load depth

w is vertical deflection of the surface

k_{wat} = g ρ_{wat} (load per unit depth)

k_{sub} = g ρ_{sub} (response per unit deflection)

g = 9.8 m/s^2 (gravity)

$$\nabla^4 = \left(\frac{\partial^2 \partial}{\partial x^2} + \frac{\partial^2 \partial}{\partial x^2}\right)^2$$ (bi-harmonic differential operator)

The plate flexural parameter $\boldsymbol{D}$ is a measure of the resistance to bending.

For a plate with thickness $\boldsymbol{T}$,
elastic rigidity $\boldsymbol{\mu}$, and Poisson ratio $\boldsymbol{\nu}$, the value is

$$D = \frac{\mu \, T^3}{6(1-\nu)}$$

We adopt values of $\nu = 1/2$ and $\mu = 32 \; GPa$,
but leave plate thickness T as a free parameter.

elastic plate model

elastic plate model

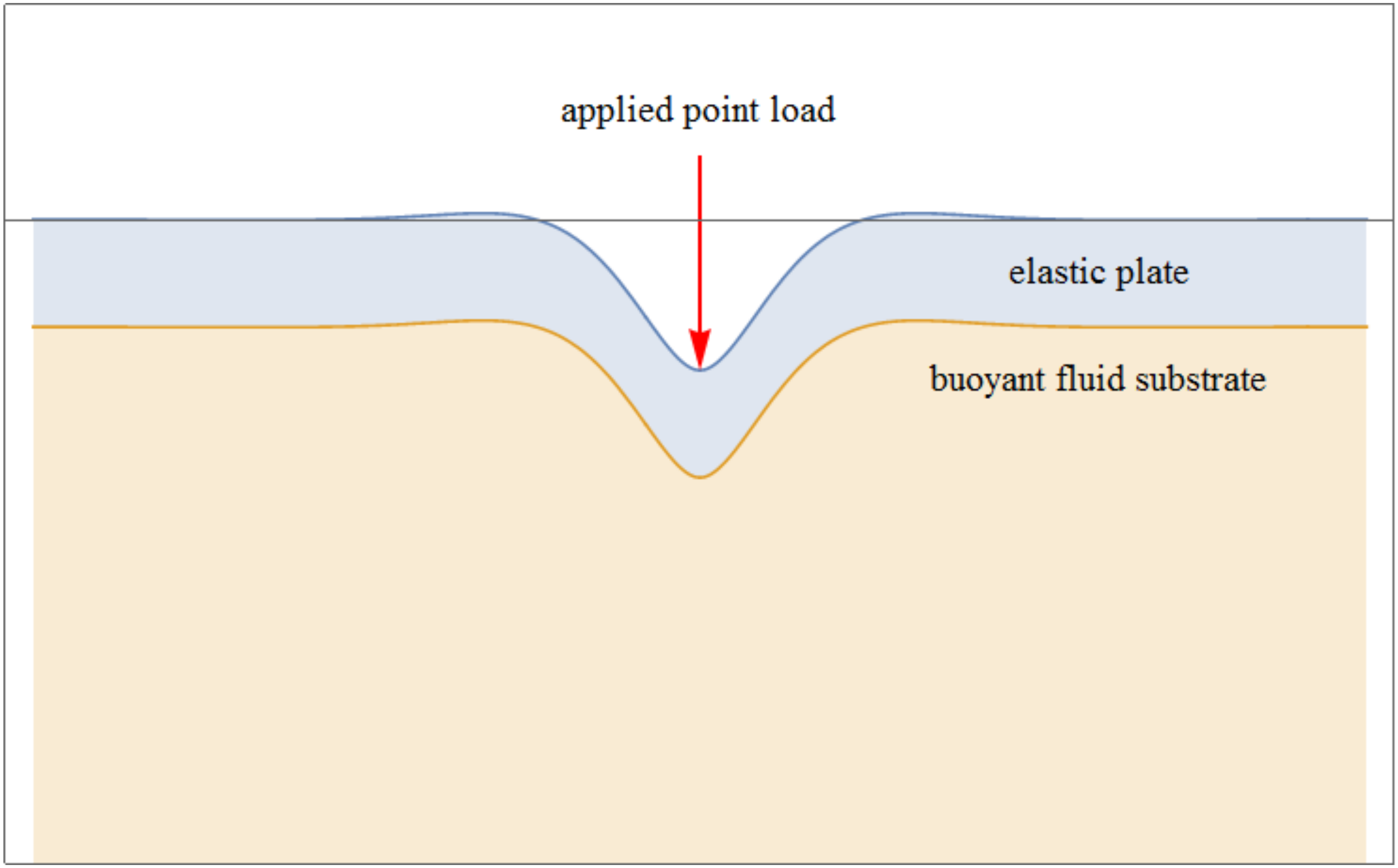

In practice, our elastic plate model has 3 free parameters:

- z lake water surface elevation
- T elastic plate thickness
- ρ_{sub} substrate density

The first parameter determines the depth and areal extend of the load.

The last 2 parameters characterize the solid Earth resistance to the load.

One of our objectives is to see if there is a single Earth model (T, ρ_{sub}) which works well for both Bonneville and Provo shorelines.

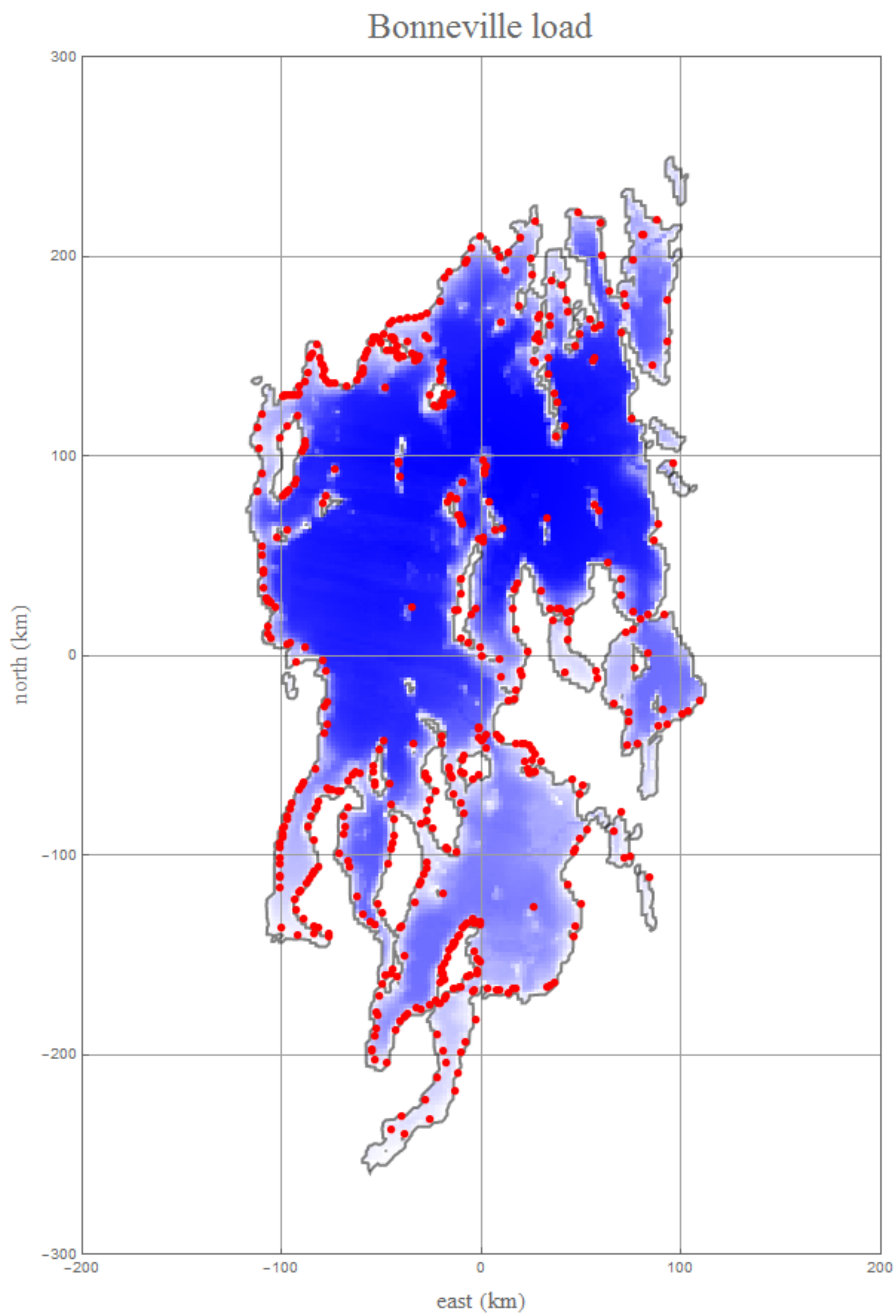
Bonneville load
300
200
100
0
-100
-200
-300
-200
-100
0
100
200
north (km)
east (km)

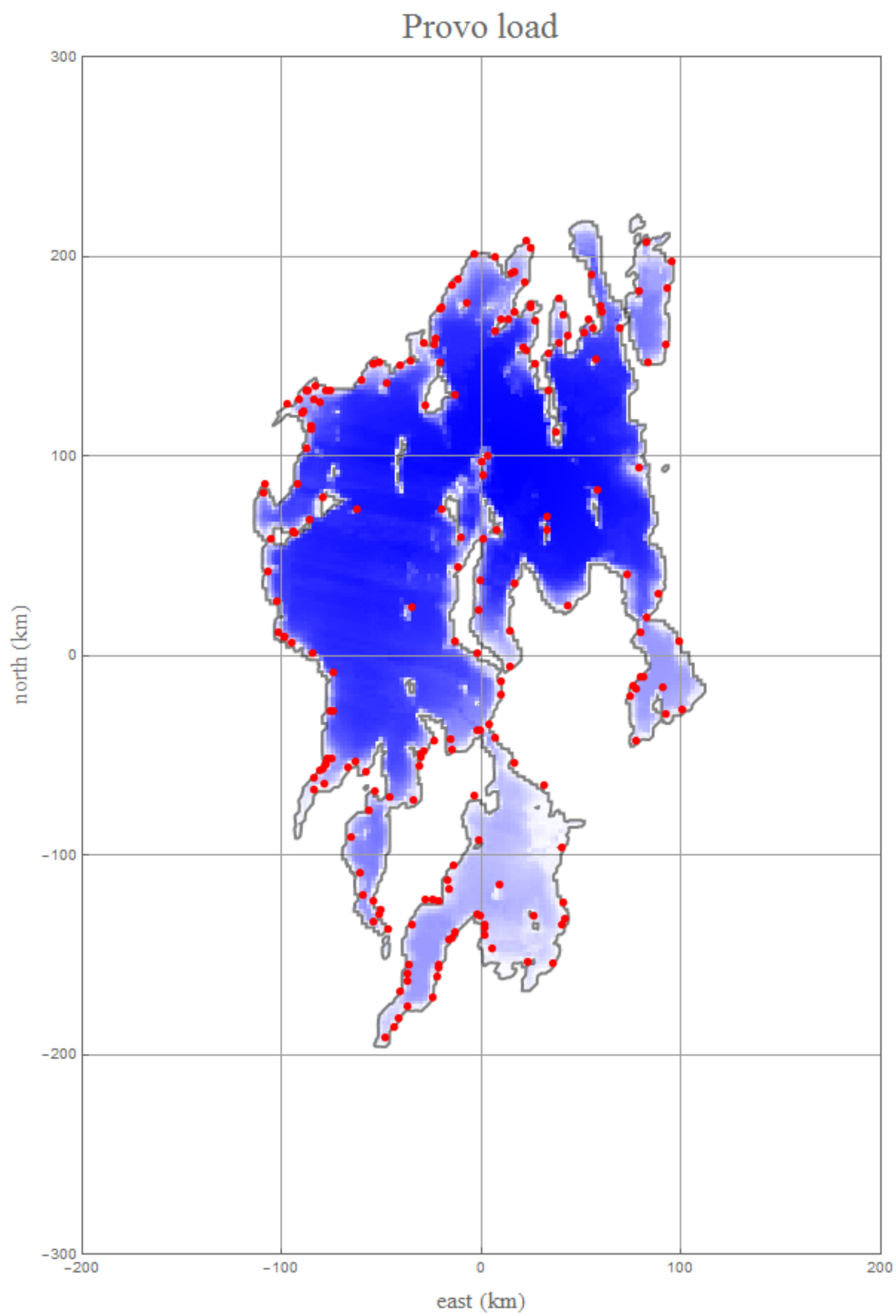

Provo load
300
200
100
0
−100
−200
−300
north (km)
−200
−100
0
100
200
east (km)

best-fitting parameter values for Bonneville

plate thickness:	(19.94	$\pm$ 0.10)	km
substrate density:	(3813	$\pm$ 15)	kg/m^3
water surface elevation:	(1553.42	$\pm$ 0.10)	m

data variance:	278.7 m^2
model variance:	266.6 m^2
residual variance:	10.0 m^2

best-fitting parameter values for Provo

plate thickness:	(15.65 ± 0.22)	km
substrate density:	(3726 ± 30)	kg/m^3
water surface elevation:	(1453.30 ± 0.14)	m

data variance:	149.9 m^2
model variance:	133.6 m^2
residual variance:	15.3 m^2

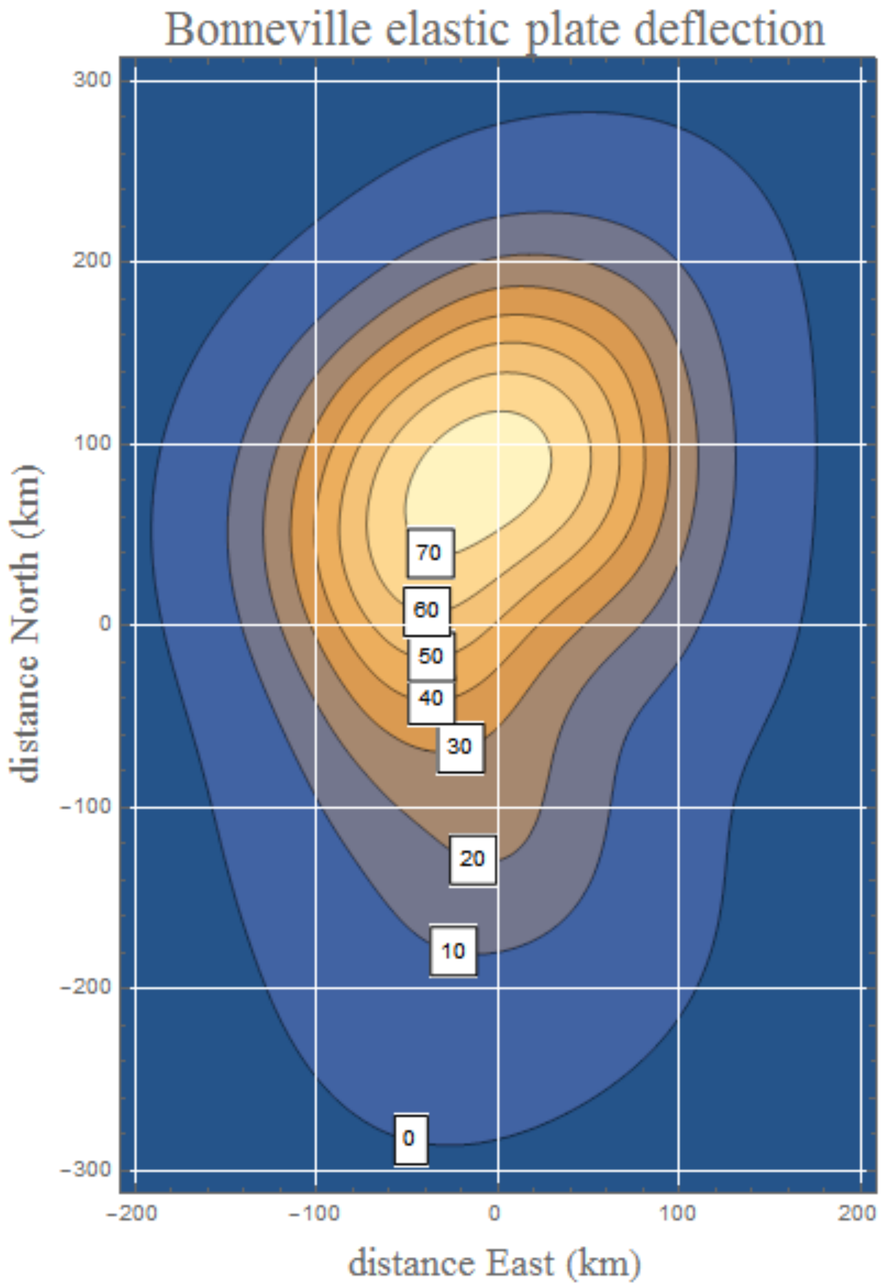

Bonneville elastic plate deflection
distance North (km)
distance East (km)
300
200
100
0
-100
-200
-300
-200
-100
0
100
200
70
60
50
40
30
20
10
0

Bonneville elastic plate deflection

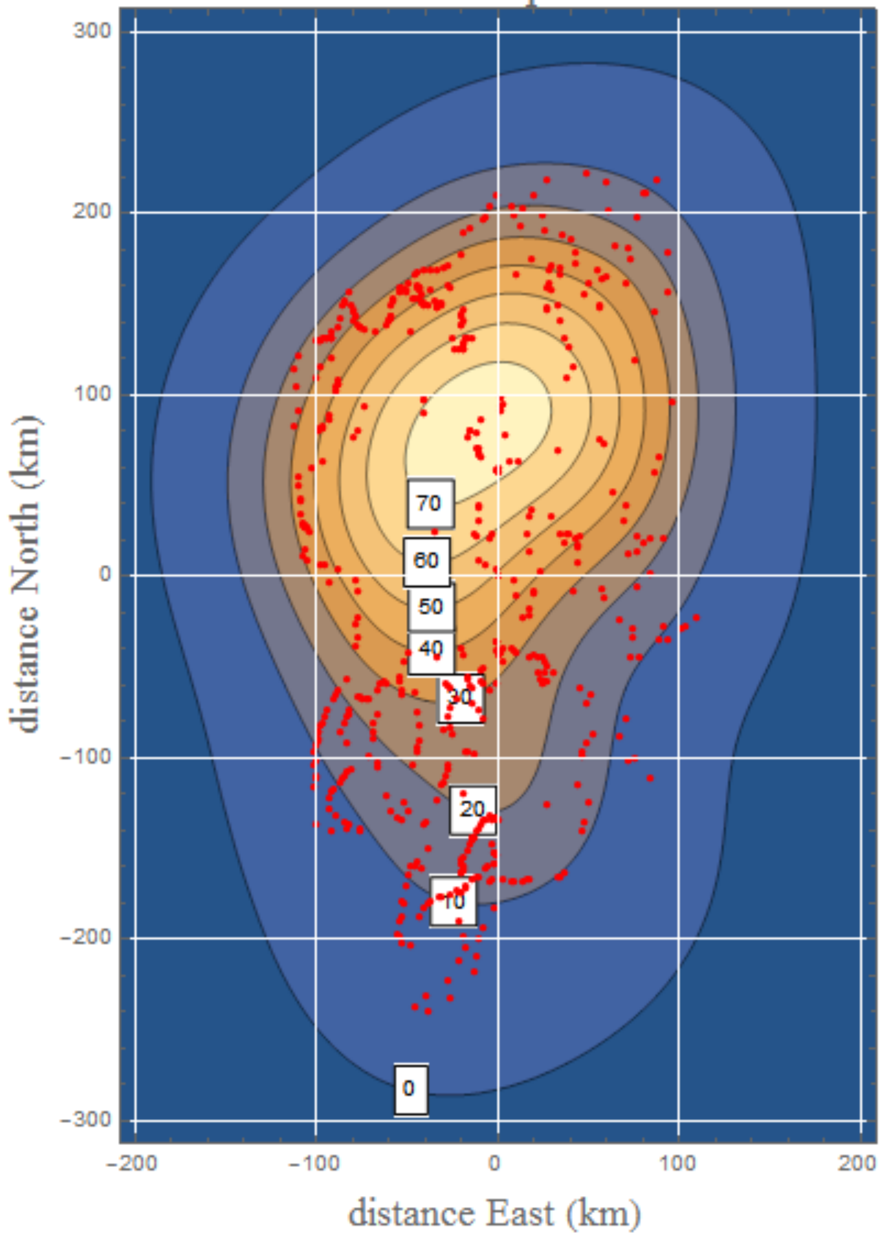

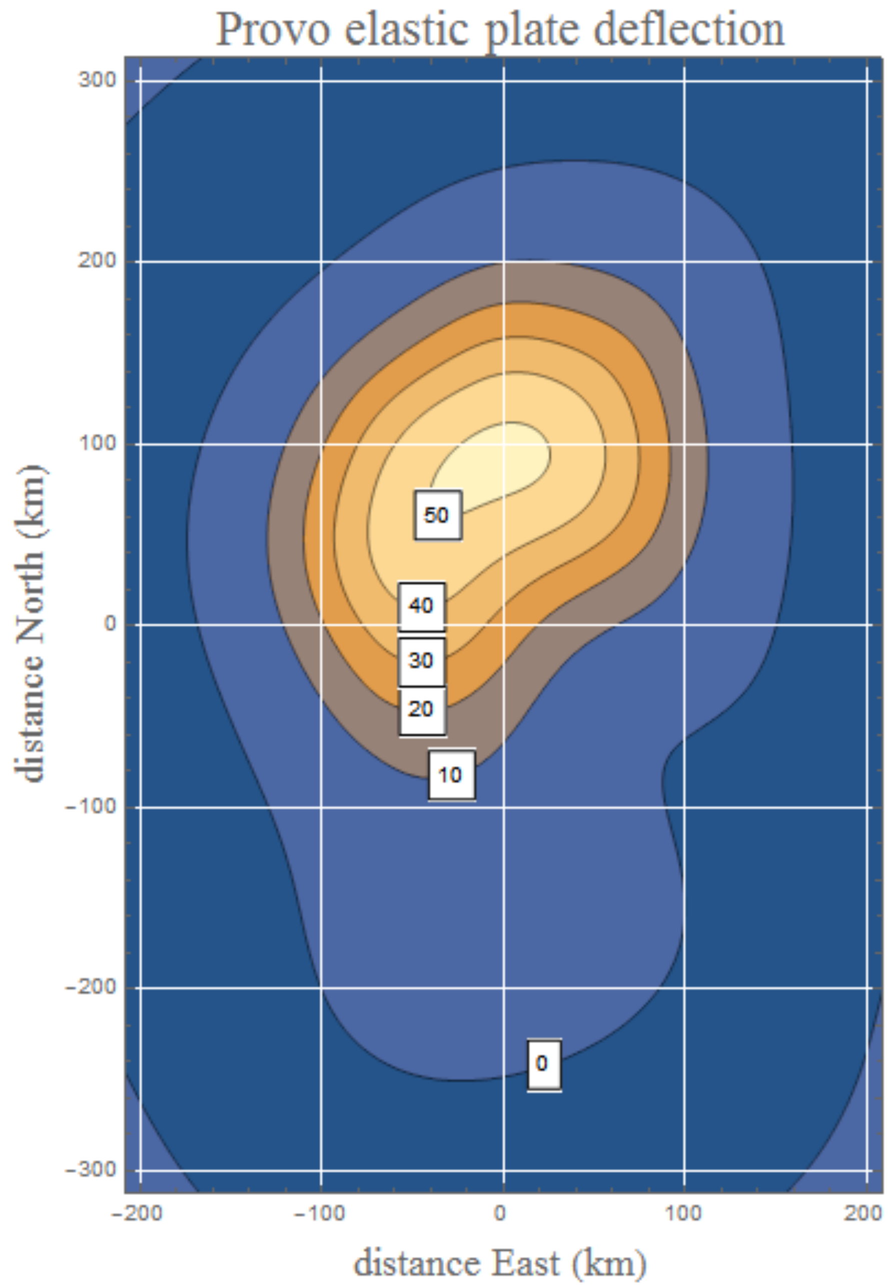

Provo elastic plate deflection
300
200
100
0
-100
-200
-300
-200
-100
0
100
200
distance North (km)
distance East (km)
50
40
30
20
10
0

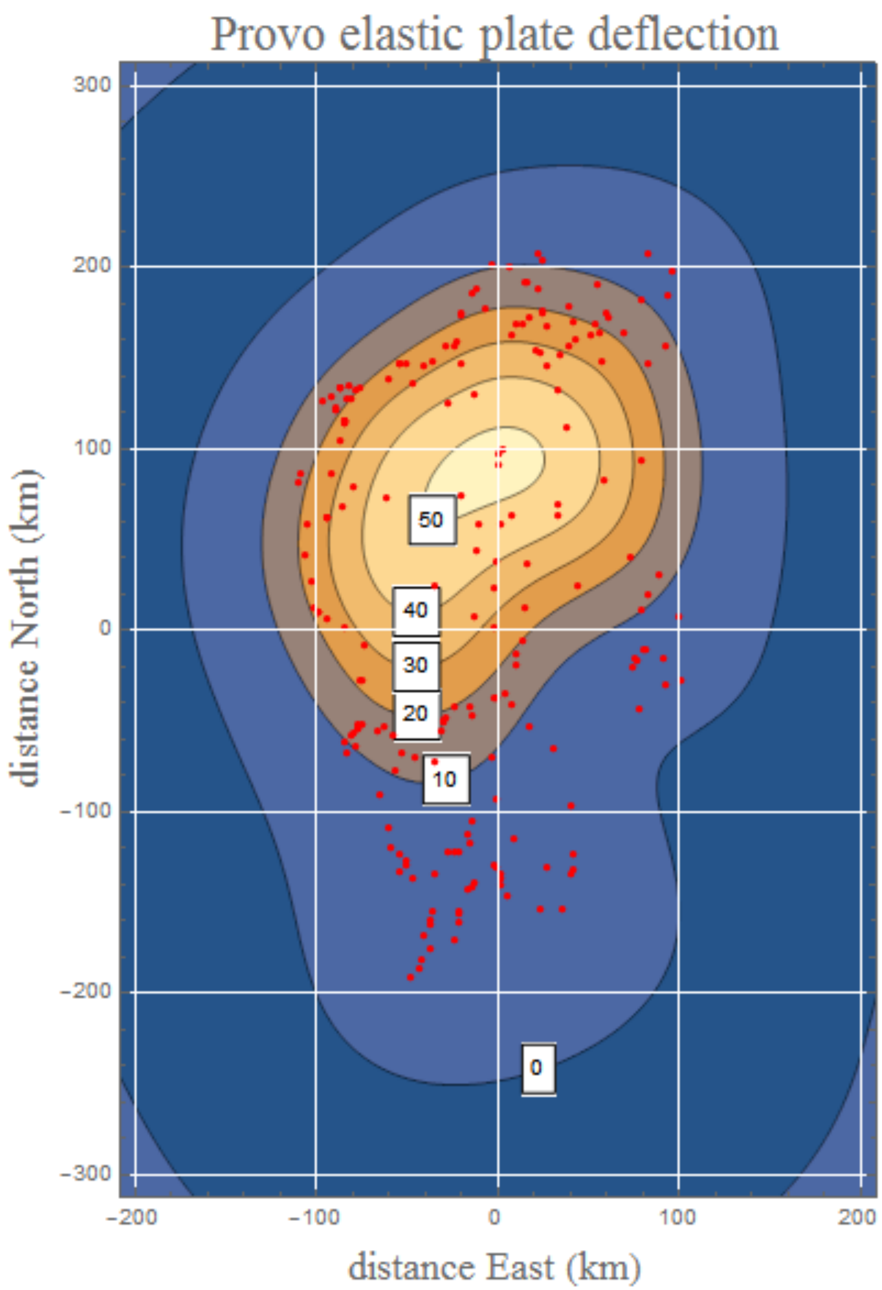

Provo elastic plate deflection
distance North (km)
distance East (km)
300
200
100
0
-100
-200
-300
-200
-100
0
100
200
50
40
30
20
10
0

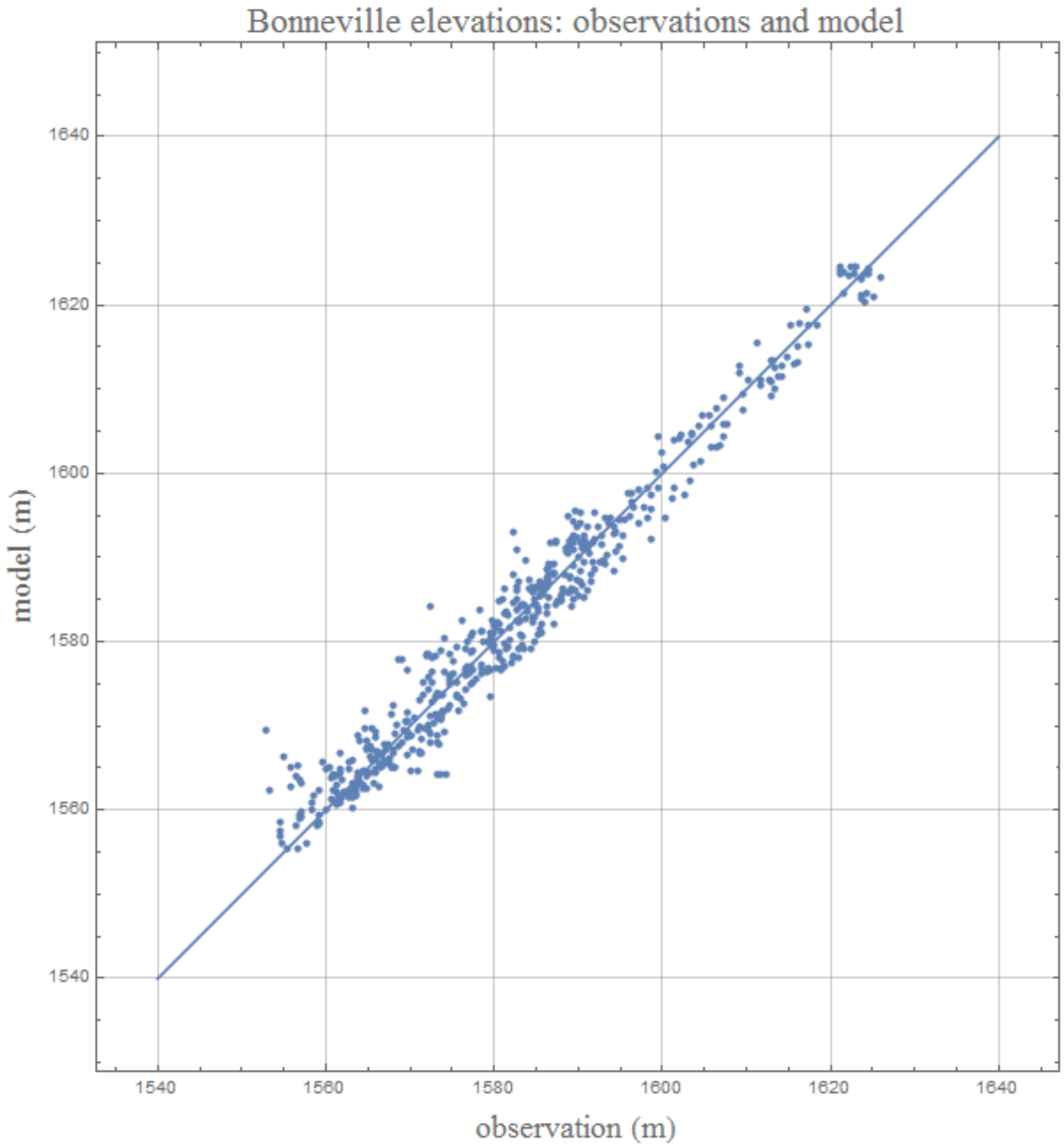

Bonneville elevations: observations and model
model (m)
1540
1560
1580
1600
1620
1640
observation (m)

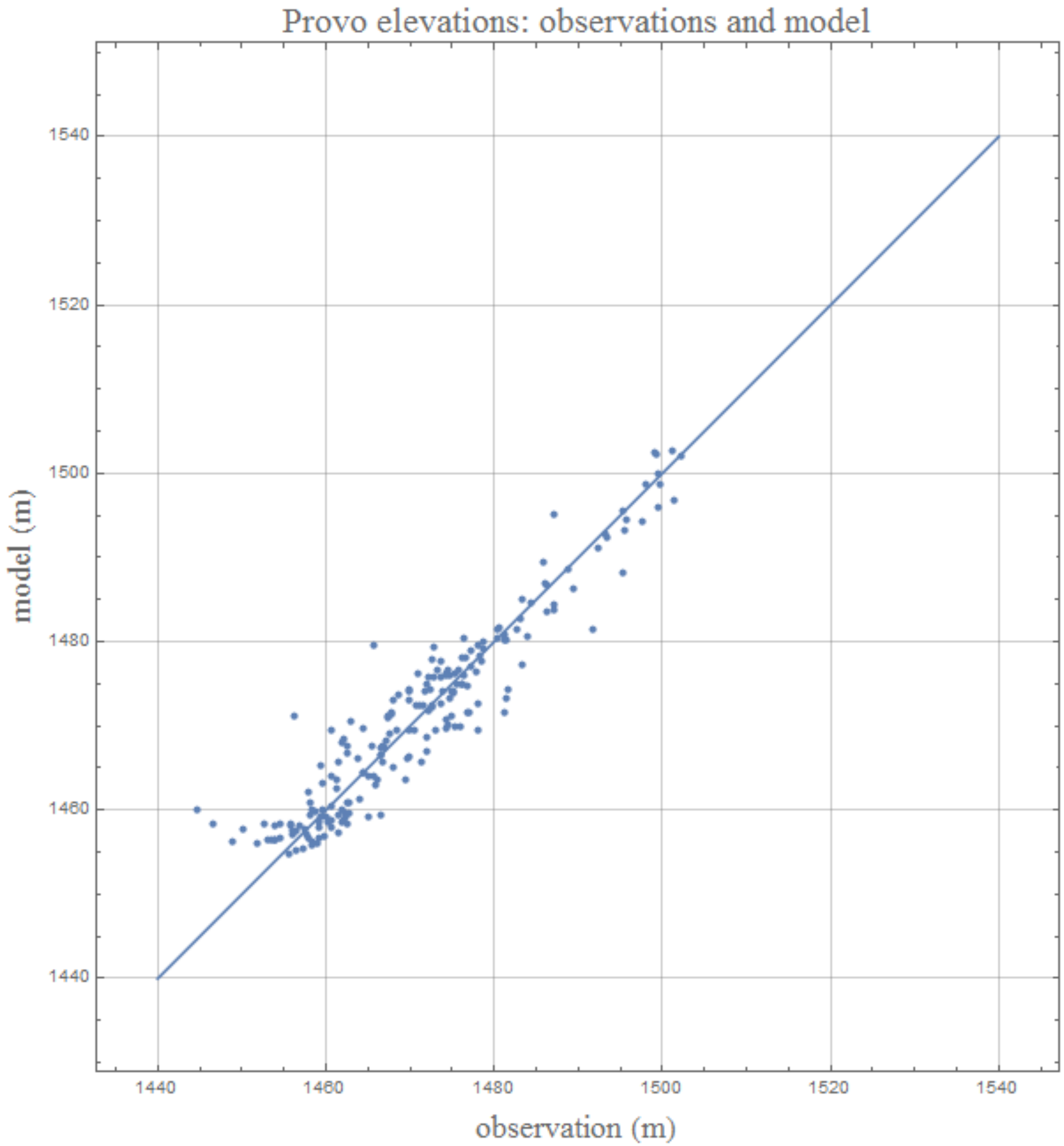
Provo elevations: observations and model
model (m)
observation (m)
1440
1460
1480
1500
1520
1540
1440
1460
1480
1500
1520
1540

residual = observed - computed

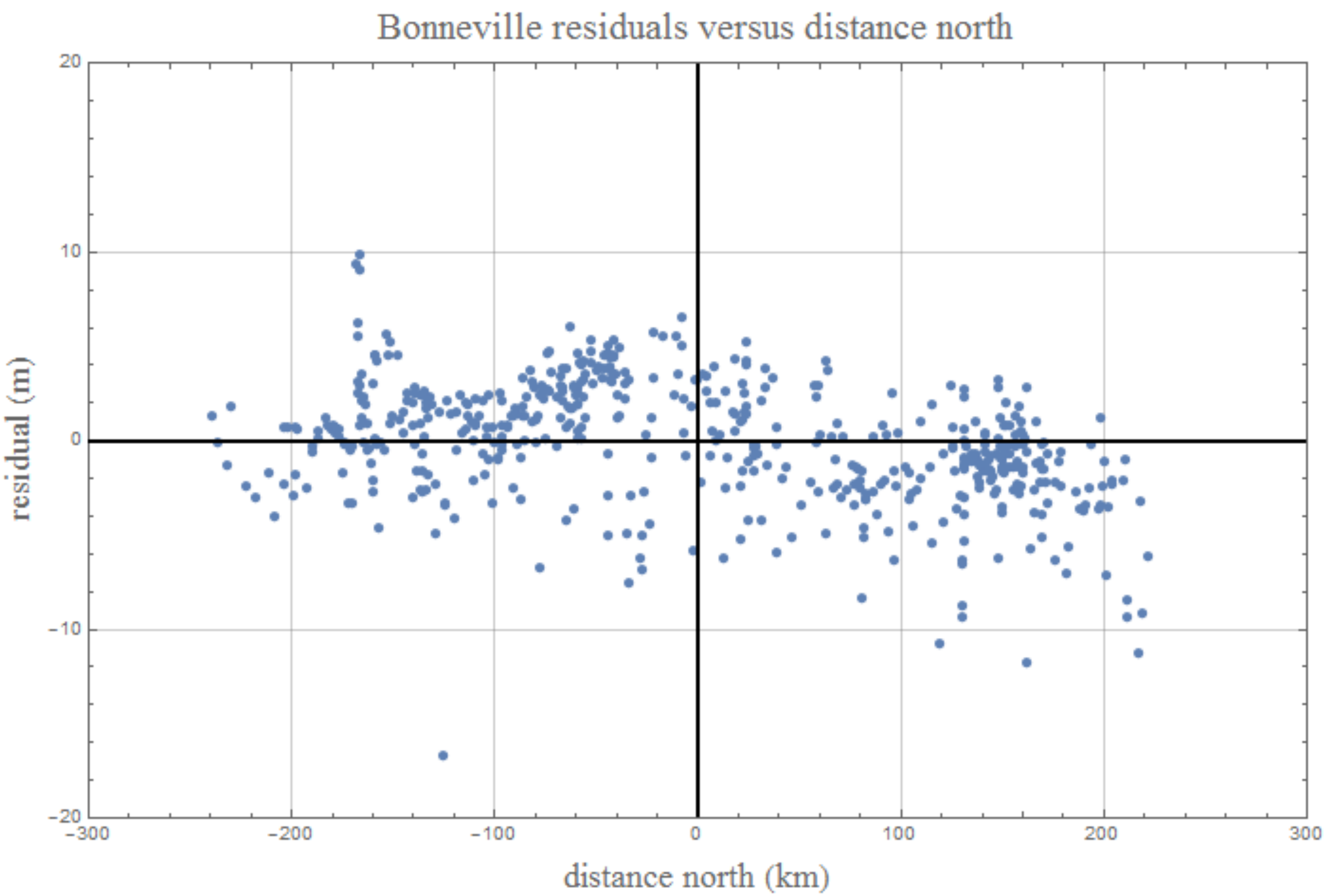

residual = observed - computed

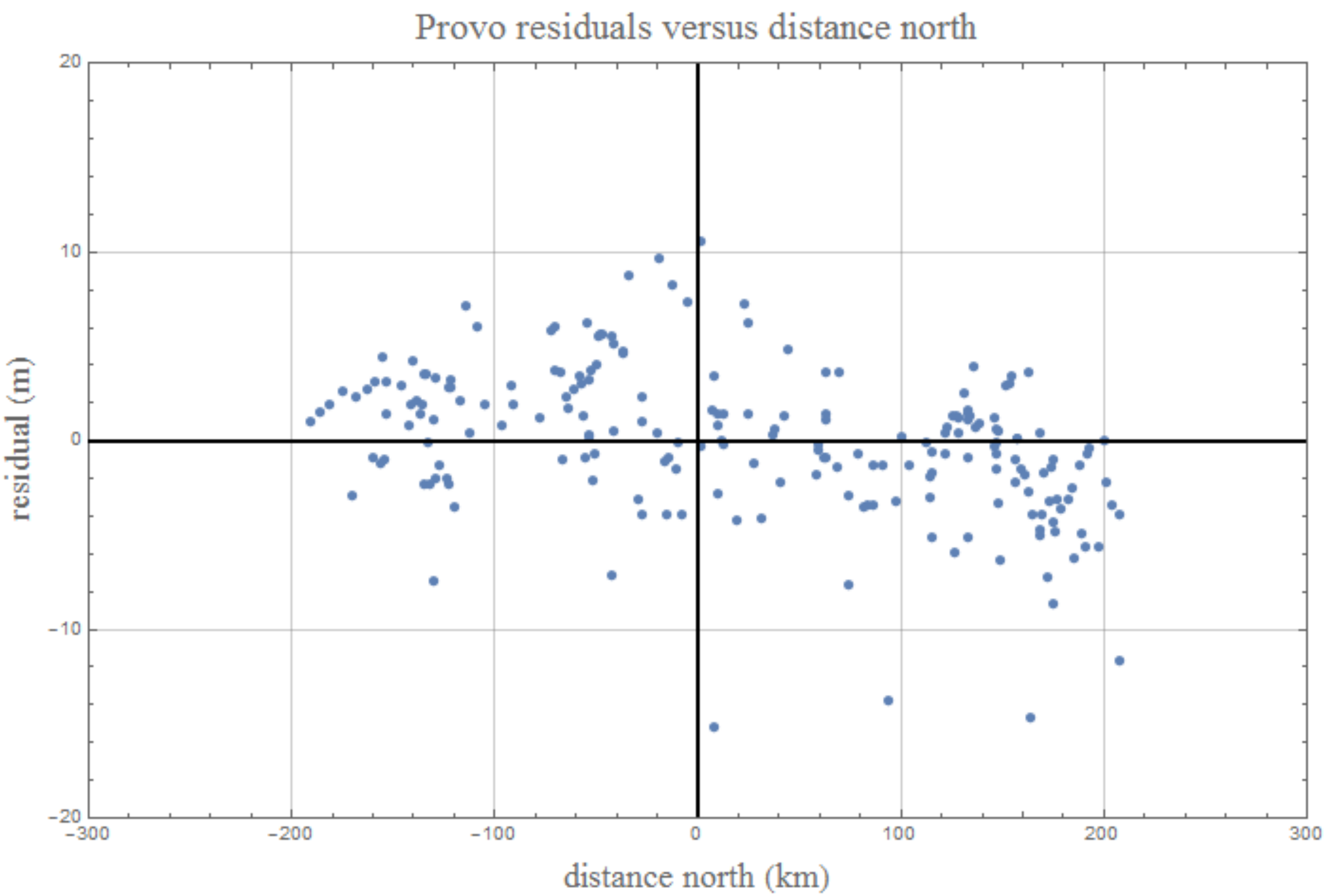

If these models were "properly" fitting the data, we would expect the residuals to be random, and not spatially coherent.

Instead, we find that there are coherent patterns in the residuals.

We expect that they are due to:

1. sedimentary loads
2. volcanic offsets
3. faulting offsets
4. other effects

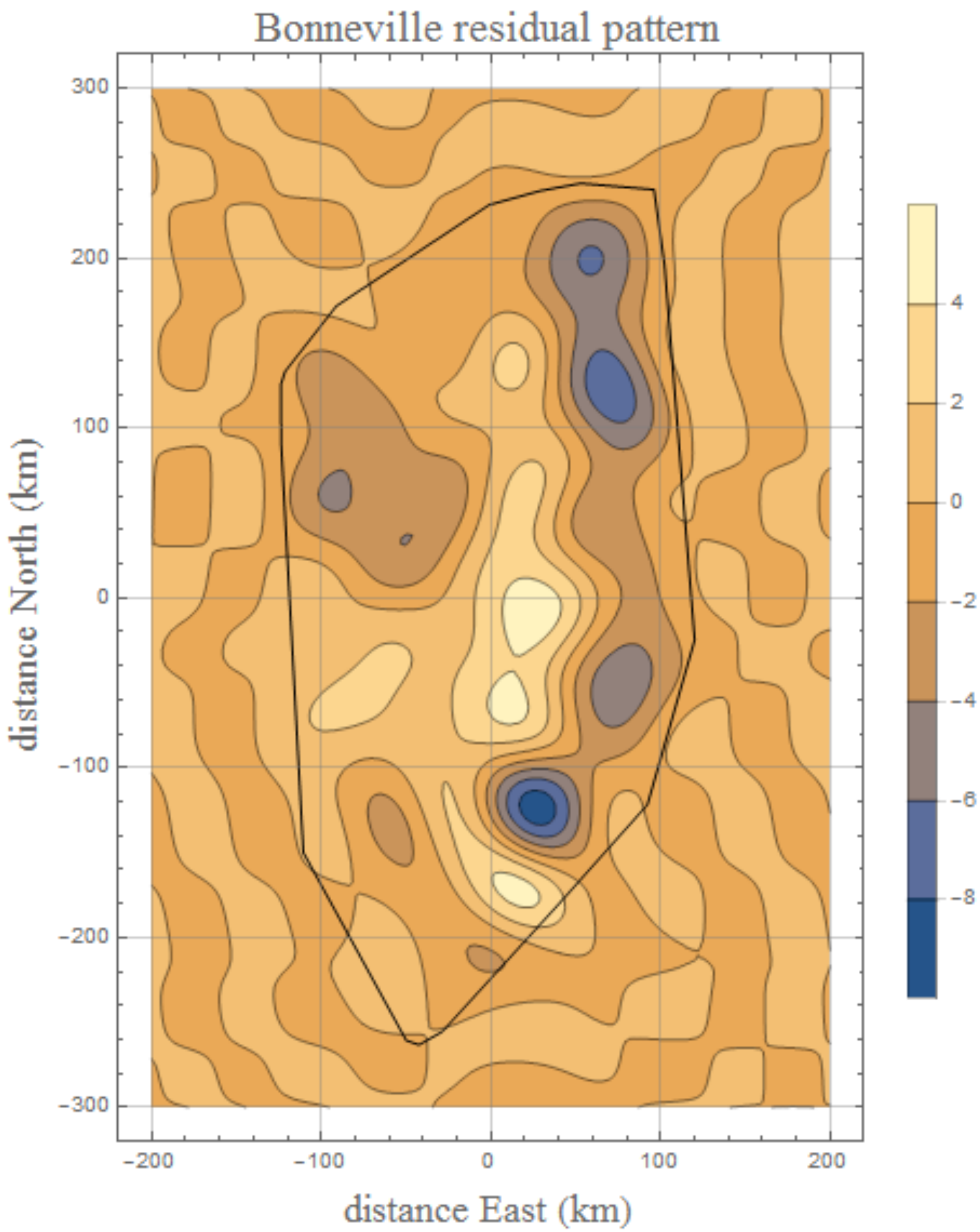

Bonneville residual pattern
300
200
100
0
-100
-200
-300
-200
-100
0
100
200
distance North (km)
distance East (km)
4
2
0
-2
-4
-6
-8

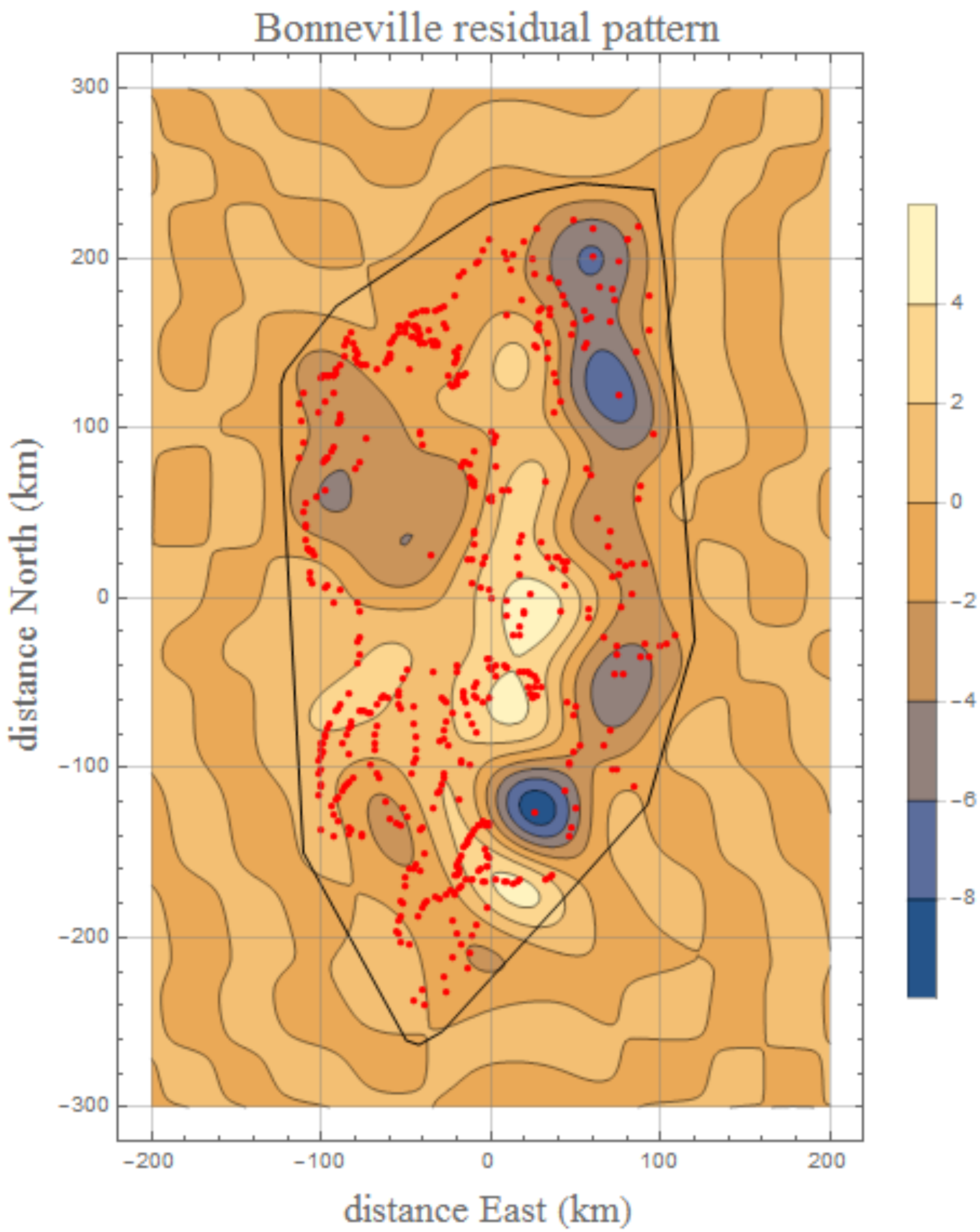
Bonneville residual pattern
300
200
100
0
-100
-200
-300
-200
-100
0
100
200
distance North (km)
distance East (km)
4
2
0
-2
-4
-6
-8

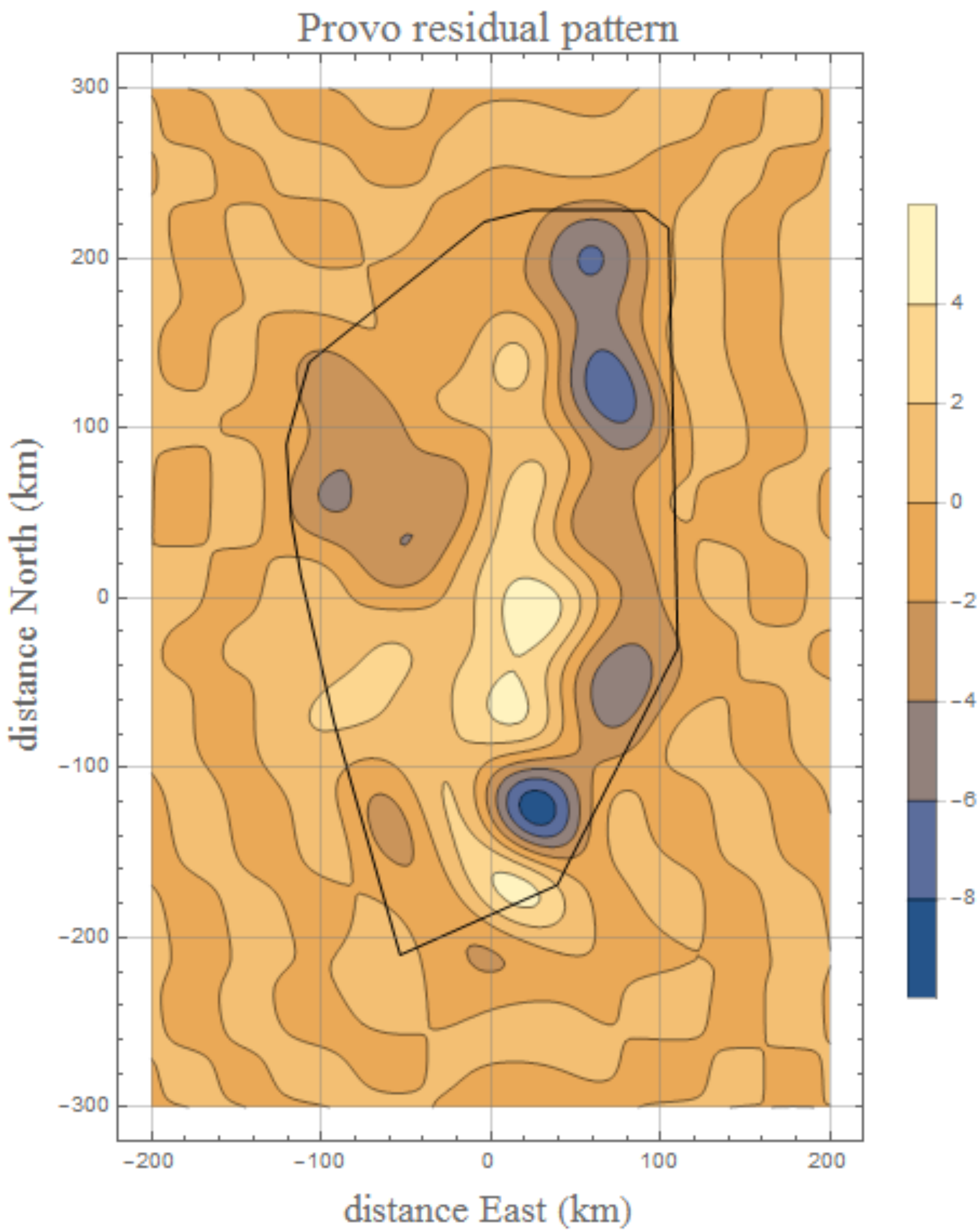
Provo residual pattern
distance North (km)
distance East (km)
300
200
100
0
-100
-200
-300
-200
-100
0
100
200
4
2
0
-2
-4
-6
-8

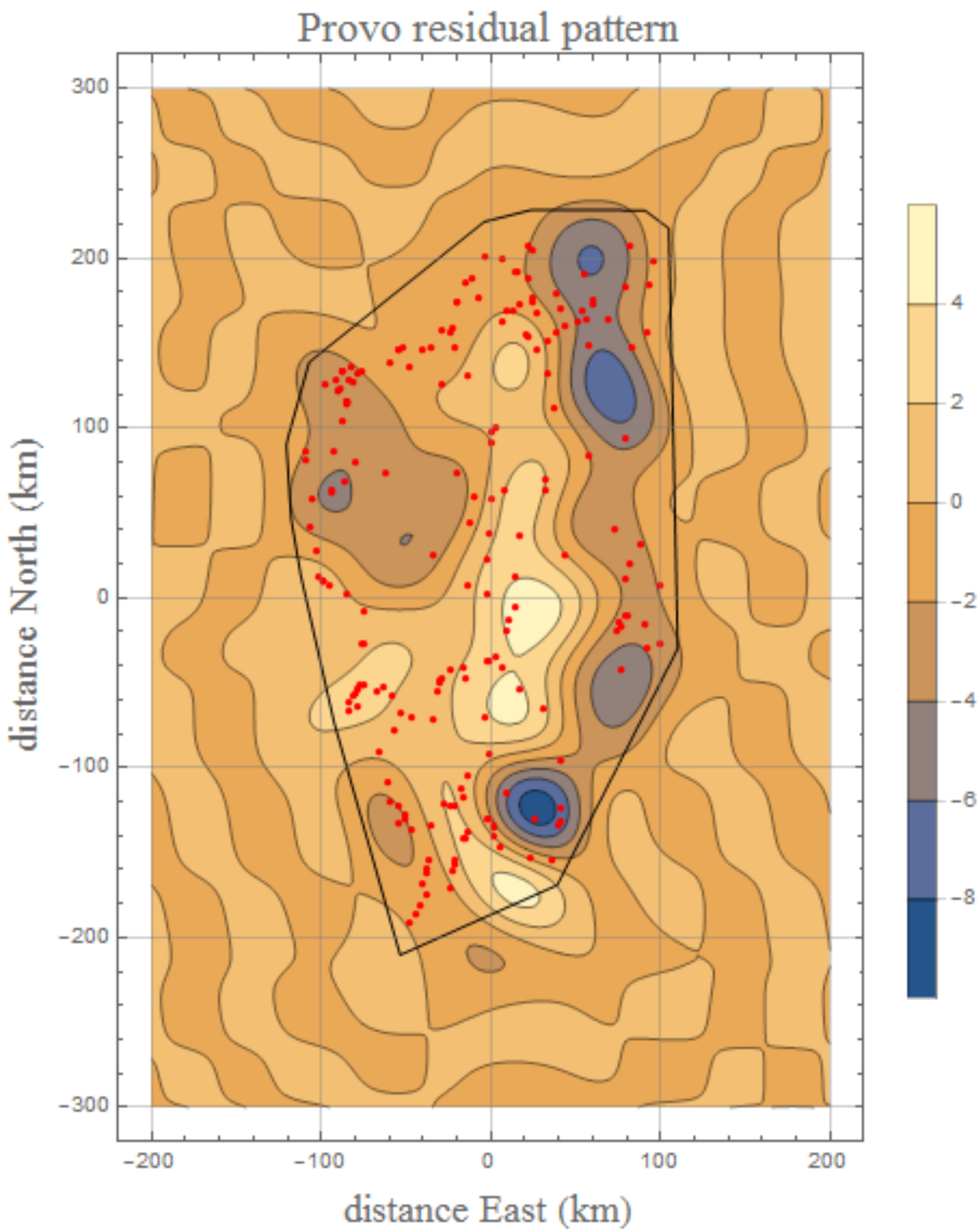
Provo residual pattern
distance North (km)
distance East (km)
300
200
100
0
-100
-200
-300
-200
-100
0
100
200
4
2
0
-2
-4
-6
-8

Using the Bonneville-derived model parameters, we can examine the expected rebound associated with various lake surface elevations.

The next few figures summarize the results.

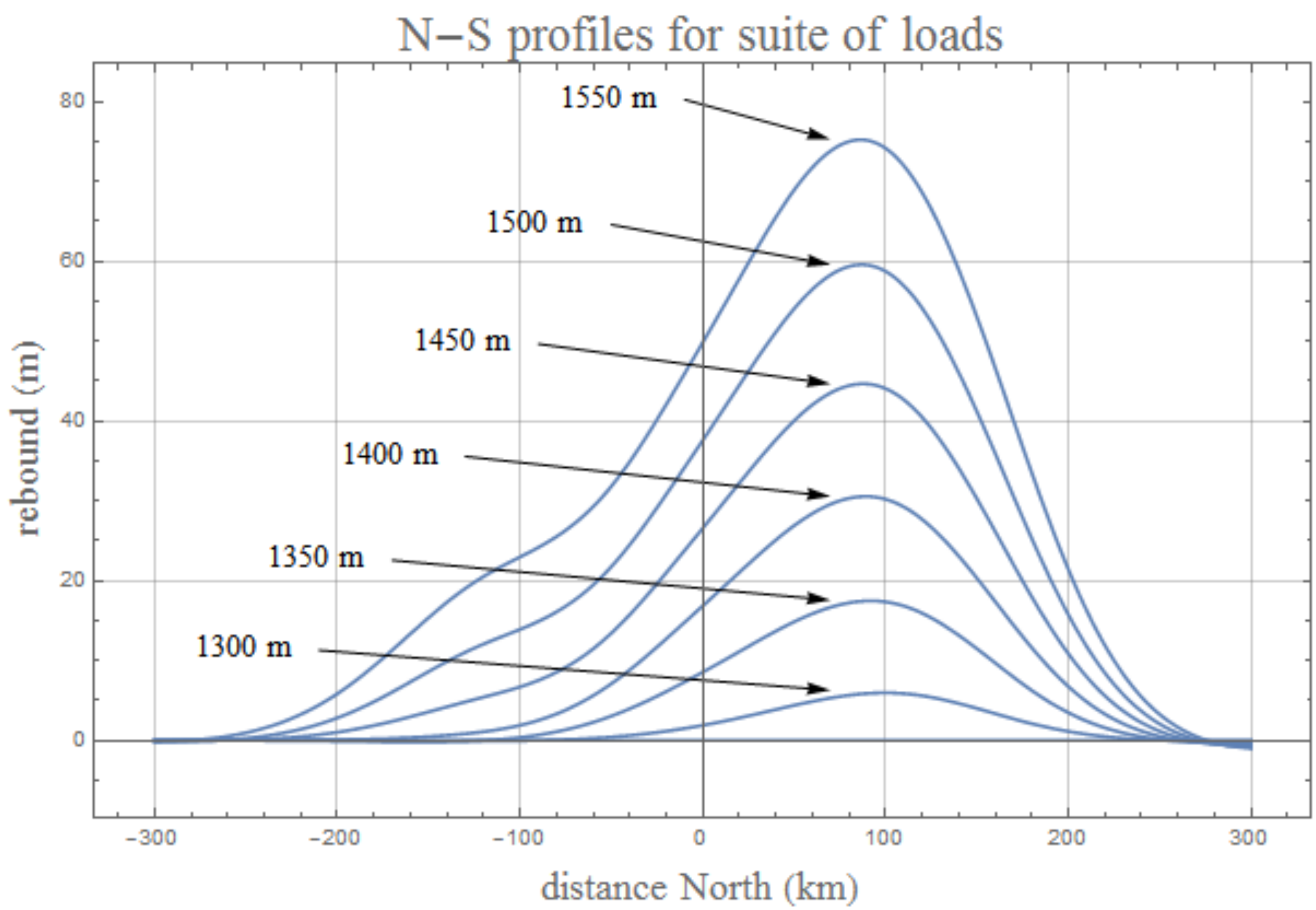
N−S profiles for suite of loads
1550 m
1500 m
1450 m
1400 m
1350 m
1300 m
rebound (m)
distance North (km)
80
60
40
20
0
−300
−200
−100
0
100
200
300

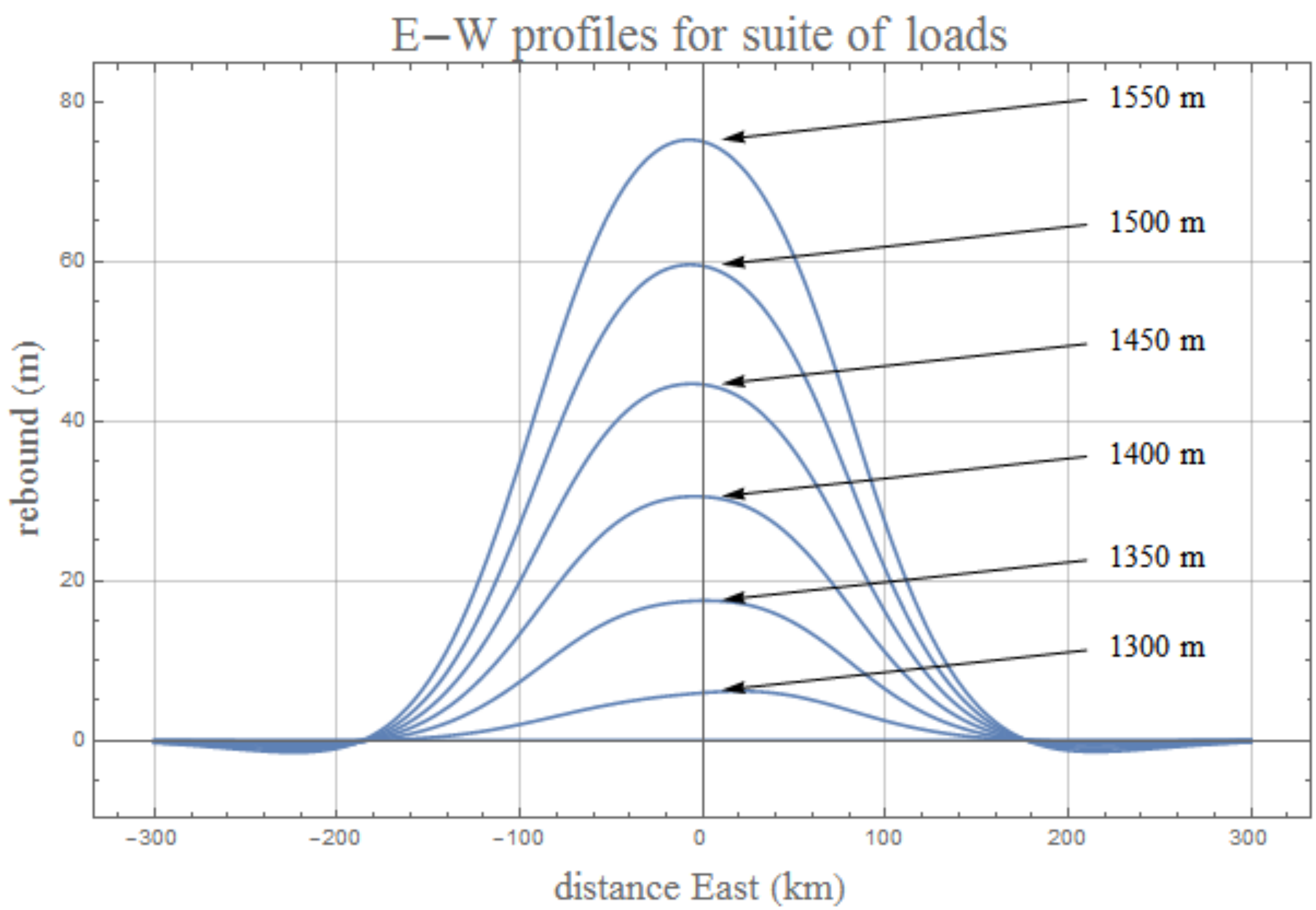
E–W profiles for suite of loads
1550 m
1500 m
1450 m
1400 m
1350 m
1300 m
80
60
40
20
0
rebound (m)
-300
-200
-100
0
100
200
300
distance East (km)

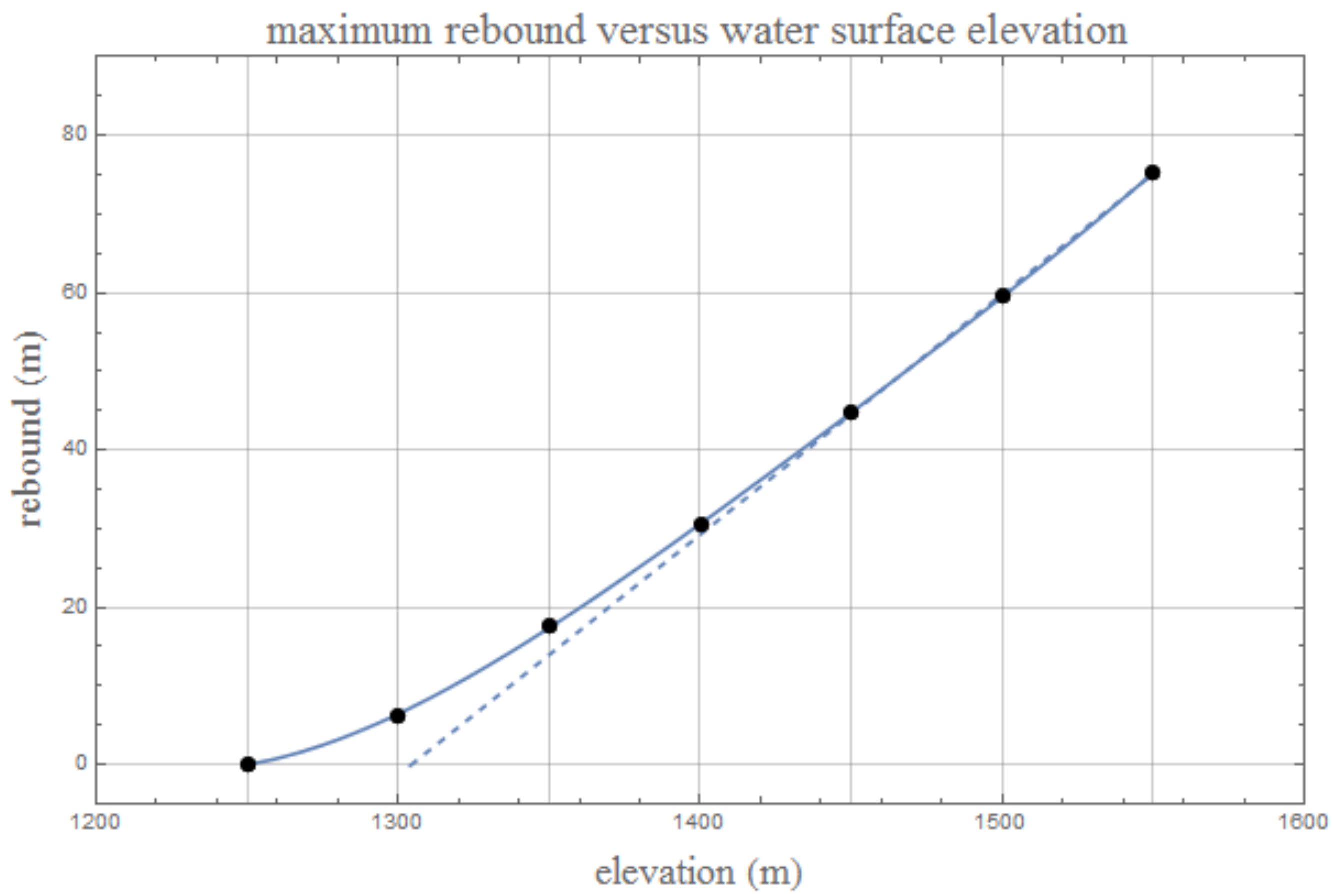

maximum rebound versus water surface elevation
rebound (m)
80
60
40
20
0
1200
1300
1400
1500
1600
elevation (m)

conclusions

An elastic plate model gives

- good fit to Bonneville
- worse fit to Provo

Best-fitting Provo parameters have

- thinner plate
- lower density substrate

compared to Bonneville

Both of these features yield larger response for a given load

Provo did not reach equilibrium.

Provo elevations record memory of a larger load in the past

NEW AGE CONTROL ON OLD LAKE CYCLES, EVIDENCE FROM LUMINESCENCE AGES FROM NORTHERN UTAH AND SOUTHERN IDAHO

Tammy M. Rittenour, Joel L. Pederson, Robert Q. Oaks Jr., Susanne U. Jänecke, Michelle S. Nelson

Department of Geology, Utah State University, Logan, UT 84322

Corresponding author (Rittenour): tammy.rittenour@usu.edu

ABSTRACT

Age control for lake phases of pluvial Lake Bonneville has largely been accomplished using radiocarbon dating. However, radiocarbon results can have inherent errors related to old and young carbon contamination, interpreted association of the material dated and the depositional context, and added uncertainty related to the need to calibrate ages into calendar years. Optically stimulated luminescence (OSL) affords an independent dating method for sediment deposition by providing an age estimate of the last time sediment was exposed to light. Samples for OSL dating (n=60) have been collected from a number of sites associated with Lake Bonneville in northern Utah and southern Idaho as a part of student and faculty projects at Utah State University. Most of these results have not yet been published, but they contain valuable information about the age of deposits associated with the Provo, Bonneville, Cutler Dam and Little Valley lake cycles and associated alluvial and lacustrine deposits in Thatcher basin. OSL results reported here and others from the literature (e.g., Kaufman and others, 2001; Oviatt and others, 2005; Spencer and others, 2015) are summarized in reference to the available radiocarbon chronology (for the youngest lake cycles) and compared to reconstructed lake-level sequences. A subset of the OSL chronology is reported in Oaks and others (this volume) along with stratigraphic evidence for four pluvial lake cycles in Cache Valley. We highlight differences and similarities between the OSL and radiocarbon chronologies and discuss implications for the timing of Bear River diversion and paleoclimate/paleoenvironmental interpretations of the OSL-based Bonneville Basin pluvial record.

REFERENCES

Kaufman, D.S., Forman, S.L. and Bright, J., 2001, Age of the Cutler Dam alloformation (late Pleistocene), Bonneville basin, Utah: Quaternary Research, v. 56, p. 322–334.

Oaks, R.Q., Jr., Jänecke, S.U., Rittenour, T.M., Erickson, T.L., and Nelson, M.S., 2019, OSL age dating of two, perhaps three, pre-Bonneville deep-water pluvial lakes in Cache Valley, Utah-Idaho—Implications of their unexpected high altitudes for excavation of Cutler Narrows from a level above 1494 m (4901'), down to the present level of 1314 m (4310') mainly during the Bonneville lake cycle, *in* Lund, W.R., McKean, A.P., and Bowman, S.D., editors, Proceedings volume 2018 Lake Bonneville geologic conference and short course: Utah Geological Survey Miscellaneous Publication 170.

Oviatt, C.G., Miller, D.M., McGeehin, J.P., Zachary, C., and Mahan, S., 2005, The younger Dryas phase of Great Salt Lake, Utah, USA: Palaeogeography, Palaeoclimatology, Palaeoecology, v. 219, p. 263–284.

Spencer, J.Q., Oviatt, C.G., Pathak, M., and Fan, Y., 2015, Testing and refining the timing of hydrologic evolution during the latest Pleistocene regressive phase of Lake Bonneville: Quaternary International, v. 362, p. 139–145.

This content is a PDF version of the author's PowerPoint presentation.

New Age Control on Old Lake Cycles: through the use of luminescence dating

Tammy Rittenour, Joel Pederson, Robert Oaks and Susanne Jänecke

UtahState University
DEPARTMENT OF GEOLOGY

USU LUMINESCENCE LABORATORY
http://usu.edu/geo/luminlab
1770 North Research Parkway, Suite 123, North Logan, Utah 84341

Age control is key to understanding past processes and events....

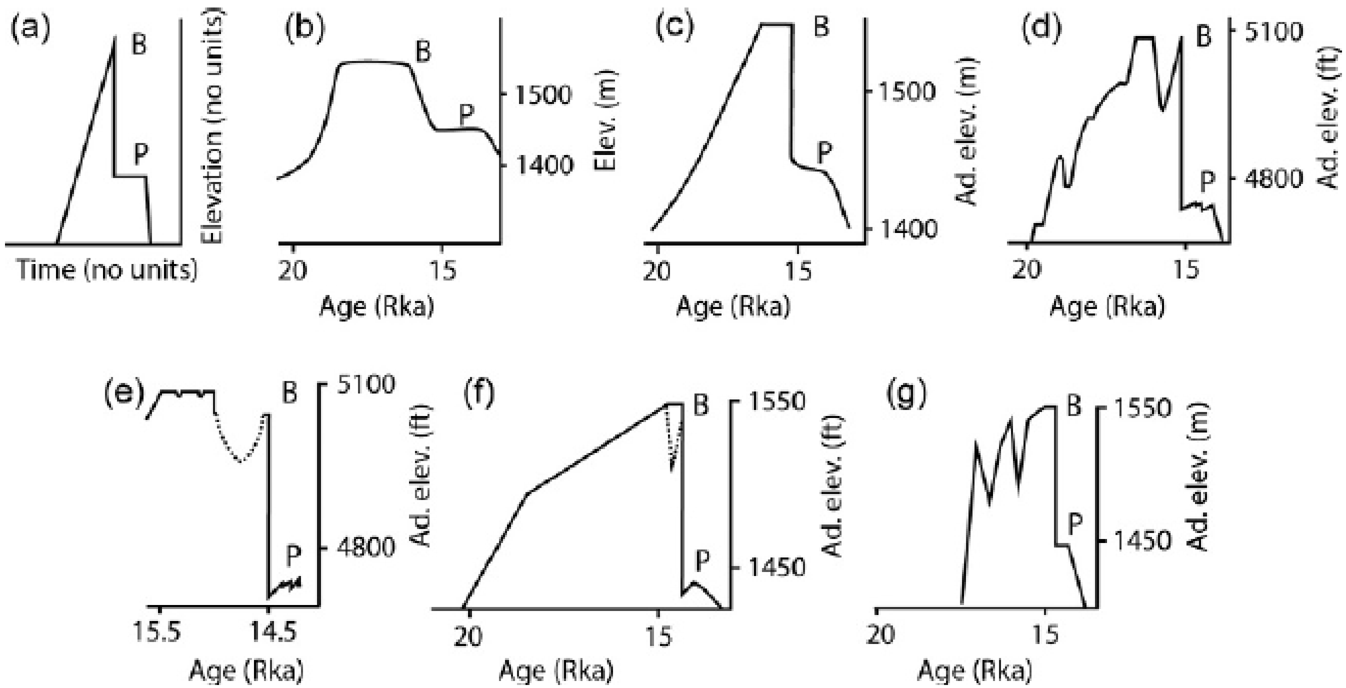

Oviatt and Jewell, 2016

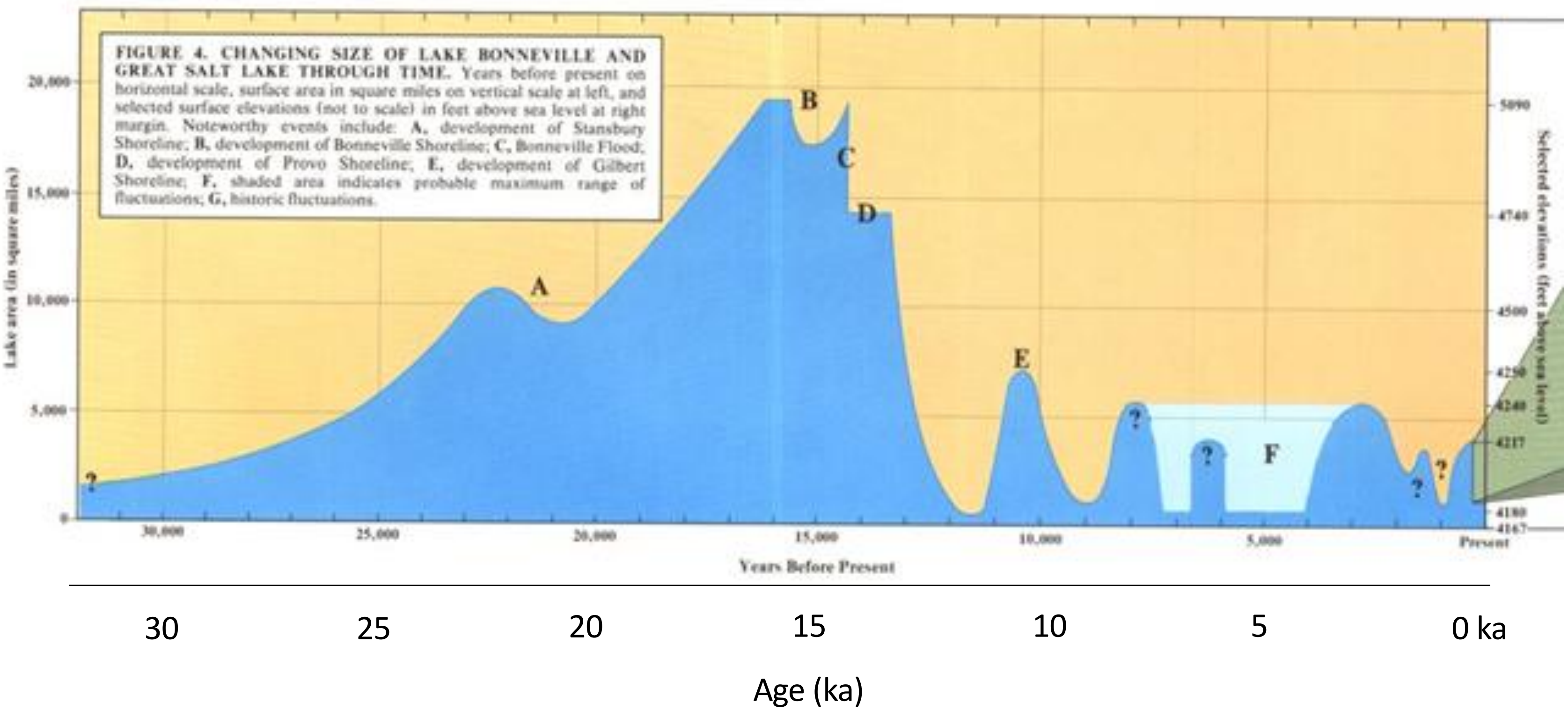

FIGURE 4. CHANGING SIZE OF LAKE BONNEVILLE AND GREAT SALT LAKE THROUGH TIME. Years before present on horizontal scale, surface area in square miles on vertical scale at left, and selected surface elevations (not to scale) in feet above sea level at right margin. Noteworthy events include: A, development of Stansbury Shoreline; B, development of Bonneville Shoreline; C, Bonneville Flood; D, development of Provo Shoreline; E, development of Gilbert Shoreline; F, shaded area indicates probable maximum range of fluctuations; G, historic fluctuations.
Lake area (in square miles)
20,000
15,000
10,000
5,000
0
A
B
C
D
E
F
?
30,000
25,000
20,000
15,000
10,000
5,000
Present
Years Before Present
Selected elevations (feet above sea level)
5090
4740
4500
4250
4240
4217
4180
4167
30
25
20
15
10
5
0 ka
Age (ka)

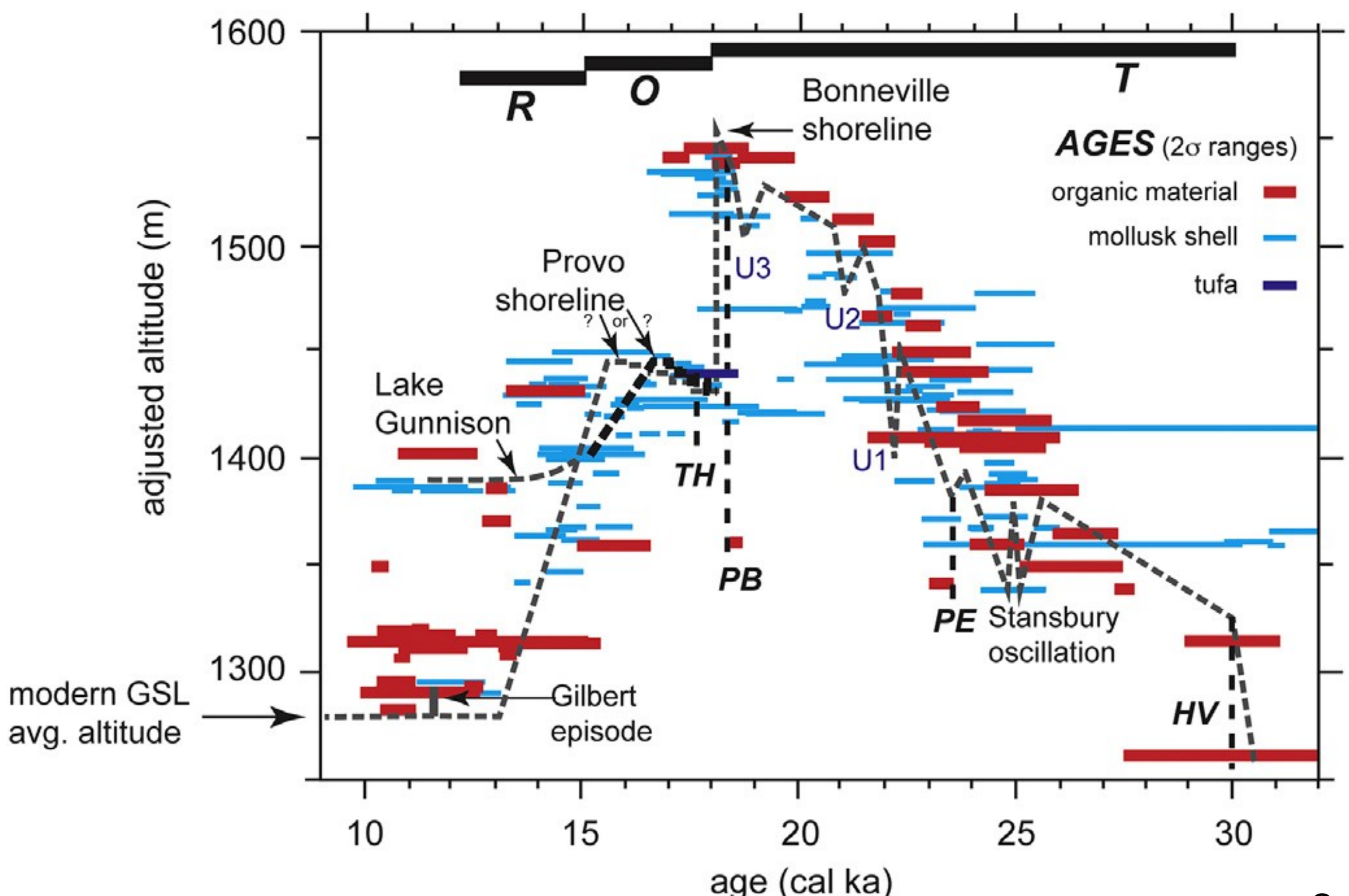
1600
1500
1400
1300
adjusted altitude (m)
10
15
20
25
30
age (cal ka)
R
O
T
Bonneville shoreline
AGES (2σ ranges)
organic material
mollusk shell
tufa
Provo shoreline
? or ?
U3
U2
U1
Lake Gunnison
TH
PB
PE
Stansbury oscillation
HV
modern GSL avg. altitude
Gilbert episode

Oviatt, 2015

Bonneville hydrograph using radiocarbon ages and corrected elevations

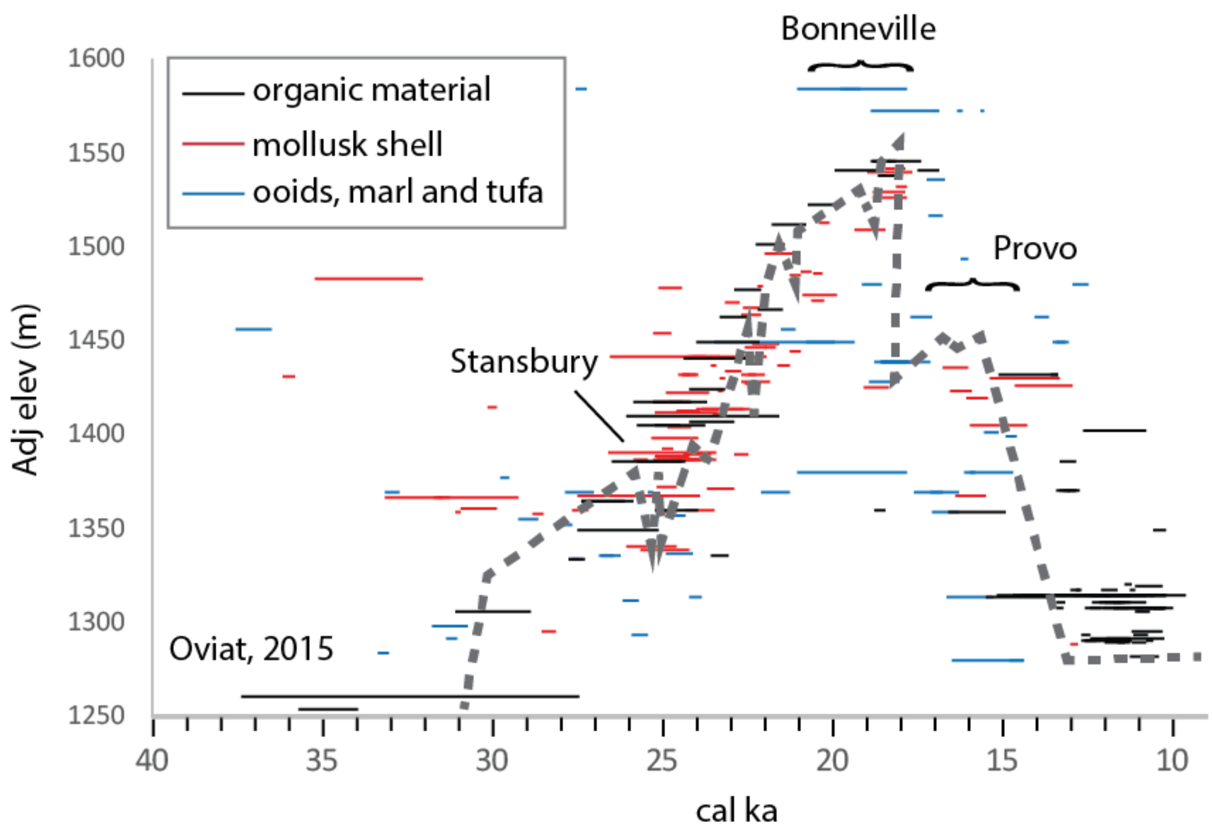

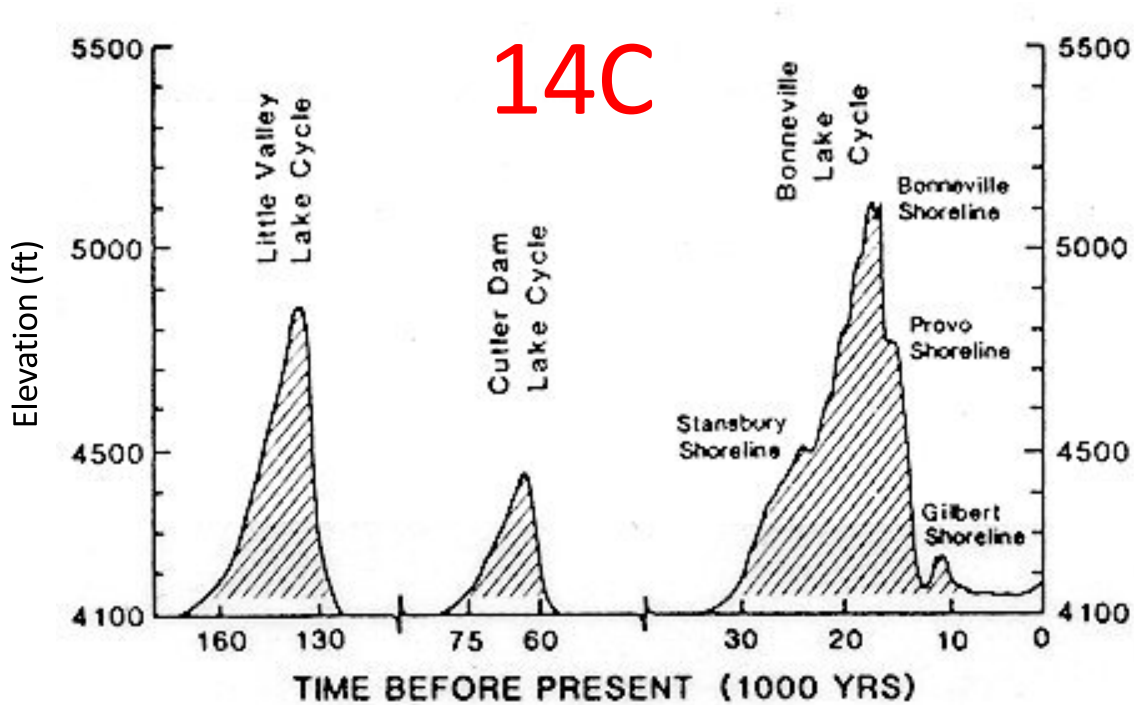

Note uneven x-axis time scale

Luminescence Dating: provides an age estimate for the last time sediment was exposed to light/heat

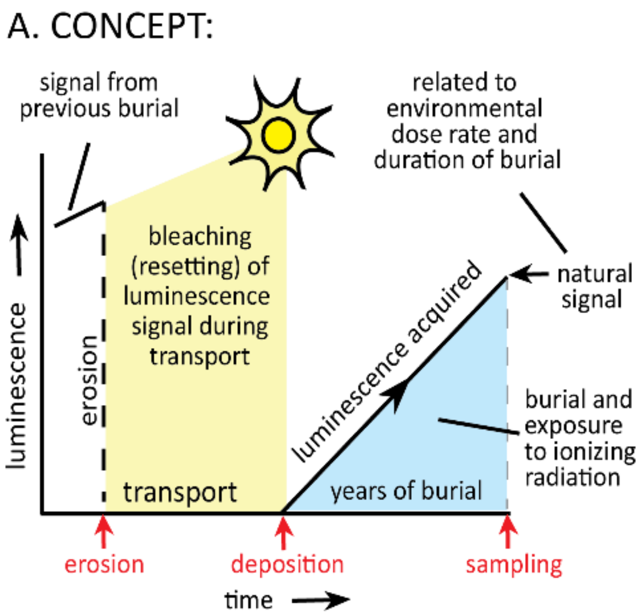

$$\text{Age (ka)} = \frac{\text{equivalent dose (Gy)}}{\text{dose rate (Gy/ka)}}$$

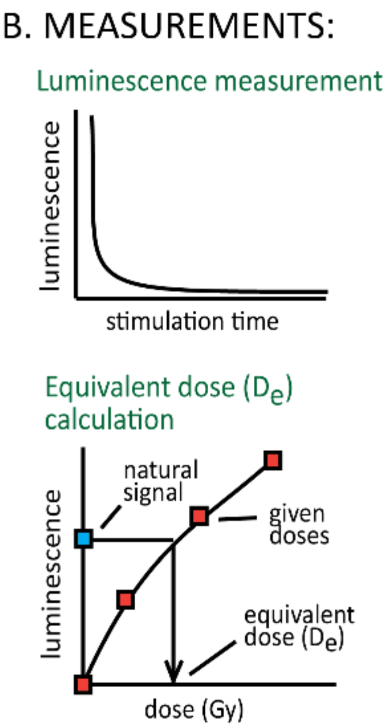

Gy = Gray = 1 Joule/kg energy
ka = kiloannum, thousand year

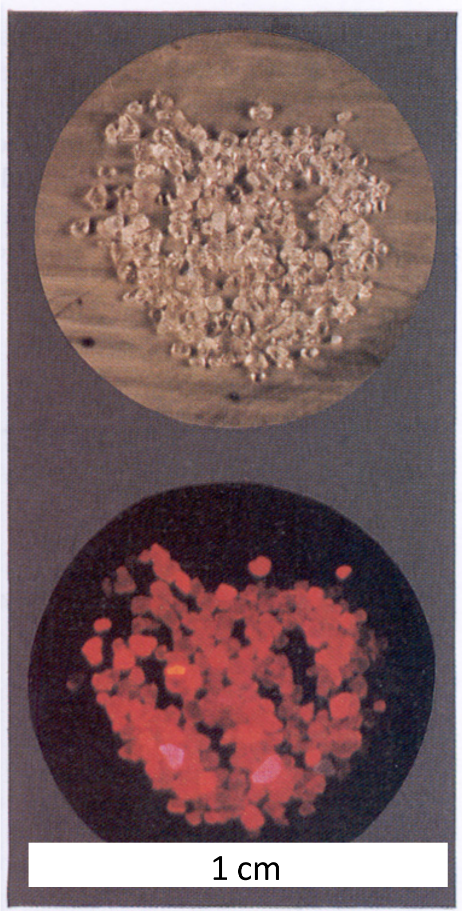

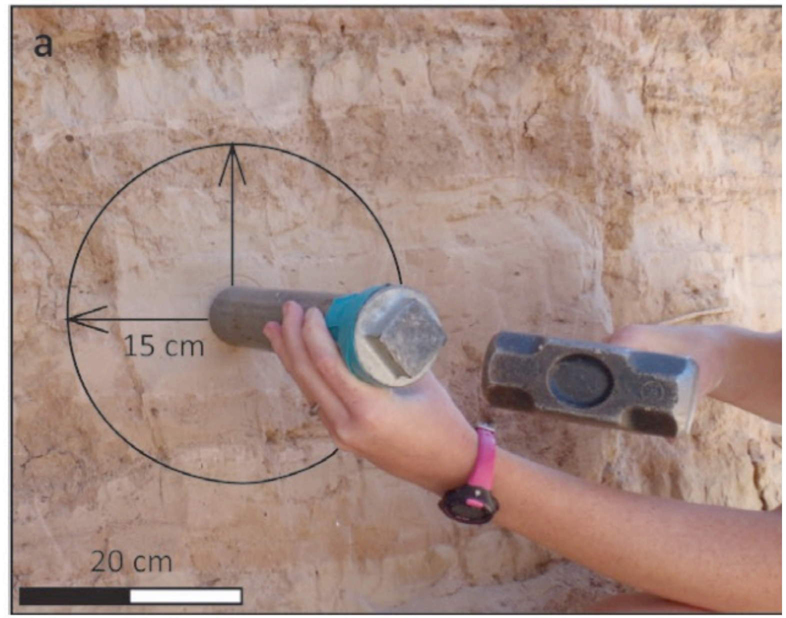
a
15 cm
20 cm


a
b
c
d
e
f
g
h
i
j
k
l
NATIONAL

Luminescence Chronology:

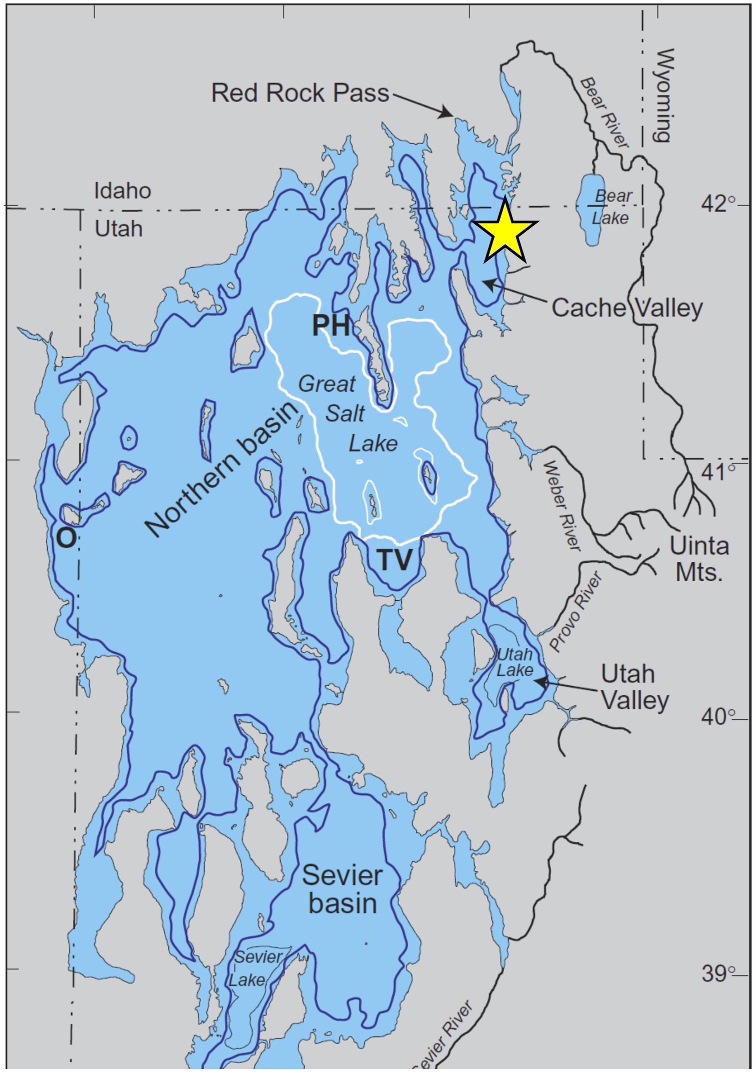

Northern Utah and Cache Valley focus

88 Luminescence samples collected over the last decade

Samples from lake Bonneville or related deposits

63 samples complete and used here

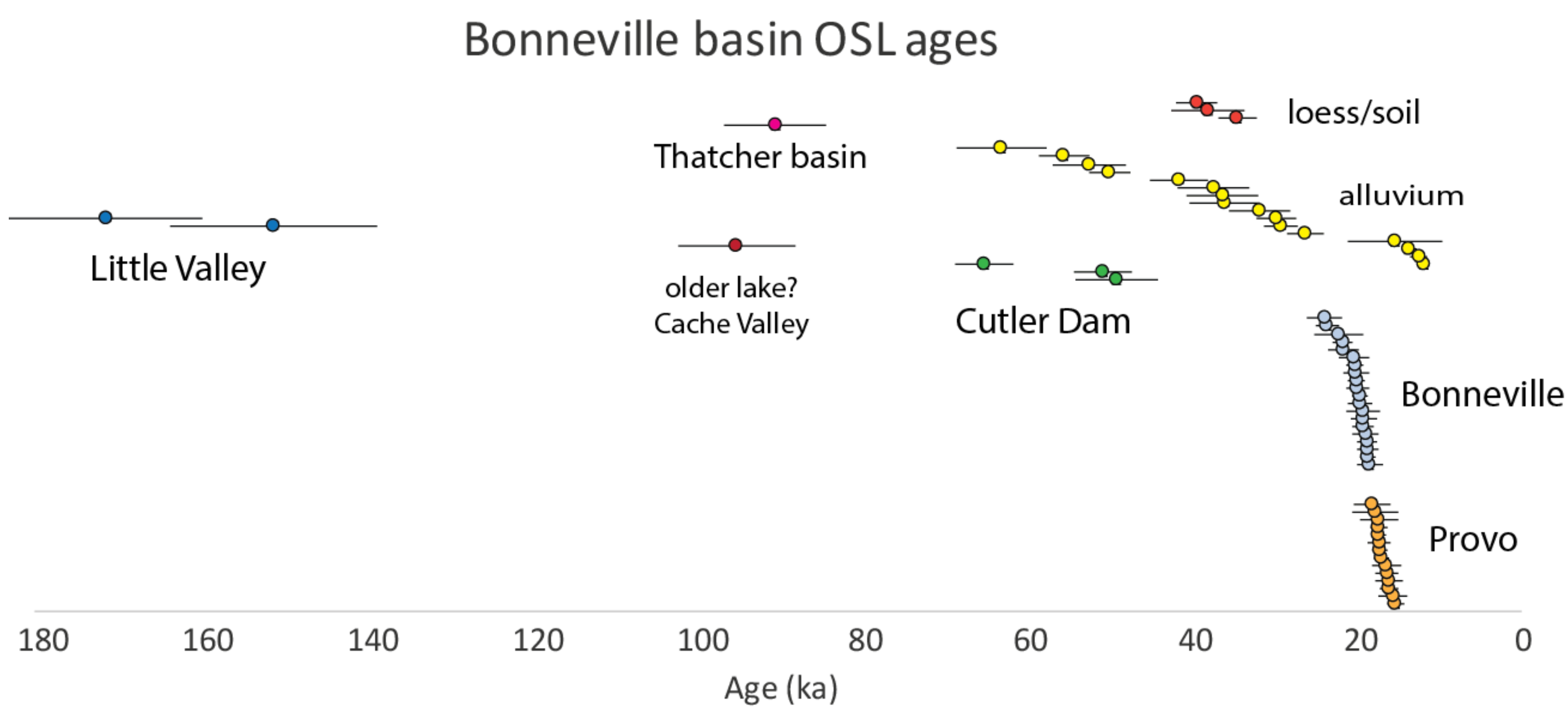

Bonneville basin OSL ages
loess/soil
Thatcher basin
alluvium
Little Valley
older lake?
Cache Valley
Cutler Dam
Bonneville
Provo
180
160
140
120
100
80
60
40
20
0
Age (ka)

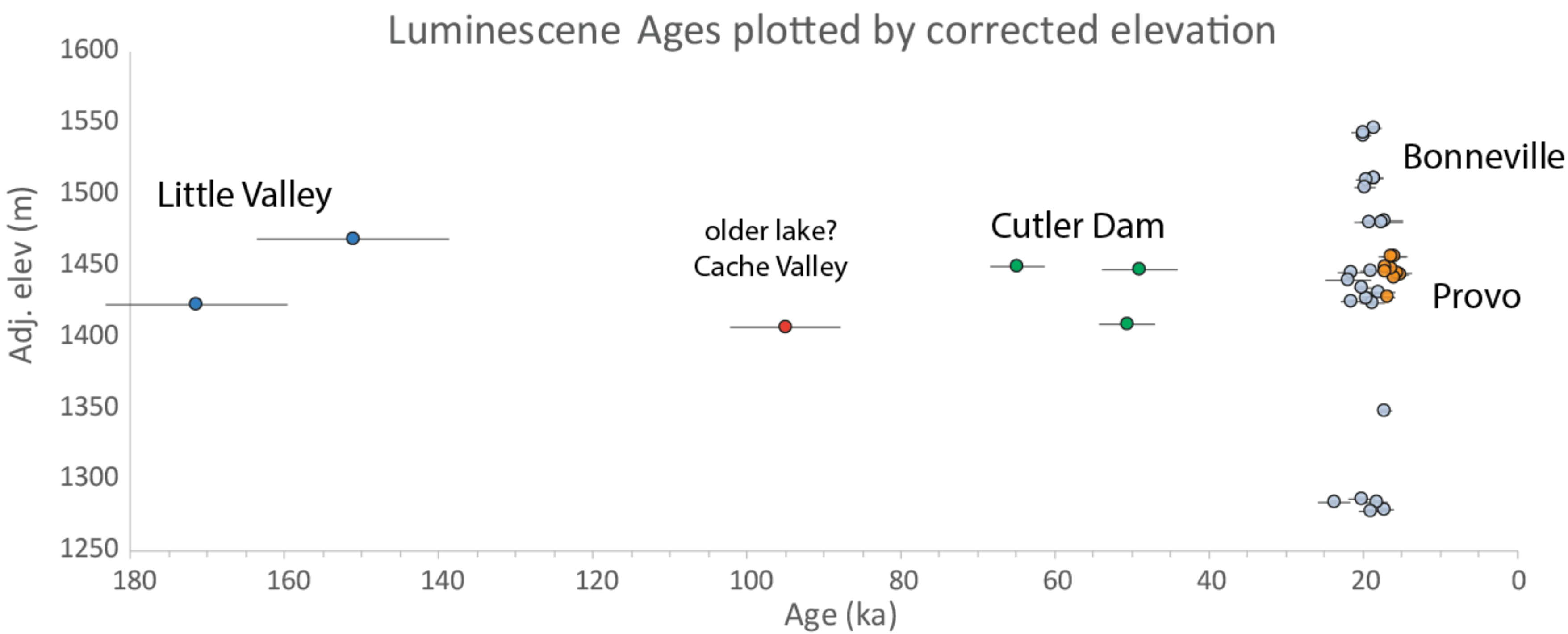

Luminescene Ages plotted by corrected elevation
Adj. elev (m)
1600
1550
1500
1450
1400
1350
1300
1250
180
160
140
120
100
80
60
40
20
0
Age (ka)
Little Valley
older lake?
Cache Valley
Cutler Dam
Bonneville
Provo

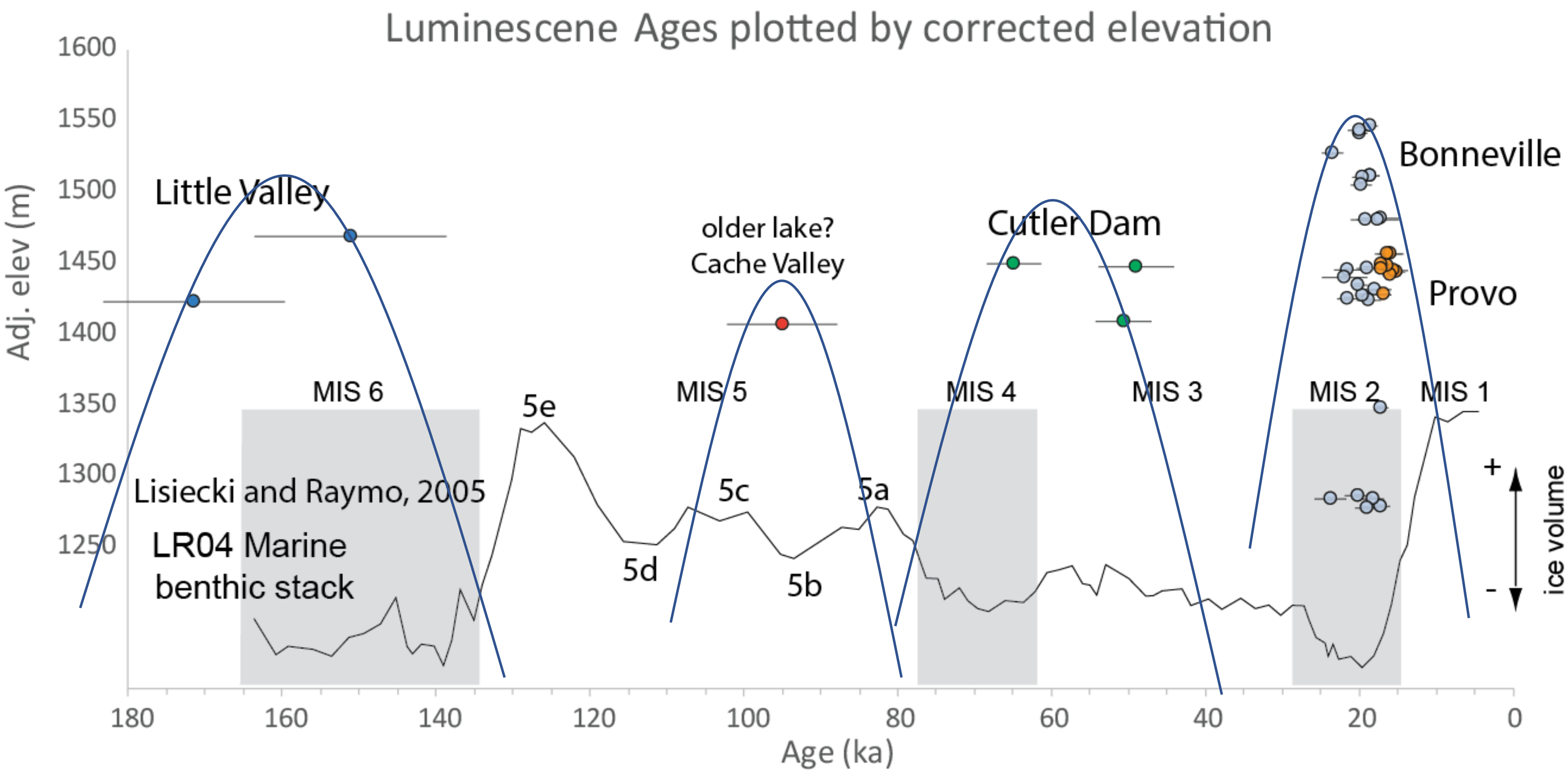

Luminescene Ages plotted by corrected elevation
Adj. elev (m)
1600
1550
1500
1450
1400
1350
1300
1250
Little Valley
older lake?
Cache Valley
Cutler Dam
Bonneville
Provo
MIS 6
5e
MIS 5
MIS 4
MIS 3
MIS 2
MIS 1
Lisiecki and Raymo, 2005
5c
5a
LR04 Marine
benthic stack
5d
5b
+
-
ice volume
180
160
140
120
100
80
60
40
20
0
Age (ka)

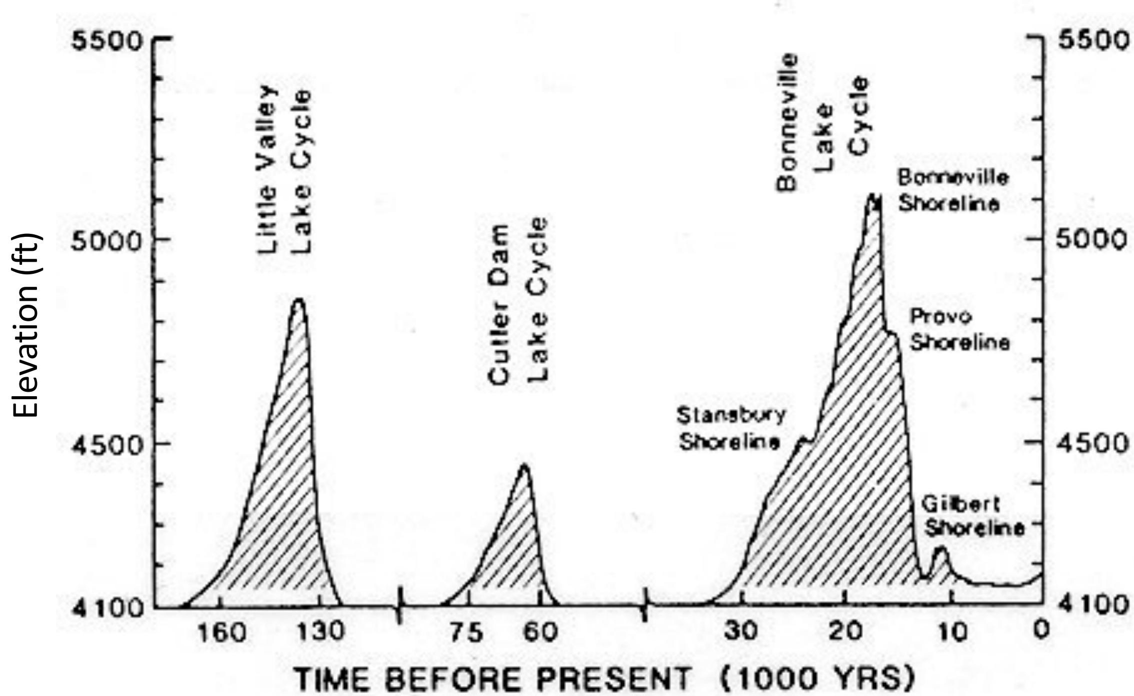

Note uneven x-axis time scale

Luminescence ages vs corrected deposit elevation

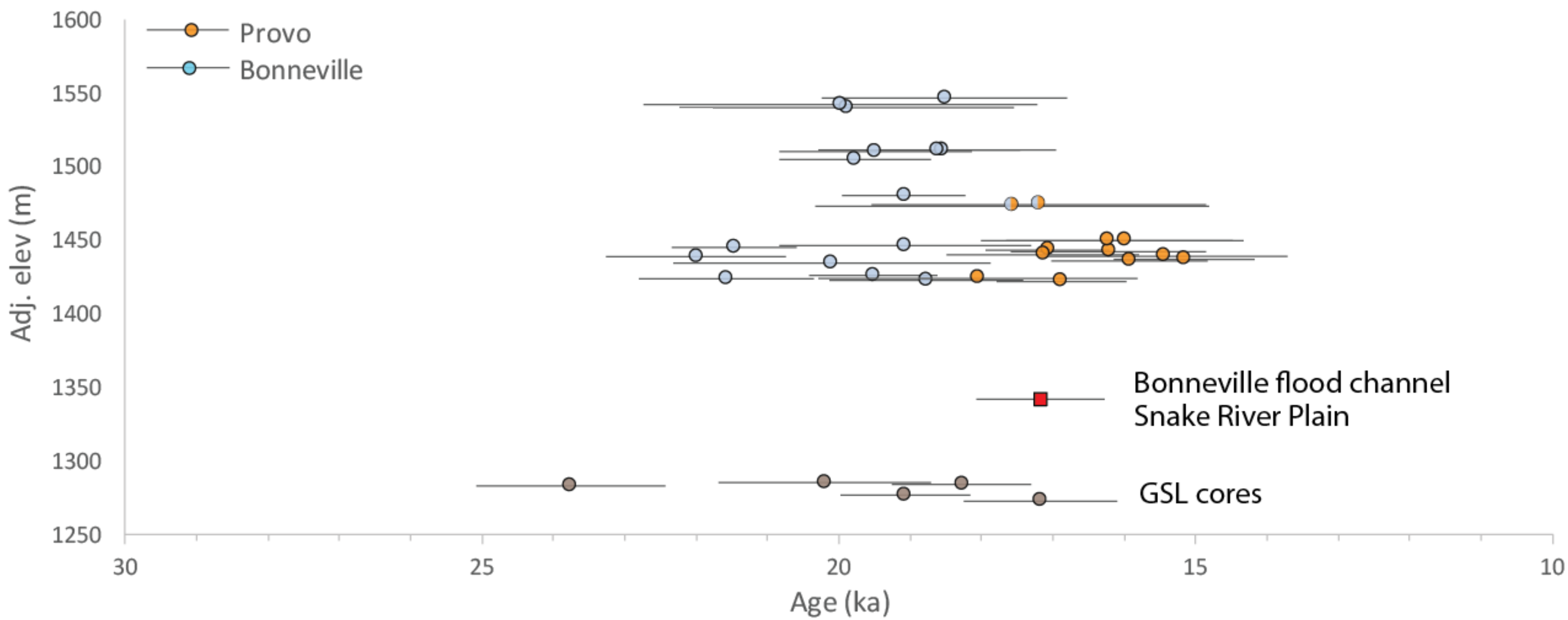

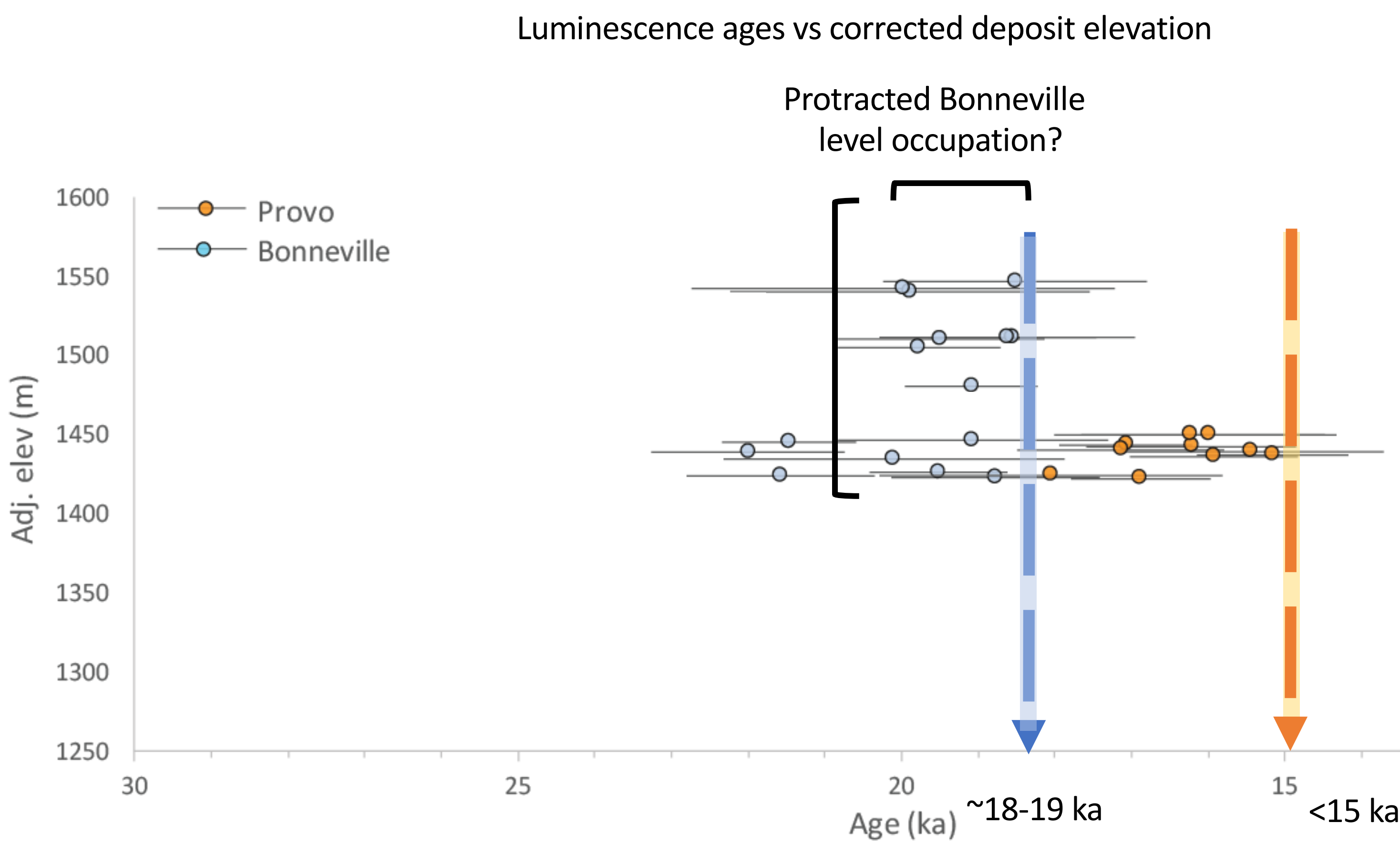
Luminescence ages vs corrected deposit elevation
Protracted Bonneville level occupation?
Provo
Bonneville
Adj. elev (m)
1600
1550
1500
1450
1400
1350
1300
1250
30
25
20
15
10
Age (ka)
~18-19 ka
<15 ka

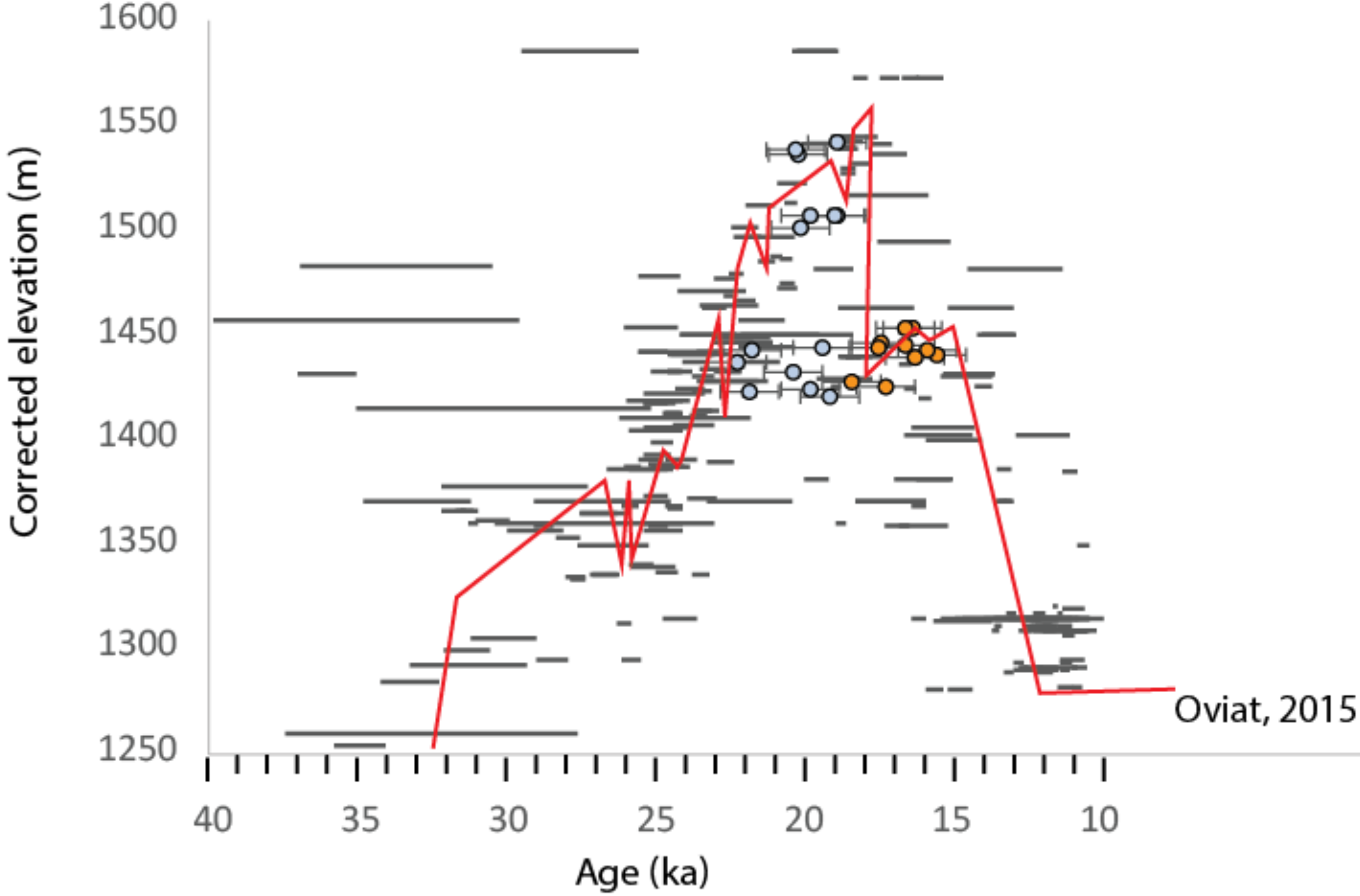

Corrected elevation (m)
1600
1550
1500
1450
1400
1350
1300
1250
40
35
30
25
20
15
10
Age (ka)
Oviat, 2015

New Age Control on Old Lake Cycles: through the use of luminescence dating

CACHE VALLEY: A CRITICAL PART OF LAKE BONNEVILLE PRESERVES EVIDENCE FOR A PROTRACTED BONNEVILLE HIGHSTAND, POSSIBLE TECTONIC TRIGGERS OF THE BONNEVILLE FLOOD, LIQUEFACTION, AND CLUSTERED EARTHQUAKES ON THE EAST AND WEST CACHE FAULT ZONES

Susanne U. Jänecke, Robert Q. Oaks, Jr., Tammy M. Rittenour, A.J. Knight, Justin Oakeson, and Nathan Ellis

Department of Geology, Utah State University, Logan, UT 84322

Corresponding author (Jänecke): susanne.janecke@usu.edu

ABSTRACT

Geologic, geomorphic, and geophysical analyses of landforms, sediments, and structures in conjunction with new radiocarbon (^{14}C) and optically stimulated luminescence (OSL) age determinations document a revised history of flooding and recession of Lake Bonneville in Cache Valley, Idaho and Utah. The presence of wave-cut cliffs in bedrock throughout the Bonneville basin show that the Bonneville highstand was protracted. Triangular facets were cut into bedrock in the footwalls of normal faults, and were steepened significantly by wave erosion at the highest Bonneville shoreline.

Crosscutting relations associated with the Riverdale fault in SE Idaho suggest that a major surface-rupturing earthquake occurred near the Zenda threshold at the north end of Cache Valley around the time of the Bonneville flood (Jänecke and Oaks, 2011a, 2011b). Thus, it is likely that fluctuating loads, rebound, and/or pore pressures induced by changing lake levels may have triggered a large earthquake that in turn initiated the Bonneville flood. The flood ended centuries of stable outflow through the Zenda threshold.

G.K. Gilbert (1880, 1890) first observed that the Bonneville flood scoured a major flood channel from Cache Valley northward that shifted the outlet of Lake Bonneville a great distance southward into Cache Valley. The bedrock sill at the south end of this Swan Lake scour channel became the new threshold for the main 1455 ± 3 m Provo shoreline, 10 m above the commonly accepted altitude of 1445 m (Jänecke and Oaks, 2011a, 2011b). The 1445 m contour in northern Cache Valley coincides instead with a lower Provo shoreline (1446 ± 3 m) that was controlled by a second bedrock sill southeast of Clifton, Idaho. The sparse record of shorelines rebounded from the ~1445 m level in Cache Valley indicate that the outlet at Clifton, Idaho, was quickly abandoned when Lake Bonneville reverted to closed-basin conditions. A dry meandering riverbed connects the Clifton and Swan Lake outlets and preserves evidence of the large northward-flowing Bonneville River across Round Valley. The Great Basin's modern divide at Red Rock Pass formed in the Holocene, after Lake Bonneville, when an eastern tributary near the midpoint of the relict flood channel of the Bonneville River built a small alluvial fan across the Swan Lake scour channel and created a subtle drainage divide (Gilbert 1880, 1890; Jänecke and Oaks, 2011a, 2011b). Gilbert was the first to recognize that that the modern drainage divide at Red Rock Pass is unrelated to Lake Bonneville.

The possibility that an earthquake triggered the Bonneville flood (Jänecke and Oaks, 2011a, 2011b) led us to explore the late Pleistocene activity of normal faults in and near Cache Valley. Just west of Cache Valley, the Wasatch fault zone has increased its slip rate since the Bonneville flood (Hetzel and Hampel, 2005; Karow and Hampel, 2010 and citations therein), but little is known about the response of active normal faults in Cache Valley to loading and unloading by Lake Bonneville. To examine the relations between ancient seismicity and lake history, we re-excavated deformed Upper Pleistocene sandy lake beds along a ~50 m by 5 m collapsed north wall of an abandoned gravel pit at the mouth of Green Canyon in Cache Valley, Utah. Utah State University faculty identified two liquefaction events in the outcrop in the 1980s during class trips, and we sought to determine the number, nature, and age of the paleo-earthquakes responsible for the strong deformation there.

The exposure of the paleodelta of Green Canyon is within the boundary between the northern and central Utah segments of the East Cache fault zone (McCalpin, 1994). It is ~25 m to ~170 m basinward, respectively, of two diverging fault strands of the East Cache fault zone, and there might be additional buried faults at lower elevation than the exposure near the main upper Provo shoreline (McCalpin, 1989; this study).

Deposition of upward coarsening lacustrine deposition in the delta of Green Canyon started before 22.4 ± 0.4 cal kyr B.P. (^{14}C) with deposition of prodelta clay, mud, and silt, and continued after 20.1 ± 0.3 cal kyr B.P. (^{14}C) as sand and gravel were laid down in a prograding delta. Nearshore lacustrine deposition is indicated by ripples, cross beds, other sedimentary structures, lacustrine *Stagnicola* gastropod shells throughout the exposure, and the position of the beds ~40–45 m below the Bonneville shoreline at Green Canyon.

Fifteen new age determinations indicate early onset of deep lake conditions in Cache Valley at or higher than 1515 to 1510 m (corrected for rebound)(this study and Rittenour and others, 2019). The high altitude of the lake provides additional evidence for Oaks and others' (2019; this volume) interpretation of Cache Valley Bay. Oaks and others (2019) dated prior lake cycles in Cache Valley, documented their unexpectedly high altitudes, and concluded that Cache Valley was filled by a separate pluvial lake from the main Bonneville basin until the rise to the Bonneville highstand connected them across the Junction Hills. Integration of Cache Valley lake into the main Bonneville basin must postdate the lake beds in Cache Valley that were deposited at higher altitudes than predicted by the Bonneville hydrograph, like the transgressive sediment in the paleodelta at Green Canyon.

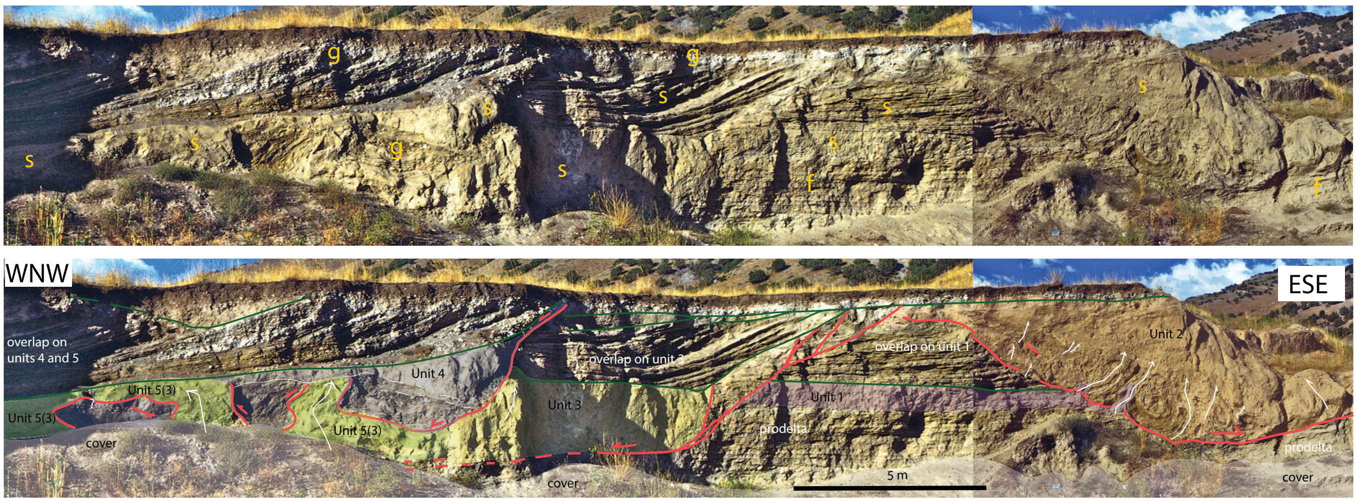

Figure 1. *View to north-northeast of deltaic sediment of Green Canyon in 1980. Colored units are liquefied masses of event horizons 1-5. Unit 3 was activated a second time in a diapiric mode during event 5. Undeformed cap of alluvial gravel is probably flood related (?), and overlies deformed deltaic sand (s) and gravel (g) from the last pluvial along an angular unconformity. Each green line is an angular unconformity. Lower one-third of exposure contains mostly prodelta fine sand, silt and clay (f=fines). Orange lines are slip surfaces of nested slumps in lateral spreads. Each event bed has a major unconformity at the upper surface (green lines).*

We uncovered multiply deformed shallow lake beds and one capping fluvial gravel in the exposure at Green Canyon. Listric faults in the exposure sole into prodelta clay beds beneath the sandy and gravelly deltaic part of the succession. West-dipping slip surfaces in the exposure are part of nested lateral spreads, not tectonic faults. Cross-cutting relations are exceptionally clear. The deltaic sediment of Green Canyon was deposited, seismically deformed, and slumped in at least four strong earthquakes under subaqueous conditions in a shallow-water, deltaic part of Cache Valley lake. Six ^{14}C ages on *Stagnicola* sp. shells and three OSL ages are stratigraphically consistent within error, and confirm that the lacustrine sediment was deposited and deformed during ~2–5 kyr of high lake levels prior to the Bonneville flood. The geometry and position in the landscape of a laterally continuous alluvial gravel bed, which overlies the highly deformed sandy lake beds in angular unconformity, suggest that the gravel bed was probably laid down immediately after the erosional stripping of the highest units during the Bonneville flood. The gravel cap may be a flood deposit or barely postdate the Bonneville flood because it predates focused downcutting along the modern channel of Green Canyon Wash that began with the Bonneville flood and occupation of the Provo shorelines ~70 m lower in the landscape. All the deformation in the exposure must therefore predate the Bonneville flood at ~18 ka.

The Green Canyon site exposes three listric slip surfaces of lateral spreads, four sequential thick liquefied units, and less deformed flat and cross-stratified lacustrine and deltaic sediment. Each thick liquefied mass of sand is a different age, yet all of the deformation occurred when the sediment was saturated by the pluvial lake as it approached or stabilized at its highest shoreline. Three of the liquefied units (0.75 to 5 m thick) are localized and displaced in the hanging walls of listric east- and west-dipping slip surfaces of lateral spreads that appear to be coeval with the liquefied fault-graded beds above them. Deposition was ongoing, and produced multiple cross-cutting relations that constrain the relative ages of three similar lateral-spread-liquefaction pairs (LSLP) and one underlying strata-bound liquefied mass (SBLM) that deforms a possible weak geosol. Each LSLP and SBLM formed during a discrete event.

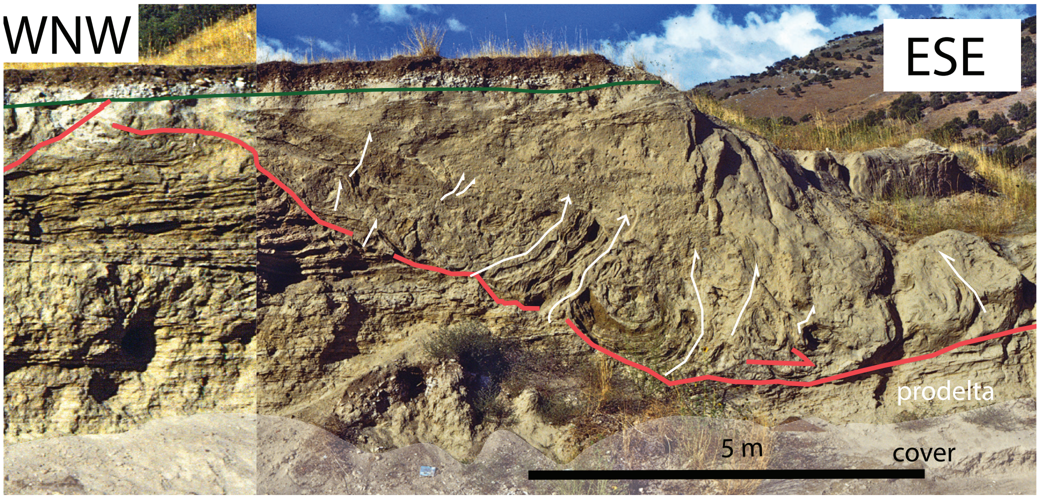

Figure 2. *Fault-graded beds of event bed number 2, as it was exposed in the 1980s above a listric slip surface (longest red line). See figure 1 for its position in the exposure. The largest pseudonodule is about 2.5 m across. Fluid escape (white arrows trace sand dikes and sills) created the pseudonodules low in the event layer. The upper two-thirds of the event layer is massive and disaggregated due to protracted shaking and liquefaction. Fault-graded bedding like this is diagnostic of seismic shaking of sediment under a body of water (Rodriguez and others, 2000). View to north-northeast. Red contacts within the event bed separate more deformed above from less-deformed part of the fault-graded bed, below. Note the fluvial gravel at the top of the outcrop, which might be related to the Bonneville flood.*

Each was subsequently capped by a major erosional surface, upon which 1–2 m of stratified sediment was deposited. The youngest LSLP deformed twice, and its diapirically deformed slip surface records deformation during two strong earthquakes. Seiches likely produced each erosion surface. Truncations at slip surfaces, fault wedges, disconformities and angular unconformities, overlapping sediment, onlapping sediment, sand dikes and sills, and growth strata separate the three LSLP and one SBLM from one another. Less extreme deformation modified the intervening lake beds.

The most extreme deformation is expressed in fault-graded beds that are 1–5 m thick. The similarity between the LSLP and SBLM in the Green Canyon pit and secondary deformation generated by the 1934 M 6.6 Hansel Valley earthquake (McCalpin and others, 1992) indicate that seismic shaking is the most likely explanation for the five largest deformational events recorded at the mouth of Green Canyon. The smaller deformation features may have formed during subsequent aftershock sequences.

Other evidence for a tectonic trigger includes the presence of small fault wedges, alternating brittle and ductile deformation, brittle fluid-escape structures, buried scarps, sand dikes, erosion of each fault-graded bed, and angular unconformities. We propose that five separate moderate to large earthquakes shook and liquefied the sediment between ~22.4 ka and the Bonneville flood (~ 18 ka; age from Miller, 2016). Those earthquakes probably ruptured the nearby central or northern segments of the East Cache fault because other gravel pits lack liquefied sediment in coeval deposits elsewhere in Cache Valley.

If we are correct that each liquefaction and major diapiric re-liquefaction event records a moderate to large earthquake when a deep pluvial lake filled Cache Valley, then the adjacent part of the East Cache fault zone generated at least five major earthquakes during the last pluvial between about 22.4 ka and the Bonneville flood at about 18 cal kyr B.P.. The paleoseismic data of McCalpin (1994) documents one additional earthquake along the East Cache fault zone as Lake Bonneville paused at the Provo shoreline. The temporal clustering of the ≥ 6 syn-Bonneville paleoearthquakes, their strong spatial association with the East Cache fault zone, the paucity of deformation at the site after the Bonneville flood, and the absence of liquefaction in coeval sediment elsewhere in Cache Valley, are all consistent with a high frequency of liquefaction-inducing earthquakes along the central or northern segment of the East Cache fault during the transgression and highstand of the pluvial lake in Cache Valley. A single mid-Holocene earthquake that occurred ~ 4–5 ka is the only earthquake known to have ruptured the East Cache fault zone during the Holocene (McCalpin, 1994). Altogether, there has been a significant decline in earthquake frequency since the deep-water phase of the Bonneville lake cycle along the East Cache fault zone.

The low earthquake frequency along the Utah part of the East Cache fault zone documented here in the Holocene is in marked contrast to the history of the West Cache fault zone and the Wasatch fault zone; those western fault zones generated numerous Holocene earthquakes (Black and others, 1999, 2000; Solomon, 1999; Hetzel and Hampel, 2005; Ellis and Jänecke, 2018). We explain the opposite earthquake histories of the East and West Cache fault zones as the consequence of opposite flexural stresses induced by the loading and later rebound produced by pluvial lakes along an upper monoclinal hinge (near the East Cache fault zone) and along a lower monoclinal hinge (near the West Cache fault zone and the Wasatch fault zone) at the eastern

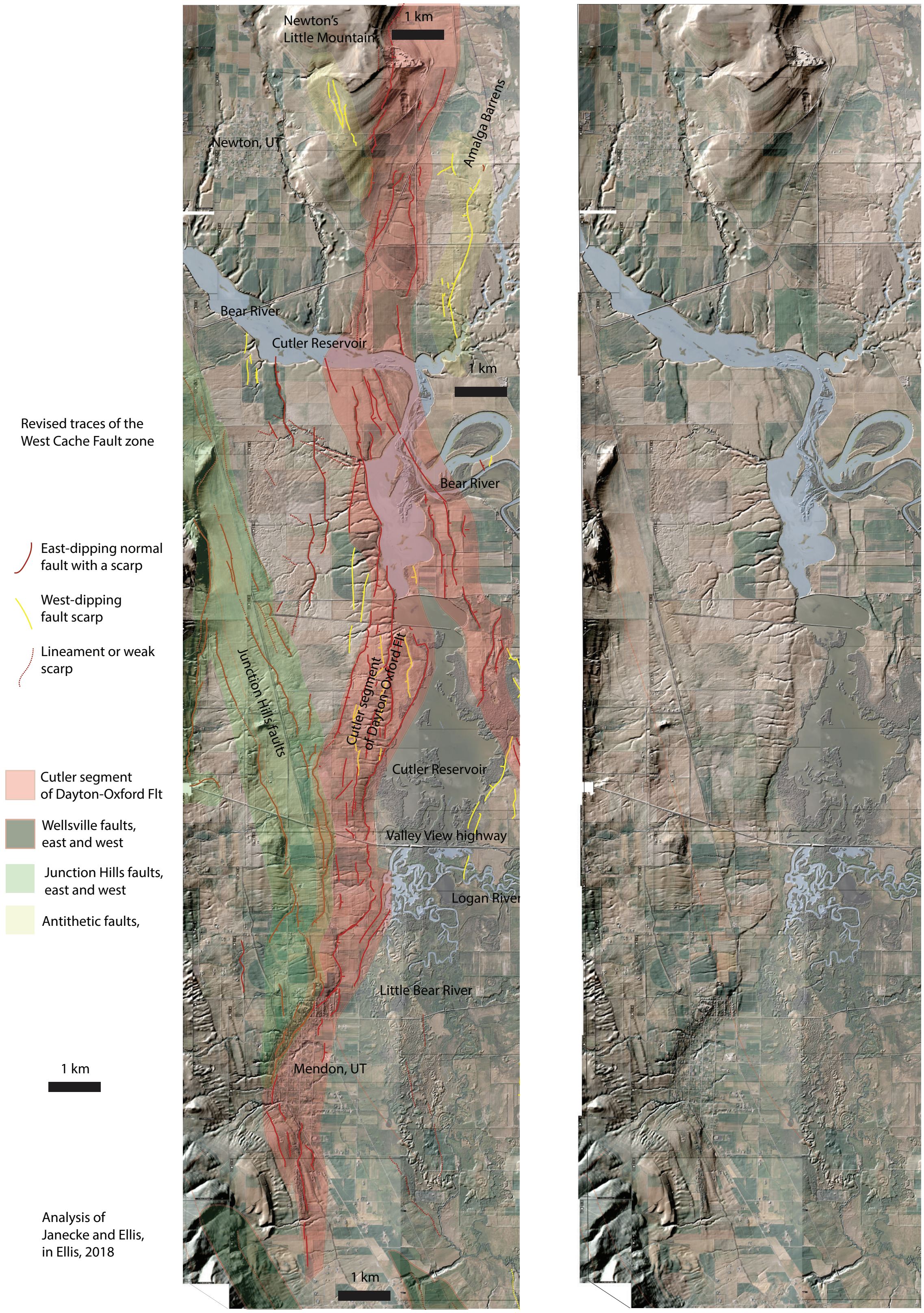

Figure 3. *New traces of the West Cache fault zone identified using lidar by Ellis and Jänecke (2018) on the floor of Cache Valley. Fault zones are up to 1 km wide and contain both east- and west-dipping traces. Geophysical datasets support this interpretation (Evans and Oaks, 1996). The Dayton-Oxford fault is much longer than previously known, connects with both the Junction Hills and Wellsville faults, and joins these other faults to form a very high fault scarp in Mendon, Utah. Jänecke and Evans (2017) identified a small subset of these faults.*

margin of Lake Bonneville and Cache Valley lake. Lateral changes in loading within Lake Bonneville and Cache Valley lake could explain clustered earthquake activity by changing the loading stresses in the crust, by modulating rebound-related stresses, and/or by raising the pore pressure along the slip surfaces with circulating groundwater. Similar processes might explain the rough coincidence of the Bonneville flood and the last major earthquake on the Riverdale fault zone in northern Cache Valley (Jänecke and Oaks, 2011a, 2011b).

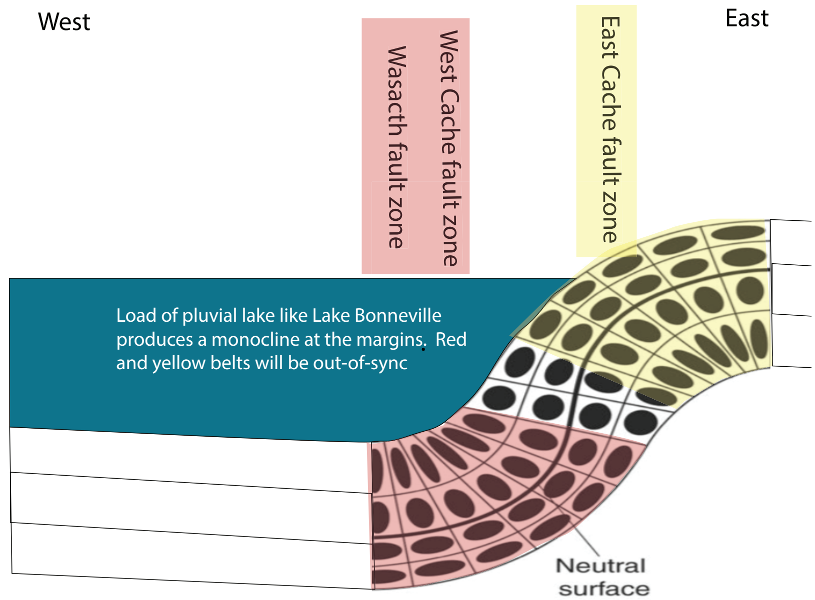

Figure 4. *Conceptual model of enhanced extension along the East Cache fault zone during the last pluvial. Rebound during the Holocene caused the western faults to be more active than the eastern fault zone.*

The West Cache fault zone ruptured at least three times in the Holocene (Black and others, 1999, 2000; Solomon, 1999), and a fourth Holocene earthquake is likely because it displaces Holocene marsh deposits on the floor of Cache Valley along newly identified traces of the Cutler Reservoir segment of the Dayton-Oxford fault zone (Ellis and Jänecke 2018). This fault segment links the Wellsville, Junction Hills, and Dayton-Oxford faults with one another (Jänecke and Evans, 2017; Ellis and Jänecke, 2018; Jänecke and others, 2019). Holocene scarps along most of the new traces nearly double the length of active fault traces mapped in the West Cache fault zone. At least one additional surface-rupturing earthquake is needed to explain the plethora of Holocene fault scarps on the floor of Cache Valley. Altogether these data suggest that the West Cache fault zone and the Wasatch fault zone, were positioned near the lower monoclinal hinge of the flexurally bending lithosphere, and both have been particularly active since Lake Bonneville disappeared.

REFERENCES

Black, B.D., Giraud, R.E., and Mayes, B.H., 2000, Paleoseismic investigation of the Clarkston, Junction Hills, and Wellsville faults, West Cache fault zone, Cache County, Utah—Paleoseismology of Utah, Volume 9: Utah Geological Survey Special Study 98, 23 p.,

Black, B.D., Solomon, B.J., and Giraud, R.E., 1999, Surficial geology and paleoseismicity of the West Cache fault zone, Cache County, Utah, *in* Spangler, L.E., and Allen, C.J., editors, Geology of Northern Utah and Vicinity: Utah Geological Association Publication 27, p. 181–202.

Ellis, N.R., and Jänecke, S.U., advisor, 2018, LIDAR results in a revised map and analysis of active faults in West Cache fault zone, Utah (Senior thesis): Utah State University Geology Department, https://works.bepress.com/susanne_janecke/228/.

Evans, J.P., and Oaks, R.Q., Jr., 1996, Three-dimensional variations in extensional fault shape and basin form—The Cache Valley basin, eastern Basin and Range Province, United States: Geological Society of America Bulletin, v. 108, no. 12, p. 1580–1593.

Gilbert, G.K., 1880, The outlet of Lake Bonneville: American Journal of Science, 19, p 341–349.

Gilbert, G.K., 1890, Lake Bonneville: United States Geological Survey Monograph 1, 438 p.

Hetzel, R., and Hampel, A., 2005, Slip rate variations on normal faults during glacial-interglacial changes in surface loads: Nature, v. 435, p. 81–84, doi.org/10.1038/nature03562.

Jänecke S.U., and Evans, J.P., 2017, Revised structure and correlation of the East Great Salt Lake, North Promontory, Rozel, and Hansel Valley fault zones revealed by the 2015-2016 low stand of Great Salt Lake, in Lund, W.R., Emerman, S.H., Wang, W., Zanazzi, A., editors, Geology and Resources of the Wasatch: Back to Front: Utah Geological Association Publication 46, p. 295–360.

Jänecke, S.U., and Oaks, R.Q., Jr., 2011a, Reinterpreted history of latest Pleistocene Lake Bonneville—Geologic setting of threshold failure, Bonneville flood, deltas of the Bear River, and outlets for two Provo shorelines, southeastern Idaho, USA, in Evans, J.P., and Lee, J., editors, Geologic Field Trips to the Basin and Range, Rocky Mountains, Snake River Plain, and Terranes of the U.S. Cordillera: Geological Society of America Field Guide 21, p. 193–220, doi:10.1130/2011.0021(09).

Jänecke, S.U., and Oaks, R.Q., Jr., 2011b, New insights into the outlet conditions of late Pleistocene Lake Bonneville, southeastern Idaho, USA: Geosphere, v. 7, no. 6, p. 1369–1391.

Jänecke, S.U., Oaks, R.Q., Jr., Ellis, N., Evans, J.P., Knight, A.J., and Oakeson, J., 2019, Cache Valley—liquefaction, out-of-sync earthquakes, Lake Bonneville, and revising the West Cache fault zone: UQFPWG Annual meeting, Utah Geologic Survey, Feb 2019.

Karow, T., and Hampel, A., 2010, Slip rate variations on faults in the Basin-and-Range Province caused by regression of Late Pleistocene Lake Bonneville and Lake Lahontan: International Journal of Earth Sciences (Geol Rundsch) v. 99 p. 1941–1953, https://doi.org/10.1007/s00531-009-0496-3.

McCalpin, J.P., 1989, Surficial geologic map of the East Cache fault zone, Cache County, Utah: U.S. Geological Survey Miscellaneous Field Studies Map MF-2107, scale 1:50,000.

McCalpin, J.P., 1994, Neotectonic deformation along the East Cache fault zone, Cache County, Utah—Paleoseismology of Utah, Volume 5: Utah Geological Survey, Special Study 83, 37 p.

McCalpin, J.P., Robison, R.M., and Garr, J.D., 1992, Neotectonics of the Hansel Valley—Pocatello Valley corridor, northern Utah and southern Idaho, *in* Gori, P.L., and Hays, W.W., editors, Assessment of regional earthquake hazards and risk along the Wasatch Front, Utah: U.S. Geological Survey Professional Paper 1500-G, 18 p.

Oaks, R.Q., Jr., Jänecke, S.U., Rittenour, T.M., Erickson, T.L., and Nelson, M.S., 2019, OSL age dating of two, perhaps three, pre-Bonneville deep-water pluvial lakes in Cache Valley, Utah-Idaho—Implications of their unexpected high altitudes for excavation of Cutler Narrows from a level above 1494 m (4901'), down to the present level of 1314 m (4310') mainly during the Bonneville lake cycle: *in* Lund, W.R., McKean, A.P., and Bowman, S.D., editors, Proceedings volume 2018 Lake Bonneville geologic conference and short course: Utah Geological Survey Miscellaneous Publication 170.

Rittenour, T. M., Pederson, J. L., Oaks, R. Jr., Jänecke, S. U., Nelson, M., 2019, New age control on old lake cycles, evidence from luminescence ages from northern Utah and southern Idaho: *in* Lund, W.R., McKean, A.P., and Bowman, S.D., editors, Proceedings volume 2018 Lake Bonneville geologic conference and short course: Utah Geological Survey Miscellaneous Publication 170.

Rodriguez-Pascua, M.A., Calvo, J.P., De Vicente, G., and Gómez-Gras, D., 2000, Soft-sediment deformation structures interpreted as seismites in lacustrine sediments of the Prebetic Zone, SE Spain, and their potential use as indicators of earthquake magnitudes during the Late Miocene: Sedimentary Geology, v. 135, nos. 1–4, p.117–135.

Solomon, B.J., 1999, Surficial geologic map of the West Cache fault zone and nearby faults, Box Elder and Cache Counties, Utah: Utah Geological Survey Map 172, 20 p. pamphlet, 2 sheets, scale 1:50,000.

This content is a PDF version of the author's PowerPoint presentation.

Cache Valley: clustered earthquakes, liquefaction, possible triggers of the Bonneville flood

See our abstract for other topics

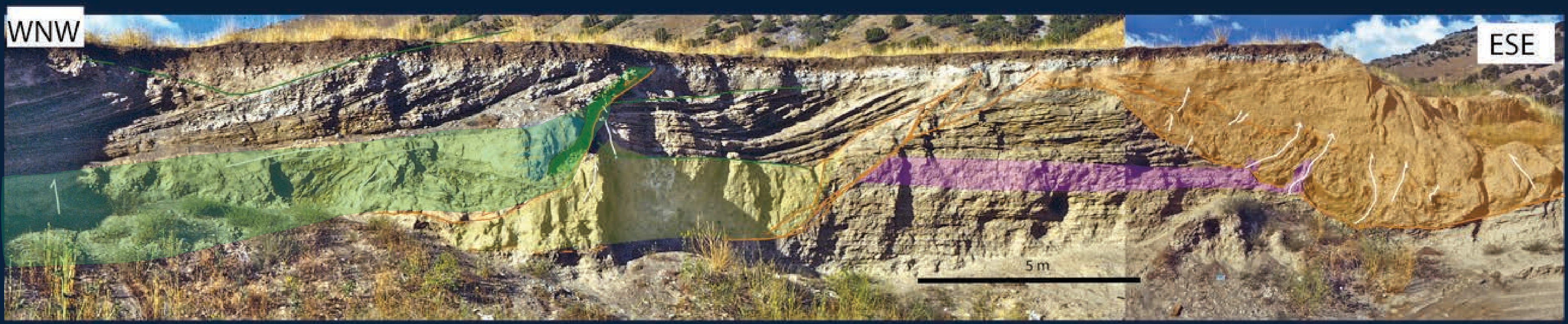

All views of exposure are to the NNE

Susanne Janecke
Robert Q. Oaks, Jr.
Tammy Rittenour
A.J. Knight
and Justin Oakeson

UtahState University Geology

Each colored unit is liquefied

Why are we discussing liquefaction and earthquakes in a Bonneville symposium?- 2 main reasons

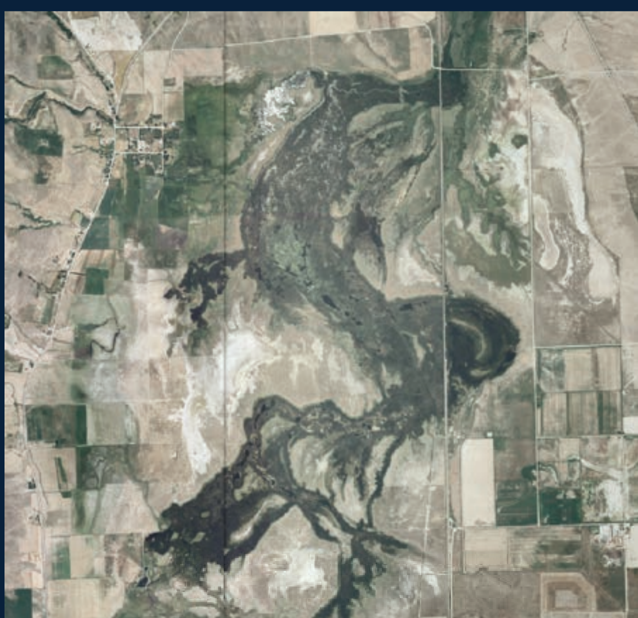

Dry bed of the Bonneville river in northern Cache Valley

UtahState UNIVERSITY Geology

Susanne U. Janecke and
Robert Q. Oaks, Jr.
Department of Geology
Geosphere 2011

Reason 1: Riverdale fault, Idaho, produced a major surface-rupturing scarp across the Bonneville delta around the time of the Bonneville flood. That earthquake might have triggered the Bonneville flood.
Janecke and Oaks, 2011

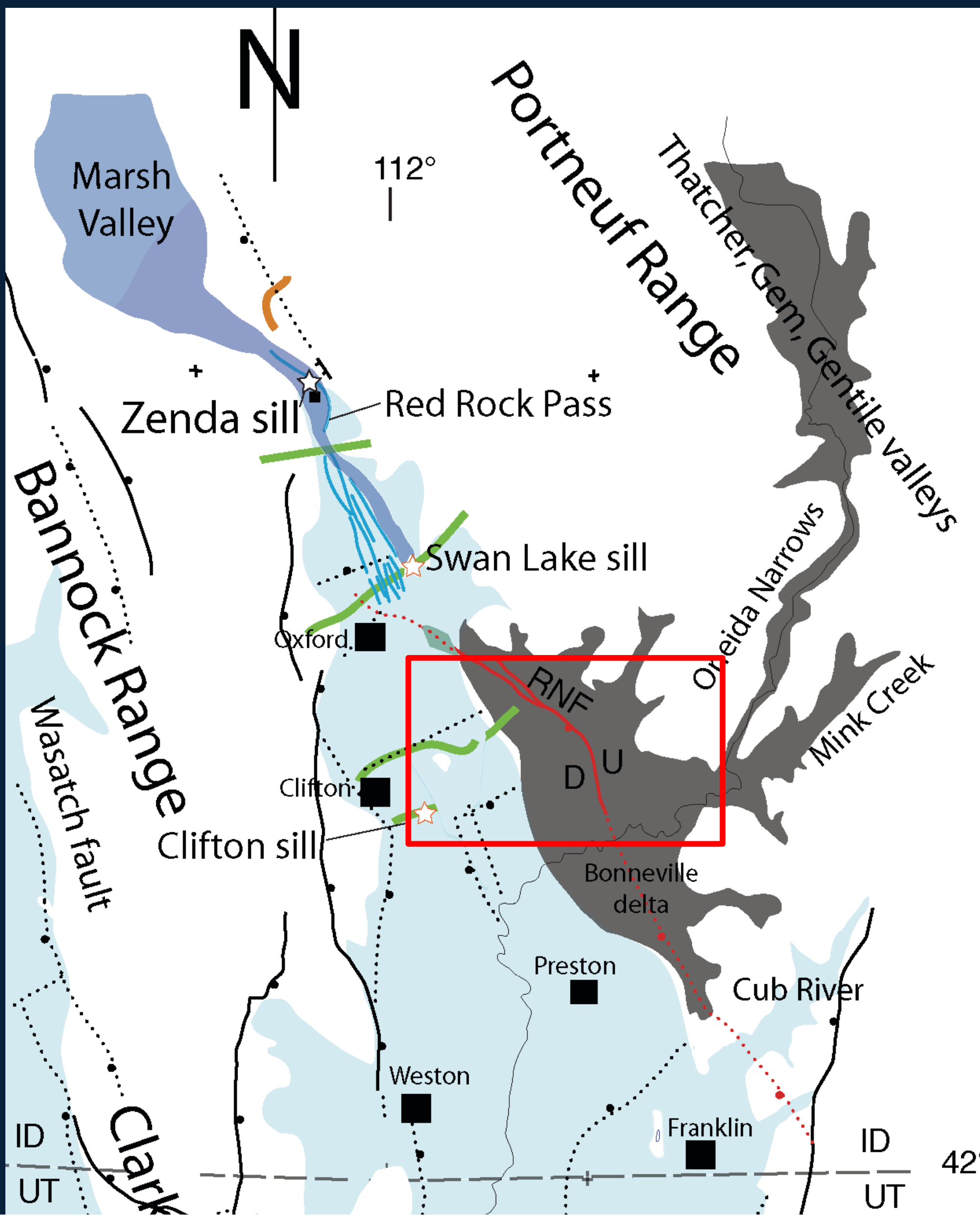

Bonneville delta at max extent

THEN

Riverdale Fault cuts it

THEN

Provo delta of Bear River

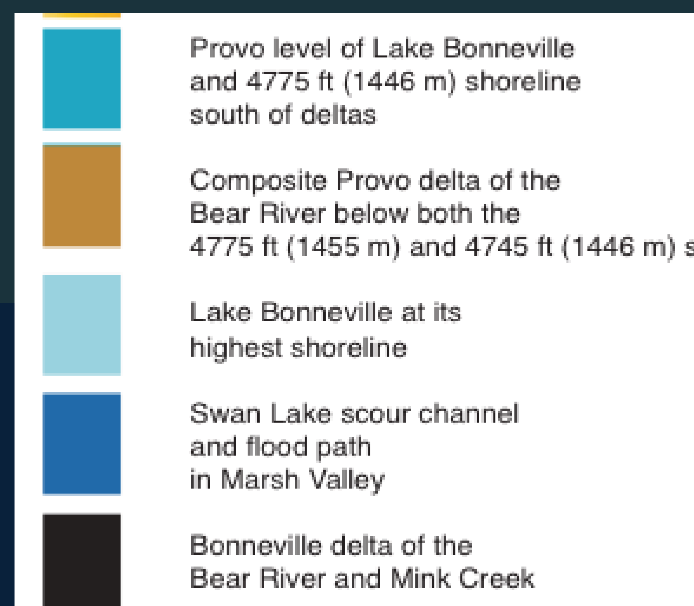

This normal fault is 50 km long and cuts Bonneville deposits for ~10 km across the delta topset

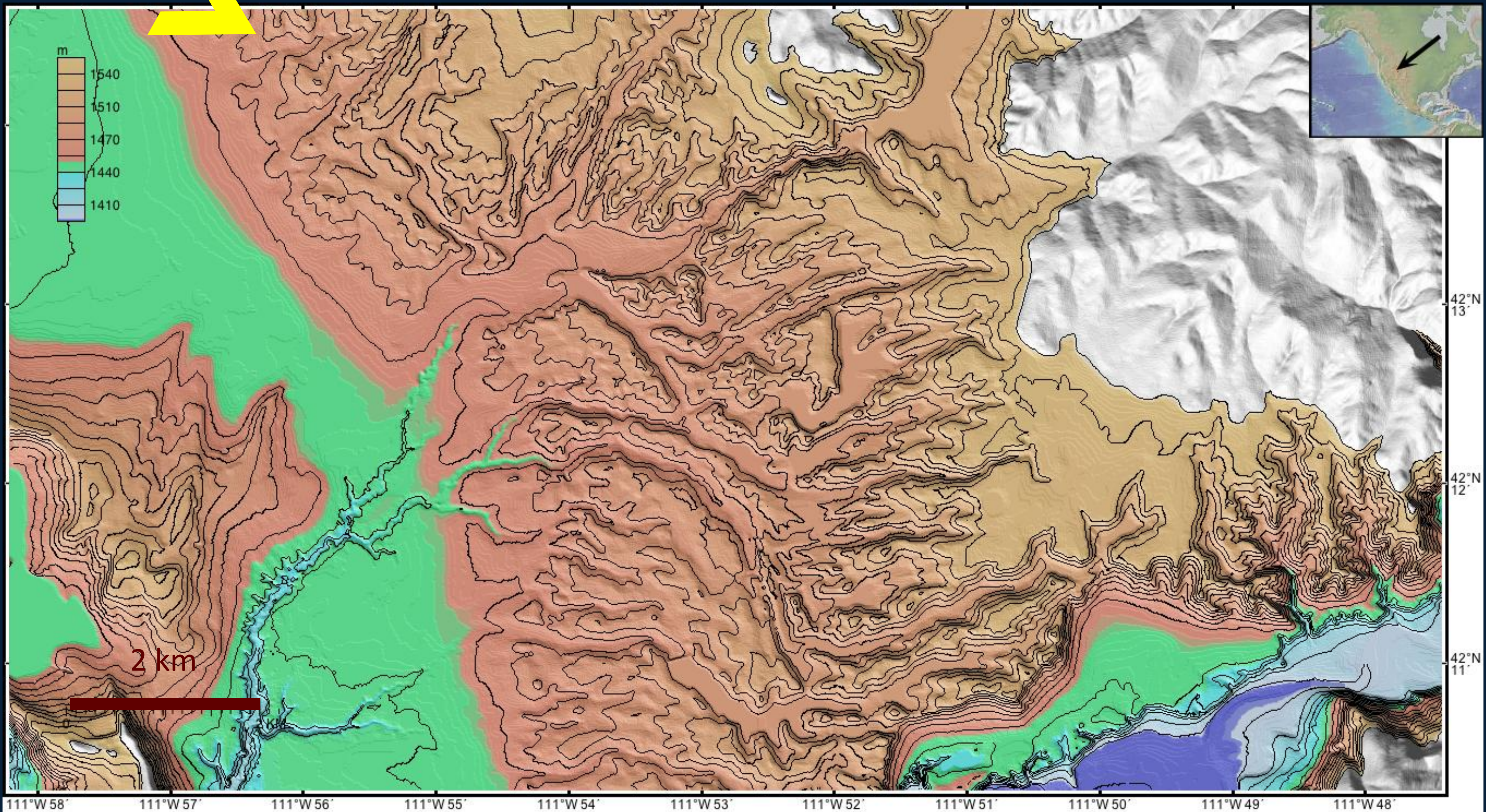

REASON 2: Landscape suggests that Lake Bonneville must have been stable at its highest shoreline for many centuries, maybe >1000 yrs(?)

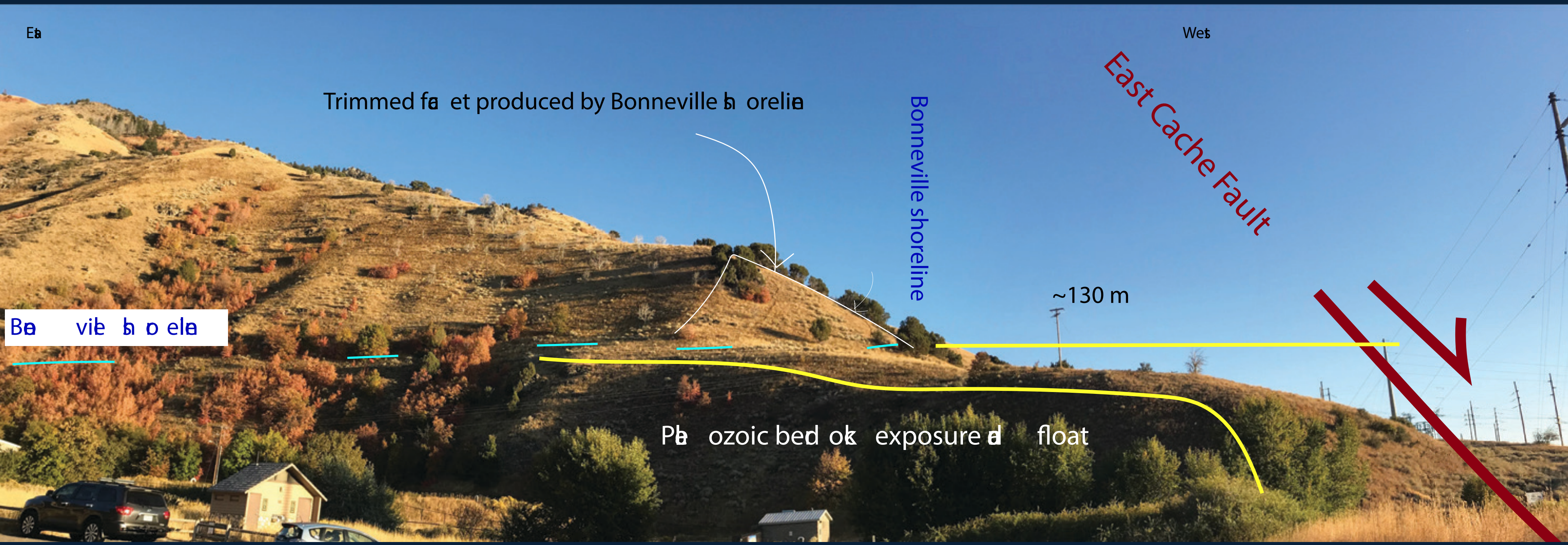

Lake carved cliffs and terraces across hard bedrock
The B. shoreline trimmed and steepened triangular facets
in the footwalls of active faults everywhere

Facet composed of Paleozoic bedrock at Green Canyon, near liquefied outcrop

Triangular facets of East Cache fault are steepest where Lake Bonneville trimmed them. 100-400 m east of fault

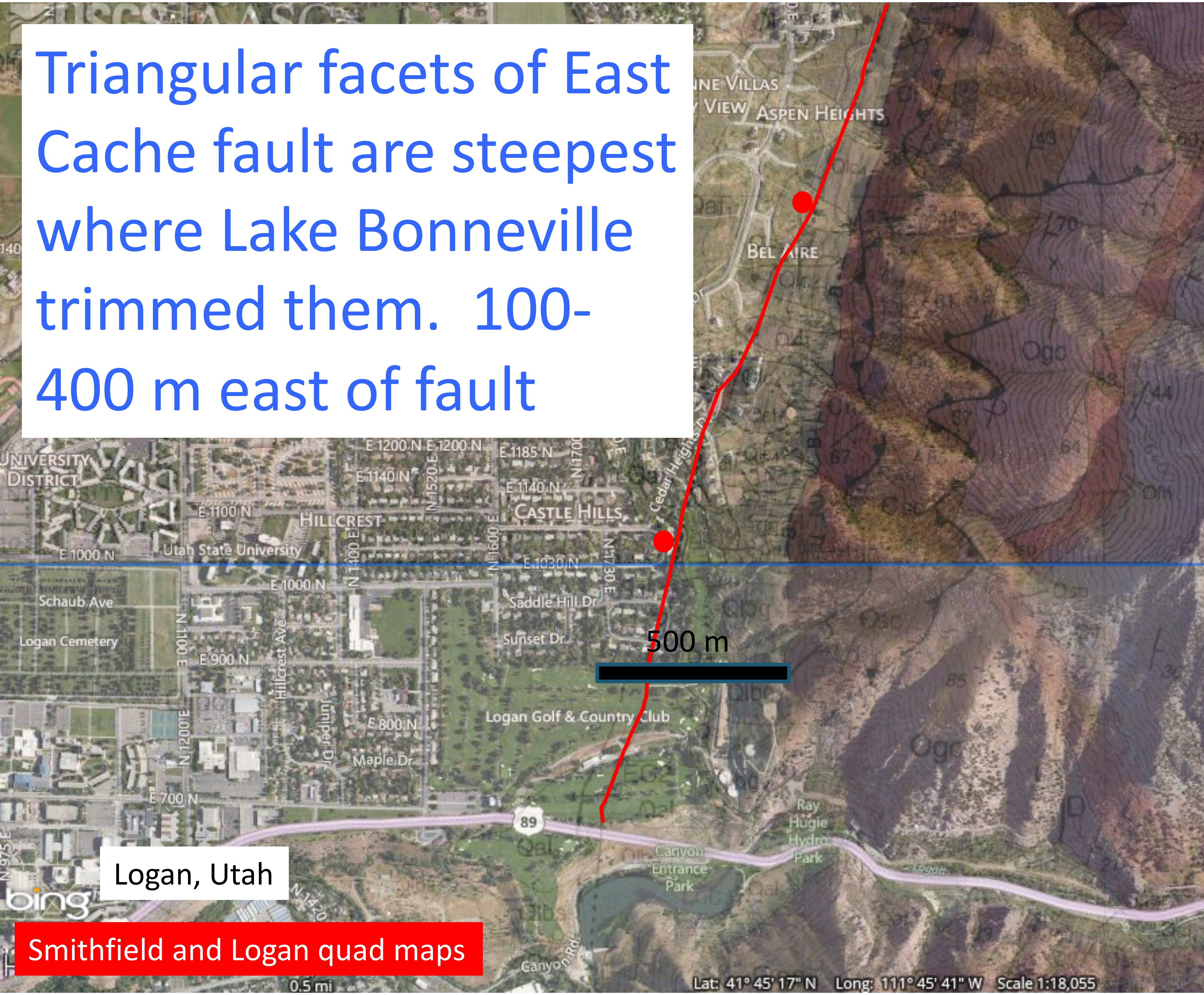

Facets at the B. shoreline are up to 100-80 m high

Lake Bonneville must have been pounding on these cliffs for centuries as it was stable and flowing across its threshold at Zenda

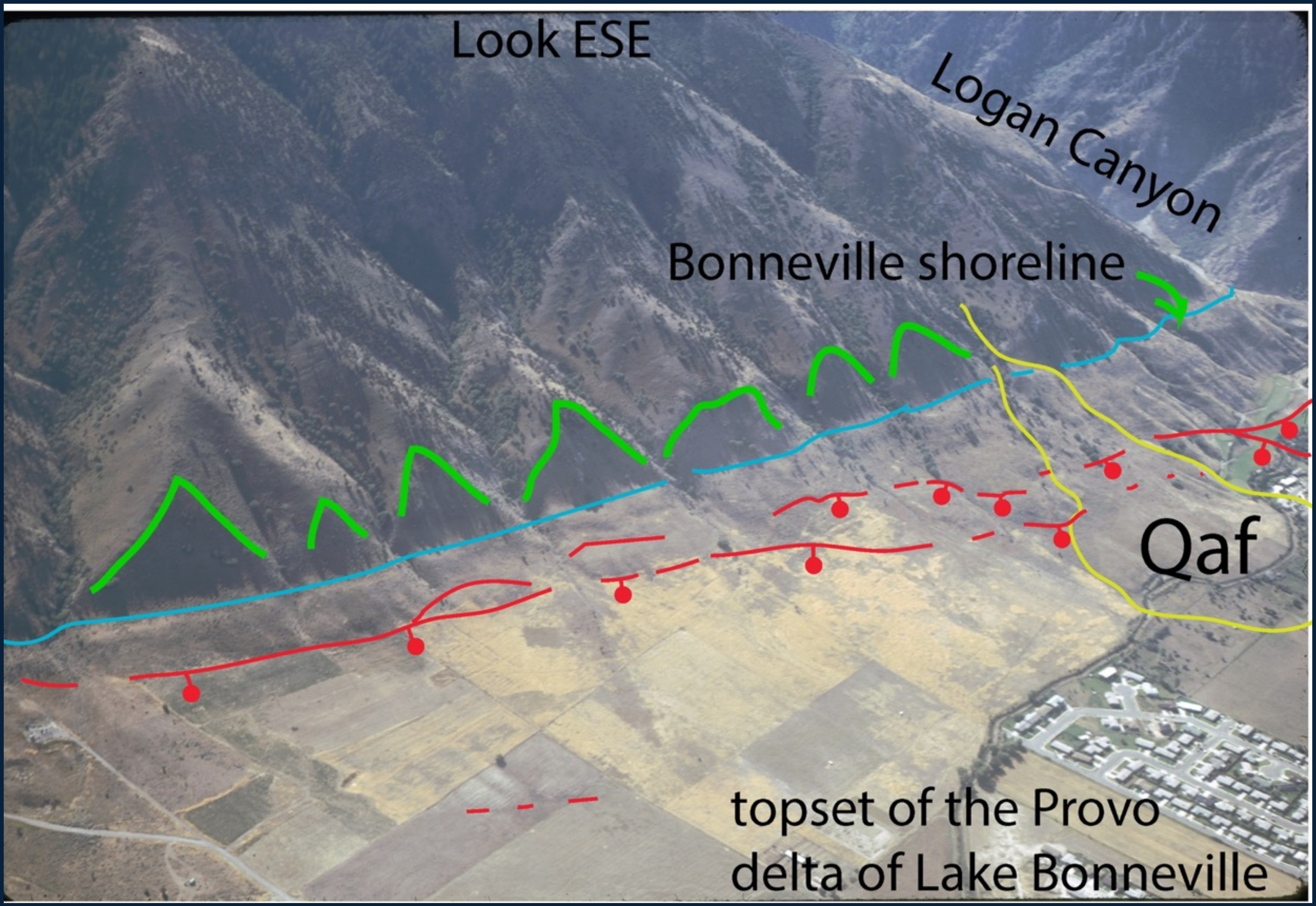

- The possibility that an earthquake triggered the Bonneville flood led us to examine a highly deformed outcrop of Bonneville deposits near Logan, Utah
- Might it record THE earthquake that triggered the Bonneville flood?
- If not, what does it record?

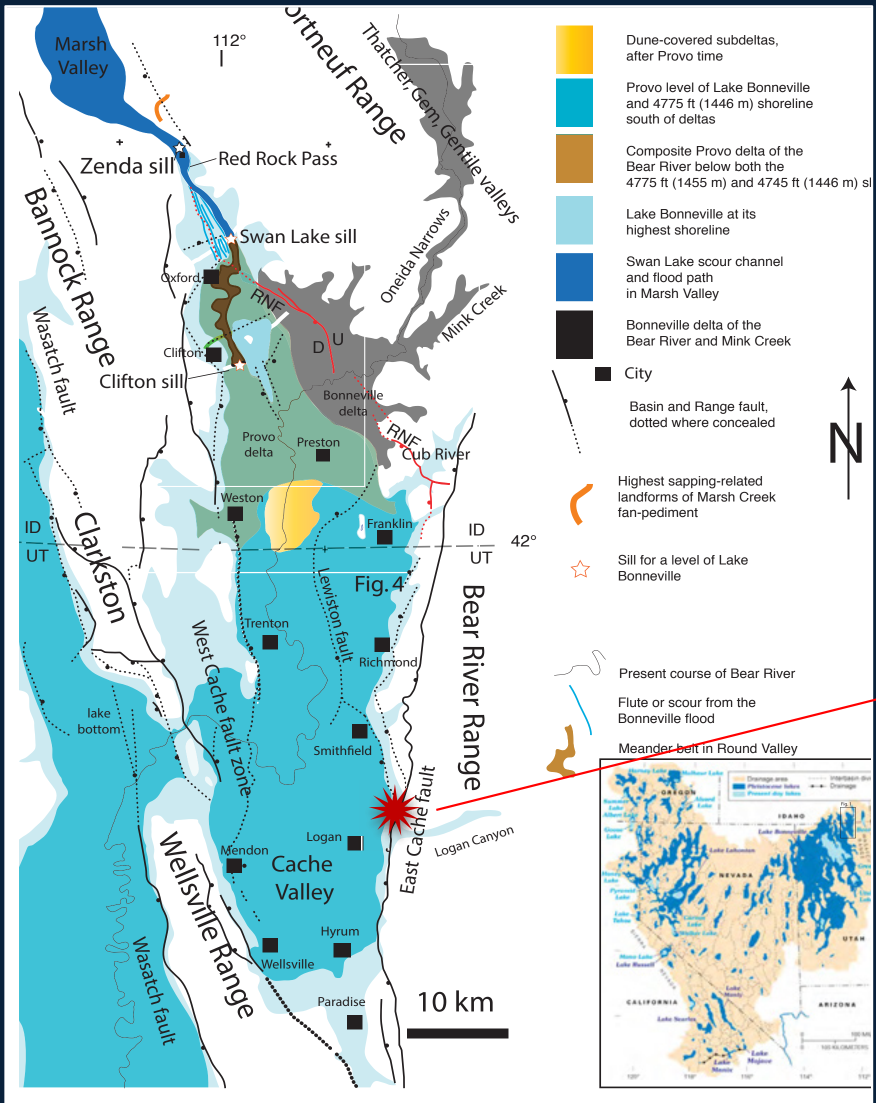

Figure 1. Map of lake levels within Cache Valley. Deltas of the Bear River are differentiated from other lacustrine deposits.

Consider how deformation like this might destabilize the outlet of Lake Bonneville if it occurred near Zenda

The liquefied outcrop of Green Canyon, North Logan, Utah

On the 1980's the outcrop was using in field trips by USU faculty. Our current work shows that 4 major earthquakes produced each of 4 major liquefaction zones -in color. Additional events are possible.

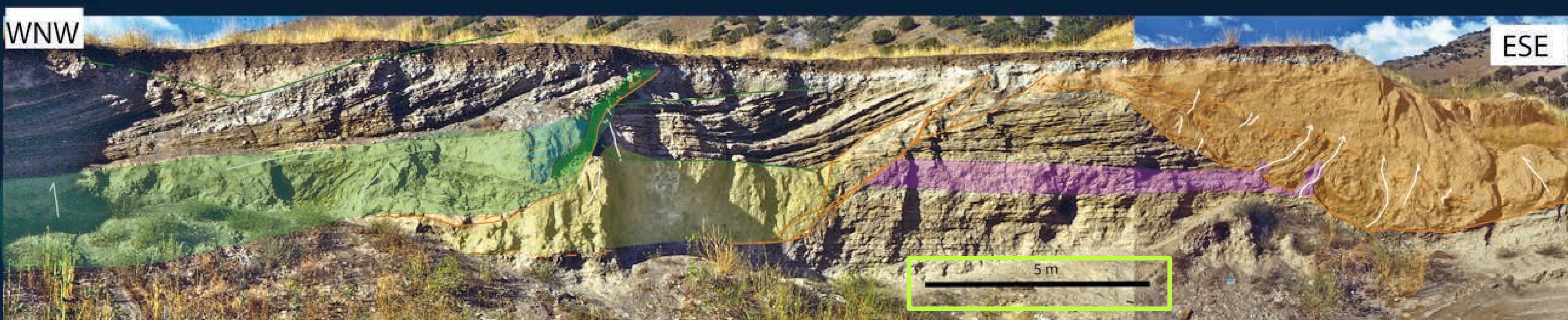

Study site is between Bonneville and Provo shoreline, 225 m west of Bonneville shoreline

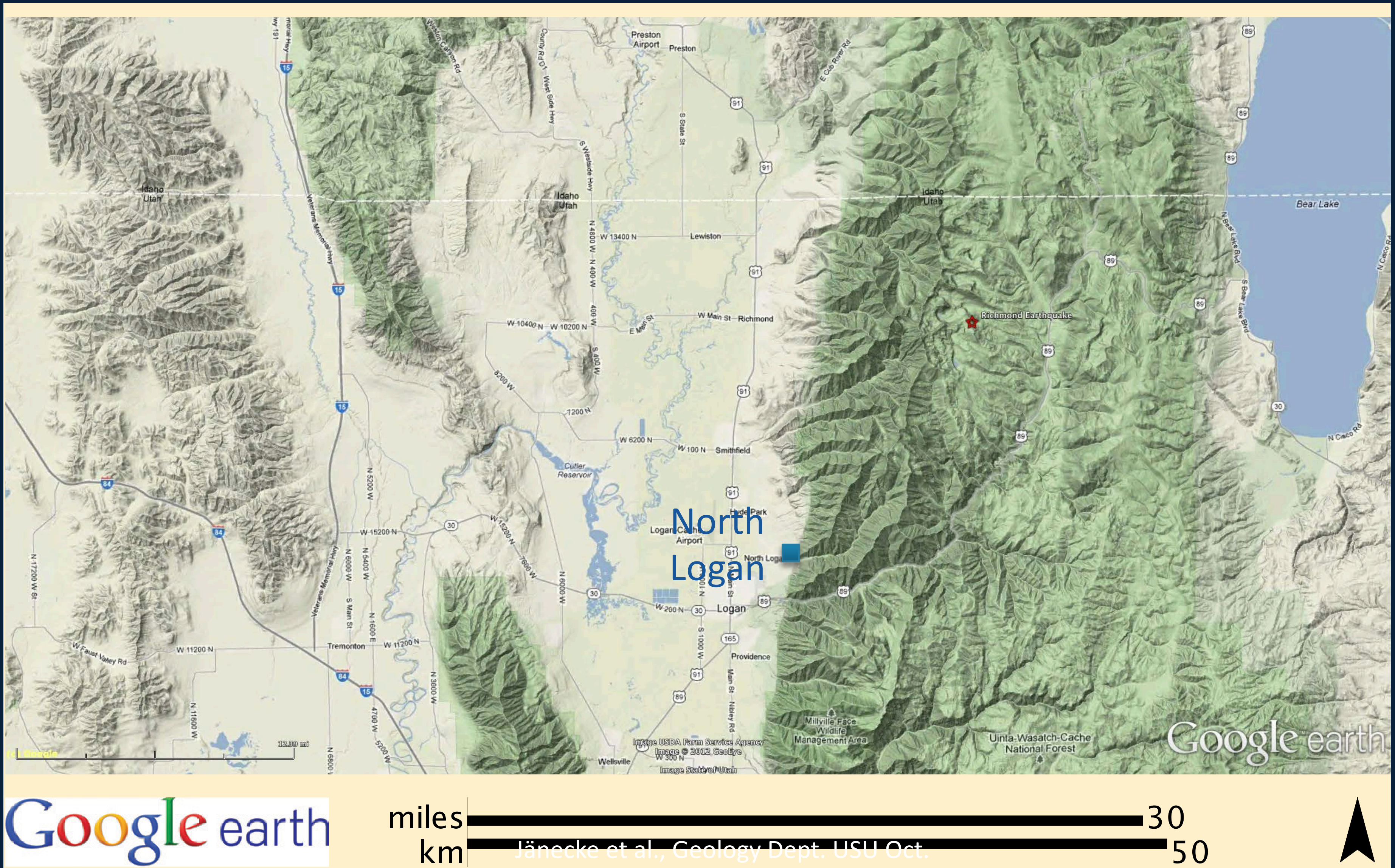

Jänecke et al., Geology Dept. USU Oct. 2018

Since Lake Bonneville, normal faults in Cache Valley slipped at low rates with long recurrence intervals.

West Cache fault was fairly active in Holocene (Black et al., 2000), Janecke and Ellis, 2018

Site is at a segment boundary, where several faults branch

Central segment of ECF:
MRE 4.5 ka
Penultimate event was 15.6 to 18.5 ka during Provo time

Northern segment:
No evidence of latest Quaternary slip except for a lateral spread
(McCalpin, 1987, 1994)

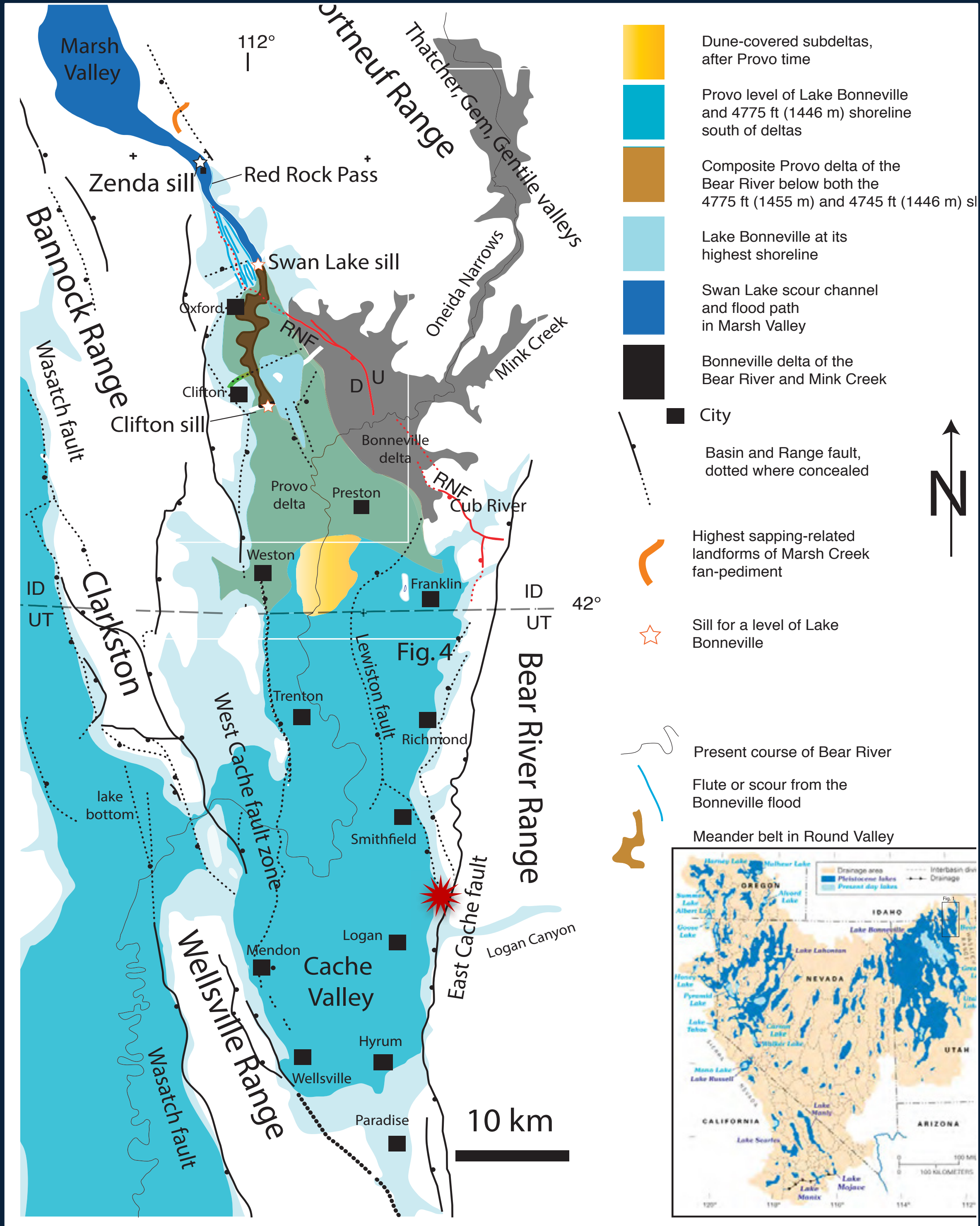

Figure 1. Map of lake levels within Cache Valley. Deltas of the Bear River are differentiated from other lacustrine deposits.

East Cache fault surrounds the Green Canyon site

There are strands of East Cache fault around the site

One inactive strand is ~200 m to E along mountain front (McCalpin, 1989) and second buried strand is even closer

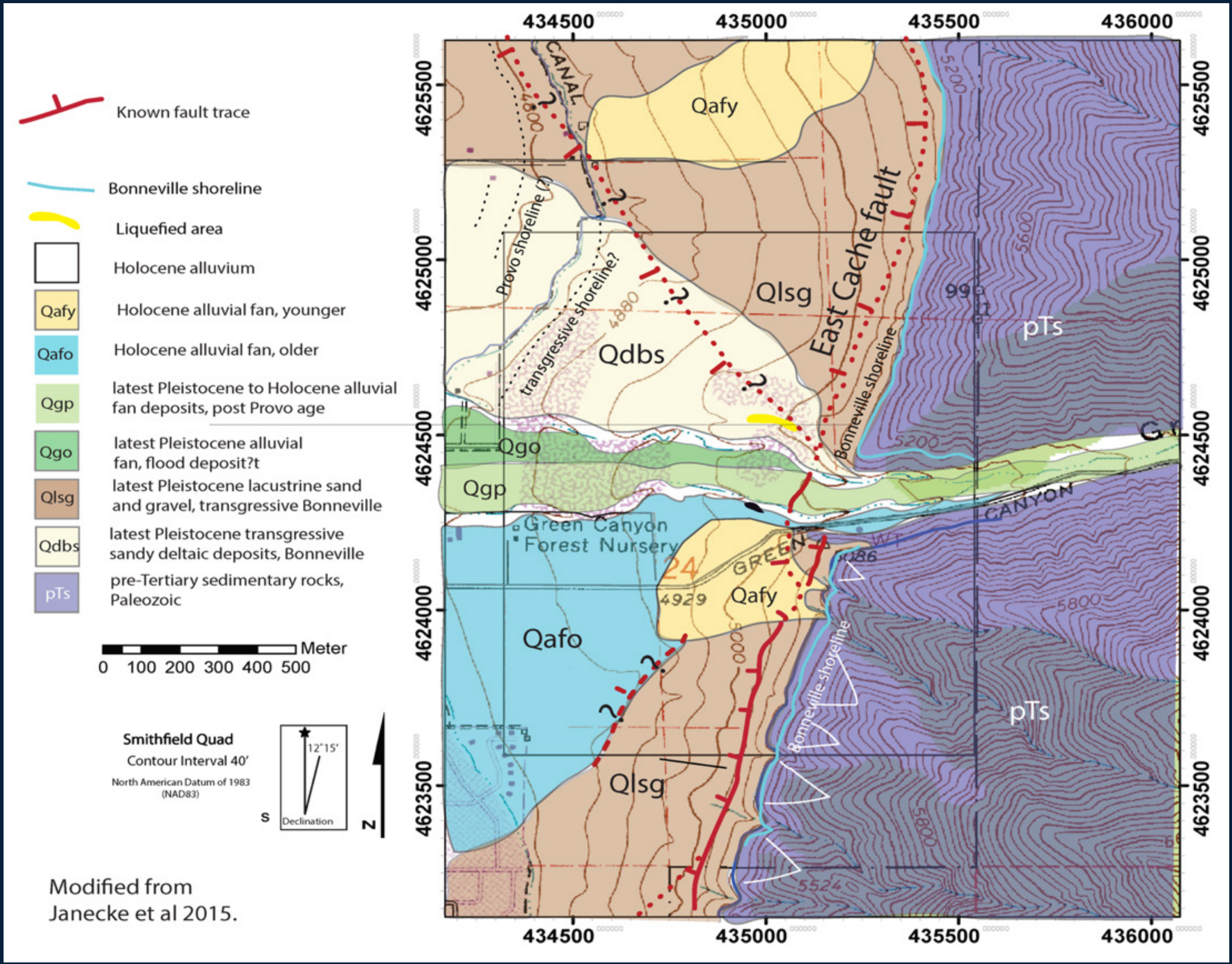

Deposition of seds was within 40-45 m

Then of highstand of Lake Bonneville

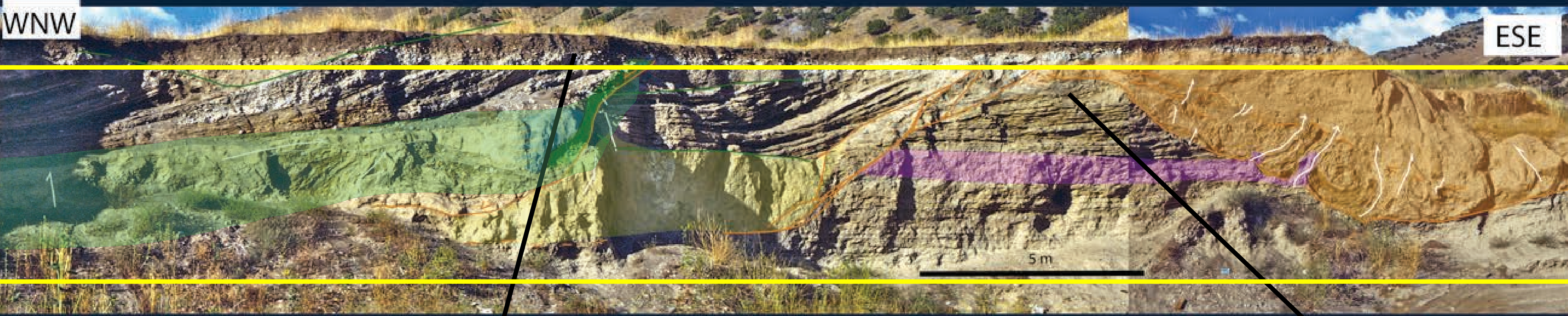

Stage 2

*40-45 m below Bonneville Shoreline

*Colors denote liquefied units

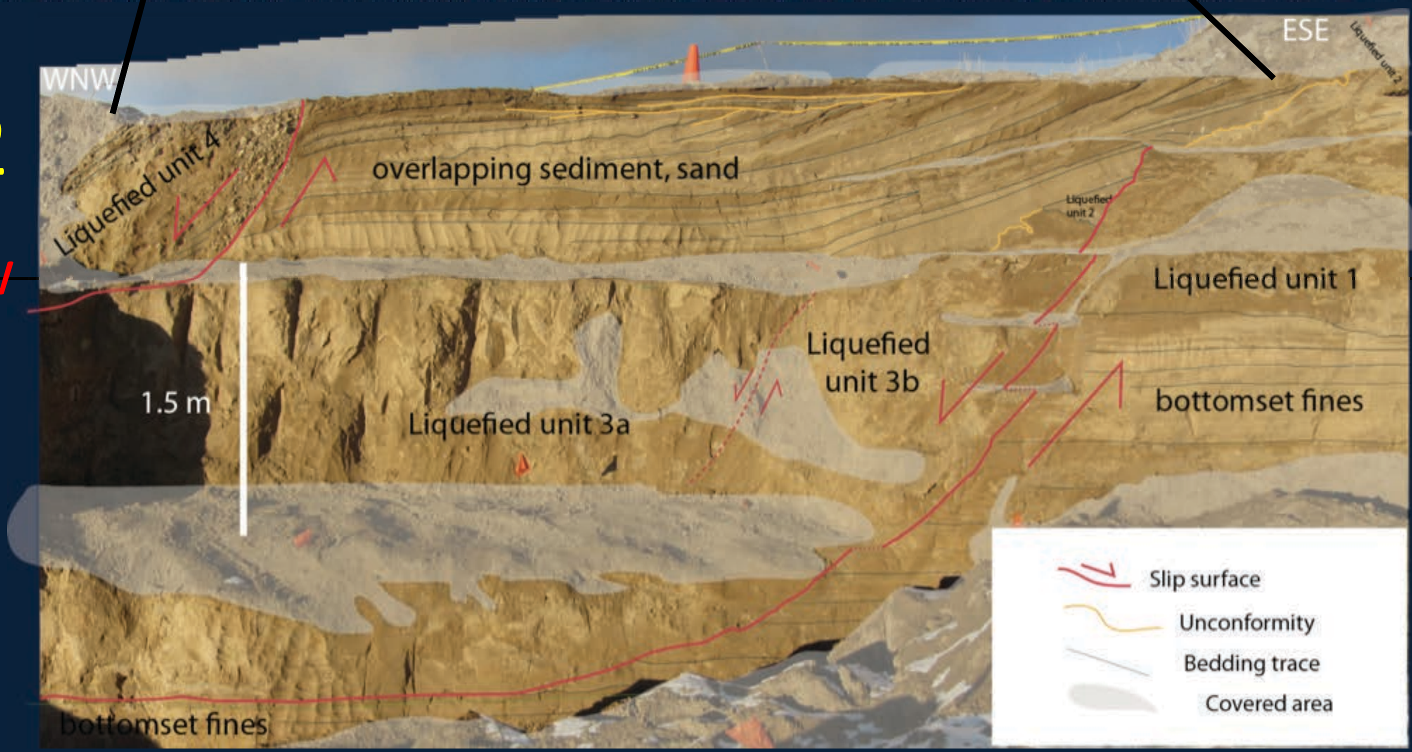

Except for capping gravel and soil, all sediment was deposited in shallow part of Lake Bonneville

Evidence:
1. Gastropod shell,
2. ripples,
3.cross beds,
4.sedimentary facies,
5.radiocarbon and OSL ages

Gastropod shells are common in sandy deltaic beds

There is pervasive liquefaction as well
Pseudonodules of all sizes

All views of exposure are to the NNE

The liquefied beds are full of round features called pseudonodules, flames, fluid escape structures and load casts

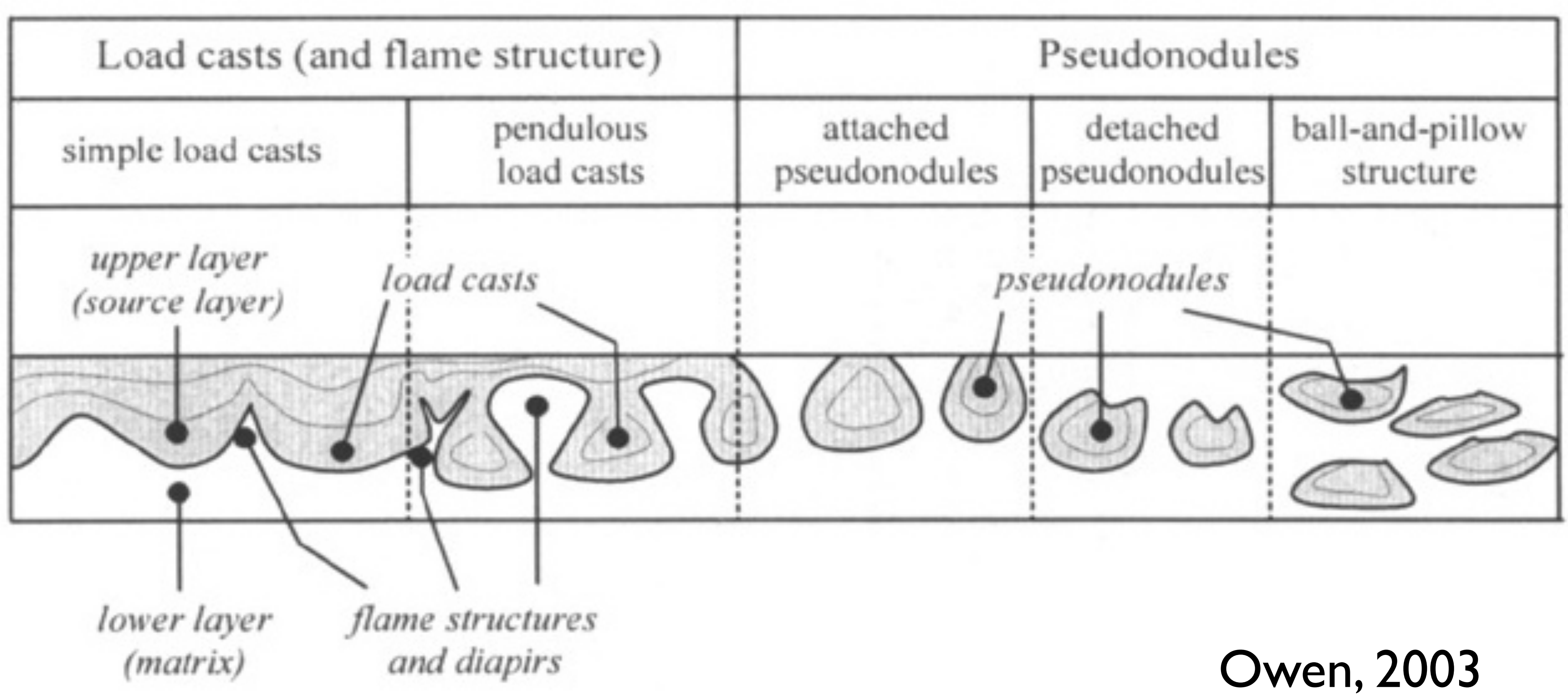

Owen, 2003

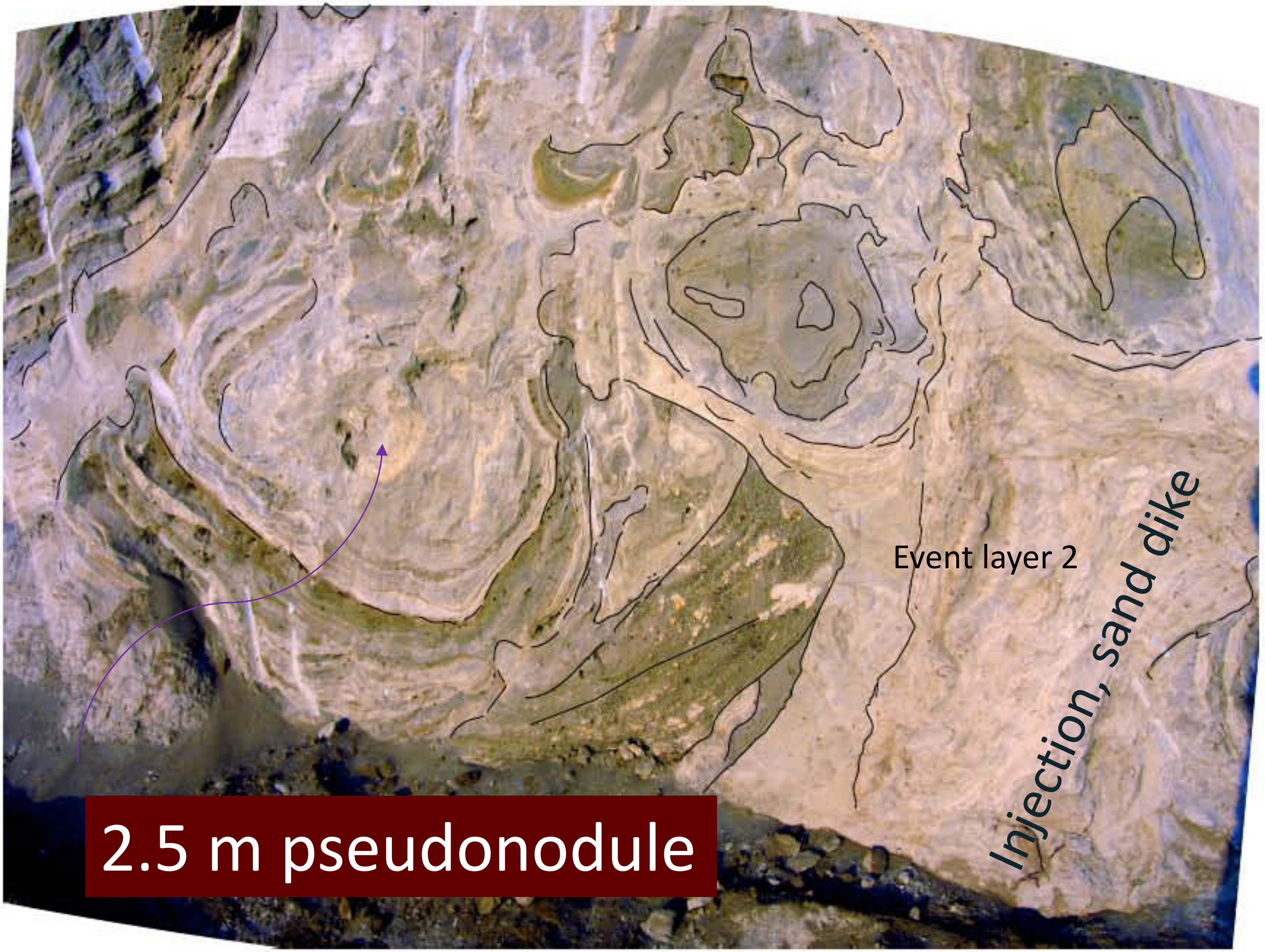
Event layer 2
Injection, sand dike
2.5 m pseudonodule

Stratigraphy

1980's photo of ~half of outcrop:

WNW ESE

- Soil
- Intact cap of alluvial gravel, Flood-related (?)
- over deformed Bonneville deltaic sand (s) and gravel (g)
- over deformed Bonneville prodelta fine sand, silt and clay (f, fines)
- Less deformed Bonneville foresets of gravel (g)

All the deformation was during Bonneville transgression, before the flood,
-before gravel cap and incision of inset channels

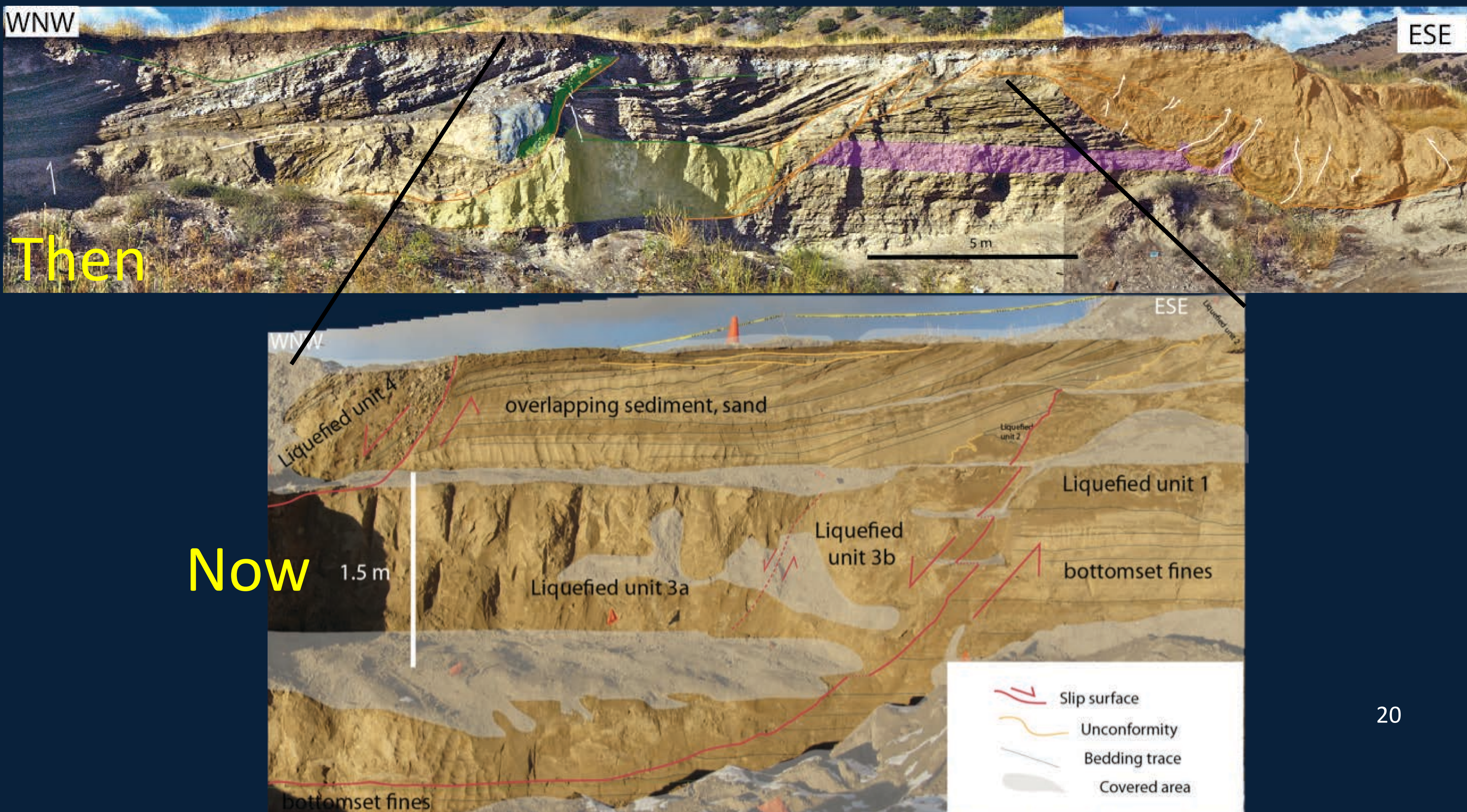

Research questions during initial research:

1. Does the deformed outcrop at Green Canyon record an earthquake at the time of the Bonneville flood?
2. Are there exposed strands of the East Cache fault?

1. No-all deformation dates from the Bonneville transgression close to highstand
2. No-All “Faults” are slip surfaces of nested lateral spreads

Overlapping beds are less deformed, but cut by slip surface in west

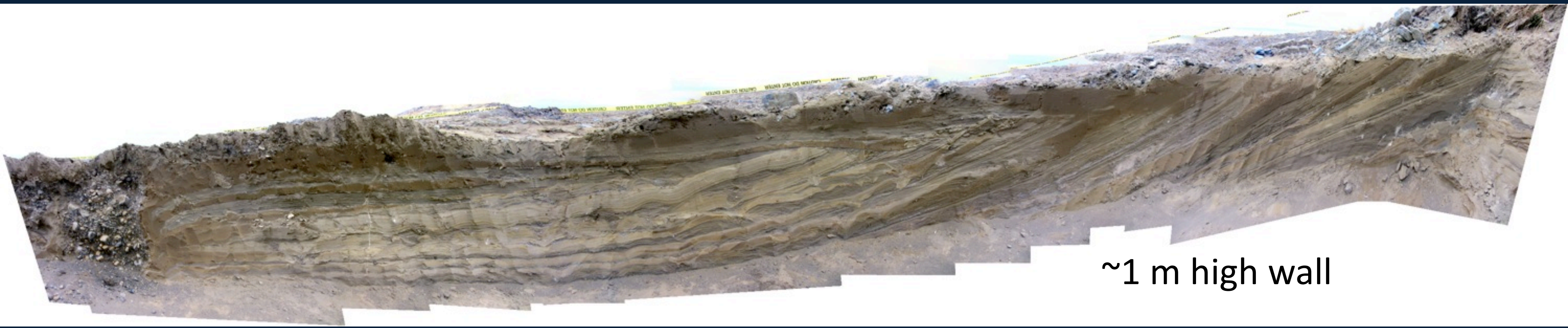

Sediment draped across scarps on bed of Lake Bonneville

2012


Depositional onlap
10 cm

Lacustrine fault wedge contains blocks of footwall

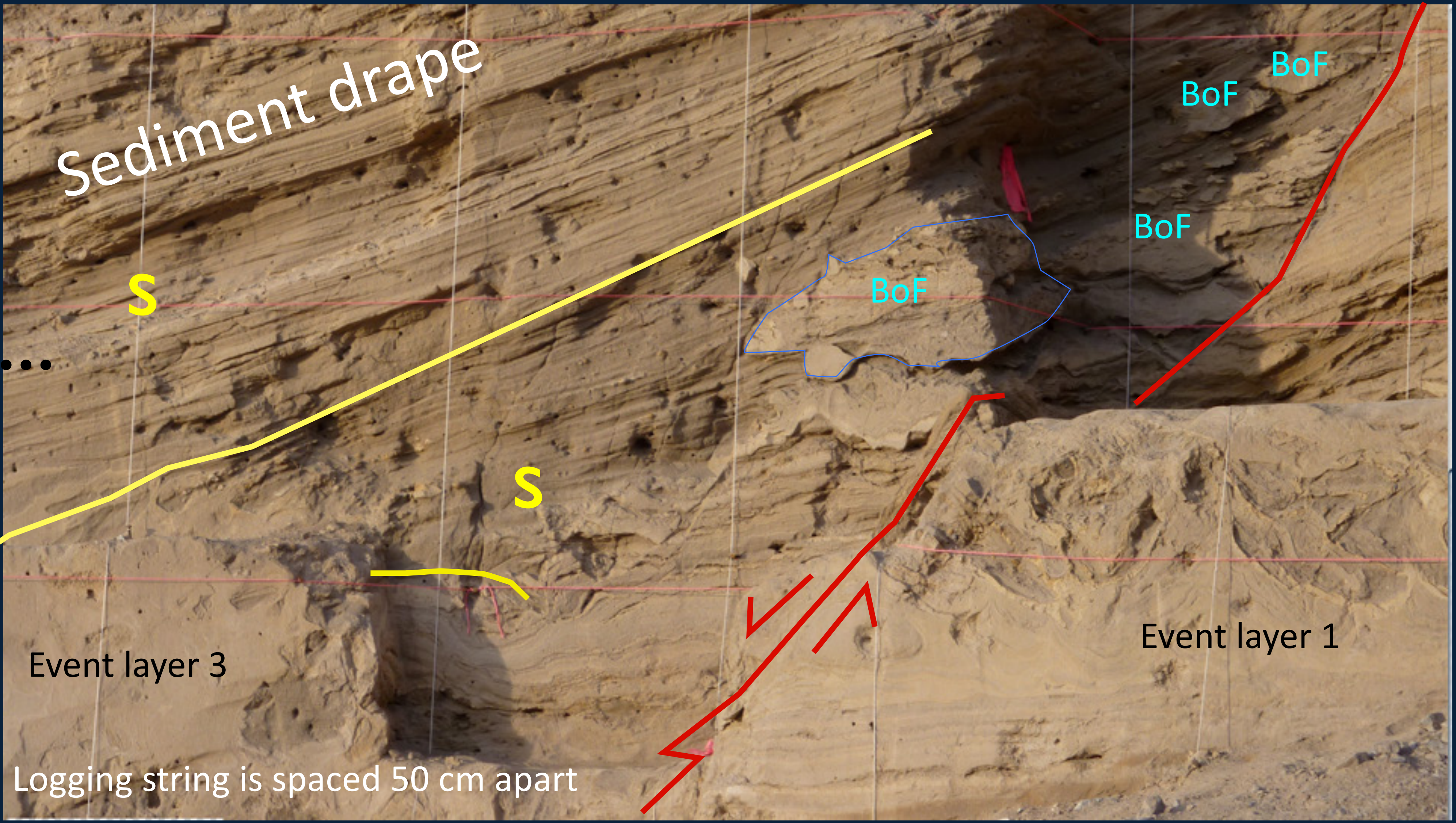

This is analogous to a colluvial wedge along a normal fault

There is a slip surface below all major liquefied masses except the purple one

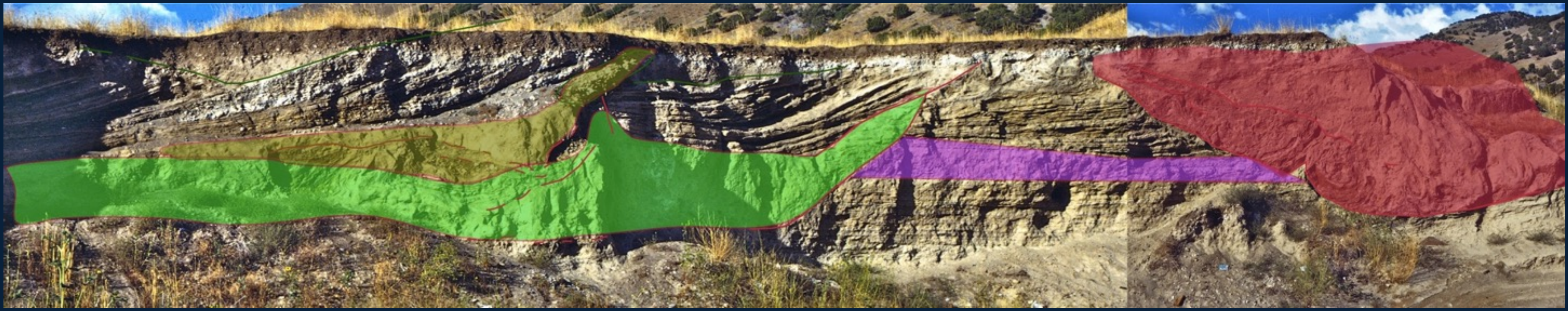

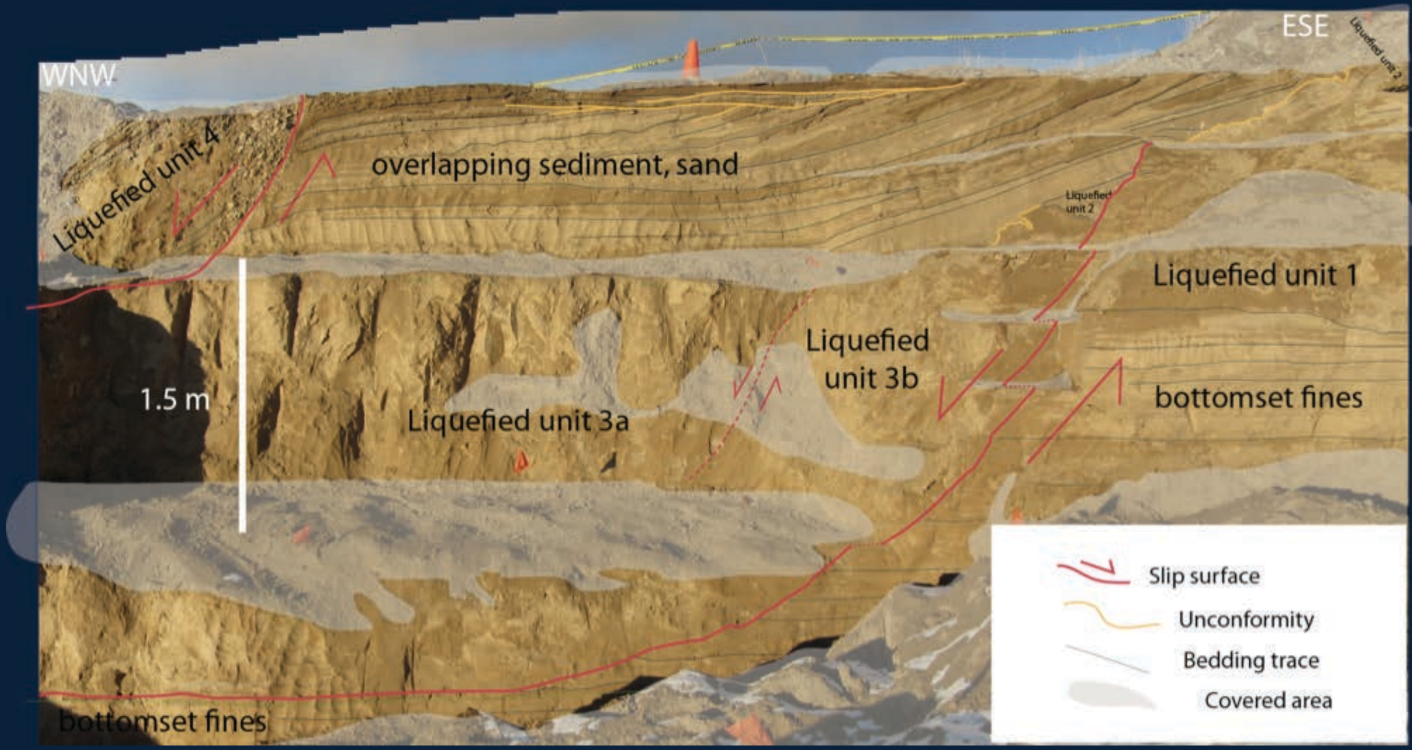

Basal slip surface of the lateral spread

About 1.5 m high

Relative ages are very clear due to cross-cutting relationships

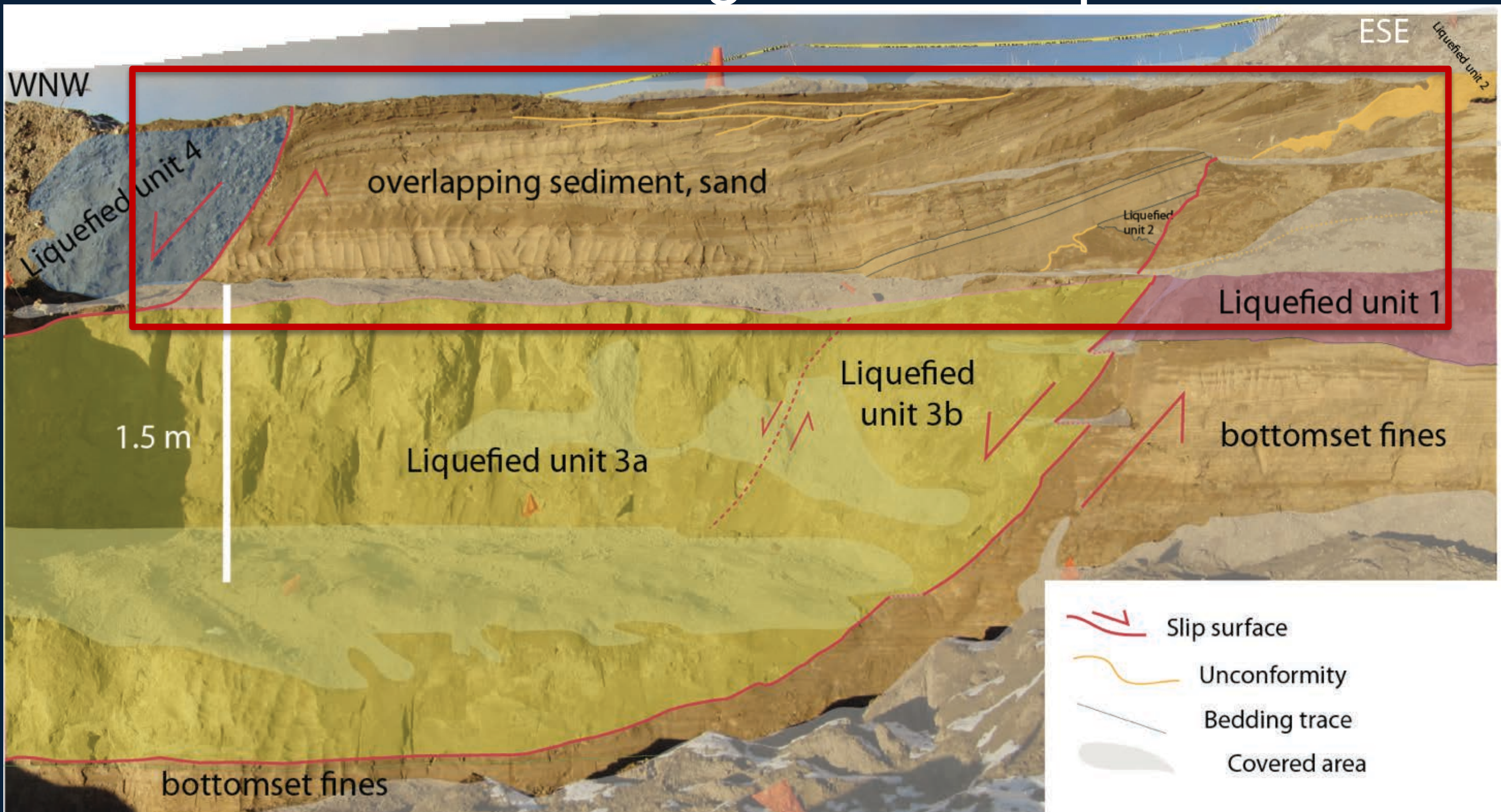

The 4 THICK liquefied intervals: numbered and colored from oldest to youngest

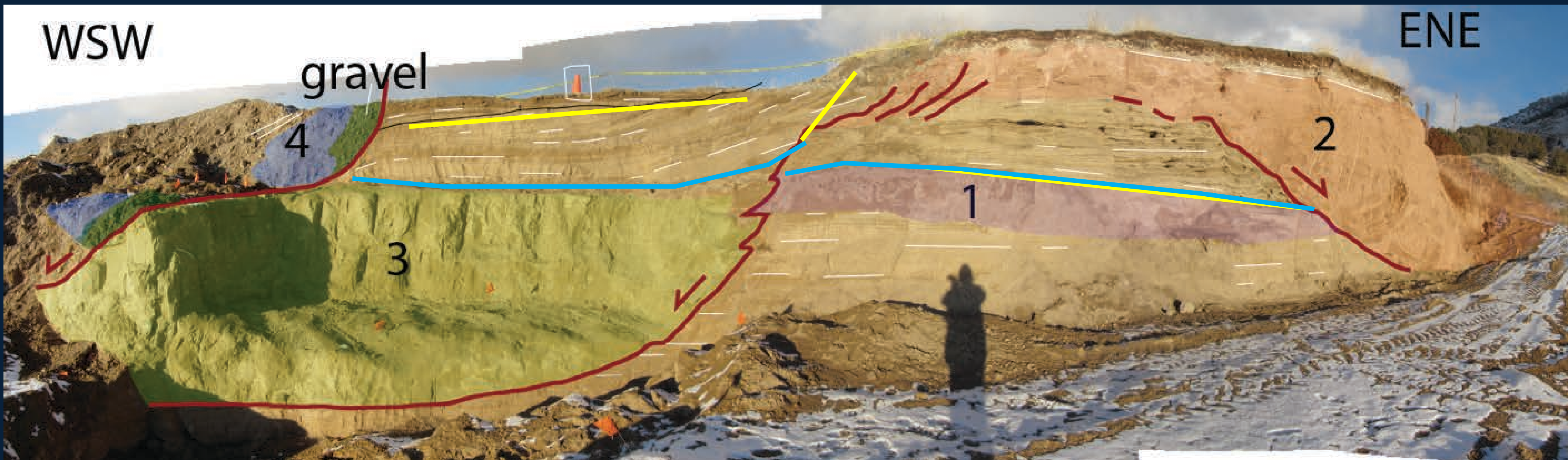

Each bench is 1.5 m high

Cross-cutting relationships between these beds and show that each is a different age, from 1 to 4

Unconformities,
slip surfaces and
overlapping beds

Detailed Chronology
deposit, liquefy, erode, REPEAT

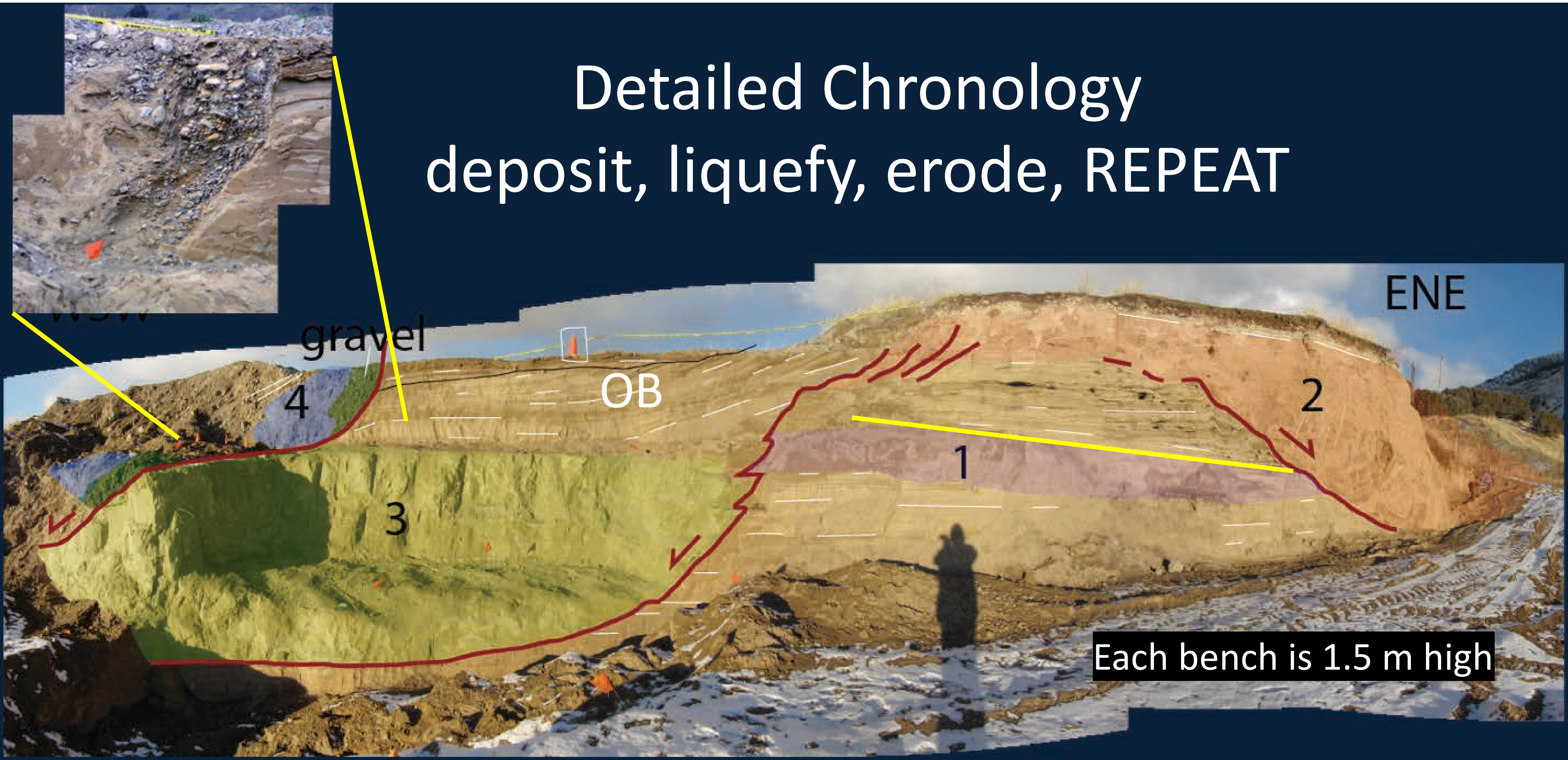

- Lake rises to ~ 40 m below the high stand
- Event bed number 1, possibly after a brief regression
- Erosion of liquefied bed 1
- Deposition of more lake beds
- Event bed 2 ± lateral spreading
- Deposition of more lake beds
- Event 3 and slip surface

- Overlap beds (OB) are deposited across lateral spread
- Shaking causes Event bed 3 to invade overlap succession
- Lateral spread slips again, cuts overlap and event 3 bed
- Event bed 4 activated the western slip surface
- More deltaic deposition

Summary at outcrop

- Deltaic transgressive sand of Lake Bonneville
- Contain 4 thick liquefied units
- That formed sequentially >4 times
- Outcrop is cut by 3 listric slip surfaces within a slump or lateral-spread complex,
- Those slip surfaces were active at least 4 times.

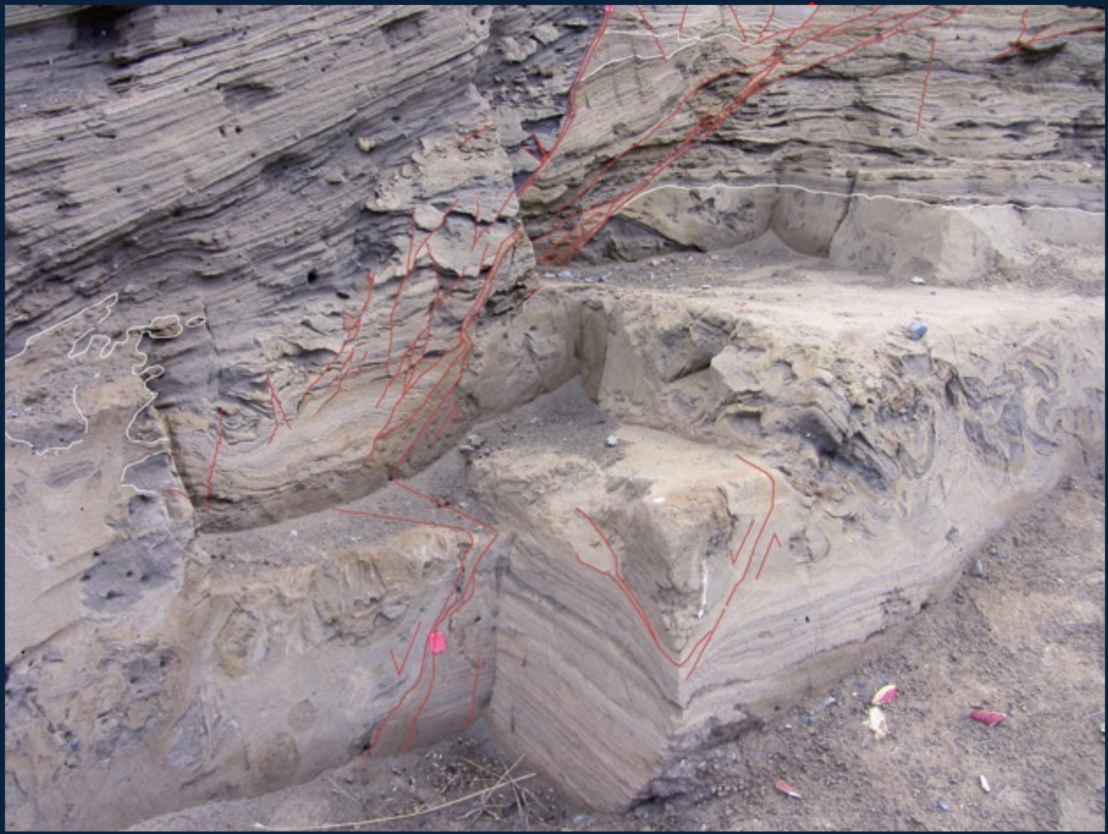

Consider how deformation like this might destabilize the outlet of Lake Bonneville if it occurred near Zenda

3. Were the lateral spreads and overlying liquefied masses of sand activated by earthquakes?

Lateral spread triggered by 1964 Alaska earthquake
USGS pics

Some features only form during earthquakes

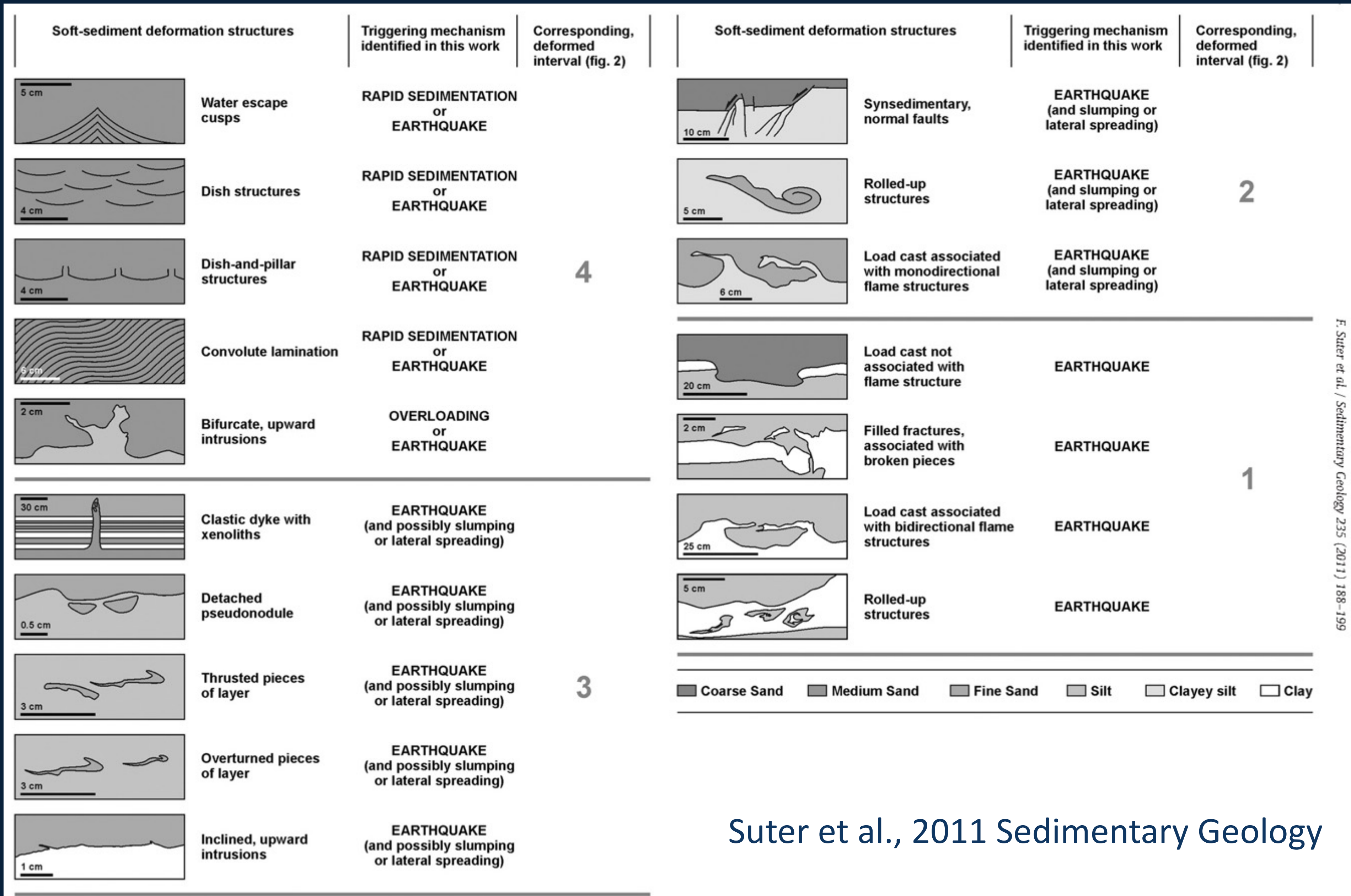

Suter et al., 2011 Sedimentary Geology

Fig. 7. Summary of the 17 types of soft-sediment deformation structures found in each of the 4 deformed intervals of the Aeropuerto section, with their respective triggering mechanism identified in the scope of this study. Numbers correspond to the deformed interval they belong to, labelled in Fig. 2. Soft-sediment deformation structures appear in stratigraphic order, except for deformed interval no. 3, where the clastic dyke crosscuts the entire deformed interval.

Soft sediment deformation or seismite?

Or some of each?

- Features consistent with loading processes

  -Delta fronts are known to fail in lateral spreads and slumps

  -Possible association of loading structure and regressions in Paola et al's lab experiments

- Features consistent with seismite interpretation
  - Location near E Cache Flt.
  - Great thickness of structureless, liquefied beds
  - Injections, sand dikes and sills
  - The G.C. delta seems too small and gentle for such massive and repeated collapses
  - "Fault-graded bedding" is present
  - Fluid escape across brittle faults from oscillatory conditions
  - Hansel Valley earthquake produced similar liquefaction, slumping and lateral spreads (Robison, McCalpin)
  - Repeat events on thin delta
  - Sand volcano and sand dikes

Fluid escape strcts, sand dikes and slip surfaces/faults

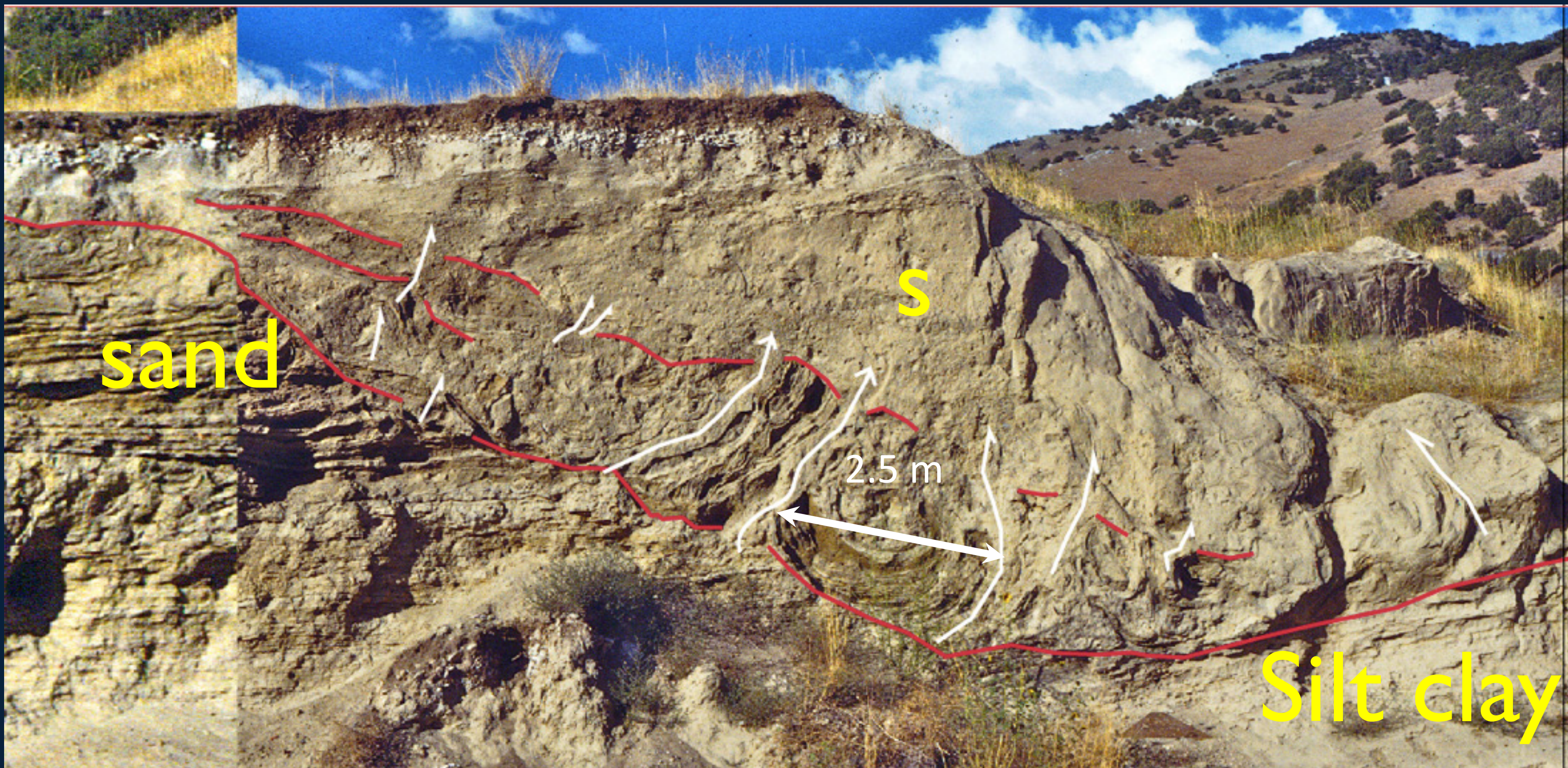

1980's outcrop

Fluid-escape paths are white

Fault-graded bedding is diagnostic of seismic shaking of a lake bed

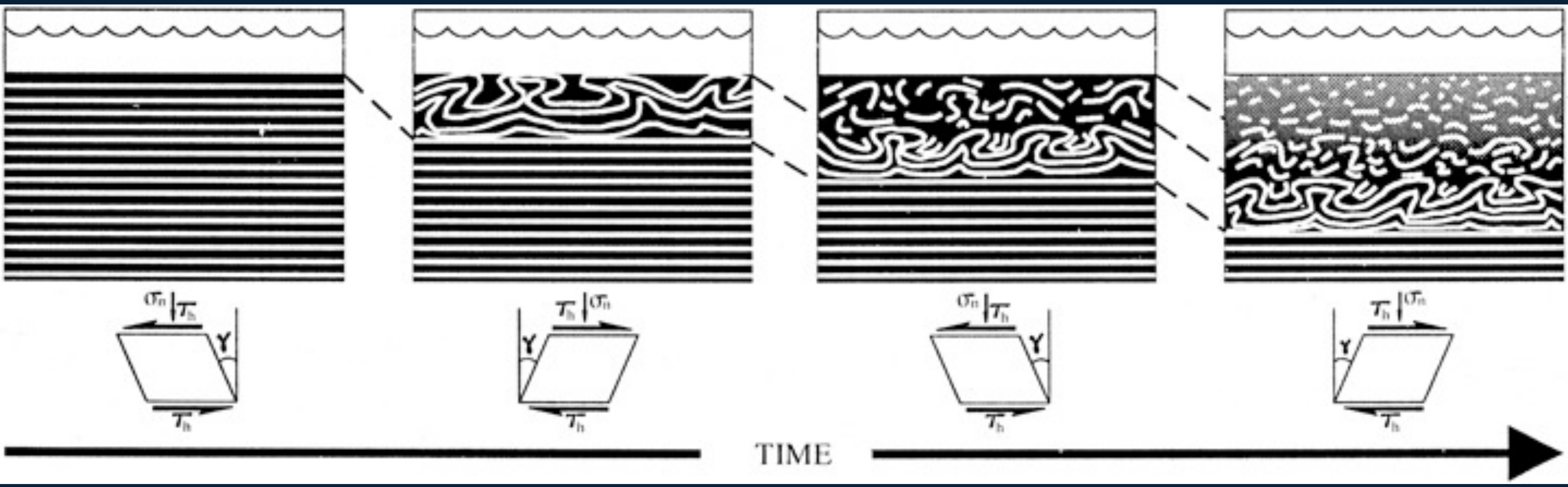

Rodriguez et al., 2000

Fault-graded beds

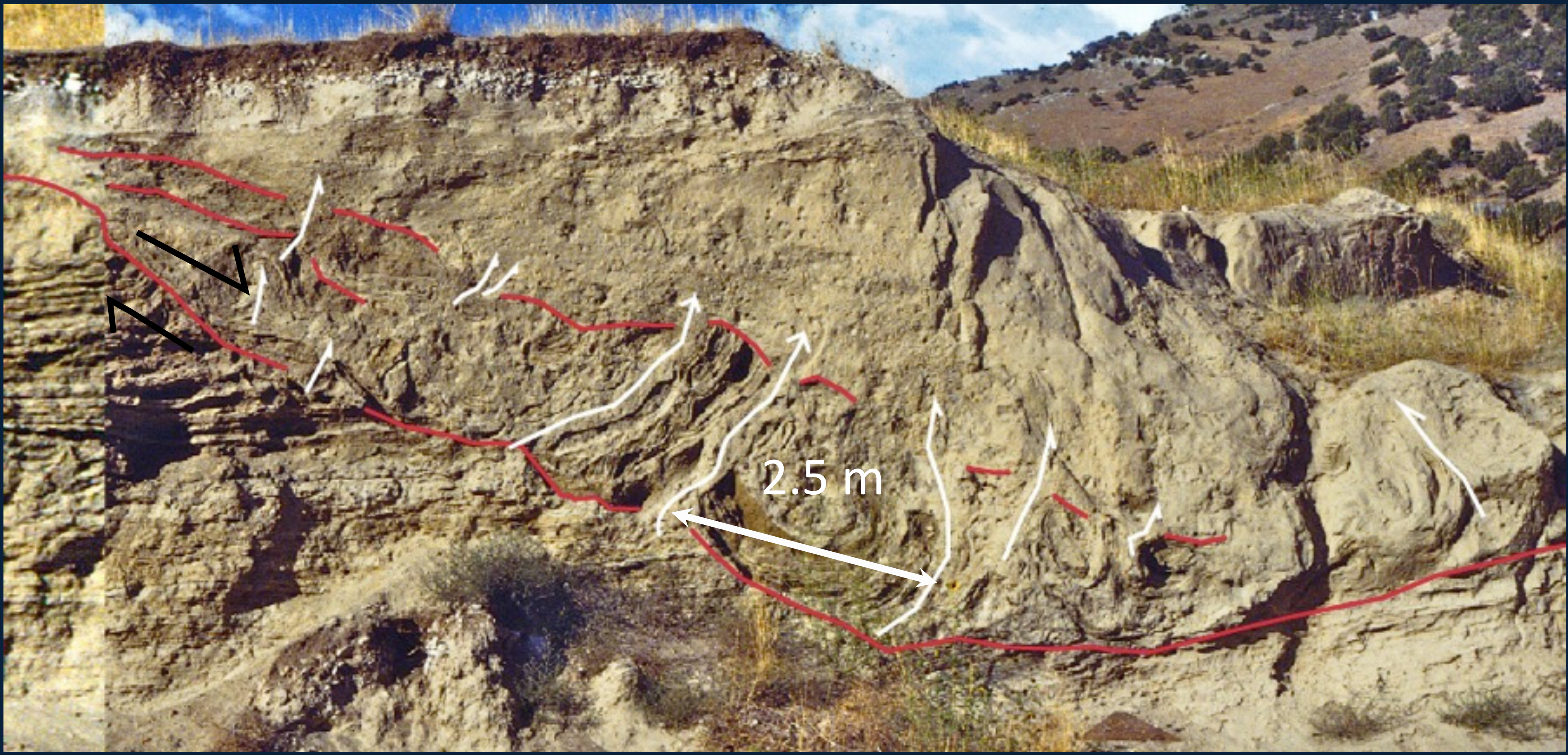

~6 m high exposure, 1980s

15 cm wide sand volcano

Fluid escape across brittle slip surfaces consistent with oscillatory conditions

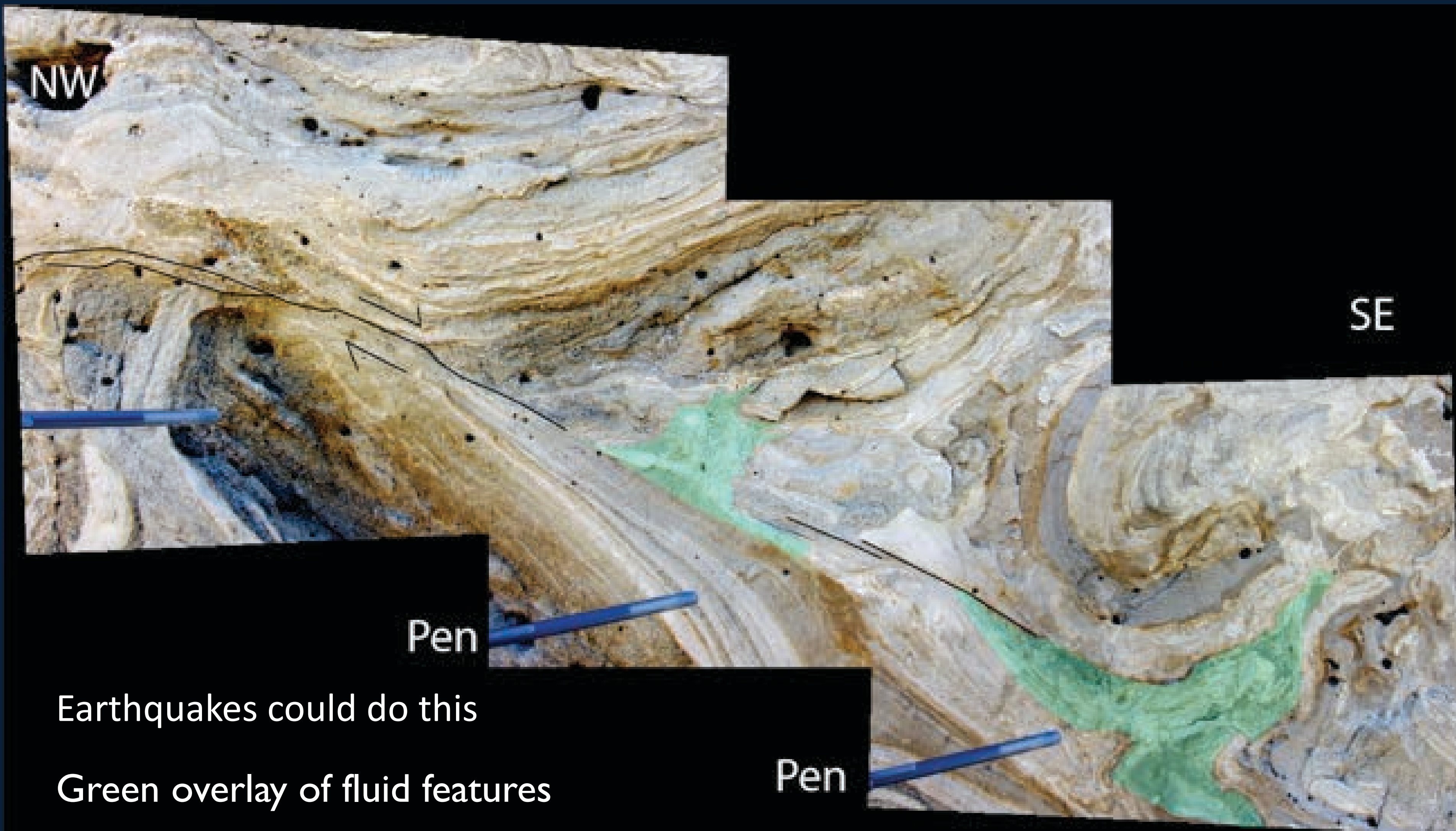

Earthquakes could do this

Green overlay of fluid features

Large clast within liquefied sand body- High energy is needed to churn the sediment

Smaller deformational events may reflect aftershocks

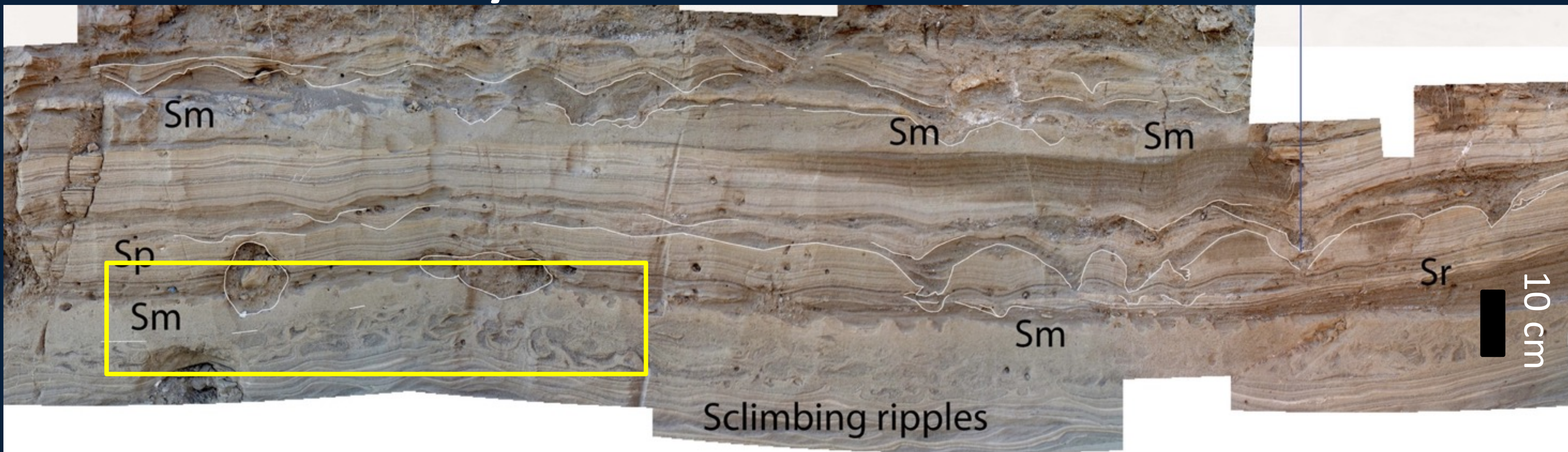

Summary

- Liquefaction occurred at least 4 times under Lake Bonneville (~22 ka to B flood).

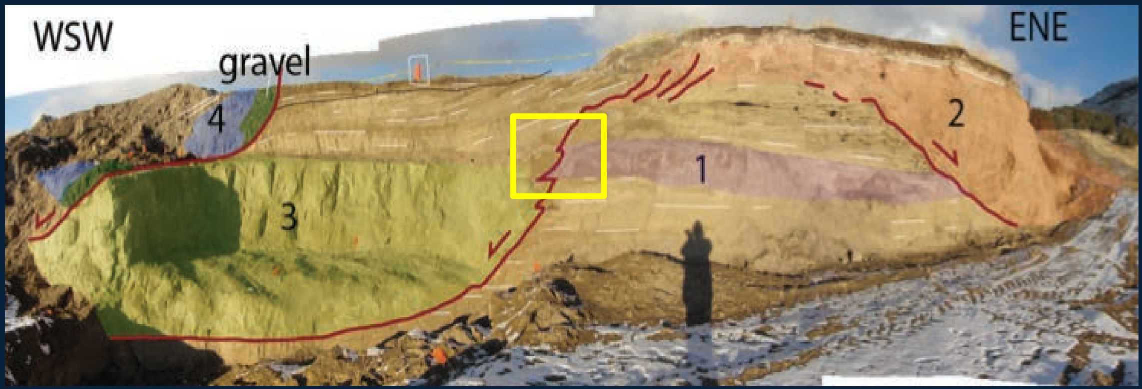

Research questions

3. Did large earthquakes trigger the liquefaction (and the associated slumps)?-YES

4. How many liquefaction events are there?->4

5. Could liquefaction like this trigger or facilitate the Bonneville flood? YES.

6. Why were earthquakes so clustered under L. Bonneville?

Next figure plots the 4 triggered events in time

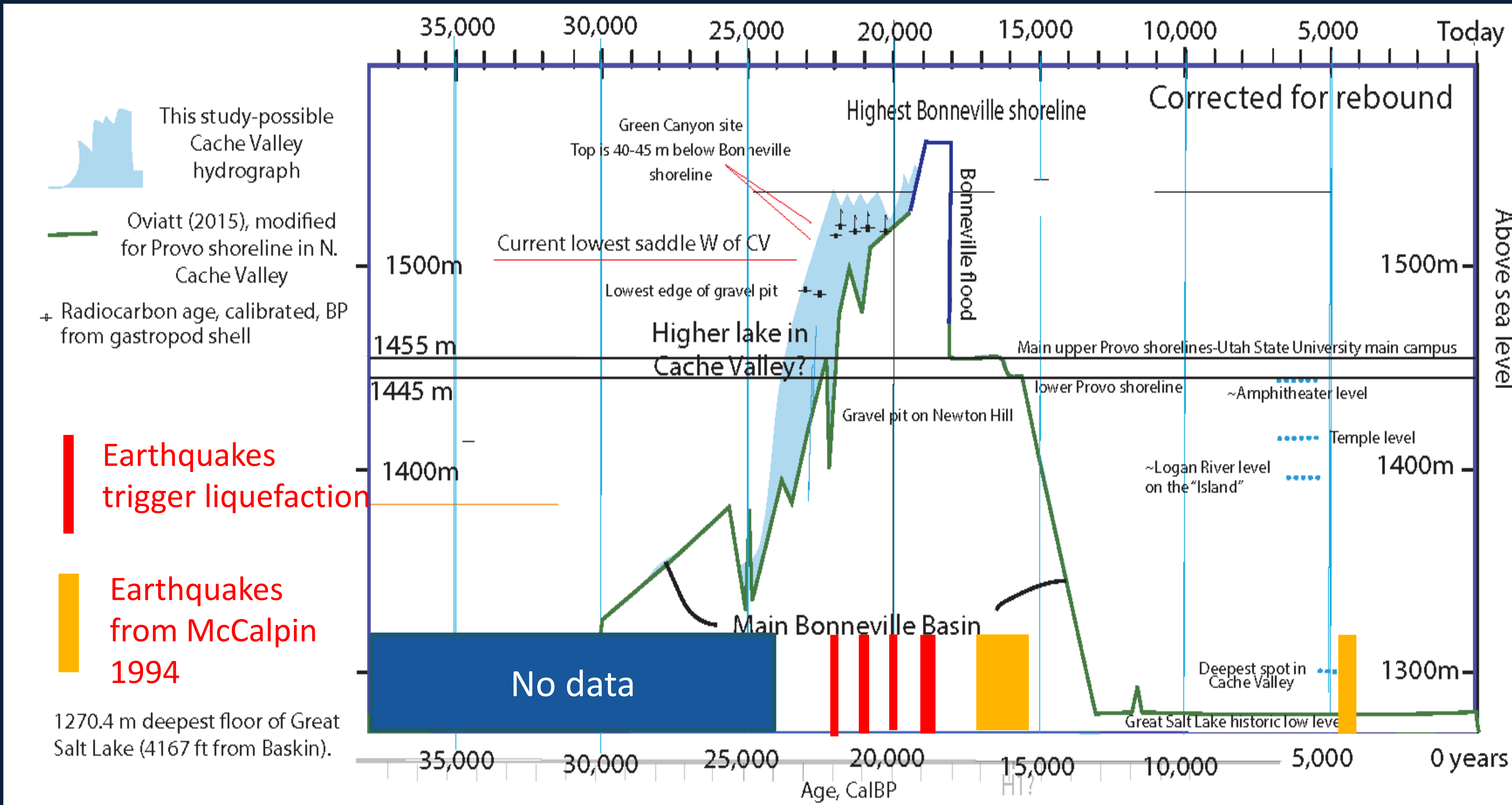

4 events in 5 or 2 ky for depending on hydrograph of Cache Valley (7 Radiocarbon ages are all higher and older than hydrograph predicts. Was Cache Valley separate from Lake Bonneville until the flood? See Oaks et al this meeting)

Earthquakes clustered when lake was high
Why? Hetzel and Hampel, 2005 suggest an answer: Stresses and flexure

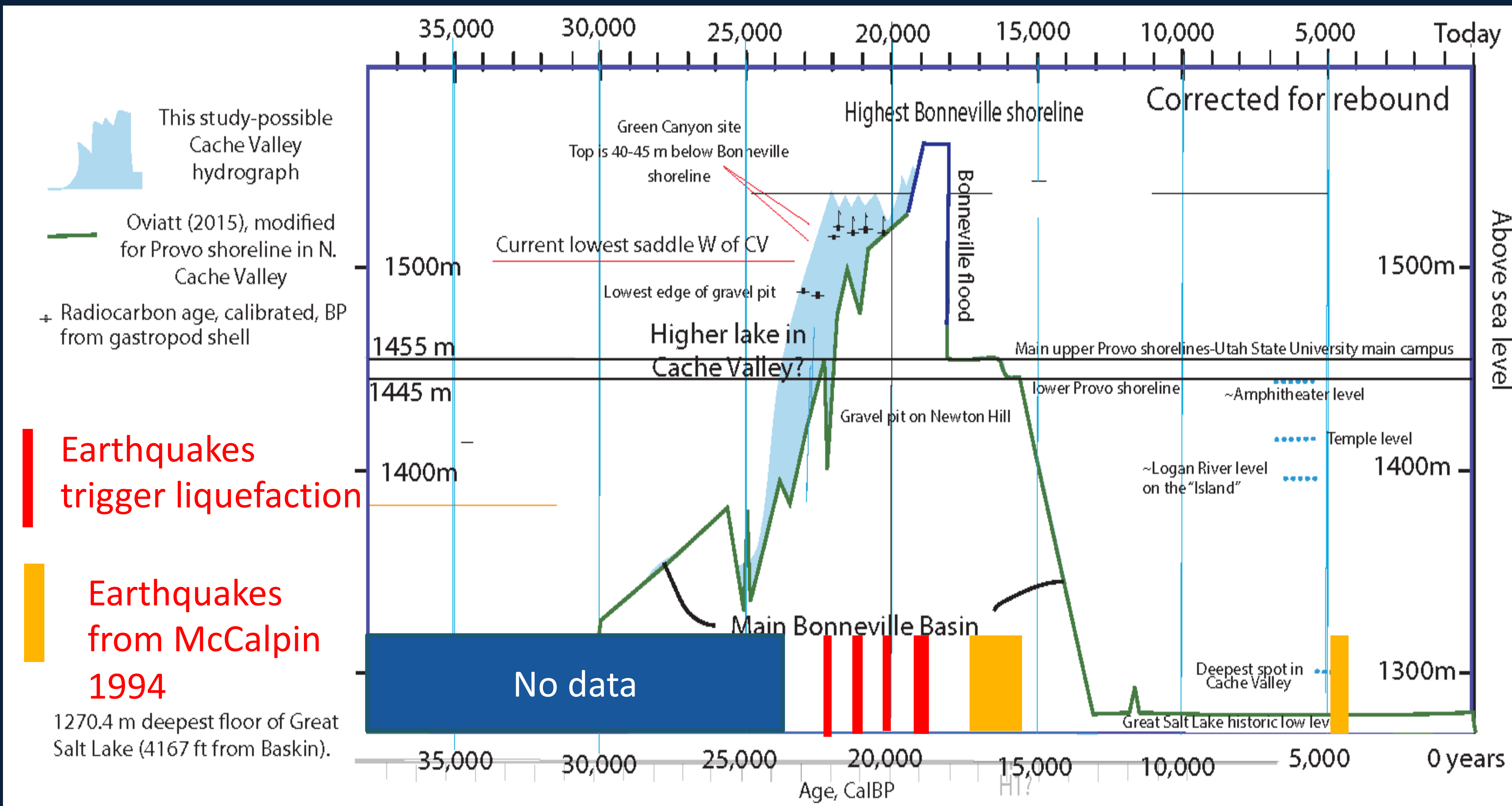

Consider east edge of Lake Bonneville: a monocline from loading

Load of lake Bonneville produces a monocline at the margins

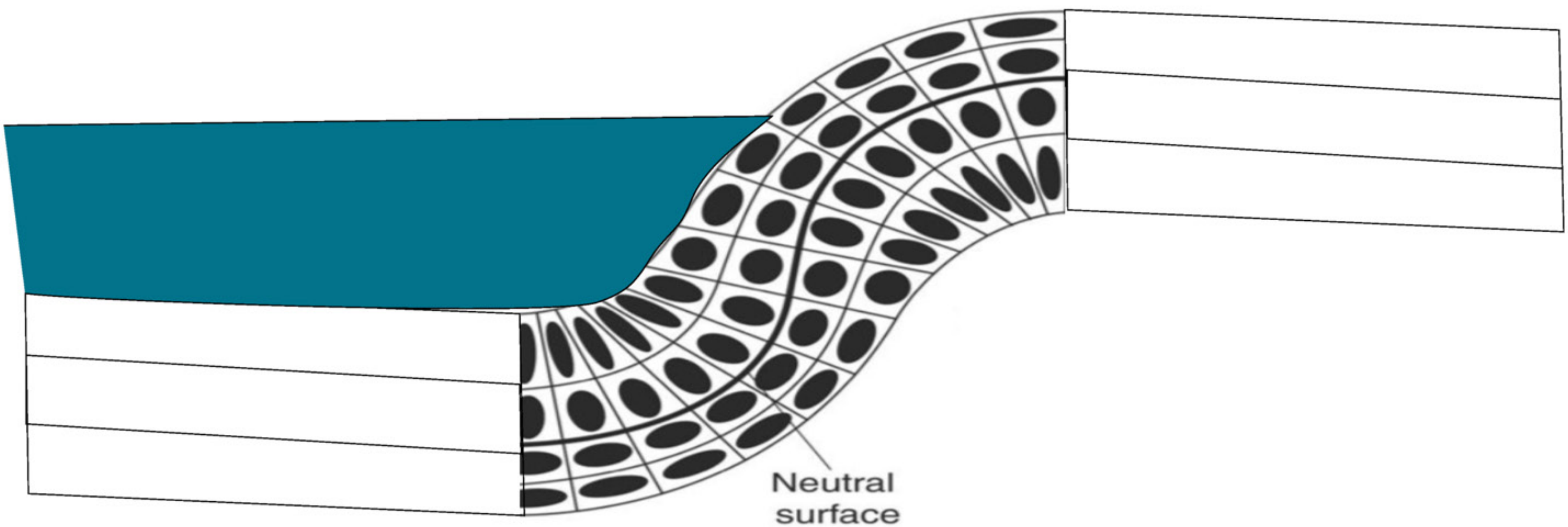

Much vertical exaggeration, view north

Upper hinge is zone of enhanced extension

Load of lake Bonneville produces a monocline at the margins

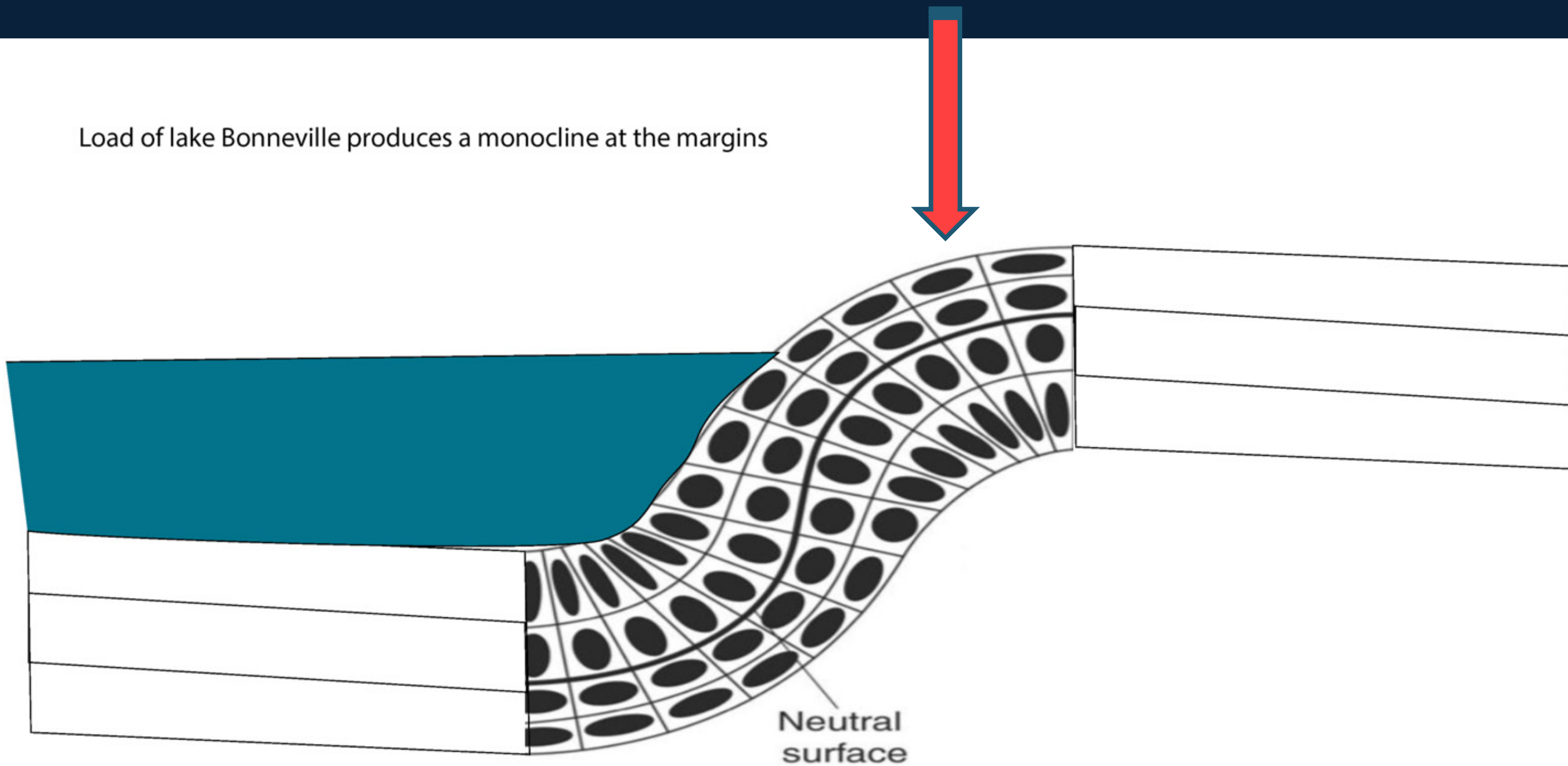

Much vertical exaggeration

Whereas lower hinge is zone of reduced extension

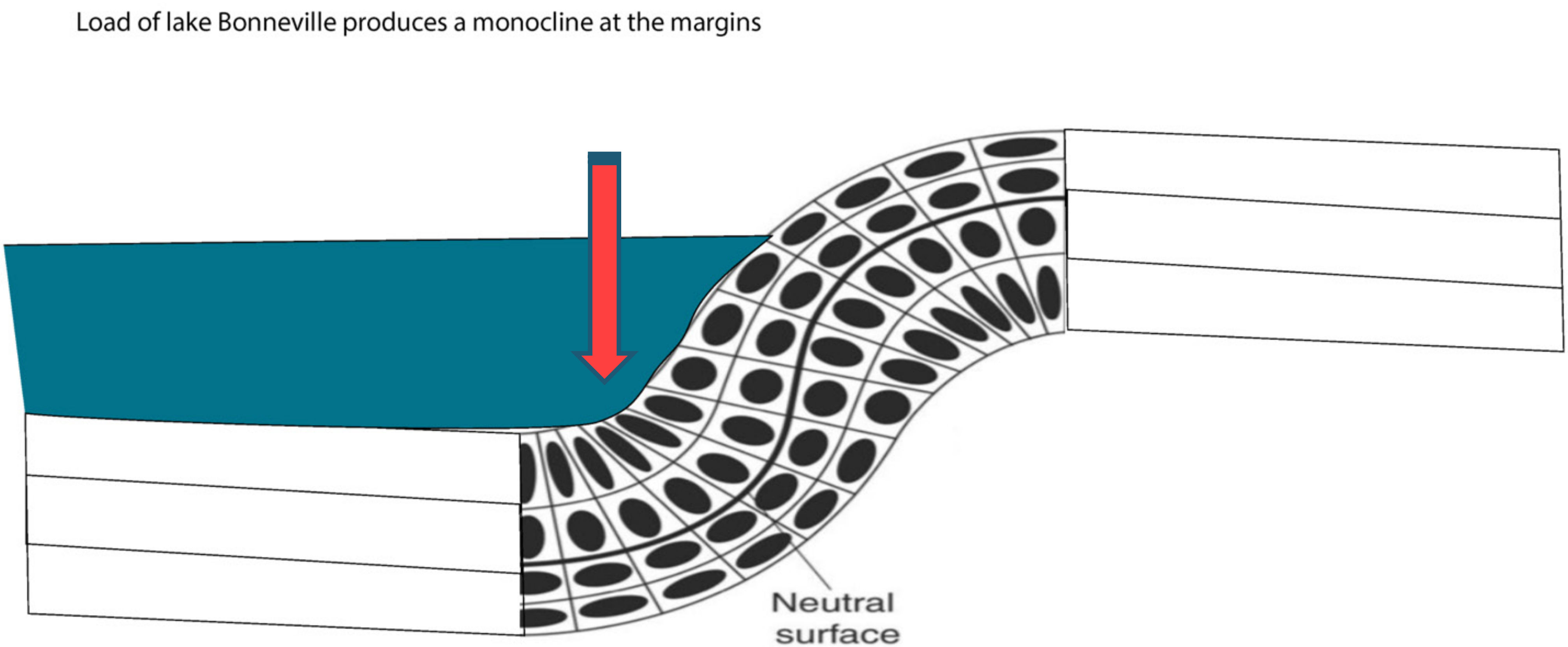

Much vertical exaggeration

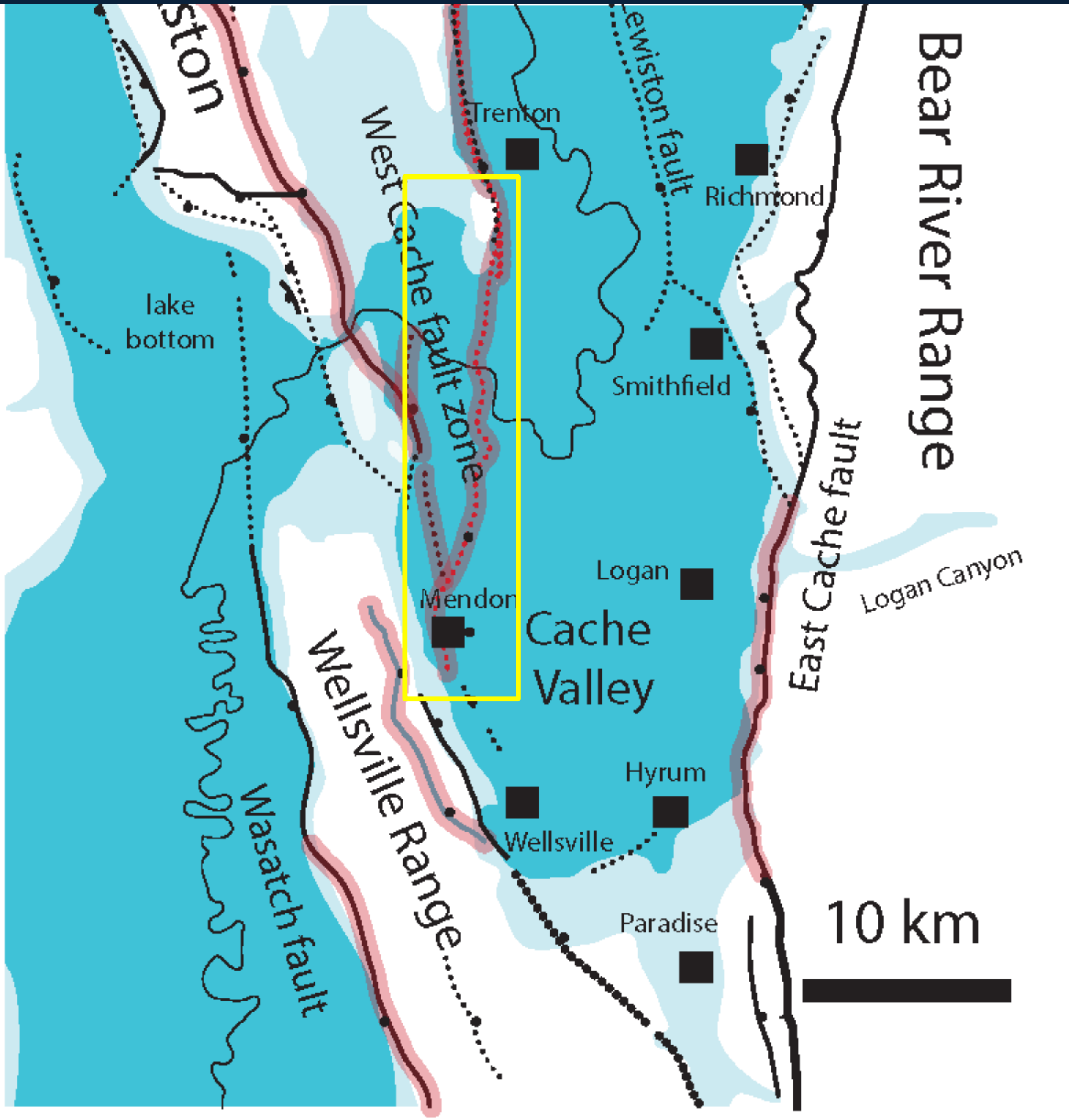

Figure 1. Map of lake levels within Cache Valley. Deltas of the Bear River a shoreline is simplified west of Cache Valley. RNF—Riverdale normal fau Great Basin (modified from Morrison, 1991). Geosphere, December 2011

West Cache fault zone was unusually active in Holocene and created a 1-km-wide fault zone on floor of Cache Valley around Cutler reservoir.

Janecke and Evans, 2016,
Janecke and Ellis, 2018

Janecke and Oaks, 2011

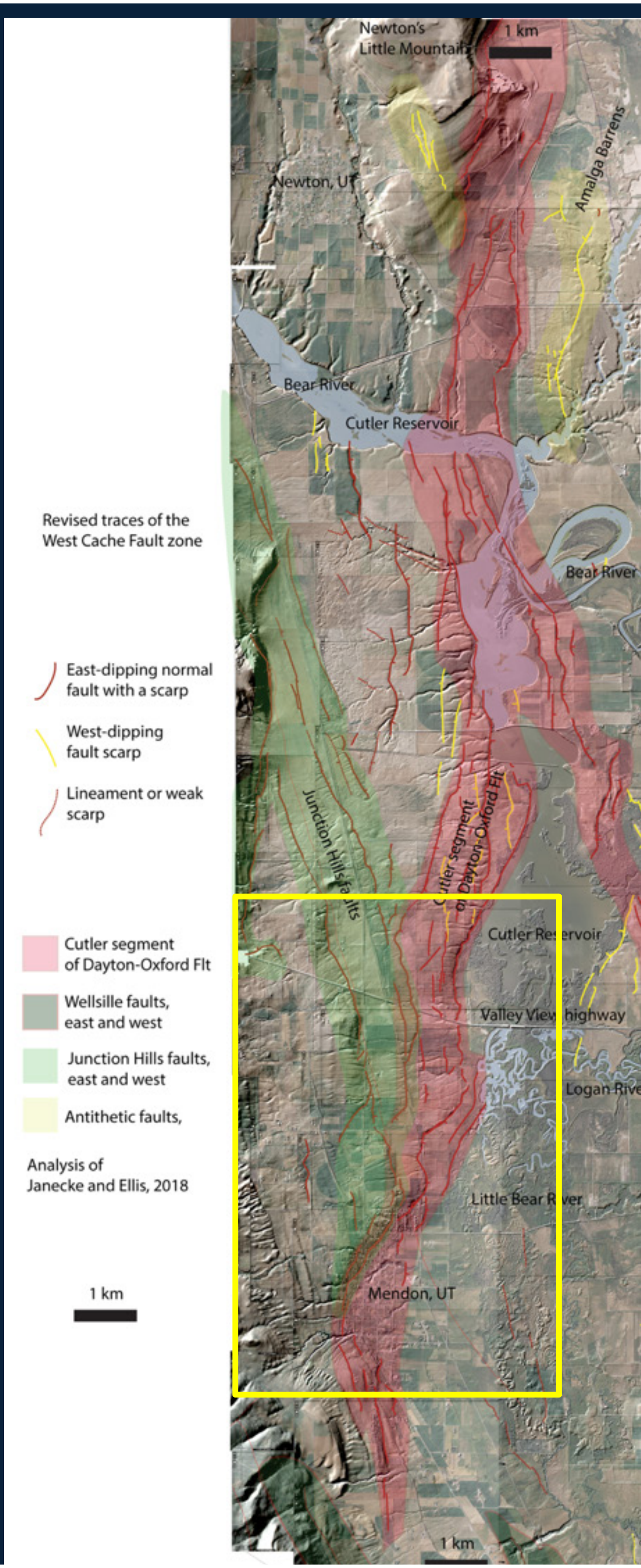

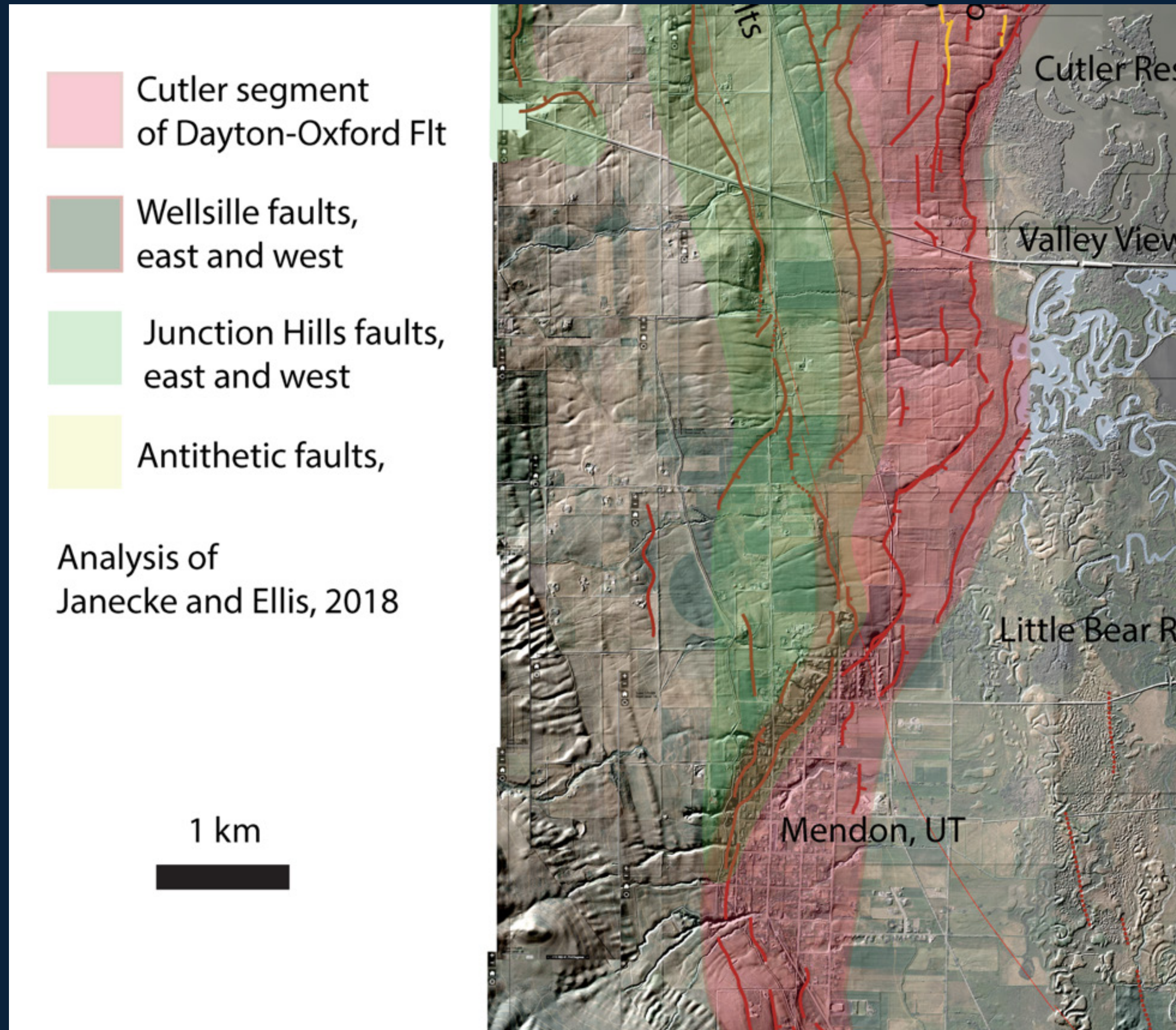

Janecke and Evans, 2016, Janecke and Ellis, 2018

Such bending could produce episodic slip and two parallel belts

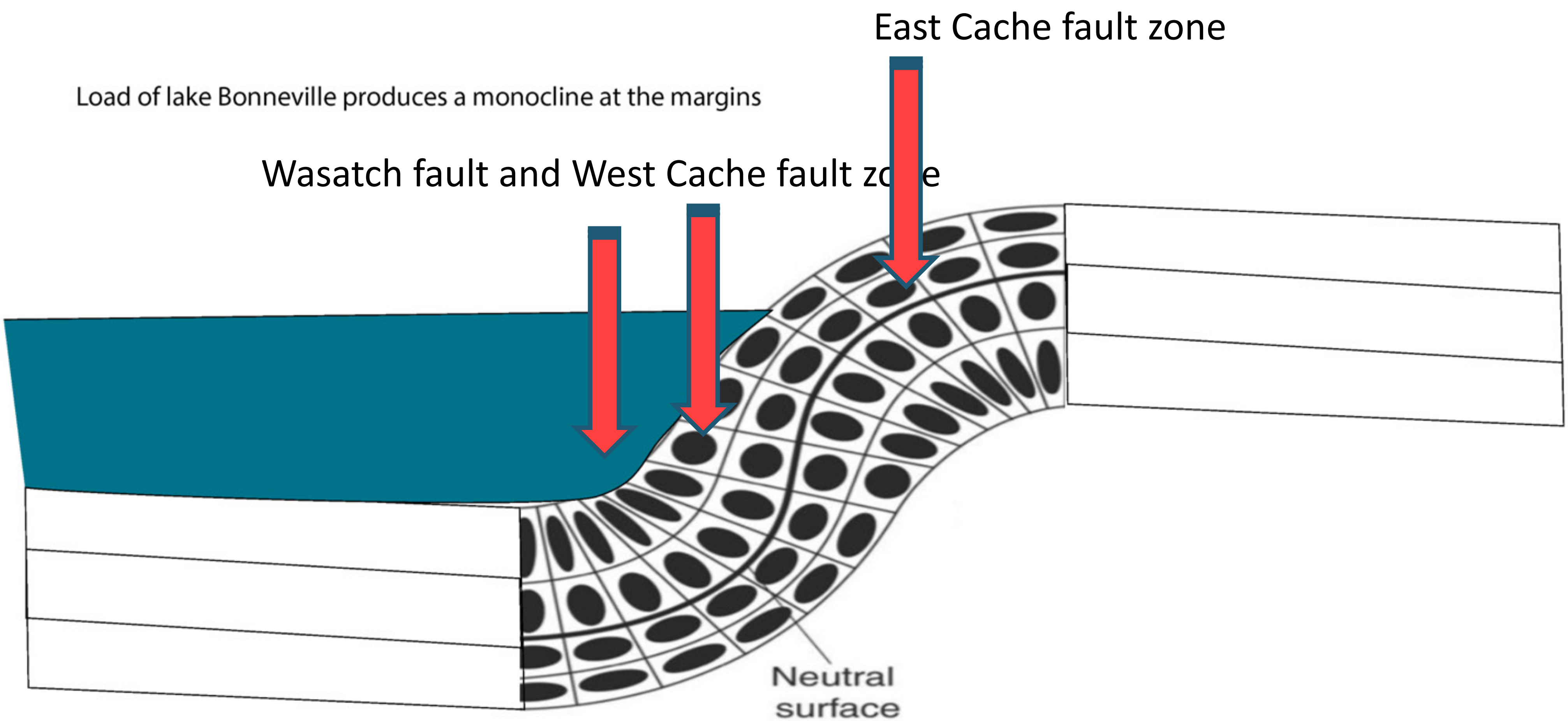

Much vertical exaggeration

- The load of Lake Bonneville created parallel belts of activity.
- East Cache-Riverdale fault belt was more active under Lake Bonneville due to outer arc stretching across an upper monoclinal hinge
- Wasatch-West Cache fault belt was less active at the time.

as doi:10.1130/GES00587.1 Janecke and Oaks

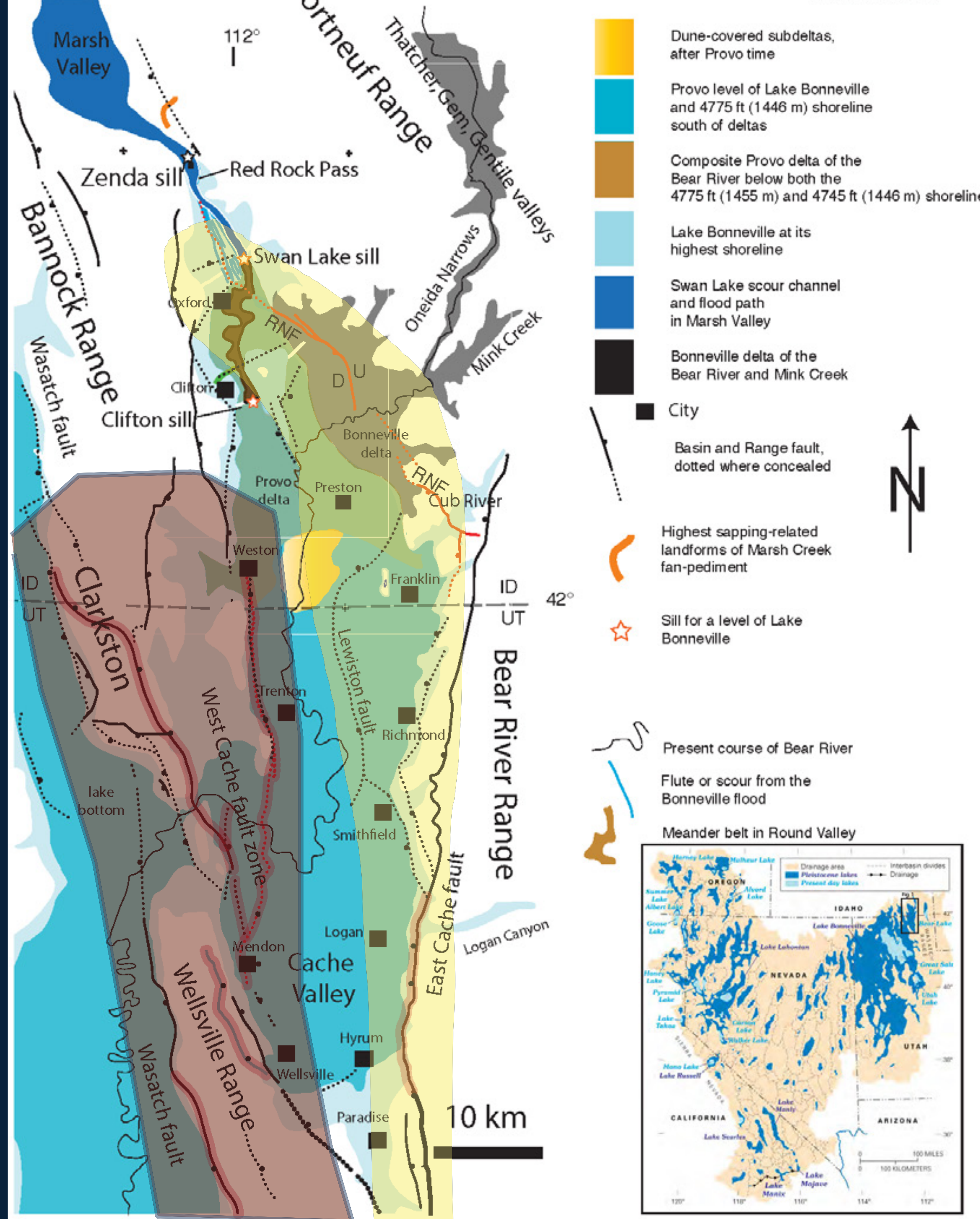

Figure 1. Map of lake levels within Cache Valley. Deltas of the Bear River are differentiated from other lacustrine deposits. Provo shoreline is simplified west of Cache Valley. RNF—Riverdale normal fault (+landslide?). Inset map shows location within the Great Basin (modified from Morrison, 1991). Geosphere, December 2011

In Holocene, activity leveled caught up/or slowed

An earthquake similar to the ones recorded in Green Canyon area, in east belt, could have triggered the Bonneville flood—

BUT ONLY after many centuries of stable outflow. It took time to build the lg. Bonneville delta of Bear River and the wave-cut landforms.

as doi:10.1130/GES00587.1 Janecke and Oaks

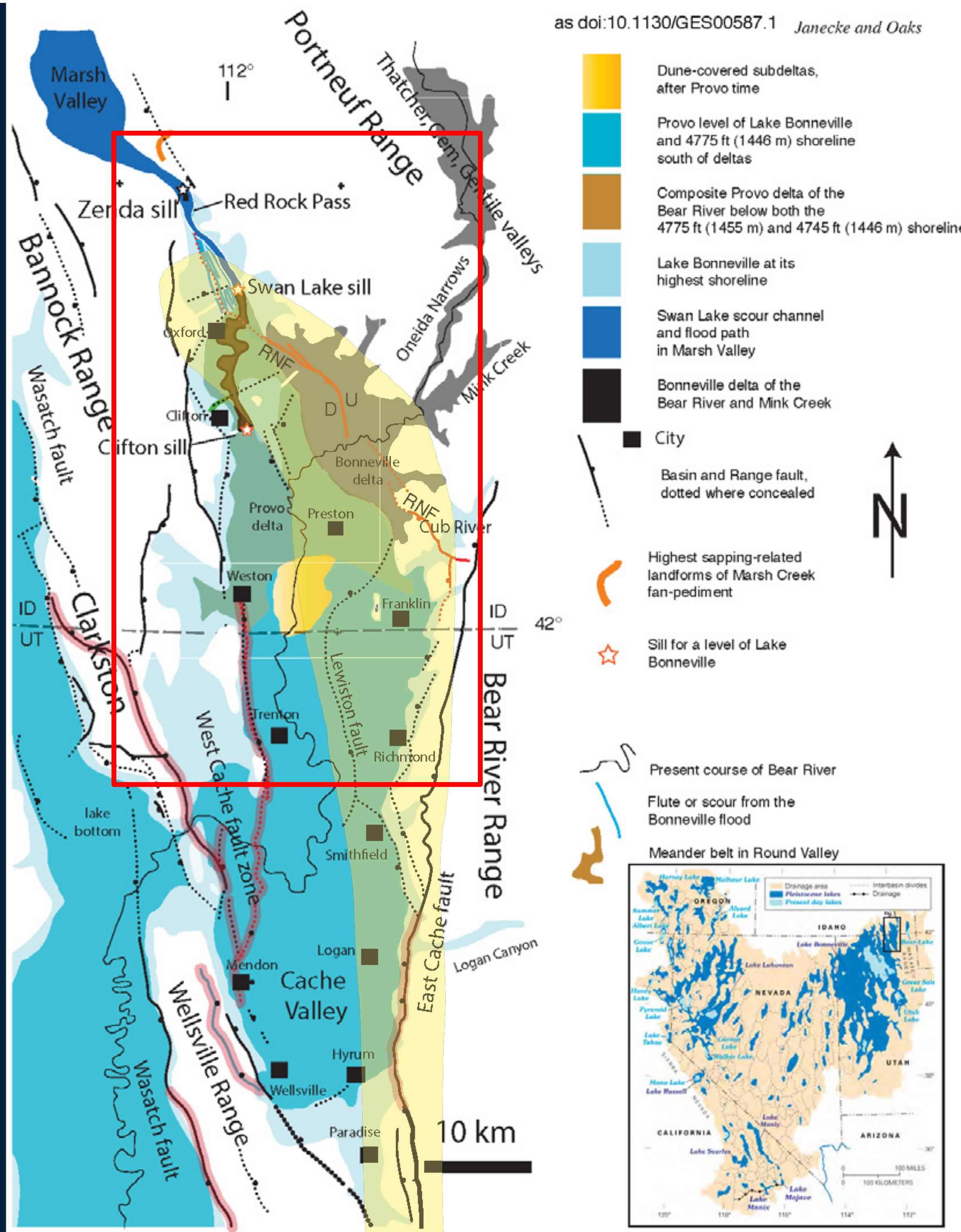

Figure 1. Map of lake levels within Cache Valley. Deltas of the Bear River are differentiated from other lacustrine deposits. Provo shoreline is simplified west of Cache Valley. RNF—Riverdale normal fault (+landslide?). Inset map shows location within the Great Basin (modified from Morrison, 1991). Geosphere, December 2011

An earthquake along Riverdale fault or other structure in east belt could have triggered the Bonneville flood after many centuries of stable outflow at Zenda.

How?

Janecke and Oaks 2011

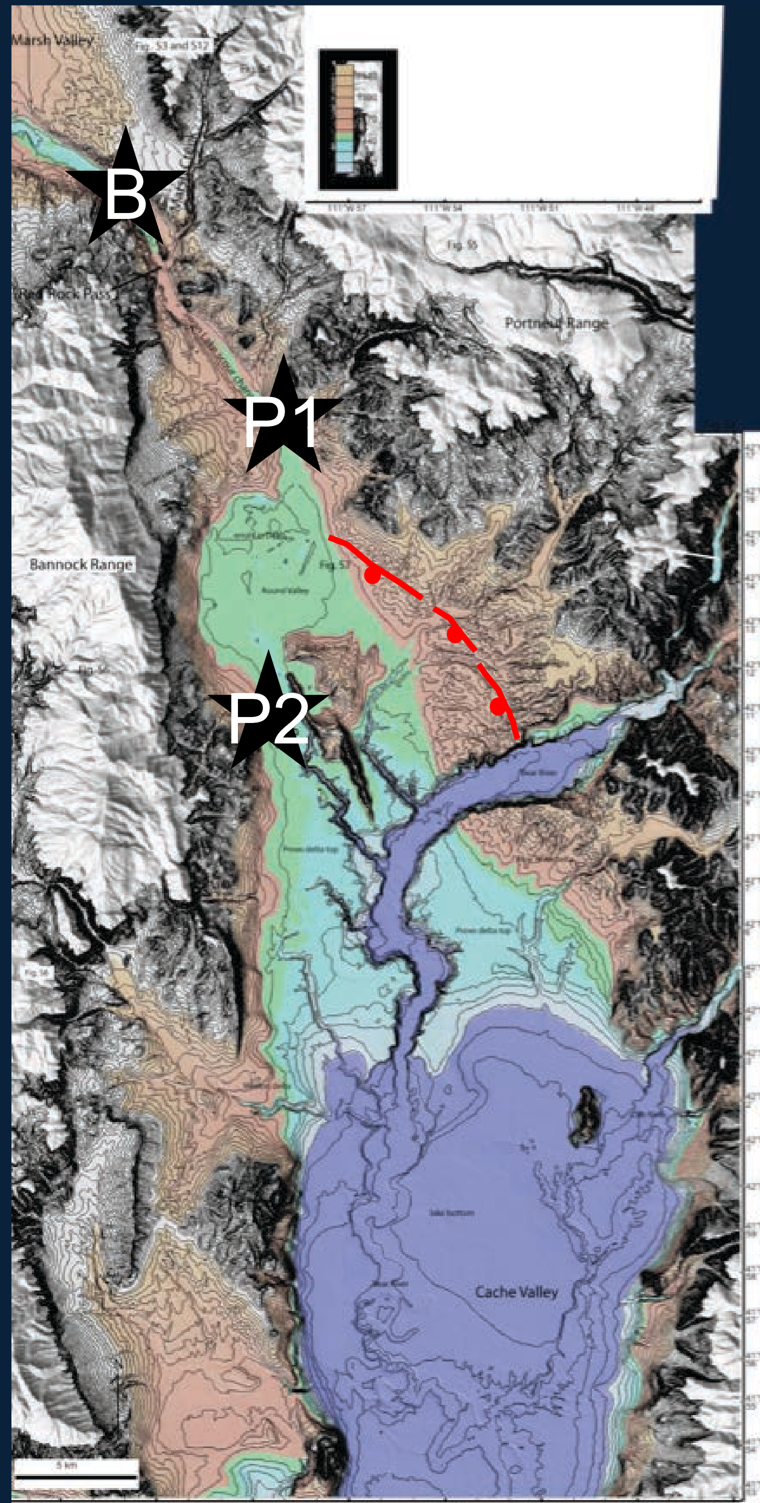

Bonneville s.l.

U. Provo s.l.

L. Provo s.l.

Below Provo

Possible impacts of large earthquakes on the Lake Bonneville?

- Seiches from earthquakes and secondary processes
- Shaking and breaking of natural dam composed of Salt Lake Formation
- Scenario like Lituya bay 1958 is possible with an earthen dam

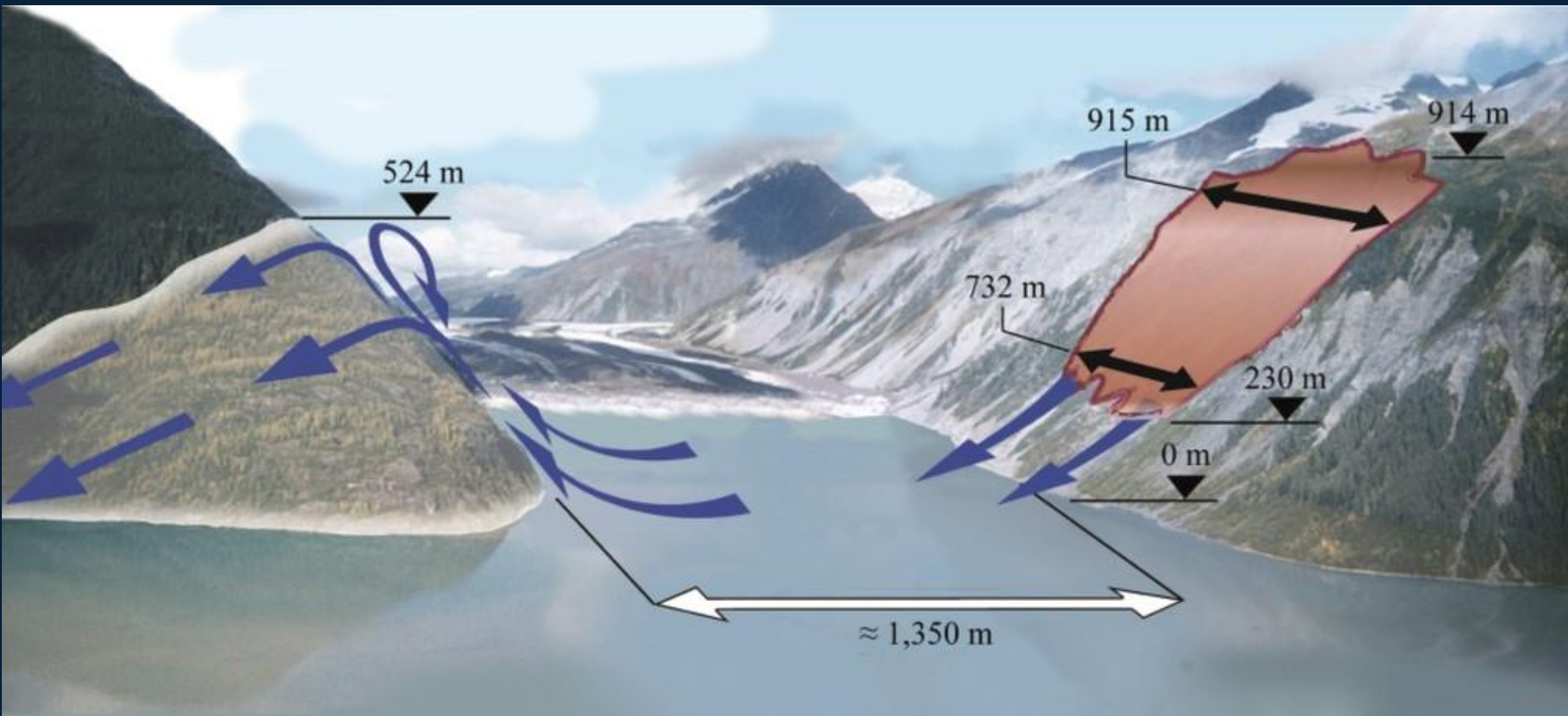

Two additional event layers ?

Cache Valley: A critical part of Lake Bonneville tells a unique tale of shorelines, thresholds, clustered earthquakes, liquefaction, possible triggers of the Bonneville flood, and late integration with the main basin.

Jänecke, Susanne U., Oaks, Robert Q. Jr, Rittenour, Tammy M., Knight, A.J., and Oakeson, Justin, Department of Geology, Utah State University, 4505 Old Main Hill, Logan, UT 84322-4505, susanne.janecke@usu.edu

Geologic, geomorphic, and geophysical analyses of landforms, sediments, and structures in conjunction with new ^{14}C and OSL age determinations document a revised history of flooding and recession of Lake Bonneville in Cache Valley, Idaho and Utah. The presence of wave-cut cliffs in bedrock throughout the Bonneville basin show that the Bonneville highstand was protracted and probably lasted for centuries. Triangular facets were cut into bedrock in the footwalls of normal faults and were steepened significantly by wave erosion at the highest Bonneville shoreline. Crosscutting relationships further suggest that the Riverdale fault, Idaho, produced a major surface-rupturing earthquake near the Zenda threshold around the time of the Bonneville flood. Thus, fluctuating loads, rebound, and/or pore pressures induced by changing lake levels may have triggered a large earthquake that initiated the Bonneville flood and ended the stable outflow that occurred at the Bonneville highstand.

G.K. Gilbert first observed that the Bonneville flood scoured a major flood channel into Cache and Marsh Valleys, and shifted the outlet of Lake Bonneville a great distance southward into Cache Valley during the occupation of the Provo shorelines. The bedrock ridge at the south end of this Swan Lake scour channel became the new threshold for the outflow that produced the main 4775 ± 10 ft (1455 ± 3 m) Provo shoreline, 10 m above the commonly accepted altitude of 1445 m. The 1445 m contour coincides instead with a lower Provo shoreline (4745 ± 10 ft (1446 ± 3 m) that was controlled by a second bedrock ridge and younger threshold at Clifton, Idaho. The sparse record of shorelines rebounded from the ~1445 m level in Cache Valley indicate that the outlet at Clifton, ID was quickly abandoned when Lake Bonneville reverted to a closed condition. A dry meandering riverbed connects the Clifton and Swan Lake outlets and preserves evidence of the large northward-flowing Bonneville River in Round Valley. The Great Basin's modern divide at Red Rock Pass formed in the Holocene, after Lake Bonneville, when a tributary built a small alluvial fan across the midpoint of the Swan Lake scour channel and created a subtle dam (Gilbert 1880, 1890). Thus, Gilbert showed that the modern drainage divide at Red Rock Pass is unrelated to Lake Bonneville.

The possibility that an earthquake triggered the Bonneville flood led us to explore the late Pleistocene activity of normal faults in Cache Valley. The Wasatch fault has increased its slip rate since the Bonneville flood, but little is known about the response of active normal faults in Cache Valley to loading and unloading by Lake Bonneville. To examine the relationships between ancient seismicity and lake history, we re-excavated deformed Upper Pleistocene sandy lake beds along an ~50 m by 5 m collapsed north wall of an abandoned gravel pit at the mouth of Green Canyon, Cache Valley, northern Utah. USU faculty identified 2 liquefaction events in the outcrop in the 1980's during class trips, and we sought to determine the number, nature, and age of the paleo-earthquakes responsible for the strong deformation there.

The exposure of the paleodelta of Green Canyon coincides with the boundary between the northern and central segments of the East Cache fault. It is ~25 m to ~170 m basinward of two diverging fault strands of the East Cache fault and there are additional buried faults close to the outcrop that roughly follow the main upper Provo shoreline (McCalpin, 1994; this study).

Upward coarsening lacustrine deposition at the site started before 22.4 ± 0.4 ky cal BP (^{14}C) with deposition of prodelta clay, mud and silt, and continued after 18.1 ± 0.3 ky cal BP (^{14}C) as sand and gravel were laid down in a prograding delta. Nearshore lacustrine deposition is indicated by ripples, cross beds, other sedimentary structures, lacustrine shells throughout the exposure, and the position of the beds ~40-45 m below the Bonneville shoreline at Green Canyon.

Ten new age determinations indicate early onset of deep lake conditions in Cache Valley, at or higher than 40-45 m from the highstand. The high altitude of the lake provides additional evidence for Oaks et al (this volume)'s interpretation of Cache Valley Bay. Oaks et al. (2018) dated prior lake cycles in Cache Valley and conclude that Cache Valley Bay was a separate pluvial lake until it became fully integrated into the Bonneville basin in the middle of the Bonneville lake cycle. The integration must postdate the lake beds in Cache Valley that were deposited at higher altitudes than predicted by the Bonneville hydrograph.

We uncovered multiply-deformed shallow lake beds and one capping fluvial gravel in the exposure in the Bonneville delta at Green Canyon. Listric faults in the exposure sole into prodelta clay beds beneath the sandy and gravelly deltaic part of the succession. West-dipping slip surfaces in the exposure are part of nested lateral spreads, not tectonic faults. Cross-cutting relationships are exceptionally clear. The deltaic sediment of Green Canyon was deposited, seismically deformed, and slumped in at least 4 events under subaqueous conditions in a shallow-water, deltaic part of Lake Bonneville. Six ^{14}C ages on *Stagnicola* sp. shells and three OSL ages are stratigraphically consistent within error, and confirm that the lacustrine sediment was deposited and deformed during 4-5 ky of high lake levels prior to the Bonneville flood. The geometry and position in the landscape of a laterally continuous alluvial gravel bed, which caps the highly deformed sandy lake beds in angular unconformity, suggest that the gravel bed was probably laid down immediately after the erosional stripping of the highest units by the Bonneville flood. The gravel cap may be a flood deposit or barely postdate the Bonneville flood because it predates the significant, focused downcutting along the modern channel of Green Canyon Wash that coincided with the occupation of the Provo shorelines ~70 m lower in the landscape. All the deformation in the exposure must therefore predate the earliest occupation of the main Provo shoreline.

The Green Canyon site exposes 3 listric slip surfaces of lateral spreads, 4 sequential thick liquefied units, undeformed flat and cross-stratified lacustrine and deltaic sediment, thin deformed beds. Each thick liquefied mass of sand is a different age, yet all of the deformation occurred when the sediment was saturated by Lake Bonneville and was within ~40 m of its highest altitude. Three of the liquefied units (0.75 to 5 m thick) are localized and displaced in the hanging walls of listric east- and west-dipping slip surfaces of lateral spreads that appear to be coeval with the liquefied sediment above them. Deposition was ongoing, and produced multiple cross-cutting relationships that constrain the relative ages of three similar lateral-spread-liquefaction pairs (LSLP) and one underlying strata-bound liquefied mass (SBLM) that deforms a possible weak paleosol that contains rootlets. Each LSLP and SBLM formed during a discrete event and was followed by deposition of 1-2 m of stratified sediment. Truncations at slip surfaces, fault wedges, disconformities and angular unconformities, overlapping sediment, onlapping sediment, sand dikes and sills, and growth strata separate the 3 LSLP and 1 SBLM from one another. Less extreme deformation modified the intervening lake beds.

The most extreme deformation is expressed in fault-graded beds that are more than 5 m thick. The similarity between the LSLP and SBLM in the Green Canyon pit and secondary deformation generated by the 1934 M 6.6 Hansel Valley earthquake (McCalpin et al., 1992) indicate that seismic shaking is the most likely explanation for the four largest deformational features at the mouth of Green Canyon. The smaller deformational features may have formed during subsequent aftershock sequences. Other evidence for a tectonic trigger includes the presence of small fault wedges, alternating brittle and ductile deformation, buried scarps, small sand dikes, and angular unconformities. We propose that four separate, moderate to large earthquakes shook and liquefied the sediment between ~23 ka and the Bonneville flood (~17 to 18 ky). Those earthquakes triggered each LSLP or SBLM, and also produced listric top-basinward and top-toward-the-range-front slip surfaces.

If each liquefaction event records a moderate to large earthquake between about 23 and 17 ky cal BP, the earthquake frequency along the adjacent part of the East Cache fault zone was high when the basin was full. This evidence plus the paleoseismic data of McCalpin (1994) for one additional earthquake shortly after the Bonneville flood and another major earthquake since then, show that there has been a significant decline in earthquake frequency on adjacent segments of the East Cache fault zone since the deep-water phases of the Bonneville lake cycle. The temporal clustering of the liquefaction triggered by the syn-Bonneville paleo-earthquakes, their position near the East Cache fault zone, and the lack of deformation at the site since the Bonneville flood, are consistent with a high frequency of seismicity during the transgression and high stand of Lake Bonneville. The lake could explain this clustered activity by changing the loading stresses in the crust, by modulating rebound-related stresses, and/or by raising the pore pressure along the slip surfaces with circulating pore water. Similar processes might explain the rough coincidence of the Bonneville flood and last major earthquake on the Riverdale fault zone in northern Cache Valley (Janecke and Oaks, 2011a and b).

The increase in earthquake frequency along part of the East Cache fault zone documented here is in marked contrast to that of the Wasatch fault zone, which had a reduced slip rate during the occupation of Lake Bonneville (Hetzel and Hampel 2005). We explain the opposite responses of the two fault zones as the consequence of opposite flexural stresses induced by the loading and rebound produced by Lake Bonneville along an upper monoclinal hinge (near the East Cache fault) and that along a lower monoclinal hinge (near the Wasatch fault) at the eastern margin of Lake Bonneville. The fact that most of the West Cache fault zone, including 18 long of newly identified faults around Cutler Reservoir, ruptured in the Holocene (Black et al., 2000; Janecke and Evans, 2017; Ellis and Janecke et al., 2018 in prep) suggest that the West Cache fault zone be in synch with the Wasatch fault zone and reflect the stresses near the lower monoclinal hinge of the flexurally bending lithosphere.

Jake staff is 160 cm long

Deformation in a very short time interval- ^{14} C

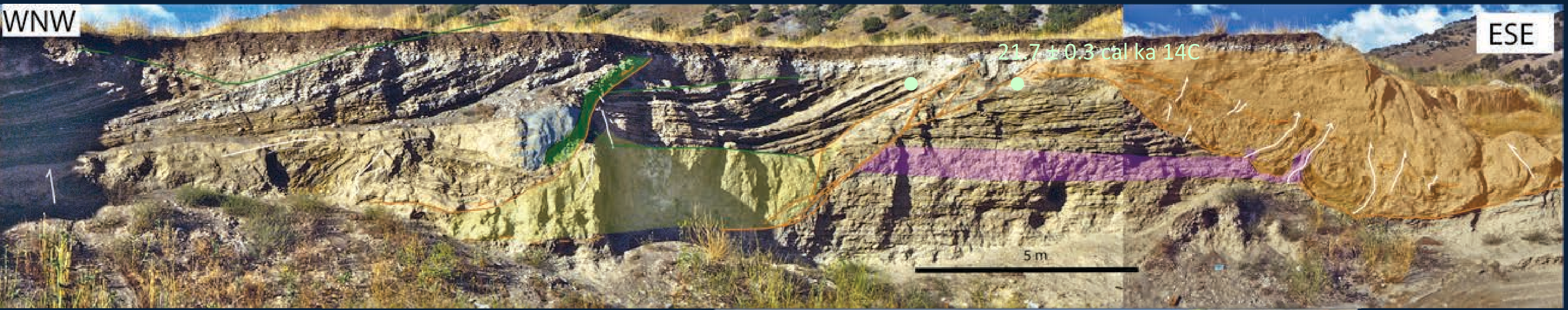

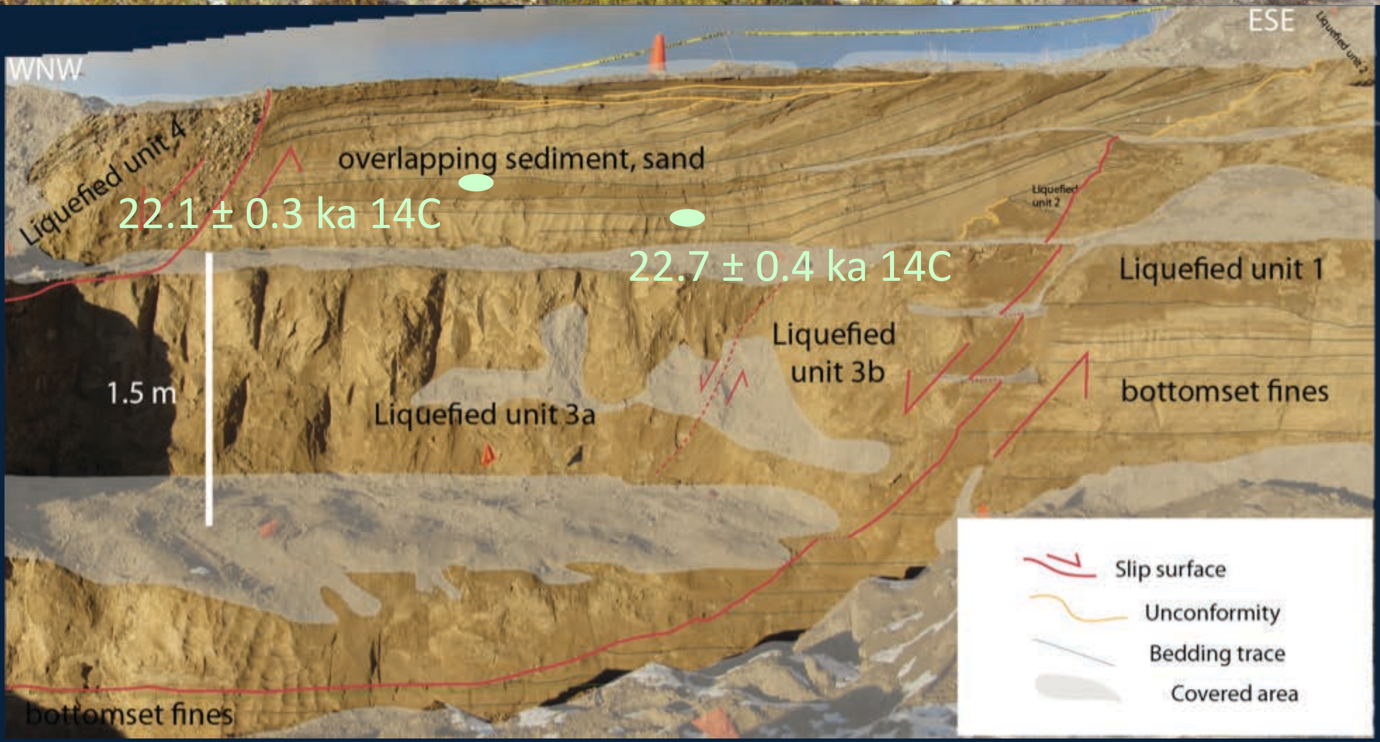

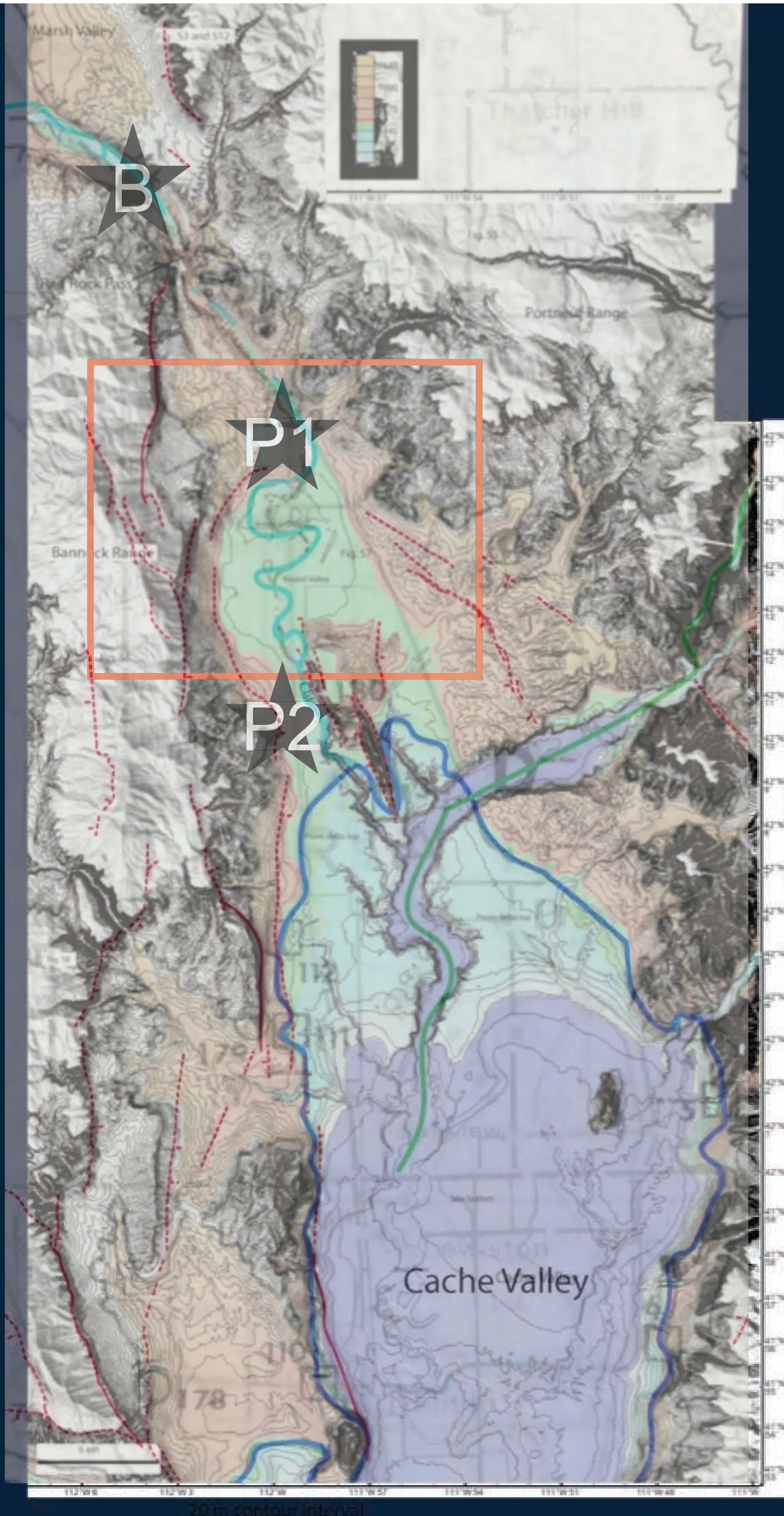

The 1445 m shoreline of Currey 1982 (BLUE) does not connect to the scour channel of Gilbert according to the map.

THE LAST PLEISTOCENE GLACIATION IN THE UINTA MOUNTAINS: UPDATED CHRONOLOGY AND CONNECTIONS TO LAKE BONNEVILLE

Benjamin J. Laabs[1] and Jeffrey S. Munroe[2]

[1]Department of Geosciences, North Dakota State University, Fargo, ND 58102;
[2]Department of Geology, Middlebury College, Middlebury, VT 05753

Corresponding author (Laabs): benjamin.laabs@ndsu.edu

ABSTRACT

Mountain glaciation in the vicinity of Lake Bonneville included numerous valley glaciers and ice fields in the Uinta and Wasatch Mountains, and some smaller glaciers in mountains of the western Lake Bonneville basin. Understanding of glacial chronologies in these mountains has lagged that of the last cycle of Lake Bonneville, due in part to the lack of preserved organic matter suitable for radiocarbon dating in most glacial deposits. Cosmogenic exposure dating of moraines has helped constrain the timing of mountain glaciation, but has been limited until recently by uncertainty of the in situ production of beryllium-10 (^{10}Be). Previously reported cosmogenic ^{10}Be exposure ages of moraines in mountains neighboring Lake Bonneville are recalculated here using newer production rates and scaling models. Recalculated cosmogenic exposure ages are 10–14% older than reported in previous studies, which significantly shifts the apparent relative timing of mountain glaciation and the phases of Lake Bonneville. In the Uinta Mountains, glaciers in eastern valleys last occupied their terminal moraines prior to the overflowing phase of Lake Bonneville, whereas glaciers in the central and western valleys occupied their terminal moraines while the lake overflowed. Glaciers in the western Wasatch Mountains attained their maxima prior to and during the overflowing phase of Lake Bonneville. The updated cosmogenic glacial chronologies still permit the possibility that Lake Bonneville impacted glacier mass balance in neighboring mountains. Ice retreat began by ~18–17 ka while the lake overflowed, suggesting a climatic shift that initiated ice retreat but still supported a high lake.

INTRODUCTION

The rich record of Pleistocene mountain glaciation in the Lake Bonneville basin (LBB) affords an opportunity to study the possible hydrologic and climatic connections between mountain glaciers and Lake Bonneville. Glacial mapping and reconstructions in the Uinta Mountains (Munroe and Mickelson, 2002; Munroe and others, 2006; Munroe and Laabs, 2009), which featured the vast majority of ice in the LBB, and in other mountains around Lake Bonneville (figure 1; Laabs and others, 2011; Laabs and Munroe, 2016; Quirk and others, 2018) reveal the following pattern of glaciation in space and time: (1) the total volume of mountain glaciers in the LBB was less than 5% of the volume of Lake Bonneville, (2) mountain glaciers expanded before and during the overflowing phase of Lake Bonneville, and (3) glacier equilibrium-line altitudes were lowest in mountains surrounded by and immediately east (downwind) of Lake Bonneville. These observations support the possibility that Lake Bonneville impacted regional climate and was a local moisture source for mountain glaciers (Munroe and Mickelson, 2002) if mountain glaciers persisted through the Last Glacial Maximum (ending at 19 ka) to the overflowing phase of Lake Bonneville at 18.0–15.5 ka (Oviatt, 2015).

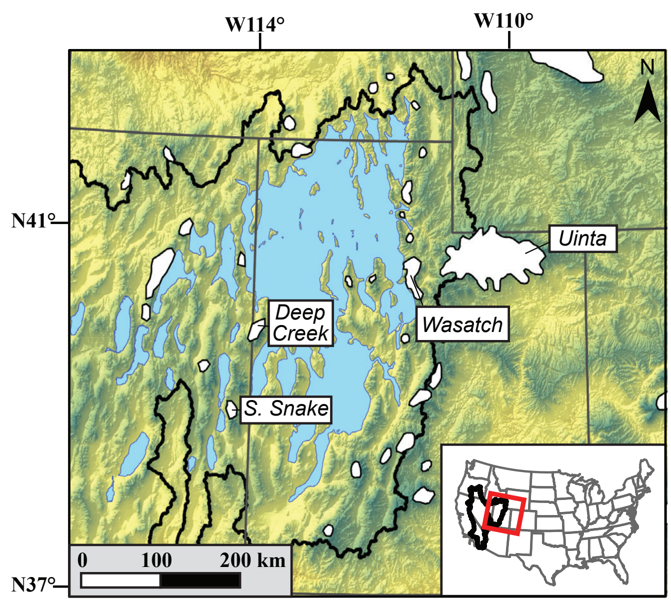

Figure 1. Shaded relief map of the northeastern Great Basin, western United States with extents of Great Basin lakes (blue) and mountain glacier systems (white) produced from a 30-m DEM from the National Elevation Dataset (https://catalog.data.gov/dataset/usgs-national-elevation-dataset-ned). Lake extents are from Reheis (1999) and glacier systems are from Pierce (2003). Mountain glacier systems with cosmogenic ^{10}Be exposure chronologies are labeled.

Until recently, understanding the relative timing of mountain glaciation and the transgressive (30–18 ka), overflowing (18.0–15.5 ka), and regressive (15.5–12.0 ka) phases of Lake Bonneville (as outlined by Oviatt, 2015) has been limited by several factors. Chiefly, age limits on mountain glacial deposits in the Uinta Mountains and elsewhere in the LBB have been few, due in large part to the lack of preserved organic matter available for radiocarbon dating in glacial deposits, and the fact that nearly all mountain glaciers in the LBB terminated high above the lake shoreline, thereby limiting to a single location at Little Cottonwood Canyon, at the western front of the Wasatch Mountains, where stratigraphic relations between glacial and lacustrine deposits can be observed. There, privatization and modification of the land surface have resulted in removal of outcrops displaying stratigraphic relations of lacustrine and glacial sediment described in previous studies (Madsen and Curry, 1979; Scott, 1988). More recent work by Godsey and others (2005) at a new exposure describes interlayering of glacial sediment with nearshore deposits of Lake Bonneville near the mouth of Little Cottonwood Canyon, suggesting that the glacier was at or near its known terminus during the Bonneville highstand.

The application of cosmogenic nuclide surface exposure dating to Pleistocene glacial deposits in the Uinta Mountains and elsewhere in the LBB has started to reveal the relative timing of mountain glaciation and the last cycle of Lake Bonneville. Several studies, all focusing on deposits of the last glaciation in the Uinta Mountains, report cosmogenic beryllium-10 (^{10}Be) exposure ages of erratic boulders atop terminal moraines (Munroe and others, 2006; Laabs and others, 2007; Refsnider and others, 2008; Laabs and others, 2009). Additionally, cosmogenic ^{10}Be exposure dating has been applied to terminal moraines in the western Wasatch Mountains (Laabs and others, 2011; Quirk and others, 2018) and in mountains west of Lake Bonneville (Laabs and Munroe, 2016). All of these studies have reported cosmogenic ^{10}Be exposure ages of terminal moraines that closely correspond to the late transgressive or early overflowing phase of Lake Bonneville.

Until recently, the direct comparison of cosmogenic ^{10}Be exposure ages of moraines with age limits on the last Lake Bonneville cycle (chiefly based on calendar-corrected radiocarbon dates) was complicated by a limited understanding of *in situ* production of cosmogenic ^{10}Be. Specifically, determining the sea-level high-latitude production rate of *in situ* ^{10}Be had been limited by the small number of locations where the production rate could be calibrated (Balco and others, 2008). Further, the most commonly used models for scaling *in situ* ^{10}Be production for altitude, geomagnetic latitude, and time yielded variable production rates in mountains of the LBB, and some of these models performed poorly in a recent statistical analysis by Borchers and others (2016). An important step forward was provided by recent work calibrating the ^{10}Be production rate at an independently dated surface in the LLB (Lifton and others, 2015, 2016), and development of a new model for scaling *in situ* production of ^{10}Be in space and time (Lifton and others, 2014). Such improvements to cosmogenic nuclide production models reduce variability among cosmogenic ^{10}Be exposure age estimates and permit more accurate comparison of cosmogenic ^{10}Be exposure ages of moraines to the chronology of Lake Bonneville. These newer ^{10}Be production models are now incorporated into online exposure age calculators (Balco and others, 2008; Marrero and others, 2016; Martin and others, 2017), providing accessible and consistent calculation and comparison of cosmogenic ^{10}Be exposure ages in the LBB and elsewhere.

This paper updates the cosmogenic chronology of glacial deposits in the Uinta Mountains based on newer models of *in situ* production of ^{10}Be. Although no new cosmogenic ^{10}Be exposure ages are available since the reporting on this subject by Laabs and Munroe (2016), the incorporation of newer ^{10}Be production models in online cosmogenic exposure age calculators affords a more consistent comparison of the cosmogenic exposure ages of moraines to the chronology of Lake Bonneville. Additionally, cosmogenic ^{10}Be exposure ages of moraines are updated in parts of the western Wasatch Mountains (not including Big Cottonwood Canyon; the reader is referred to Quirk and others [2018] for a report on this area), and in two ranges in the western LBB, the South Snake and Deep Creek Ranges. The updated cosmogenic chronologies of glacial deposits support our previous reporting (Laabs and Munroe, 2016) that Pleistocene glaciers in the LLB reached expanded positions before and during the overflowing phase of Lake Bonneville, and began retreating before the lake ceased overflowing at the Provo shoreline.

METHODS

Cosmogenic ^{10}Be exposure ages of terminal moraines of the last glaciation in the LBB are recalculated here using newer production models for *in situ* ^{10}Be that take advantage of a calibrated spallogenic production rate from within the LBB (Lifton and others, 2015, 2016) and an updated version of the time-dependent production scaling model of Lifton and others (2014), termed "LSDn" in a statistical analysis of the model by Borchers and others (2016). The production rate calibration site in the LBB is an erosional surface below the highest shoreline of Lake Bonneville at the southern end of the Promontory Mountains in northern Utah. The surface formed by wave cutting along the mountain front during the transgressive phase of Lake Bonneville and was exposed during the Bonneville flood at ca. 18.0 ka (Lifton and others, 2015). The calibration at this site yields a sea-level, high-latitude spallogenic production rate of *in situ* ^{10}Be statistically similar to other calibration sites worldwide and represents the only ^{10}Be production rate calibration of an independently dated surface in western North America. Given the geographic and temporal proximity of this calibration site to late Pleistocene moraines in the LBB, it provides the best available production model for computing cosmogenic ^{10}Be exposure ages associated with the moraines. We combined this calibration set with the LSDn scaling model of Lifton and others (2014) as implemented in Version 3.0 of the online calculator formerly known as the CRONUS calculator (Balco and others, 2008) to compute cosmogenic ^{10}Be exposure ages of moraines in the LBB excluding those in Big Cottonwood Canyon of the western Wasatch Mountains. The reader is referred to Quirk and others (2018) for cosmogenic ^{10}Be exposure ages and data for that location, which were calculated in the same way as the cosmogenic exposure ages reported here.

RESULTS AND DISCUSSION

Recalculated cosmogenic ^{10}Be exposure ages in the Uinta and Wasatch Mountains are 10–14% (about 2 kyr) older than originally reported by Laabs and others (2009, 2011). Older exposure ages are to be expected because the production rates used here are proportionately less than those used in the original studies. The newly calculated older exposure ages prompt reconsideration of the relative timing of moraine occupation and the last cycle of Lake Bonneville.

In most studies of cosmogenic moraine chronologies, the mean of boulder exposure ages of terminal moraines is considered the best estimate of when ice last occupied the moraine (figure 2). This interpretive approach is based on the observation that cosmogenic ^{10}Be exposure ages atop a single moraine are normally distributed and vary as expected given measurement errors (e.g., internal uncertainty shown in table 1). This is the case for 8 or 10 dated terminal moraines in the Uinta Mountains. Individual exposure ages of boulders atop the moraines at Smiths Fork and North Fork Provo (terminal) show a bimodal distribution (even after outliers identified by Laabs and others [2009] are removed), suggesting that the moraines are either degrading or were occupied twice during the last glaciation. Other moraines have a single mode (figure 3), with ages varying as expected as indicated by reduced chi-squared values (χ^2r in table 1) close to or slightly greater than unity (c.f., Rood and others, 2011). In these cases, the mean age (table 1, figure 2) closely corresponds to the most probable age as indicated by relative probability plots (figure 3). In cases where cosmogenic ^{10}Be exposure age distributions are bimodal, it is unclear whether (1) the moraines were occupied twice, (2) have undergone a period of degradation (represented by the younger mode) since the time of ice abandonment, or (3) some other factor has contributed to the apparent bimodal exposure history of boulders atop the Smiths Fork and North Fork Provo moraines. For this reason, the mean exposure ages of these two moraines are considered the best estimates of the time when ice last occupied the moraines. For all other moraines in the Uinta Mountains and elsewhere in the LBB, the mean exposure age is also considered the best limit on the time when ice last occupied the moraines.

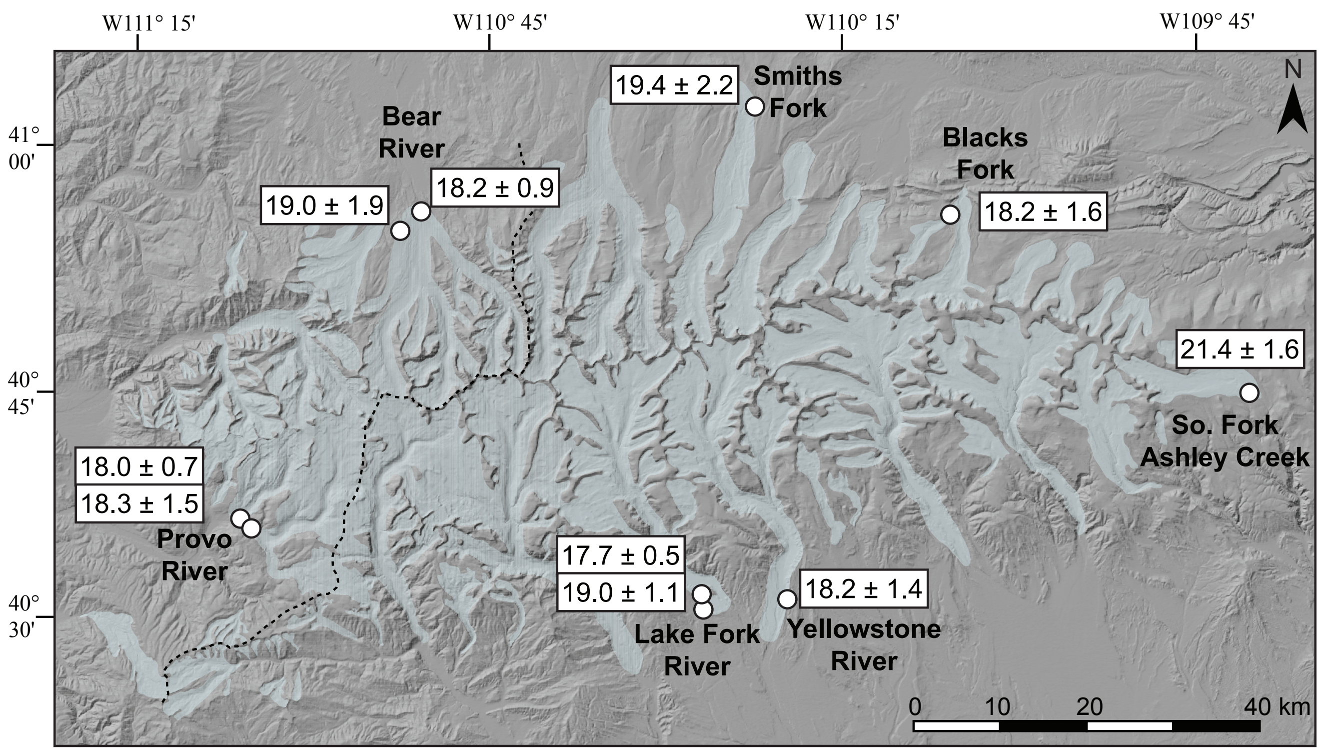

Figure 2. Shaded relief with reconstructed maximum ice extents of the last glaciation in the Uinta Mountains, Utah produced from a 30-m DEM from the National Elevation Dataset (https://catalog.data.gov/dataset/usgs-national-elevation-dataset-ned). Recalculated mean cosmogenic ^{10}Be exposure ages (ka) of terminal moraines in glacial valleys are described in the text (see table 1 for individual cosmogenic exposure ages).

Mean and maximum probable cosmogenic ^{10}Be exposure ages of moraines in the Uinta Mountains, Wasatch Mountains, and western LBB mountains overlap, with some variability relative to the overflowing phase of Lake Bonneville (figure 3). In the Uinta Mountains, terminal moraines were last occupied by ice prior to or during the overflowing phase of Lake Bonneville. Ice retreat began earliest in the South Fork Ashley Creek valley in the eastern Uinta Mountains, where the mean cosmogenic ^{10}Be exposure age of the terminal moraine is 21.4 ± 1.6 ka. This valley was farthest from Lake Bonneville and had one of the highest equilibrium-line altitudes (ELAs) in the Uinta Mountains, suggesting that its mass balance was less impacted by a lake effect from Lake Bonneville compared to other valleys closer to the lake. In the Burnt Fork valley, also far from Lake Bonneville compared to other glacial valleys, cosmogenic exposure ages are highly variable (table 1, figure 3). If, as Laabs and others (2009) suggested, such high variability suggests the oldest exposure age of this moraine best represents the time when it was last occupied by ice, then the ice retreat here also began prior to the overflowing phase of Lake Bonneville.

Terminal moraine exposure ages are generally younger in the middle and western valleys of the Uinta Mountains, corresponding to the overflowing phase of Lake Bonneville. In the middle valleys of the Uinta Mountains, exposure ages of terminal moraines range from 19.4 ± 2.2 ka in the Smiths Fork valley to 18.2 ± 1.4 ka in the Yellowstone River valley. In western valleys, exposure ages range from 19.0 ± 1.9 ka in the East Fork Bear River valley to 18.0 ± 0.7 ka in the North Fork Provo River valley.

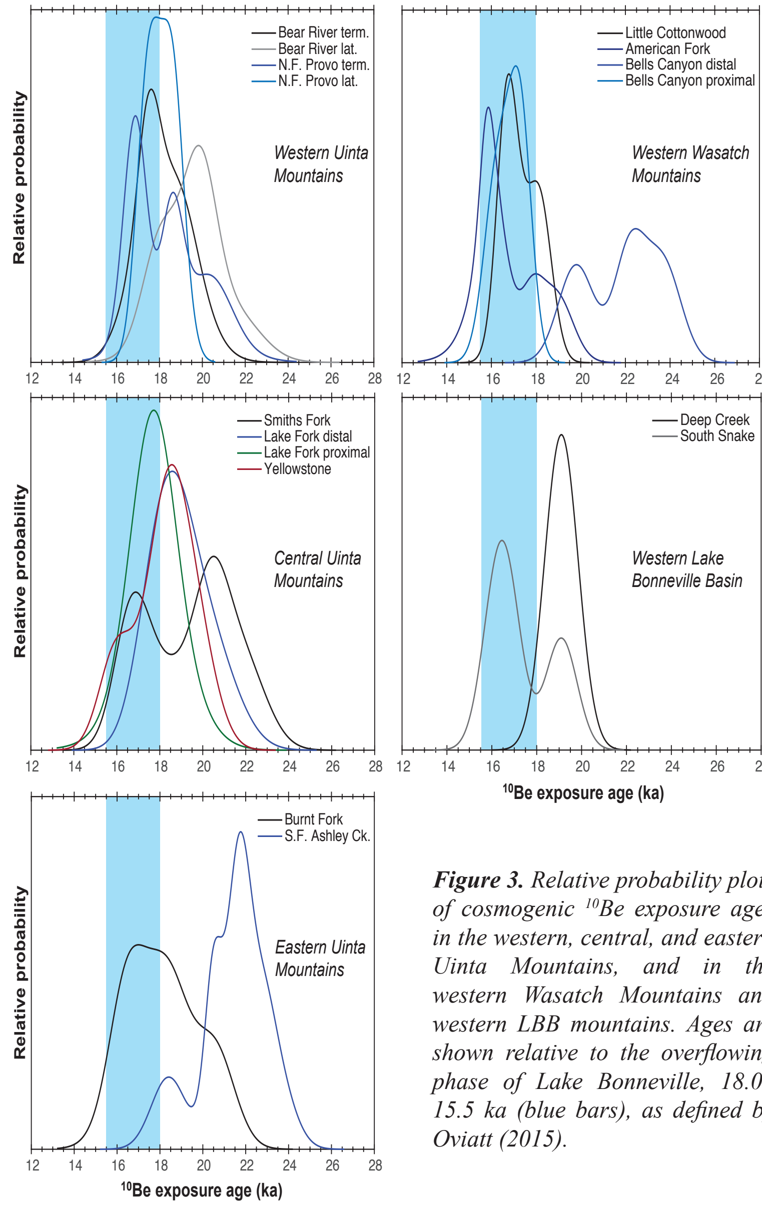

***Figure 3.** Relative probability plots of cosmogenic ^{10}Be exposure ages in the western, central, and eastern Uinta Mountains, and in the western Wasatch Mountains and western LBB mountains. Ages are shown relative to the overflowing phase of Lake Bonneville, 18.0–15.5 ka (blue bars), as defined by Oviatt (2015).*

Changes in mountain glacier length immediately after the time when terminal moraines were abandoned is difficult to assess in these areas, except in the Lake Fork valley of the southern Uinta Mountains (figure 2). There, an ice proximal crest nested into the ice-distal crest of the terminal moraine has a mean exposure age of 17.7 ± 0.5 ka. The moraine age suggests that ice re-advanced to or persisted at its maximum length during the early part of the overflowing phase of Lake Bonneville, but like glaciers elsewhere in the Uinta Mountains, began retreating while the lake continued to overflow. This observation differs significantly from the original reports of Laabs and others (2009) and Laabs and others (2011), where cosmogenic ^{10}Be exposure ages of moraines (calculated with the consensus production rate at the time) suggested that ice persisted at terminal moraines until the end of the overflowing phase of Lake Bonneville at ca. 15.5 ka.

In the Wasatch Mountains, cosmogenic ^{10}Be exposure ages of terminal moraines differ across three valleys. Terminal moraines in American Fork and Little Cottonwood Canyons are younger than the small number (n = 3) of boulder exposure ages from atop the ice-distal crest of the terminal moraine in Bells Canyon (figure 3). The exposure ages from atop the ice-distal moraine crest in Bells Canyon suggest that ice occupied the terminal moraine at 21.9 ± 2.0 ka, prior to the overflowing phase of Lake Bonneville during the global Last Glacial Maximum. The younger terminal moraine exposure ages from American Fork Canyon (16.8 ± 1.4 ka) and Little Cottonwood Canyon (17.3 ± 0.7 ka) overlap with exposure ages from the ice-proximal moraine crest in Bells Canyon (16.8 ± 0.7 ka), indicating that glaciers occupied terminal moraines during the overflowing phase of Lake Bonneville.

Table 1. *Cosmogenic beryllium-10 exposure ages of moraines in the Lake Bonneville basin.*

Mountains	Valley/Moraine	Sample ID	Cosmogenic Exposure Age (ka)	Internal uncertainty (kyr)	External uncertainty (kyr)
Uinta west	Bear River - Main Valley	EBBF-1	17.0	0.9	1.1
		EBBF-2	18.9	0.9	1.2
		EBBF-3	17.5	0.5	0.8
		EBBF-4	18.3	1.0	1.2
		EBBF-5	19.2	1.2	1.4
			18.2 ± 0.9	**χ^2r = 1.28**	
	Bear River - East Fork	EFBR-1	15.0	1.5	1.6
		EFBR-4A	22.2	4.1	4.2
		EFBR-4B	19.9	0.8	1.1
		EFBR-5	19.8	0.9	1.2
		EFBR-7	19.5	1.8	2.0
		EFBR-8	19.9	0.7	1.0
		EFBR-9A	18.3	0.8	1.1
		EFBR-9B	21.6	1.2	1.5
		EFBR-9C	17.8	0.8	1.1
			19.0 ± 1.9	**χ^2r = 1.83**	
	N.F. Provo terminal	NFP-1	12.9	0.6	0.8
		NFP-4C	14.7	0.7	0.9
		NFP-4B	15.2	0.8	1.0
		NFP-2B	16.8	0.6	0.9
		NFP-5	16.9	0.5	0.8
		NFP-4A	18.6	0.5	0.9
		NFP-3A	19.0	2.0	2.2
		NFP-4D	20.4	1.0	1.2
			18.3 ± 1.5	**χ^2r = 5.32**	
	N.F. Provo lateral	NFP-12	17.3	0.5	0.8
		NFP-13	17.7	0.5	0.9
		NFP-14	18.6	0.5	0.9
		NFP-15	18.6	0.6	0.9
			18.0 ± 0.7	**χ^2r = 1.58**	
Uinta middle	Smiths Fork	EFSF-2	18.5	1.3	1.5
		EFSF-4	20.4	0.8	1.1
		EFSF-5	16.7	0.8	1.0
		EFSF-7	30.3	1.7	2.1
		EFSF-8	21.8	1.1	1.3
		EFSF-9	51.8	3.8	4.3
		EFSF-10	27.0	1.2	1.6
			19.4 ± 2.2	**χ^2r = 5.90**	
	Lake Fork distal	LF04-3	11.2	0.6	0.8
		LF04-1	17.5	0.9	1.1
		LF04-2	18.3	0.9	1.1
		LF04-5B	18.6	1.0	1.2
		LF04-5A	19.1	1.0	1.2
		LF-RK-5	19.9	1.4	1.6
		LF04-4	20.5	1.2	1.4
			19.0 ± 1.1	**χ^2r = 1.15**	
	Lake Fork proximal	LFR-1	17.8	0.9	1.1
		LFR-3	18.7	1.3	1.4
		LFR-4	17.2	1.0	1.2
		LFR-5	17.4	1.8	1.9
		LFR-6	17.3	1.1	1.2
		LFR-7	17.9	1.0	1.2
		LFR-9	17.9	1.0	1.2
			17.7 ± 0.5	**χ^2r = 0.24**	

Table 1. *Continued*

	Yellowstone	YS-RK-11	12.8	0.6	0.8
		YS-RK-6	14.2	0.7	0.9
		YS-RK-7	16.0	0.8	1.0
		YS-RK-9	18.3	0.9	1.1
		YS-RK-3	18.2	1.0	1.2
		YS-RK-10	18.6	0.9	1.1
		YS-RK-8	19.8	0.9	1.1
			18.2 ± 1.4	**χ^2r = 4.45**	
Uinta east	Burnt Fork	BF-13	14.1	0.7	0.8
		BF-15	16.4	0.8	1.0
		BF-16	17.3	1.2	1.4
		BF-9	18.0	1.6	1.8
		BF-17	18.5	0.9	1.1
		BF-12	20.6*	0.9	1.2
			18.2 ± 1.6	**χ^2r = 3.28**	
	S.F. Ashley	SFA-9	18.4	0.8	1.0
		SFA-10	20.5	0.4	0.9
		SFA-5	21.3	0.9	1.2
		SFA-1	21.6	0.5	1.0
		SFA-8	21.8	0.5	1.0
		SFA-4	22.7	0.6	1.0
		SFA-2	23.4	0.8	1.2
		SFA-7	39.2	1.0	1.8
		SFA-11	53.9	2.4	3.2
		SFA-6	56.2	1.7	2.8
			21.4 ± 1.6	**χ^2r = 5.37**	
Wasatch	American Fork	AF-7	13.9	0.6	0.8
		AF-2	15.5	0.7	0.9
		AF-6	15.6	1.2	1.4
		AF-11	15.8	0.3	0.7
		AF-9	16.0	0.5	0.8
		AF-10	16.2	0.7	0.9
		AF-1	16.3	0.6	0.9
		AF-4	17.8	0.5	0.8
		AF-3	18.7	0.8	1.0
		AF-8	19.0	0.7	1.0
			16.8 ± 1.4	**χ^2r = 4.80**	
	Little Cottonwood	02-UT-LCC-01	17.8	0.6	0.9
		02-UT-LCC-02	16.7	0.5	0.8
		02-UT-LCC-04	17.0	0.5	0.8
		02-UT-LCC-05	18.0	0.5	0.9
		02-UT-LCC-06	16.7	0.4	0.8
		02-UT-LCC-07	16.6	0.5	0.8
		02-UT-LCC-08	18.4	0.5	0.9
			17.3 ± 0.7		
	Bells distal	BCR-1	19.8	0.8	1.1
		BCR-2	23.7	0.8	1.2
		BCR-4	22.2	0.7	1.1
			21.9 ± 2.0	**χ^2r = 6.13**	
	Bells proximal	BCLR-1	16.3	0.6	0.9
		BCLR-2	17.3	0.5	0.8
			16.8 ± 0.7	**---**	

Table 1. *Continued*

Western LBB	Deep Creek Range	DC-02	11.5	0.5	0.6
		DC-05	18.8	0.7	1.0
		DC-06	19.1	0.7	1.0
		DC-03	19.4	0.7	1.0
		DC-04	30.4	5.0	5.1
			19.1 ± 0.3	**χ^2r = 0.22**	
	South Snake Range	DL-1	16.7	0.7	1.0
		DL-2	19.1	0.7	1.0
		DL-4	16.2	0.7	0.9
		DL-6	13.5	0.5	0.7
			17.3 ± 1.6	**χ^2r = 5.40**	

Note: *all ages are calculated using version 3.0 of the online calculator formerly known as CRONUS (Balco and others, 2008) based on a calibrated production rate at Promontory Point, Utah (Lifton and others, 2015) and LSDn scaling (Lifton and others, 2014). Mean exposure ages of moraines with 1s are shown in bold. Internal uncertainty is based on the AMS measurement of beryllium-10 concentration and external uncertainty is based on the measurement uncertainty and the uncertainty of the scaled production rate. Ages shown in gray were identified as outliers by Laabs and others (2009). Sample data are given in Laabs and others (2009) and Laabs and Munroe (2016).*

**Considered by Laabs and others (2009) to be the best estimate of the moraine age.*

As reported by Laabs and Munroe (2016), the preservation of multiple crests (ice-proximal and ice-distal) along the Bells Canyon terminal moraine affords an opportunity to more precisely identify temporal changes in glacier length. The distinct cosmogenic exposure ages of the distal and proximal moraine crests in Bells Canyon suggest multiple intervals of ice occupation of the terminal moraine complex; one interval prior to the overflowing phase of Lake Bonneville and one interval during the overflowing phase. New cosmogenic exposure age limits from Big Cottonwood Canyon of Quirk and others (2018) also reveal evidence of an earlier glacial maximum prior to the overflowing phase of Lake Bonneville. There, ice occupied a lateral moraine delimiting the time of maximum glacier length at 20.2 ± 1.1 ka. To summarize, evidence that glaciers were expanded to their terminal moraine positions during the overflowing phase of Lake Bonneville is present in American Fork, Little Cottonwood, and Bells Canyons. In contrast, a moraine representing a later glacial maximum in the Wasatch Mountains was not found in Big Cottonwood Canyon. There, Quirk and others (2018) report an exposure age of 17.9 ± 0.5 ka for a bedrock surface just above the dated lateral moraine, which suggests that overall ice retreat began during the overflowing phase of Lake Bonneville, as was the case in neighboring glacial valleys in the Wasatch Mountains.

Cosmogenic exposure ages of terminal moraines in mountains in the western LBB are few but are consistent with exposure ages of moraines in the Uinta and Wasatch Mountains. The bimodal distribution of exposure ages of the moraine in the South Snake Range suggests multiple intervals of ice occupation, although more data are needed to more accurately determine the age of this single crested moraine, and to evaluate if it was constructed by multiple episodes of ice advance to the same position. Cosmogenic exposure ages of the moraine in the Deep Creek Range indicate that ice last occupied the terminal moraine at 19.1 ± 0.3 ka, prior to the overflowing phase of Lake Bonneville.

CONCLUSIONS

Overall, the recalculated cosmogenic chronology of terminal moraines in the Uinta, Wasatch, and western LBB mountains displays some correspondence between the time when mountain glaciers last occupied terminal moraines and the overflowing phase of Lake Bonneville. Only a small number of instances suggest that terminal moraines were abandoned prior to the overflowing phase of Lake Bonneville; these are far downwind of the lake in the eastern Uinta Mountains, terminal moraines of an earlier glacial maximum in Big Cottonwood Canyon of the Wasatch Mountains, and in the Deep Creek Range, where more data are needed to better assess the timing of glaciation. In most valleys, glaciers occupied (or reoccupied) terminal moraines during the overflowing phase of Lake Bonneville. Mean exposure ages of terminal moraines in the central and western Uinta Mountains correspond to the late transgressive/early overflowing phase (20–18 ka), whereas exposure ages of terminal moraines in the Wasatch Mountains closer to the lake suggest that moraines were occupied until ~17 ka. No terminal moraines correspond to the end of the overflowing phase of Lake Bonneville as originally reported by Laabs and others (2009, 2011), unless the lake dropped from the Provo shoreline earlier than suggested in recent reports by Oviatt (2015) and Miller (2016).

An impact by Lake Bonneville on glacier mass balance in the Uinta and Wasatch Mountains remains possible based on the updated moraine chronology reported here. If the lake was near its maximum size just prior to the start of its overflow at 18 ka, as suggested by the hydrograph of Oviatt (2015), then it may have been a moisture source for glaciers in the Uinta and Wasatch Mountains even prior to 18 ka. If so, lake-effect precipitation in the central and western Uinta Mountains, where paleo-glacier ELAs were among the lowest in the range (Munroe and Mickelson, 2002) and recalculated cosmogenic ages range from ~20–18 ka, could have impacted glacier mass balance. Ice retreat during the overflowing phase in the central and western Uinta Mountains could have been caused by a reduced lake effect resulting from a 25% decline in lake surface area at the Provo shoreline. Even in the valleys of the western Wasatch Mountains immediately downwind of Lake Bonneville, glaciers began retreating at ~17 ka while the lake overflowed. This observation supports the possibility of a climatic shift during the overflowing phase of the lake to conditions that no longer favored glacier maxima.

Although the potential impact of Lake Bonneville on glacier mass balance in the Uinta and Wasatch Mountains is supported by ELA reconstructions and the recalculated chronology summarized here, it is still complicated by several uncertainties. First, whether the lake was seasonally frozen during the latter part of the transgressive phase and the overflowing phase is uncertain, although clumped isotope data from Mering (2015) suggest that the average lake temperature was warm enough to remain ice free. Additionally, the frequency of lake-effect storms to enhance moisture, the impact of the lake on near surface lapse rates in neighboring mountains, and seasonal differences in temperature and precipitation changes relative to the modern climate are unclear. Ongoing reconstructions of hydroclimate in the LBB during the last glaciation and Bonneville lake cycle (e.g., Oster and Ibarra, 2019) and refinements to the chronologies of Lake Bonneville and Pleistocene mountain glaciers may help resolve remaining questions regarding the hydrologic and climatic relationship of the lake and mountain glaciers.

REFERENCES

Balco, G., Stone, J., Lifton, N., and Dunai, T., 2008, A complete and easily accessible means of calculating surface exposure ages or erosion rates from ^{10}Be and ^{26}Al measurements: Quaternary Geochronology, v. 3, p. 174–195.

Borchers, B., Marrero, S., Balco, G., Caffee, M., Goehring, B., Lifton, N., Nishiizumi, K., Phillips, F., Schaefer, J., and Stone, J., 2016, Geological calibration of spallation production rates in the CRONUS-Earth project: Quaternary Geochronology, v. 31, p. 188–198.

Godsey, H.S., Atwood, G., Lips, E., Miller, D.M., Milligan, M., and Oviatt, C.G., 2005, Don R. Currey Memorial Field Trip to the shores of Pleistocene Lake Bonneville, *in* Pederson, J., and Dehler, C.M., editors, Interior Western United States: Geological Society of America Field Trip Guide 6, p. 419–448.

Laabs, B.J., Marchetti, D.W., Munroe, J.S., Refsnider, K.A., Gosse, J.C., Lips, E.W., Becker, R.A., Mickelson, D.M., and Singer, B.S., 2011, Chronology of latest Pleistocene mountain glaciation in the western Wasatch Mountains, Utah, USA: Quaternary Research, v. 76, no. 2, p. 272–284.

Laabs, B.J.C., and Munroe, J.S., 2016, Late Pleistocene mountain glaciation in the Lake Bonneville Basin, *in* Oviatt, C.G., and Schroeder, J., editors, Developments in Earth Surface Processes, v. 20, Lake Bonneville—A Scientific Update: Elsevier, p. 462–503.

Laabs, B.J., Munroe, J.S., Rosenbaum, J.G., Refsnider, K.A., Mickelson, D.M., Singer, B.S., and Caffee, M.W., 2007, Chronology of the last glacial maximum in the upper Bear River basin, Utah: Arctic, Antarctic, and Alpine Research, v. 39, no. 4, p. 537–548.

Laabs, B.J., Refsnider, K.A., Munroe, J.S., Mickelson, D.M., Applegate, P.J., Singer, B.S., and Caffee, M.W., 2009, Latest Pleistocene glacial chronology of the Uinta Mountains—support for moisture-driven asynchrony of the last deglaciation: Quaternary Science Reviews, v. 28, nos. 13–14, p. 1171–1187.

Lifton, N., Caffee, M., Finkel, R., Marrero, S., Nishiizumi, K., Phillips, F.M., Goehring, B., Gosse, J., Stone, J., Schaefer, J., Theriault, B., Jull, A.J.T., and Fifield, K., 2015, In situ cosmogenic nuclide production rate calibration for the CRONUS-Earth project from Lake Bonneville, Utah, shoreline features: Quaternary Geochronology, v. 26, p. 56–69.

Lifton, N.A., Phillips, F.M., and Cering, T.E., 2016, Using Lake Bonneville features to calibrate in situ cosmogenic nuclide production rates, *in* Oviatt, C.G., and Schroeder, J., editors, Developments in Earth Surface Processes, v. 20, Lake Bonneville—A Scientific Update: Elsevier, p. 165–183.

Lifton, N., Sato, T., and Dunai, T.J., 2014, Scaling in situ cosmogenic nuclide production rates using analytical approximations to atmospheric cosmic-ray fluxes: Earth and Planetary Science Letters, v. 386, p. 149–160.

Madsen, D.B., and Currey, D.R., 1979, Late Quaternary glacial and vegetation changes, Little Cottonwood Canyon area, Wasatch Mountains, Utah: Quaternary Research, v. 12, p. 254–270.

Marrero, S.M., Phillips, F.M., Borchers, B., Lifton, N., Aumer, R., and Balco, G., 2016, Cosmogenic nuclide systematics and the CRONUScalc program: Quaternary Geochronology, v. 31, p.160–187.

Martin, L.C.P., Blard, P.H., Balco, G., Lavé, J., Delunel, R., Lifton, N., and Laurent, V., 2017, The CREp program and the ICE-D production rate calibration database: a fully parameterizable and updated online tool to compute cosmic-ray exposure ages: Quaternary Geochronology, v. 38, p. 25–49.

Mering, J.A., 2015, New constraints on water temperature at Lake Bonneville from carbonate clumped isotopes: University of California Los Angeles, M.S. thesis, 176 p.

Miller, D.M, 2016. The Provo shoreline of Lake Bonneville, *in* Oviatt, C.G., and Schroeder, J., editors, Developments in Earth Surface Processes, v. 20, Lake Bonneville—A Scientific Update: Elsevier, p. 127–144.

Munroe, J.S., and Laabs, B.J.C., 2009, Glacial geology of the Uinta Mountains area, Utah and Wyoming: Utah Geological Survey Miscellaneous Publications, 09-4DM, DVD, 1 pl., scale 1:100,000, contains GIS data and text, ISBN 1-55791-825-2.

Munroe, J.S., Laabs, B.J., Shakun, J.D., Singer, B.S., Mickelson, D.M., Refsnider, K.A., and Caffee, M.W., 2006, Latest Pleistocene advance of alpine glaciers in the southwestern Uinta Mountains, Utah, USA—Evidence for the influence of local moisture sources: Geology, v. 34, no. 10, p. 841–844.

Munroe, J.S., and Mickelson, D.M., 2002, Last glacial maximum equilibrium-line altitudes and paleoclimate, northern Uinta Mountains, Utah, USA: Journal of Glaciology, v. 48, no. 161, p. 257–266.

Oster, J., and Ibarra, D.E.,2019, Glacial hydroclimate of western North America, insights from proxy-model comparison, records from key locations, and implications for Lake Bonneville, *in* Lund, W.R., McKean, A.P., and Bowman, S.D., editors, Proceedings volume 2018 Lake Bonneville geologic conference and short course: Utah Geological Survey Miscellaneous Publication 170.

Oviatt, C.G., 2015, Chronology of Lake Bonneville, 30,000 to 10,000 yr BP: Quaternary Science Reviews, v. 110, p. 166–171.

Pierce, K.L., 2003, Pleistocene glaciations of the Rocky Mountains: Developments in Quaternary Sciences, v. 1, p. 63–76.

Quirk, B.J., Moore, J.R., Laabs, B.J., Caffee, M.W., and Plummer, M.A., 2018, Termination II, Last Glacial Maximum, and late glacial chronologies and paleoclimate from Big Cottonwood Canyon, Wasatch Mountains, Utah: Geological Society of America Bulletin, v. 130, p. 1889–1902., doi:10.1130/B31967.1.

Refsnider, K.A., Laabs, B.J.C., Plummer, M.A., Mickelson, D.M., Singer, B.S., and Caffee, M.W., 2008, Last glacial maximum climate inferences from cosmogenic dating and glacier modeling of the western Uinta ice field, Uinta Mountains, Utah: Quaternary Research, v. 69, p. 130–144.

Reheis, M.C., 1999, Extent of Pleistocene lakes in the western Great Basin: U.S. Geological Survey Miscellaneous Field Studies Map 2323, scale 1:800,000, https://doi.org/10.3133/mf2323.

Rood, D.H., Burbank, D.W., and Finkel, R.C., 2011, Chronology of glaciations in the Sierra Nevada, California, from ^{10}Be surface exposure dating: Quaternary Science Reviews, v. 30, nos. 5–6, p.646–661.

Scott, W.E., 1988, Temporal relations of lacustrine and glacial events at Little Cottonwood and Bells canyons, Utah, *in* Machette, M.N., editor, In the footsteps of G.K. Gilbert; Lake Bonneville and neotectonics of the eastern Basin and Range Province; guidebook for field trip twelve: Utah Geological Survey Miscellaneous Publication 88-1, p. 78–81.

This content is a PDF version of the author's PowerPoint presentation.

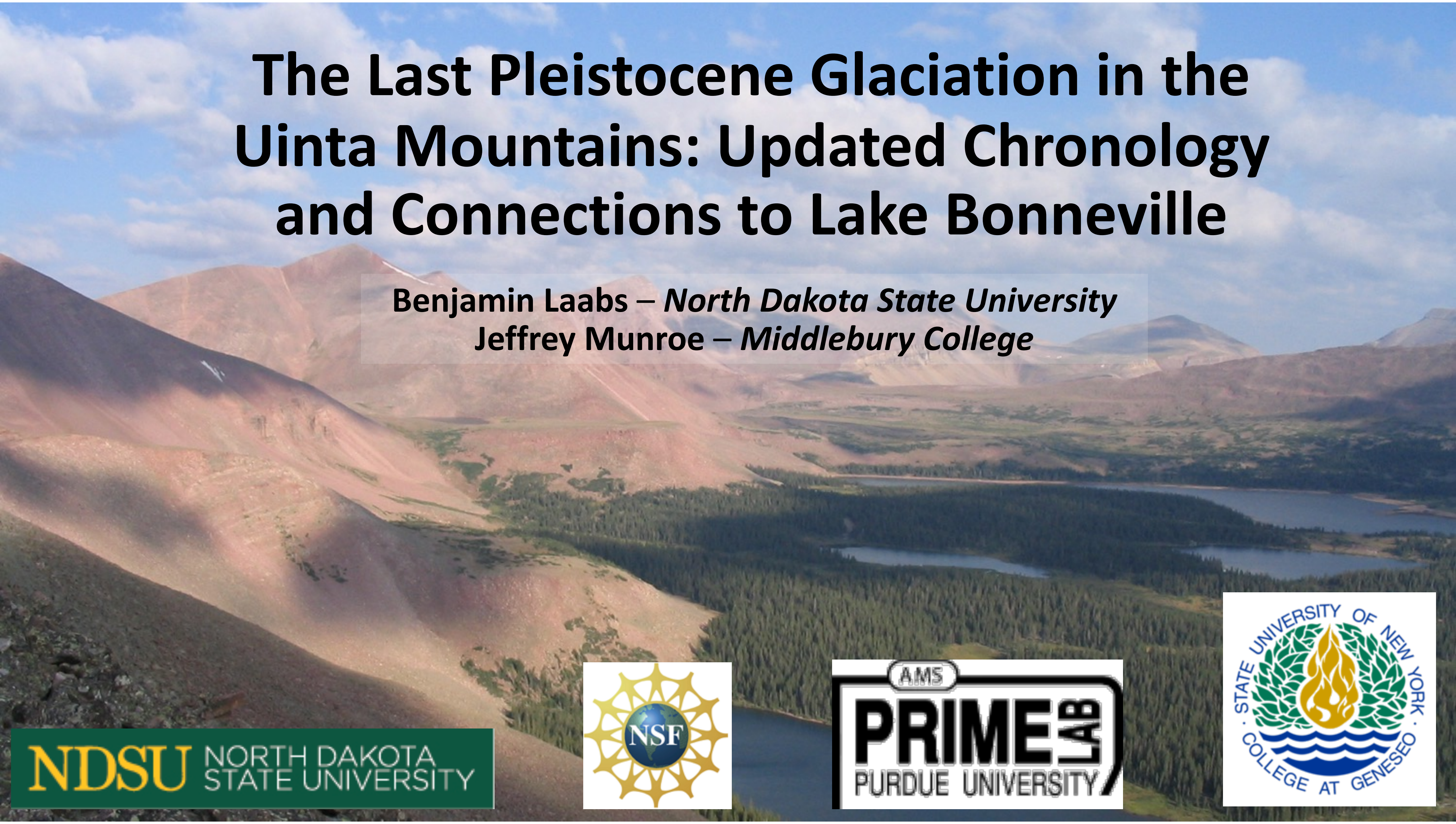

The Last Pleistocene Glaciation in the Uinta Mountains: Updated Chronology and Connections to Lake Bonneville

Benjamin Laabs – ***North Dakota State University***
Jeffrey Munroe – ***Middlebury College***

NDSU NORTH DAKOTA STATE UNIVERSITY

NSF

AMS PRIME LAB PURDUE UNIVERSITY

STATE UNIVERSITY OF NEW YORK · COLLEGE AT GENESEO

The last glaciation in the Bonneville Basin

- Evidence of mountain glaciation in at least 15 separate ranges
- Reconstructions of glacier shapes and equilibrium-line altitudes (ELAs)
- Cosmogenic exposure ages of moraines in several mountains
- Pattern of glaciation in space and time suggests a hydrologic/climatic connection between Lake Bonneville and mountain glaciers

The last glaciation

- Generalized ice extents during the last glaciation (*Biek et al., 2010*)
- Greatest volume of glacier ice in the Uinta and Wasatch Ranges
- Ice volume << lake volume
  - Glaciers did not contribute significantly to Bonneville transgression

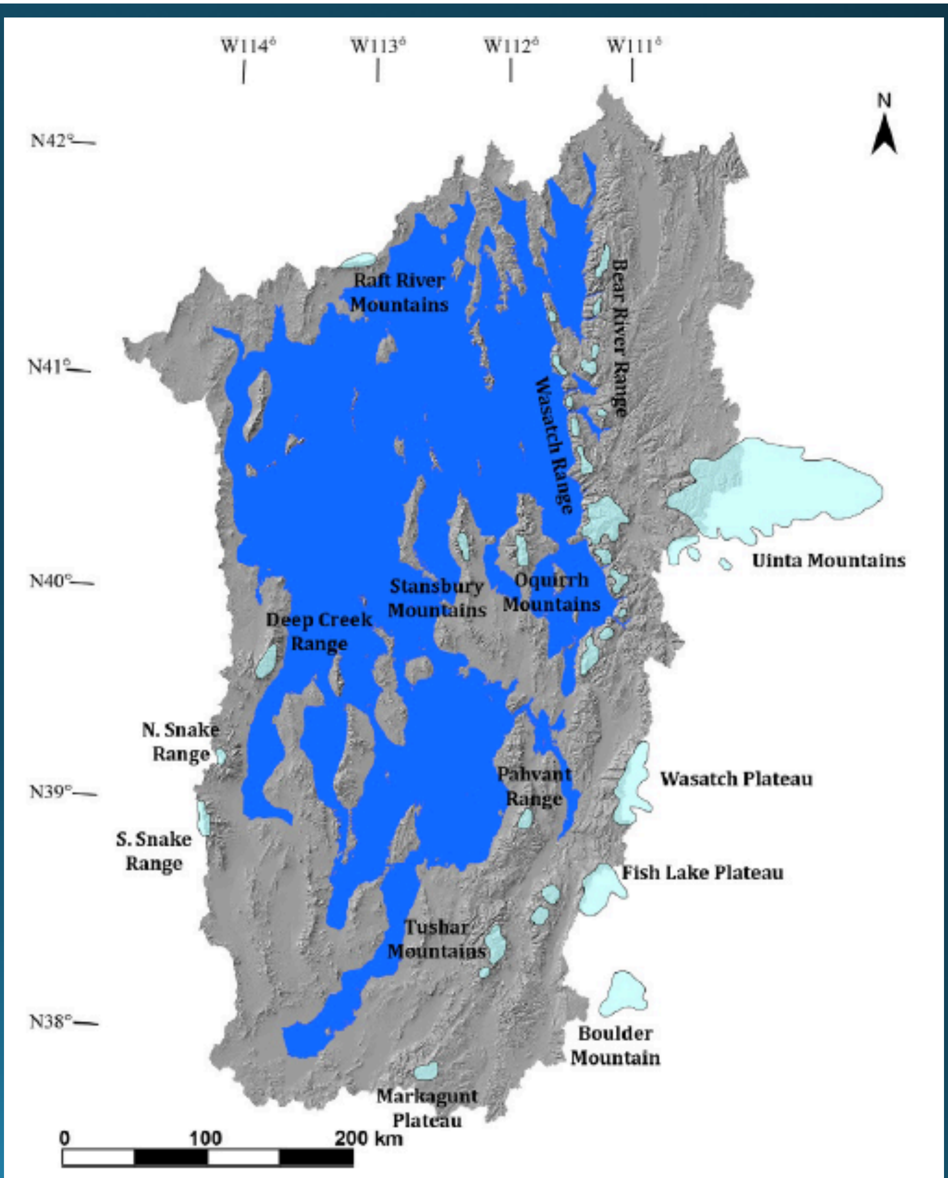

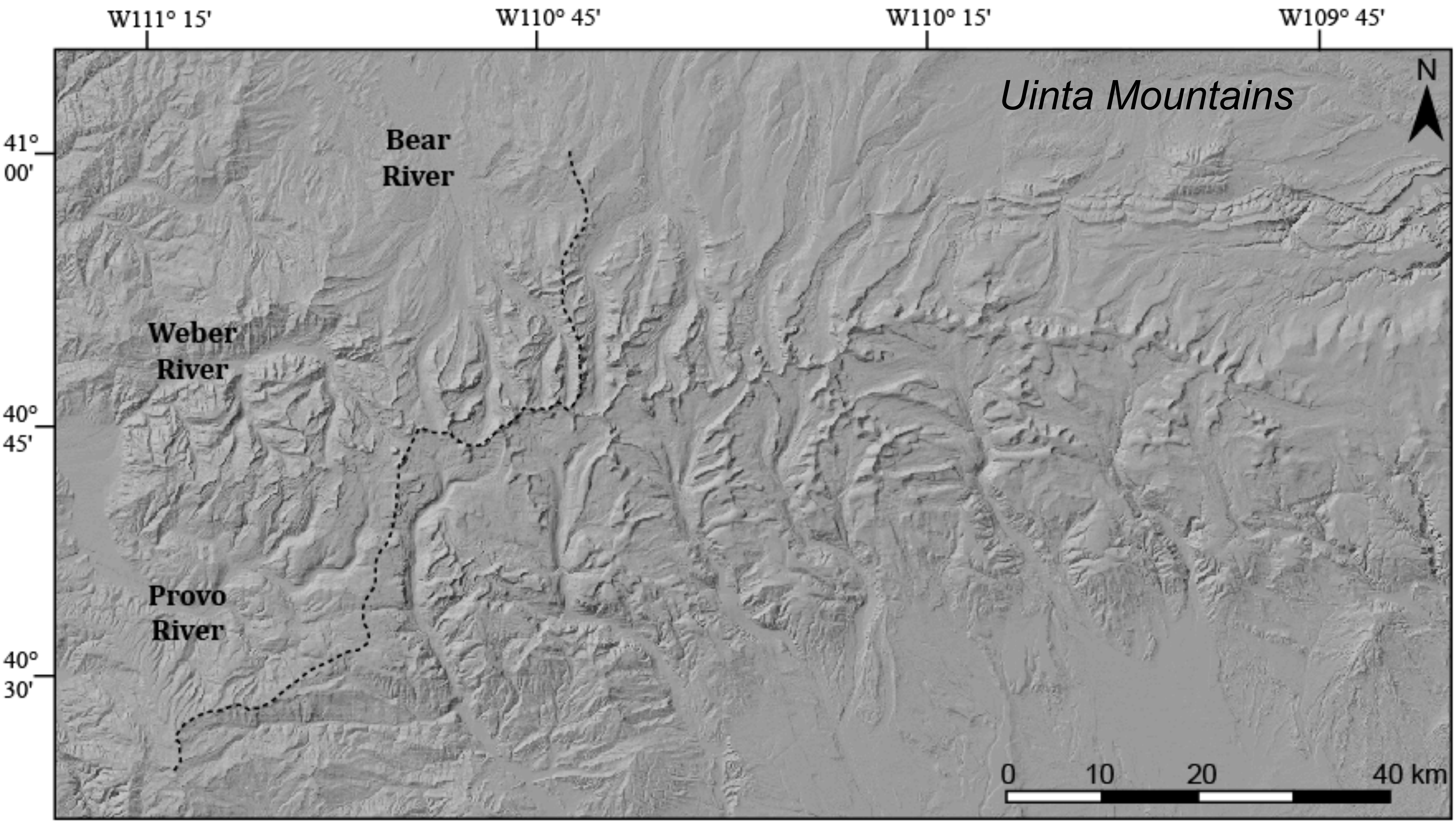
W111° 15'
W110° 45'
W110° 15'
W109° 45'
41° 00'
40° 45'
40° 30'
Uinta Mountains
N
Bear River
Weber River
Provo River
0
10
20
40 km

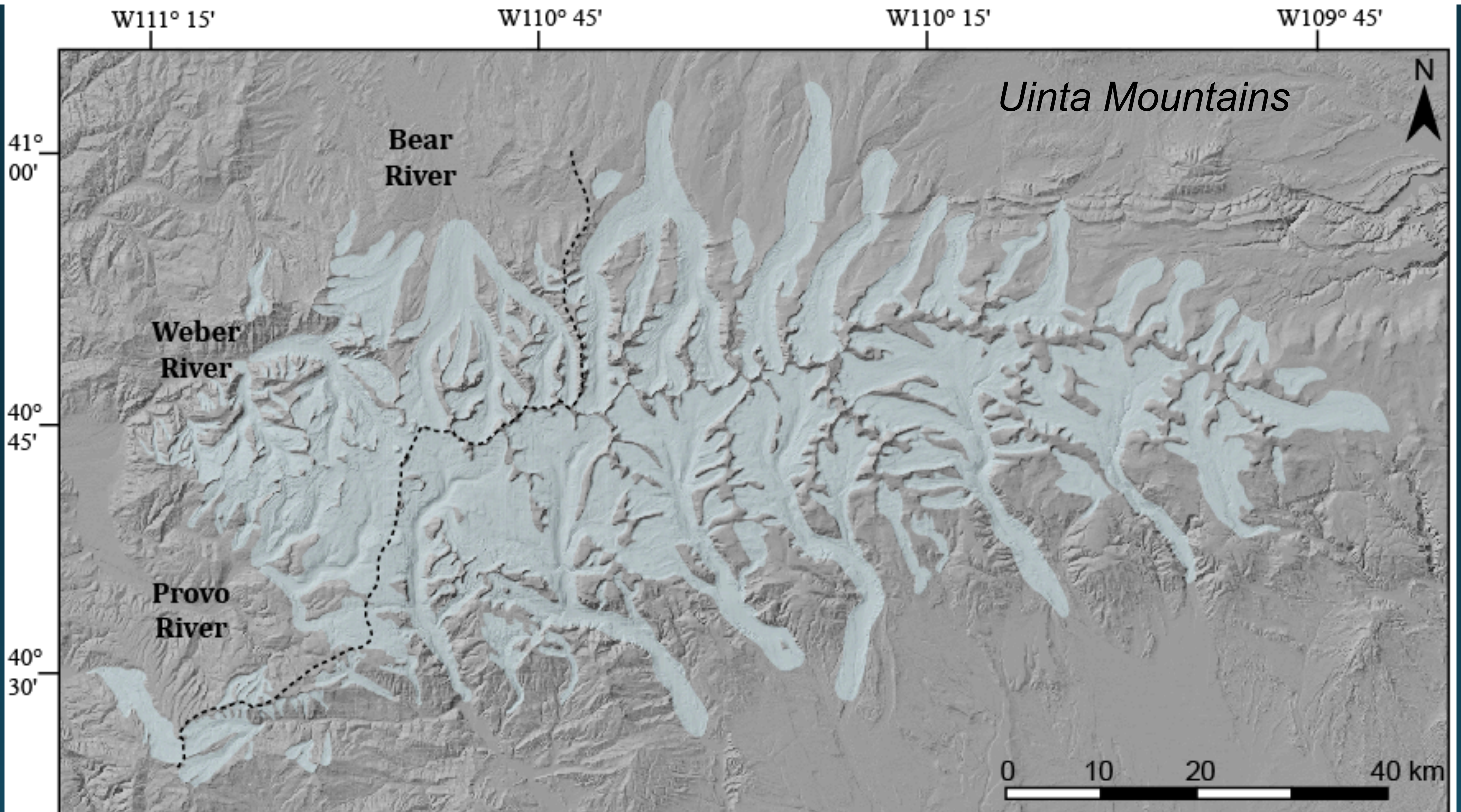
W111° 15'
W110° 45'
W110° 15'
W109° 45'
Uinta Mountains
N
41°
00'
40°
45'
40°
30'
Bear
River
Weber
River
Provo
River
0
10
20
40 km

The last glaciation

Glaciers occupied the upper ~5% of the basin

Lake Bonneville occupied the lower 35% of the basin

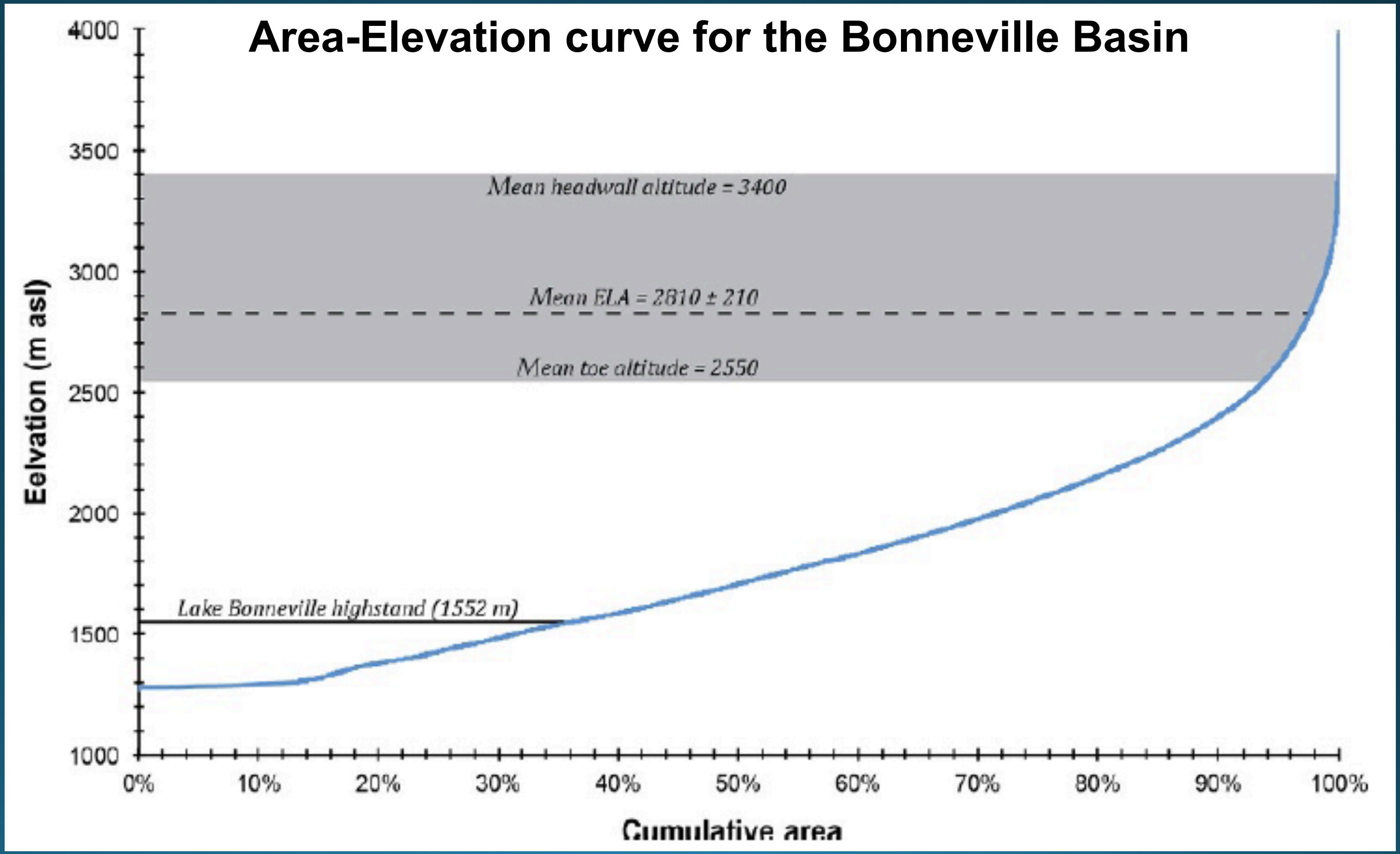

The last glaciation

Glacier ELAs within and beyond the Bonneville basin

Across most of the western U.S., ELAs *rise* from west to east

Across Lake Bonneville, ELAs *decline* from west to east

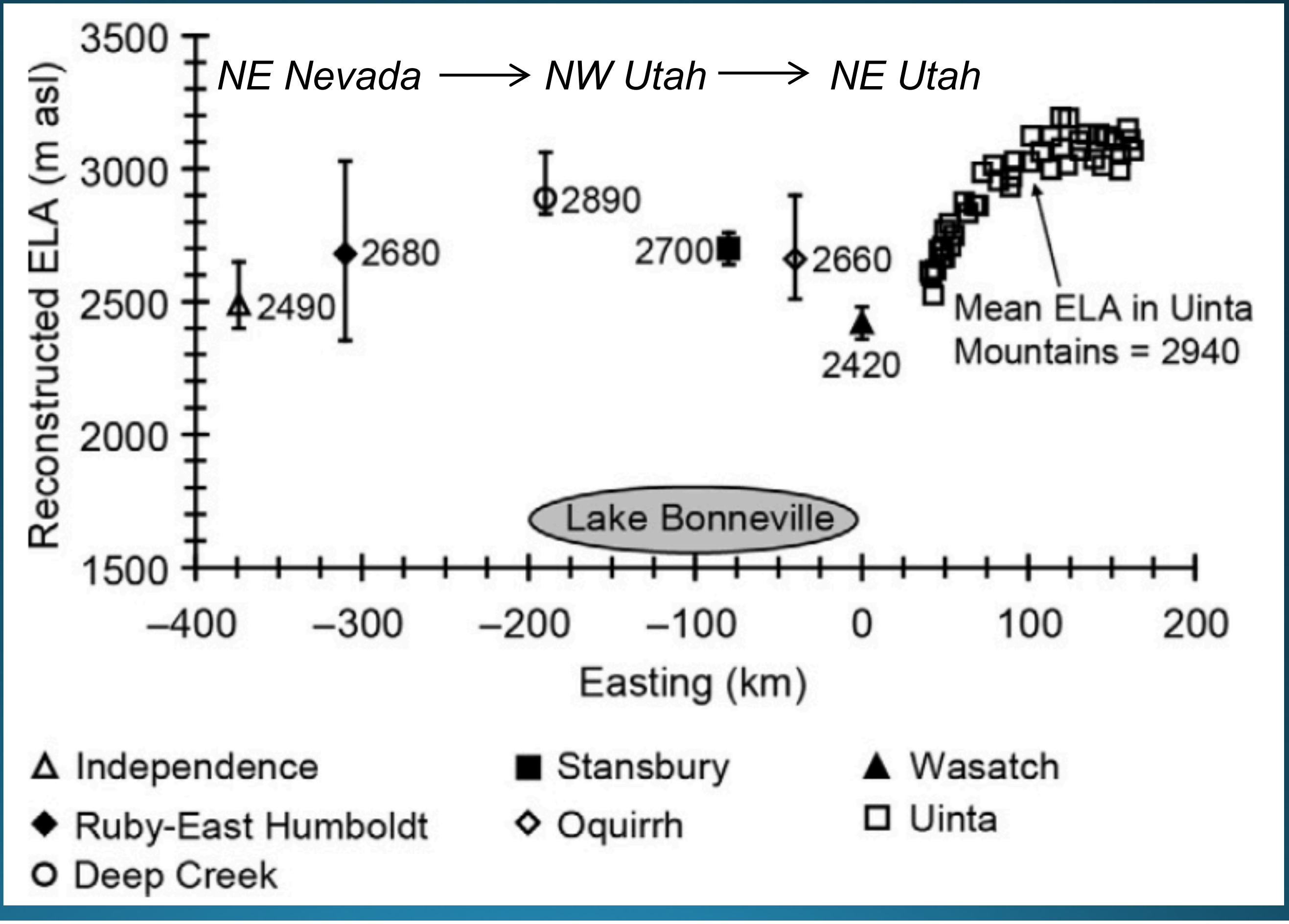

The last glaciation – temporal patterns

- **Timing of glaciation relative to Lake Bonneville is becoming clear**
  - Stratigraphic relationships observed only at the Wasatch Front
  - Radiocarbon dating of glacial deposits is unavailable nearly everywhere
- **Cosmogenic surface exposure dating of glacial features has grown**
  - Cosmogenic beryllium-10 (^{10}Be) exposure ages of moraines
  - Improved estimates of cosmogenic nuclide production rates

Cosmogenic ^{10}Be surface exposure dating

Assume that only "fresh" boulders are deposited at crest, constant exposure history

Average boulder exposure age = last time ice occupied the moraine

Production rates of ^{10}Be and ^{3}He are calibrated → comparison of moraine ages with Bonneville deposits

The last glaciation

- Average cosmogenic ^{10}Be exposure ages of **terminal moraines** in the Bonneville Basin (ka)
- Ice retreat from some terminals begins during Bonneville transgression

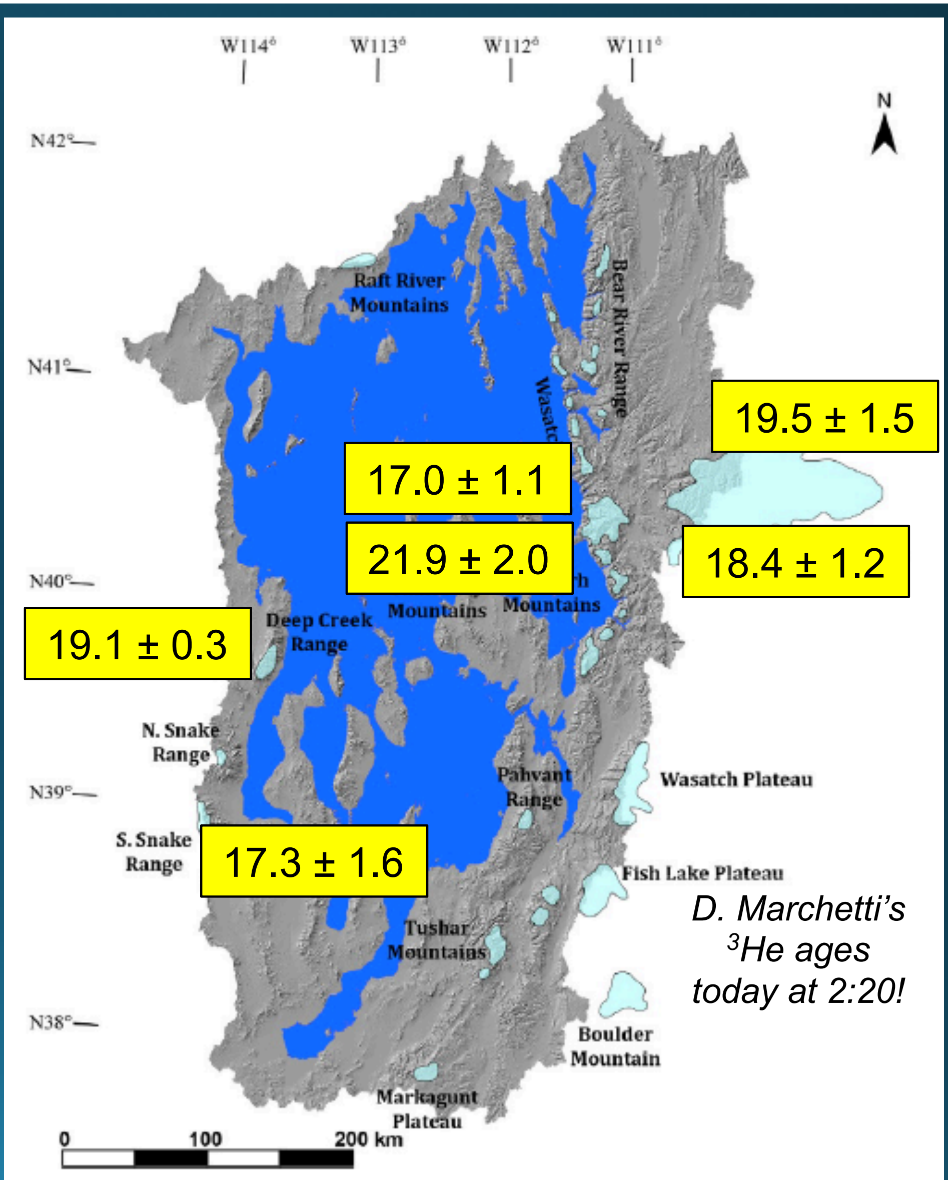

D. Marchetti's ^{3}He ages today at 2:20!

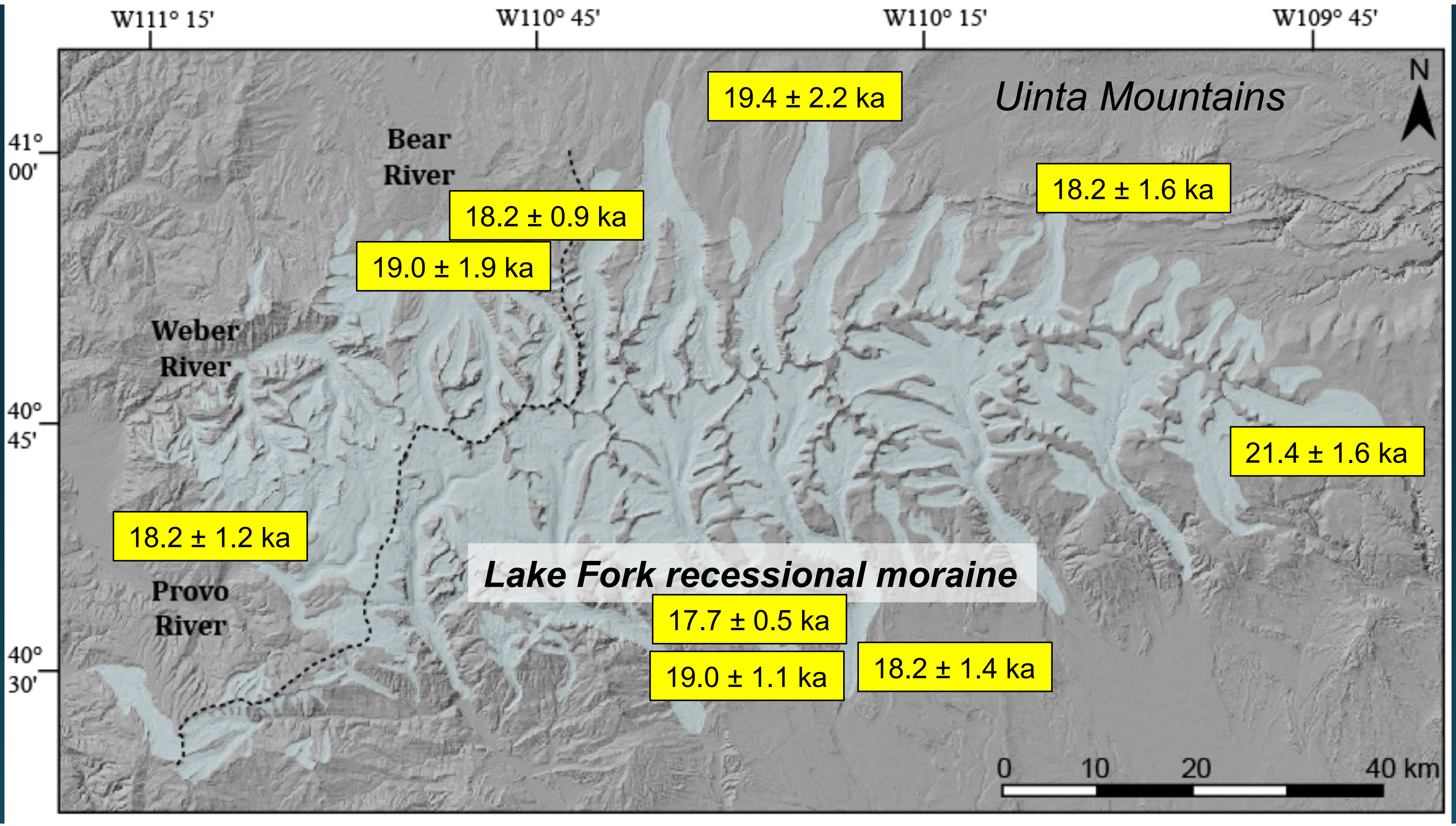
W111° 15'
W110° 45'
W110° 15'
W109° 45'
41° 00'
40° 45'
40° 30'
N
Uinta Mountains
19.4 ± 2.2 ka
18.2 ± 1.6 ka
Bear River
18.2 ± 0.9 ka
19.0 ± 1.9 ka
Weber River
21.4 ± 1.6 ka
18.2 ± 1.2 ka
Provo River
Lake Fork recessional moraine
17.7 ± 0.5 ka
19.0 ± 1.1 ka
18.2 ± 1.4 ka
0
10
20
40 km

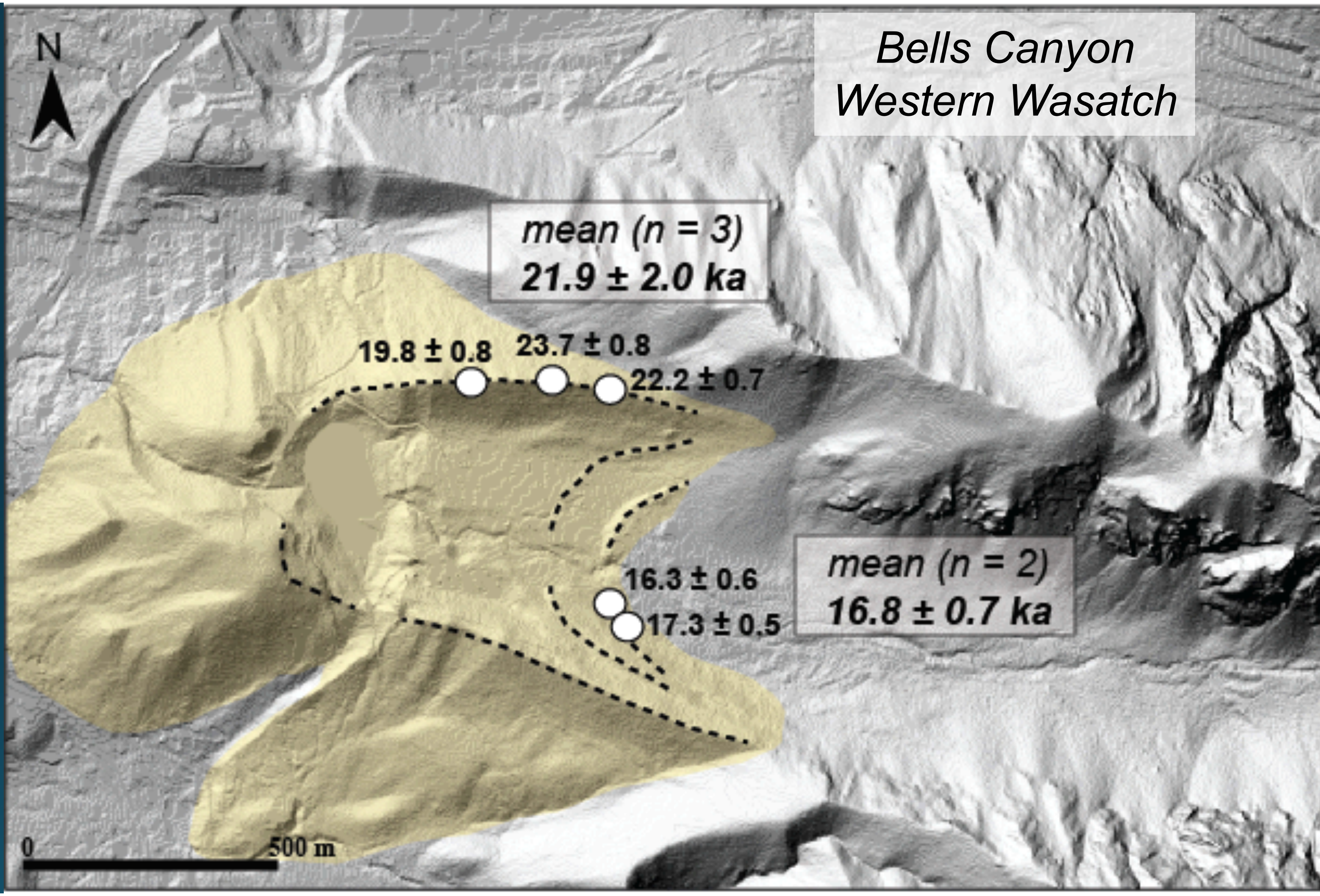
Bells Canyon
Western Wasatch
N
mean (n = 3)
21.9 ± 2.0 ka
19.8 ± 0.8
23.7 ± 0.8
22.2 ± 0.7
16.3 ± 0.6
17.3 ± 0.5
mean (n = 2)
16.8 ± 0.7 ka
0
500 m

The last glaciation - summary

- Most terminal moraines were occupied during the transgressive phase of Lake Bonneville (before 18 ka)
- Nested recessional moraines and younger terminals were occupied during the early part of the overflowing phase (~18-17 ka)
    - Favorable climate for glaciers and lakes → ***D. Ibarra and K. Fleming talks!***
- Ice retreated during the later part of the overflowing phase (after 17 ka), with pauses in the Wasatch → ***B. Quirk's talk!***
- Bonneville lake effect in the Wasatch and western Uinta supported by ELAs, chronology, and glacier modeling (Quirk et al., 2018)

Terminus

Cosmogenic ^{10}Be surface exposure dating

Theory:

Cosmic radiation bombards surface materials, reacts with elements in minerals

Reactions produce cosmogenic isotopes (^{10}Be in quartz)

Concentrations of ^{10}Be are proportional to **exposure age** of a surface

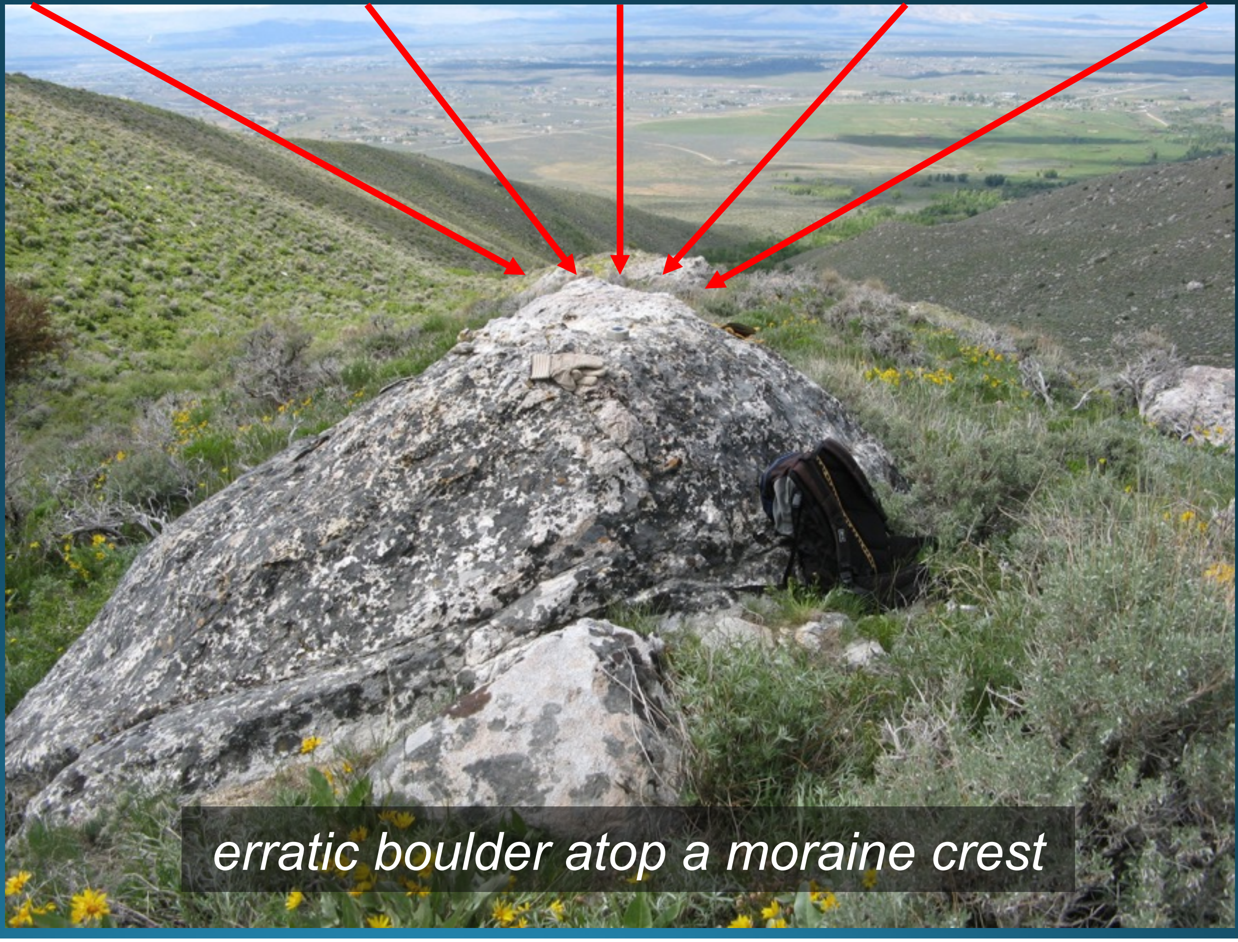

erratic boulder atop a moraine crest

VISUALIZATION OF A LAKE BONNEVILLE SHORELINE DEPOSIT IN PILOT VALLEY, UTAH

Katelynn M. Smith, John H. McBride, Stephen T. Nelson, R. William Keach, II,
Samuel M. Hudson, David G. Tingey, Kevin A. Rey, and Gregory T. Carling

Department of Geological Sciences, Brigham Young University, Provo, UT 84602

Corresponding author (McBride): john_mcbride@byu.edu

ABSTRACT

Pilot Valley in the eastern Basin and Range Province, western Utah, USA, contains numerous shorelines and depositional remnants of late Pleistocene Lake Bonneville. These remnants present excellent ground-penetrating radar (GPR) targets due to their coherent stratification, low-clay, low-salinity, and low-moisture content. Three-dimensional (3D) GPR imaging can resolve fine-scale stratigraphy of these deposits down to a few centimeters, and when combined with detailed outcrop characterization, can provide an in-depth look at the architecture of these deposits. On the western side of Pilot Valley, a well-preserved late Pleistocene gravel bar records shoreline depositional processes associated with the Provo shoreline period. Three-dimensional GPR data, measured stratigraphic sections, cores, paleontological sampling for paleo-ecology and radiocarbon dating, and mineralogical analysis permit a detailed reconstruction of the depositional environment of this prograding gravel bar, which is well-exposed and similar to many Bonneville shoreline deposits throughout the area. Contrary to other described Bonneville shoreline deposits, however, calibrated radiocarbon ages range from 16.5 to 14.3 cal kyr B.P., and show that this bar was stable and active during an overall regressive stage of the lake as it dropped from the Provo shoreline.

Our study provides a comprehensive model for an ancient pluvial lake-shore depositional environment in the Basin and Range Province using an integration of geological and geophysical data, and suggests that stable, progradational bedforms common to the various stages of Lake Bonneville are likely not all associated with periods of shoreline stability as is commonly assumed. The high-resolution 3D GPR visualization demonstrates the high degree of compartmentalization possible for a potential subsurface reservoir target based on ancient shoreline sedimentary facies.

IMAGING THE MARGINS OF PLEISTOCENE LAKE DEPOSITS WITH HIGH-RESOLUTION SEISMIC REFLECTION IN THE EASTERN BASIN AND RANGE: PILOT VALLEY, UTAH (USA)

John V. South[1], John H. McBride[2], Greg T. Carling[2], Alan L. Mayo[2],
David G. Tingey[2], Kevin A. Rey[2], and Stephen T. Nelson[2]

[1]Dominion Energy Wexpro, Salt Lake City, UT 84111;
[2]Department of Geological Sciences, Brigham Young University, Provo, UT 84604

Corresponding author (South): johnvsouth@gmail.com

ABSTRACT

A vast area of the northeastern Great Basin of the western USA was inundated by a succession of Plio-Pleistocene lakes, including Lake Bonneville. Playa sediment deposition from these lakes onlapped onto pre-existing alluvial fans that blanketed the slope of adjacent mountain ranges to create prominent angular unconformities. Understanding these unconformities is useful for constraining understanding of the geologically recent tectonic evolution of the Basin and Range Province. The Pilot Valley playa, just east of the Utah-Nevada border near Wendover, Utah, represents a remnant of these lakes. In order to investigate the interaction of lake sedimentation and alluvial-fan development, high-resolution seismic profiles were acquired near the base of the bounding mountain ranges. The profiles reveal the stratigraphic relationships between Quaternary pluvial sediments as a shoreline depositional facies and the adjacent bounding fan deposits. On the western side of the basin, these profiles image sub-horizontal playa sediments prograding over inclined alluvial fans. The boundary between the playa and fan sediments is marked by a prominent angular unconformity. Seismic images from the opposite side of the basin reveal a more heterogeneous structural and stratigraphic style, including down-to-the-basin normal faulting of shallow Paleozoic bedrock overlain by alluvial-fan deposits, which are in turn on-lapped by a thin veneer of playa sediments. The new geophysical images, when integrated with available geologic mapping, aid in constraining how deep aquifers are locally recharged from an adjacent range. The results also demonstrate the strong structural asymmetry of the range and playa system, consistent with a classic half-graben structure. Lastly, this study demonstrates the utility of shallow seismic reflection as a tool to provide high-resolution subsurface images in the geophysically challenging environment of alluvial fan-playa geology.

This content is a PDF version of the author's PowerPoint presentation.

IMAGING THE MARGINS OF PLEISTOCENE LAKE DEPOSITS WITH HIGH-RESOLUTION SEISMIC REFLECTION IN THE EASTERN BASIN AND RANGE: PILOT VALLEY, UTAH (USA)

John V. South†
John McBride
Greg Carling
Alan Mayo
David Tingey
Kevin Rey
Stephen Nelson

Department of Geological Sciences
Brigham Young University
Provo, UT

†*Now at*
Dominion Energy Wexpro
Salt Lake City, UT

Objectives

- Investigate use of shallow high-resolution seismic reflection profiles to ***image margins of a pluvial basin*** in a typical Basin and Range valley-playa system.

- Determine ***degree of shallow geological variability*** on opposite sides of and along the playa system in the basin.

- Investigate ***geometrical relation between playa sediments and alluvial fan sediments*** in a Basin and Range setting and (provides a geometrical setting for interpreting the salt and fresh groundwater boundary relationships.)

Index Map

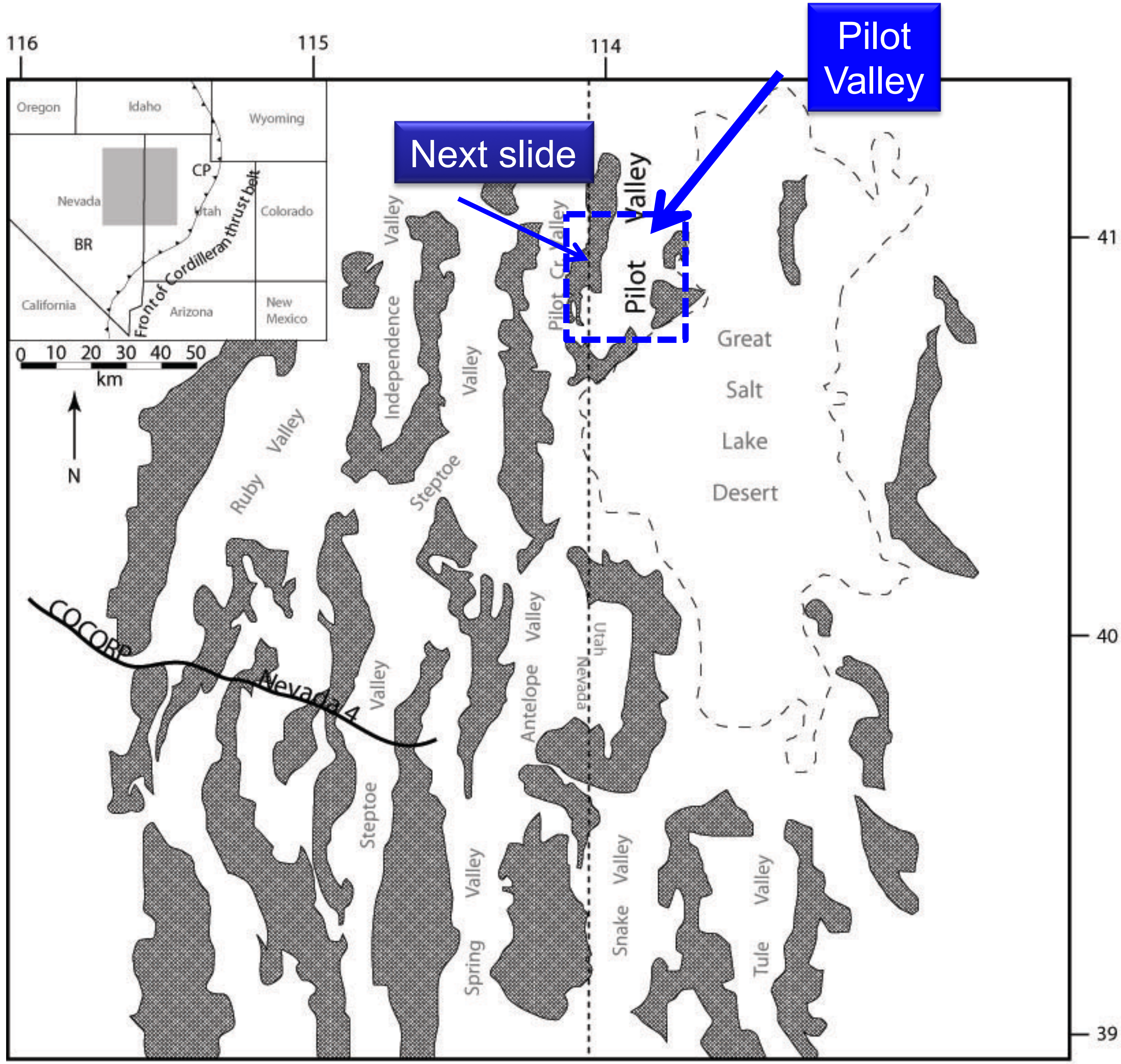

116
115
114
41
40
39
Oregon
Idaho
Wyoming
Nevada
CP
Utah
Colorado
BR
California
Arizona
New Mexico
Front of Cordilleran thrust belt
0 10 20 30 40 50
km
N
Pilot Valley
Next slide
Valley
Pilot
Pilot Cr. Valley
Independence Valley
Valley
Ruby Valley
Steptoe
Great
Salt
Lake
Desert
Antelope Valley
Utah
Nevada
COCORP
Nevada 4
Steptoe Valley
Spring Valley
Snake Valley
Tule Valley

Simplified Geology with Seismic Lines Overlain

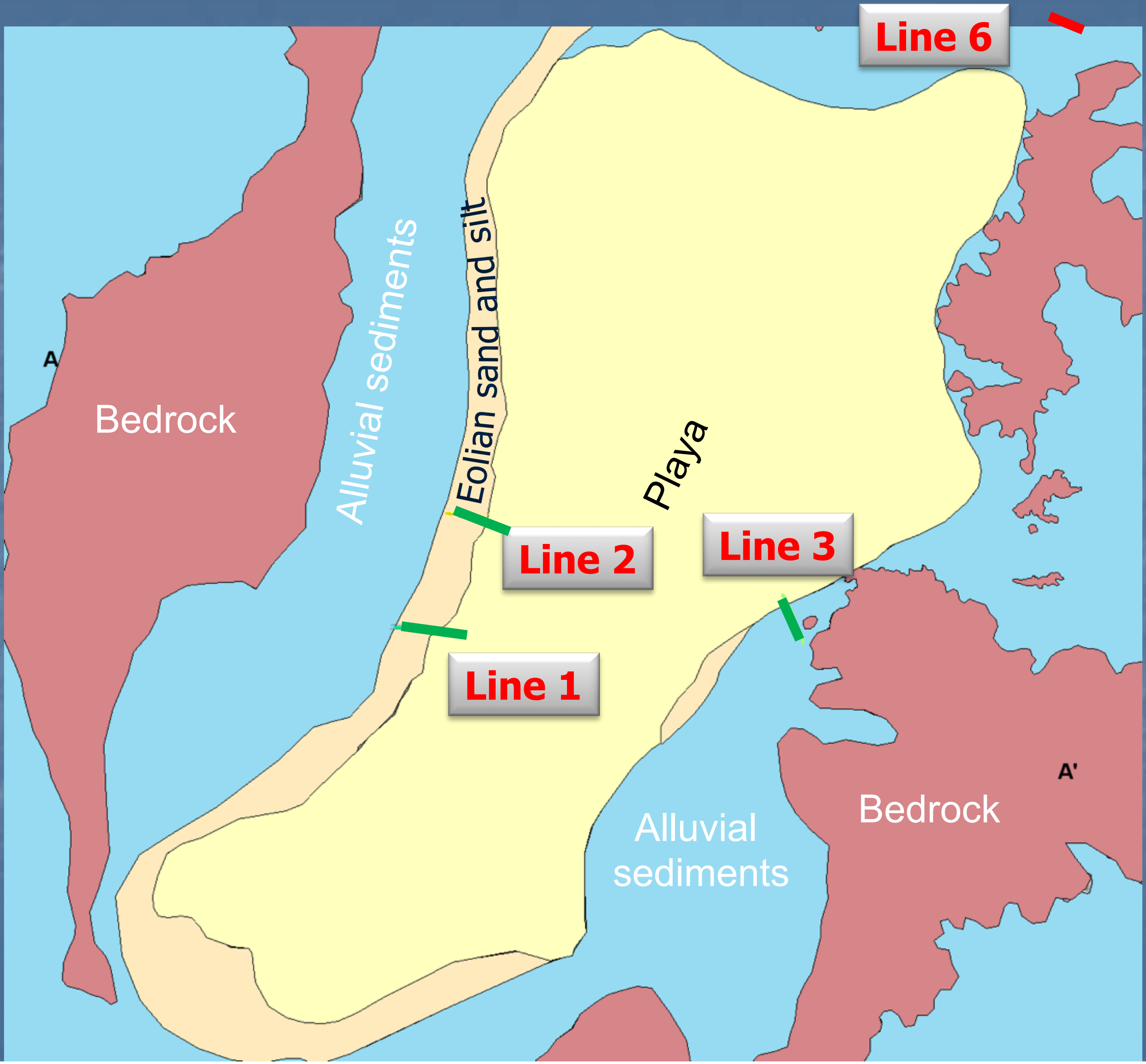

Data collection on the alluvial fan/playa

- 10-ft station intervals (5 ft CDP interval)
- 48-96-channel (24-72 fold)
- 28-Hz phones
- Conventional CDP roll-along (“push the spread”)
- Accelerated weight drop (with 100 lb. hammer)
- Four Profiles (three are ~1 mile long; one is shorter)

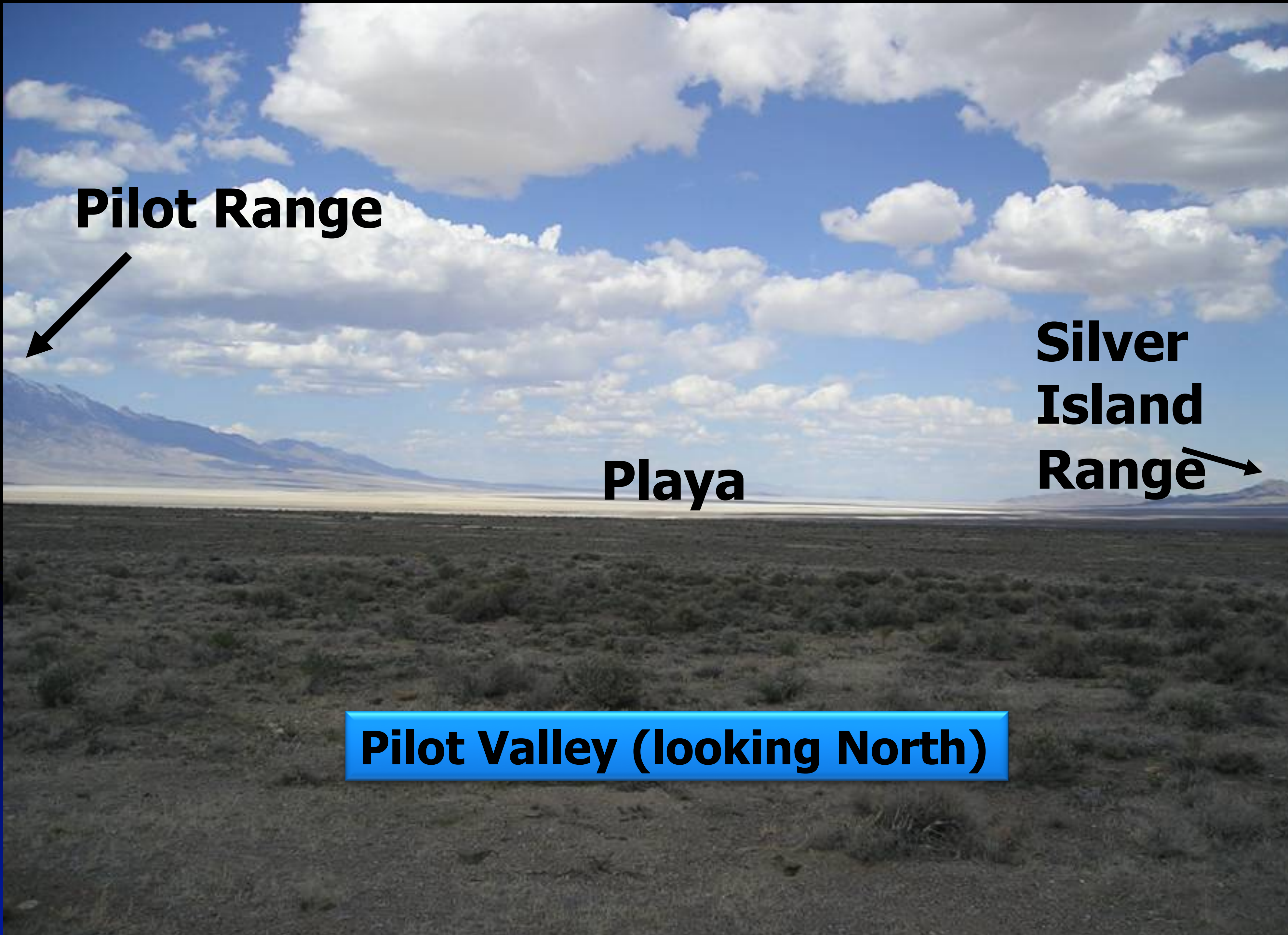
Pilot Range
Silver Island Range
Playa
Pilot Valley (looking North)

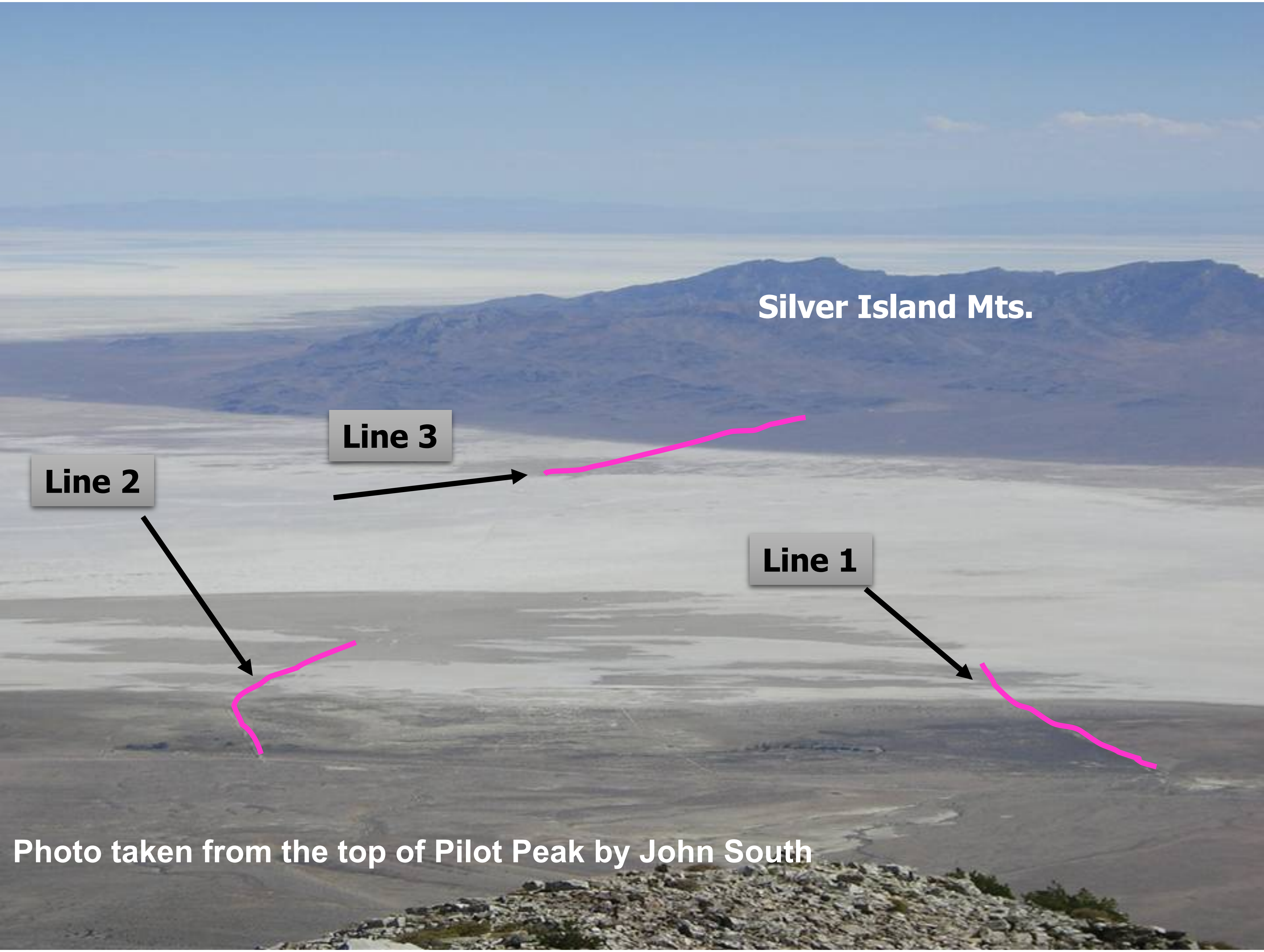
Silver Island Mts.
Line 3
Line 2
Line 1
Photo taken from the top of Pilot Peak by John South

West side of Pilot Valley

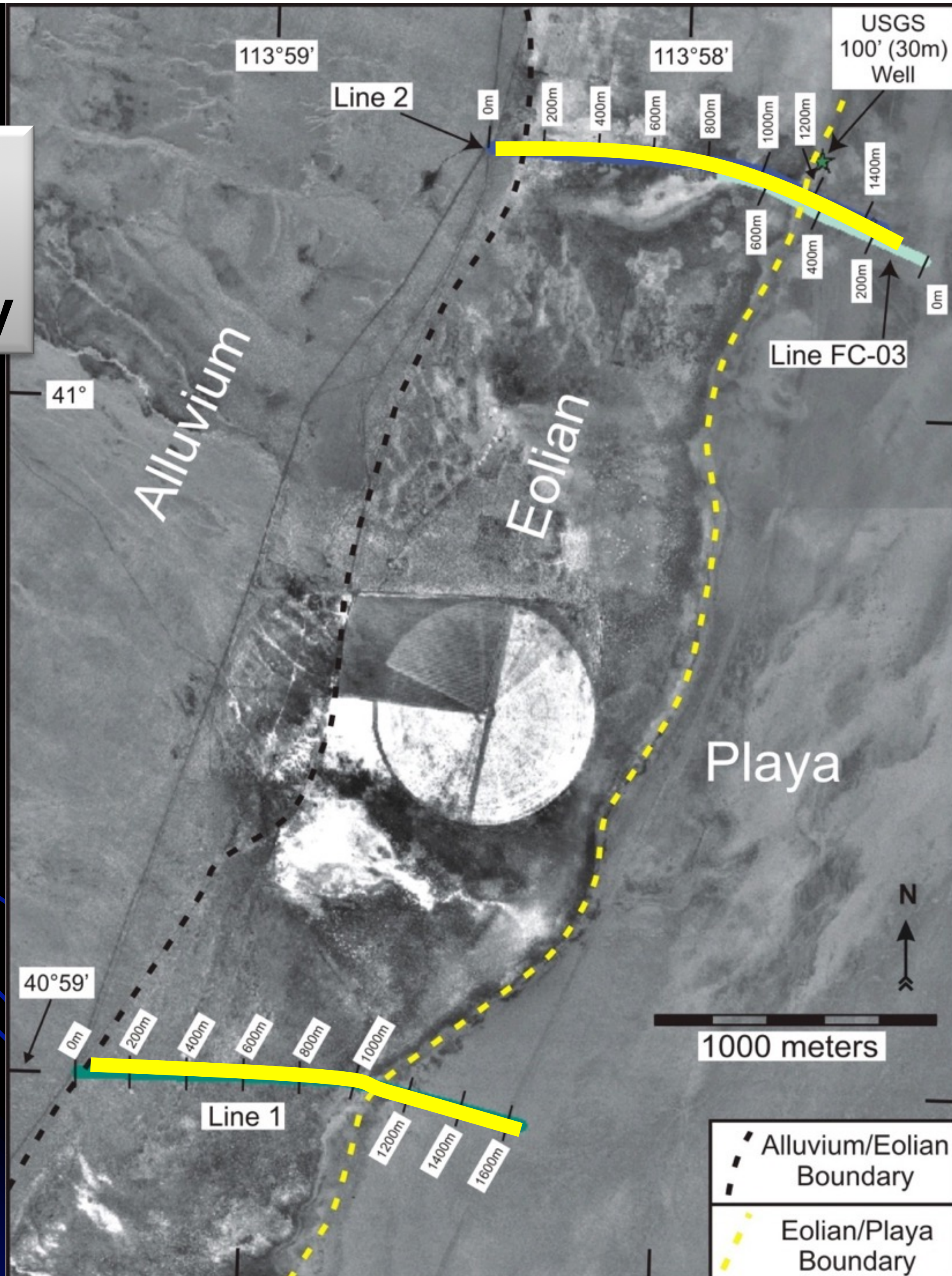

Line 2

Line 1


Pilot Valley, Utah, Nevada looking west at Pilot Range
Line 2

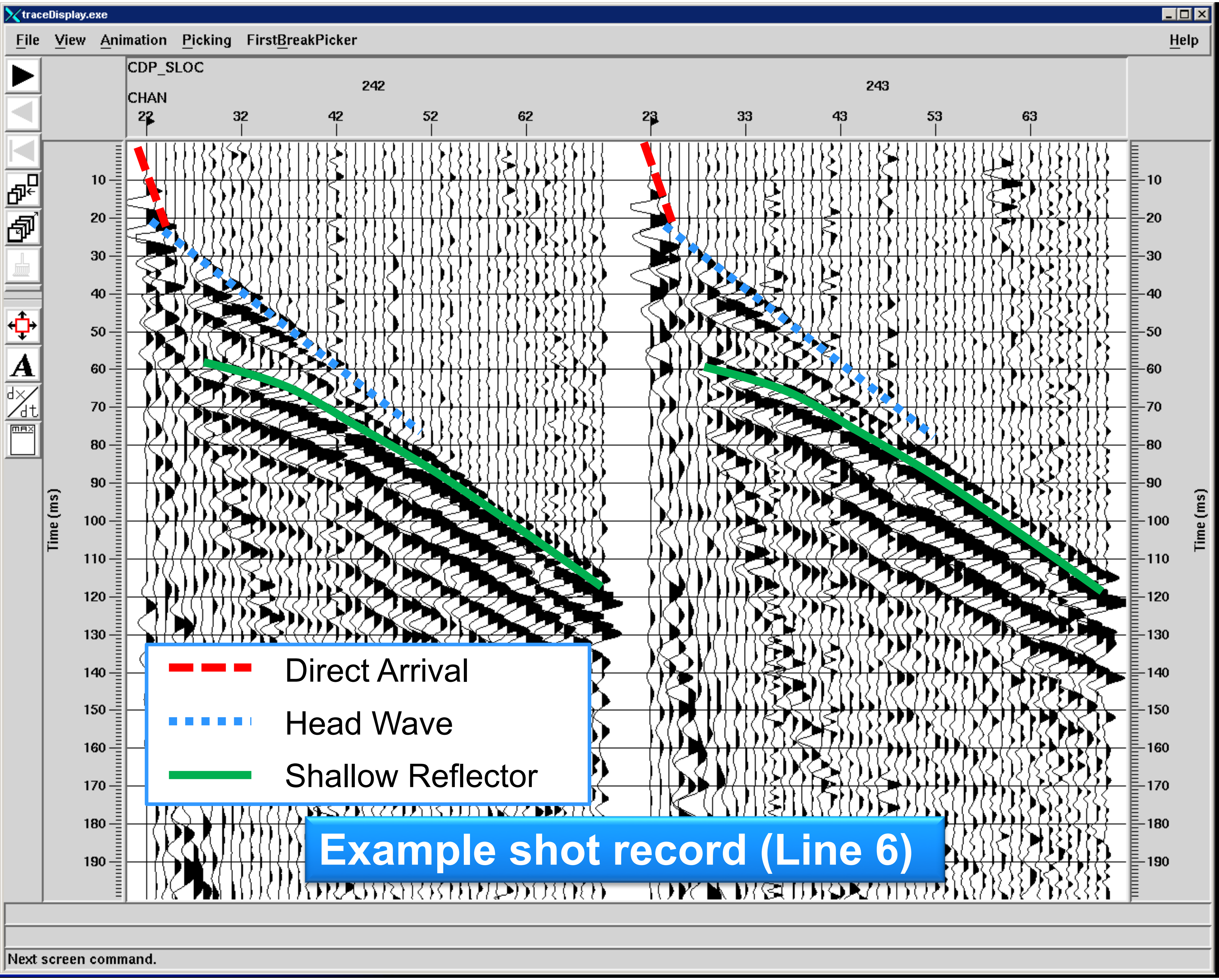

Example shot record (Line 6)

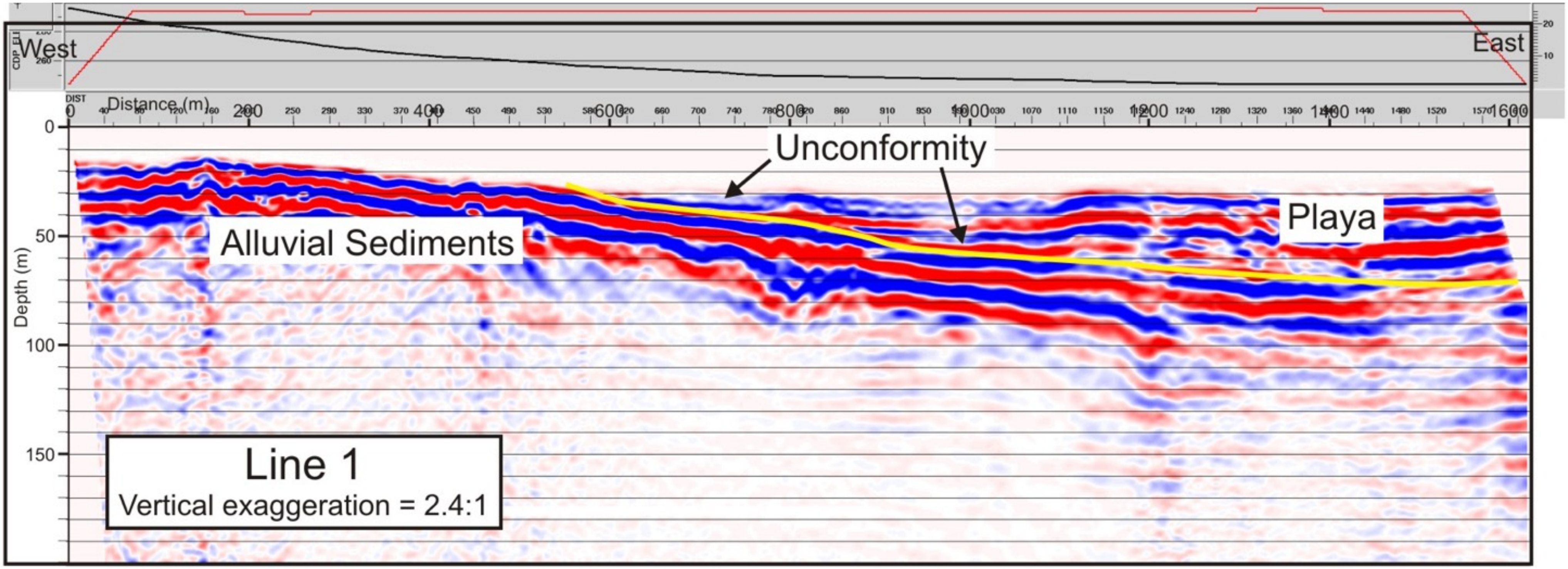

Line 1

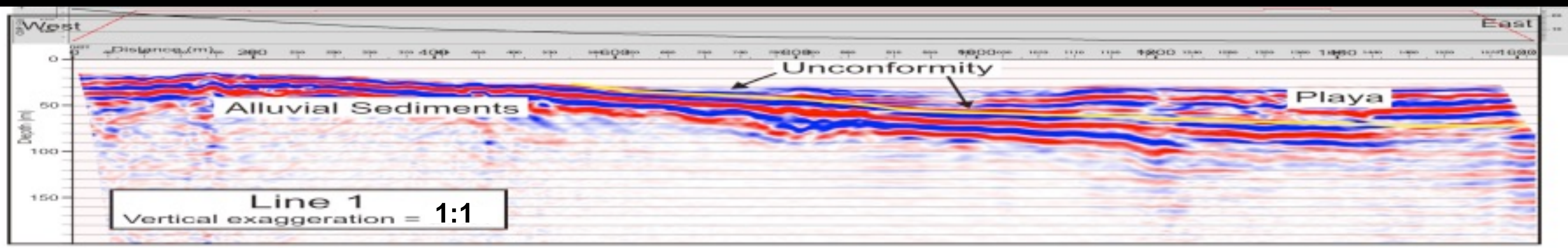

Vertically squashed to illustrate "true" scale

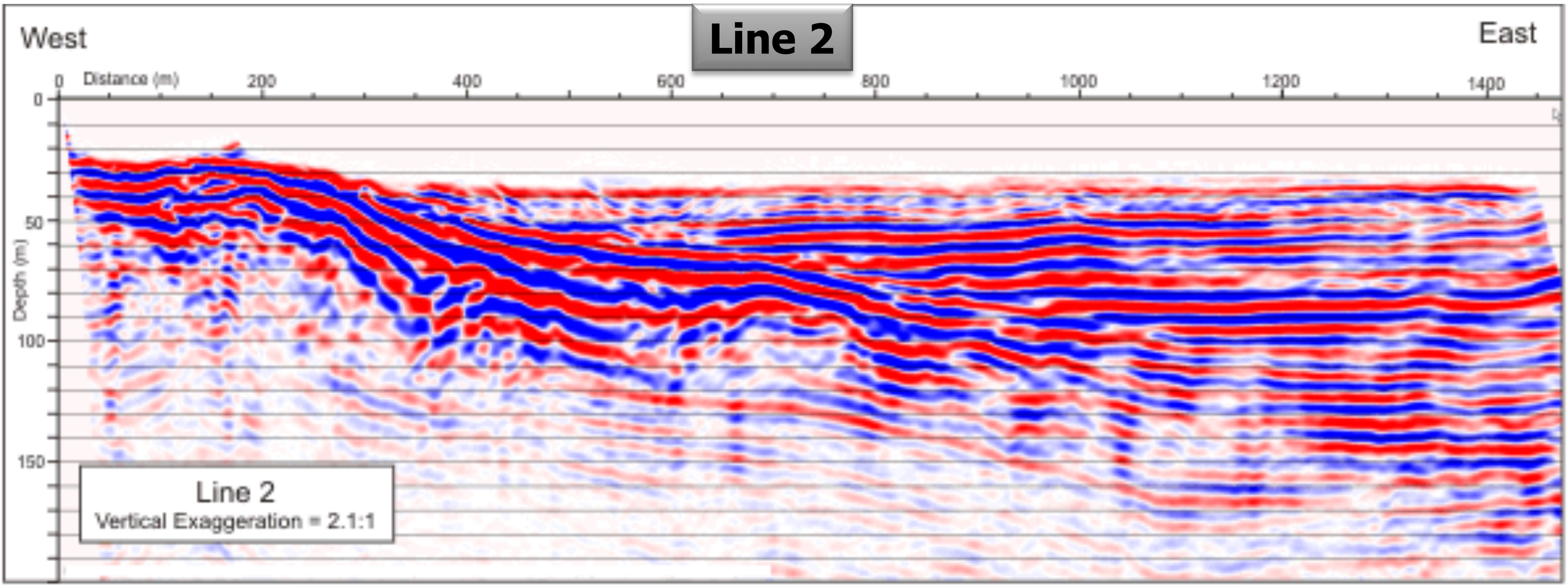

Pilot Valley Line 2, P-wave

Pilot Valley Profile 2, P-wave

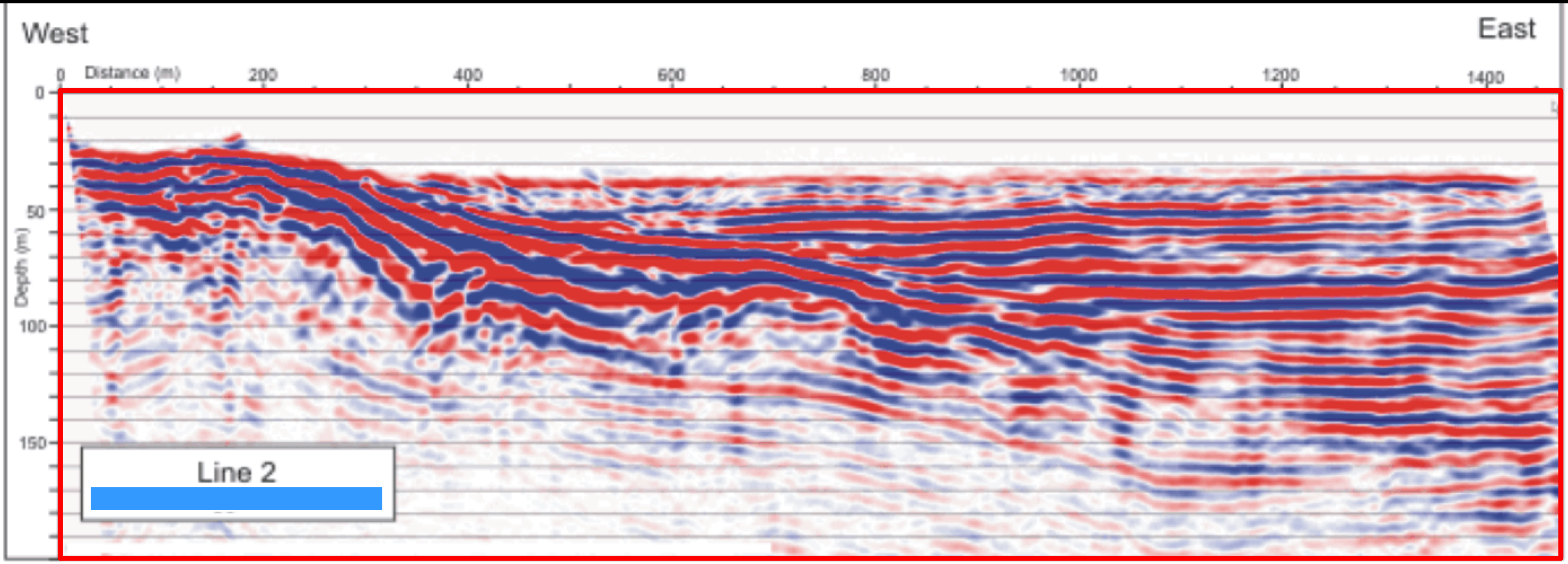

Pilot Valley Profile 2, P-wave with SH-wave superimposed

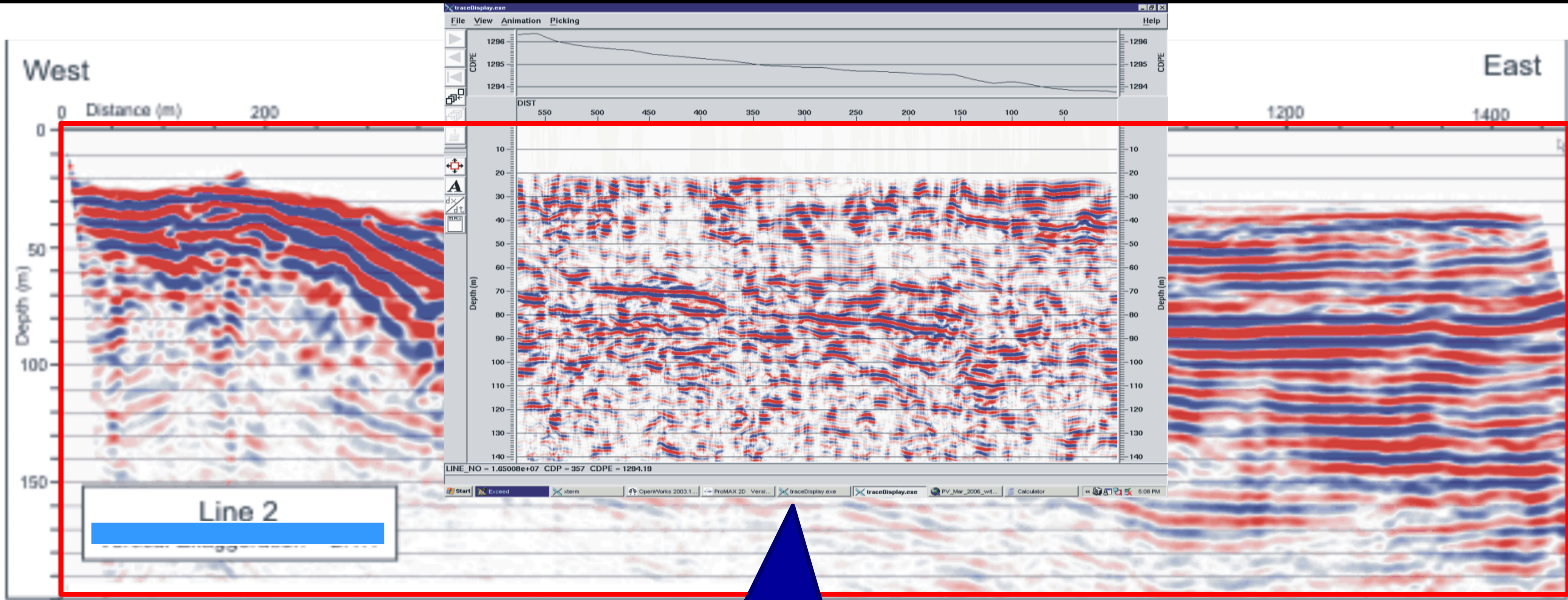

Horizontally polarized shear wave seismic profile yields higher resolution, closer spatial sampling

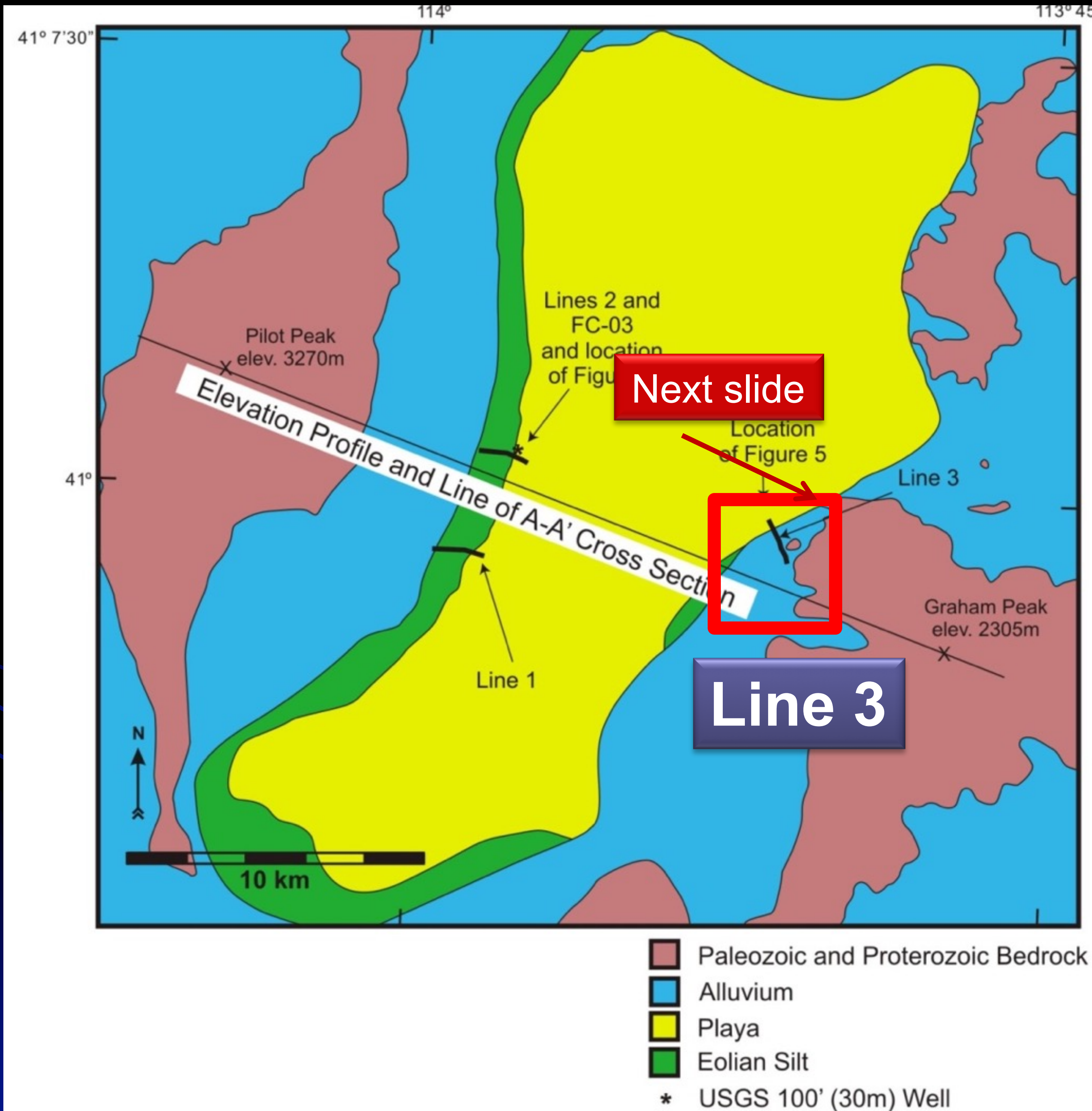

114°
113° 45
41° 7'30"
41°
Pilot Peak
elev. 3270m
Elevation Profile and Line of A-A' Cross Section
Lines 2 and
FC-03
and location
of Figu
Next slide
Location
of Figure 5
Line 3
Graham Peak
elev. 2305m
Line 1
Line 3
N
10 km
Paleozoic and Proterozoic Bedrock
Alluvium
Playa
Eolian Silt
* USGS 100' (30m) Well

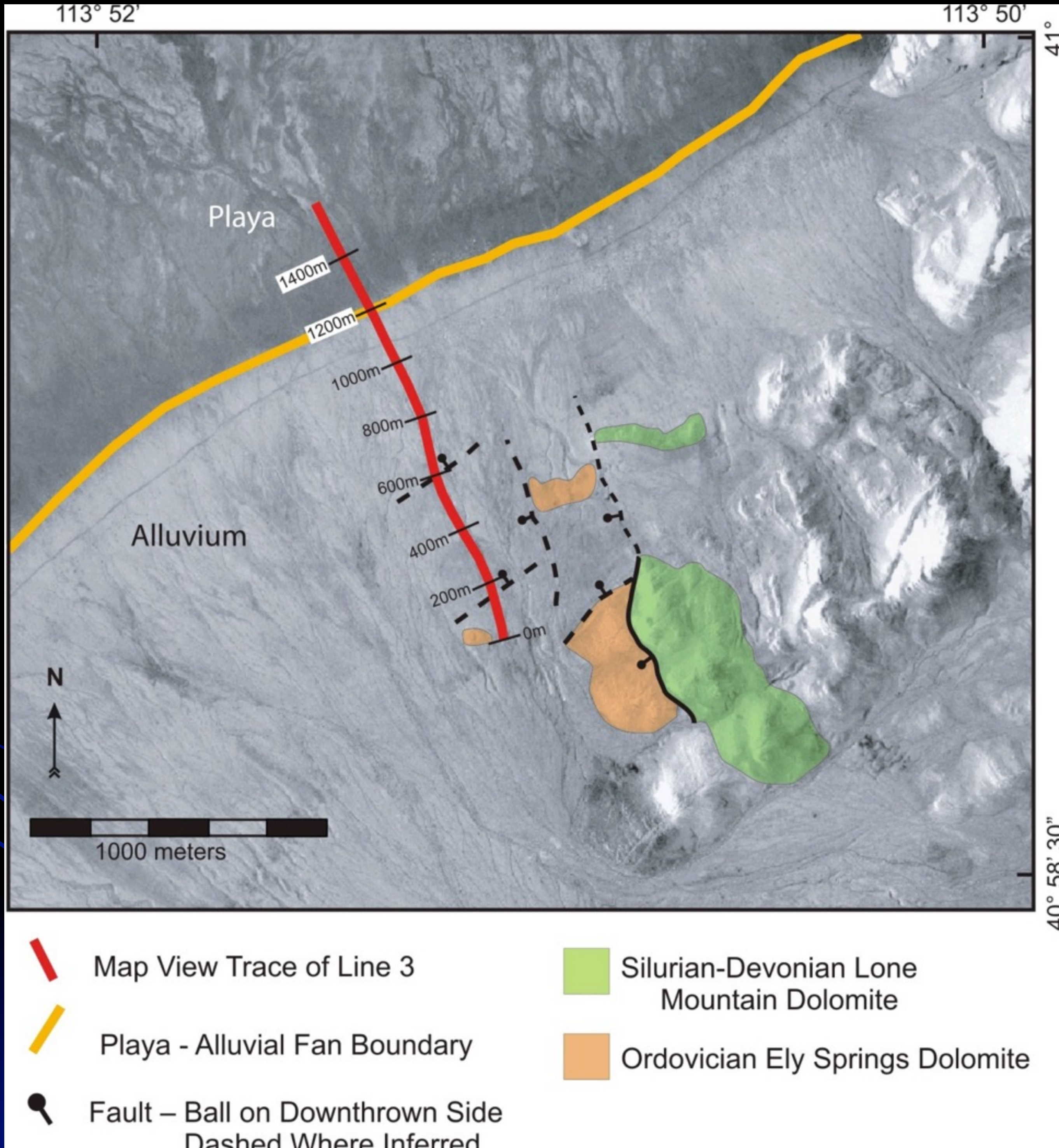

Line 3

East side of Pilot Valley

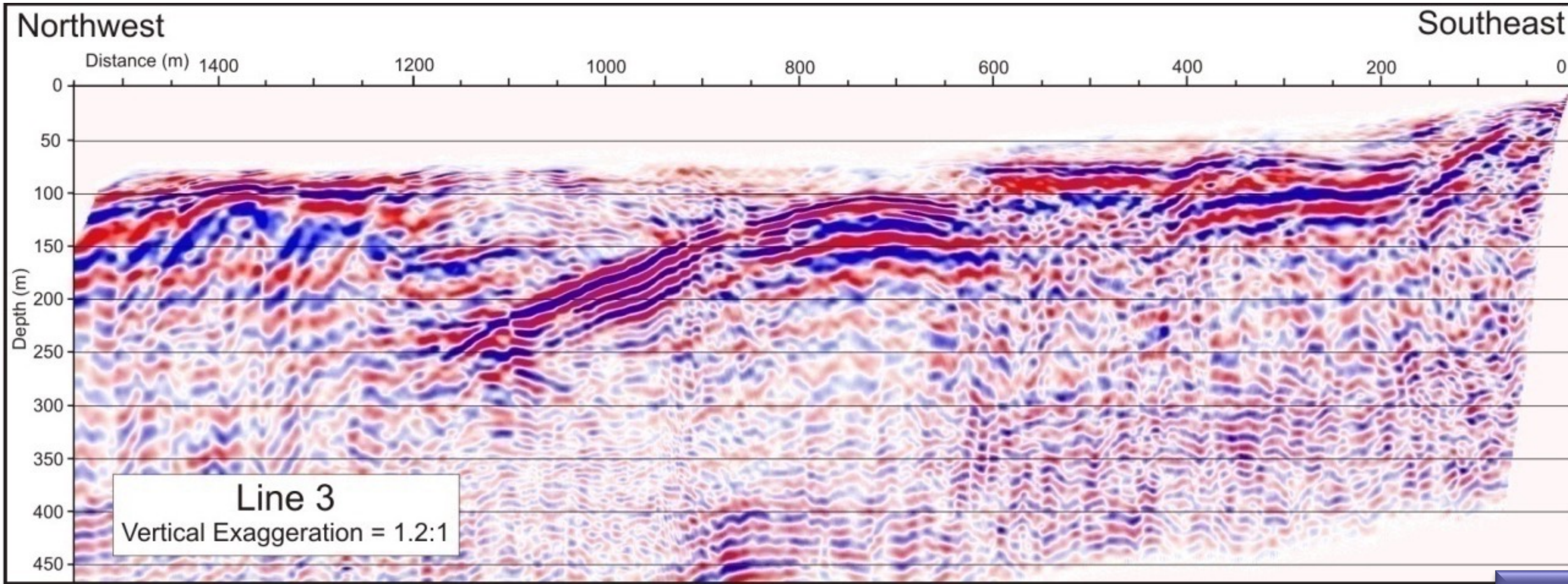
Northwest
Southeast
Distance (m)
1400
1200
1000
800
600
400
200
0
Depth (m)
0
50
100
150
200
250
300
350
400
450
Line 3
Vertical Exaggeration = 1.2:1

Line 3

Line 6

East side of Pilot Valley


Crater Island Range, view looking ESE
Line 6
Duralast

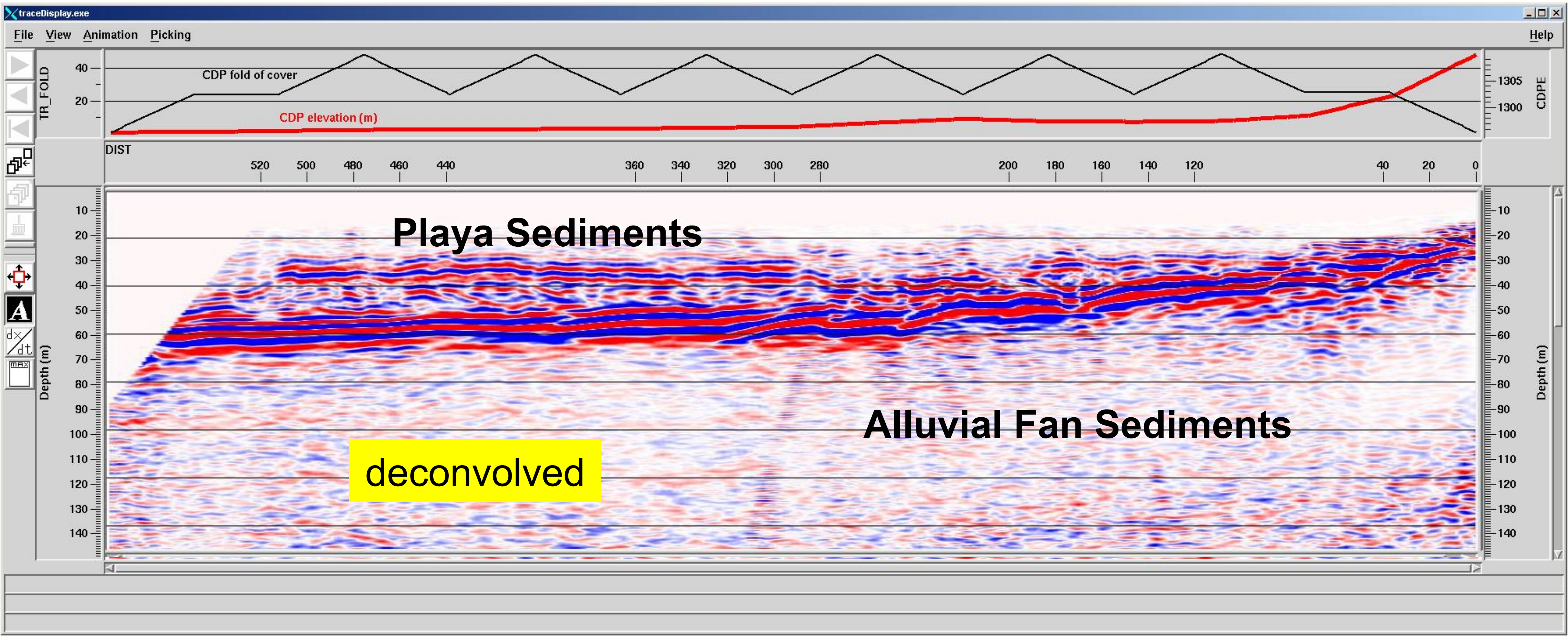
traceDisplay.exe
File
View
Animation
Picking
Help
TR_FOLD
40
20
CDP fold of cover
CDP elevation (m)
1305
1300
CDPE
DIST
520
500
480
460
440
360
340
320
300
280
200
180
160
140
120
40
20
0
Depth (m)
10
20
30
40
50
60
70
80
90
100
110
120
130
140
Playa Sediments
Alluvial Fan Sediments
deconvolved

Index Map

Note location of COCORP Nevada Line 4 and its relation to Pilot Valley

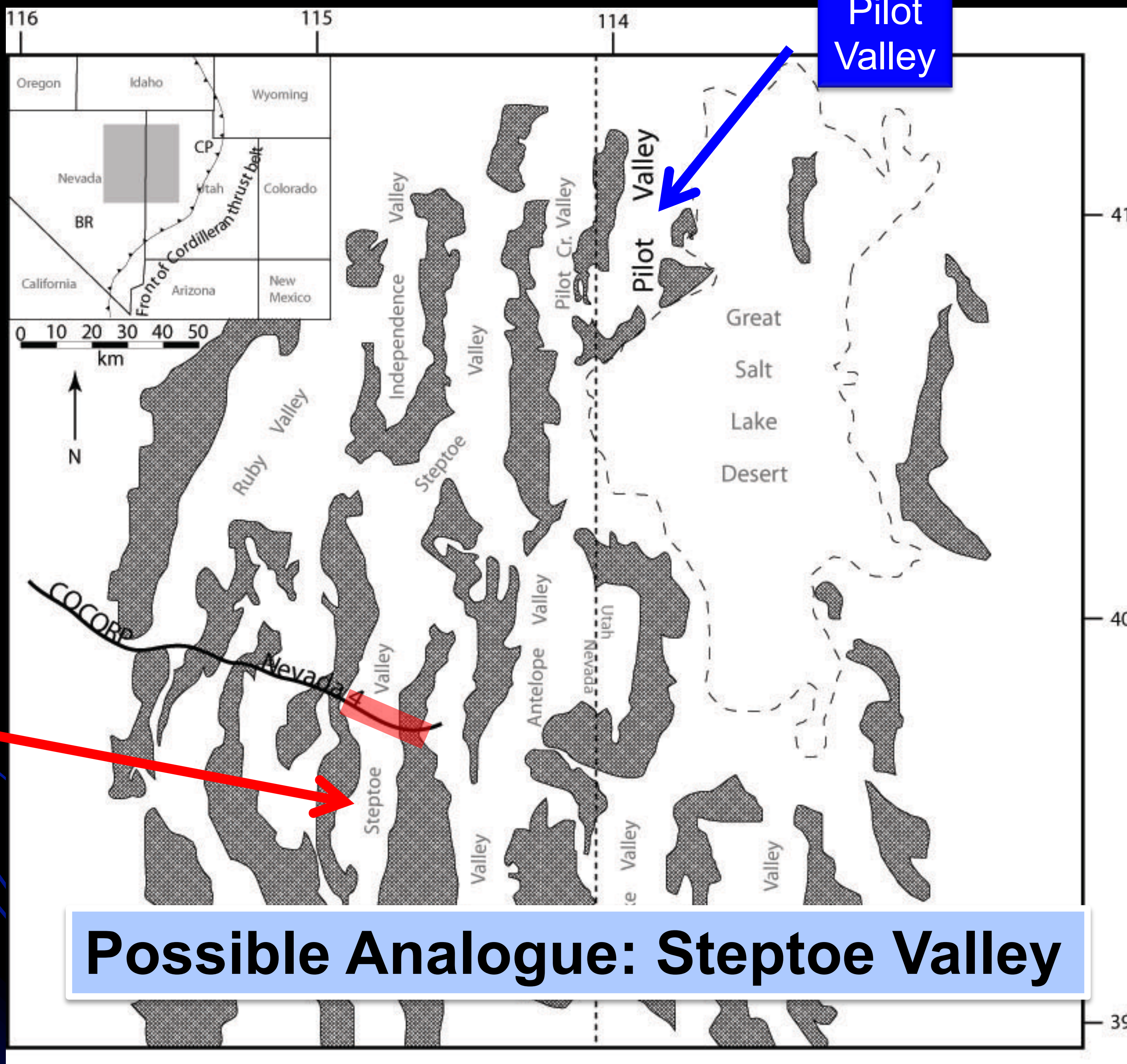

Possible Analogue: Steptoe Valley

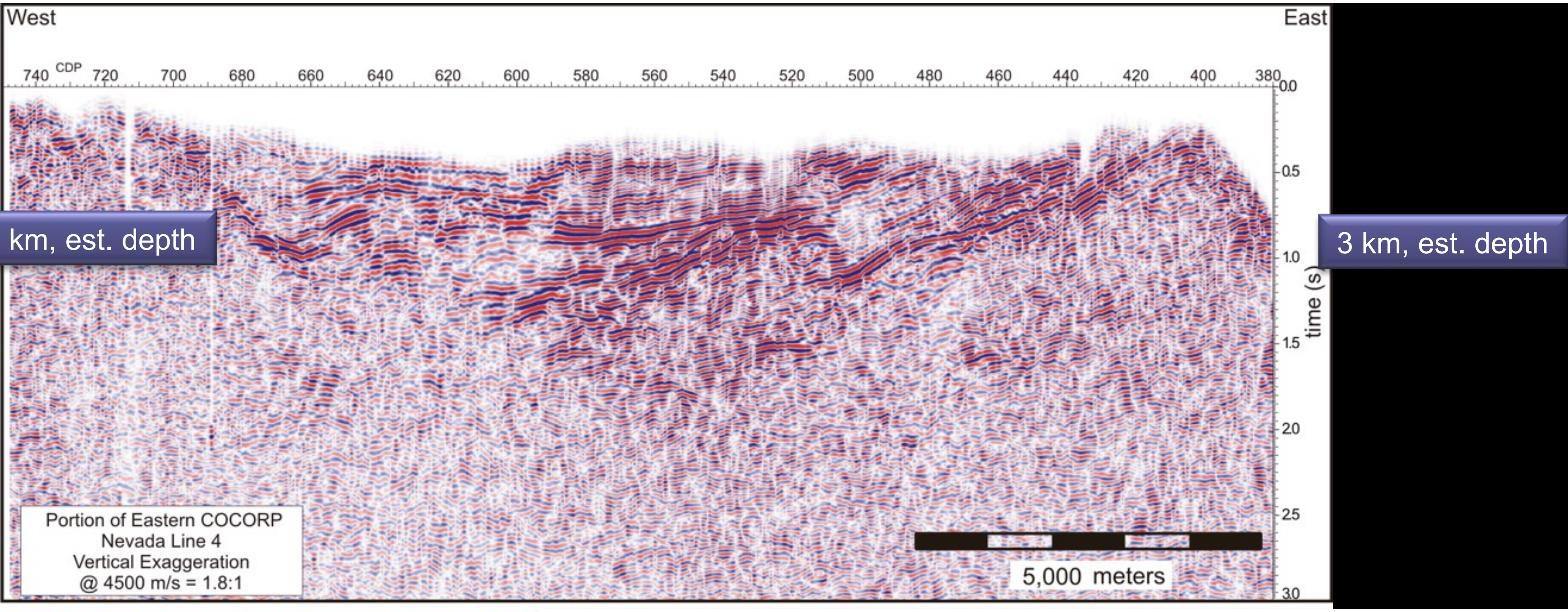

Possible Analogue: Steptoe Valley

Simplified and interpretive cross-section of Pilot Valley

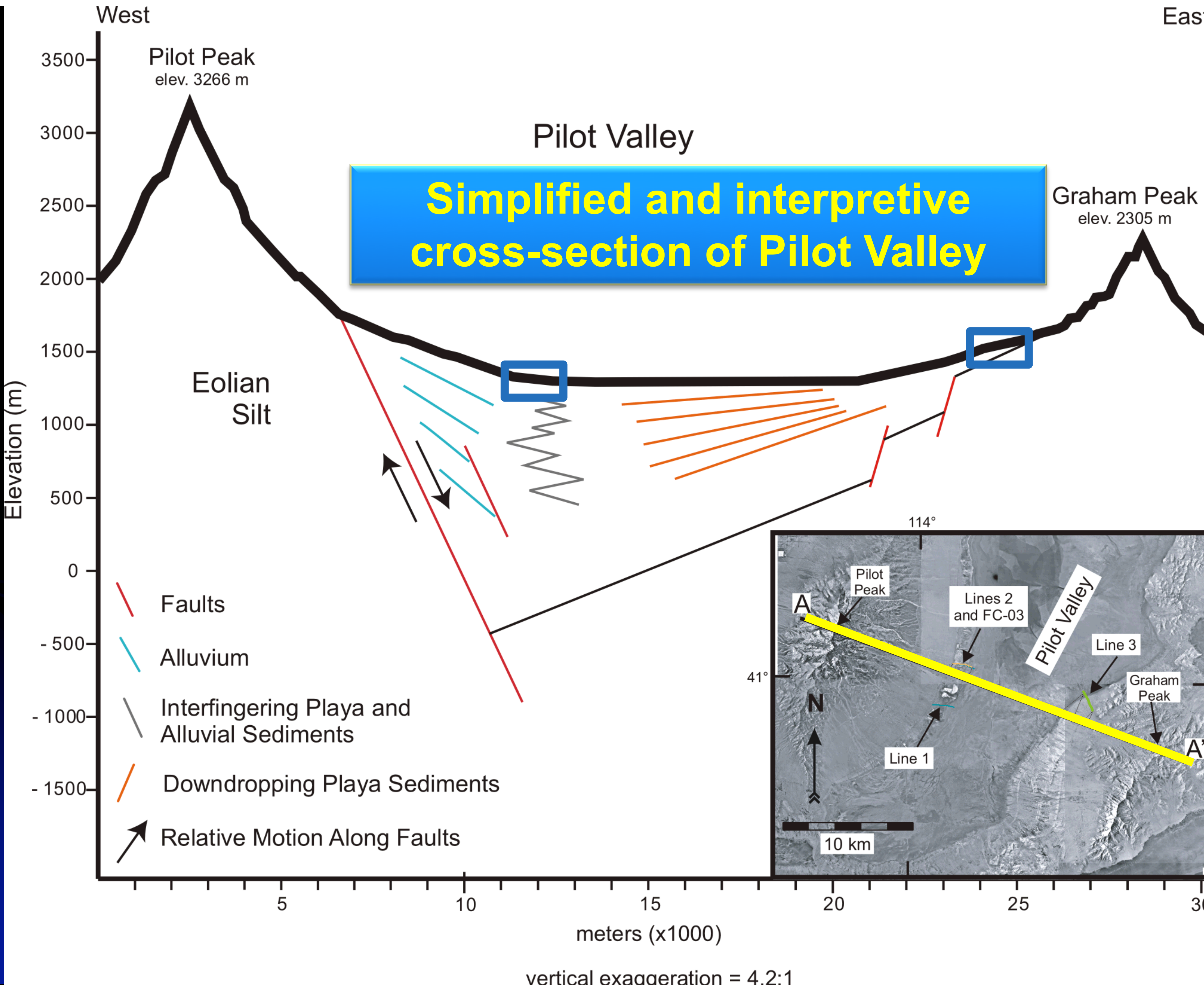

Conclusions/Summary

- Playa-alluvial fan environment ideal for seismic data acquisition
- Significant amount of geological variation from east to west in Pilot Valley, as well as from south to north
- Playa sediments onlap alluvial fan on west side, along the line of springs of Pilot Valley
- Apparent absence of faults along point of spring discharge on the west side of Pilot Valley
- Heavily faulted structural environment along the east side, nearer bedrock outcrops

acknowledgements

HALLIBURTON Solving challenges.™

IHS

DIATOM, MINERALOGICAL, AND GEOCHEMICAL PROXIES PROVIDE A NEW VIEW OF THE PALEOLIMNOLOGY OF LAKE BONNEVILLE (WESTERN USA) AS OBSERVED IN THE RESTRICTED PILOT VALLEY SUB-BASIN

Stephen Nelson and Kevin Rey

Department of Geological Sciences, Brigham Young University, Provo, UT 84604

Corresponding author: (Nelson) oxygen.isotope@gmail.com

ABSTRACT

Between 30 and 13 ka, pluvial Lake Bonneville (western US) rivaled Lake Michigan in terms of surface area, depth, and volume, and its marls represent an important archive of climate and paleolimnological processes. We report the first diatom record anywhere in the basin for the complete Bonneville lake cycle from core taken in the Pilot Valley sub-basin, Utah. Combined with geochemical and mineralogical records, the proxies represent closed-basin transgression, the catastrophic Bonneville flood, open-lake conditions, and closed-basin regression and desiccation cycles.

Diatoms record pH and salinity, and vary from alkalibiontic/brackish (early transgression), alkaliphilous/fresh-brackish (deep lake) and back to alkalibiontic/brackish (late regression) conditions, and mesotraphentic to eutraphentic nutrient loads. The Bonneville flood produced freshening recorded in marls by a decrease in the ratio of carbonate minerals to quartz, a decrease in Sr, and minima in carbon and oxygen isotopes after the flood.

Pennate diatoms reveal passage through and back into the euphotic zone during transgression and regression by sufficient light penetration through the water column to support an active benthos. As such, the base of the euphotic zone (~35 m depth?) can be established through time. However, establishing time-depth relations in the core required an unusual model-based approach because reservoir effects and detrital carbonate influence ^{14}C activities in marl and detrital Th makes U-series ages impractical.

Restriction and evaporation within the Pilot Valley arm of Lake Bonneville during times of shallow water produced high endogenic carbonate production, an order of magnitude higher than during deep-water phases. This is revealed in the age-depth model, carbon and oxygen isotopes, and relative diatom abundances, requiring a major re-evaluation of the position of the previously published Bonneville flood horizon within the sediments of Pilot Valley. In summary, lacustrine sediments from restricted arms of large pluvial lakes may vary significantly from complementary records from an open basin.

This content is a PDF version of the author's PowerPoint presentation.

Diatom, mineralogical, and geochemical proxies provide a new view of the paleolimnology of Lake Bonneville (western USA) as observed in the restricted Pilot Valley sub-basin

◊ Stephen T. Nelson & Kevin A. Rey, Dept. of Geological Sciences, Brigham Young University, Provo, UT 84602

JOURNAL OF QUATERNARY SCIENCE (2005) **20**(1) 3–19

Published online in Wiley InterScience (www.interscience.wiley.com). DOI: 10.1002/jqs.889

Shoreline Tufa and Tufaglomerate from Pleistocene Lake Bonneville, Utah, USA: stable isotopic and mineralogical records of lake conditions, processes, and climate

STEPHEN T. NELSON,[1]* M. JAY WOOD,[1] ALAN L. MAYO,[1] DAVID G. TINGEY[1] and DENNIS EGGETT[2]
[1] Department of Geology, S389 ESC, Brigham Young University, Provo, UT 84602, USA
[2] Department of Statistics, 230 TMCB, Brigham Young University, Provo, UT 84602, USA

Nelson, S. T., Wood, M. J., Mayo, A. L., Tingey, D. G. and Eggett, D. 2005. Shoreline Tufa and Tufaglomerate from Pleistocene Lake Bonneville, Utah, USA: stable isotopic and mineralogical records of lake conditions, processes, and climate. *J. Quaternary Sci.*, **Vol. 20** pp. 3–19. ISSN 0267-8179.

Received 22 February 2004; Revised 2 August 2004; Accepted 5 August 2004

Outline

- ◊ Overview of Lake Bonneville
- ◊ Geochemistry & mineralogy of Bonneville marls from core PV-15 as well as shoreline tufas
- ◊ What diatoms add to the story
  - "diatoms: helping you breathe since the Jurassic"
  - biogenic silica cell walls
- ◊ Conclusions

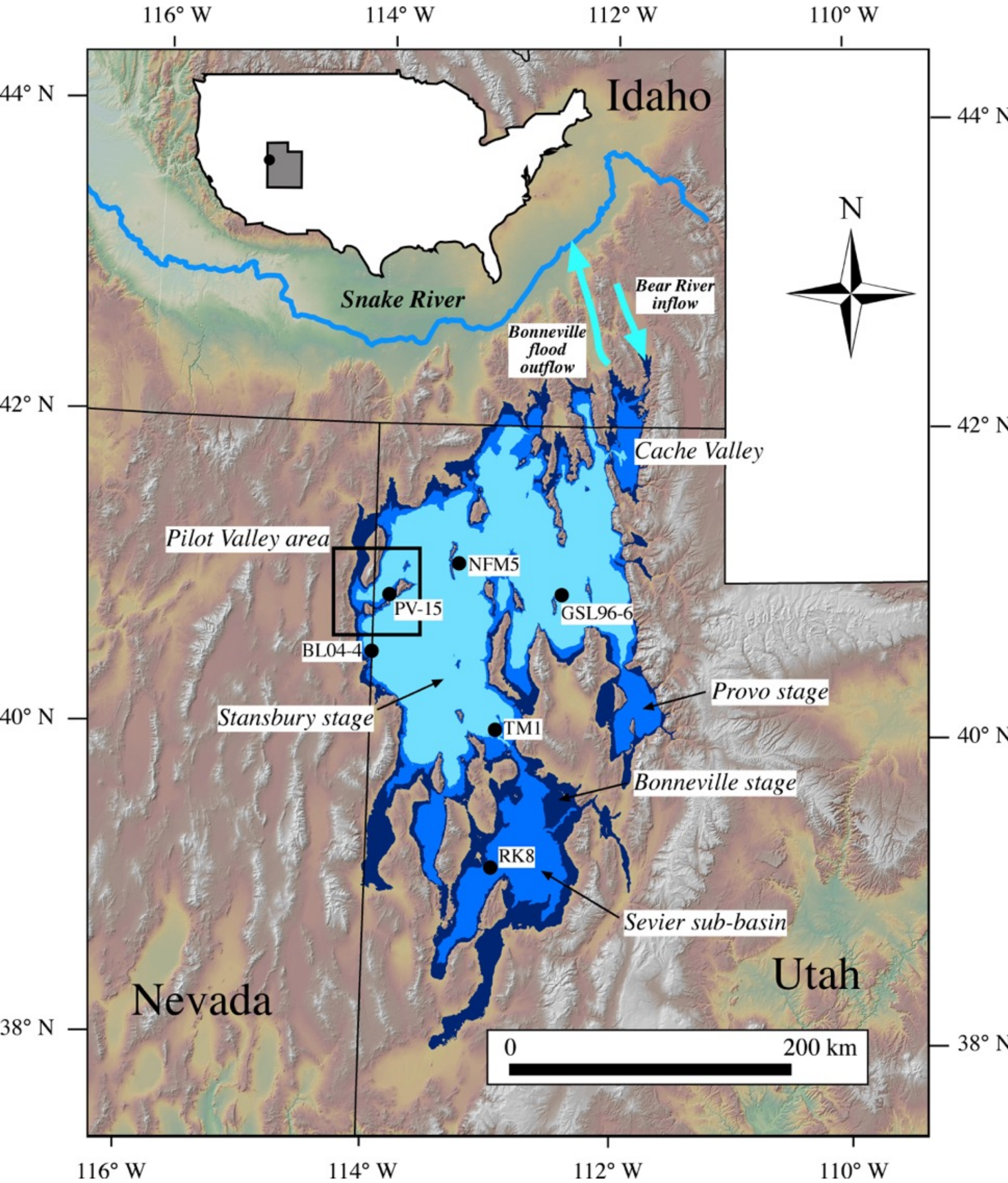

Lake Bonneville

- ◊ Similar surface area, depth, and volume to modern Lake Michigan
- ◊ 390 hits in GEOREF with Lake Bonneville in ***title***

Lake Bonneville

Lake Bonneville

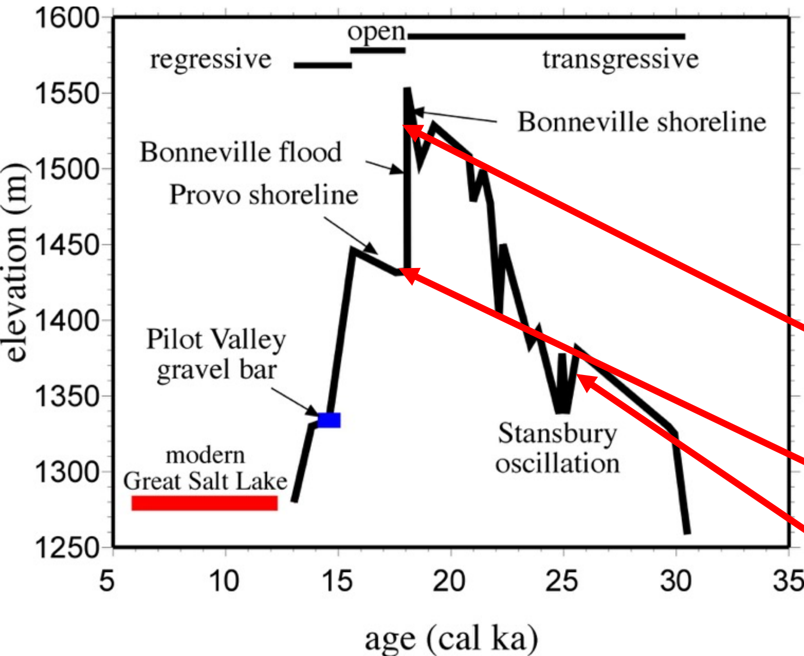

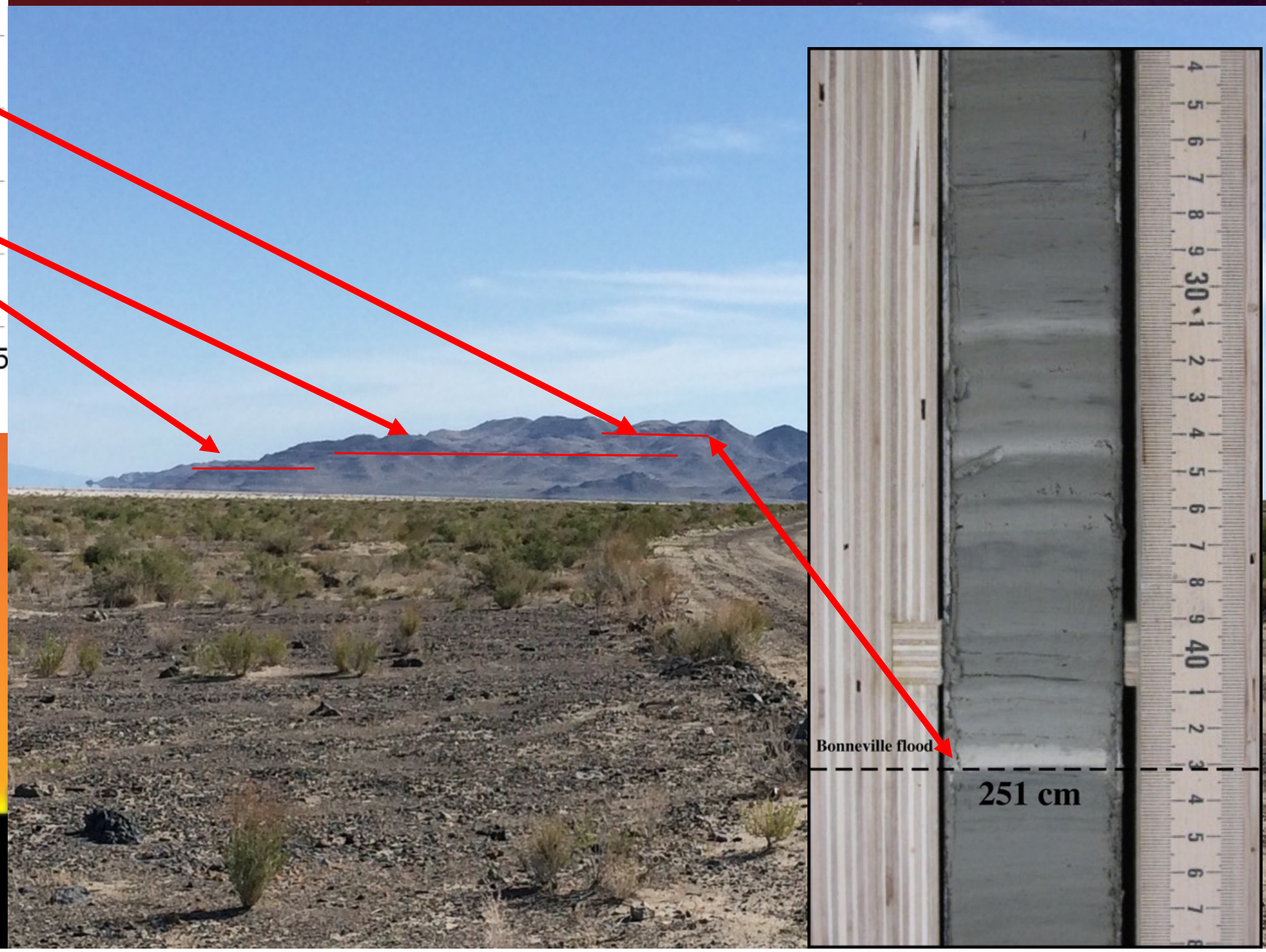

modified from Oviatt (2015)

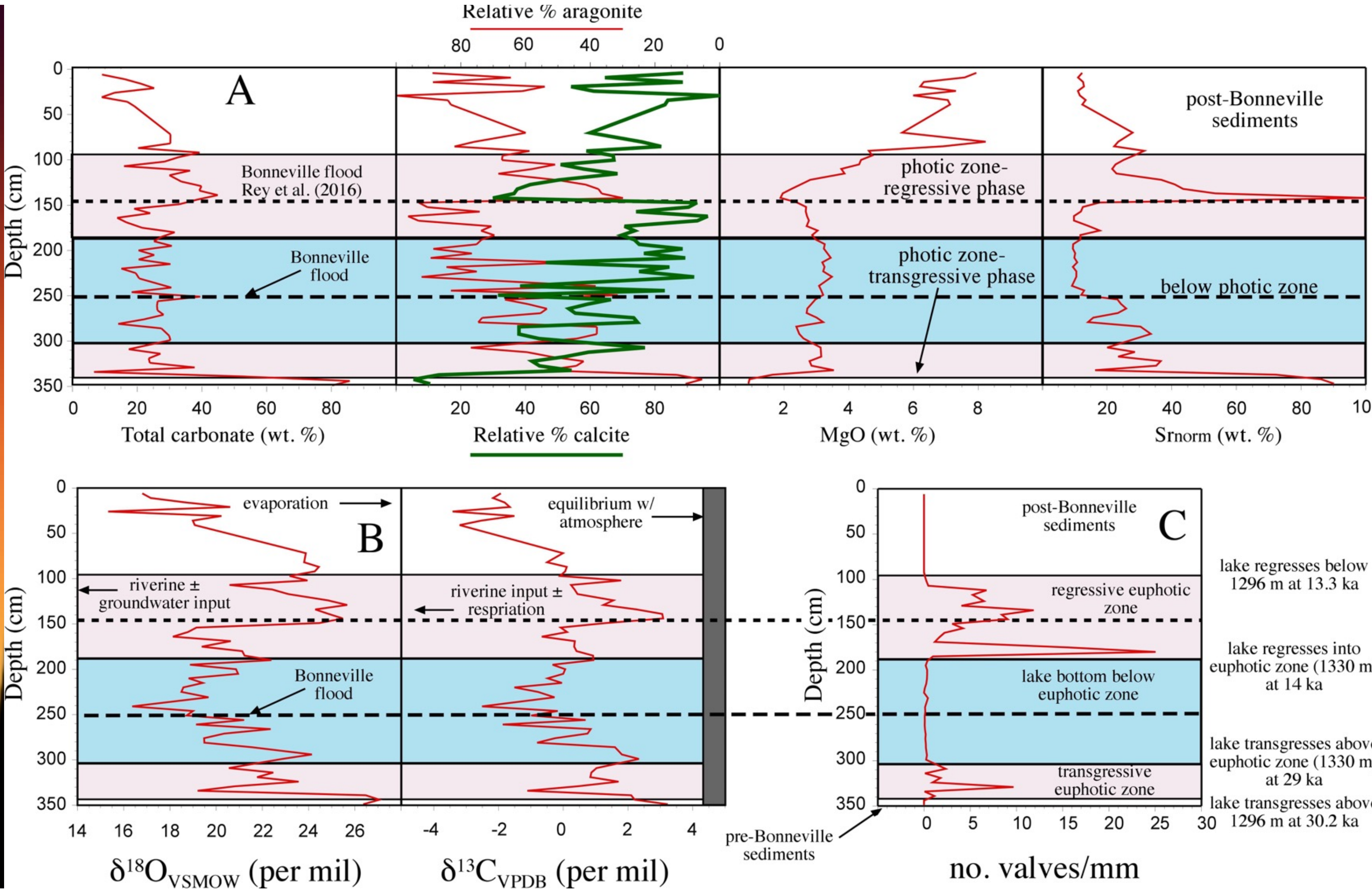
Relative % aragonite
A
post-Bonneville sediments
Bonneville flood Rey et al. (2016)
photic zone-regressive phase
Bonneville flood
photic zone-transgressive phase
below photic zone
Depth (cm)
Total carbonate (wt. %)
Relative % calcite
MgO (wt. %)
Srnorm (wt. %)
evaporation
equilibrium w/ atmosphere
B
riverine ± groundwater input
riverine input ± respriation
Bonneville flood
$\delta^{18}O_{VSMOW}$ (per mil)
$\delta^{13}C_{VPDB}$ (per mil)
pre-Bonneville sediments
post-Bonneville sediments
C
regressive euphotic zone
lake bottom below euphotic zone
transgressive euphotic zone
no. valves/mm
lake regresses below 1296 m at 13.3 ka
lake regresses into euphotic zone (1330 m) at 14 ka
lake transgresses above euphotic zone (1330 m) at 29 ka
lake transgresses above 1296 m at 30.2 ka

Net water balance

net flux > Bear River

Table 4. Modern long-term fluxes of Utah streams as they enter the Bonneville basin (NWIS, 2017b). The Bear River discharge was measured at Corrine, Utah. Thus, it captures the modern fluxes of the Bear River and all its tributaries in Cache Valley.

Stream	Discharge ($m^3 s^{-1}$)
Bear River	77.0
Weber River	34.8
Ogden River	6.1
Provo River	10.0
American Fork River	3.9
Little Cottonwood Creek	2.3
Sevier River	17.1
Hobble Creek	3.3
Salt Creek	2.0
Red Butte Creek	0.4
Spanish Fork River	14.8
Beaver River	4.0

Lake Bonneville

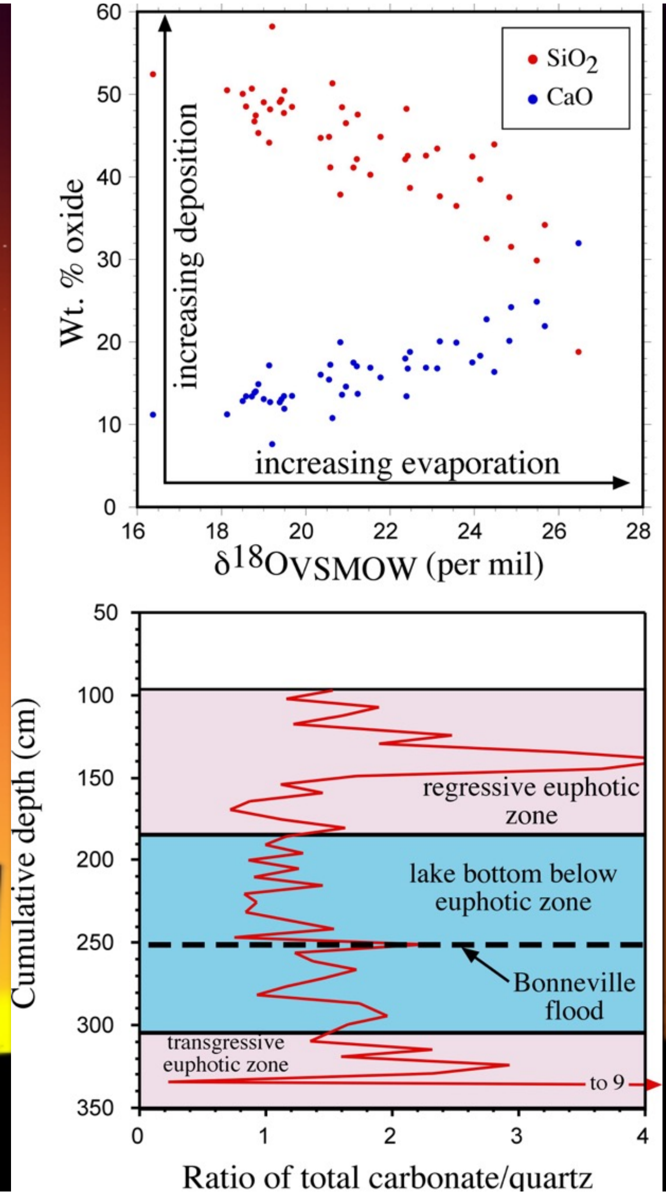

Lake Bonneville

extensive atmos. exchange—
small res. effect?

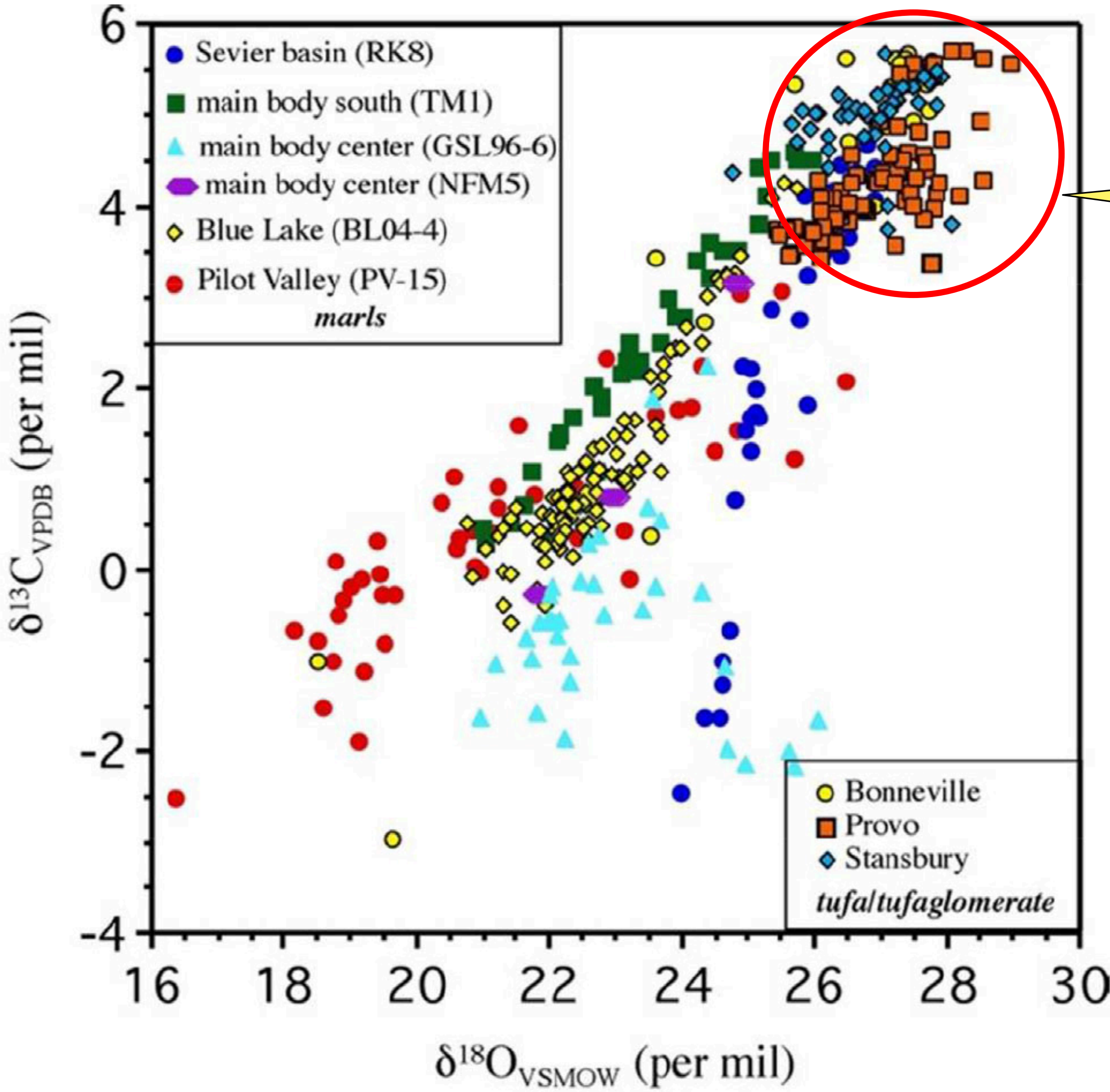

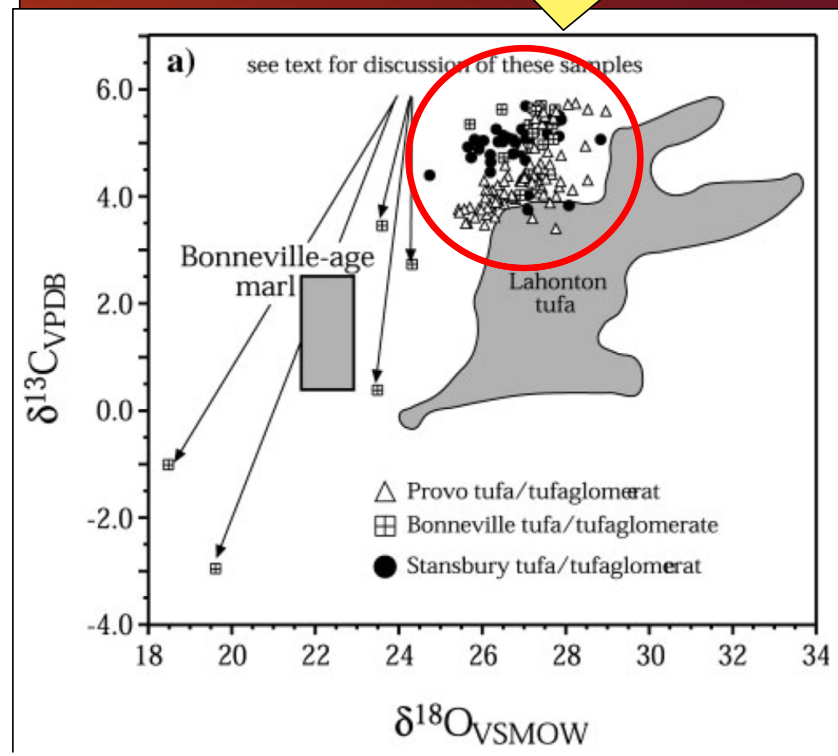

Lake Bonneville

5 to 85% evaporation

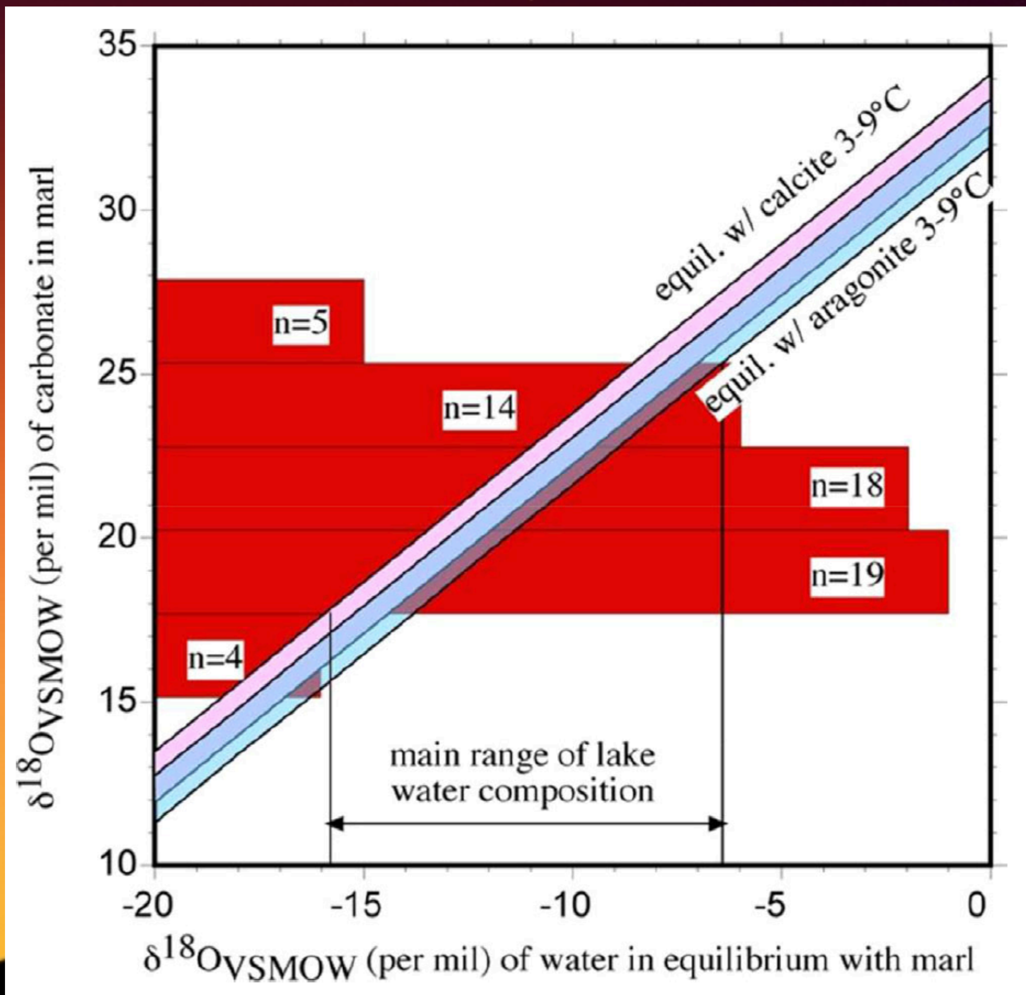

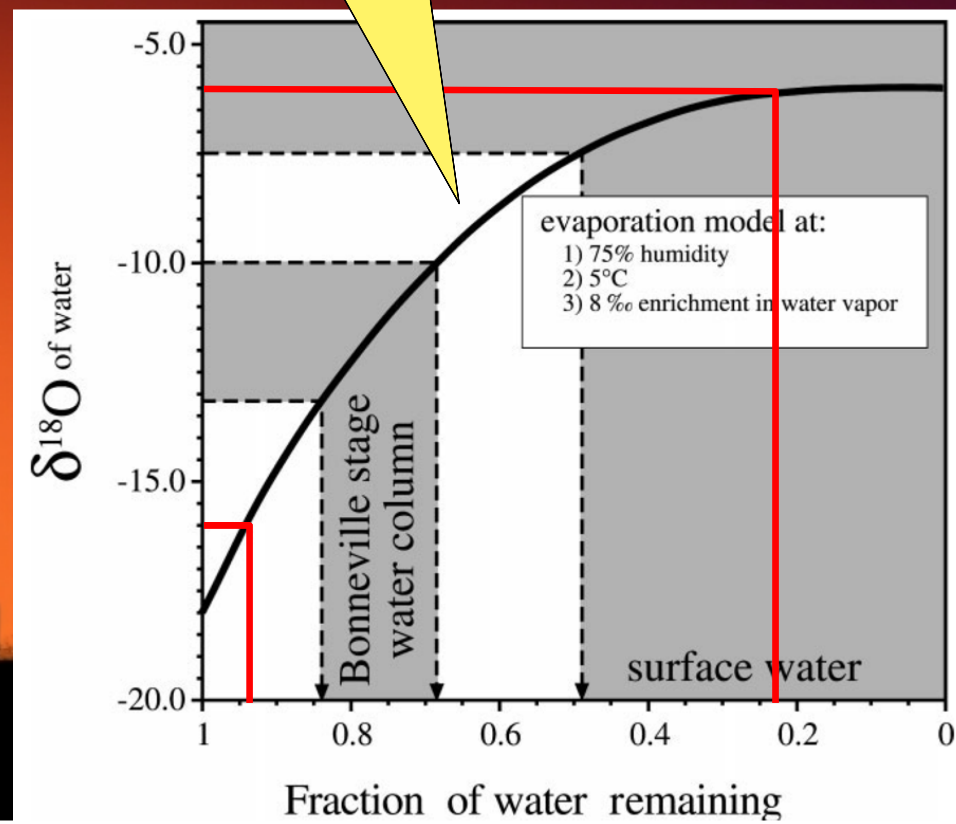

Lake Bonneville

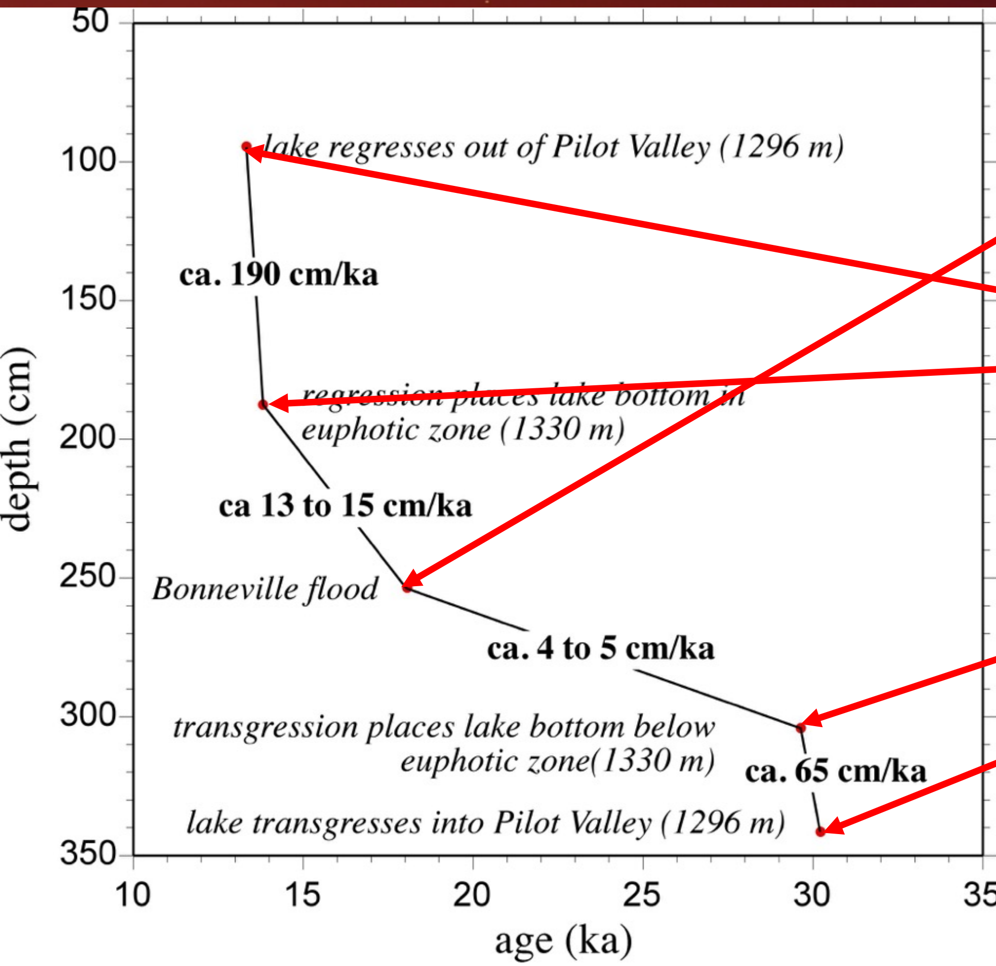

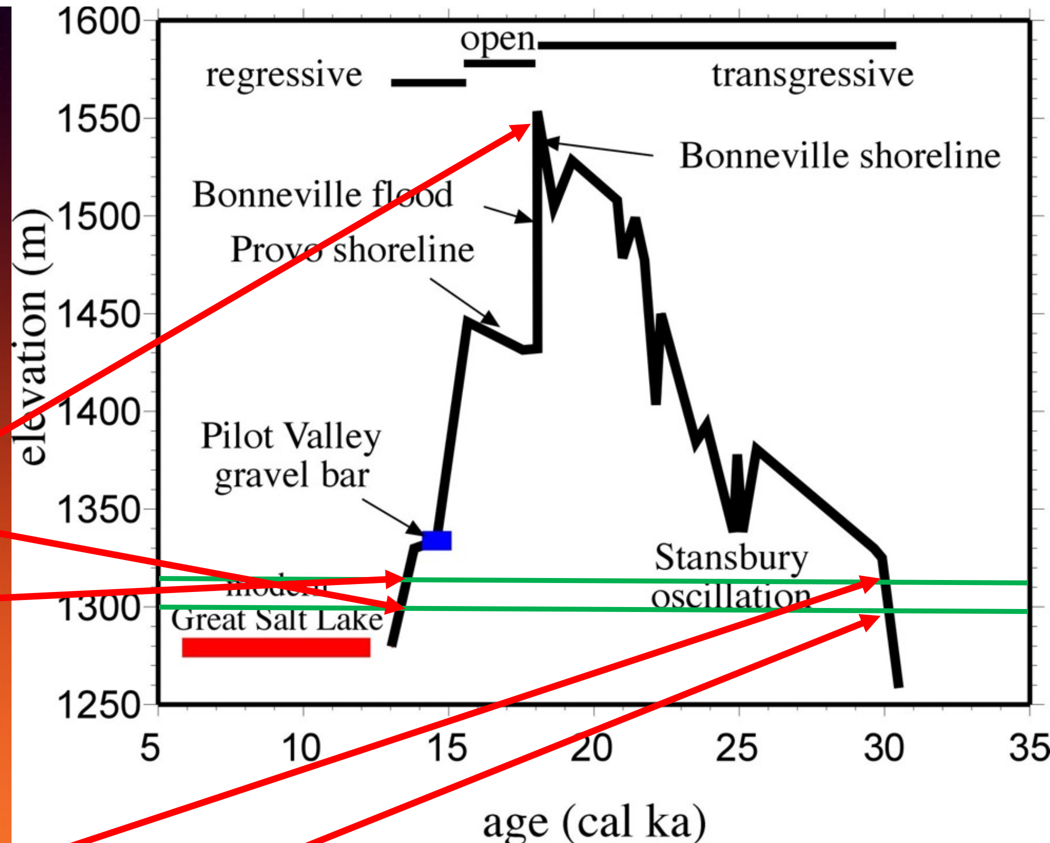

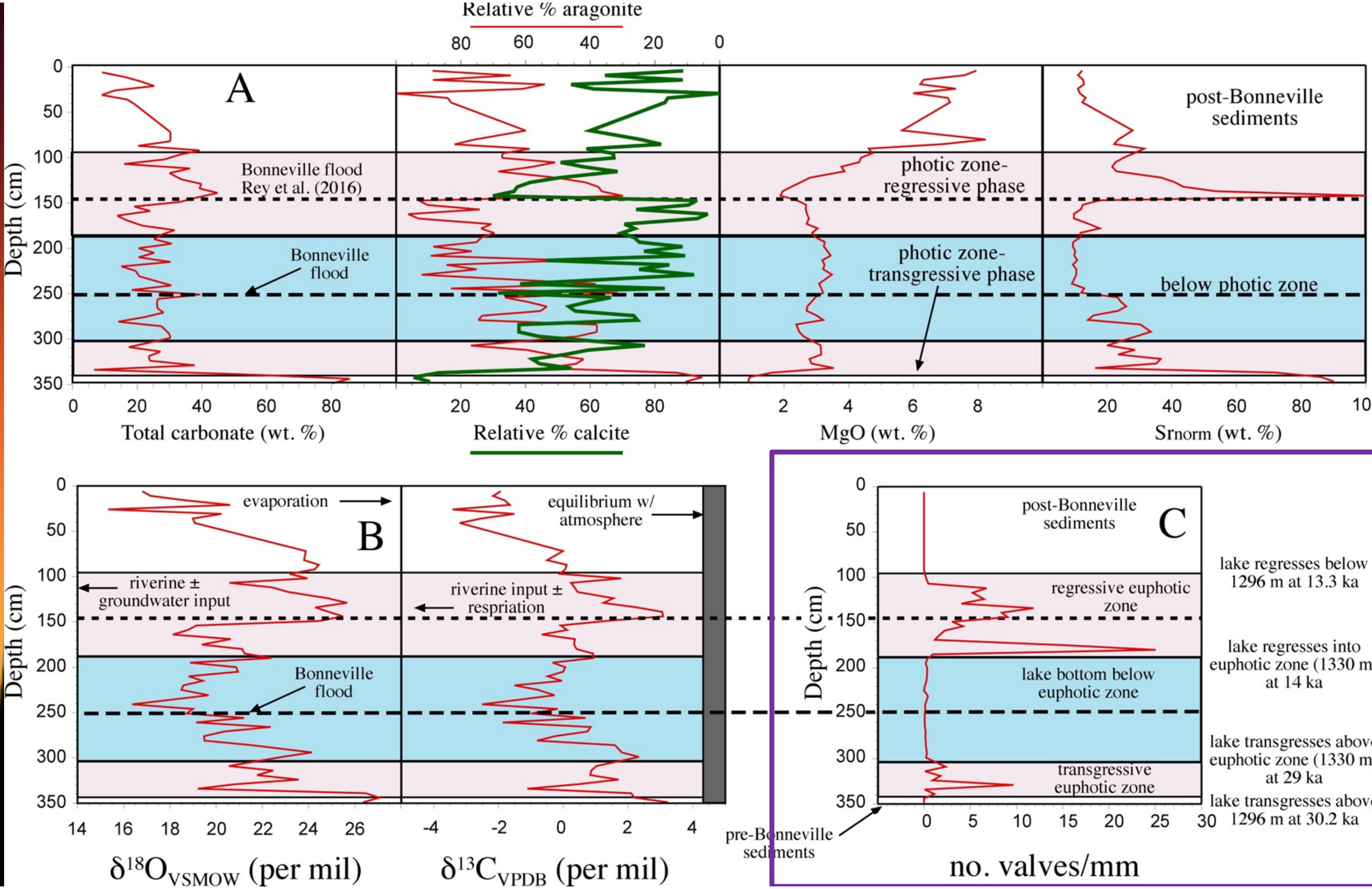

Relative % aragonite
A
Depth (cm)
Bonneville flood
Rey et al. (2016)
Bonneville flood
photic zone-
regressive phase
photic zone-
transgressive phase
post-Bonneville
sediments
below photic zone
Total carbonate (wt. %)
Relative % calcite
MgO (wt. %)
Srnorm (wt. %)
B
evaporation
riverine ±
groundwater input
Bonneville
flood
equilibrium w/
atmosphere
riverine input ±
respriation
δ18OVSMOW (per mil)
δ13CVPDB (per mil)
C
post-Bonneville
sediments
regressive euphotic
zone
lake bottom below
euphotic zone
transgressive
euphotic zone
lake regresses below
1296 m at 13.3 ka
lake regresses into
euphotic zone (1330 m)
at 14 ka
lake transgresses above
euphotic zone (1330 m)
at 29 ka
lake transgresses above
1296 m at 30.2 ka
pre-Bonneville
sediments
no. valves/mm

Tufa

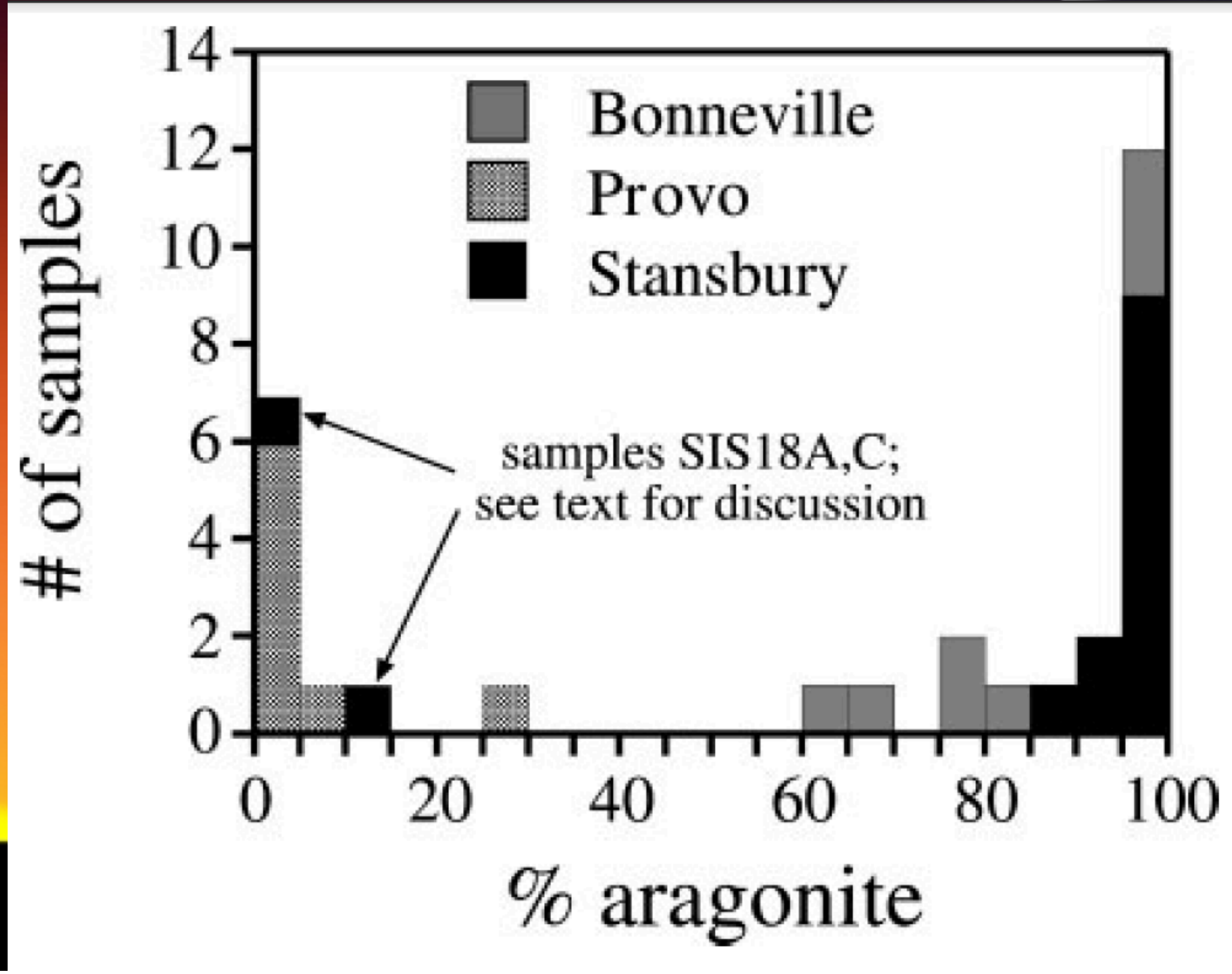

Bonneville
Provo
Stansbury
samples SIS18A,C;
see text for discussion
# of samples
% aragonite
0
2
4
6
8
10
12
14
0
20
40
60
80
100

Restriction

when the lake was shallow, PV was a marl factory

- surface area connection
  - Bonneville stage: 17%
  - Stansbury stage: 8%
  - 1315 m reference: 7%
- cross sectional areas of sills
  - Provo: 1.2×10^{6} m^2
  - Stansbury: 3.9×10^{5} m^2
  - 1315 m reference: 1.3×10^{5} m^2

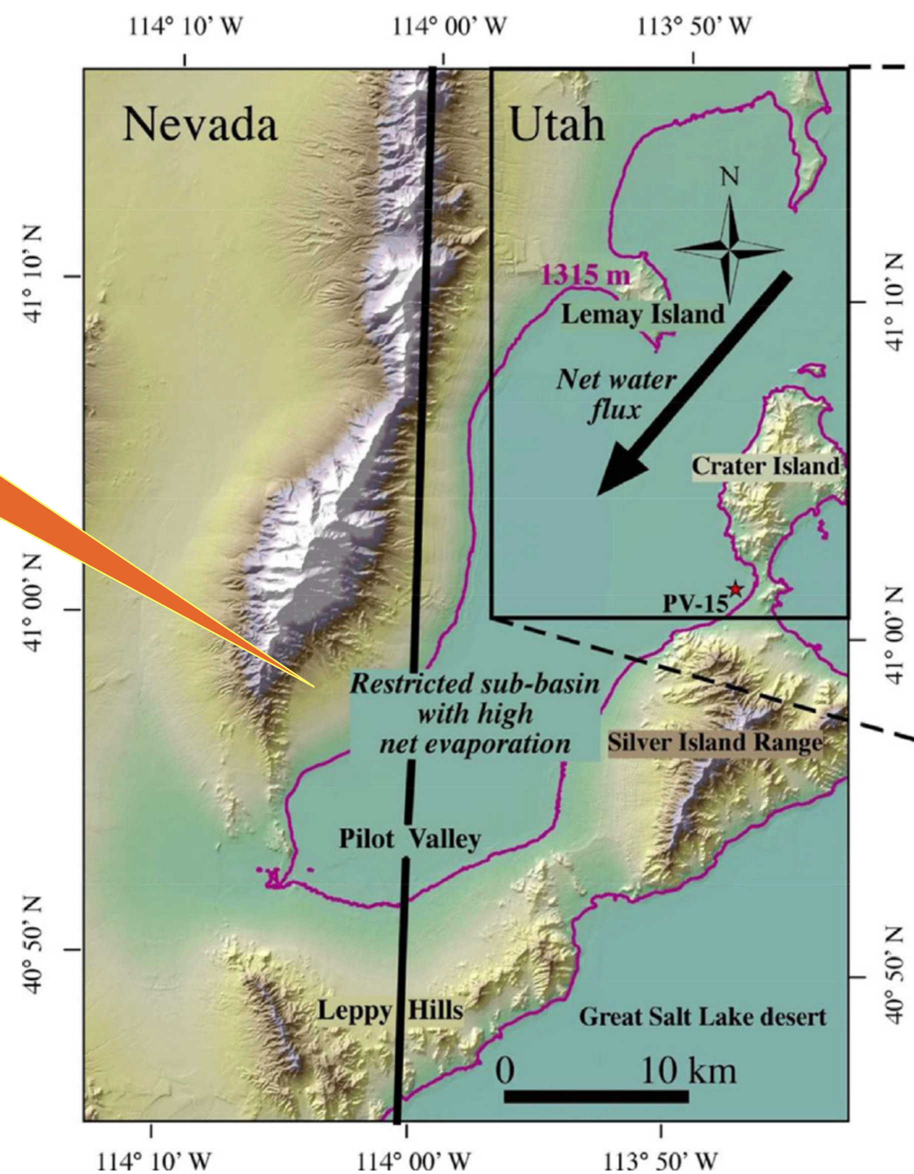

Lake Bonneville

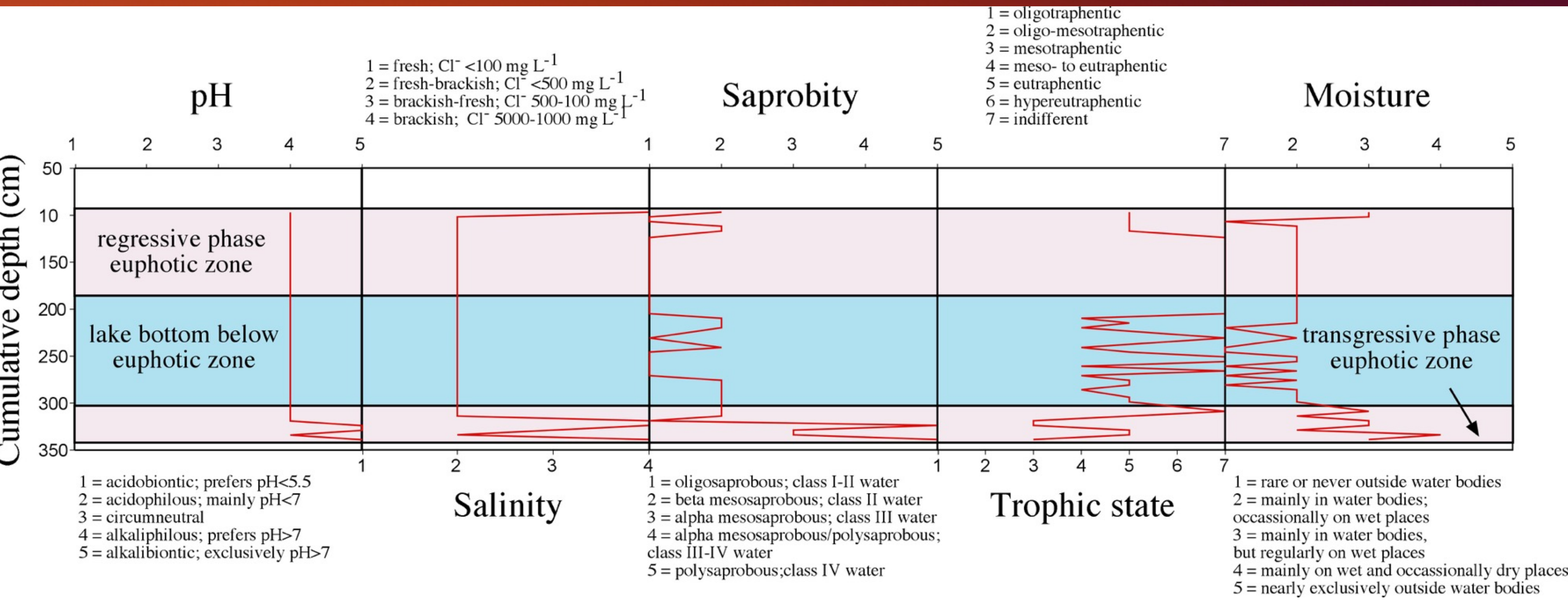

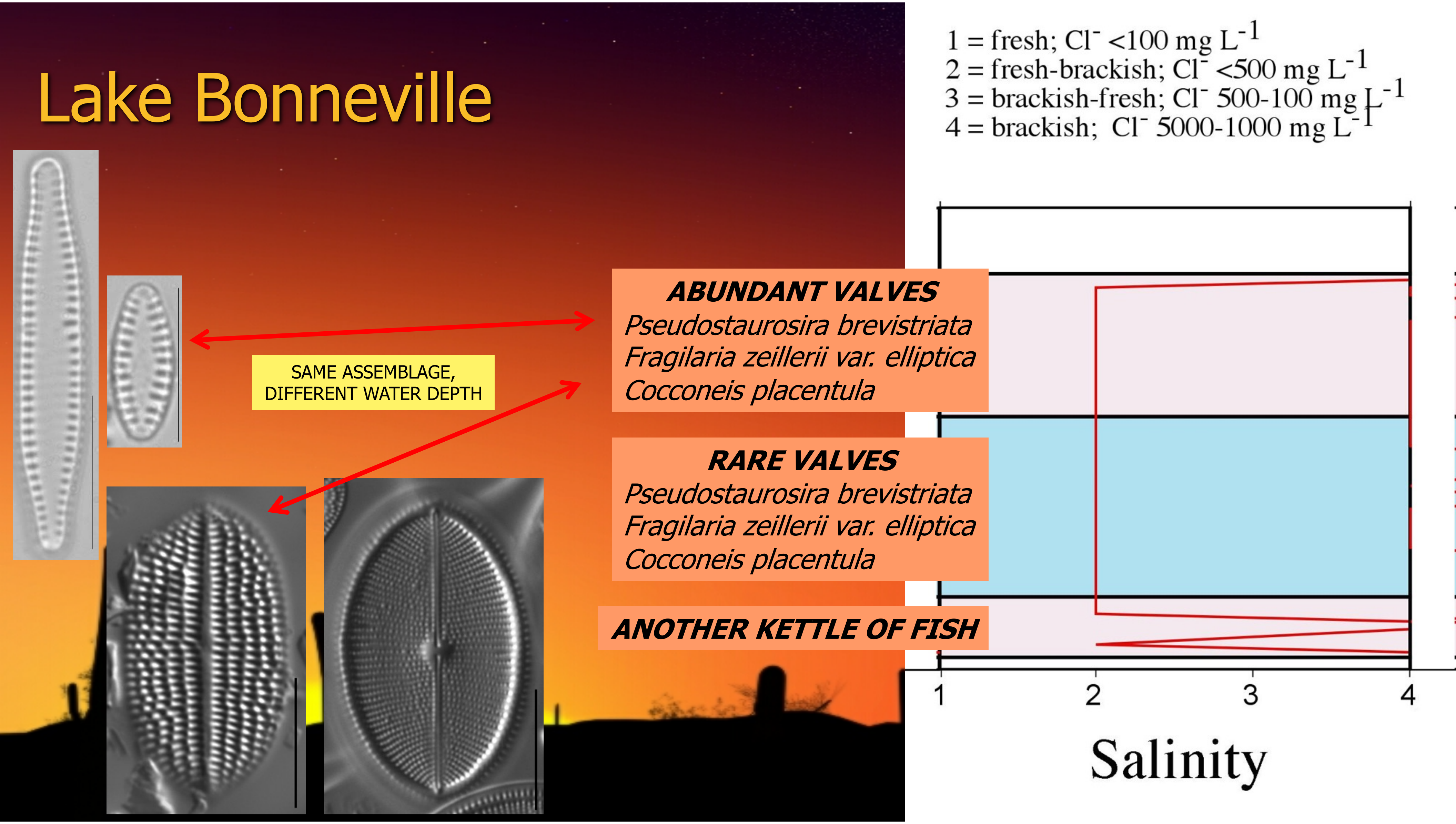
Lake Bonneville
SAME ASSEMBLAGE, DIFFERENT WATER DEPTH
ABUNDANT VALVES
Pseudostaurosira brevistriata
Fragilaria zeillerii var. elliptica
Cocconeis placentula
RARE VALVES
Pseudostaurosira brevistriata
Fragilaria zeillerii var. elliptica
Cocconeis placentula
ANOTHER KETTLE OF FISH
1 = fresh; Cl⁻ <100 mg L-1
2 = fresh-brackish; Cl⁻ <500 mg L-1
3 = brackish-fresh; Cl⁻ 500-100 mg L-1
4 = brackish; Cl⁻ 5000-1000 mg L-1
1
2
3
4
Salinity

Lake Bonneville

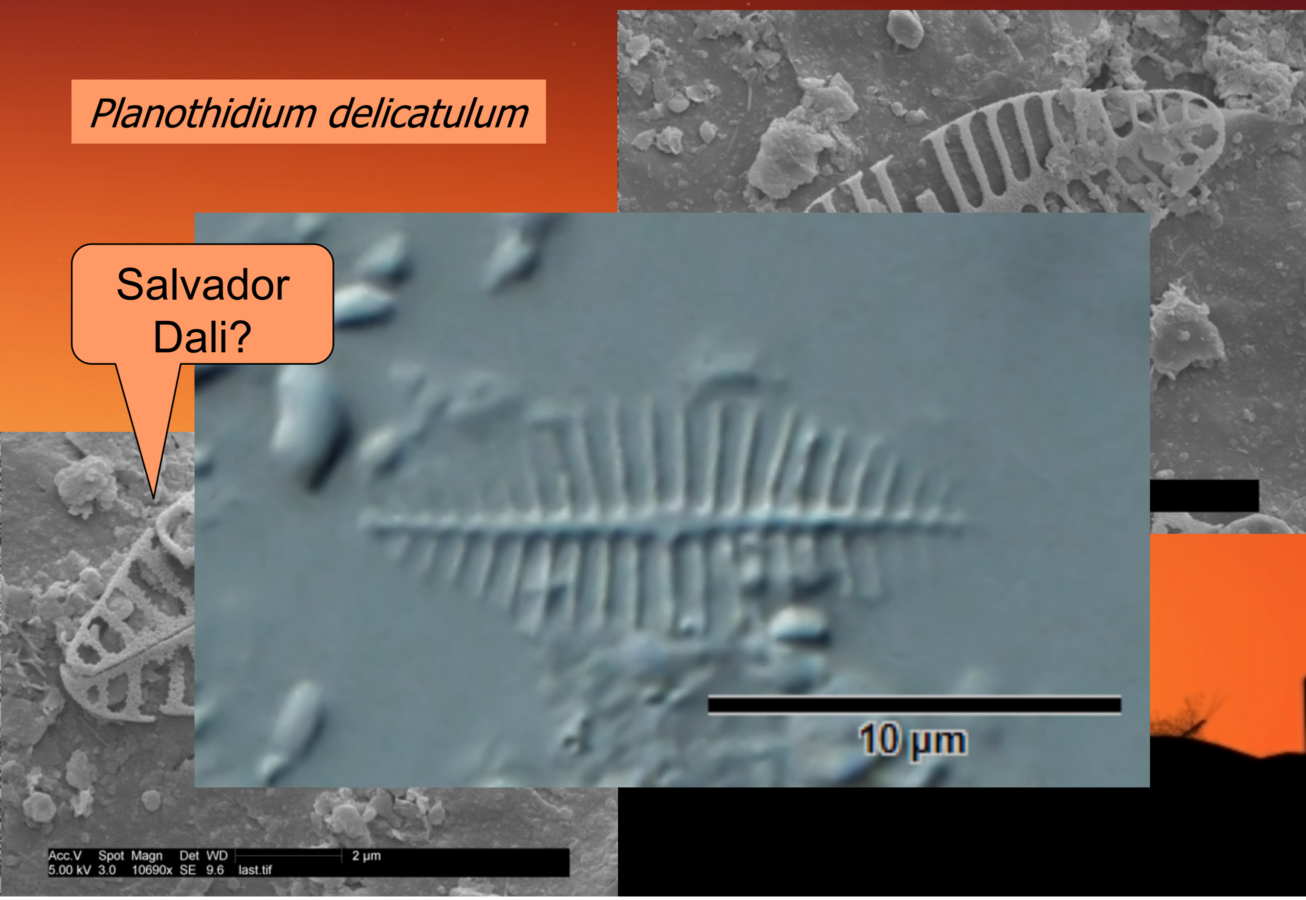

1 = fresh; Cl^- <100 mg L^{-1}
2 = fresh-brackish; Cl^- <500 mg L^{-1}
3 = brackish-fresh; Cl^- 500-100 mg L^{-1}
4 = brackish; Cl^- 5000-1000 mg L^{-1}

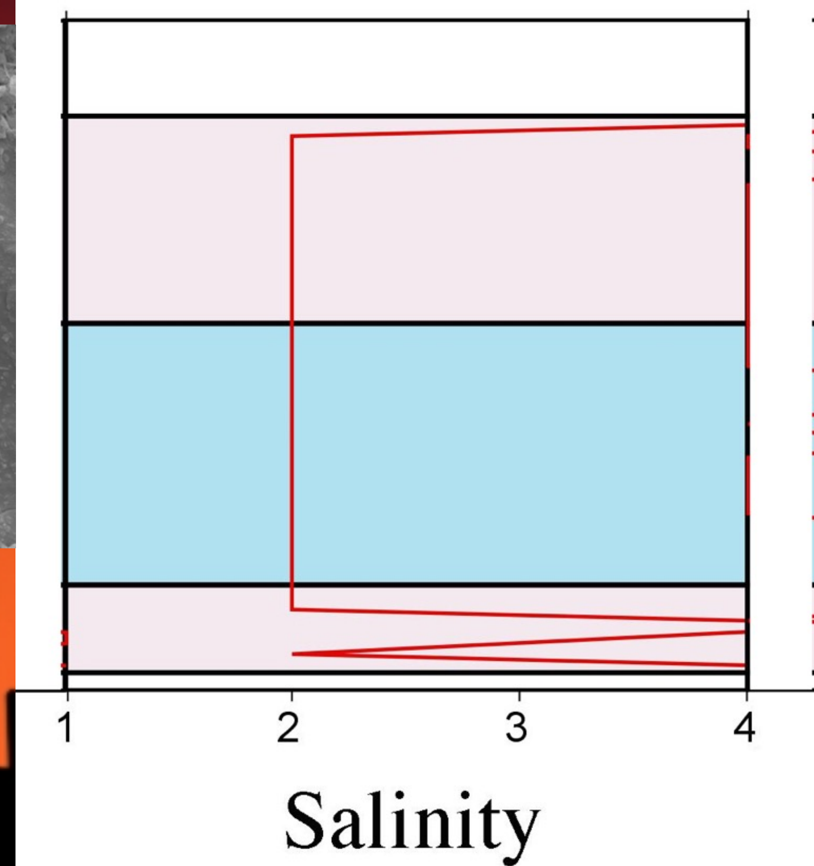

Lake Bonneville

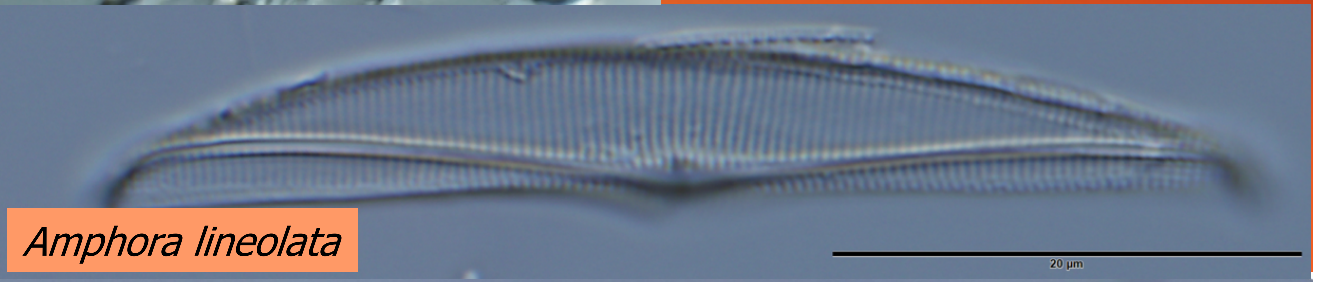

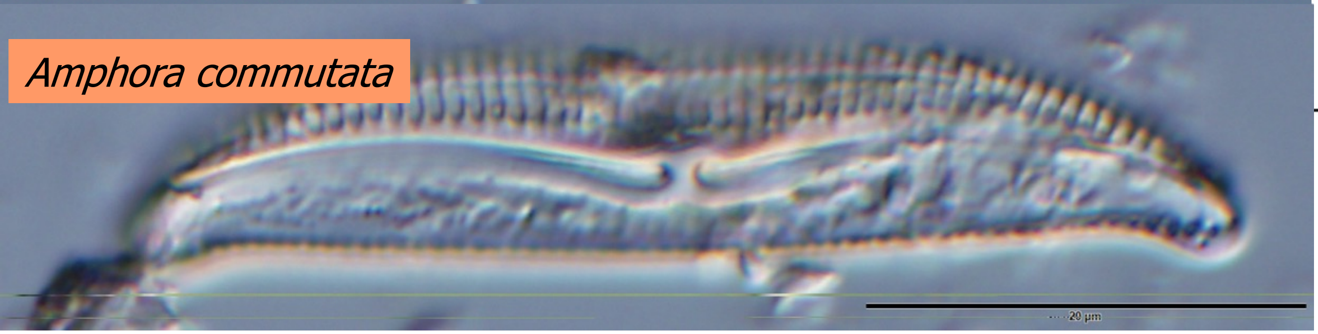

1 = fresh; Cl^- <100 mg L^{-1}
2 = fresh-brackish; Cl^- <500 mg L^{-1}
3 = brackish-fresh; Cl^- 500-100 mg L^{-1}
4 = brackish; Cl^- 5000-1000 mg L^{-1}

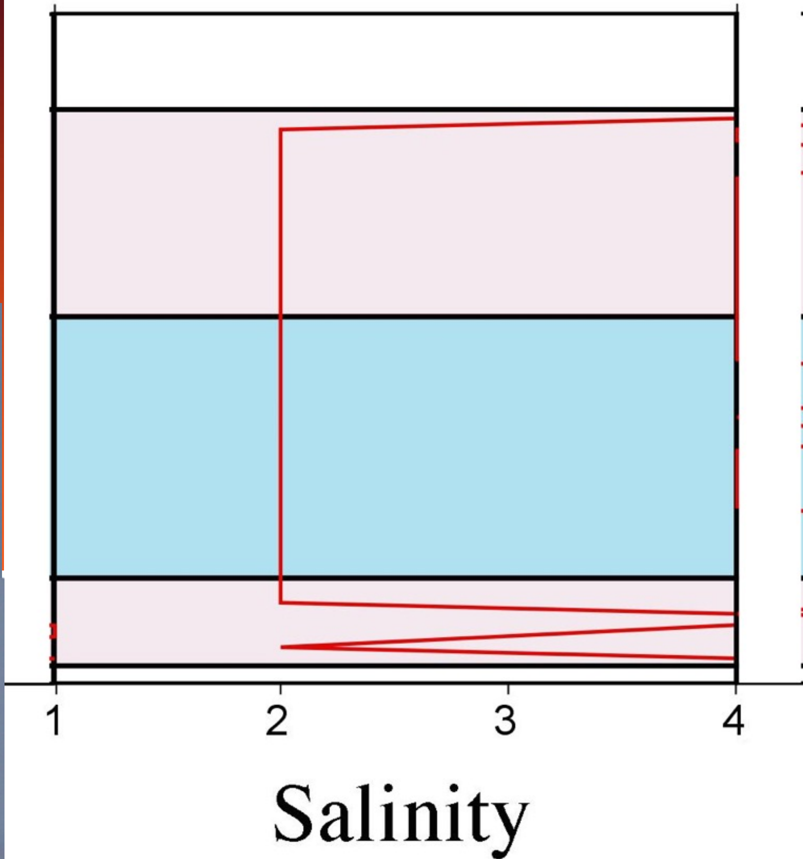

Lake Bonneville

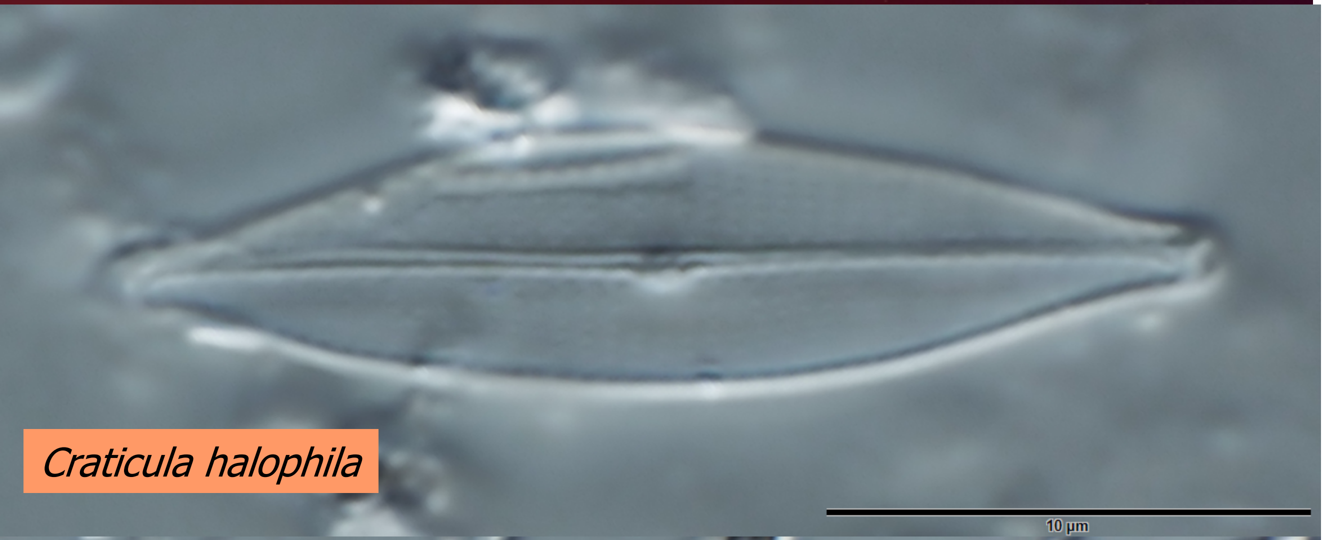

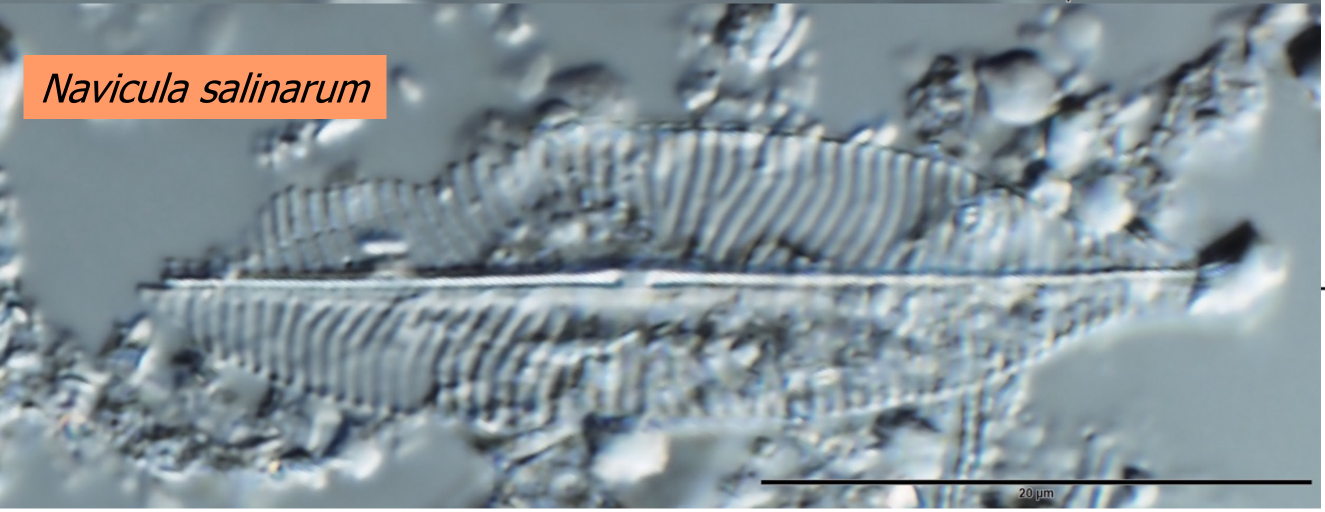

1 = fresh; Cl^- <100 mg L^{-1}
2 = fresh-brackish; Cl^- <500 mg L^{-1}
3 = brackish-fresh; Cl^- 500-100 mg L^{-1}
4 = brackish; Cl^- 5000-1000 mg L^{-1}

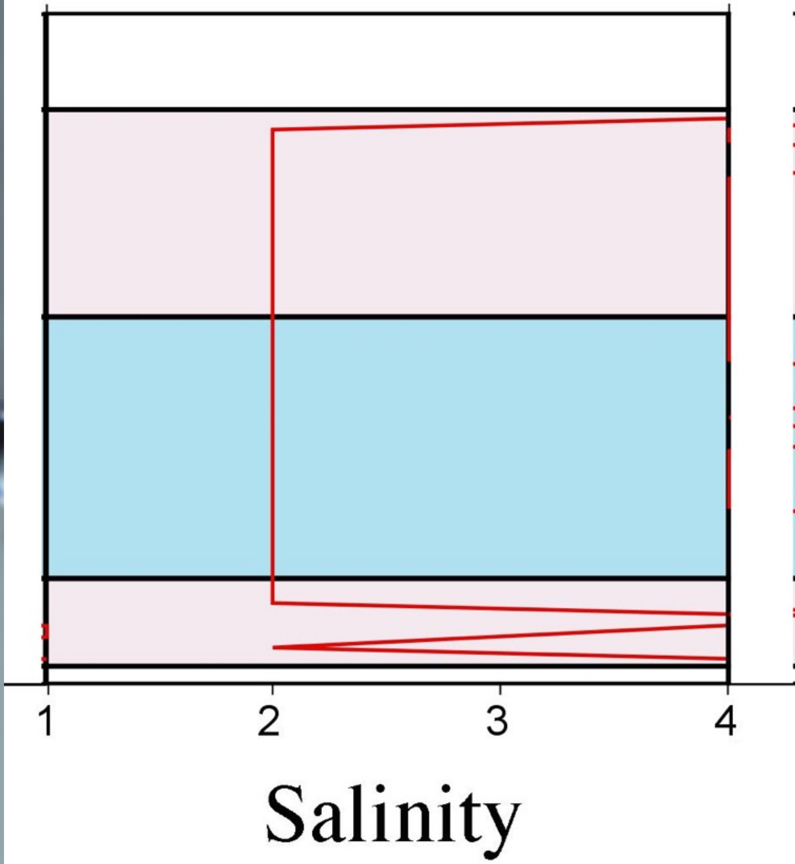

Lake Bonneville

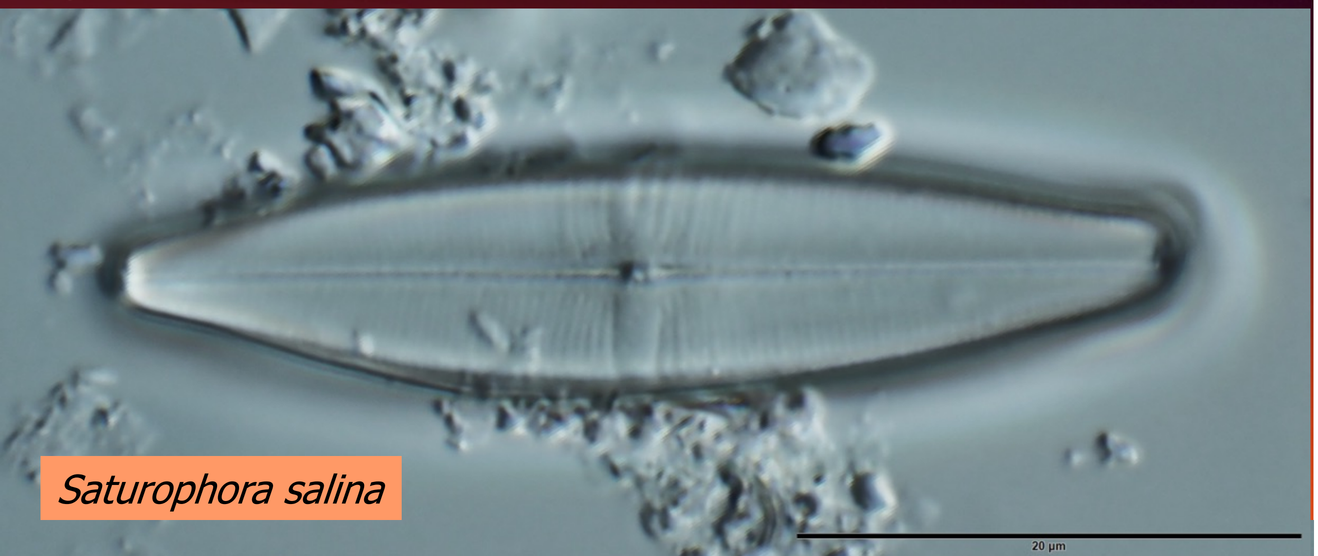

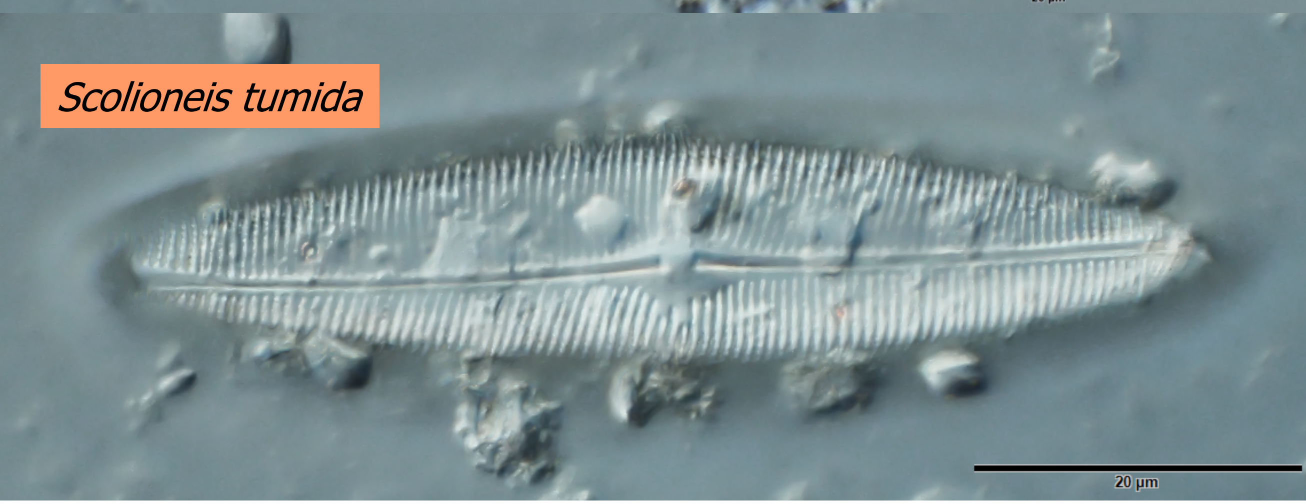

1 = fresh; Cl^- <100 mg L^{-1}
2 = fresh-brackish; Cl^- <500 mg L^{-1}
3 = brackish-fresh; Cl^- 500-100 mg L^{-1}
4 = brackish; Cl^- 5000-1000 mg L^{-1}

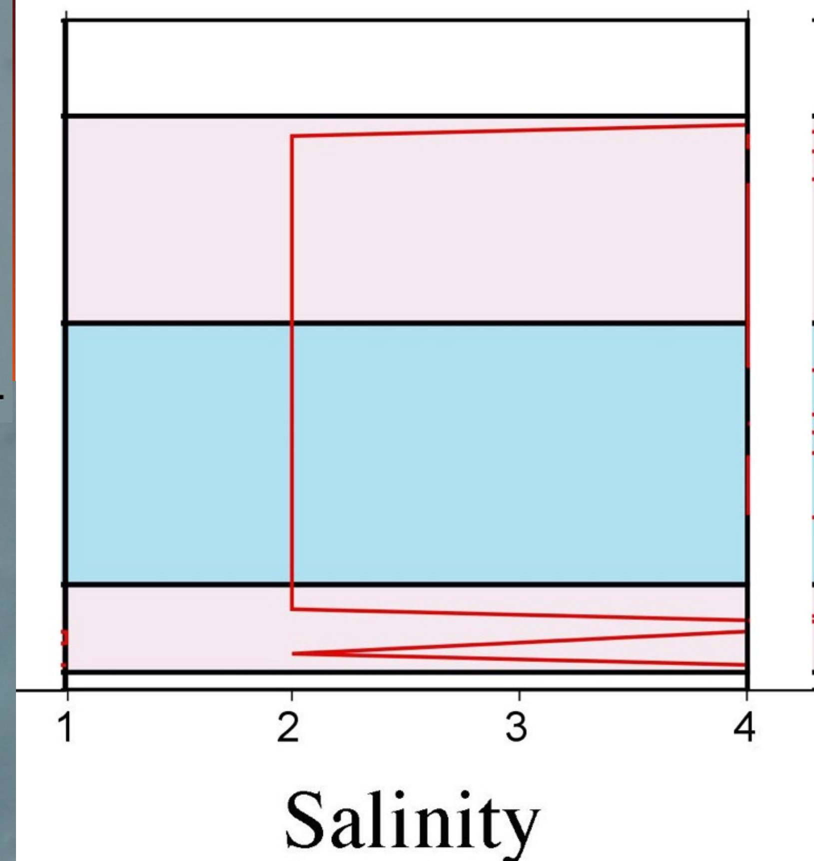

High salinity early

Enormous amount of salt flushed out of Bonneville basin!

Conclusions

◊ Sedimentation rates vary enormously
  - high when PV was restricted (shallow water)
  - endogenic carbonate production was high

◊ Relative diatom abundance shows passage from deep to shallow water
  - this includes the catastrophic Bonneville flood

◊ High salinity in early transgressive phase dissolved near-surface salts
  - mixed marine/continental taxa

◊ Large volumes of salt transported out of the basin

◊ Salinity rose during late regressive phase, but not to levels experienced early on

LAKE BONNEVILLE GEOSITES AND ANALOGS TO MARS

Marjorie A. Chan[1], Holly S. Godsey[1], Paul W. Jewell[1], Timothy J. Parker[2], Jens Ormo[3], Chris H. Okubo[4], and Goro Komatsu[5]

[1] Department of Geology & Geophysics, University of Utah, Salt Lake City, UT 84112;
[2]Jet Propulsion Laboratory, California Institute of Technology, Pasadena, CA 91125;
[3]Centro de Astrobiologı´a (CSIC-INTA), Torrejo´n de Ardoz, Spain;
[4]U.S. Geological Survey, Tucson, AZ 85719;
[5]Università degli Studi G. d'Annunzio, Chieti e Pescara, Italy

Corresponding author (Chan): marjorie.chan@utah.edu

ABSTRACT

An international geoheritage movement focuses on the scientific and educational value of geologically diverse areas. Geosites are important, natural records of Earth's surface processes, environments, and geological history. A variety of distinctive geosites formed near and around Pleistocene Lake Bonneville in northwestern Utah, and include shorelines, moraines, salt flats, playas, and fault scarps. Lake Bonneville is a large, geologically young, terrestrial lake system with exemplary well-preserved shoreline characteristics that formed on the order of a thousand years or less. Therefore, these features provide essential analogs for interpreting ancient shorelines on Mars which are also thought to have formed quite rapidly. In addition, much is known about Bonneville lake levels, tectonic history of the basin, sediment supply, climate, and fetch, providing a wealth of information from which to interpret the Mars landforms. The collective terrestrial lessons provide a framework to evaluate possible boundary conditions for ancient Mars hydrology and the environmental feedback of large bodies of water. This knowledge of shoreline characteristics, processes, and environments can support explorations of habitable environments and guide future planetary mission explorations.

These Lake Bonneville geosites are geologically young, unconsolidated deposits that are easily removed or destroyed, particularly in or near population centers of rapid urban growth where they are accessible for housing development or sand and gravel extraction. In the Bonneville basin, several major Pleistocene landforms are being altered or destroyed at alarming rates. Protection of geosites can take a number of forms, but all conservation efforts depend upon the collective cooperative involvement of many stakeholders, as well as the scientific community. Ultimately, protection of geosites relies upon an informed and involved citizenry who speak out and work to promote best practices in sustainability and land-use management.

This content is a PDF version of the author's PowerPoint presentation.

Lake Bonneville Geosites and Analogs to Mars

Marjorie A. Chan

Holly S. Godsey, Paul W. Jewell, Timothy J. Parker, Jens Ormo, Chris H. Okubo, Goro Komatsu

University of Utah, Jet Propulsion Lab - Calif. Institute of Technology, Center for Astrobiology – Madrid Spain, U.S. Geological Survey, Flagstaff, School of Planetary Sciences - Pescara,Italy

THE UNIVERSITY OF UTAH

1. **Geoconservation**
   Geoheritage = scientific, educational geologically diverse areas
   Geosites = natural records of Earth's surface processes, environments, & geological history
2. **Analogs to Mars**

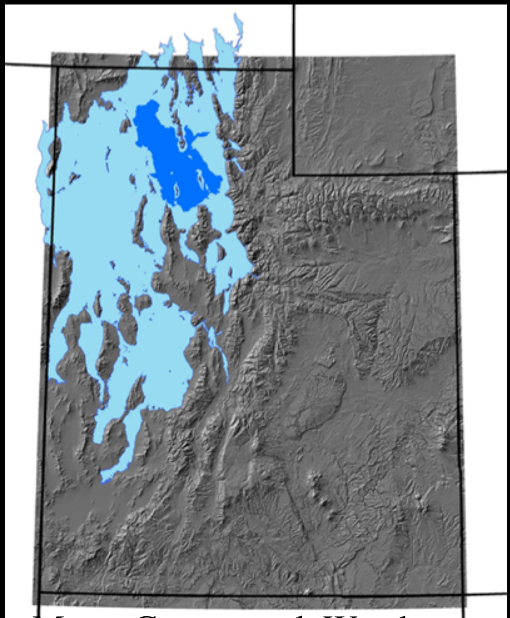

Maps: Currey et al, Wambeam

1. Geoconservation = International

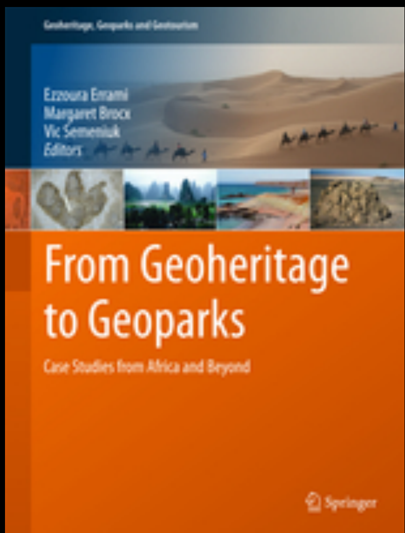

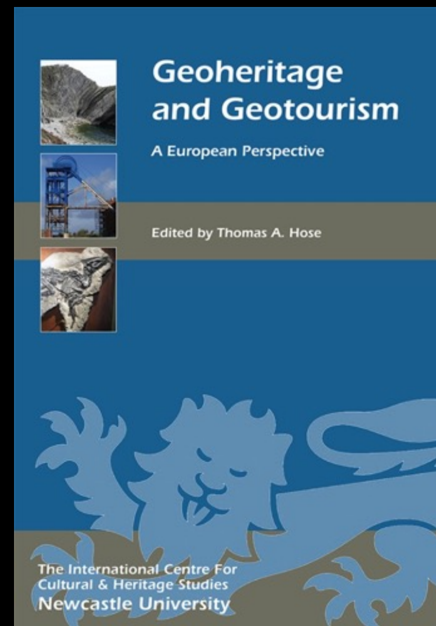

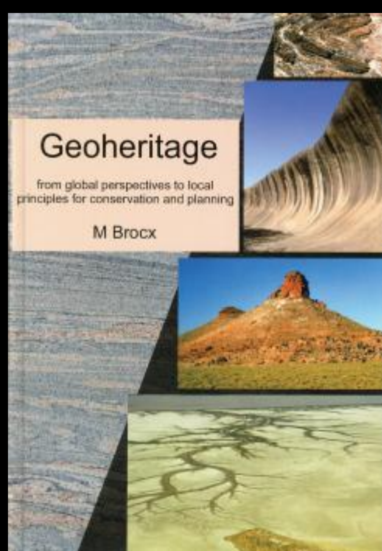

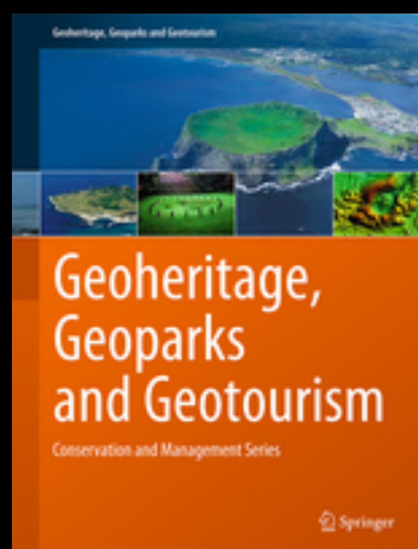

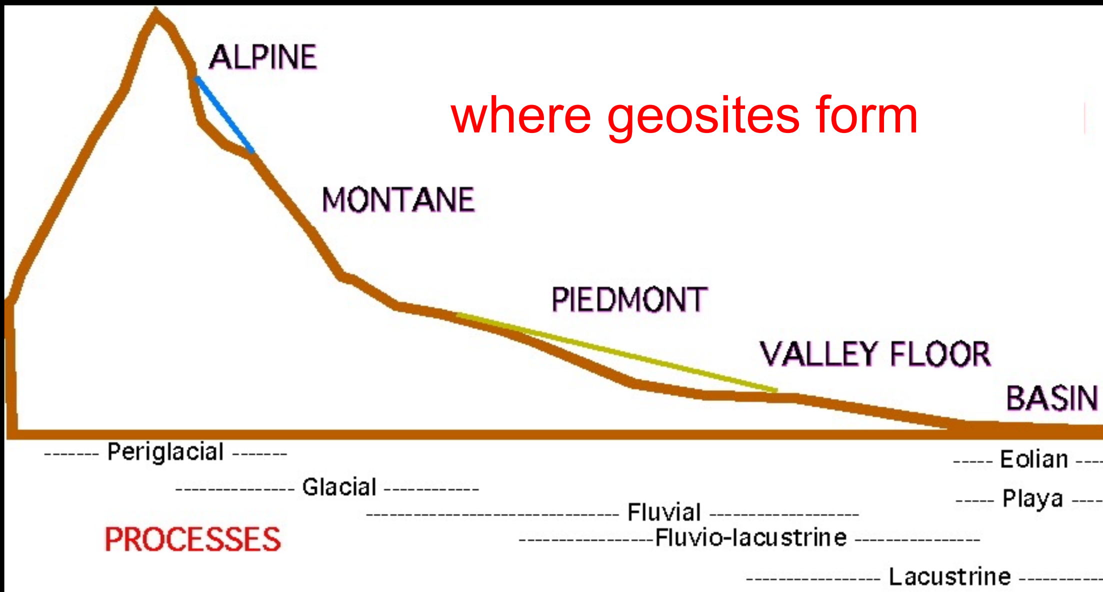

Lake Bonneville's Geoheritage Diversity

- shorelines wave-cut erosional terraces
- spits,bay mouth barriers
- deltas
- gullies
- outburst channels
- playa lake features
  - -- patterned grounds
  - -- eolian systems
  - -- evaporite deposits

Landforms:
shorelines,
beach ridges,
bars, spits, &
tombolos.

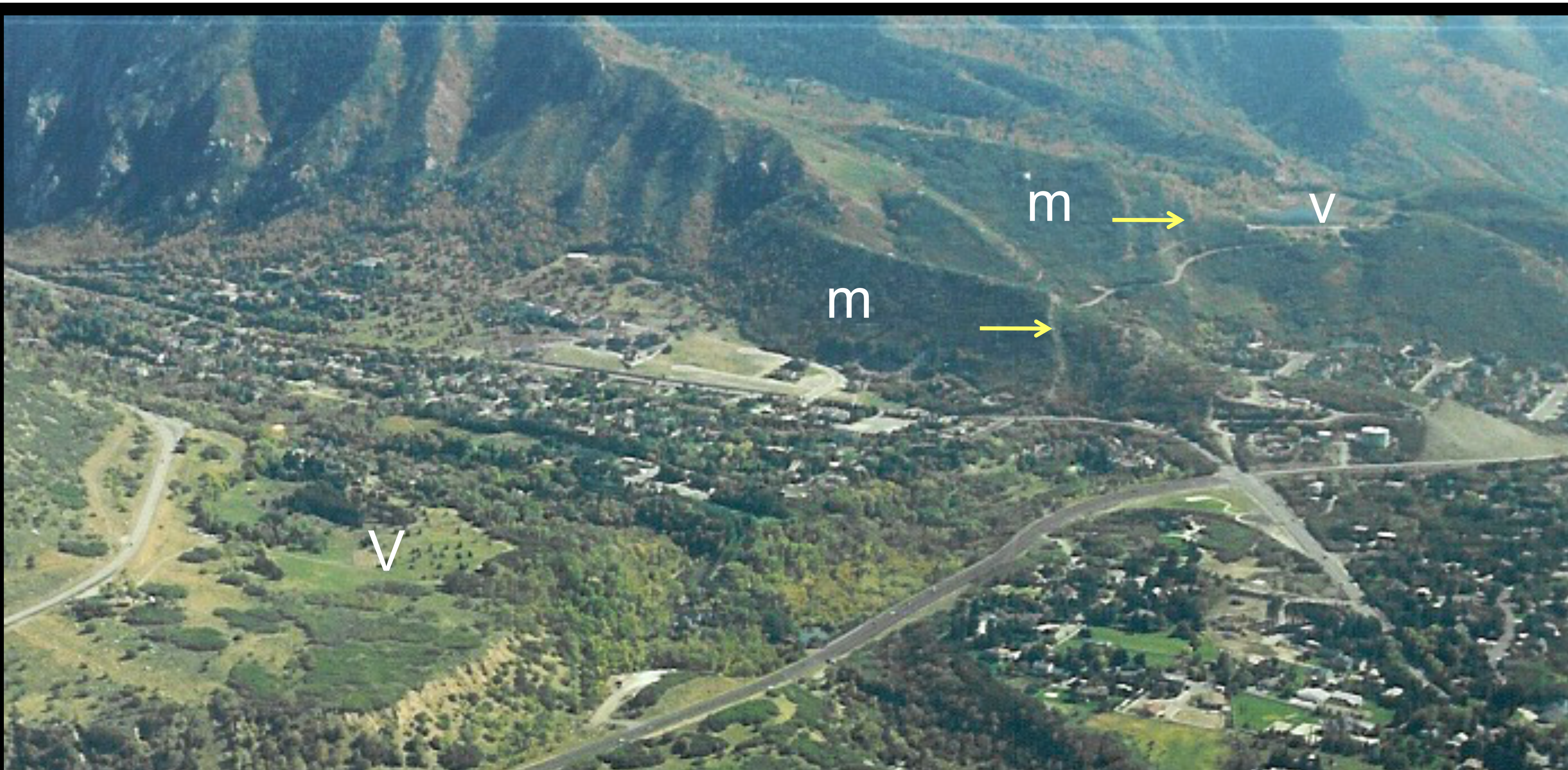

Glacial valleys, moraines, fault scarps, more….

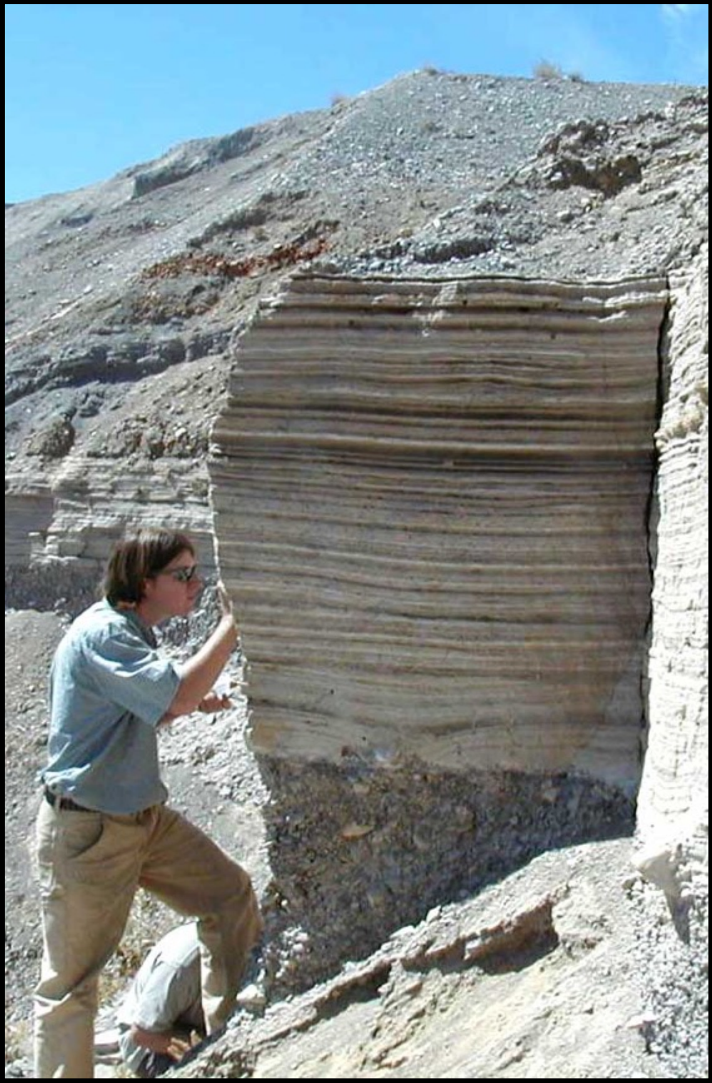

Sediment record:
clastic sediments & marl

W

Rills, Gullies

Point of the Mountain,
Traverse Range

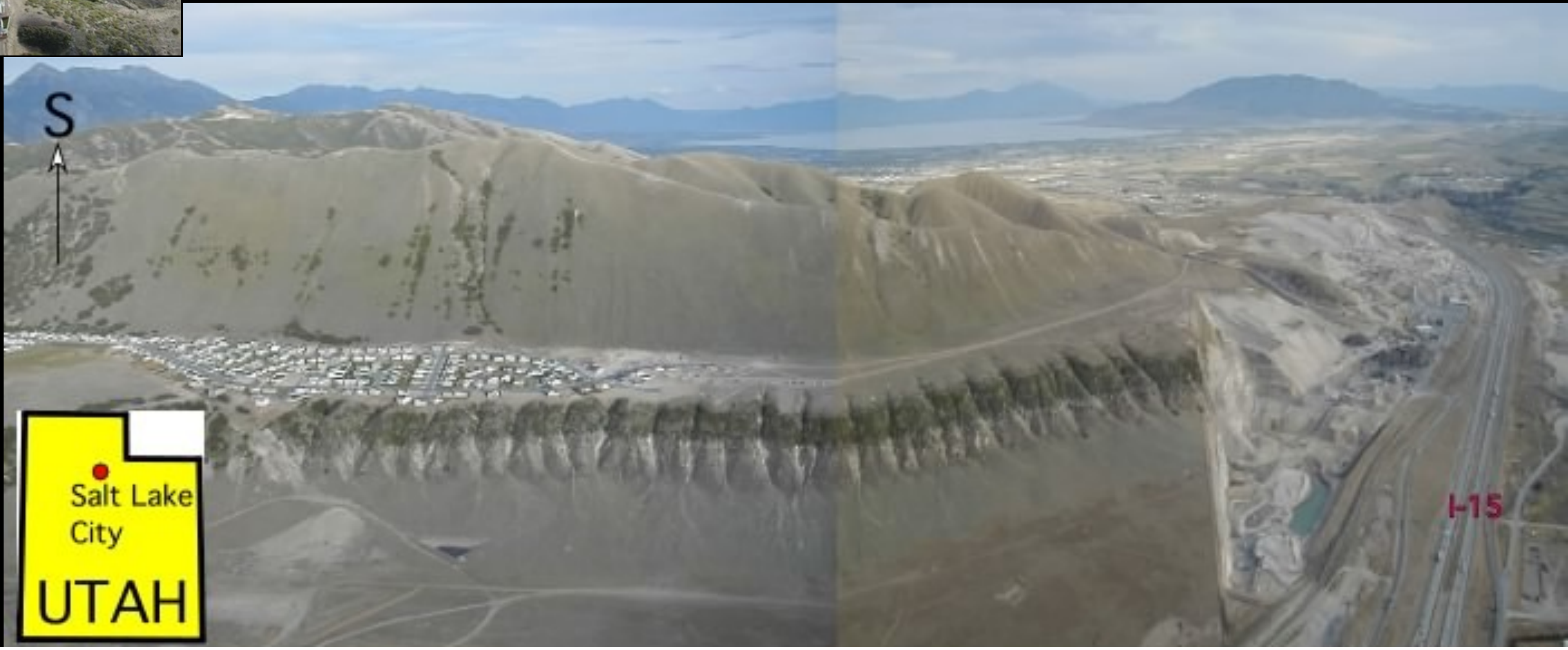

c2005

Outburst floods
with giant boulders

Red Rock Pass, UT/ID border

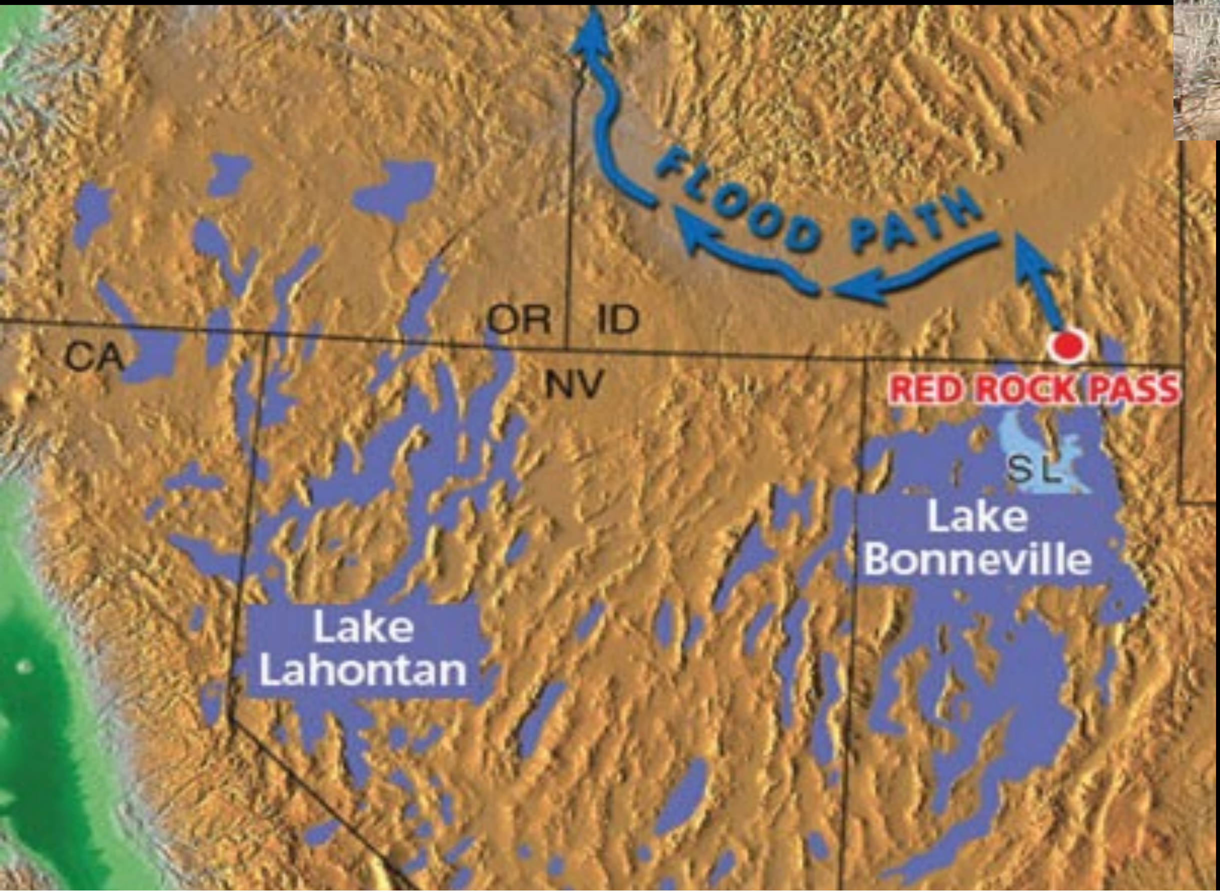

Red Rock Pass looking northeast across the spillway of the Bonneville Flood. Photo by Ann Yearsley.

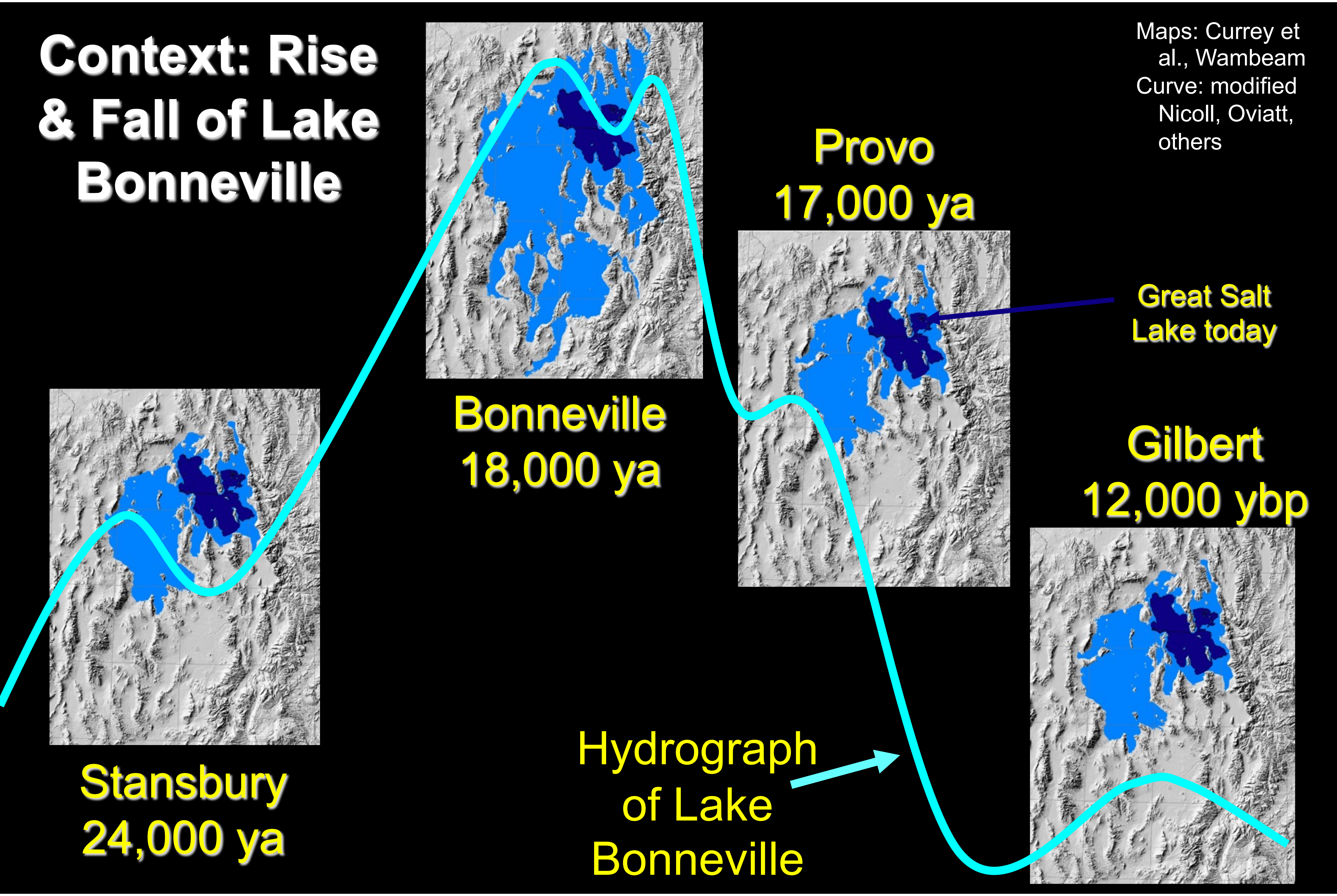
Context: Rise & Fall of Lake Bonneville
Maps: Currey et al., Wambeam
Curve: modified Nicoll, Oviatt, others
Bonneville
18,000 ya
Provo
17,000 ya
Great Salt Lake today
Stansbury
24,000 ya
Gilbert
12,000 ybp
Hydrograph of Lake Bonneville

Geosites = Target for modification/ removal in urban region

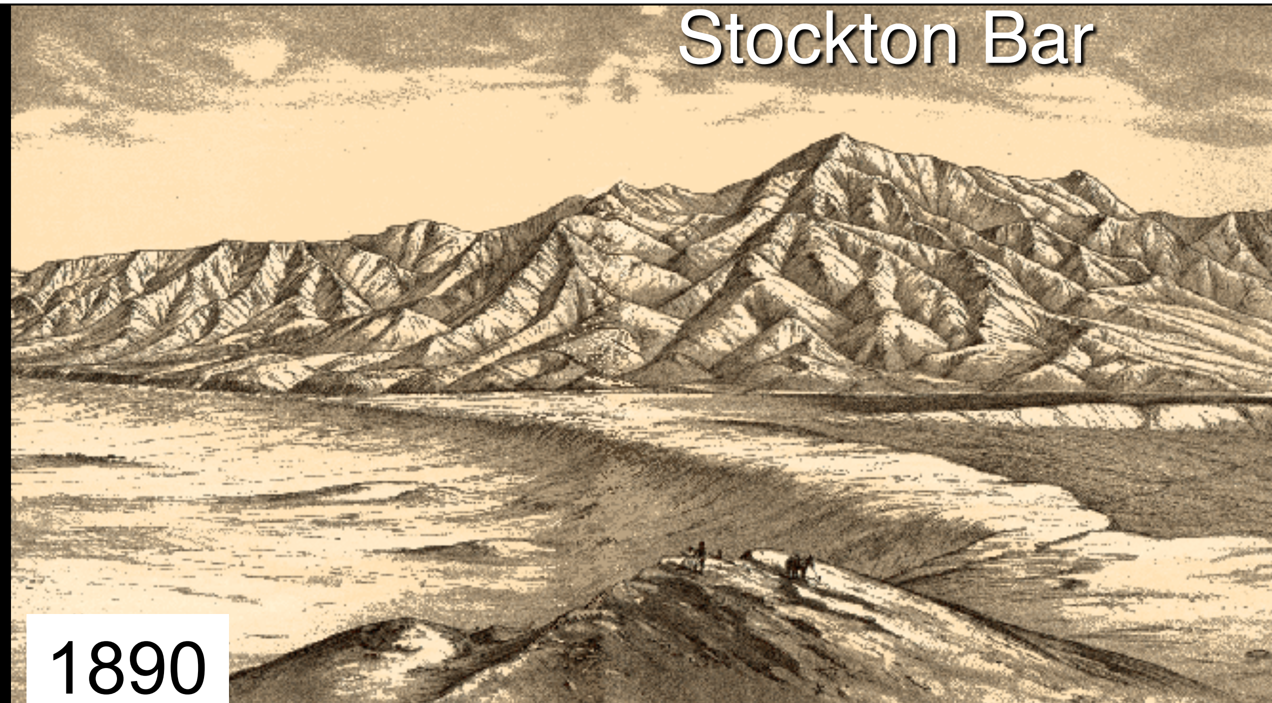

- Prominent ridge of sand & gravel deposited by waves in Lake Bonneville
- Natural barrier between Rush & Tooele Valleys
- ~2500 m across x 400 m wide, southern 1000 m extension
- Ice age record, most complete & largest of its kind in W. hemisphere

GK Gilbert 1890 “Great Bar at Stockton”

2009 Rezoning hearings

Community involvement = crucial!

Photos: Maegan Burr

SOS = Save Our Stockton sandbar

Sand & gravel rezone denied, but future still uncertain

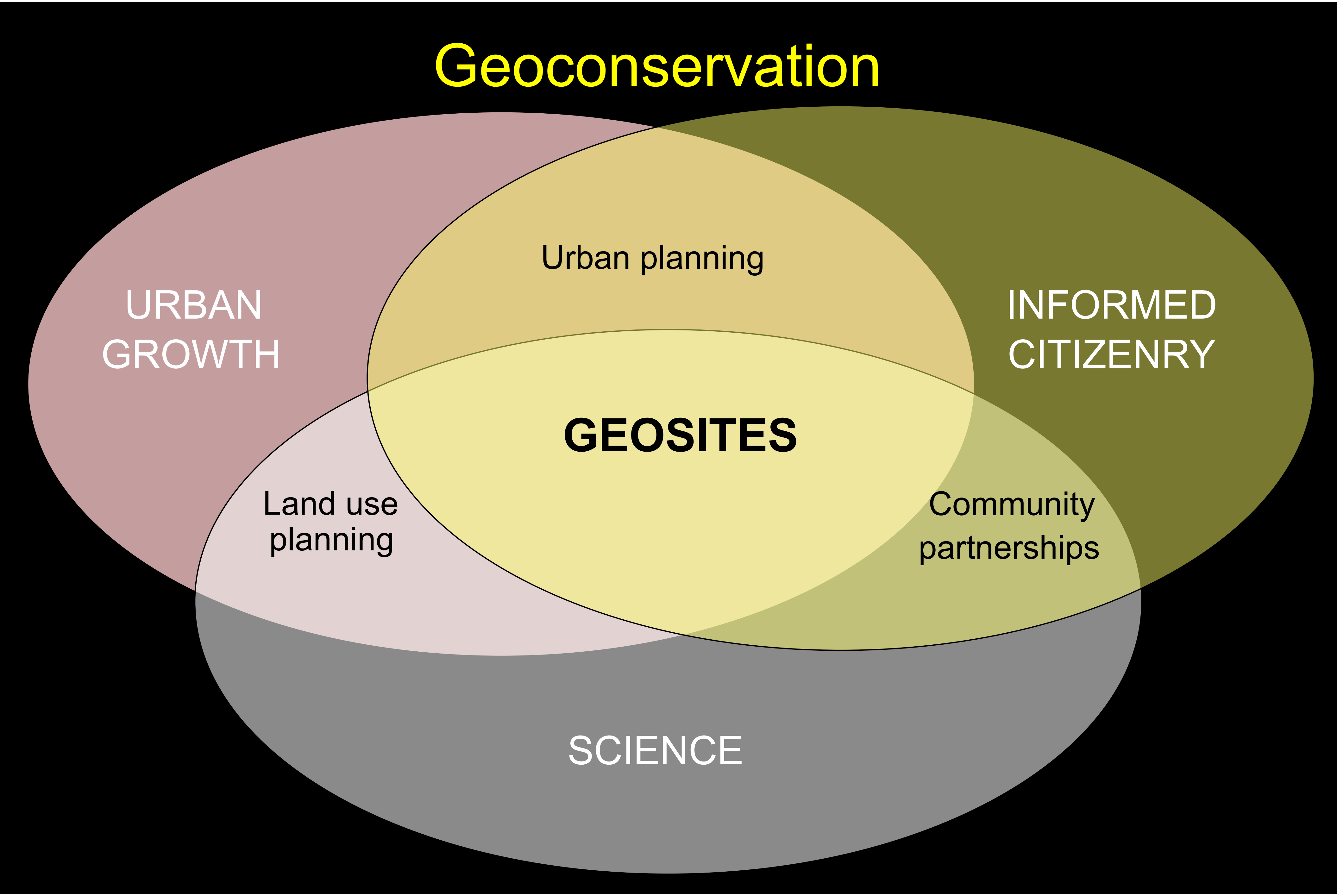
Geoconservation
Urban planning
URBAN GROWTH
INFORMED CITIZENRY
GEOSITES
Land use planning
Community partnerships
SCIENCE


GEOSITES
Challenge: endangered in urban setting,
little/no protection on private land
1. Identify, inventory, prioritize heritage for scientific & societal value
2. Plan for conservation, quality of life, open space
3. Foster education & community partnerships
utah.com

2. Analogs to Mars

Lake Bonneville -> process constraints for shorelines on Mars

- Large (~50,000 km^2) terrestrial closed lake during LGM (~20 kya)
- Well-preserved geomorphic features
- Highstand until catastrophic outburst flood (~17.4 kya)
- Warming climate lowered its volume

Lake Bonneville shoreline characteristics

- geomorphic expression (e.g. erosional vs. depositional, pristine vs. modified)
- dimensions and slope (e.g., original vs. resurfaced)
- topographic profile in cross section
- sediment storage
- degree of preservation

Bonneville Example DEM shorelines

Oquirrh Mtns

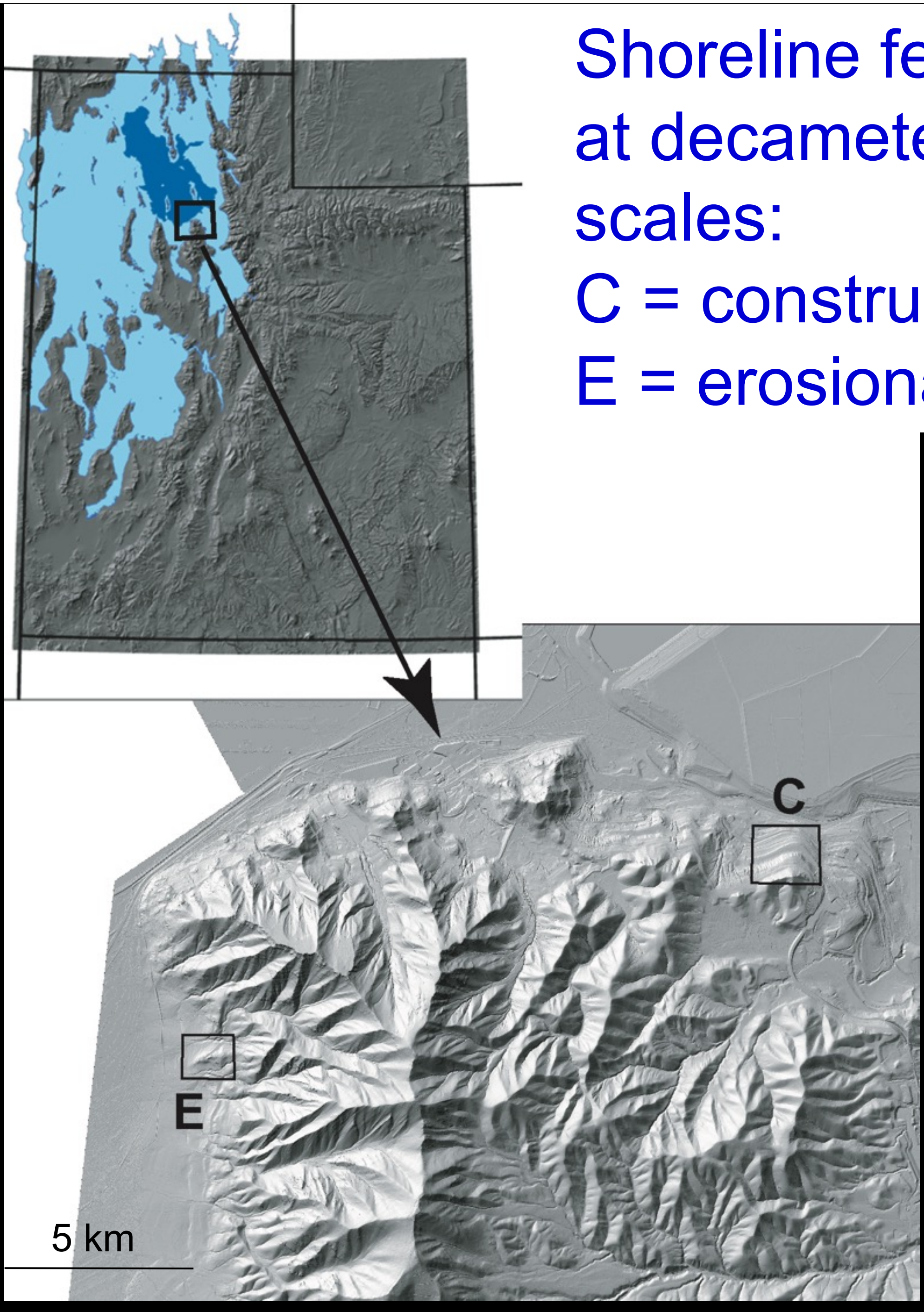

Shoreline features at decameter scales:
C = constructional
E = erosional

Bonneville level constructional shoreline - DEM

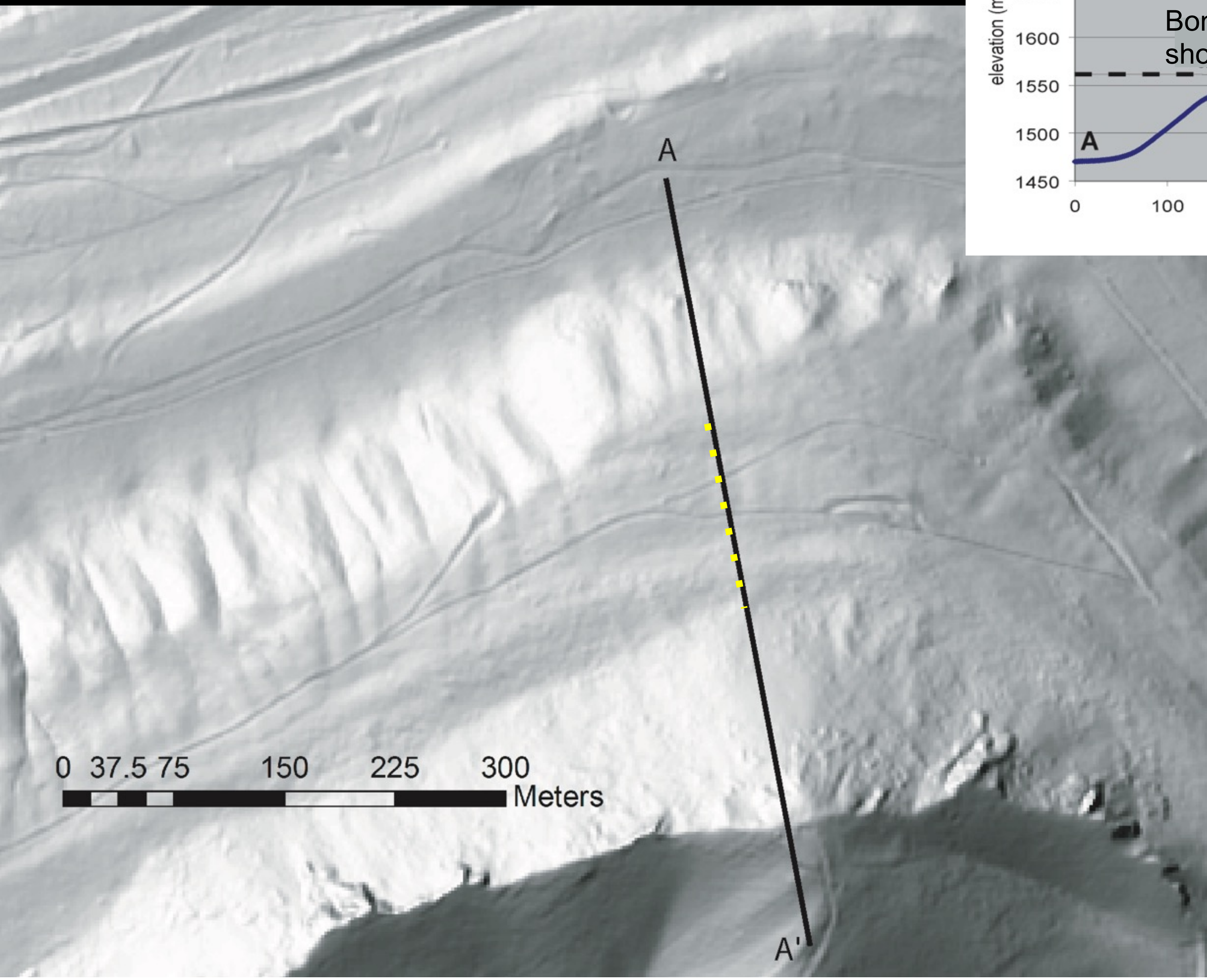

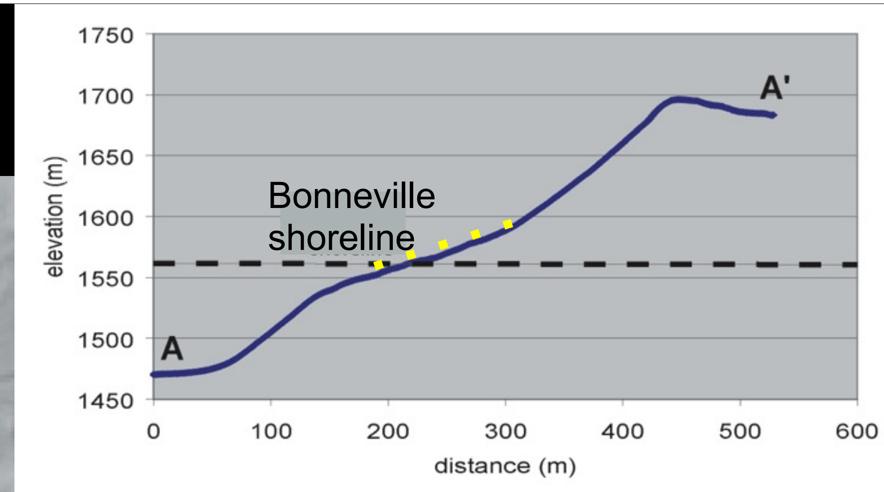

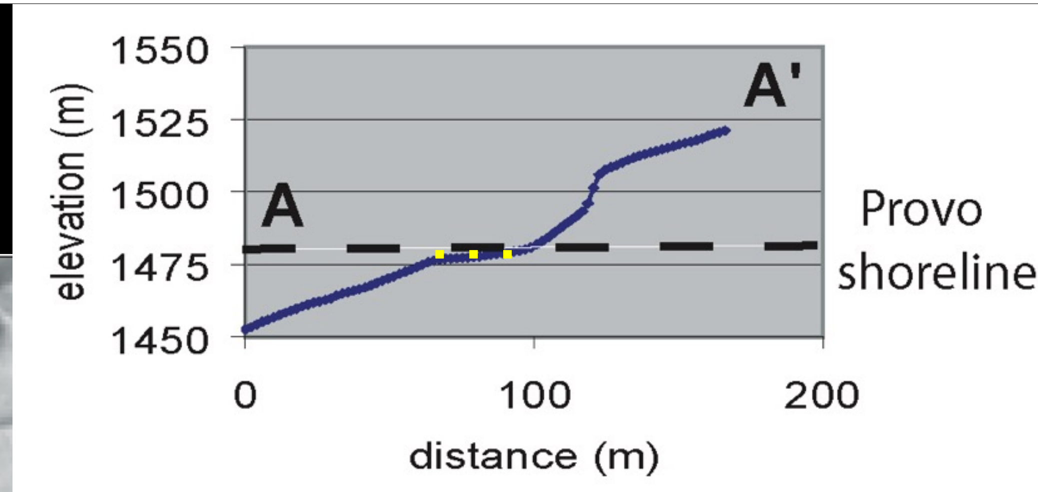

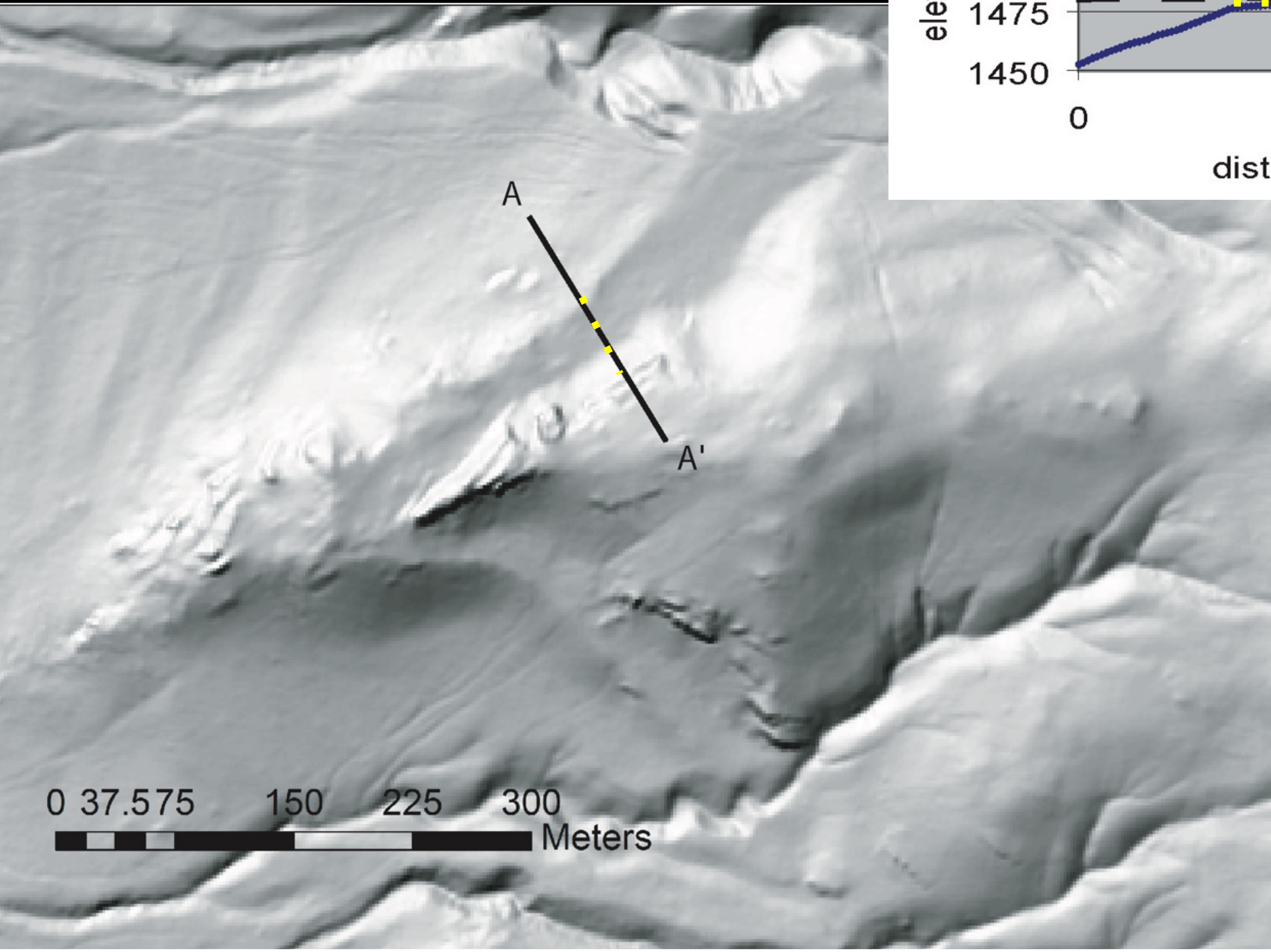

Provo level erosional shoreline - DEM


Farmington Bay,
GSL
Weber River Delta
Egg Island
©2007 Google™


Rock Creek, Utah County

Deltas

Modern Spit, Antelope Island, UT

UGS photograph, 1988

Scales, Features, and Areas for Advances

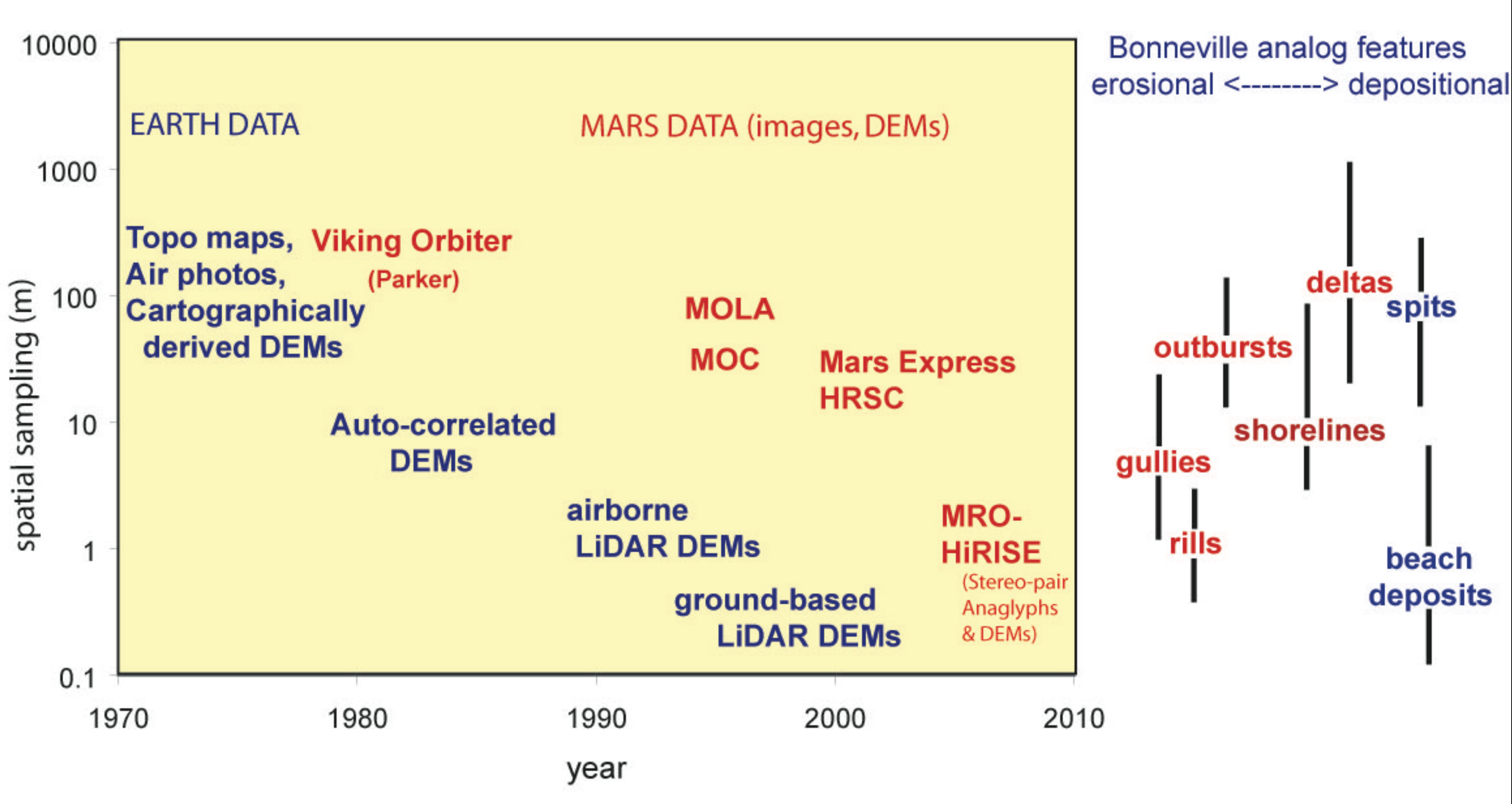

CONCEPTS

- Compare recent data of putative shorelines on Mars with Earth's best paleoshorelines
- Develop recognition criteria to constrain geomorphic processes and landforms

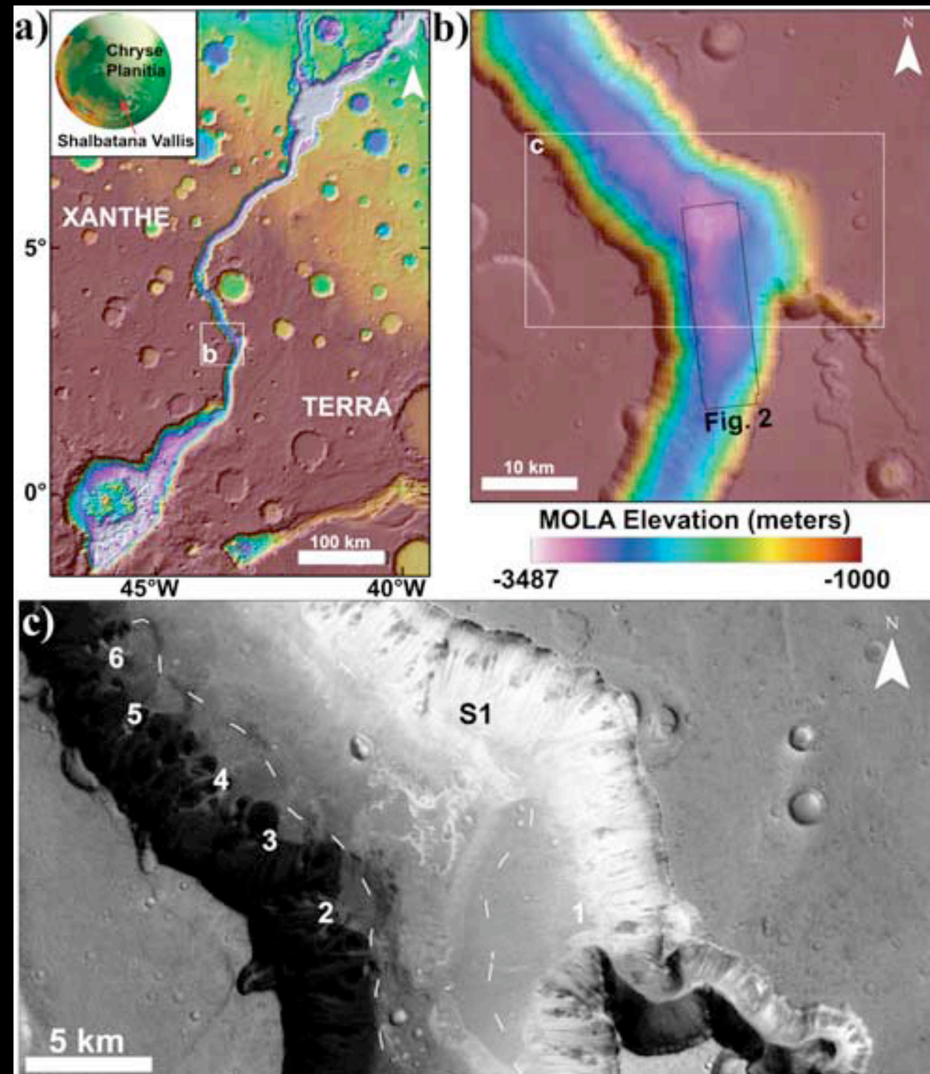

"unequivocal shorelines"?
Shalbatana Vallis
(Achille et al. 2009)

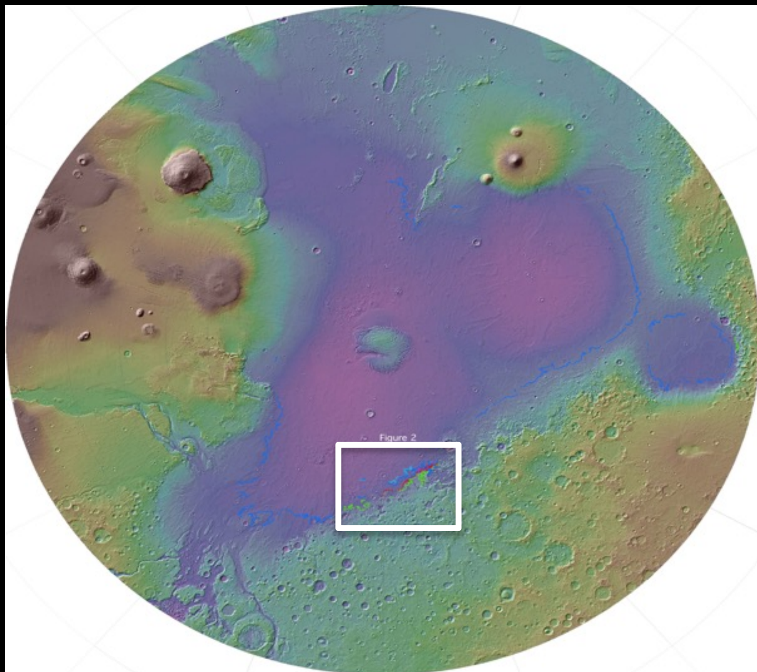

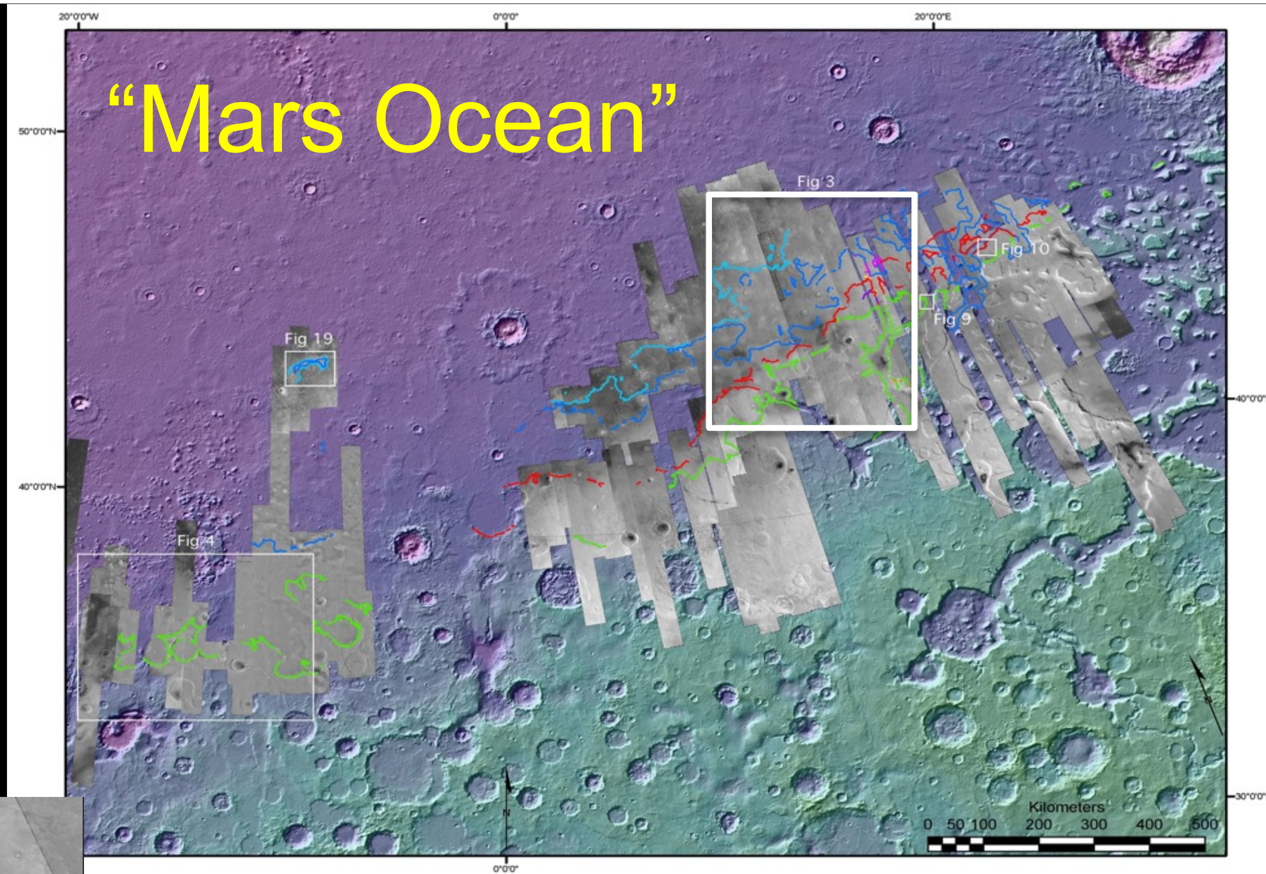

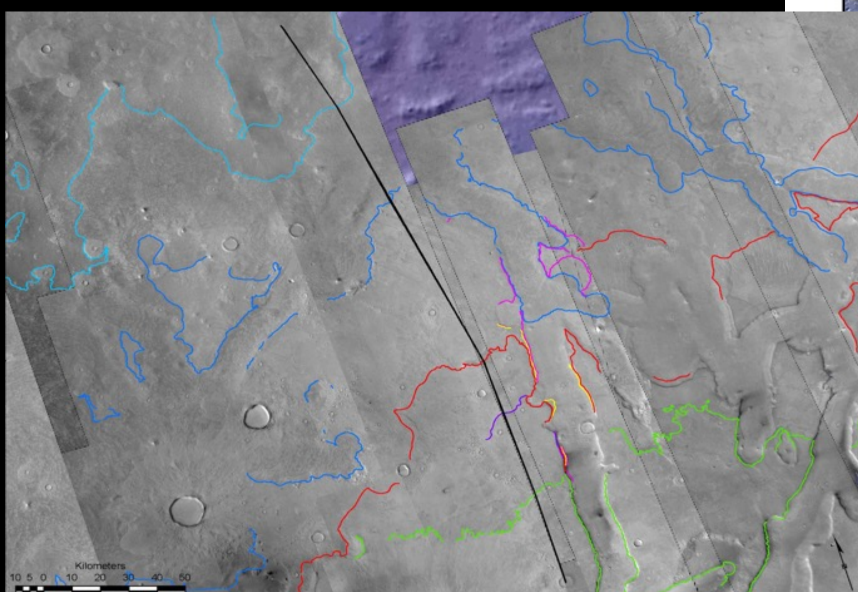

Mapped shorelines of W. Deuteronilus Mensae, Northern plains

(Late Noachian – Hesperian)

Parker et al. 2010

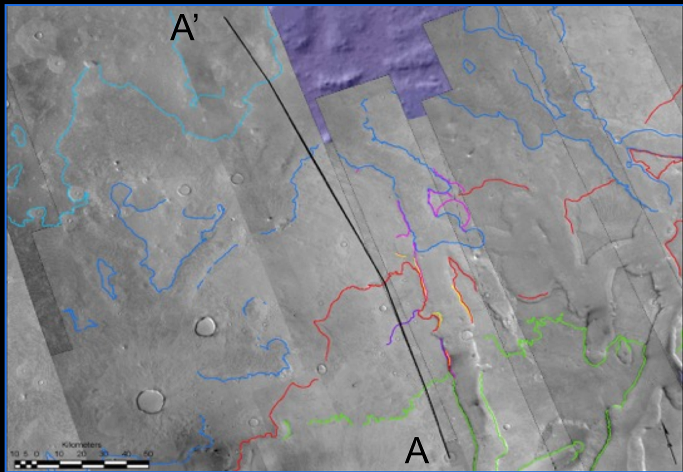

- Arabia: local terracing
- Ismenius: some rills
- Deuteronilus: prominent tilt west & towards basin interior, lobate flows
- Acidalia: transition of plains textures

Tim J. Parker (unpublished)

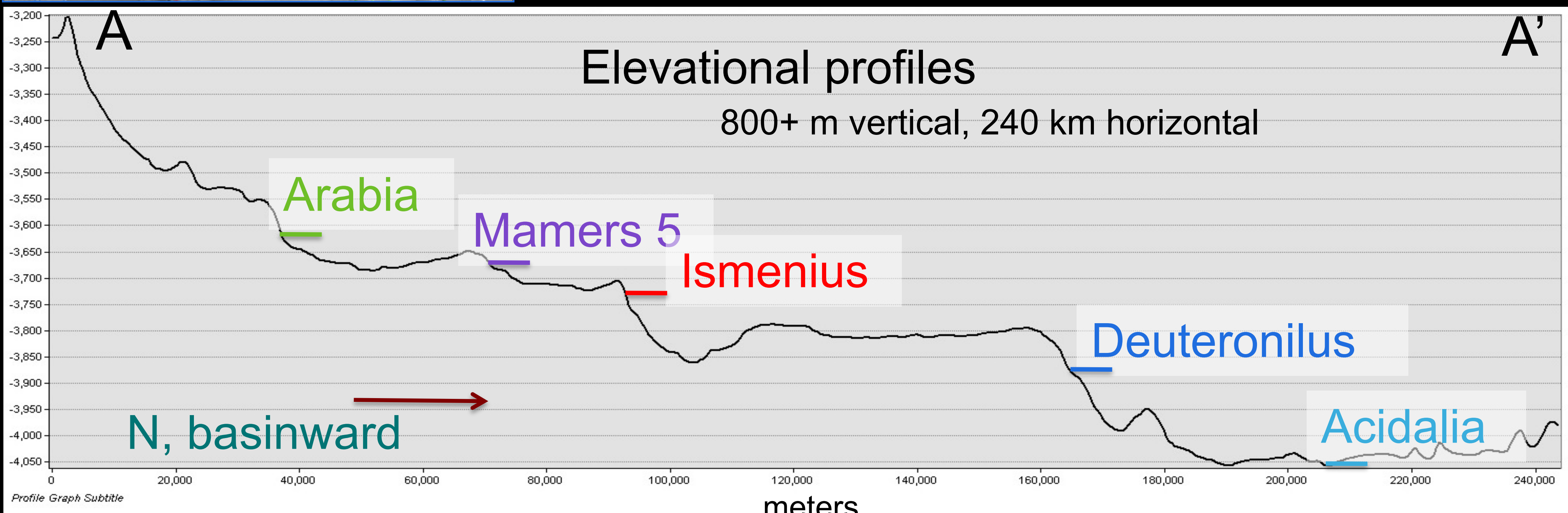

Shorelines usually constant elevation (equipotential surface)
Mars shorelines N. plains vary up to sev. kms: maybe affected by Tharsis volcanism – big mass bulge (Citron et al. 2018)

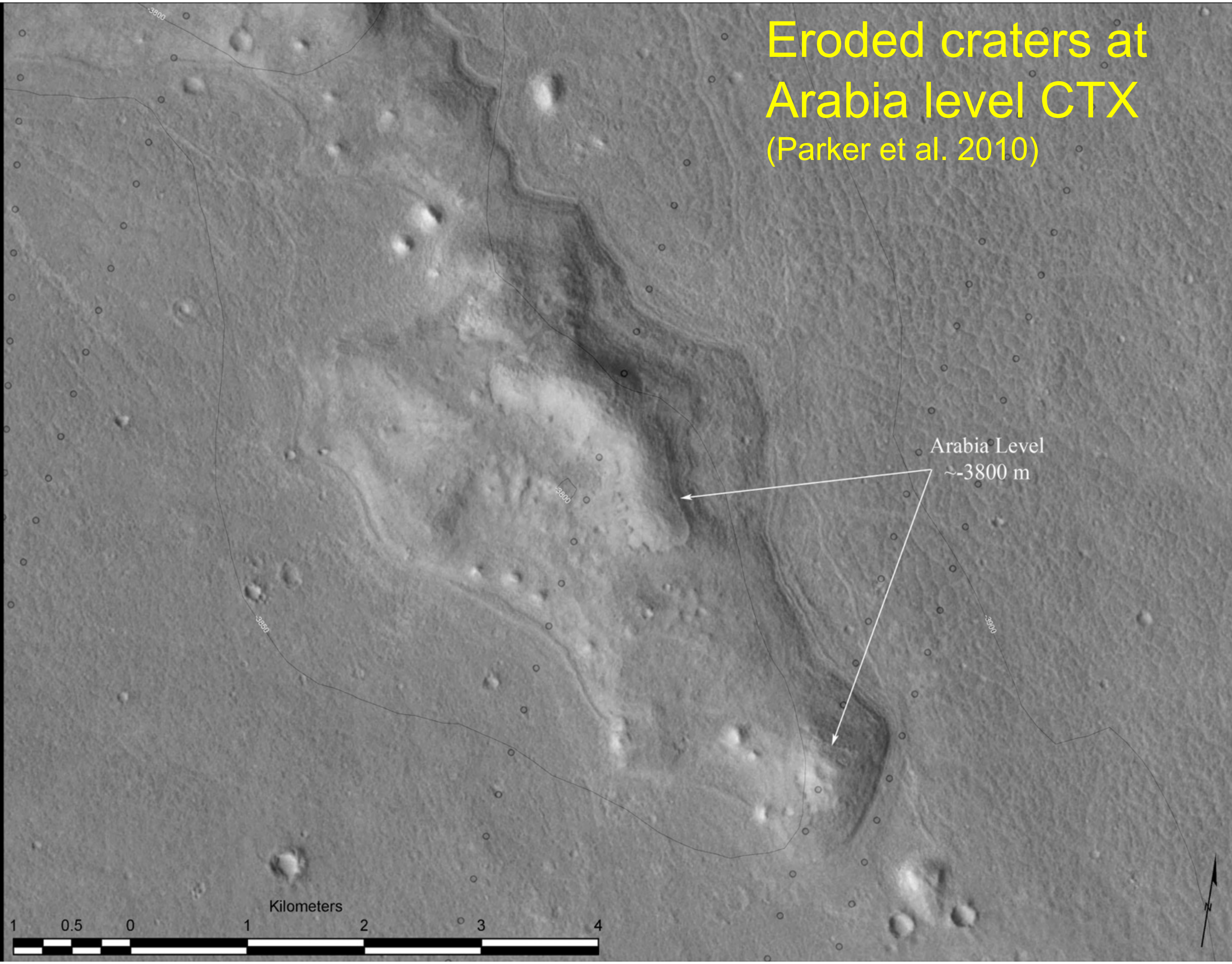
Eroded craters at
Arabia level CTX
(Parker et al. 2010)
Arabia Level
~-3800 m
Kilometers
1 0.5 0 1 2 3 4

Water and geologic development of early Mars

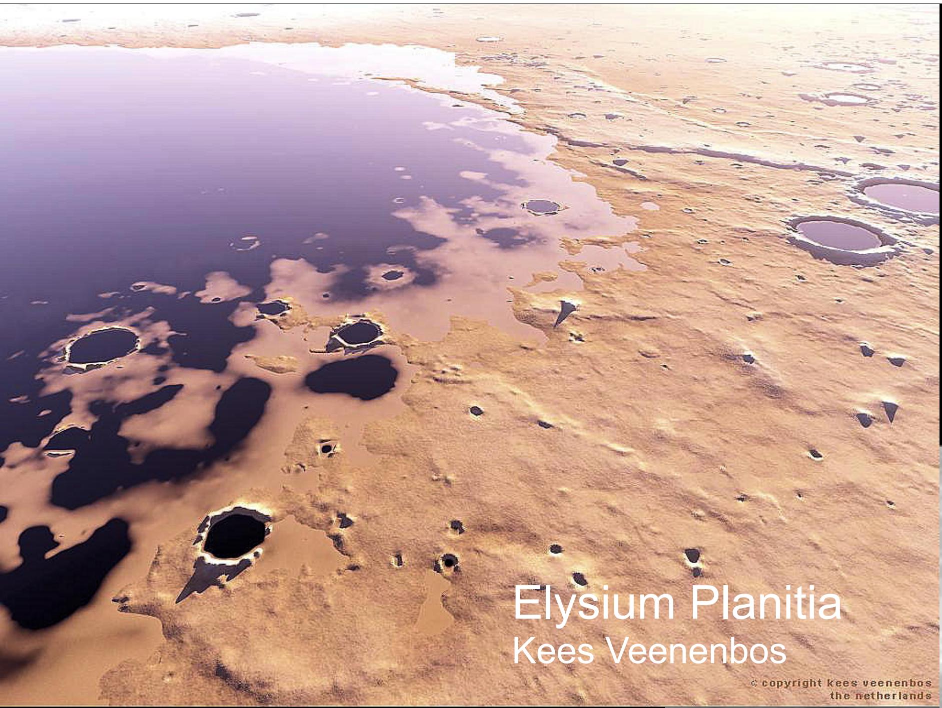

How was standing water on Mars geomorphically effective, and for how long?

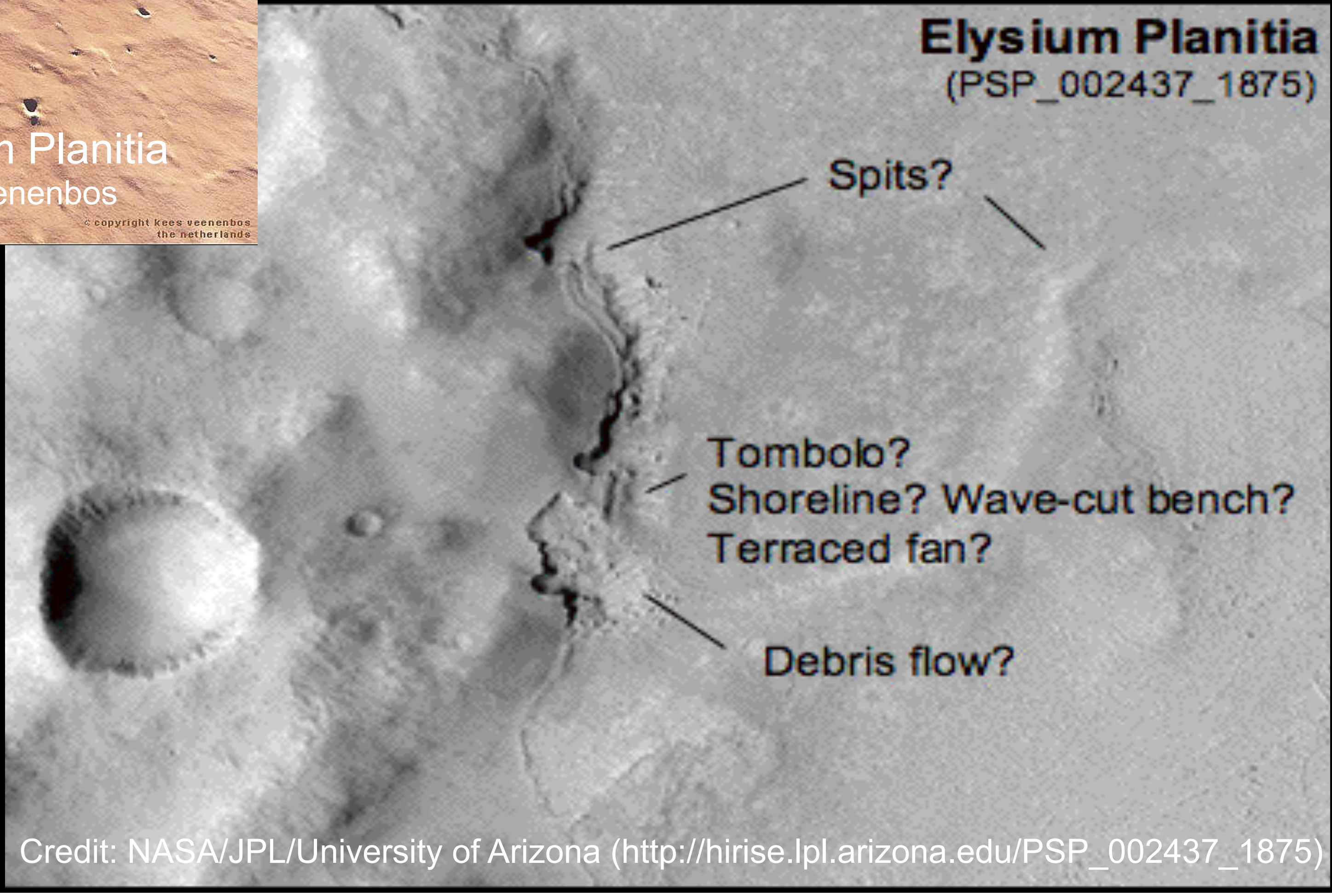

Credit: NASA/JPL/University of Arizona (http://hirise.lpl.arizona.edu/PSP_002437_1875)

Evidence for ancient ocean in N. Plains?

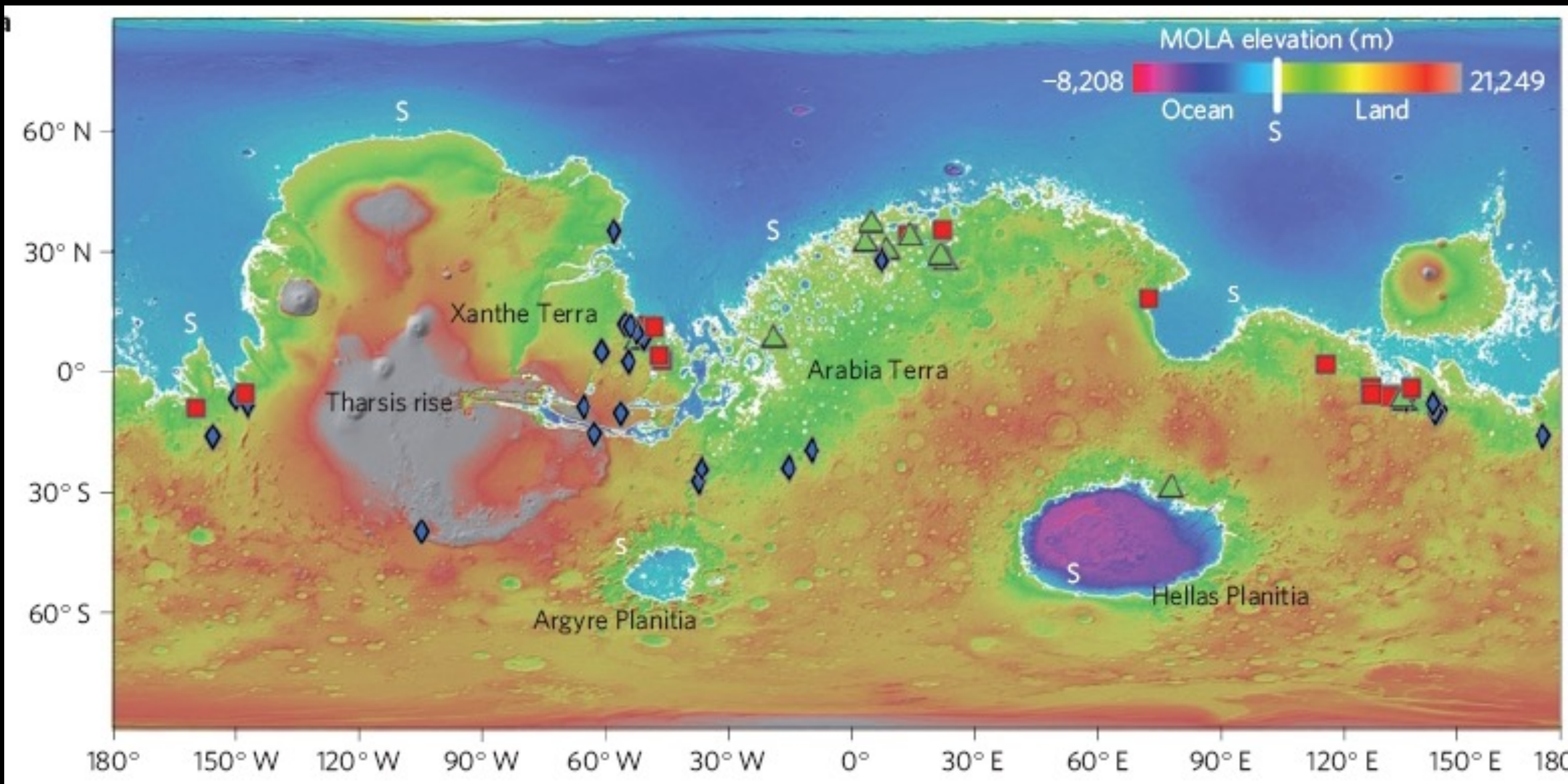

(DiAchille & Hynek 2010)

Deltas along dichotomy (highland-lowland) boundary

Shorelines on Mars shaped by impact mega tsunamis?

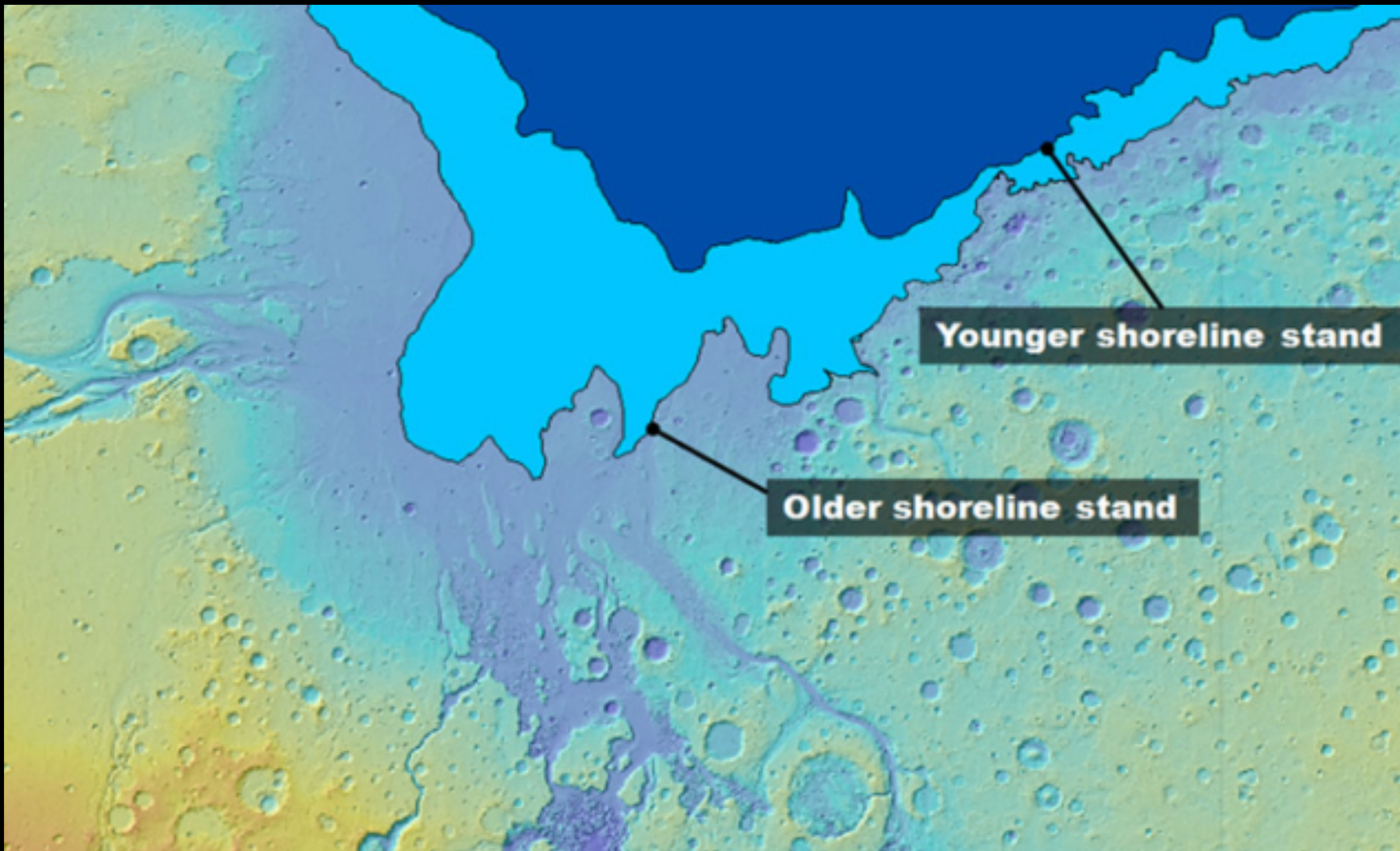

Circum-Chryse & Arabia Terra of N. Plains

Rodriguez et al. 2016

Lake Bonneville Analog justification

- Better than Earth's tidal oceans given Mars' small moons and its distance from sun
- Extensional setting -> steep sided water bodies like Mars
- Wide range of landforms & processes
- Rapid climate change (since LGM)
- Framework for imagery comparisons

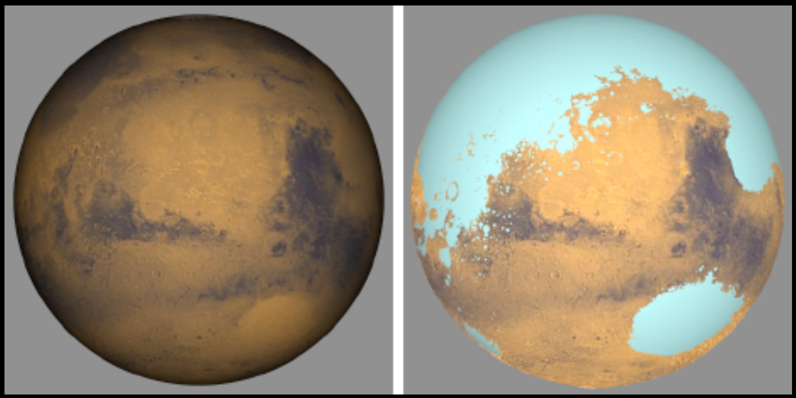

Analog Summary

Mars ocean shorelines:

- shows 4+ major levels
- correlative segments with different topo elevations
- likely constructional & erosional
- remain pristine after ~ 3 b.y.

Lake Bonneville shorelines:

- good terrestrial analog
- surficial dynamics
- temporal constraints
- characteristics linked to processes
- best pristine terrestrial shorelines

Ocean
Crater fills
Valley lakes

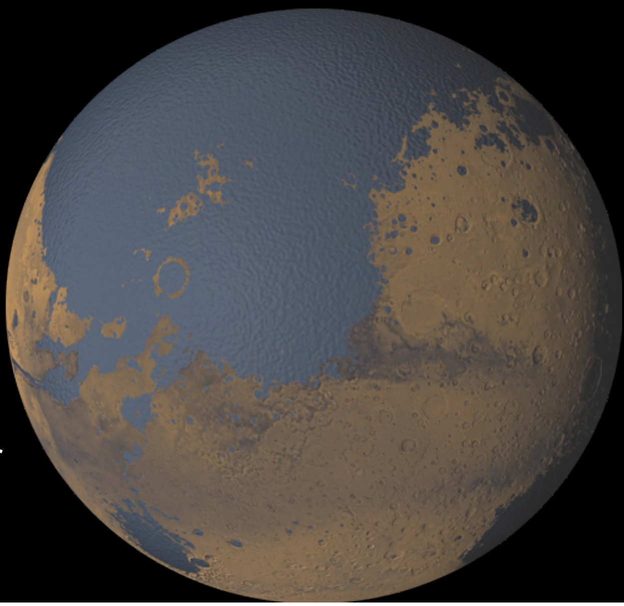

NASA/Goddard Space Flight Center Scientific Visualization Studio

+

Conclusions

- Lake Bonneville: Remarkable geosites for science, education, landscape quality
- Worthy of geoconservation, analogs application

Acknowledgments

Don R. Currey
Genevieve Atwood
Andrea Dion

NSF Grants:

DEB-9817777
EAR-9809241
ESI-0329669

Photo: D. LaMacchia

COSMOGENIC ^{10}BE SURFACE EXPOSURE DATING AND NUMERICAL MODELING OF LATE PLEISTOCENE GLACIERS IN NORTHWESTERN NEVADA

Kaitlyn Fleming[1] and Benjamin Laabs[2]

[1]Environmental and Conservation Program, North Dakota State University, Fargo, ND 58102;
[2]Department of Geosciences, North Dakota State University, Fargo, ND 58102

Corresponding author (Fleming): kaitlyn.fleming@ndsu.edu

ABSTRACT

The Great Basin region of the southwestern United States features a rich geologic record of Pleistocene climate change. This study focuses on the glacial record in the Pine Forest and Santa Rosa Ranges in northwestern Nevada west of the Pleistocene Lake Bonneville basin. Preliminary cosmogenic exposure ages in these two ranges are consistent with observations elsewhere in the Great Basin where glacier maxima (or near maxima) and lake highstands in the northwestern Great Basin occurred at ~18–17 ka. Here, we apply numerical modeling of glaciers in both ranges to limit the range of temperature and precipitation combinations accompanying glacier maxima. Numerical model experiments simulating maximum ice extent in the Pine Forest Range and near maximum ice extent in the Santa Rosa Range yield differing results. If precipitation in the Pine Forest Range was similar to modern during a glacial maximum at 21–20 ka, then temperature depressions during this time were -9 to -8°C. If precipitation in the Santa Rosa Range was similar to modern at 18–17 ka, then temperature ranges were -6 to -5°C. Temperature-precipitation combinations for the Pine Forest Range compare favorably with results of model applications to other mountains in the northern Great Basin. To better limit precipitation in the Santa Rosa Range at 18–17 ka, glacier model results are compared with water-budget modeling results for pluvial lakes in northeastern Nevada. This comparison suggests that temperature depression at 18–17 ka was -4 to -10°C and precipitation was 1.5 to 2 times greater than modern. Overall, the chronology of glacial deposits in the northwestern Great Basin and inferred climate during the last glaciation show consistency across the northern Great Basin.

INTRODUCTION

The rich geologic record of Pleistocene climate change includes numerous locations in the Great Basin west of Pleistocene Lake Bonneville. Mountains and valleys in northern Nevada feature abundant records of Pleistocene mountain glaciers and pluvial lakes, which were likely coeval with Lake Bonneville (figure 1). The research described here focuses on (1) the relative timing of glacier maxima in the northwest Great Basin and (2) setting precise limits on temperature and precipitation based on combined results of numerical mountain glacier modeling. Here, we report new cosmogenic ^{10}Be exposure ages of moraines in the Santa Rosa and Pine Forest Ranges of northwestern Nevada, and compare new glacier modeling output to previously reported lake modeling results.

There are over forty glaciated mountains in the Great Basin (Osborn and Bevis, 2001), many of which are west of the Lake Bonneville basin. Partial glacial histories of ranges in the northeastern and north-central Great Basin (Laabs and others, 2013; Laabs and Munroe, 2016) suggest that mountain glaciers were at or near their maximum extent at the

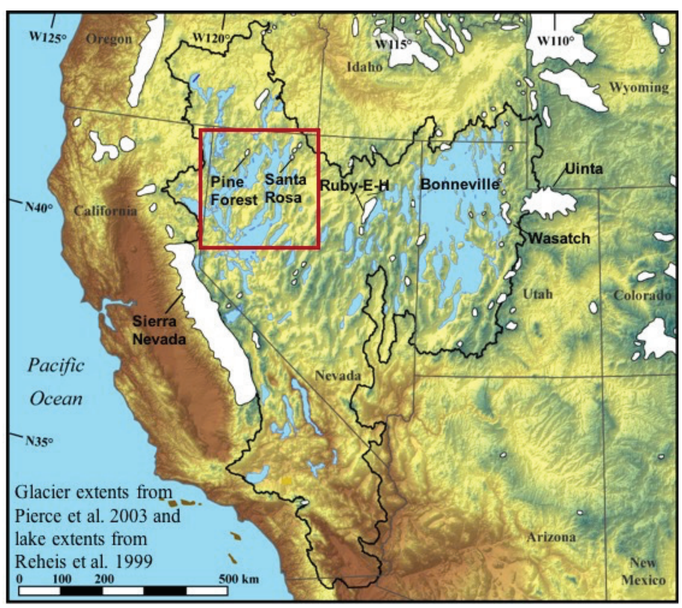

Figure 1. *Shaded relief map of the Great Basin (black outline) and neighboring regions in the western United States, with extents of Great Basin lakes (blue) and mountain glacier systems (white). Glacier systems are from Pierce et al. (2003) and lake extents are from Reheis et al. (1999). Mountain glacier systems for this study are outlined in red.*

time of pluvial lake highstands. The timing of the last Pleistocene glaciation in the Santa Rosa and Pine Forest Ranges is poorly known, particularly compared to the timing of pluvial lake highstands, including those of Jakes Lake and Lake Franklin. Developing the glacial record in the Santa Rosa and Pine Forest Ranges through new mapping, numerical glacier modeling, and cosmogenic ^{10}Be surface exposure dating of moraines can help reveal the temporal pattern of glaciation and accompanying changes in Pleistocene climate in northwestern Nevada. Specifically, identifying the relative timing of glacier maxima and the highstands of Jakes Lake and Lake Franklin, and then the changes in temperature and precipitation accompanying glacier and lake maxima can help to understand the drivers of climate change during the last glaciation and deglaciation (figures 2 and 3).

The Santa Rosa Range is in Humboldt County, Nevada. The highest peaks in the range are Granite Peak, 2,966 m (meters above sea level) and Santa Rosa Peak, 2,956 m. The range also includes Paradise peak of more modest elevation. There are over six glaciated valleys in the range, including those that head on the north flank of Granite Peak, the north and east flanks of Santa Rosa Peak, the north flank of Paradise Peak, and against unnamed headwalls 1.5 km south and 2.2 km south southwest of Paradise Peak respectively (Osborn and Bevis, 2001). The outermost terminal moraine in each valley was targeted for cosmogenic ^{10}Be surface exposure dating and numerical modeling. However, the moraines near Paradise Peak and Santa Rosa Peak do not yield well-defined morainal shapes, and cannot be used for numerical modeling or surface exposure dating.

The Pine Forest Range is also in Humboldt County, Nevada, just north of the Black Rock Desert near Denio, Nevada. The Pine Forest Range is of modest elevation with only a few closely spaced, relatively high summits, the highest of which is Duffer Peak at an elevation of approximately 2,865 m (Osborn and Bevis, 2001). This peak includes evidence for a minimum of three glaciers. The outermost terminal moraine in one of the glaciated valleys was targeted for cosmogenic ^{10}Be surface exposure dating and numerical modeling. Additionally, a recessional moraine farther up valley from the terminal moraine, close to Blue Lake, was also targeted for cosmogenic ^{10}Be surface exposure dating and numerical modeling.

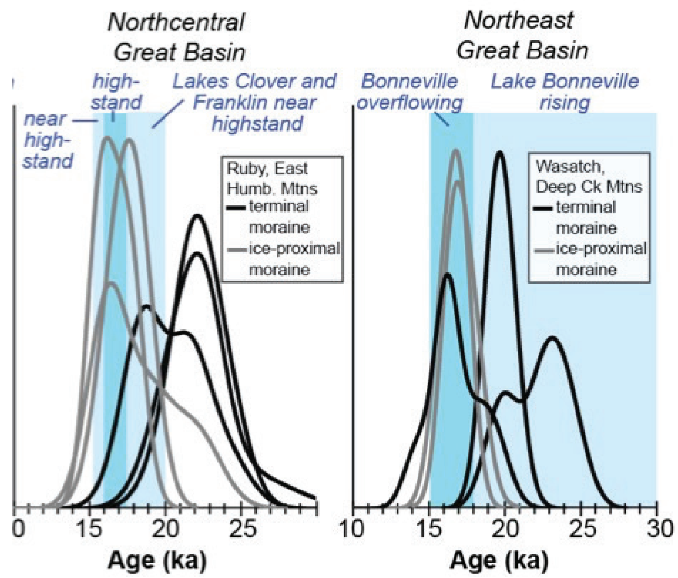

Figure 2. *Relative probability plots of cosmogenic ^{10}Be exposure ages in the northcentral and northeast Great Basin. Ages are shown relative to Lakes Clover and Franklin near highstand and relative to the overflowing phase of Lake Bonneville.*

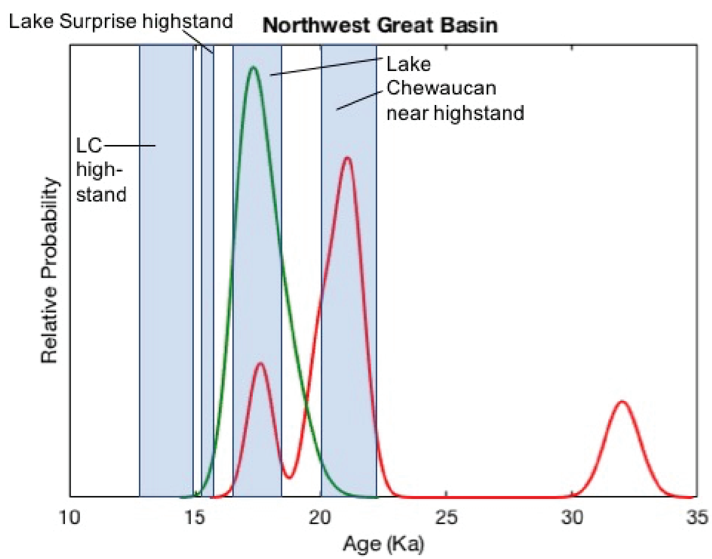

Figure 3. *Relative probability plot of cosmogenic ^{10}Be exposure ages in the northwest Great Basin, including the Pine Forest and Santa Rosa Ranges. Ages are shown relative to the Lake Surprise and Lake Chewaucan near highstands.*

Even though there have been many inferences of how climate changed in the northern Great Basin during and after the last glaciation, estimates of temperature and precipitation during times of glacier and lake maxima are variable. For example, recent hydrologic modeling studies of Lake Surprise and Jakes Lake in the northwest Great Basin, conclude that lake highstands in these valleys during the latter part of the last glaciation were accompanied by temperature depressions of 5–7°C from modern and precipitation 75–90% greater than modern (Ibarra and others, 2014; Barth and others, 2016), whereas other studies of glacial and lake records have concluded colder and drier climate accompanied lake highstands (e.g., Lyle and others, 2012). Speleothem stable isotopes are useful, continuous records of changes in effective moisture during the last glaciation (e.g., Lachniet and others, 2014; Oster and Kelly, 2016), but they do not by themselves distinguish changes in temperature and precipitation. Cosmogenic ^{10}Be surface exposure dating and glacier modeling can help identify how temperature and precipitation changed during the last glaciation in the northwestern Great Basin.

METHODS

This paper updates the cosmogenic chronology of glacial deposits in the Pine Forest and Santa Rosa Ranges based on newer models of *in situ* production of ^{10}Be. Seventeen samples, six samples from the Pine Forest Range and 11 samples from the Santa Rosa Range, were prepared in the Cosmogenic Nuclide Preparation Lab at NDSU following methods of Laabs and others (2013). Once the samples were loaded into their respective cathodes mixed with a niobium powder, they were then sent to PRIME Lab at Purdue University for ^{10}Be/^{9}Be measurement by accelerator mass spectrometer (AMS). We calculated cosmogenic ^{10}Be surface exposure ages of terminal moraines of the last glaciation and last glacial maximum using the calibrated in situ production rate for ^{10}Be determined at Promontory Point, Utah, with the LSDn production scaling model of Lifton and others (2014) as implemented in version 3.0 of the CRONUS-Earth online exposure age calculator (Balco and others, 2008; http://hess.ess.washington.edu).

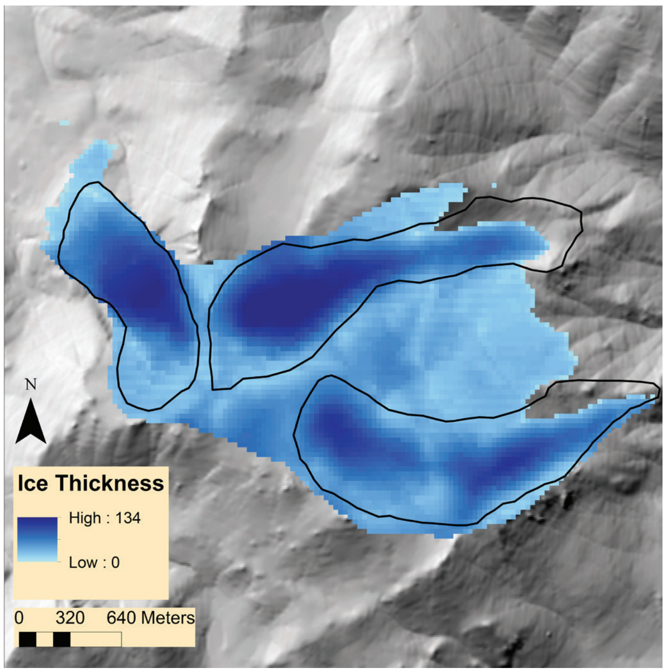

Figure 4. *The reconstructed ice extents (black line) and the modeled ice extent are shown for the Pine Forest Range, Nevada. The temperature-precipitation combination used was -9.1, 1. (https://www.usgs.gov/core-science-systems/national-geospatial-program/national-map)*

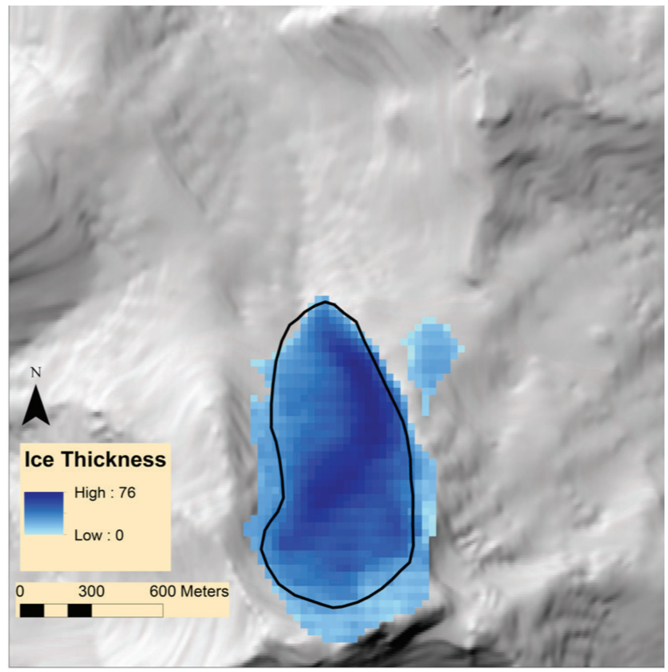

Figure 5. *The reconstructed ice extent (black line) and the modeled ice extent are shown for the Santa Rosa Range, Nevada. The temperature-precipitation combination used was -6.1, 1. (https://www.usgs.gov/core-science-systems/national-geospatial-program/national-map).*

This study also uses a forward numerical modeling approach to determine climate conditions that simulate the known maximum ice extents for the last glaciation in the Santa Rosa and Pine Forest Ranges (figures 4 and 5). The coupled energy-mass balance and ice-flow models used in this study were originally developed by Plummer and Phillips (2003), and have been used to estimate paleo-climate conditions for paleo-glaciers in various mountain glacier settings (Harrison and others, 2014; Rowan and others, 2014; Leonard and others, 2017). The modeling approach aims to match simulated ice extents produced under specific paleoclimate conditions (e.g., temperature depression from modern and precipitation) to known ice extents reconstructed from glacial deposits and landforms identified in the field (e.g., terminal and lateral moraines). The modeling approach consists of two numerical models, a mass and energy balance model and an ice-flow model. The energy-mass balance model calculates monthly snow accumulation and ablation at every cell within the model domain, a digital elevation model of a glacial valley, for the time interval of interest.

Annual mass balance depends mostly on precipitation and temperature, which are the primary inputs to the model (Plummer and Phillips, 2003). Other inputs include relative humidity, cloud cover, solar angles for the area of interest, and a digital elevation surface of the glaciated basin. Average monthly cloudiness and relative humidity are held constant at every cell and elevation within the model domain (Plummer and Phillips, 2003). The source of the inputs, including mean monthly wind speed, temperature, and precipitation, come from RAWS (remote automated weather stations). In order to get a net annual mass balance, we sum the monthly mass balance through the water year and we deviate the “modern” meteorological inputs to simulate paleo-mass balance. Sublimation and monthly snow losses due to melting are calculated from the surface-energy balance. The total is calculated only during melt season. During winter months, only the energy transfer associated with sublimation is calculated. The output is a net annual mass balance defining the areas of net accumulation and net ablation in the model domain, which is used as an input for the ice flow model.

The ice-flow model calculates the time-dependent flux of ice into or out of each cell in a grid created from a set of finite difference equations relating to flow thickness, surface slope, and bed slope (base of glacier) (Plummer and Phillips, 2003). When applying the ice-flow model to the study of geomorphic features of glaciers, we assume that major moraines represent a temporary steady-state condition. Even though the ice-flow model describes transient glacier response, we are only considering steady-state solutions. The primary variable in the model calculations is ice-free surface elevation, the behavior of which is not constant across the grid. Ice surface elevation can either increase or decrease in ice-covered portions of the grid, but can only increase or remain constant in ice-free areas (Plummer and Phillips, 2003). The output of the ice-flow model is a gridded glacier extent, which can be compared to the modeled or known ice extent. The trial-and-error method of calculating glacier mass balance based on an estimated temperature and precipitation combination and forward modeling of the glacier extent based on mass balance allows us to compare the glacier modeling results with the known ice extent. This ultimately produces a set of temperature and precipitation combinations that may have accompanied the glacier at steady state.

RESULTS AND DISCUSSION

Six cosmogenic ^{10}Be exposure ages from a terminal moraine in the Pine Forest Range range from 19.9 ka to 21.2 ka, coinciding with the latter part of the Last Glacial Maximum (21–17 ka). A single exposure age of 17.6 ± 0.5 ka on a younger moraine up valley of the terminal moraine suggests a later advance or pause in ice retreat, although additional cosmogenic exposure ages are needed to obtain an accurate numeric age of this moraine. Eleven Cosmogenic ^{10}Be surface exposure ages from a moraine in the Santa Rosa Range range from 16.8 ka to 18.7 ka. These ages provide the chronological framework for interpreting results of glacier modeling experiments in the two mountain ranges.

The glacier modeling outputs for both the Santa Rosa and Pine Forest Ranges show that modeled glacier shapes closely match the small, simple shapes that characterize the known ice extents (figures 4 and 5). The Santa Rosa numerical modeling results include a broad range of temperature and precipitation combinations that could have accompanied glacier maxima in the two mountain ranges. For example, if precipitation in the Pine Forest Range was similar to modern at the time of the local glacial maximum (~21–20 ka), then temperature depressions during the last glaciation were -9 to -8°C. If precipitation in the Santa Rosa Range was similar to modern during the later glacial maximum at ~18–17 ka, then the temperature ranges were -6 to -5°C.

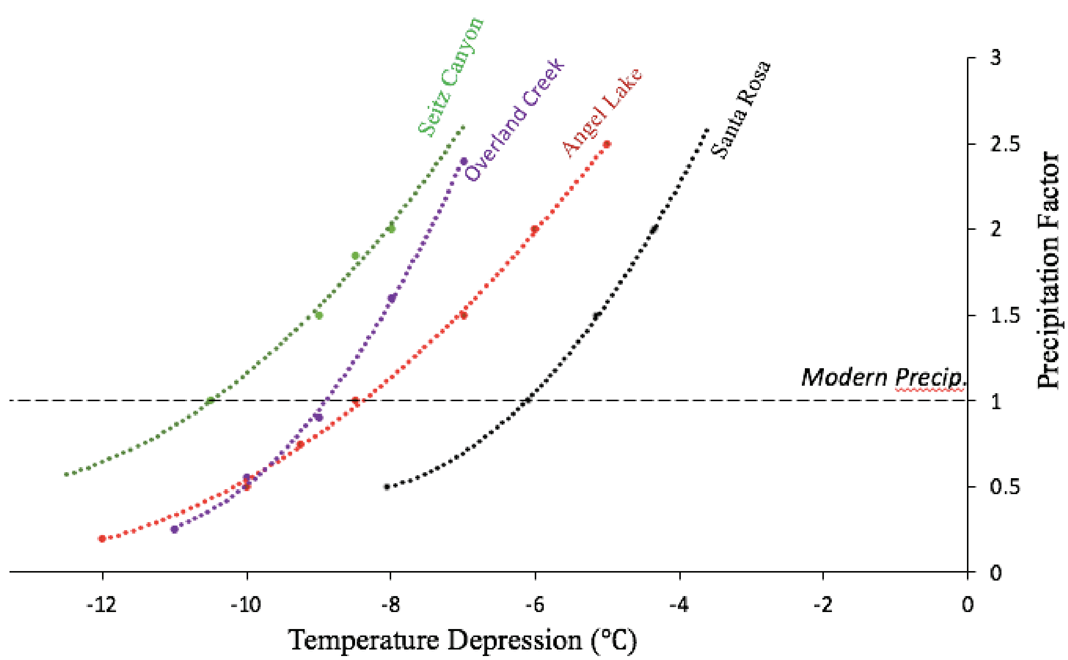

Figure 6A. Temperature-Precipitation combinations yielded from glacier modeling results west of Pleistocene Lake Bonneville. The precipitation factor is a multiplier and the precipitation factor of 1 is equal to modern precipitation.

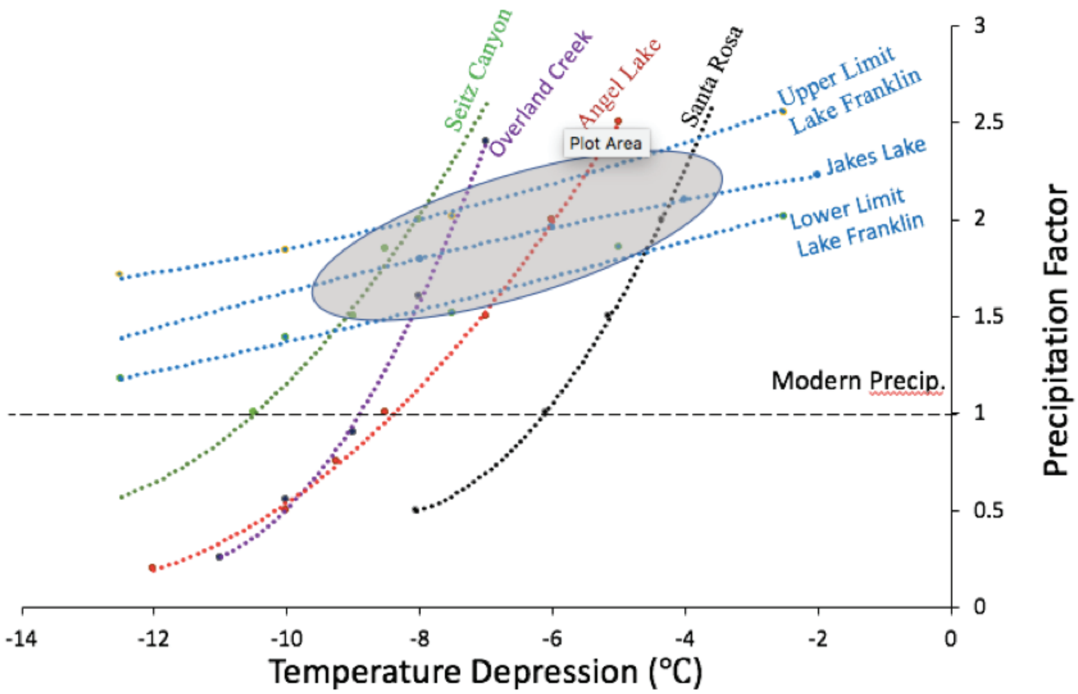

Figure 6B. *Temperature-Precipitation combinations yielded both from glacier and lake modeling results west of Pleistocene Lake Bonneville. The precipitation factor is a multiplier and the precipitation factor of 1 is equal to modern precipitation.*

It is difficult to obtain a unique temperature and precipitation value when only looking at the glacier modeling results (figure 6A). We compare modeling results reported here with others from the northern Great Basin, and with results of water-budget modeling studies of pluvial lakes to identify a unique temperature and precipitation combination for a given time interval (figure 6B). Glacier modeling results are available for the eastern Ruby Mountains (Overland Creek valley; Reimers and others, 2016) and the western Ruby Mountains (Seitz and Hennen Canyons; Truong and others, 2014) as well as the Angel Lake valley in the East Humboldt Mountains (Bradley and Laabs, 2015), providing additional limits on possible temperature and precipitation combinations for the time interval 18–17 ka. Lake-water-budget modeling results, which also provide limits on temperature-precipitation combinations for 18–17 ka, are available from Jakes Lake (Barth and others, 2016) and Lake Franklin (Ferragut and others, 2017). When comparing the Santa Rosa modeling results against other glacier modeling results, including Seitz Canyon, Overland Creek, and Angel Lake, we see that all the lines defining possible temperature-precipitation combinations run nearly parallel to one another (figure 6A). This suggests that glacier modeling results alone do not provide a unique temperature-precipitation combination for 18–17 ka. However, comparing glacier-modeling results with lake-modeling results of Barth and others (2016) and Ferragut and others (2017) reveals intersecting trajectories of possible temperature-precipitation combinations, which yield a more unique estimate of temperature and precipitation at 18–17 ka in the northern Great Basin (figure 6B). For this comparison, we include the upper and lower limits of inferred temperature and precipitation combinations for the modeling of Lake Franklin (Ferragut and others, 2017), and one range of estimates for temperature-precipitation combinations accompanying the highstand of Jakes Lake (Barth and others, 2016). For glacier and lake maxima at 18–17 ka, modeling results suggest temperature depressions from -4 to -10°C and precipitation change from 1.5 to 2 times modern. This range of temperature depressions compares favorably to clumped isotope records from Lake Chewaucan (Hudson and others, 2017), a pluvial lake that expanded in a valley just north of the Santa Rosa Range. Importantly, the combined results indicate greater-than-modern precipitation during the interval 18–17 ka, the time when most lakes of the northern Great Basin expanded (Munroe and Laabs, 2013) and the early part of Heinrich Stadial 1 (Hemming, 2004).

CONCLUSIONS

Overall, the cosmogenic chronology of a terminal moraine in the Pine Forest Range displays some coincidence with the latter parts of the Last Glacial Maximum. On the other hand, the cosmogenic chronology of a moraine in the Santa Rosa Range provides the chronological framework for interpreting results of glacier modeling experiments in the two mountain ranges. Additionally, cosmogenic ^{10}Be surface exposure ages from both the Santa Rosa and Pine Forest Ranges have ages that overlap with high lake phases of the nearby Lake Franklin and Lake Chewaucan (Munroe and Laabs, 2013; Hudson and others, 2017).

Temperature depression for Last Glacial Maximum conditions of -4 to -10°C with 2 to 1.5 times modern precipitation is consistent with estimates from western North America derived from terrestrial pollen (Worona and Whitlock, 1995), and from global climate, hydrologic, and glacial modeling studies (Birkel and others, 2012; Ibarra and others, 2014; Barth and others, 2016). Continued consideration of glacier and lake chronologies for the last glaciation along with refined modeling experiments will help to narrow estimates of temperature and precipitation across the northern Great Basin. For future work, our primary focus will be refining glacier modeling experiments summarized here and water-budget modeling of pluvial lakes of the northern Great Basin. There will also be additional cosmogenic ^{10}Be surface exposure dating of the Santa Rosa and Pine Forest Ranges.

REFERENCES

Balco, G., Stone, J., Lifton, N., and Dunai, T., 2008, A complete and easily accessible means of calculating surface exposure ages or erosion rates from ^{10}Be and ^{26}Al measurements: Quaternary Geochronology, v. 3, p. 174–195.

Barth, C., Boyle, D.P., Hatchett, B.J., Bassett, S.D., Garner, C.B., and Adams, K.D., 2016, Late Pleistocene climate inferences from a water balance model of Jakes Valley, Nevada (USA): Journal of Paleolimnology, v. 56, p. 109–122.

Birkel, S.D., Putnam, A.E., Denton, G.H., Koons, P.O., Fastook, J.L., Putnam, D.E., and Maasch, K.A., 2012, Climate inferences from a glaciological reconstruction of the late Pleistocene Wind River ice cap, Wind River Range, Wyoming: Arctic, Antarctica, and Alpine Research, v. 44, p. 265–276.

Bradley, R.A.A., and Laabs, B.J.C., 2015, Climate change during the last Pleistocene glaciation in northern Nevada inferred from numerical glacial modeling, Angel Lake type locality, East Humboldt Range, Nevada, U.S.A: Geological Society of America, Abstracts with Programs, v. 47, no. 3, p. 114.

Ferragut, G., Laabs, B.J.C., Amidon, W.A., and Munroe, J.S., 2017, Constraining Late Pleistocene climate of the northeastern Great Basin using mass balance modeling of paleolakes and glaciers: Geological Society of America, Abstracts with Programs, v. 49, no. 6, p. 361–363, doi: 10.1130/abs/2017AM-306260.

Harrison, S., Rowan, A.V., Glasser, N.F., Knight, J., Plummer, M.A., and Mills, S.C., 2014, Little Ice Age glaciers in Britain: Glacier–climate modelling in the Cairngorm Mountains: The Holocene, v. 24, p. 135–140.

Hemming, S.R., 2004, Heinrich events—massive late Pleistocene detritus layers of the North Atlantic and their global climate imprint: Reviews of Geophysics, v. 42, RG 1005.

Hudson, A.M., Quade, J., Guleed, A., Boyle, D., Bassett, S., Huntington K.W., De Los Santos, M.G., Cohen, A.S., Xiangfeng Wang, and Ke Lin., 2017, Stable C, O and clumped isotope systematics and 14C geochronology of carbonates from the Quaternary closed-basin lake system, Great Basin, USA—Implications for paleoenvironmental reconstructions using carbonates: ScienceDirect, v. 212, p. 274–302.

Ibarra, D.E., Egger, A.E., Weaver, K.L., Harris, C.R., and Maher, K., 2014, Rise and fall of late Pleistocene pluvial lakes in response to reduced evaporation and precipitation—Evidence from Lake Surprise, California: Geological Society of America Bulletin, v. 126, no. 11-12, p. 1–29.

Laabs, B.J.C., and Munroe, J.S., 2016, Late Pleistocene mountain glaciation in the Lake Bonneville basin, *in* Oviatt, C.G., and Schroeder, J., editors, Lake Bonneville—A scientific update: Amsterdam, Elsevier, p. 462–503.

Laabs, B.J., Munroe, J.S., Best, L.C., and Caffee, M.W., 2013, Timing of the last glaciation and subsequent deglaciation in the Ruby Mountains, Great Basin, USA: Earth and Planetary Science Letters, v. 361, p. 16–25.

Lachniet, M.S., Denniston, R.F., Asmerom, Y., and Polyak, V.J., 2014, Orbital control of western North America atmospheric circulation and climate over two glacial cycles: Nature Communications, v.5, p. 1–8.

Leonard, E.M., Laabs, B.J., Plummer, M.A., Kroner, R.K., Brugger, K.A., Spiess, V.M., Refsnider, K.A., Xia, Y., and Caffee, M.W., 2017, Late Pleistocene glaciation and deglaciation in the Crestone Peaks area, Colorado Sangre de Cristo Mountains, USA—chronology and paleoclimate: Quaternary Science Reviews, v. 158, p. 127–144.

Lifton, N., Sato, T., and Dunai, T.J., 2014, Scaling in situ cosmogenic nuclide production rates using analytical approximations to atmospheric cosmic-ray fluxes: Earth and Planetary Science Letters, v. 386, p.149–160.

Lyle, M. and others, 2012, Out of the tropics—The Pacific, Great Basin Lakes, and Late Pleistocene water cycle in the western United States: Science 337, p. 1629–1633.

Munroe, J.S., and Laabs, B.J., 2013, Temporal correspondence between pluvial lake highstands in the southwestern US and Heinrich Event 1: Journal of Quaternary Science, v. 28, no. 1, p. 49–58.

Osborn, G., and Bevis, K., 2001, Glaciation in the Great Basin of the western United States: Quaternary Science Reviews, v. 20, p. 1377–1410.

Oster, J.L., and Kelley N.P., 2016, Tracking regional and global teleconnections recorded by western North American speleothem records: Quaternary Science, v. 149, p. 18–33.

Pierce, K.L., 2003, Pleistocene glaciations of the Rocky Mountains: Developments in Quaternary Sciences, v. 1, p. 63–76.

Plummer, M.A., and Phillips, F.M., 2003, A 2-D numerical model of snow/ice energy balance and ice snow for paleoclimatic interpretation of glacial geomorphic features: Quaternary Science Review, v. 22, p. 1389–1406.

Reheis, M.C., 1999, Extent of Pleistocene lakes in the western Great Basin: U.S. Geological Survey Miscellaneous Field Studies Map 2323, https://doi.org/10.3133/mf2323.

Reimers, A.C., and Laabs, B.J.C., 2016, Mountain glacier retreat rates during the last Pleistocene glaciation in the western United States: Geological Society of America, Abstracts with Programs, v. 48, no. 7, p. 81—8.

Rowan, A.V., Brocklehurst, S.H., Schultz, D.M., Plummer, M.A., Anderson, L.S., and Glasser, N.F., 2014, Late Quaternary glacier sensitivity to temperature and precipitation distribution in the Southern Alps of New Zealand: Journal of Geophysical Research, Earth Surface, v. 119, p. 1064–1081.

Truong, K.T., Laabs, B.J.C., and Lam, J.J., 2014, Climate change during the last glaciation in the northern Great Basin inferred from numerical modeling of glaciers in the Ruby Mountains, northern Nevada: Geological Society of America, Abstracts with Programs, v. 46, no. 6, p. 557.

Worona, M.A., and Whitlock C., 1995, Late Quaternary vegetation and climate history near Little Lake, central Coast Range, Oregon: Geological Society of America Bulletin, v. 107, no. 7, p. 867–876.

This content is a PDF version of the author’s PowerPoint presentation.

Numerical Modeling of Late Pleistocene Glaciers and Lakes West of Lake Bonneville, Implications for Regional Climate Change

By Kaitlyn Fleming

North Dakota State University

Outline

- Study area- Pleistocene glaciers and lakes west of Lake Bonneville
- Research objectives- paleoclimate in the northwest Great Basin
- Glacier modeling
- Inferences of Late Pleistocene climate

Study Area: Santa Rosa and Pine Forest Ranges

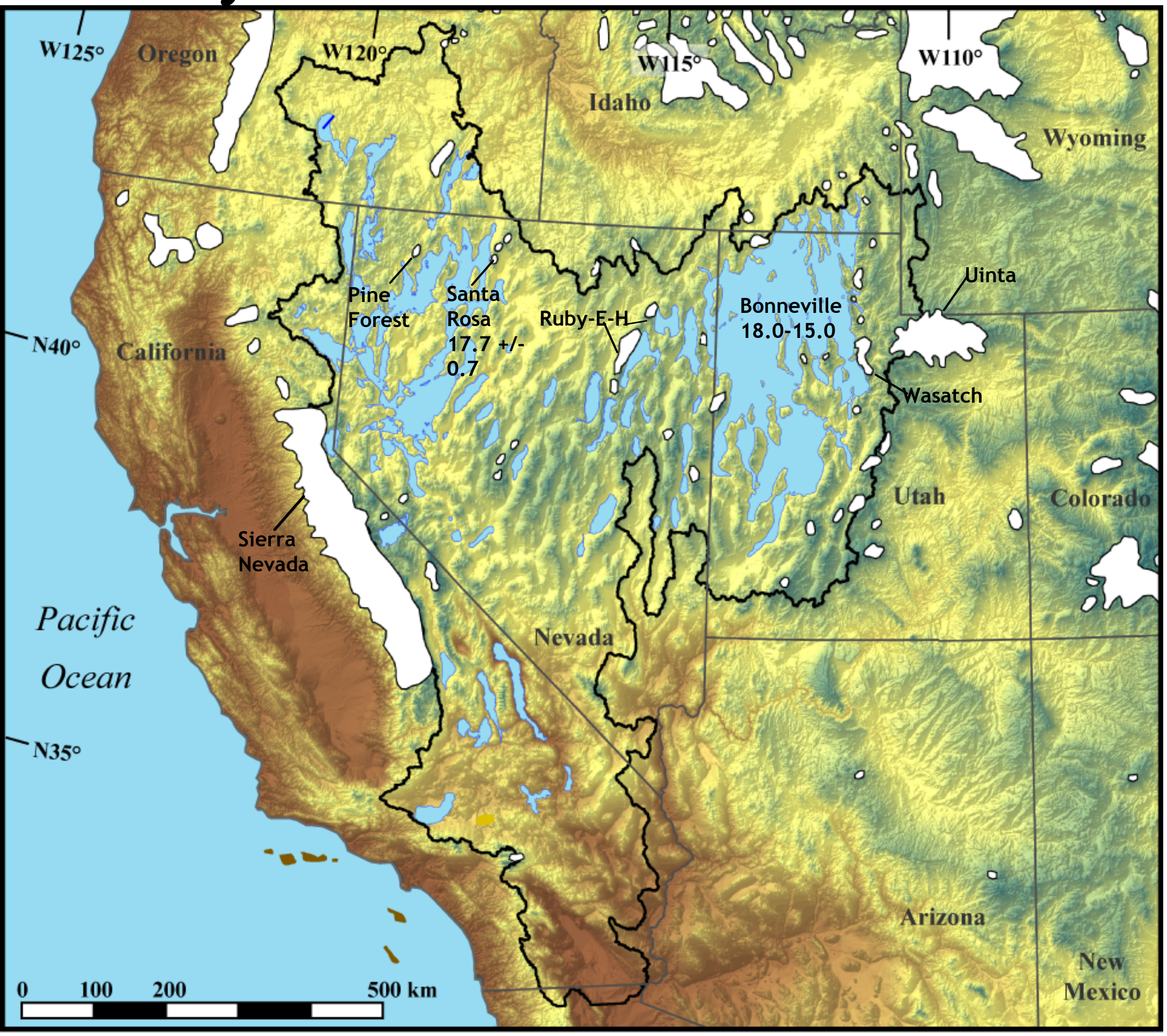

- Forty glaciated mountains in the Great Basin (Osborn and Bevis, 2001).
- Glacial histories of ranges between the Sierra Nevada and the Wasatch Mountains are partly developed (Laabs and Munroe, 2016)
- Santa Rosa and Pine Forest Ranges

Relative Timing of Moraine Deposition and Lake Highstands

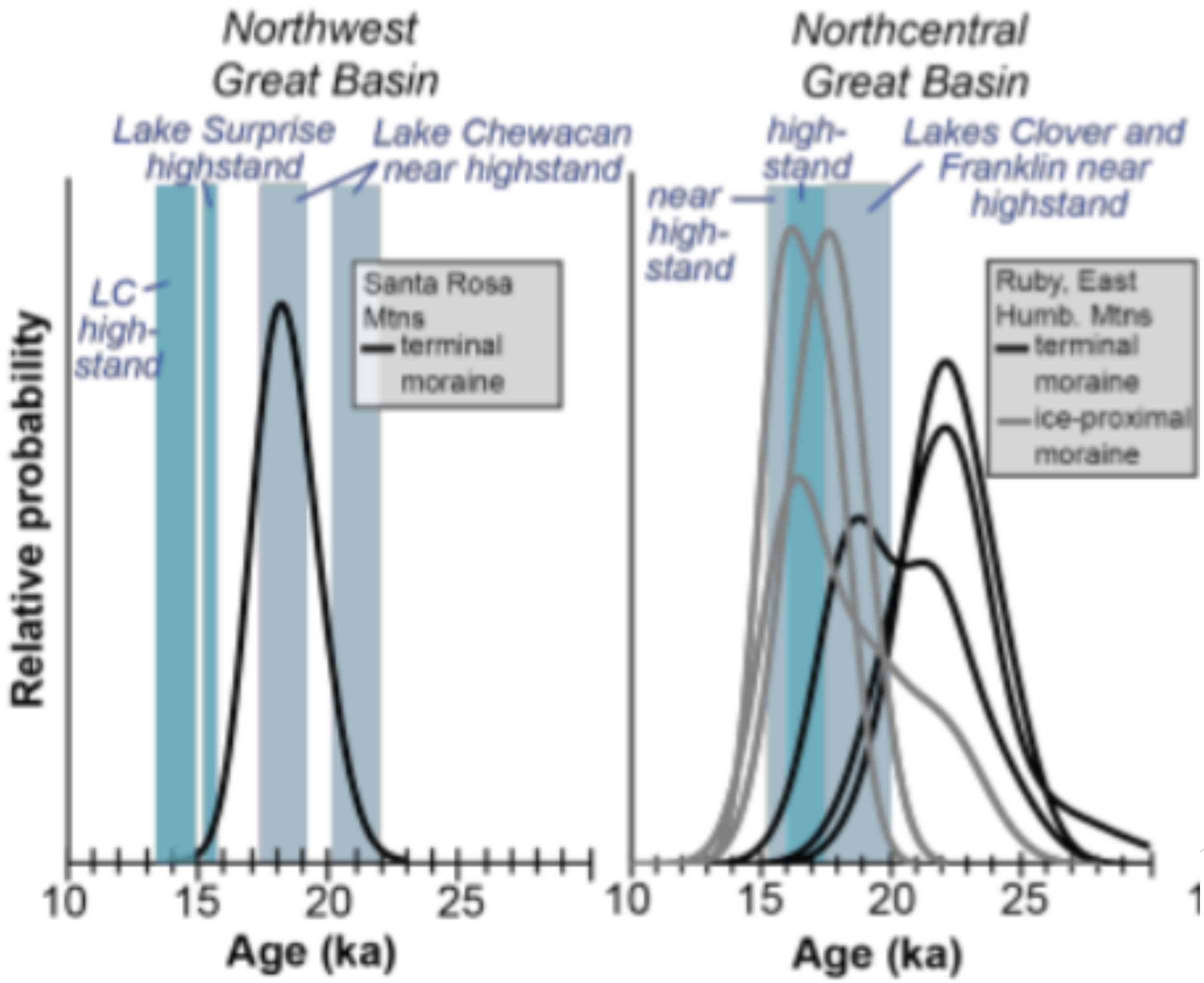

Research Objectives

- Determine the relative timing of glacier maxima and lake highstands in the northwest Great Basin
- Set precise limits on temperature and precipitation based on modeling glaciers and lakes

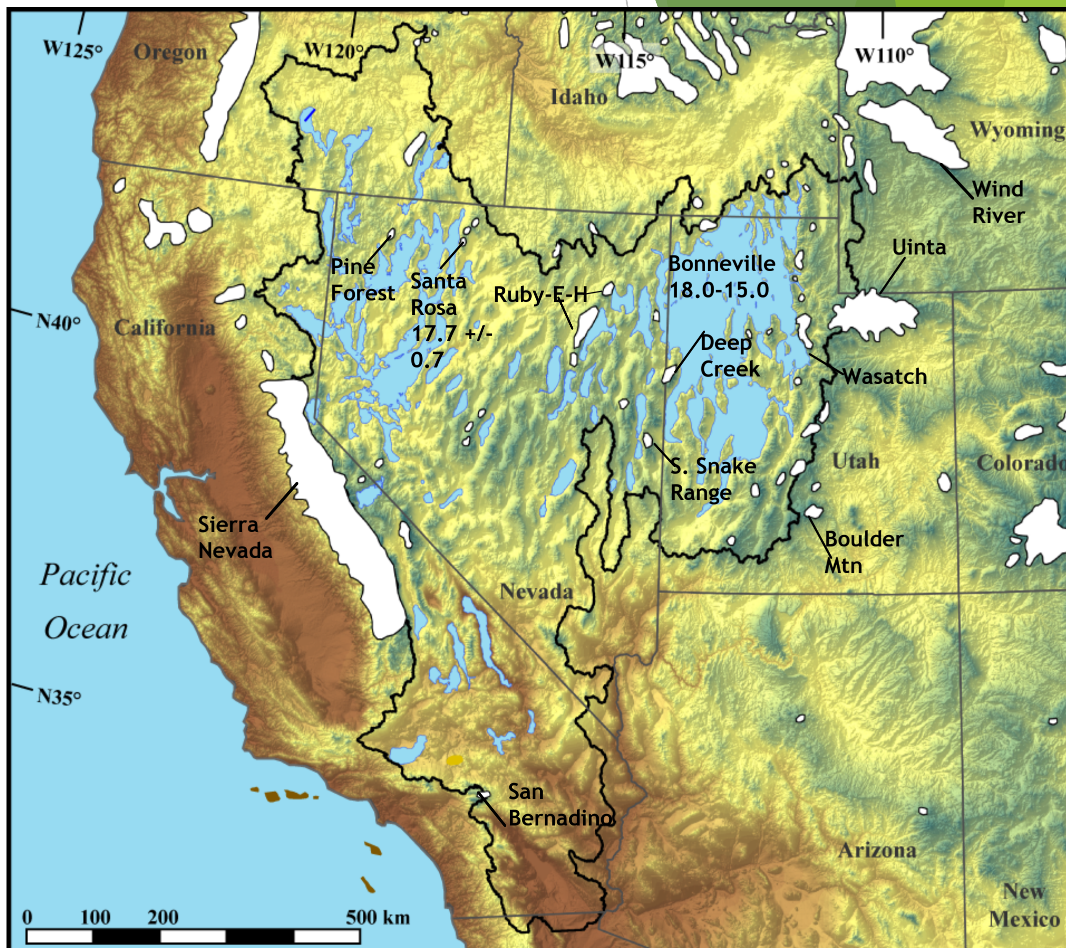

Santa Rosa Range

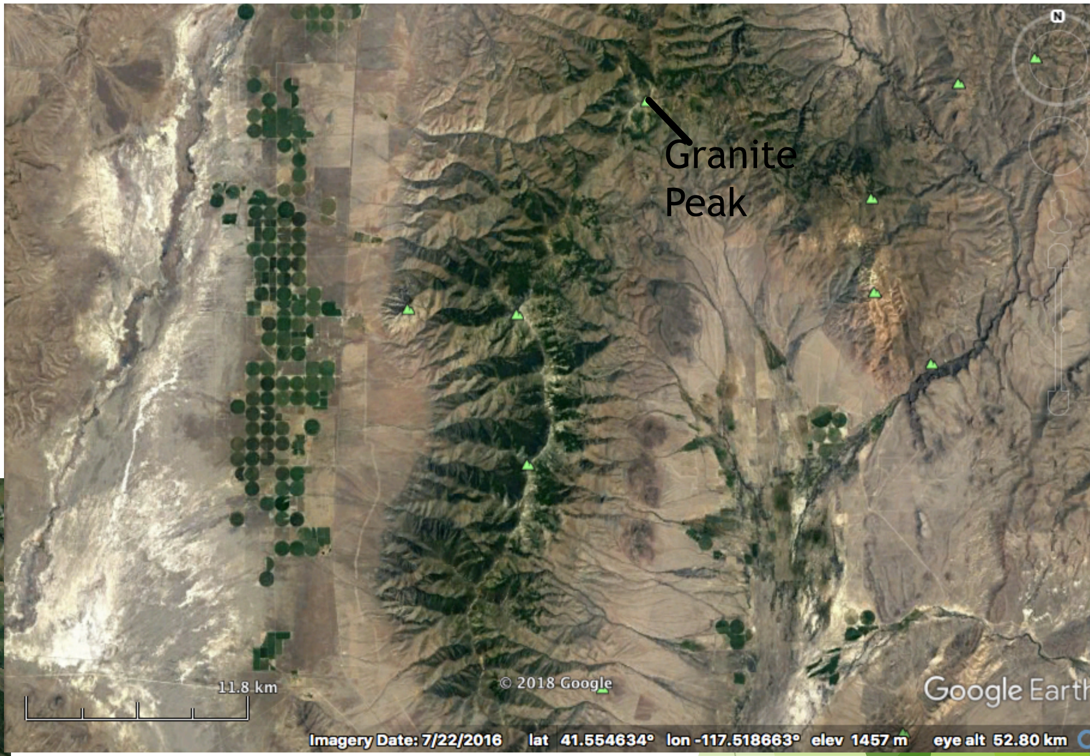

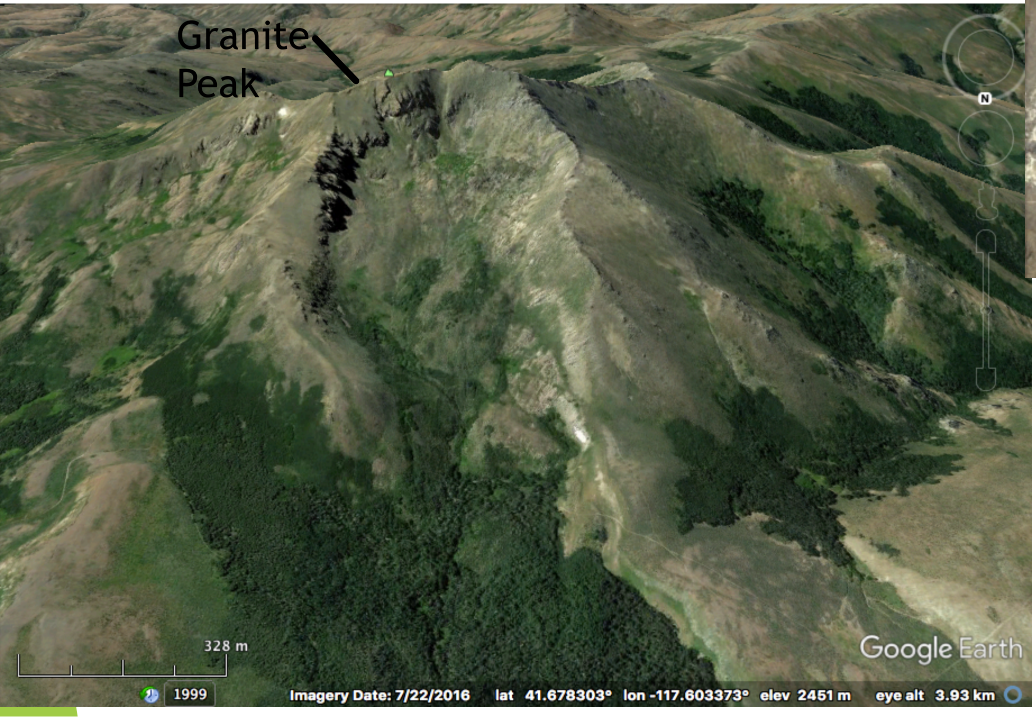

Pine Forest Range

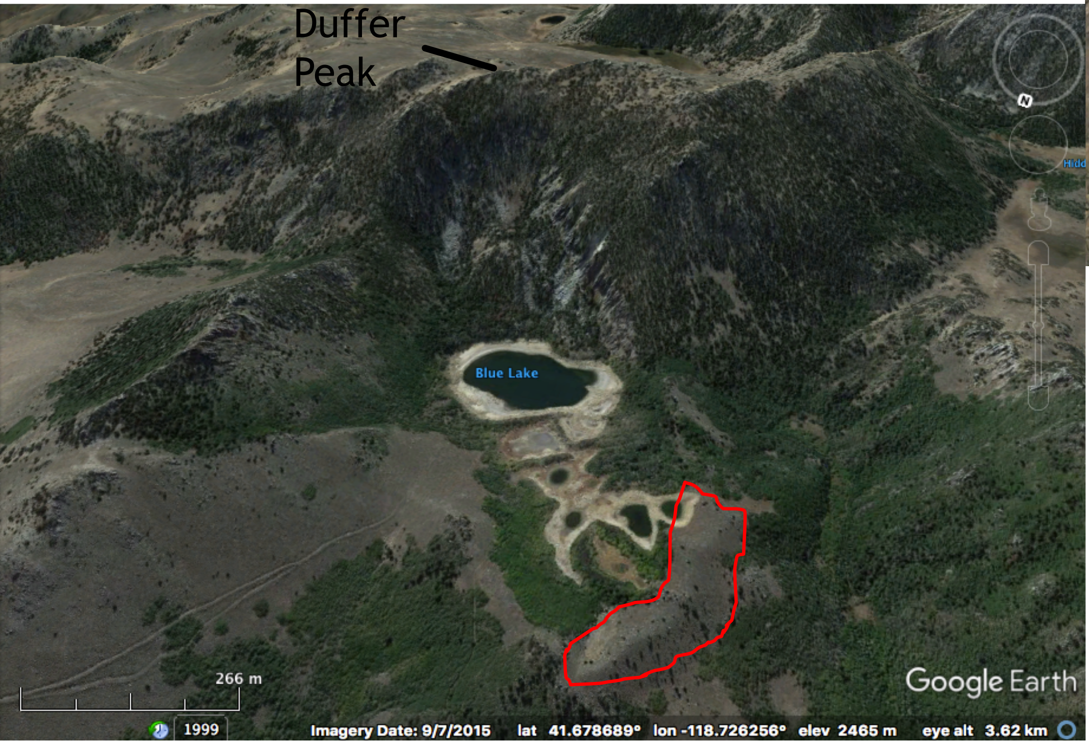

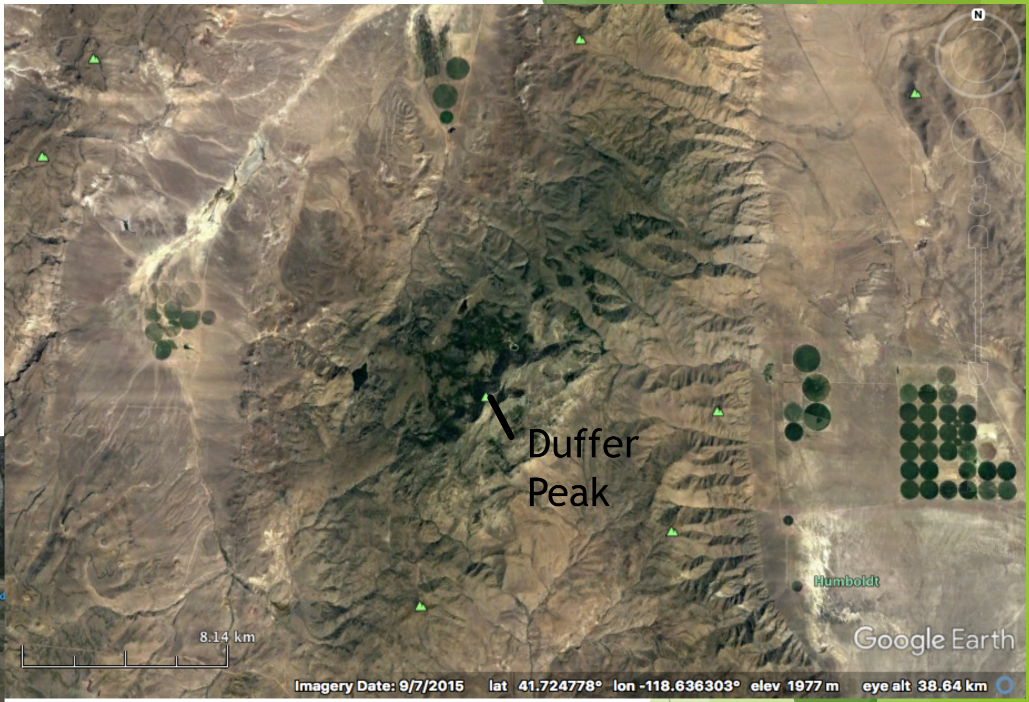

Glacier Modeling Procedure

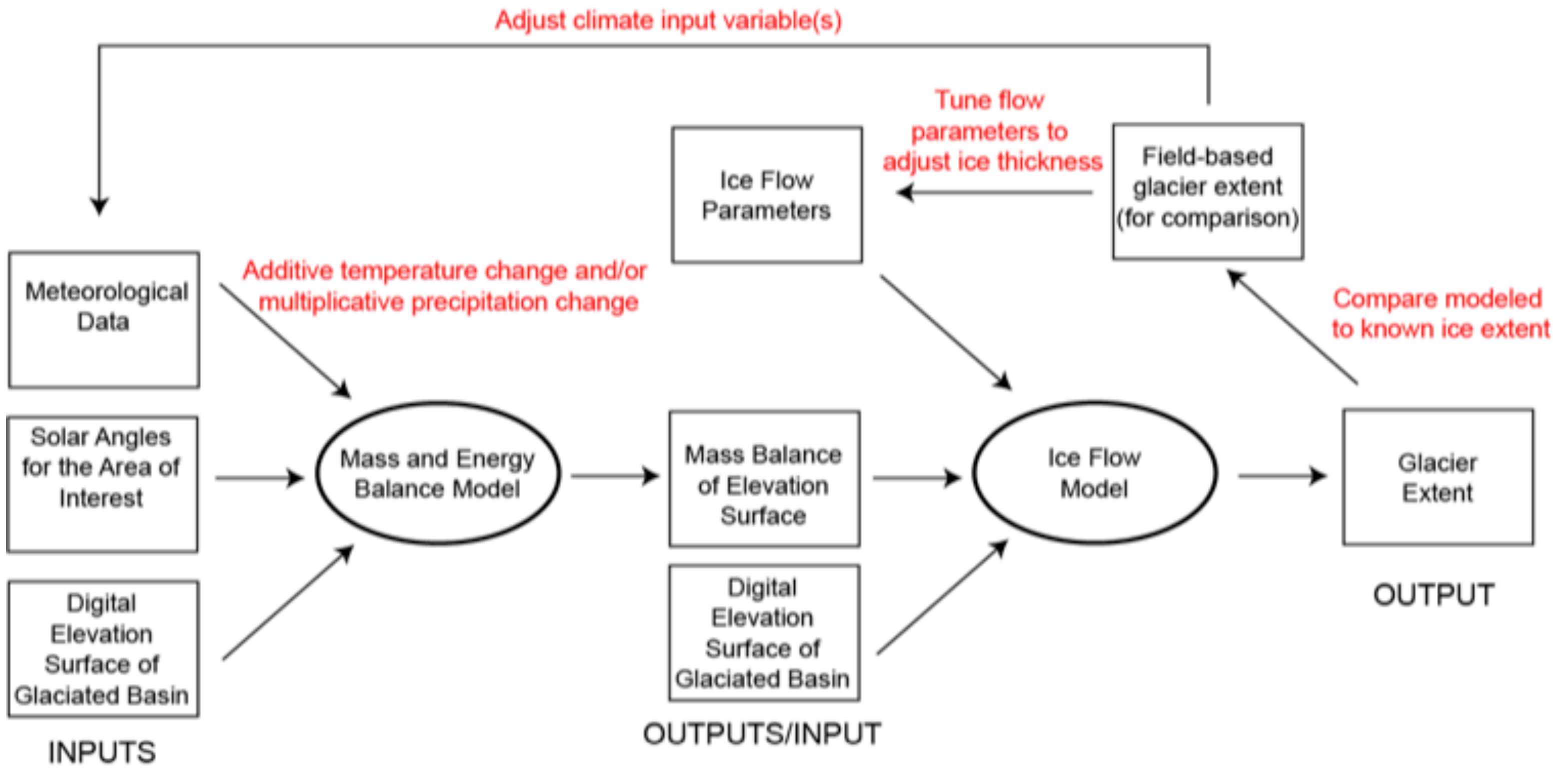

Plummer and Phillips, 2003

Glacier Modeling Results: Santa Rosa Range

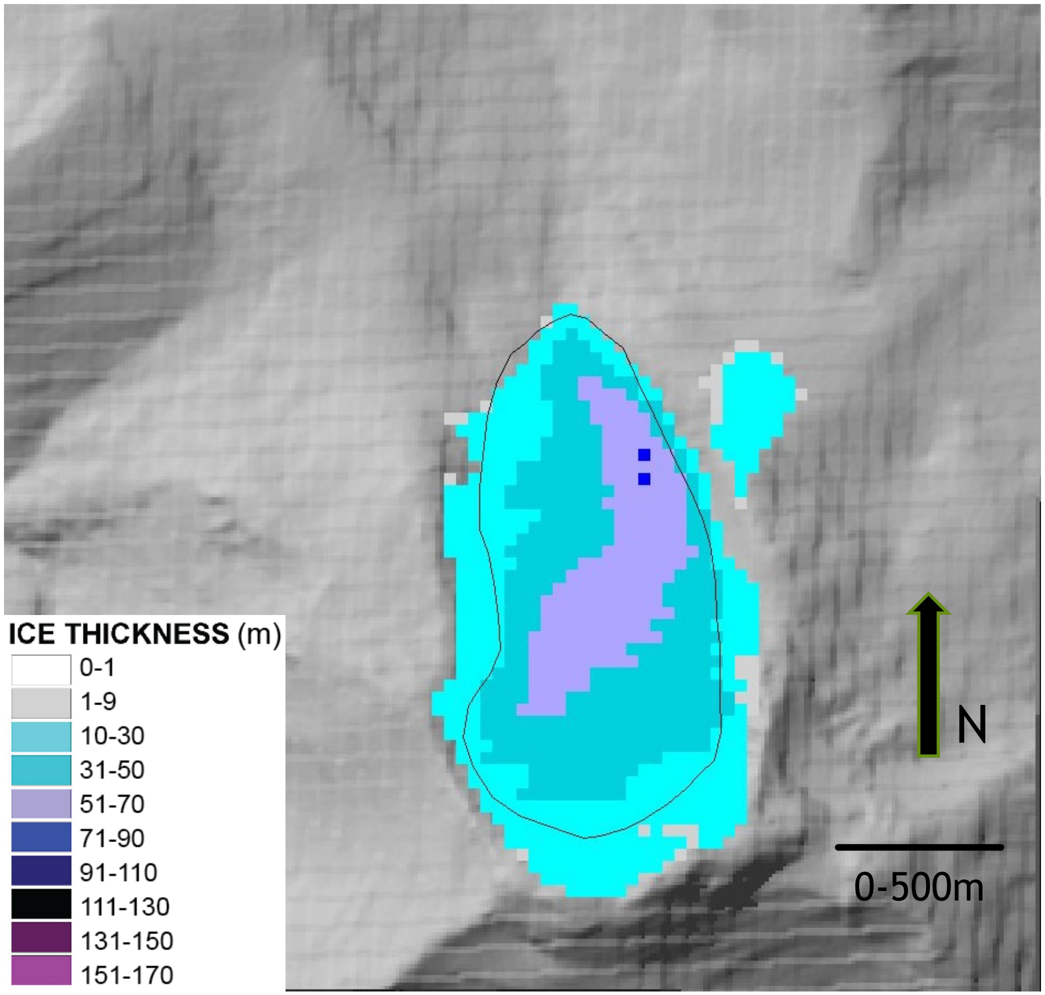

- Modeled glacier shape closely matches the known ice extent
- Temperature: -6.1
- Precipitation: 1

Glacier Modeling Results: Pine Forest Range

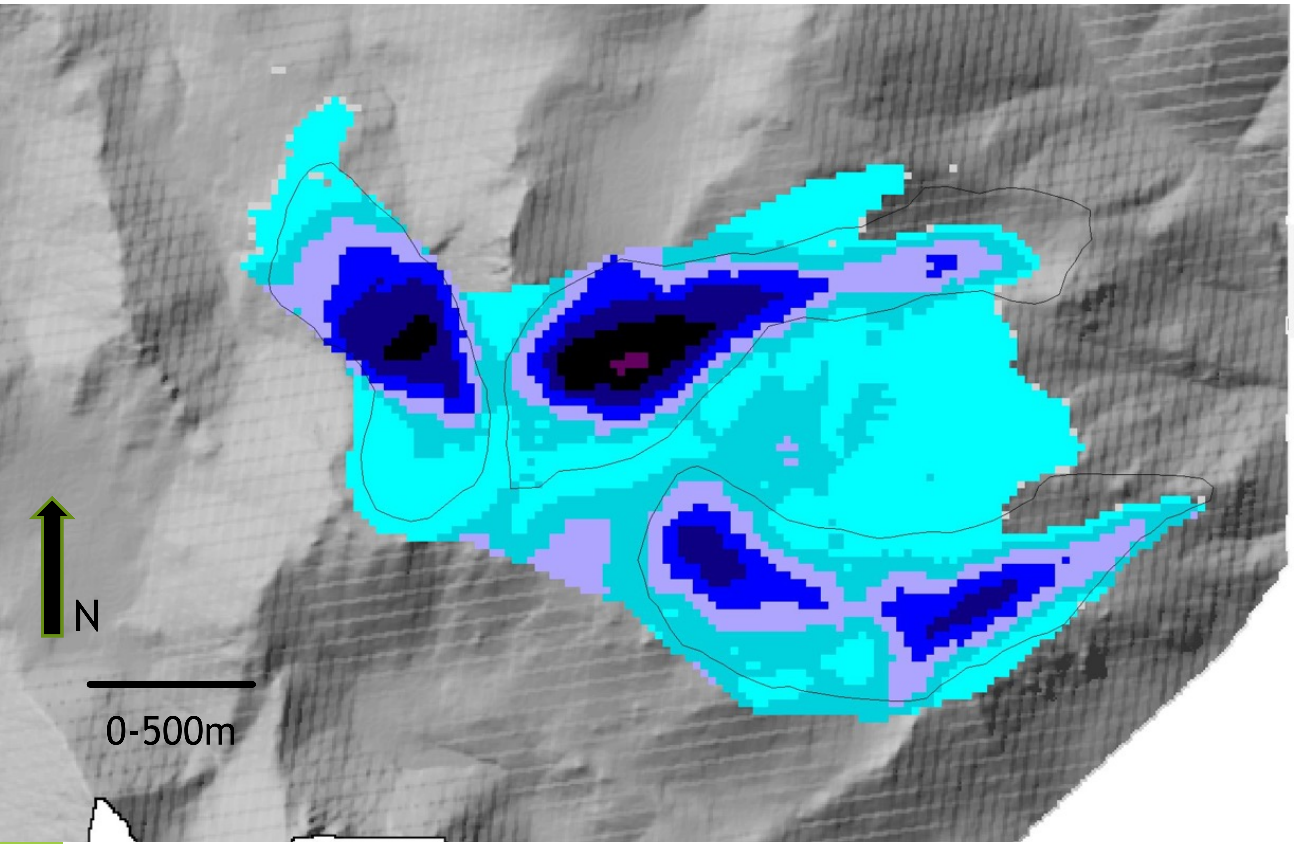

- Temperature: -10.2
- Precipitation: 1

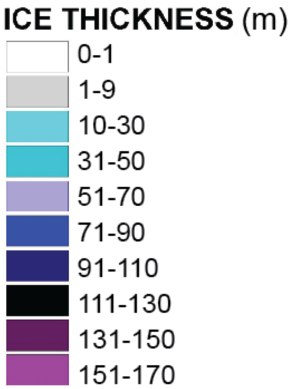

Pine Forest and Santa Rosa Glacial Model Results

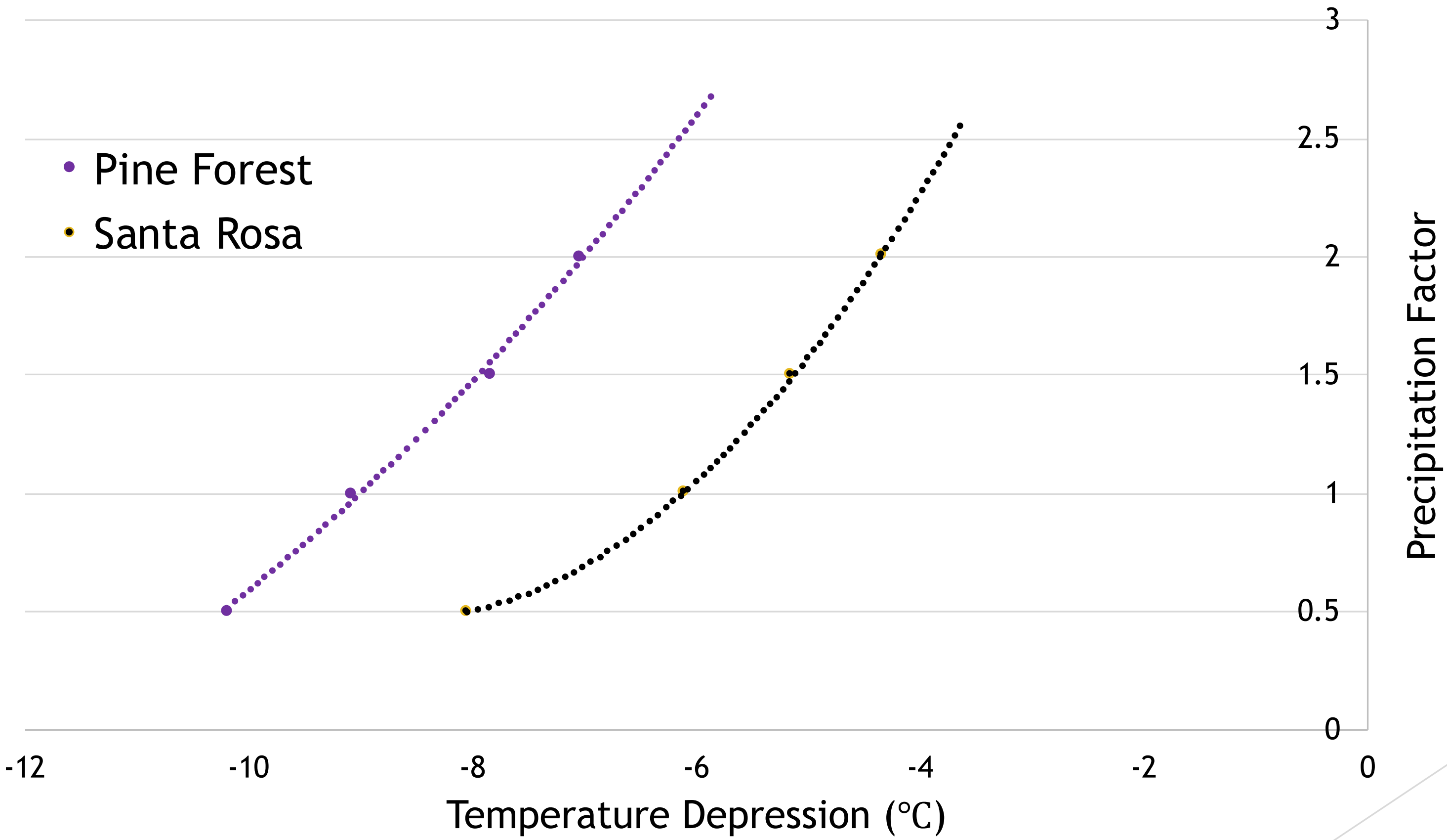

More Glacier Model Results From West of Lake Bonneville

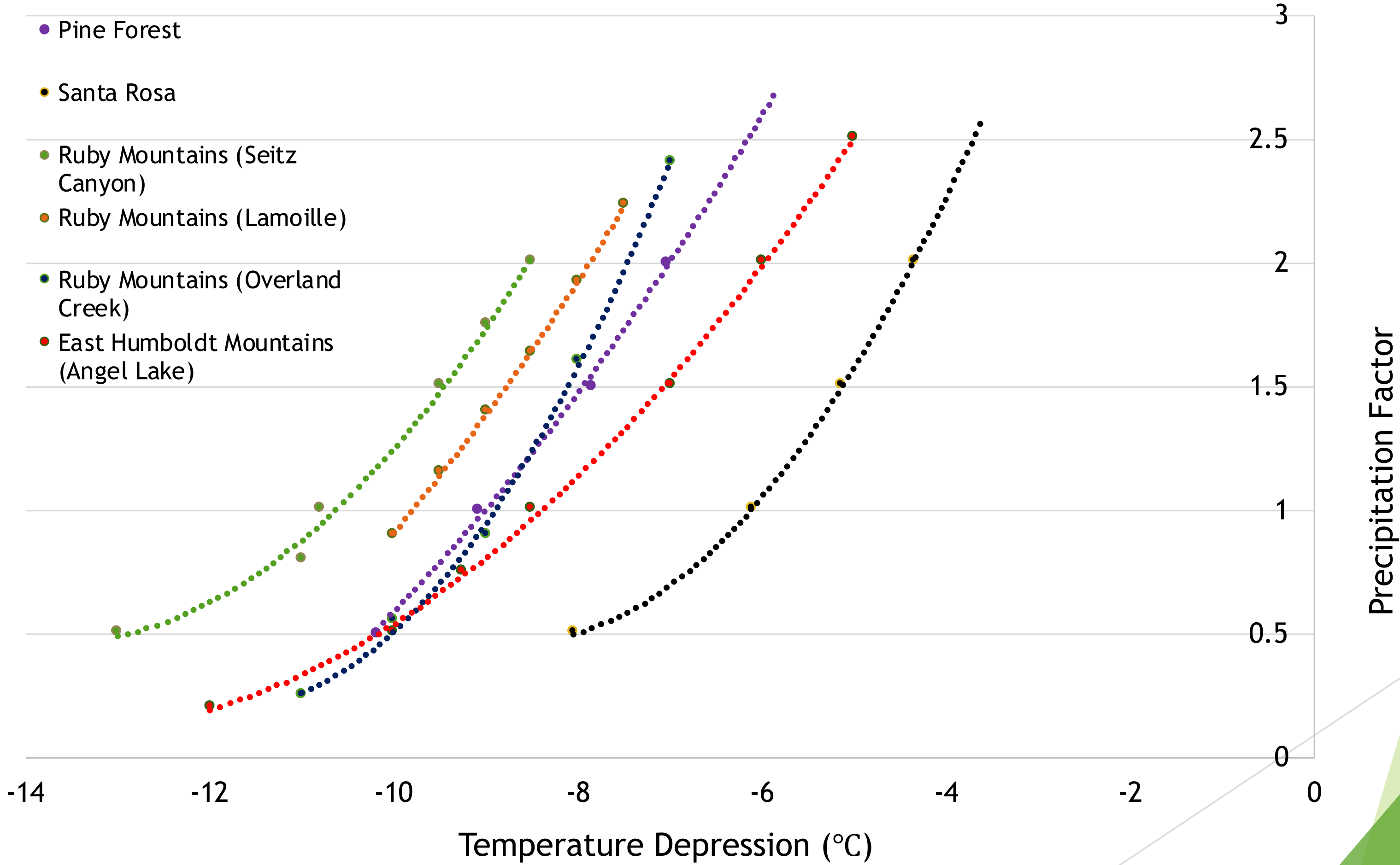

Comparison of Glacial and Lake Model Results

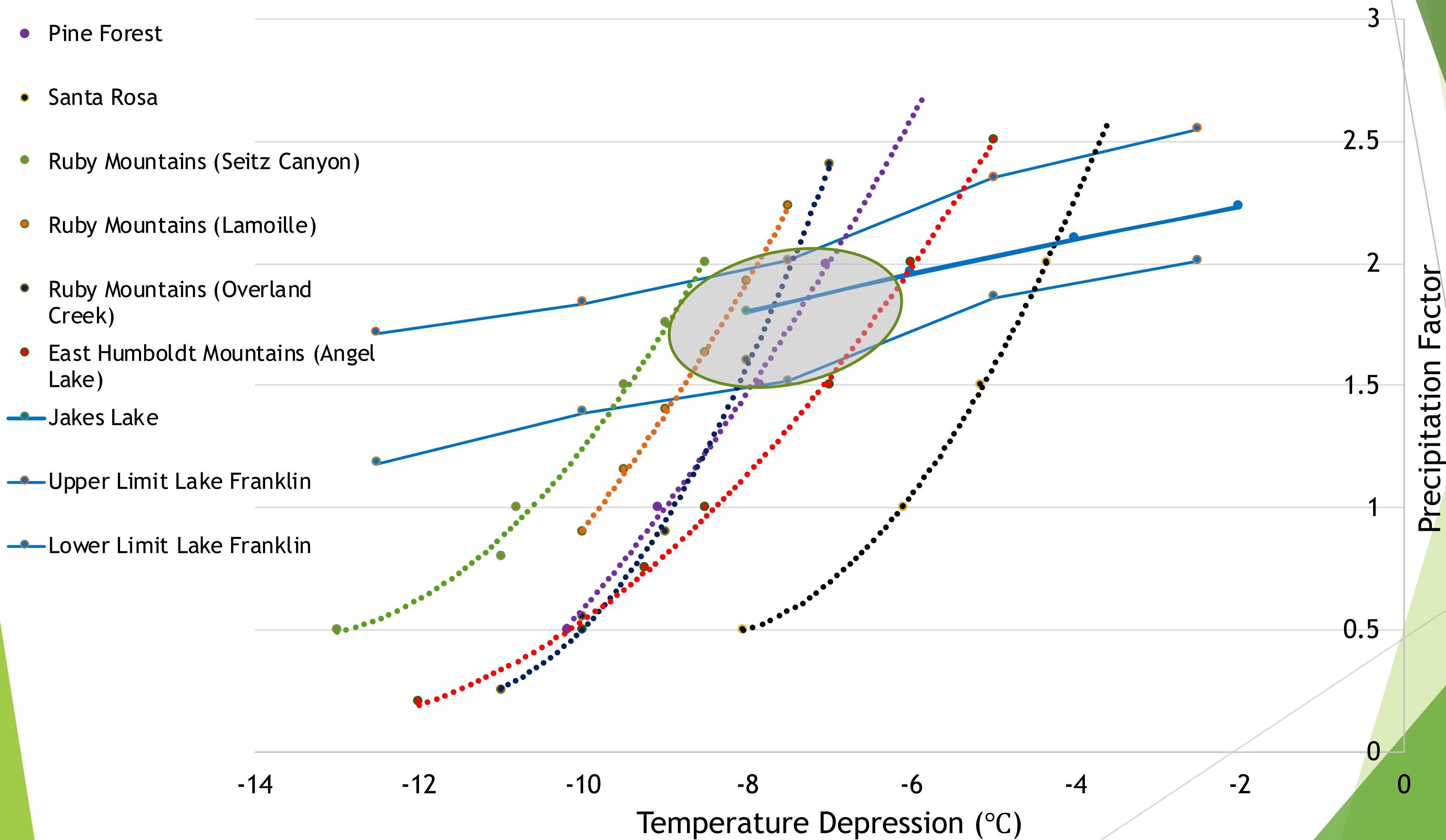

Conclusions

- Glacier modeling experiments yield a broad range of possible temperature and precipitation combinations for the northern Great Basin
- Combining glacier and lake modeling results yield temperature and precipitation combinations from -7 to -9
- Results of numerical model experiments that simulate Last Glacial Maximum (LGM) and Lateglacial ice extents include a range of temperature and precipitation combinations accompanying glacier maxima in the northwestern Great Basin
- Chronology of glacial deposits and inferred climate during the last glaciation show consistency across the northern Great Basin
  - Suggests that precipitation in the region was similar to modern

Acknowledgements

- NSF
- NDSU
- Purdue University

LAKE AREA CONSTRAINTS ON PAST HYDROCLIMATE IN THE WESTERN UNITED STATES: APPLICATION TO PLEISTOCENE LAKE BONNEVILLE

Daniel E. Ibarra[1], Jessica L. Oster[2], Matthew J. Winnick[3], Jeremy K. Caves Rugenstein[4], Michael P. Byrne[5,6], and C. Page Chamberlain[1]

[1] Earth and Planetary Science, University of California, Berkeley, 307 McCone Hall, Berkeley, CA 94720-4767, USA;
[2] Department of Earth and Environmental Sciences, Vanderbilt University, 5726 Stevenson Center; 7th Floor, Nashville, TN 37240, USA;
[3] Department of Geosciences, 611 North Pleasant Street, 233 Morrill Science Center, University of Massachusetts Amherst, Amherst, MA 01003-9297, USA;
[4] Max Planck Institute for Meteorology, Bundesstraße 53, 20146 Hamburg, Germany;
[5] School of Earth and Environmental Sciences, University of St. Andrews, Irvine Building, St. Andrews KY16 9AL, Fife, UK;
[6] Department of Physics, University of Oxford, Parks Road, Oxford OX1 3PJ, UK

Corresponding author (Ibarra): danielenriqueibarra@gmail.com

ABSTRACT

Lake shoreline remnants found in basins of the western United States reflect wetter conditions during Pleistocene glacial periods. The size distribution of paleolakes, such as Lake Bonneville, provide a first-order constraint on the competition between regional precipitation delivery and evaporative demand. In this contribution we downscale previous work using lake mass balance equations and Budyko framework constraints to determine past hydroclimate change for the Bonneville and Provo shoreline extents of Lake Bonneville during the last glacial cycle. For the Bonneville basin we derive new relationships between temperature depression and precipitation factor change relative to modern. These scaling relationships are combined with rebound-corrected estimates of lake area and volume and macrofossil-derived surface temperatures to make quantitative estimates of precipitation and water residence times for the lake. For the Bonneville shoreline (~1552 m) we calculate that, prior to spillover to the Snake River drainage, precipitation rates were ~1.37 times modern, with a water residence time of ~185 years. For the Provo shoreline (1444 m), during the period of steady-state spillover, we calculate that precipitation rates were at least 1.26 times modern, with a residence time of ~102 years. These calculations suggest minimal difference in the hydrologic regime between the Bonneville shoreline highstand and the Provo shoreline stillstand during the last glacial termination. These estimates of hydroclimate scaling relationships differ in sensitivity with previous hydrologic modeling for Lake Bonneville, and are complementary to those recently derived from glacier mass balance modeling from the Wasatch Range.

INTRODUCTION AND METHODOLOGY

The size of pluvial lakes in terminally draining basins of the western United States indicate a substantially different landscape during Pleistocene glacial periods. Building on the seminal work of G.K. Gilbert (1890) and J.C. Russell (1885), shoreline mapping and compilations of late Pleistocene lake surface areas in the western United States (e.g., Hubbs and Miller, 1948; Mifflin and Wheat, 1979; Williams and Bedinger, 1984; Reheis, 1999a; Orme, 2008; Grayson, 2011) has led to estimates of hydroclimate based on steady-state mass balance assumptions related to observed lake areas (e.g., Mifflin and Wheat, 1979; Hostetler and Benson, 1990; Reheis, 1999b; Broecker, 2010; Matsubara and Howard, 2009; Munroe and Laabs, 2013; Reheis and others, 2014; Ibarra and others, 2014; 2018; Barth and others, 2016). Geologic observations of shorelines or outcrop extent from ancient lake systems thus serve as constraints for quantitative paleoclimate reconstructions for comparison to climate model experiments (e.g., Ibarra and others, 2014; Oster and others, 2015; Barth and others, 2016; Lora and others, 2017).

One such relationship, derived from the steady-state water balance assumption, is for the area of the lake (A_L) to the area of the basin (A_B) (Hudson and Quade, 2013; Ibarra and others, 2018):

$$\frac{A_L}{A_B} = \frac{P - ET}{E_L - P + Pk} = \frac{Pk_{run}}{E_L - P + Pk_{run}} \quad (1),$$

where:

A_L and A_B = the areas of the lake and basin, respectively (km^2).
P = the basin average precipitation (mm/year).
ET = the tributary average evapotranspiration (mm/year).
E_L = the lake average evaporation (mm/yr).
k_{run} = the runoff ratio of the subaerial portion of the watershed (i.e., $P–ET = Pk_{run}$), including both groundwater and riverine runoff into the basin.

The relationship between precipitation and runoff is non-linear across climate states, and thus necessitates increased proportional runoff (higher k_{run}) with increased precipitation. To impose this non-linear relationship, we use the Budyko framework (Budyko, 1974; Fu, 1981; Broecker, 2010; Roderick and others, 2014; Greve and others, 2015), where k_{run} is determined, using the Fu (1981) formulation, as:

$$1 - k_{run} = \frac{ET}{P} = 1 + \frac{E_p}{P} - \left[1 + \left(\frac{E_p}{P}\right)^{\omega}\right]^{\frac{1}{\omega}} \quad (2),$$

where:

E_p = potential evapotranspiration, the liquid water equivalent of the net downward radiation at the Earth surface derived from energy fluxes (Roderick and others, 2014; Ibarra and others, 2018).
ω = a free parameter that integrates the hydroclimatic properties of a watershed or basin (Fu, 1981; Greve and others, 2015).

The global average ω value is ~2.6 (Roderick and others, 2014; Greve and others, 2015). Recent work has shown that more complex, spatially explicit hydrologic modeling of Pleistocene lakes follow precipitation-runoff relationships imposed by the Budyko framework (Matsubara and Howard, 2009; Barth and others, 2016), justifying this scaling approach for steady-state calculations.

In this contribution, we use the methods outlined by Ibarra and others (2018) to analyze the distribution of the precipitation and energy fields from the gridded North American Regional Reanalysis dataset (NARR). We downscale the results presented by Ibarra and others (2018) for the Bonneville basin, defined by the NARR grid cells (resolution of NARR is 32 km, n = 201 grid cells) spanning the region (37.5 to 43 °N, -114.5 to -110.5 °W), and present results based on the median change in lake area. We have confirmed that the average NARR precipitation fields (1979 to present) agree well with the 30-year normal PRISM precipitation dataset (1981 to 2010) and long-term weather station data archived by the Western Regional Climate Center. Lake evaporation (E_L) is calculated using the Priestley-Taylor equation and an E_P versus temperature scaling of 1.6%/K (Ibarra and others, 2018). To calibrate the lake area scaling relationships specifically for Lake Bonneville, we lower the Budyko ω value to 2.465, which is calibrated to the total modern lake and seasonal playa lake surface area (8924 km^2, modern A_L/A_B = 6.65%), which includes Great Salt Lake, Bear Lake, the Bonneville Salt Flats, and other seasonal playa lakes as compiled in Ibarra and others (2018).

For the latest glacial Provo and Bonneville shorelines, we use rebound corrected lake area and volume estimates determined by Adams and Bills (2016), and temperature depression estimates based on macrofossil assemblages determined by Harbert and Nixon (2018) (see table 1). Use of the non-rebounded corrected values would result in underestimates in both precipitation and lake residence times. We note that the Bonneville shoreline lake area and volume estimate reported by Adams and Bills (2016) agree well with new high-precision differential GPS measurements reported by Chen and Maloof (2017) (see also Currey, 1982; Bills and others, 2002). All contours and scaling relationships shown are the median change in precipitation and temperature (for details see Ibarra and others, 2018), intended to represent the basin average change in hydroclimate necessary to explain the observed lake areas. Medians of the calculated A_L/A_B distributions are used due to the non-normal distribution in modern precipitation and energy fluxes used for the scaling analysis. We report uncertainty ranges on our estimates, where the uncertainty reflects the full range of temperature estimates, and is asymmetric due to the Budyko scaling relationship and the non-normal distribution in modern precipitation and energy fluxes.

RESULTS AND DISCUSSION

The results of our downscaled sensitivity analysis for Lake Bonneville are displayed in figure 1A and reported in table 1. Solved for all combinations assuming a uniform temperature depression and factor change in precipitation over the basin, we plot the calculated precipitation factor change as a function of temperature depression needed to maintain a given lake area (expressed as A_L/A_B; black contours in figure 1A). The colored contours on figure 1A represent the Bonneville, Provo and modern surface area estimates.

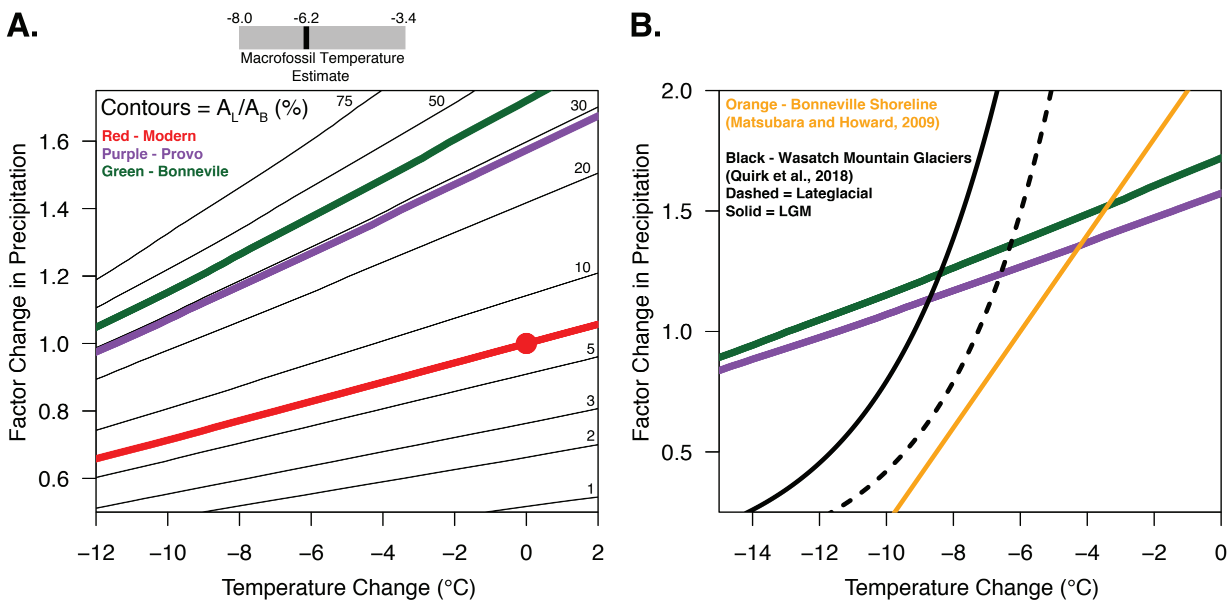

Figure 1. *Hydroclimate change inferred from Lake Bonneville shoreline areas. (A) Contoured lake area over basin area (A_L/A_B) as a function of precipitation factor change and temperature depression over the Bonneville basin (37.5 to 43 °N, -114.5 to -110.5 °W). Colored lines denote the modern (red), Provo (purple), and Bonneville (dark green) shorelines. Macrofossil temperature depression estimates are from Harbert and Nixon (2018). Note that the black contours are not linear. (B) Comparison of lake area scaling relationships with previous temperature vs. precipitation estimates from hydrologic modeling of the Bonneville shoreline (Matsubara and Howard, 2009) and glacier mass balance modeling from Big Cottonwood Canyon in the Wasatch Range (Quirk and others, 2018) on the eastern edge of Lake Bonneville. Note the axes difference between panels A and B.*

Table 1. *Modeling inputs and results for Lake Bonneville.*

Lake Stage	Lake Area [km^2][1]	Volume [km^3][1]	P/P_M vs. ΔT relationship[2]	Precipitation Factor Change	Water Residence Time (yr)
Bonneville	52,110 (A_L/A_B= 38.85%)	10,420	$P/P_M = 1.711 + 0.056 x \Delta T$	1.37 (+0.15/−0.10)	185 (+13/−16)
Provo	38,150 (A_L/A_B= 28.44%)	5290	$P/P_M = 1.572 + 0.050 x \Delta T$	> 1.26 (+0.13/−0.09)	102 (+7/−9)

[1] *Rebound-corrected lake volume and areas determined by Adams and Bills (2016).*

[2] *P/P_M = precipitation factor change; ΔT = temperature change relative to modern. Linear relationships are approximate based on linear regression fit to contours in figure 1.*

Modeling assumptions: *Budyko parameter, ω = 2.465 (calibrated to total modern lake and playa areas; 8924 km2); total basin area = 134,131 km^2; residence time calculation assumes modern precipitation rate of 338 mm/yr (NARR median; comparable to PRISM value of 344 mm/yr); median temperature depression of −6.2 (−8.0 to −3.4 °C) based on filtering of macrofossil assemblage calculation from Harbert and Nixon (2018) for all deglacial and LGM locations near Lake Bonneville; and temperature vs. potential evapotranspiration scaling of 1.6%/°C (Ibarra and others, 2018). Basin and modern lake/playa areas are from data tables in Ibarra and others (2018).*

Combining the temperature depression and lake area estimates (see above and table 1) for the Bonneville shoreline surface area prior to spill over into the Snake River (~18.5 ka), we calculate precipitation rates that were ~1.37 (+0.15/−0.10) times modern with a water residence time of 185 (+13/−16) years. This estimate is comparable but higher than the Paleoclimate Modeling Intercomparison Project (PMIP) 2 and 3 Last Glacial Maximum (LGM; n = 15) ensemble average of 1.17 (±0.47, 1σ) for Lake Bonneville determined previously by Oster and others (2015), though we note that the best performing PMIP3 models (n = 5) suggest minimal change in precipitation (1.02 ±0.19) relative to modern. Our estimates of precipitation change for the LGM are higher than the central estimates from data to the west from Newark Valley (1.14 times modern, +0.15/-0.59) and Diamond Valley (0.97 times modern, +0.10/-0.51), derived from uranium-series systematics in soil opal (Maher and others, 2014; see their table 2), but lower than estimates from lake balance modeling of Jakes Lake (~1.9 times modern produced by Barth and others (2016). Similarly, for the Provo shoreline, we calculate a minimum precipitation factor change of 1.26 (+0.13/−0.09) times modern, and a water residence time of 102 (+7/−9) years. We note that minimal change in precipitation over the Bonneville region between the LGM and ~15.5 ka is simulated by the TraCE climate model simulation of the past 22 kyr (Lora and others, 2017; see their figure 4). Given ~2.5 kyr of stable shoreline development and continual overflow (Miller and others, 2013; Oviatt, 2015), this precipitation estimate is likely a minimum value considering the balance-filled nature of the Lake Bonneville system.

The residence times of water in Lake Bonneville for the Bonneville and Provo shorelines place useful constraints on oxygen isotope measurements of sediments and shoreline tufa, though other geochemical systems, such as trace elements, are typically decoupled from water residence times. Our residence time calculations (table 1) place minimum bounds on the timescale for which oxygen isotope timeseries from cores or other high-resolution records could record rapid (sub-kyr) changes in climate (e.g., Dansgaard–Oeschger or Heinrich events) occurring within glacial-interglacial cycles (e.g., Benson and others, 1990; Oviatt and others, 1994; McGee and others, 2012; Ibarra and Chamberlain, 2015).

In figure 1B we compare the Bonneville and Provo shoreline scaling relationships with two other estimates. Previously, Matsubara and Howard (2009) produced a spatially explicit model of the Great Basin, and specifically analyzed the Bonneville region (see their figures 4 and 5). Using their hydrologic modeling simulations, Matsubara and Howard (2009) report an empirically derived multiplicative precipitation equation expressing precipitation factor change (P/P_M) as a linear relationship with temperature depression (ΔT), where $P/P_M = 2.2 + 0.2x\Delta T$ (orange line in figure 1B), a steeper slope than those derived using our approach (table 1). In a similar fashion Quirk and others (2018) recently reported relationships for LGM and post-LGM glacier extents in the Wasatch Range (shown as black lines in figure 1B). Most significantly, our relationships for the Bonneville and Provo shorelines intercept the time-equivalent, post-LGM relationships from Quirk and others (2018) at a precipitation factor change of ~1.2 to 1.3 and a temperature depression of ~7 °C, comparable to the median value from the macrofossil estimates reported by Harbert and Nixon (2018), and in agreement with the PMIP climate model ensemble average temperature depression of 7.5°C (±2.6, 1σ; n=15) for Lake Bonneville determined previously by Oster and others (2015).

CONCLUSIONS

In sum, we have downscaled the scaling analysis presented by Ibarra and others (2018) for the western United States for the Bonneville and Provo shoreline areas of Lake Bonneville during the last glacial period. These estimates are similar to previous hydrologic modeling and glacier mass balance modeling efforts. Future work will also constrain the scaling relationships associated with the pre-LGM Stansbury shoreline and post-Bonneville Gilbert episode. Furthermore, ongoing work to constrain changes in surface and lake temperature using pollen, macrofossil, and carbonate clumped isotopic techniques (e.g., Mering, 2015; Harbert and Nixon, 2018) will provide independent constraints on the regional magnitude of temperature depressions for the last glacial period. Finally, we anticipate that future more advanced spatially explicit hydrologic modeling (e.g., Matsubara and Howard, 2009; Barth and others, 2016; Hatchett and others, 2018) and isotope mass balance approaches (e.g., Ibarra and others, 2014; Hudson and others, 2017) for the Bonneville basin will provide inter-comparison between different methods for determining past changes in hydroclimate from lake area extents.

ACKNOWLEDGMENTS

Ibarra acknowledges Christine Y. Chen (MIT-WHOI), Robert S. Harbert (Stonehill College), Lauren M. Santi, Alexandrea Arnold, Juan Lora (UCLA), Kate Maher and Tyler J. Kukla (Stanford University) for discussions and suggestions. NCEP Reanalysis data provided by the NOAA/OAR/ESRL PSD, Boulder, Colorado, USA, from their website at https://www.esrl.noaa.gov/psd/. Code used to generate figure 1 can be obtained from Ibarra. This work was supported by National Science Foundation grant EAR-1450357 and the Heising-Simons Foundation to Chamberlain.

REFERENCES

Adams, K.D., and Bills, B.G., 2016, Chapter 8—Isostatic rebound and palinspastic restoration of the Bonneville and Provo shorelines in the Bonneville basin, UT, NV, and ID, *in* Oviatt, C.G., Shroder Jr., J.F., editors, Lake Bonneville—A Scientific Update: Developments in Earth Surface Processes, Elsevier, v. 20. p. 145–164.

Barth, C., Boyle, D.P., Hatchett, B.J., Bassett, S.D., Garner, C.B., and Adams, K.D., 2016, Late Pleistocene climate inferences from a water balance model of Jakes Valley, Nevada (USA): Journal of Paleolimnology, v. 56, p. 109–122, doi: 10.1007/s10933-016-9897-z.

Benson, L.V., Currey, D.R., Dorn, R.I., Lajoie, K.R., Oviatt, C.G., Robinson, S.W., Smith, G.I., and Stine, S., 1990, Chronology of expansion and contraction of four Great Basin lake systems during the past 35,000 years: Palaeogeography, Palaeoclimatology, Palaeoecology, v. 78, p. 241–286, doi: 10.1016/0031-0182(90)90217-U.

Bills, B., Wambeam, T., and Currey, D.R., 2002, Geodynamics of Lake Bonneville, *in* Gwynn, J.W., editor, Great Salt Lake—An Overview of Change: Utah Department of Natural Resources Special Publication, p. 7–32.

Broecker, W., 2010, Long-term water prospects in the western United States: Journal of Climate, v. 23, p. 6669–6683, doi: 10.1175/2010JCLI3780.1.

Budyko, M.I., 1974, Climate and life: International Geophysical Series, v. 18, 507 p.

Chen, C.Y., and Maloof, A.C., 2017, Revisiting the deformed high shoreline of Lake Bonneville: Quaternary Science Reviews, v. 159, p. 169–189, doi: 10.1016/j.quascirev.2016.12.019.

Currey, D.R., 1982, Lake Bonneville—Selected features of relevance to neotectonic analysis: U.S. Geological Survey Open-File Report 82-1070, 31 p., doi: 10.3133/ofr821070.

Fu, B.P., 1981, On the calculation of the evaporation from land surface: Scientia Atmospherica Sinica, v. 5, no. 1, p. 23–31.

Gilbert, G.K., 1890, Lake Bonneville: U.S. Geological Survey Monograph 1, 438 p.

Grayson, D., 2011, The Great Basin—A natural prehistory: University of California Press, 432 p.

Greve, P., Gudmundsson, L., Orlowsky, B., and Seneviratne, S.I., 2015, Introducing a probabilistic Budyko framework: Geophysical Research Letters, v. 42, p. 2261–2269, doi: 10.1002/2015GL063449.

Harbert, R., and Nixon, K., 2018, Quantitative late Quaternary climate reconstruction from plant macrofossil proxy in western North America: Open Quaternary, v. 4, 8 p., doi: 10.5334/oq.46.

Hatchett, B.J., Boyle, D.P., Garner, C.B., Kaplan, M.L., Bassett, S.D., and Putnam, A.E., 2018, Sensitivity of a western Great Basin terminal lake to winter northeast Pacific storm track activity and moisture transport, *in* Starratt, S.W., and Rosen, M.R., editors, From Saline to Freshwater—The Diversity of Western Lakes in Space and Time: Geological Society of America Special Papers, v. 536, 13 p., doi: 10.1130/2018/2536(05).

Hostetler, S.W., and Benson, L.V., 1990, Paleoclimatic implications of the high stand of Lake Lahontan derived from models of evaporation and lake level: Climate Dynamics, v. 4, p. 207–217, doi: 10.1007/BF00209522.

Hubbs, C.L., and Miller, R.R., 1948, The zoological evidence—Correlation between fish distribution and hydro-graphic history in the desert basins of western United States, *in* The Great Basin with emphasis on glacial and postglacial times: Bulletin of the University of Utah, v. 38, no. 20, p. 17–166.

Hudson, A.M., and Quade, J., 2013, Long-term east-west asymmetry in monsoon rainfall on the Tibetan Plateau: Geology, v. 41, p. 351–354, doi: 10.1130/G33837.1.

Hudson, A.M., Quade, J., Ali, G., Boyle, D., Bassett, S., Huntington, K.W., Marie, G., Cohen, A.S., Lin, K., and Wang, X., 2017, Stable C, O and clumped isotope systematics and 14C geochronology of carbonates from the Quaternary Chewaucan closed-basin lake system, Great Basin, USA—Implications for paleoenvironmental reconstructions using carbonates: Geochimica et Cosmochimica Acta, v. 212, p. 274–302, doi: 10.1016/j.gca.2017.06.024.

Ibarra, D.E., Egger, A.E., Weaver, K.L., Harris, C.R., and Maher, K., 2014, Rise and fall of late Pleistocene pluvial lakes in response to reduced evaporation and precipitation–Evidence from Lake Surprise, California: Geological Society of America Bulletin, v. 126, p. 1387–1415, doi: 10.1130/B31014.1.

Ibarra, D.E., and Chamberlain, C.P., 2015, Quantifying closed-basin lake temperature and hydrology by inversion of oxygen isotope and trace element paleoclimate records: American Journal of Science, v. 315, no. 9, p. 781–808, doi: 10.2475/09.2015.01.

Ibarra, D.E., Oster, J.L., Winnick, M.J., Caves Rugenstein, J.K., Bryne, M.P., and Chamberlain, C.P., 2018, Warm and cold wet states in the western United States during the Pliocene-Pleistocene: Geology, v. 46, p. 355–358, doi: 10.1130/G39962.1.

Lora, J.M., Mitchell, J.L., Risi, C., and Tripati, A.E., 2017, North Pacific atmospheric rivers and their influence on western North America at the Last Glacial Maximum: Geophysical Research Letters, v. 44, p. 1051–1059, doi: 10.1002/2016GL071541.

Maher, K., Ibarra, D.E., Oster, J.L., Miller, D.M., Redwine, J.L., Reheis, M.C., and Harden, J.W., 2014, Uranium isotopes in soils as a proxy for past infiltration and precipitation across the western United States: American Journal of Science, v. 314, p. 821–857, doi: 10.2475/04.2014.01.

Matsubara, Y., and Howard, A.D., 2009, A spatially explicit model of runoff, evaporation, and lake extent—Application to modern and late Pleistocene lakes in the Great Basin region, western United States: Water Resources Research, v. 45, p. W06425, doi: 10.1029/2007WR005953.

McGee, D., Quade, J., Edwards, R.L., Broecker, W.S., Cheng, H., Reiners, P.W., and Evenson, N., 2012, Lacustrine cave carbonates—Novel archives of paleo-hydrologic change in the Bonneville basin (Utah, USA): Earth and Planetary Science Letters, v. 351, p. 182–194, doi: 10.1016/j.epsl.2012.07.019.

Mering, J.A., 2015, New constraints on water temperature at Lake Bonneville from carbonate clumped isotopes: University of California Los Angeles, M.S. thesis, 176 p.

Mifflin, M.D., and Wheat, M.M., 1979, Pluvial lakes and estimated pluvial climates of Nevada: Nevada Bureau of Mines and Geology Bulletin, v. 95, 57 p.

Miller, D.M., Oviatt, C.G., and McGeehin, J.P., 2013, Stratigraphy and chronology of Provo shoreline deposits and lake-level implications, late Pleistocene Lake Bonneville, eastern Great Basin, USA: Boreas, v. 42, p. 342–361, doi: 10.1111/j.1502-3885.2012.00297.x.

Munroe, J.S, and Laabs, B.J.C., 2013, Latest Pleistocene history of pluvial Lake Franklin, northeastern Nevada, USA: Geological Society of America Bulletin, v. 125, p. 322–342, doi: 10.1130/B30696.1.

Orme, A.R., 2008, Pleistocene pluvial lakes of the American West—A short history of research: Geological Society, London, Special Publications, v. 301, p. 51–78, doi: 10 .1144/SP301.4.

Oviatt, C.G., 2015, Chronology of Lake Bonneville, 30,000 to 10,000 yr B.P.: Quaternary Science Reviews, v. 110, p. 166–171, doi: 10.1016/j.quascirev.2014.12.016.

Oviatt, C.G., Habiger, G.D., and Hay, J.E., 1994, Variations in the composition of Lake Bonneville marl—a potential key to lake-level fluctuations and paleoclimate: Journal of Paleolimnology, v. 11, p. 19–30, doi: 10.1007/BF00683268.

Oster, J.L., Ibarra, D.E., Winnick, M.J., and Maher, K., 2015, Steering of westerly storms over western North America at the Last Glacial Maximum: Nature Geoscience, v. 8, p. 201–205, doi: 10.1038/ngeo2365.

Quirk, B.J., Moore, J.R., Laabs, B.J.C., Caffee, M.W., and Plummer, M.A., 2018, Termination II, Last Glacial Maximum, and late glacial chronologies and paleoclimate from Big Cottonwood Canyon, Wasatch Mountains, Utah: Geological Society of America Bulletin, 14 p., doi: 10.1130/B31967.1.

Reheis, M.C., 1999a, Extent of Pleistocene lakes in the western Great Basin: U.S. Geological Survey Miscellaneous Field Studies Map MF-2323, scale 1:800,000, 1 sheet.

Reheis, M., 1999b, Highest pluvial-lake shorelines and Pleistocene climate of the western Great Basin: Quaternary Research, v. 52, p. 196–205, doi: 10.1006/qres .1999.2064.

Reheis, M.C., Adams, K.D., Oviatt, C.G., and Bacon, S.N., 2014, Pluvial lakes in the Great Basin of the western United States—a view from the outcrop: Quaternary Science Reviews, v. 97, p. 33–57, doi: 10.1016/j.quascirev.2014.04.012.

Roderick, M.L., Sun, F., Lim, W.H., and Farquhar, G.D., 2014, A general framework for understanding the response of the water cycle to global warming over land and ocean: Hydrology and Earth System Sciences, v. 18, p. 1575–1589, doi: 10.5194/hess-18-1575-2014.

Russell, I.C., 1885, Geological history of Lake Lahontan—A Quaternary lake of northwestern Nevada: U.S. Geological Survey Monograph 11, 288 p.

Williams, T.R., and Bedinger, M.S., 1984, Selected geologic and hydrologic characteristics of the Basin and Range Province, western United States; Pleistocene lakes and marshes: IMAP 1522-D, scale 1:2,500,000, 1 sheet.

This content is a PDF version of the author's PowerPoint presentation.

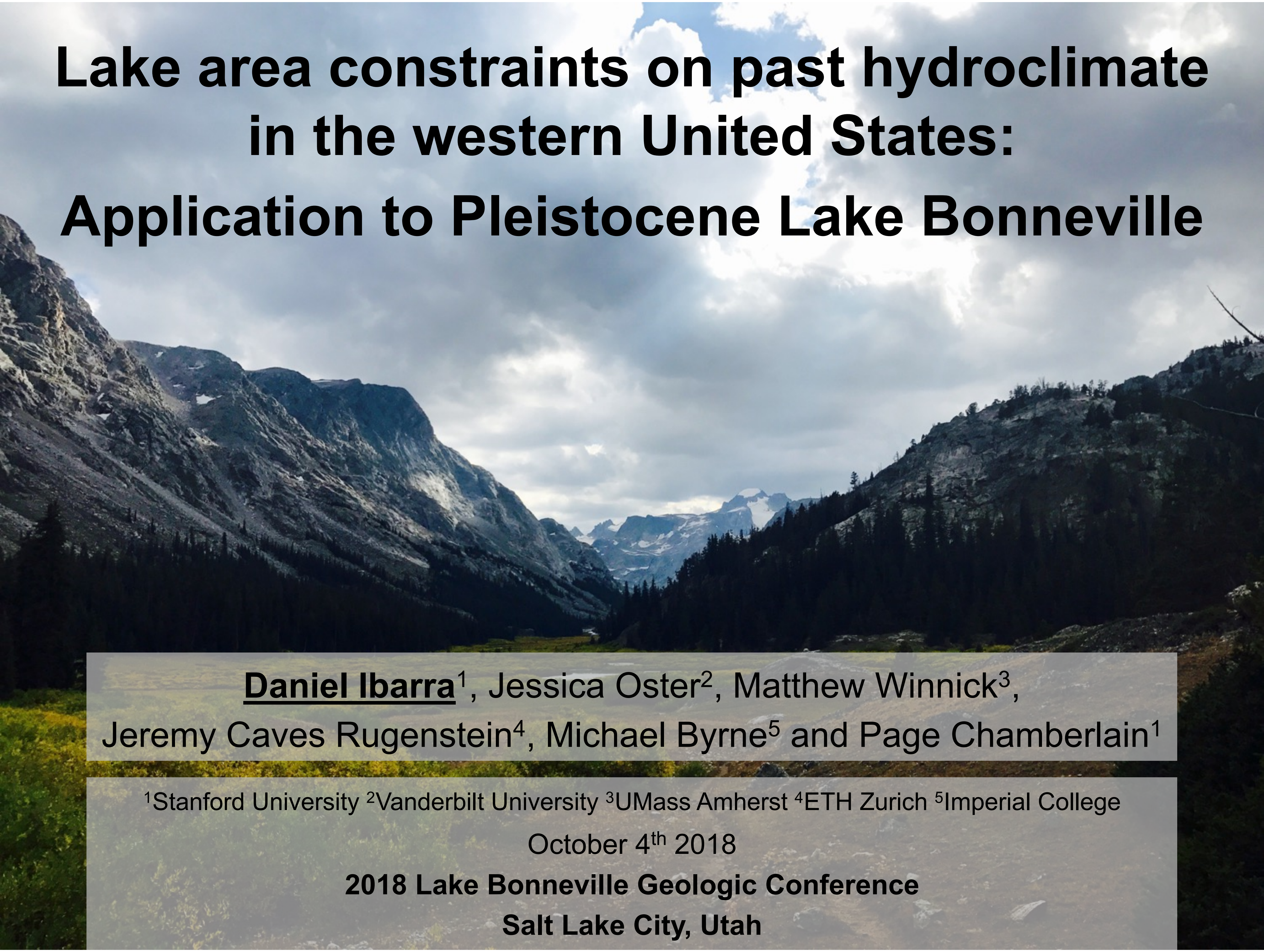

Lake area constraints on past hydroclimate in the western United States: Application to Pleistocene Lake Bonneville

Daniel Ibarra[1], Jessica Oster[2], Matthew Winnick[3], Jeremy Caves Rugenstein[4], Michael Byrne[5] and Page Chamberlain[1]

[1]Stanford University [2]Vanderbilt University [3]UMass Amherst [4]ETH Zurich [5]Imperial College

October 4th 2018

2018 Lake Bonneville Geologic Conference

Salt Lake City, Utah

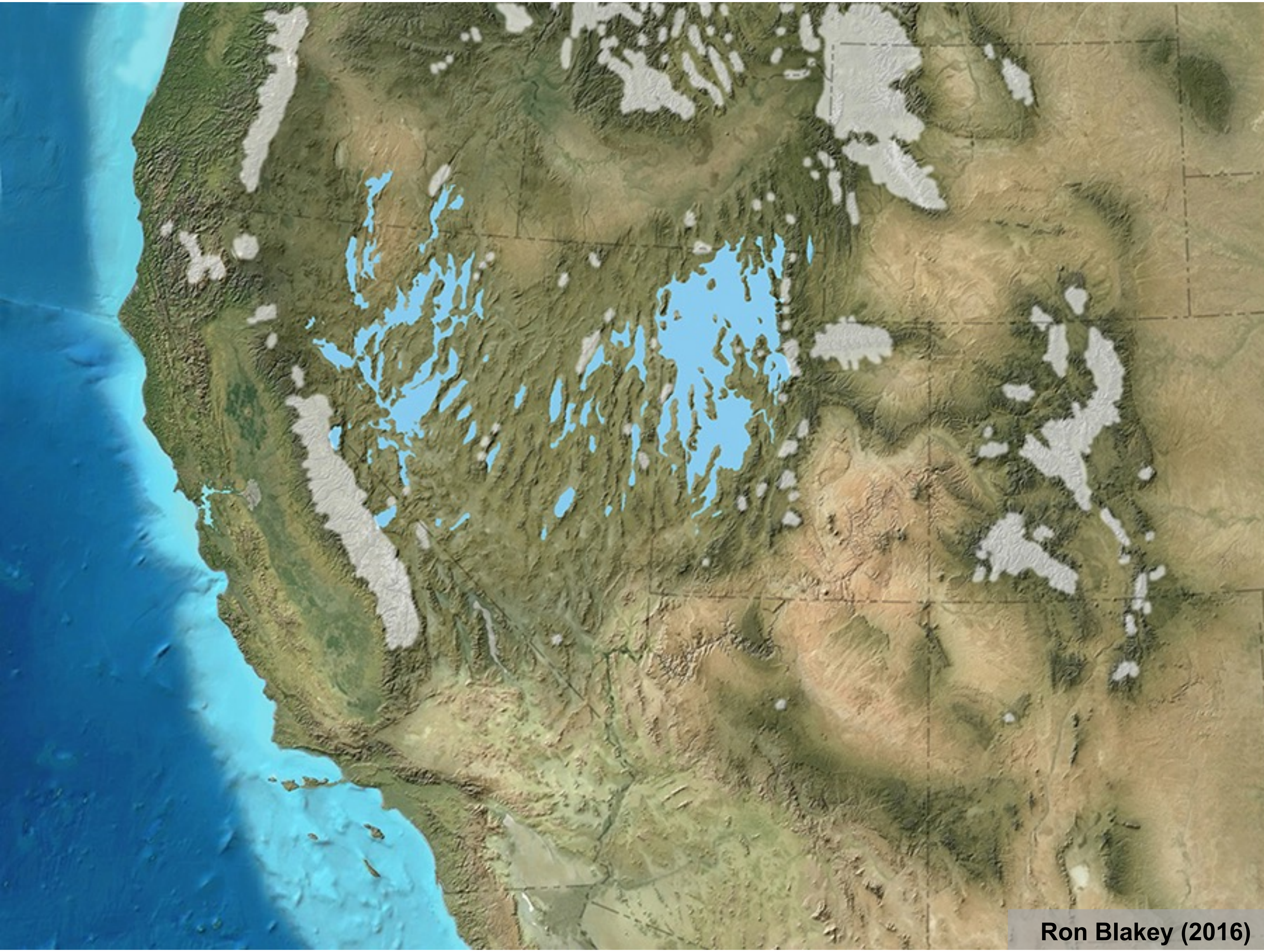
Ron Blakey (2016)

LGM Precipitation Categorical Agreement

Model/proxy agree

Model/proxy weakly disagree

Model/proxy strongly disagree

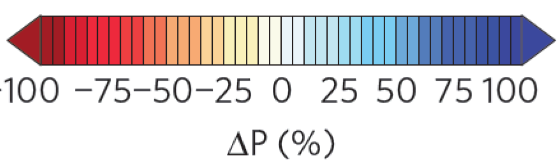

LGM Precipitation vs. Modern

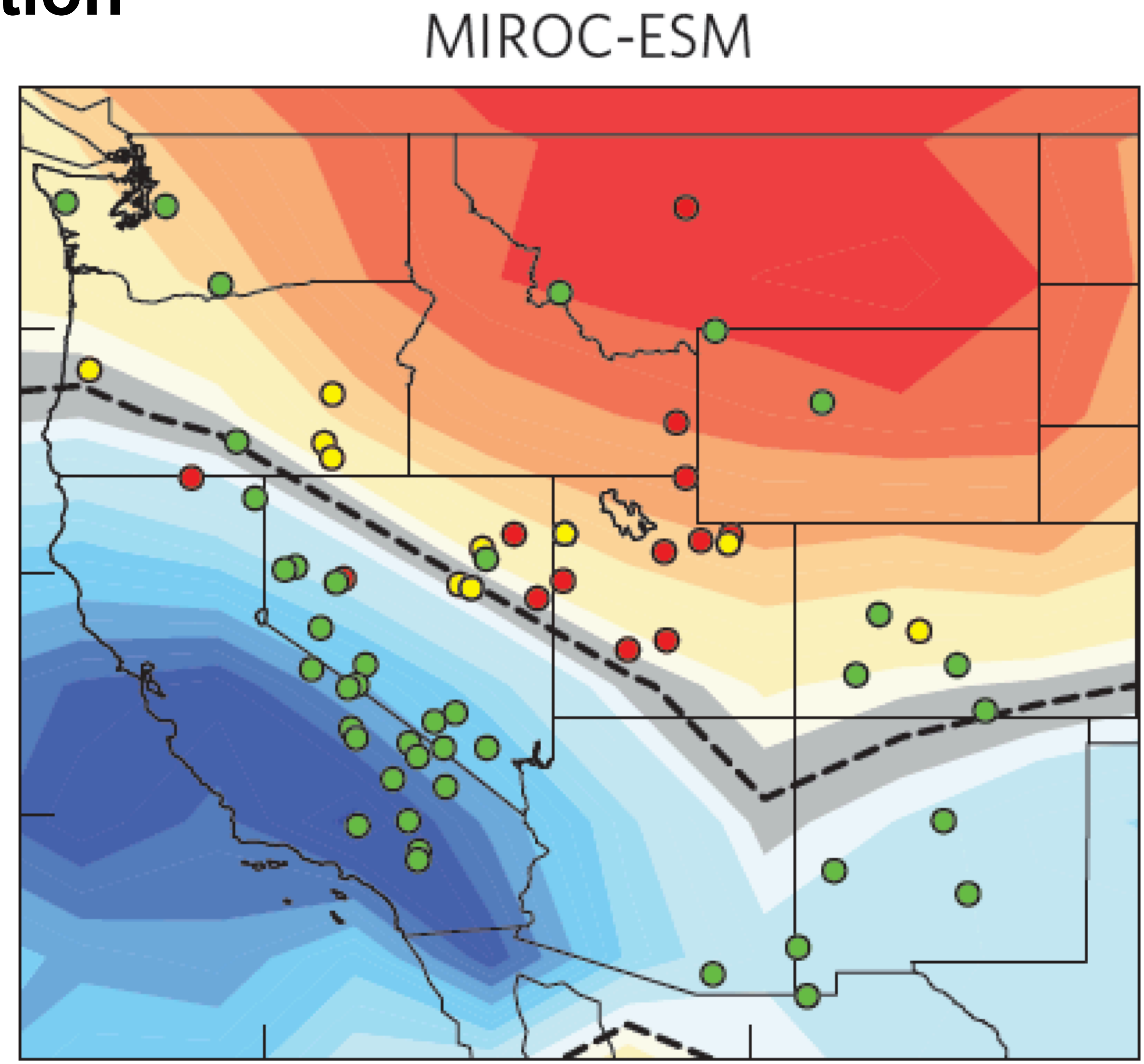

Adapted from Oster et al. (2015)

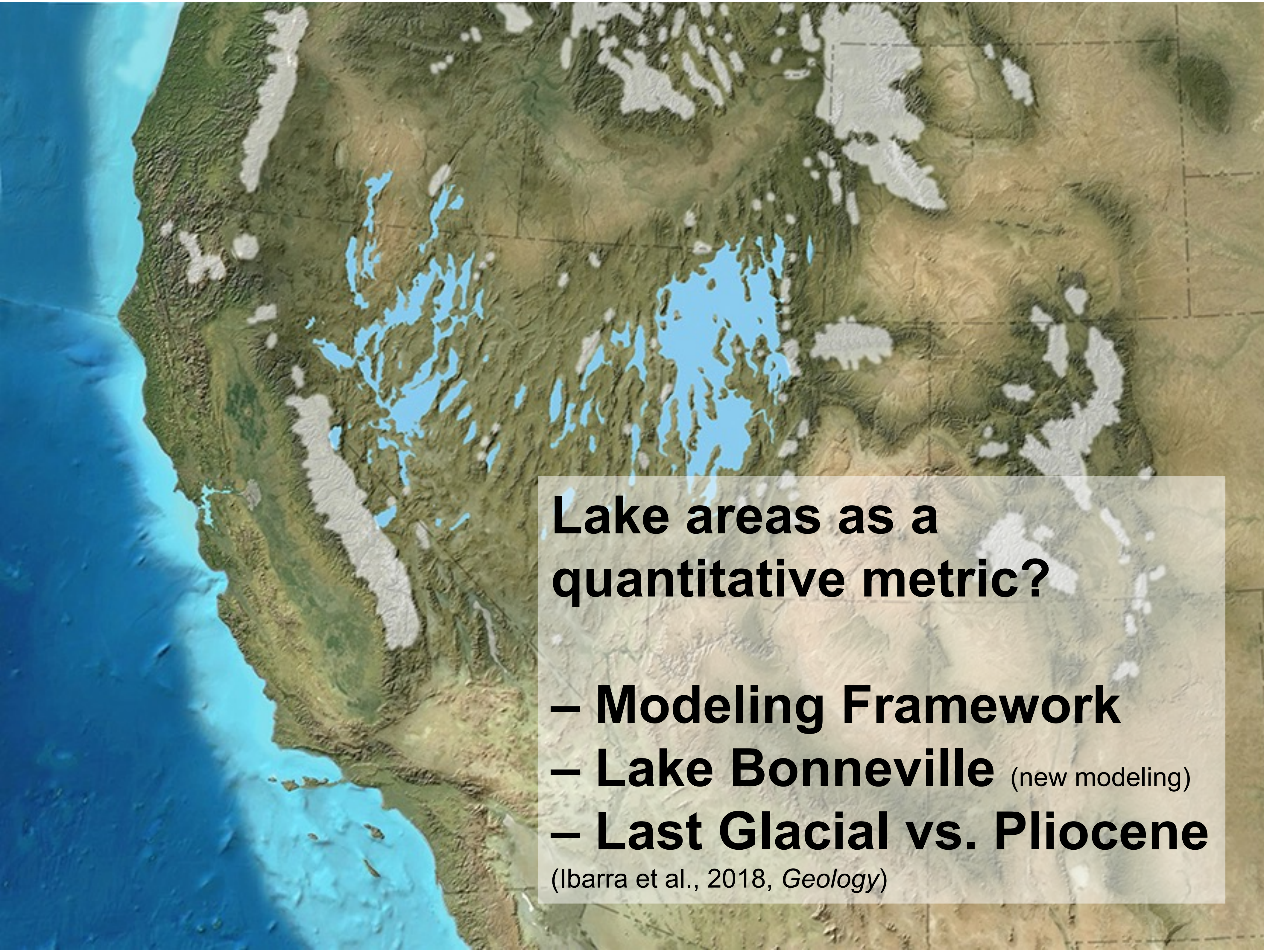

Lake areas as a quantitative metric?

– Modeling Framework
– Lake Bonneville (new modeling)
– Last Glacial vs. Pliocene
(Ibarra et al., 2018, *Geology*)

Terminal Lakes Reflect the Landscape's Water and Energy Budget

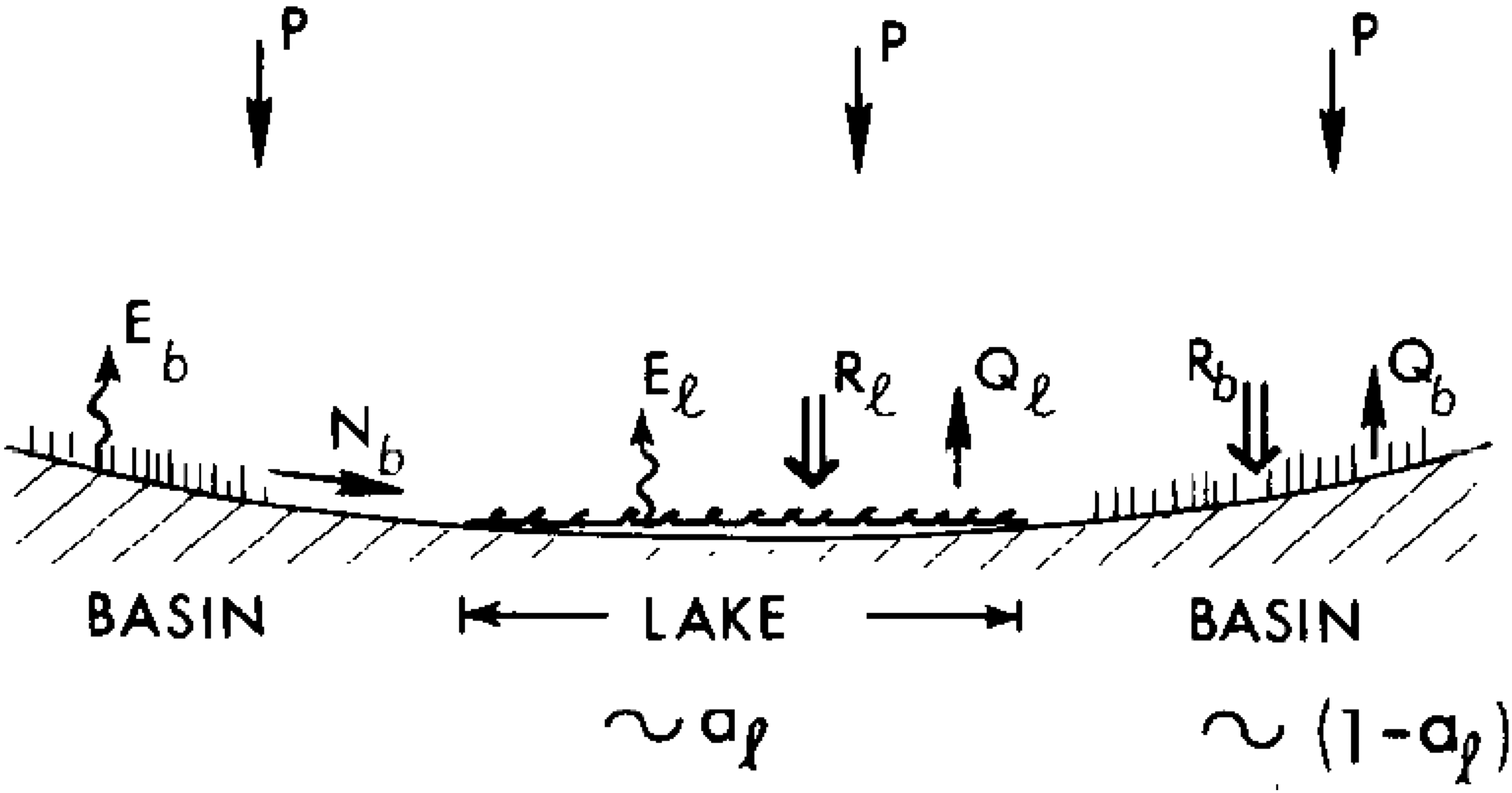

$$\frac{A_L}{A_B} = \frac{\text{Lake Area}}{\text{Basin Area}} = \frac{Pk_{run}}{E_{lake} - P + Pk_{run}}$$

John Kutzbach (1980) see also: Mifflin and Wheat (1979)

Lake Area as a Climate Indicators

$$\frac{A_L}{A_B} = \frac{\text{Lake Area}}{\text{Basin Area}} = \frac{P\boxed{k_{run}}}{\boxed{E_{lake}} - P + P\boxed{k_{run}}}$$

$$k_{run} \sim \text{f(climate, vegetation, soil type etc.)}$$
Budyko Framework

$$E_{lake} \sim \text{f(temperature, solar radiation, wind)}$$
Net Radiation with Priestley-Taylor

P – Precipitation
k_{run} – runoff coefficient
E_{lake} – lake evaporation

Broecker (2010, *Journal of Climate*); Reheis (1999, *Quaternary Research*) Hudson and Quade (2013, *Geology*)

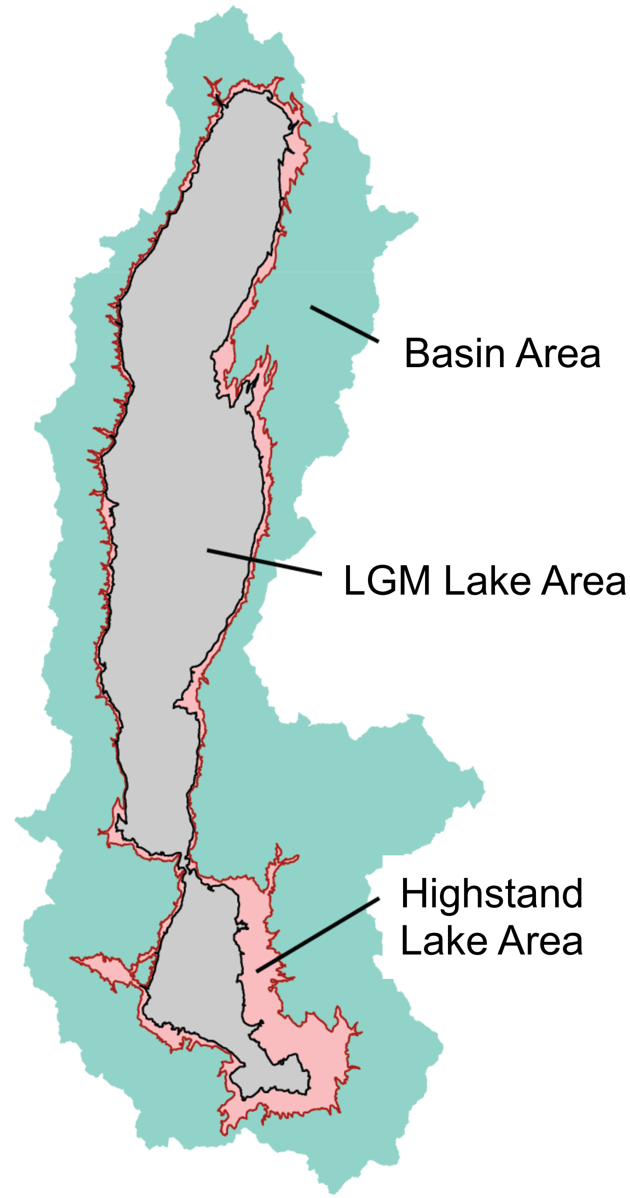

LGM Lake Surprise Ibarra et al. (2014, *GSA Bulletin*)

Budyko: Approximating Runoff (k_{run})

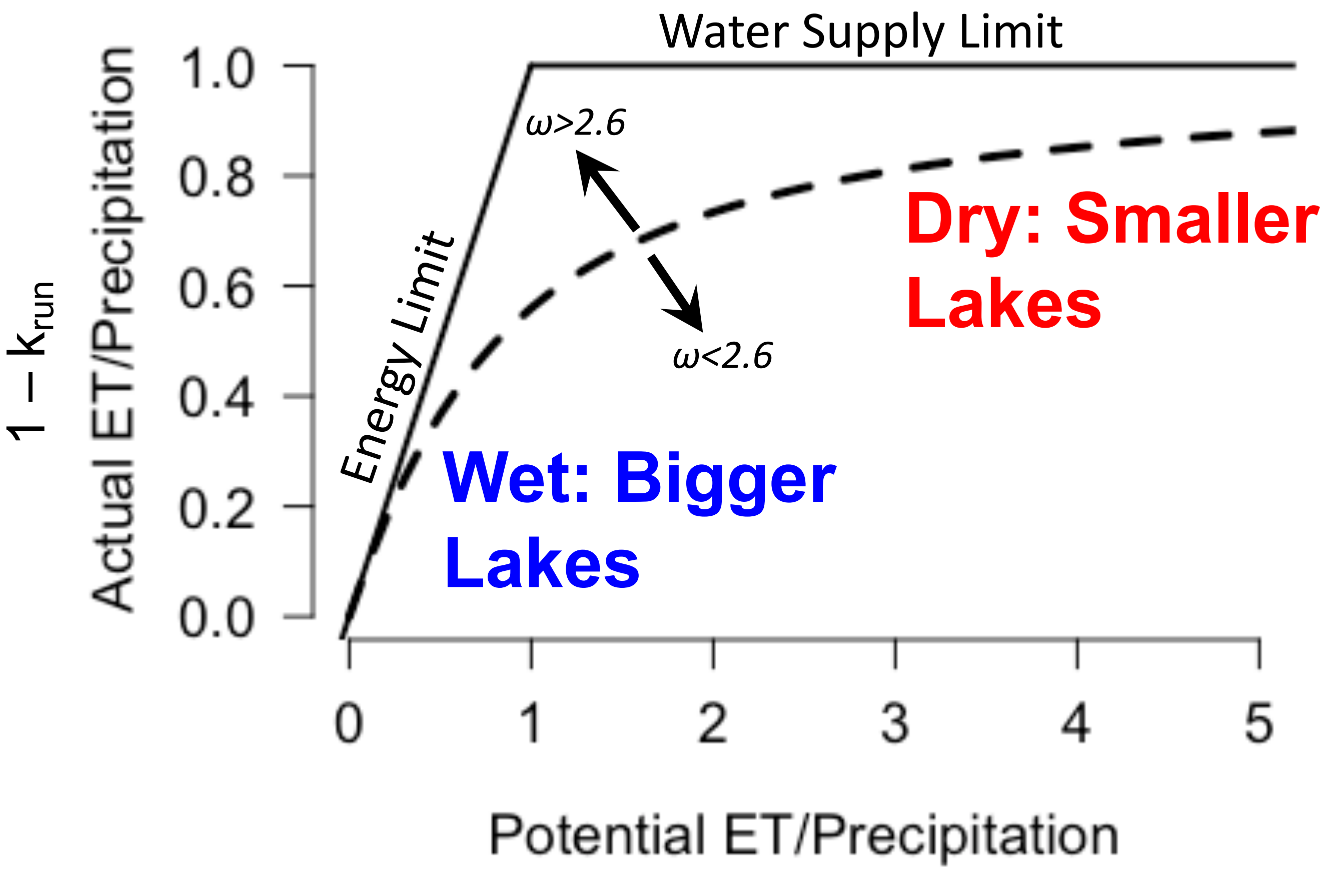

ω describes the efficiency with which P is converted to ET

Creates a positive feedback between P and k_{run}

$$1-k_{\mathrm{run}}=\frac{ET}{P}=1+\frac{E_p}{P}-\left[1+\left(\frac{E_p}{P}\right)^{\omega}\right]^{1/\omega}$$

Fu (1981)
Zhang et al. (2004, *WRR*)

Hydrologic Models Follow Budyko

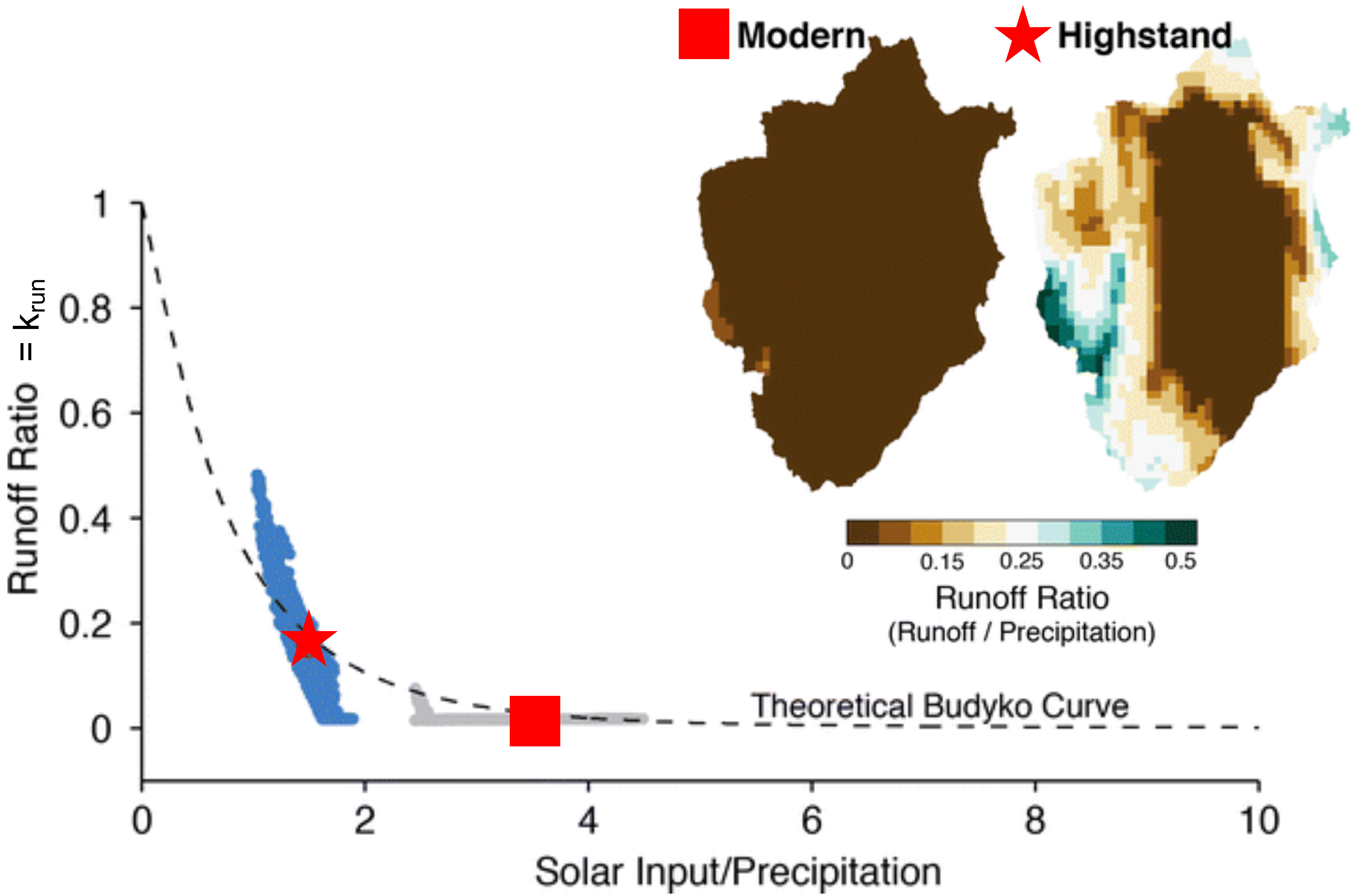

Barth et al. (2016, *J. Paleolimnology*): Pleistocene Jakes Lake, northeast NV

Energy vs. Temperature Scaling

$R_N \sim E_{lake}$ Lake Evaporation

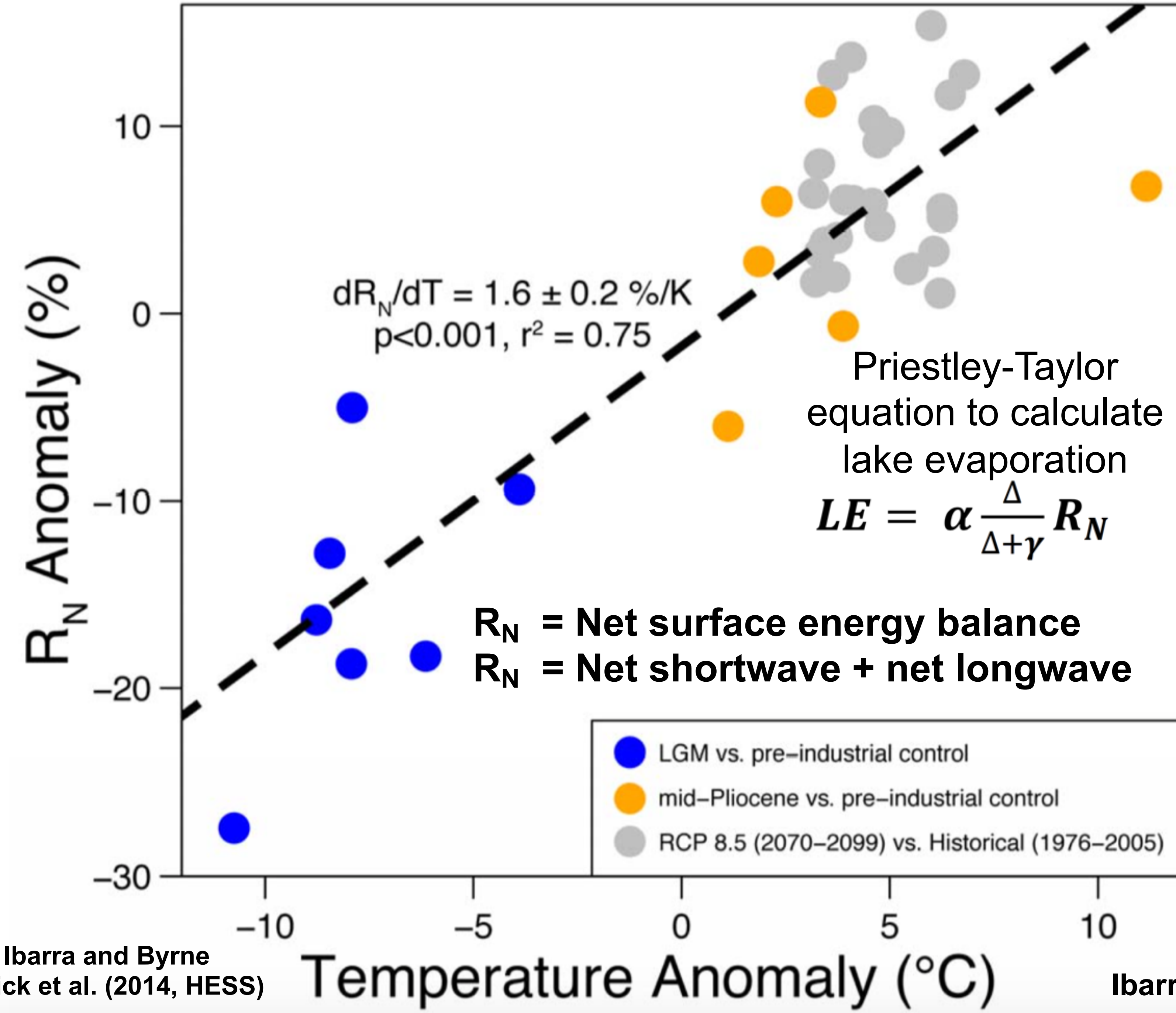

Analysis by Ibarra and Byrne
After Roderick et al. (2014, HESS)

Ibarra et al. (2018)

Lake Bonneville Application

Data sources:

- **Adams and Bills (2016) – Bonneville and Provo area and volume**
- **HydroSHEDS (USGS/WWF) basin boundary (134,131 km^2)**
- **North American Regional Reanalysis (NARR) Product**
  - **Temperature**
  - **Precipitation**
  - **Energy Fluxes**
- **Harbert and Nixon (2018) - BioArXiv Preprint**
  - **Temperature depression estimates from Macrofossils**
- **Quirk et al. (2018) – Wasatch Mountain Glacier Mass Balance (also show Stansbury estimate)**

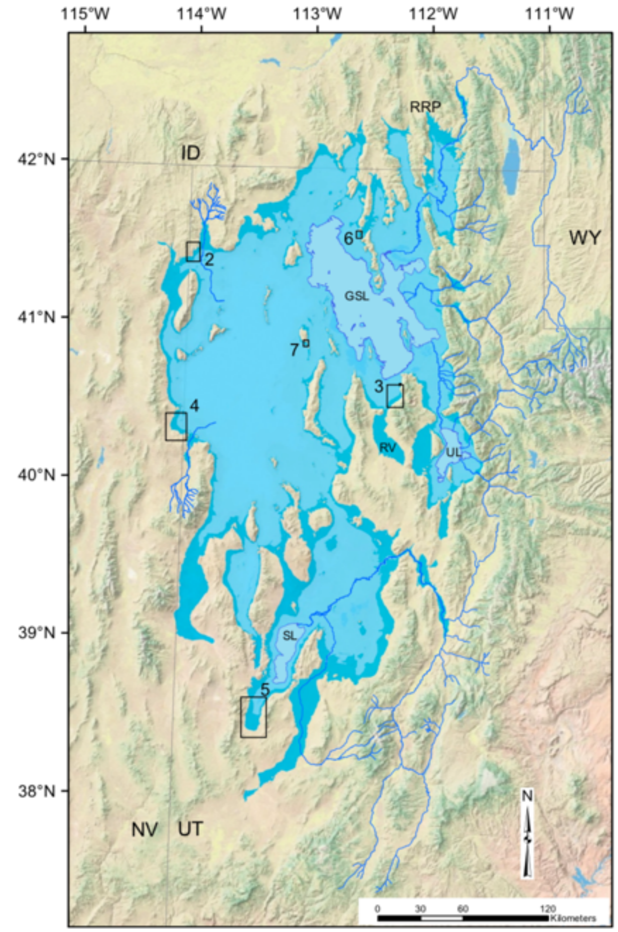

Adams and Bills (2016)

TABLE 8.1 Comparison Between Surface Areas and Volumes of Lake Bonneville Using a DEM with the Rebound Signal Removed and a Modern Topography DEM

Lake Stage	Area (km^2)	Volume (km^3)[a]
Rebound signal removed		
Bonneville	52,110	10,420
Provo	38,150	5290

Modern Bonneville Climate Space

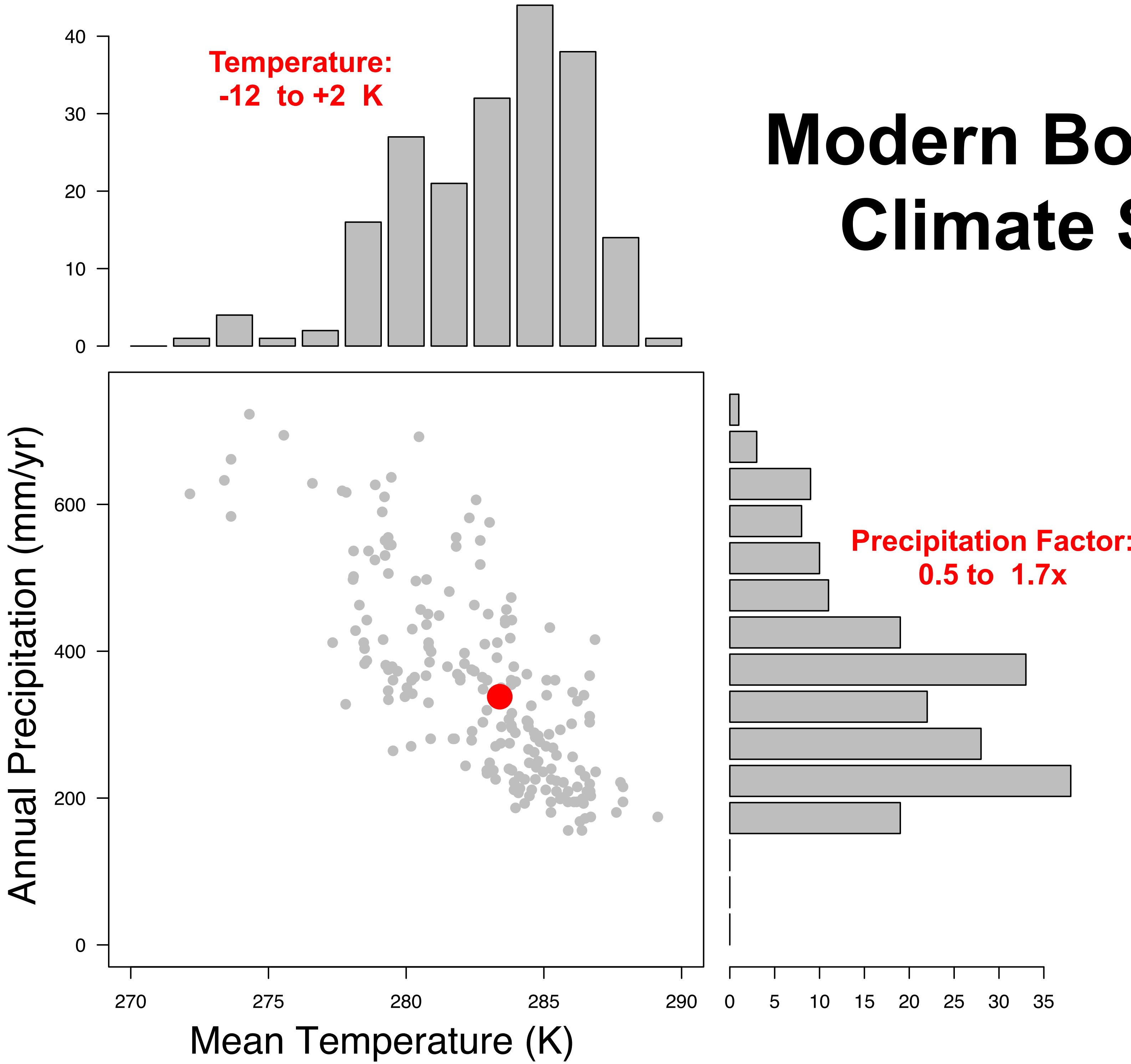

Data: NARR

Forward Model of Lake Bonneville

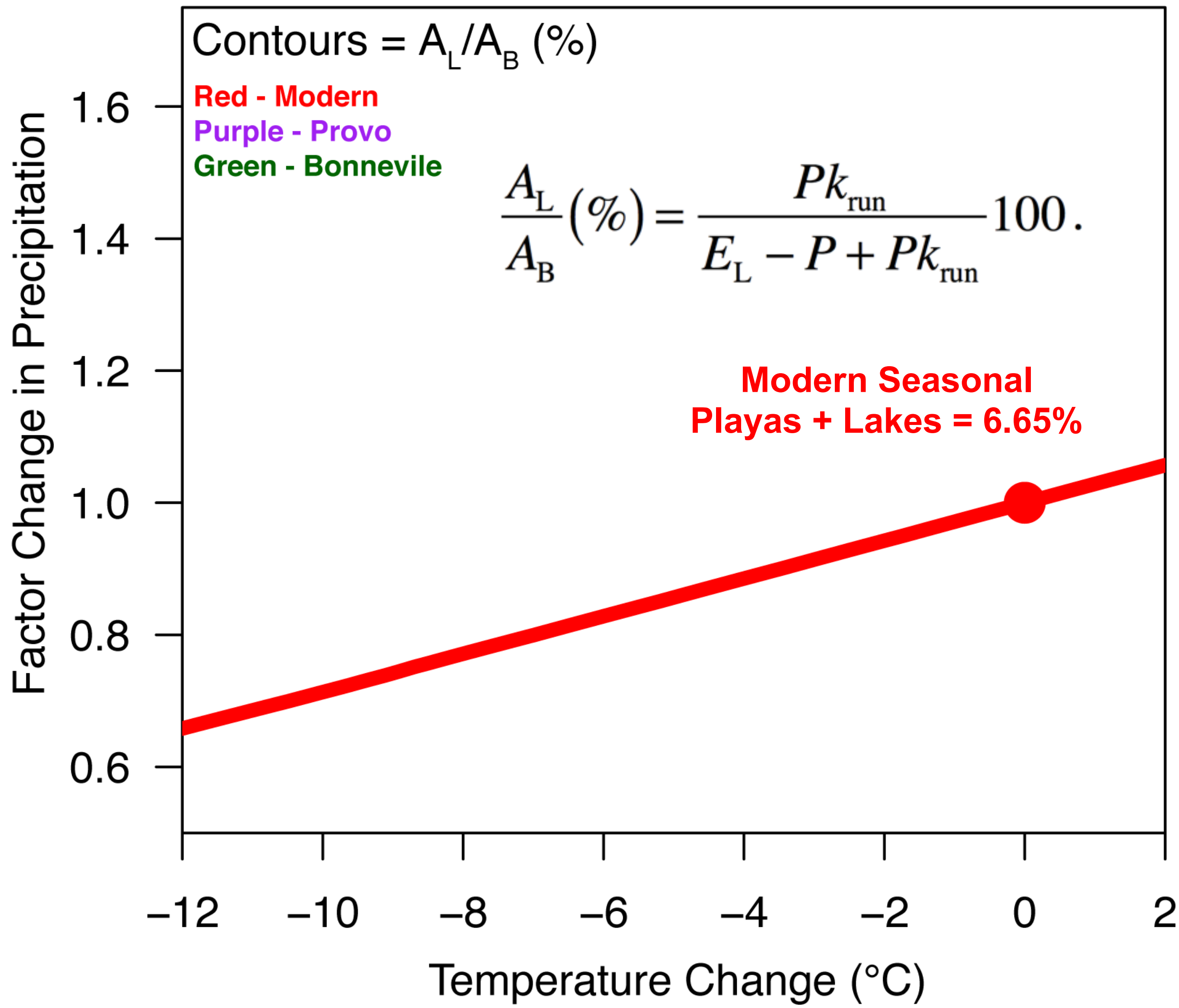

ω = 2.465

Forward Model of Lake Bonneville

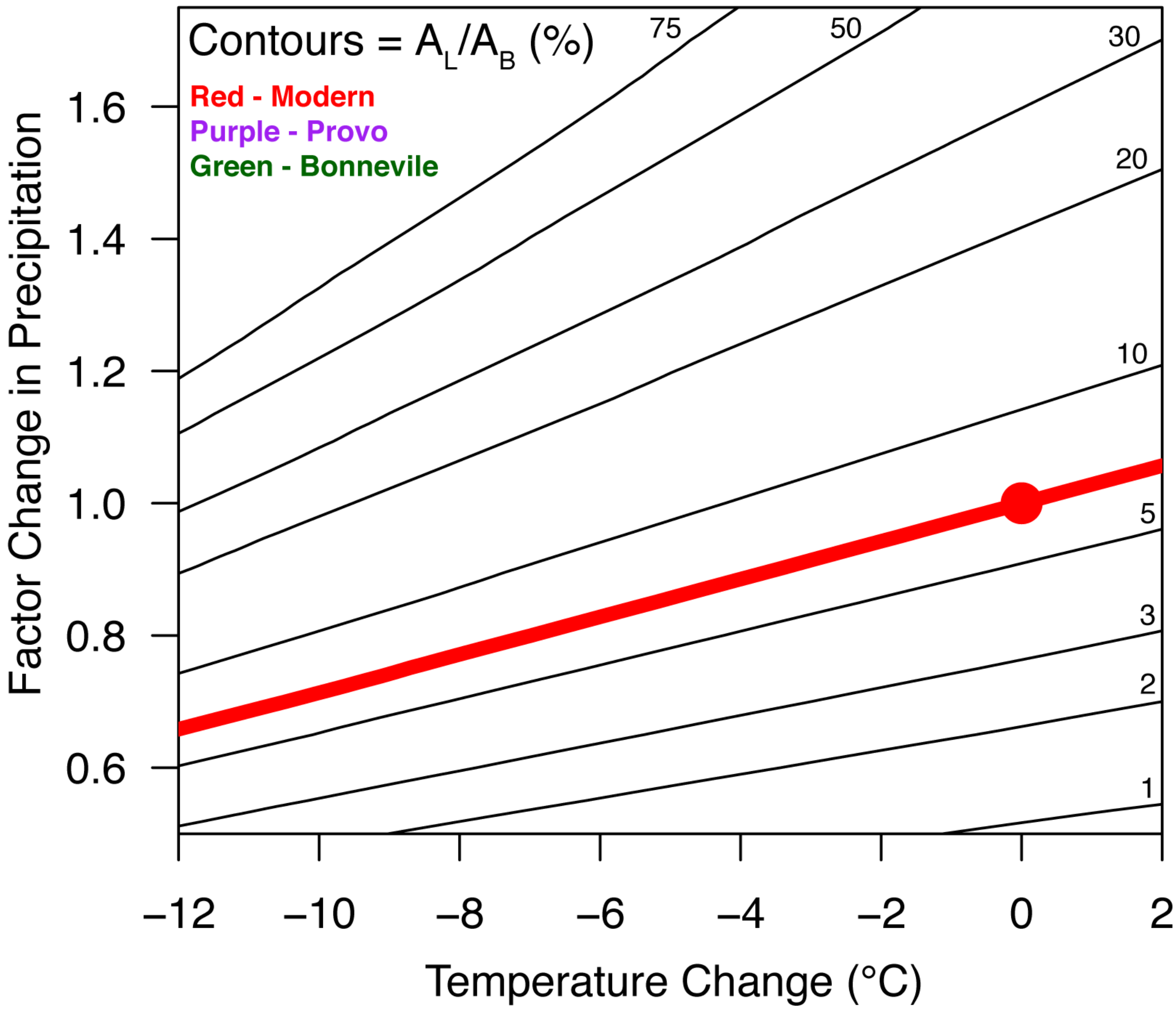

Forward Model of Lake Bonneville

Lake shoreline areas from:
Adams and Bills (2016)

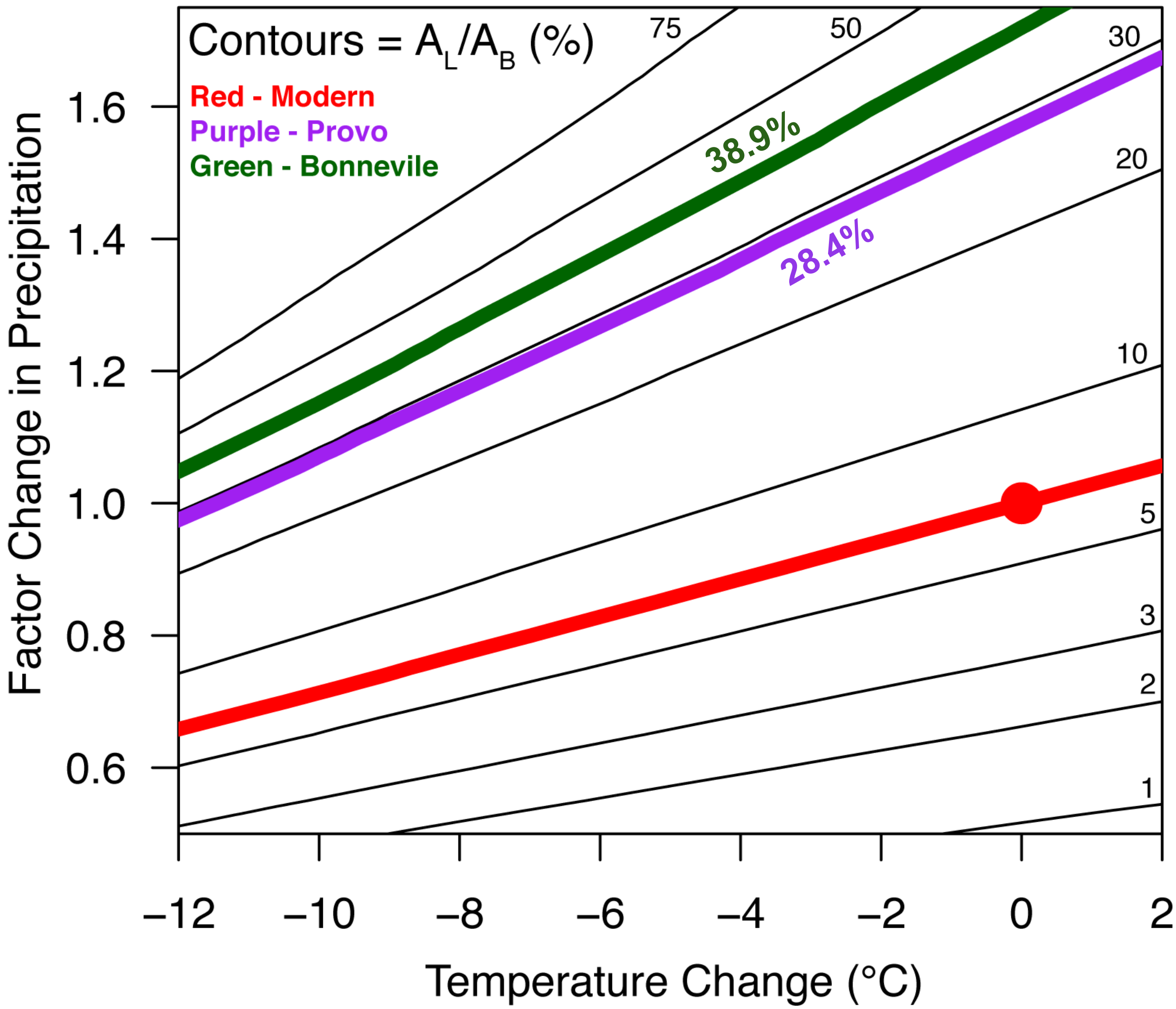

Forward Model of Lake Bonneville

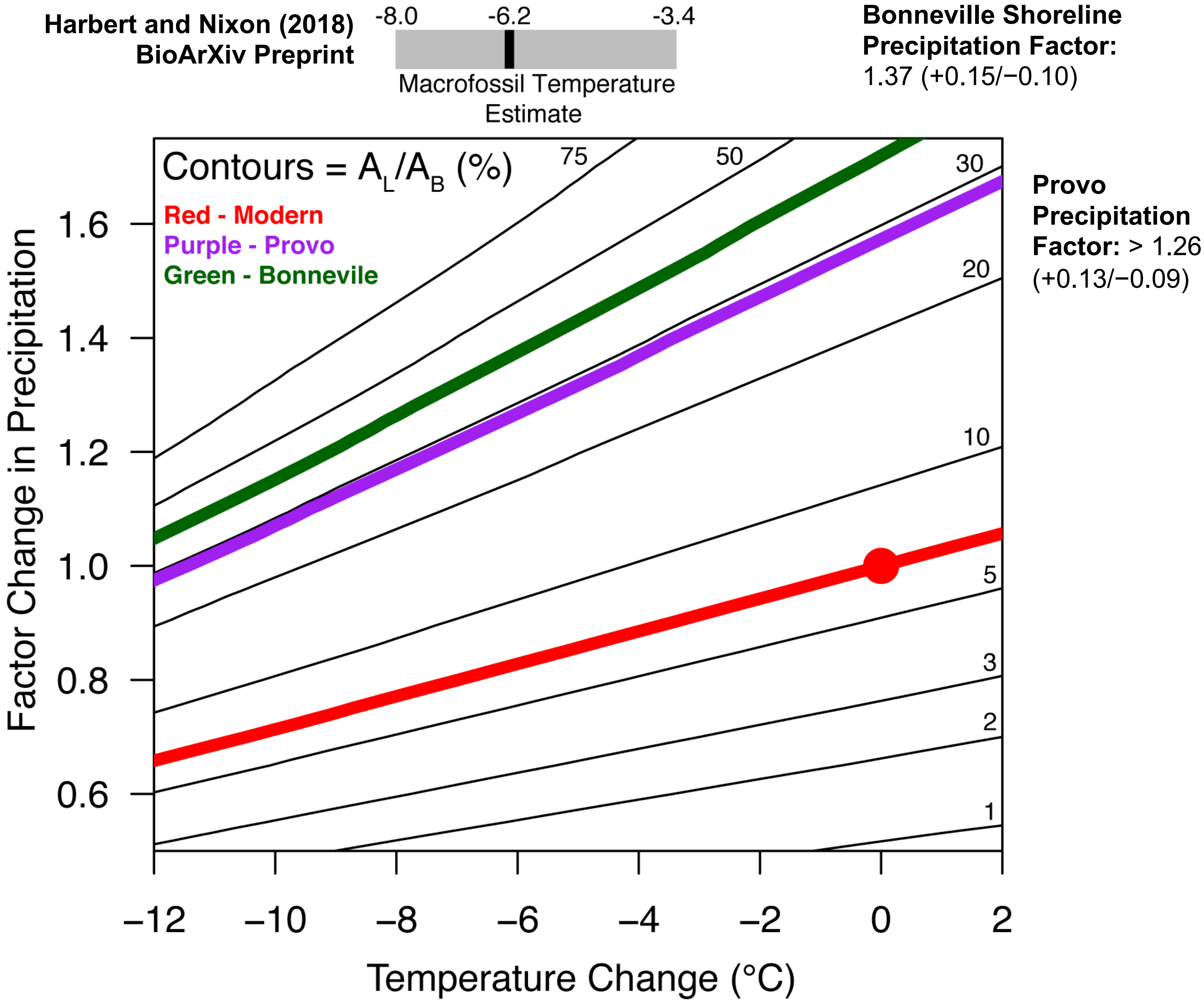

Residence Time Calculation

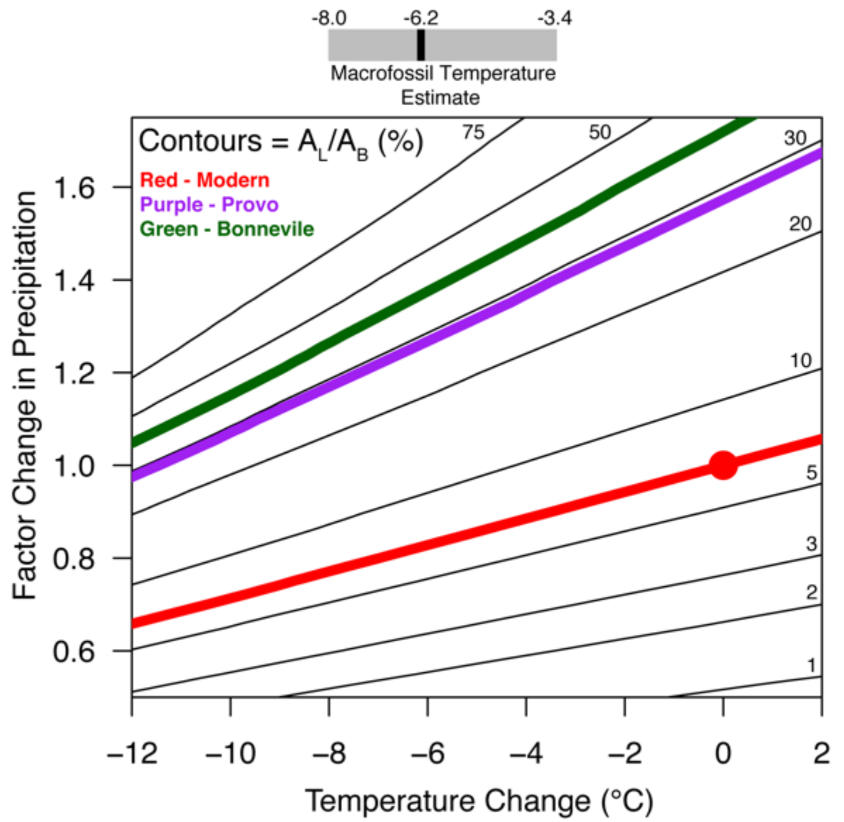

Bonneville Shoreline Precipitation Factor: 1.37 (+0.15/−0.10)

Provo Precipitation Factor: > 1.26 (+0.13/−0.09)

Residence Time (yr) = Volume (km³) / Inputs (km³/yr)

Inputs: Runoff + On-lake precipitation

Adams and Bills (2016)

TABLE 8.1 Comparison Between Surface Areas and Volumes of Lake Bonneville Using a DEM with the Rebound Signal Removed and a Modern Topography DEM

Lake Stage	Area (km^2)	Volume (km^3)[a]	Lake Water Residence Time (years)
Rebound signal removed			
Bonneville	52,110	10,420	185 (+13/−16)
Provo	38,150	5290	~102 (+7/−9)

Comparison to Other Precipitation vs. Temperature Curves

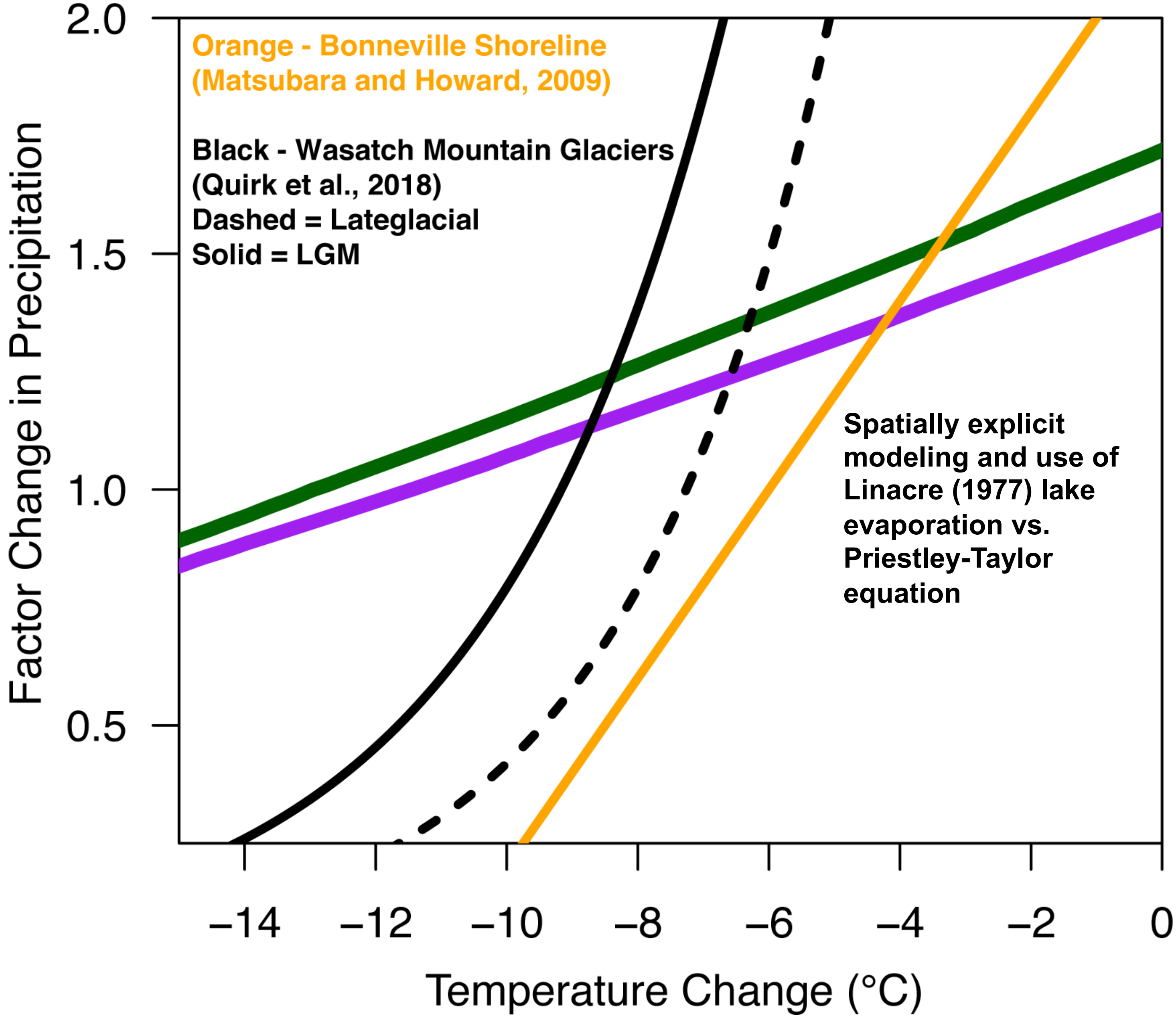

Last Glacial Maximum vs. mid-Pliocene

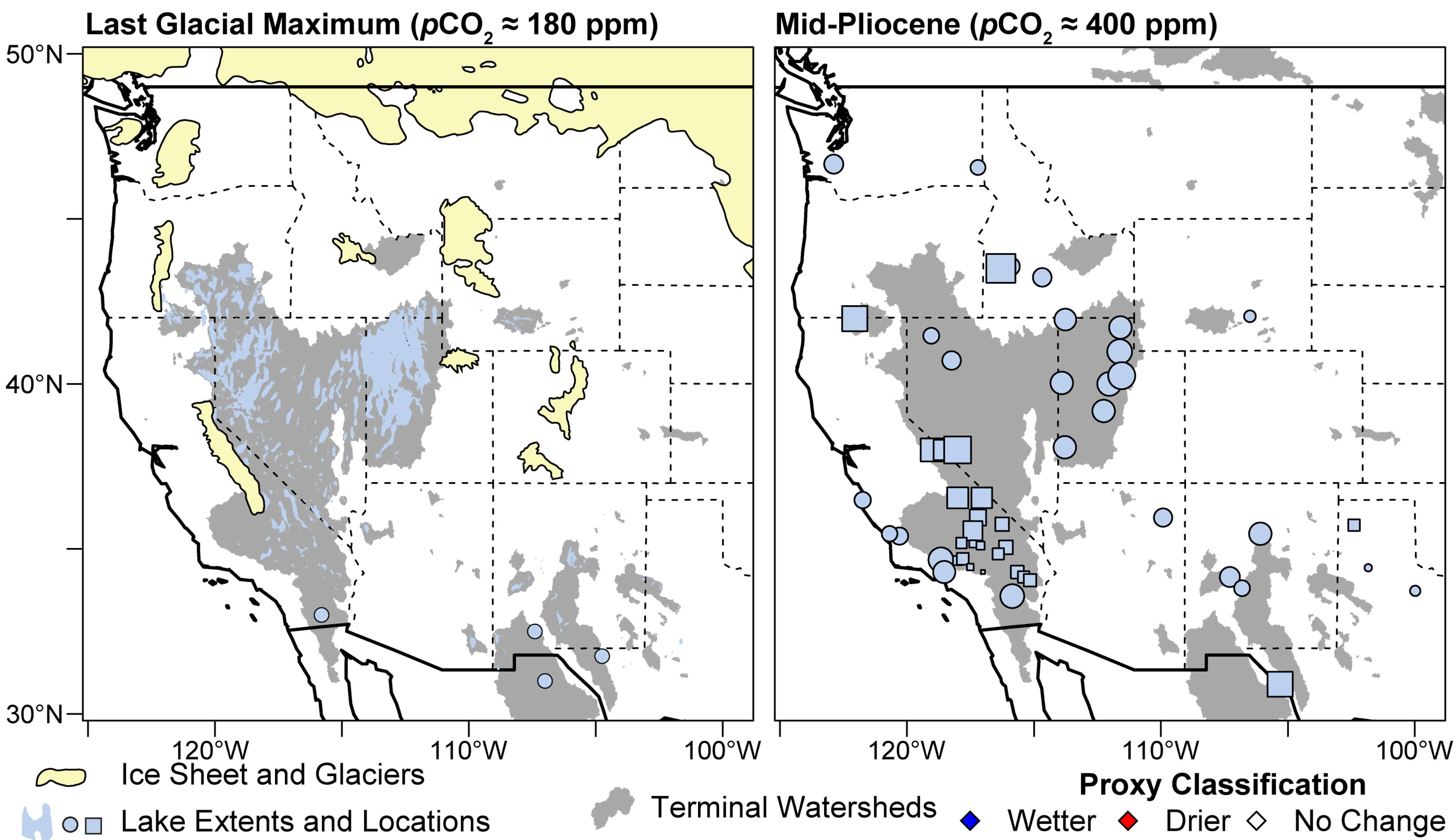

Lakes: Allen (2005); Reheis (1999); Orme (2008); Grayson (2011); Soller et al. (2009); Williams and Bedinger (1984); Milfflin and Wheat (1979) Pound et al. (2014); *Macrostrat* and *Natural Earth* databases.

Ibarra et al. (2018, *Geology*)

Lake Area Forward Model Sensitivity Analysis

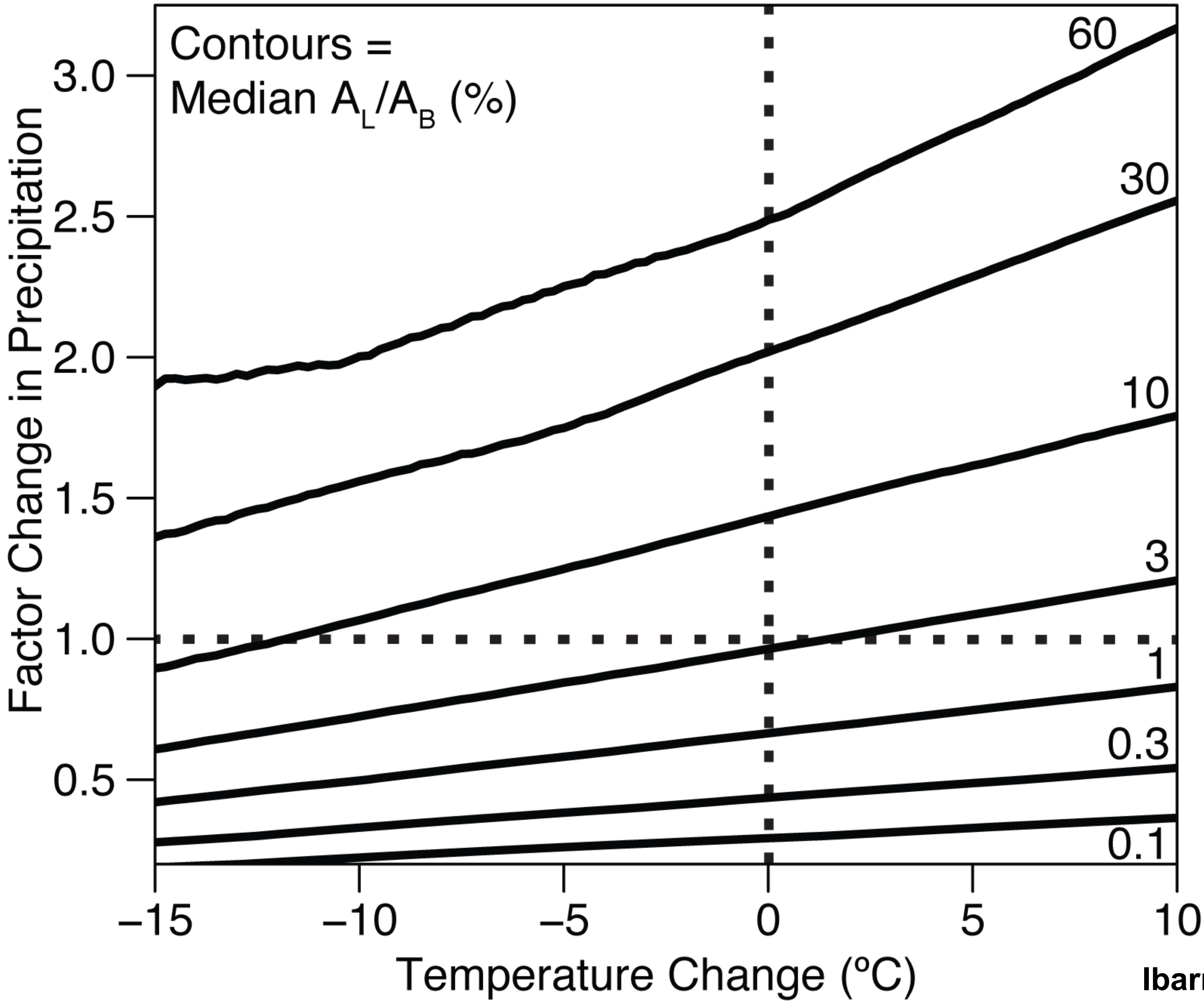

Ibarra et al. (2018)

Lake Area Forward Model Sensitivity Analysis

Analysis for entire western US domain
Temperature ranges based on independent data

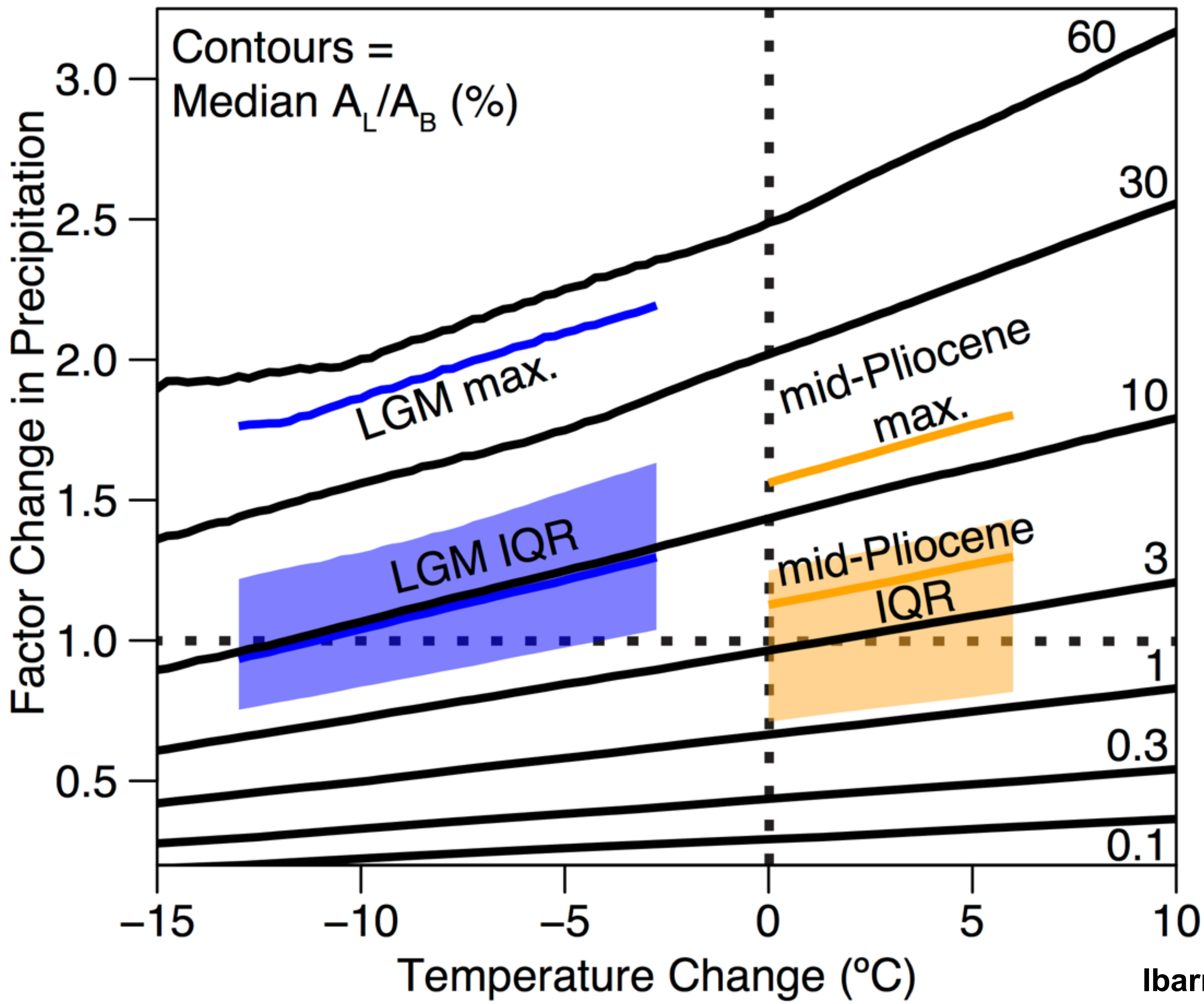

Ibarra et al. (2018)

LGM Precipitation

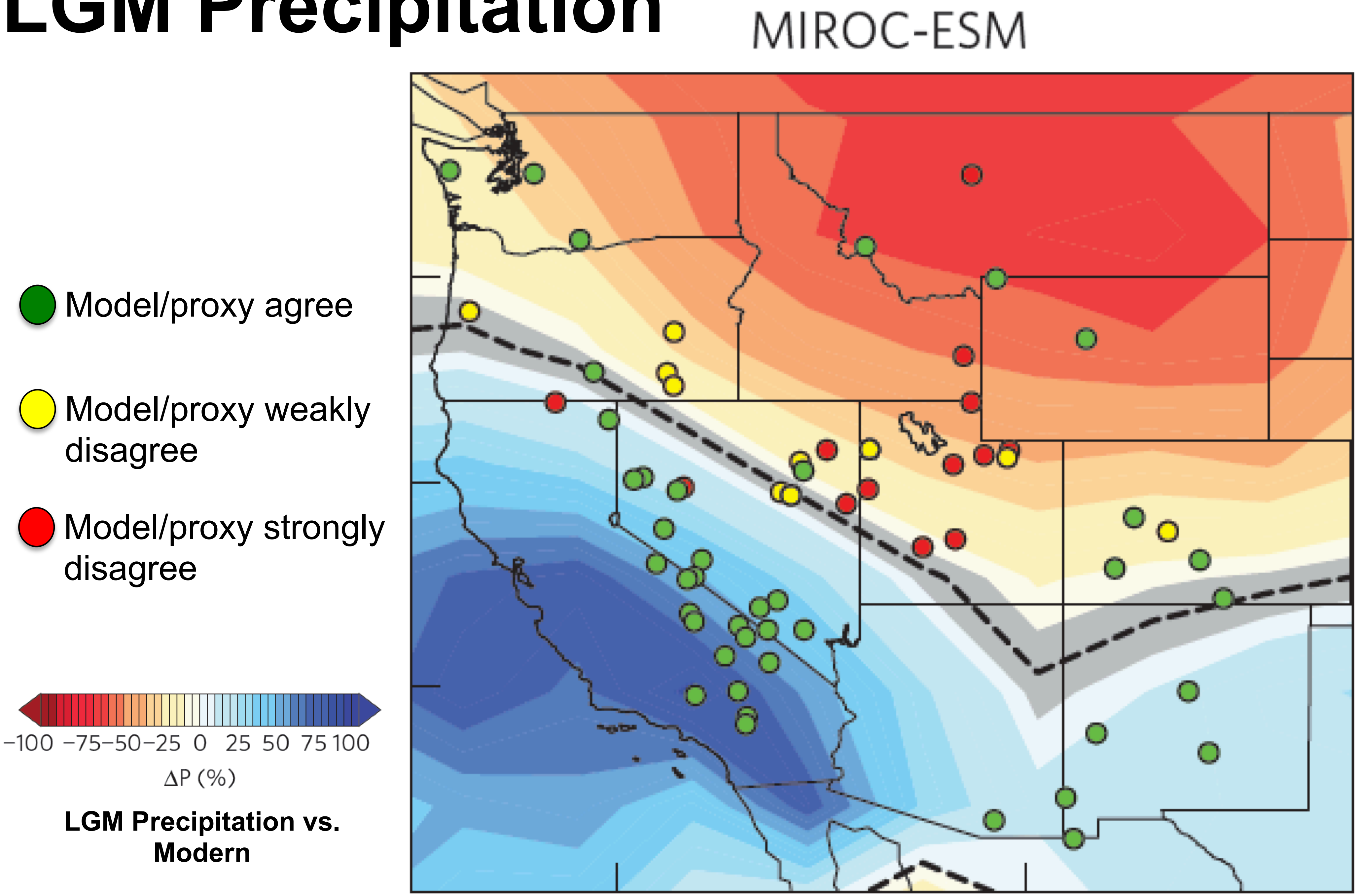

LGM Precipitation vs. Modern

Adapted from Oster et al. (2015)

Climate Model Forced Forward Model

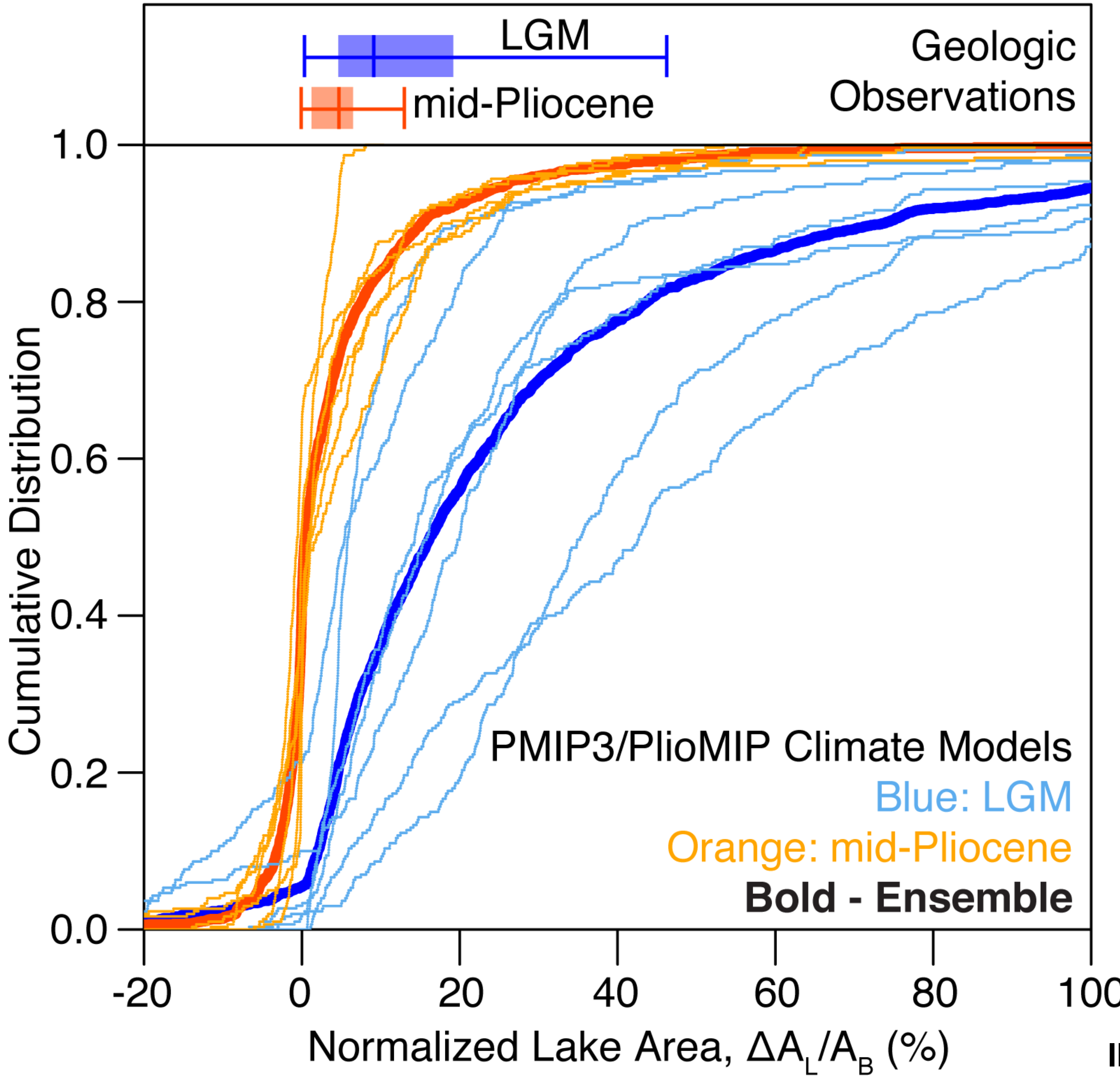

Ibarra et al. (2018)

Pliocene Lakes: Different Spatial Distribution

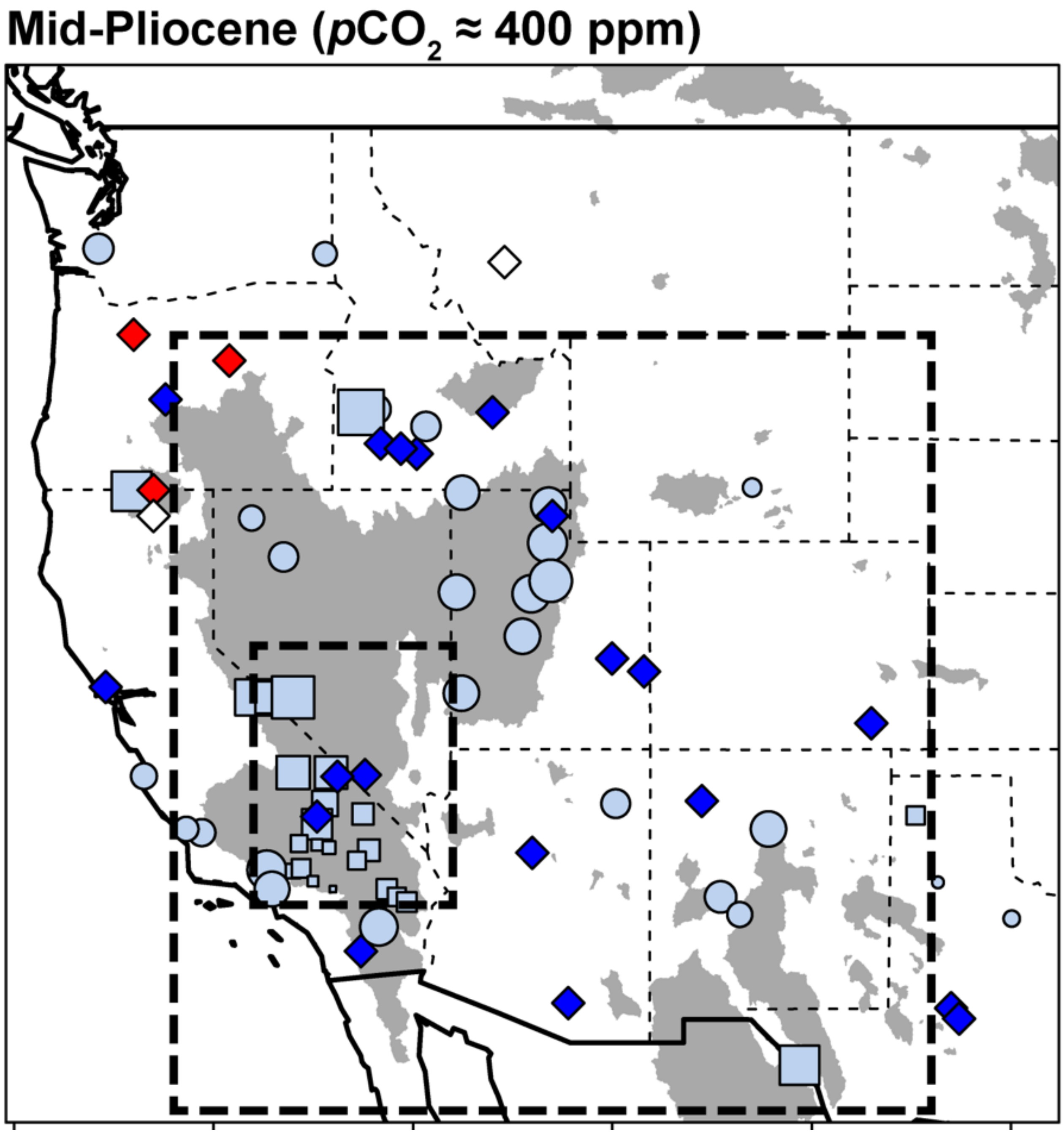

Best evidence for SW basins with Pliocene lakes compiled in Pound et al. (2014)

Ibarra et al. (2018)

Forward Modeling Lake Mass Balance

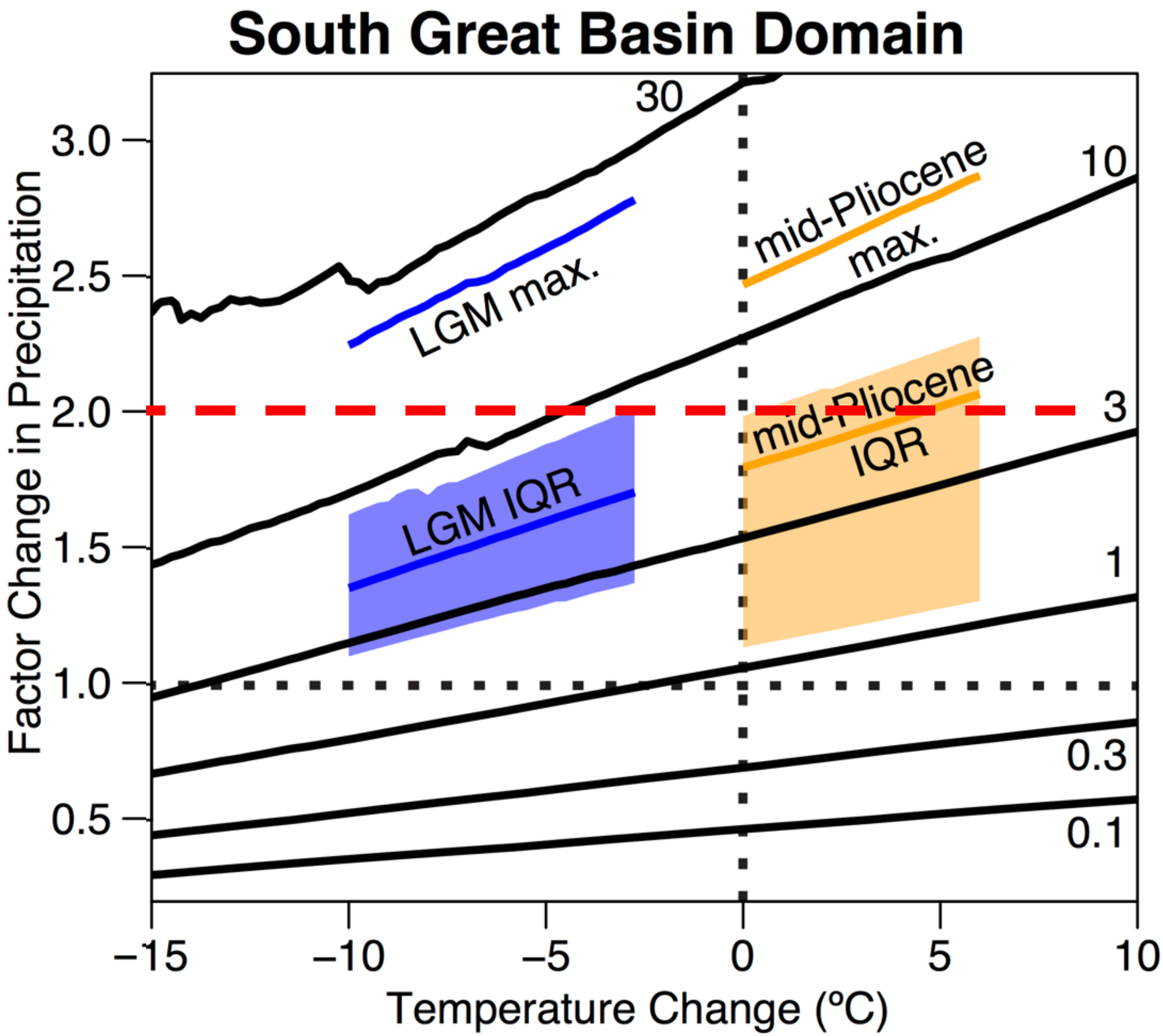

Ibarra et al. (2018)

LGM and mid-Pliocene represent <u>two wet states</u> with different hydroclimate drivers

Pleistocene Glacials

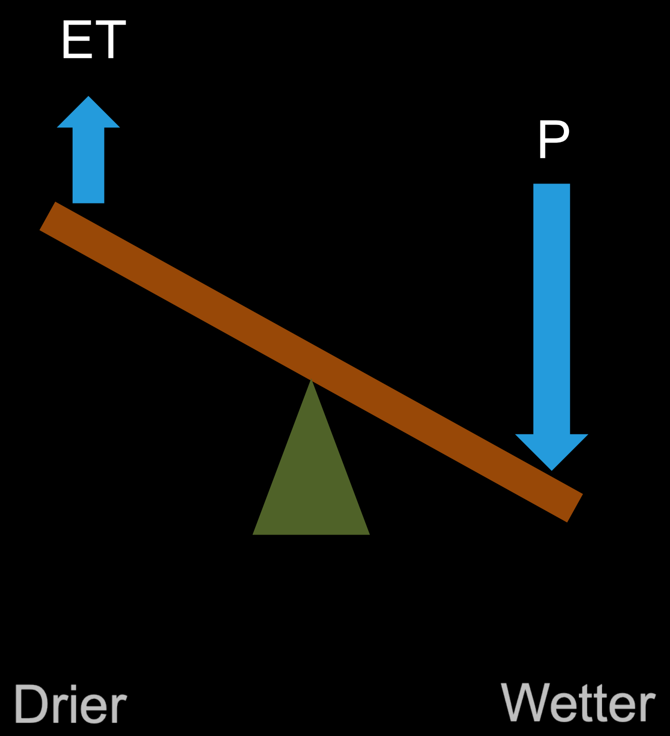

Mid-Pliocene Warm Period

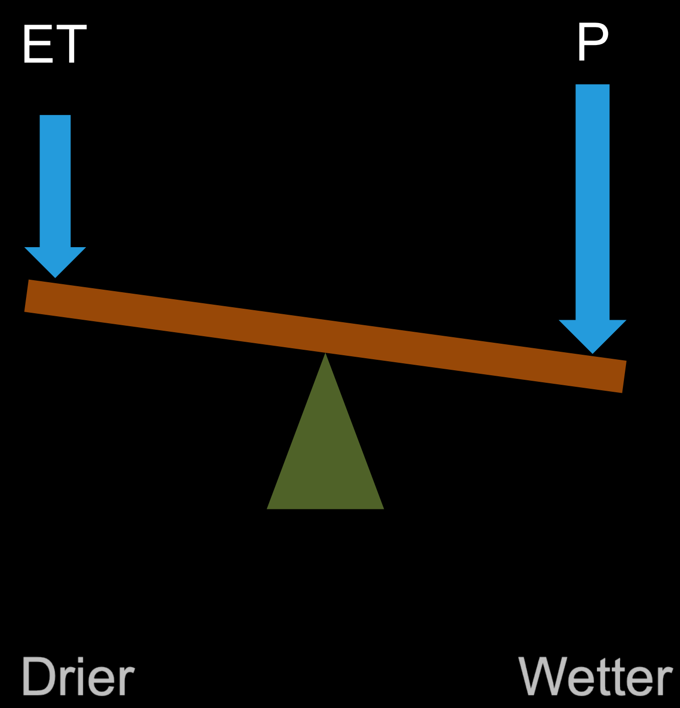

Future Work: Eocene Green River

51 Ma, $CO_2 \approx$ 600 to 1,500ppm

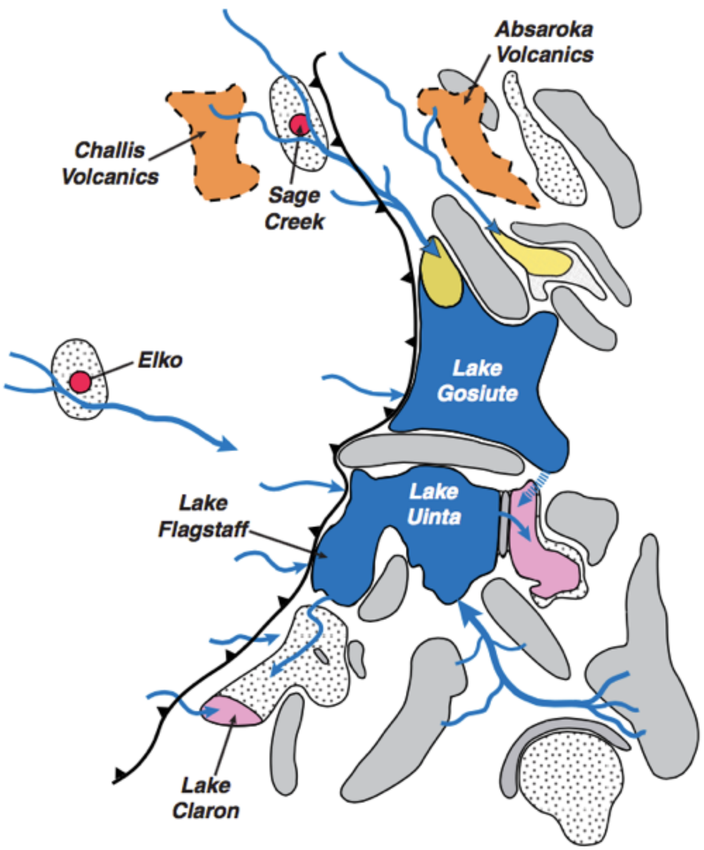

Eocene Green River (Utah and Wyoming)
Davis et al. (2009, *GSA Bulletin*)

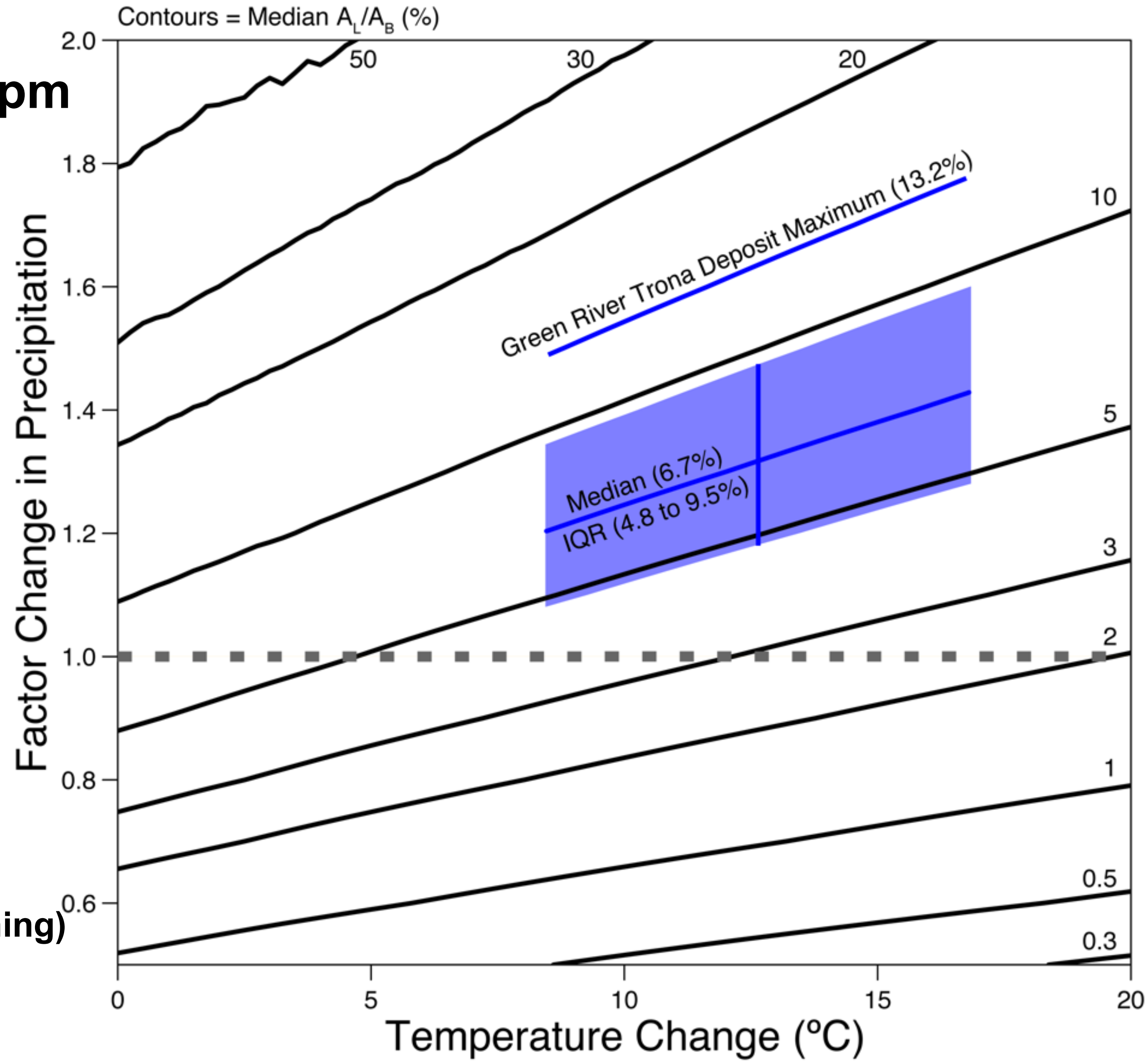

Analysis by Ibarra (*unpublished*)
Lake Gosiute constraints from Smith et al. (2008)

Takeaways

Forward model approach to link geologic observations with climate in precipitation vs. temperature space (code available)

- Bonneville and Provo shoreline precipitation estimates: 1.2 to 1.5x relative to modern
- LGM colder but spatially variable wet vs. dry
- Pliocene possibly much wetter in southwest

Possible Extensions:

- Stansbury shoreline and Gilbert episode estimates with adjusted watershed areas
- Little Valley (MIS 6) estimate with smaller watershed (remove Bear River contribution)?

Thank you!

Publication:
Ibarra et al. (2018, *Geology,* 46 (4), 355-358) *Warm and cold wet states in the western United States during the Pliocene–Pleistocene*

Acknowledgements:
James Dennedy-Frank, Kate Maher and Tyler Kukla (Stanford)
Juan Lora, Alex Arnold and Lauren Santi (UCLA)
Robert Harbert (Stonehill College)
Christine Chen (MIT-WHOI)

Funding:
- NSF EAR-1450357 to Chamberlain
- Heising-Simons Foundation
- Stanford EDGE-STEM Fellowship

Email: danieli@stanford.edu

@Dan_E_Ibarra

Office of the Vice Provost for Graduate Education

NSF

california alliance
BERKELEY UCLA STANFORD CALTECH

NARR Sensitivity Analysis Methods

- **Sensitivity of Temperature and Precipitation Changes**
- **Analyze the distributions (CDFs) for western US domain**

$$\frac{A_L}{A_B}(\%) = \frac{Pk_{run}}{E_L - P + Pk_{run}} 100.$$

Precipitation (P) factor change: 0.25x to 3.5x
Temperature anomaly: -15 °C to +10 °C

Budyko Equation (assume ω)

$$1 - k_{run} = \frac{ET}{P} = 1 + \frac{E_p}{P} - \left[1 + \left(\frac{E_p}{P}\right)^{\omega}\right]^{1/\omega},$$

Priestley-Taylor equation to calculate lake evaporation

$$\boldsymbol{LE = \alpha \frac{\Delta}{\Delta+\gamma} R_N}$$

E_p from R_N, Net Surface Radiation Balance (1.6%/K)

$$E_p = \frac{R_N}{L} = \frac{R_{S,i} - R_{S,o} + R_{L,i} - R_{L,o}}{L} = \frac{LE + H}{L}$$

Temperature Scaling of R_N

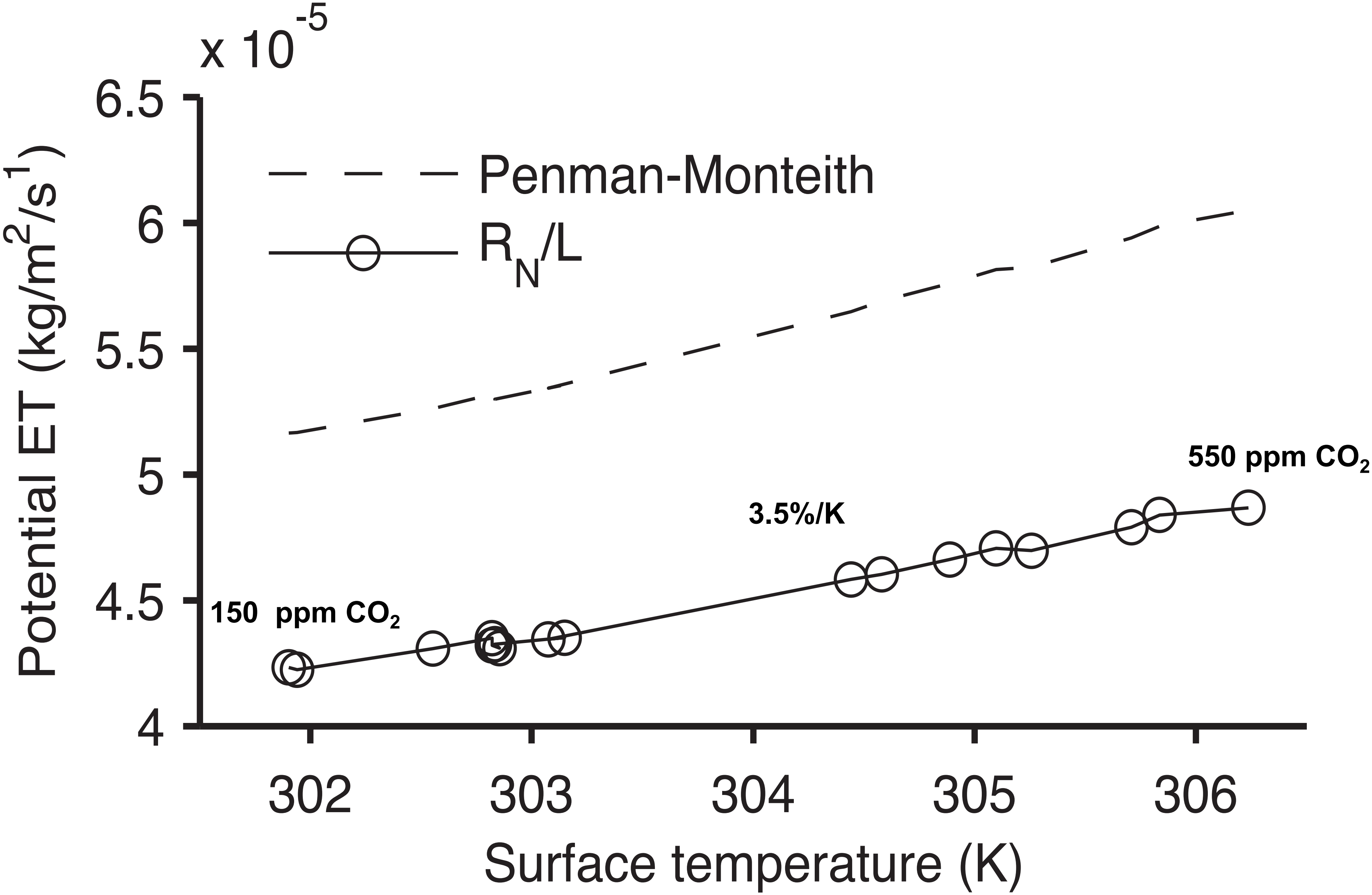

Single Column MITgcm experiments by Michael Byrne

Paleoclimate Model: Budyko Space

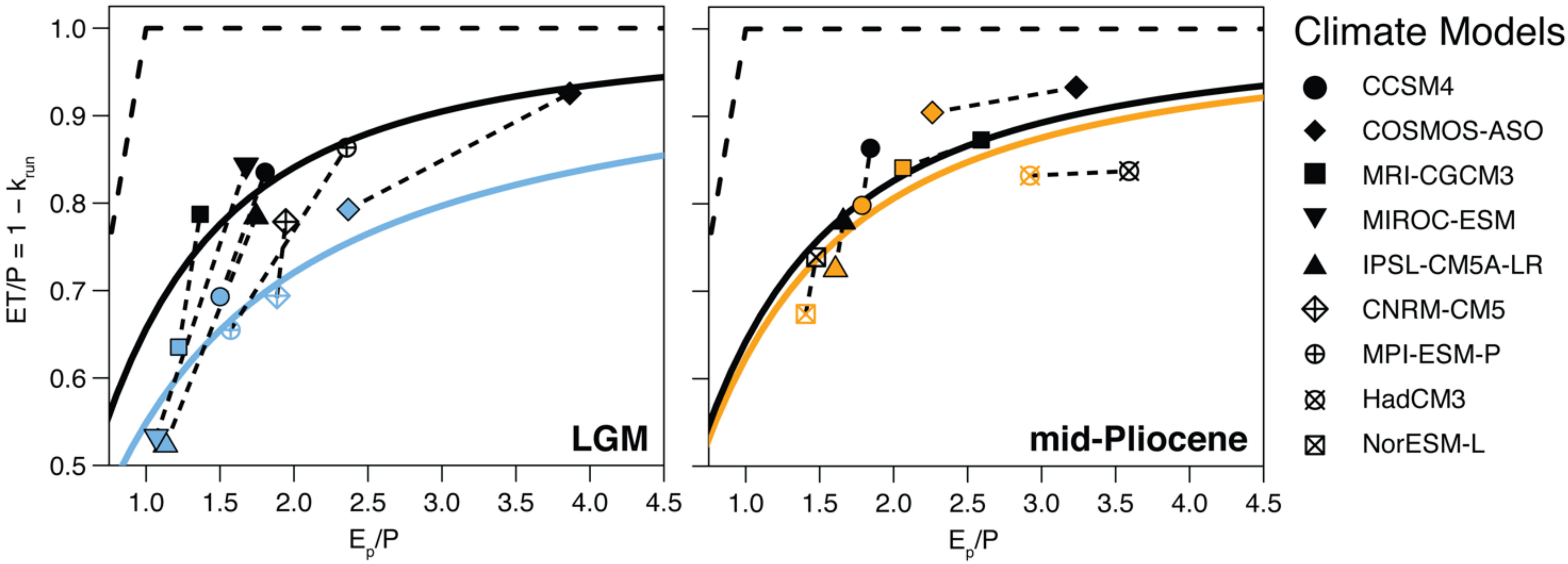

Dots → median western US values
Lines → ensemble median Budyko curves
Black = preindustrial, colored = LGM (PMIP3) and Pliocene (PlioMIP)

Ibarra et al. (2018)

Climate Models Follow Budyko

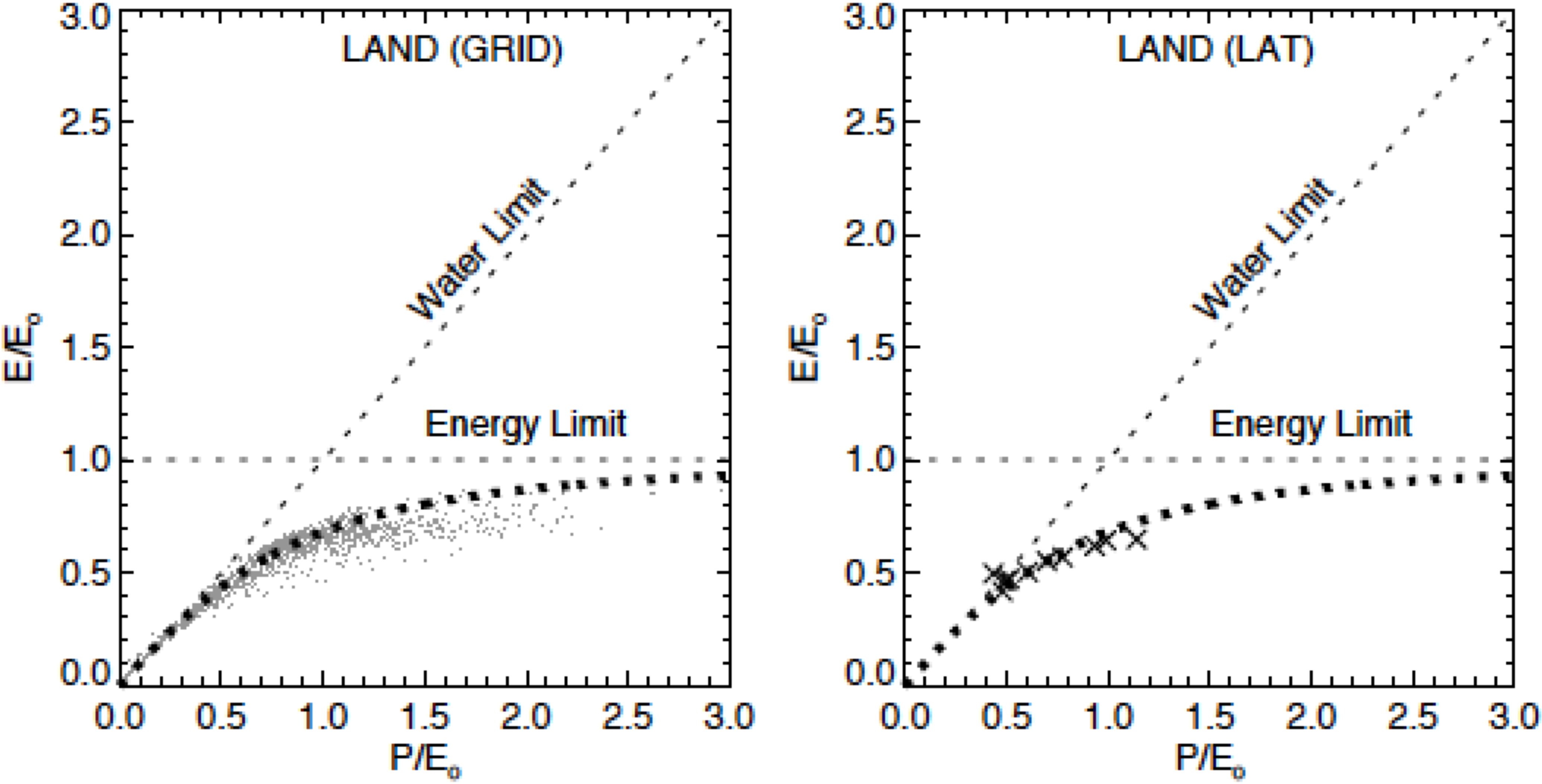

Roderick et al. (2014, *HESS*)

Sensitivity Analysis

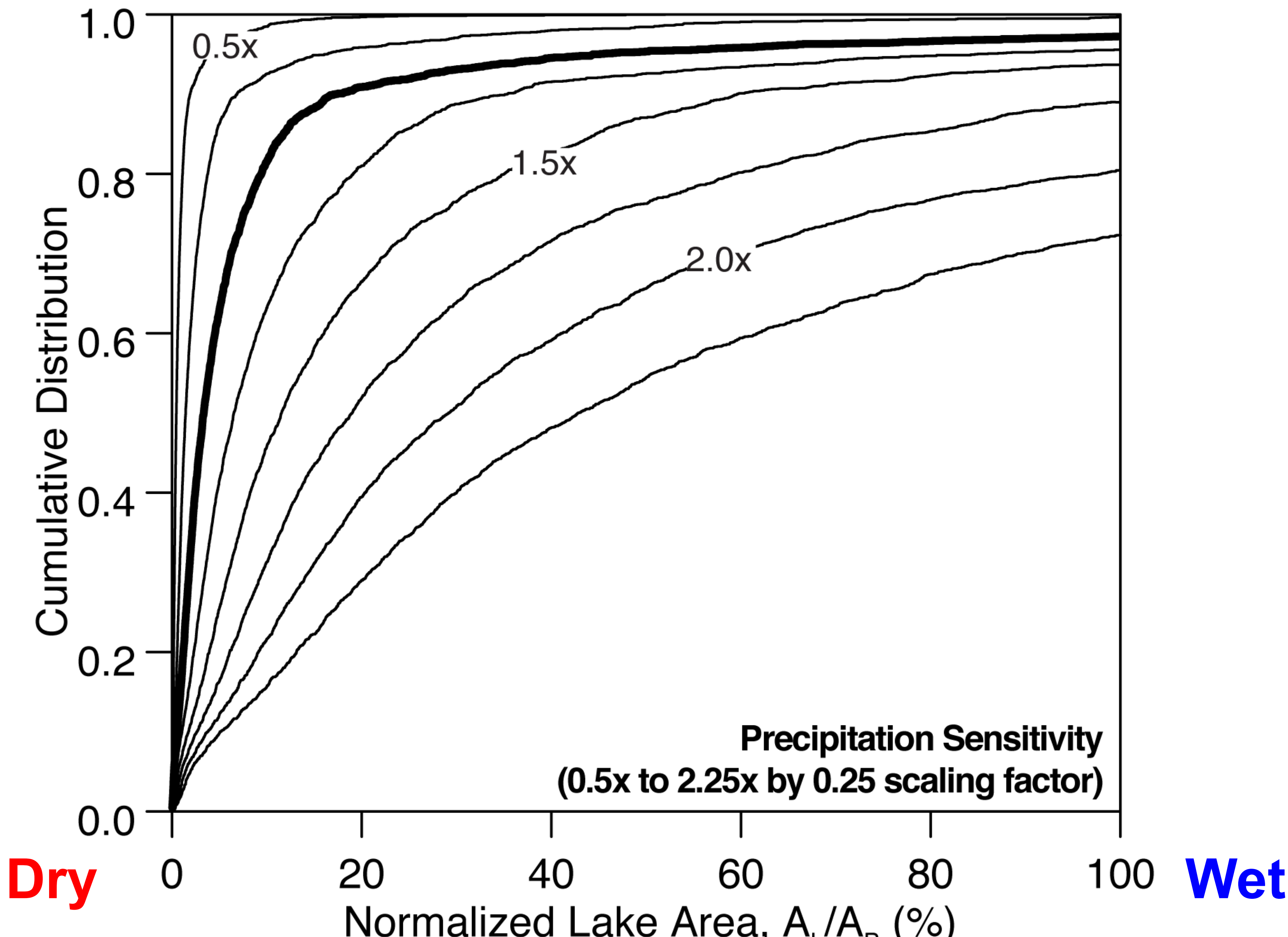

Ibarra et al. (2018)

Sensitivity Analysis

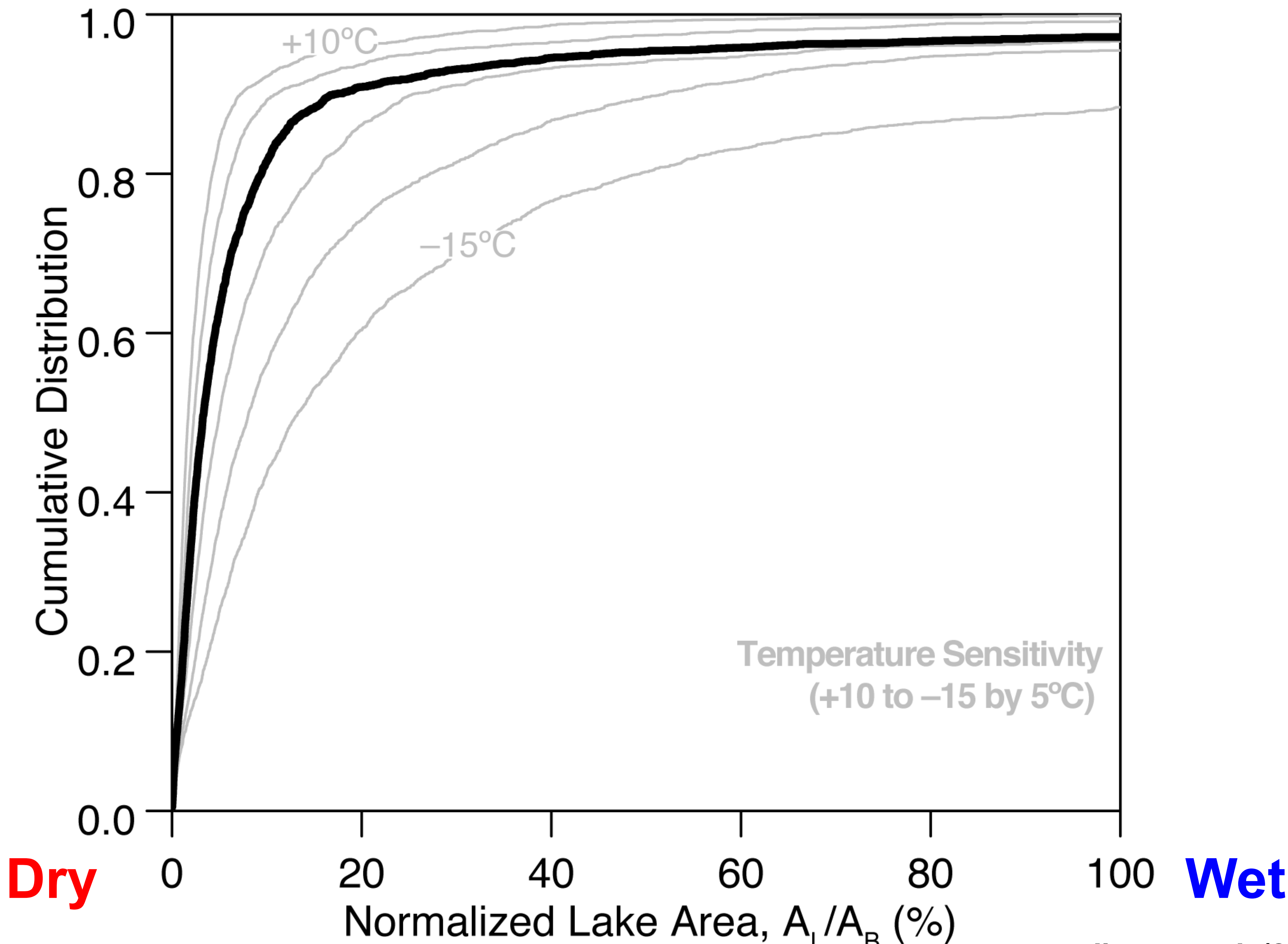

Ibarra et al. (2018)

Sensitivity Analysis

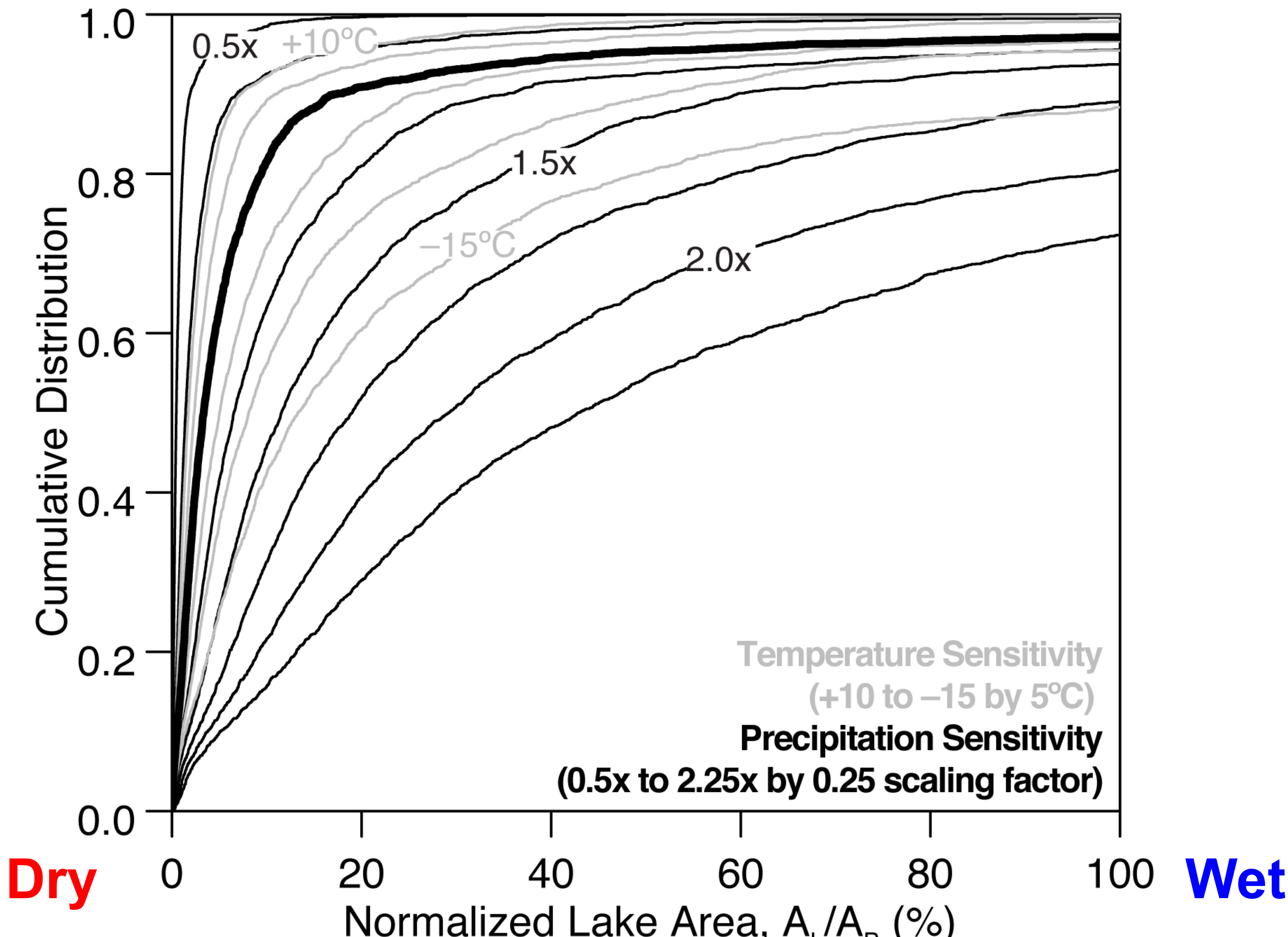

Ibarra et al. (2018)

GLACIAL HYDROCLIMATE OF WESTERN NORTH AMERICA: INSIGHTS FROM PROXY-MODEL COMPARISON AND IMPLICATIONS FOR LAKE BONNEVILLE

Jessica L. Oster[1] and Daniel E. Ibarra[2]

[1]Department of Earth and Environmental Sciences, Vanderbilt University, 5726 Stevenson Center, 7th Floor, Nashville, TN 37240;
[2]Department of Geological Sciences, Stanford University, 450 Serra Mall, Building 320, Stanford, CA 94305-2115

Corresponding author (Oster): jessica.l.oster@vanderbilt.edu

ABSTRACT

Decades of paleoclimate research have helped bring the pattern of hydroclimatic change across North America during the Last Glacial Maximum (LGM) into ever sharper focus. Despite these advances, the drivers of LGM hydroclimatic variability continue to be debated at the continental to basin scale. To explore the driving mechanisms behind LGM hydroclimatic change, we compare an updated network of moisture sensitive LGM proxy records from across North America and northern Central America with the annual precipitation output of nine simulations of LGM climate conducted as part of the Paleoclimate Model Intercomparison Project, as well as an ensemble average. The updated proxy network presented here points to wetter than modern conditions across most of the southwestern United States, with drier than modern conditions in the Pacific Northwest, Rocky Mountains, and parts of the Colorado Plateau. We find that, similar to previous work, the degree of model agreement with the proxy network is sensitive to the location and orientation of the simulated boundary between wetter and drier conditions in the western United States. The Bonneville basin occupies a key position in this context, as it is within this transition between wetter and drier conditions during the LGM. Proxy records from within and around the Bonneville basin suggest conditions that were unchanged or slightly wetter during the LGM, and the models that show the best agreement with the proxy network overall place the transition between wet and dry LGM precipitation anomalies at or near Lake Bonneville. Although models do not include pluvial lakes in their boundary conditions, our computed effective moisture anomalies as well as the model set up variables for IPSL-CM5A-LR and NCAR CCSM4, two of the models that best agree with the proxy network, demonstrate that at least these two models do include the present-day Great Salt Lake. These two models show weak positive precipitation anomalies downwind of the modern lake area and in general show good agreement with Bonneville basin proxy records. This suggests that future inclusion of pluvial lakes in model boundary conditions for the LGM could both improve proxy-model agreement and enhance our understanding of how processes such as vapor recycling influence the hydroclimate of continental interiors.

INTRODUCTION AND METHODOLOGY

Western North America has experienced a dynamic hydroclimatic history over the last glacial cycle, recorded by the growth and desiccation of large inland lakes, expansions and contractions in the ranges of vegetation, and variations in the chemical composition of pedogenic and cave minerals (Nowak and others, 1994; Maher and others, 2014; Reheis and others, 2014). More than a century of paleoclimatic research in this region has provided a wealth of information about the spatial and temporal patterns of these changes, and important insight into the drivers of hydroclimatic change can be gained by integrating these records and comparing them with paleoclimate model simulations. A network of moisture-sensitive proxies as well as pollen-based precipitation and moisture reconstructions suggest a dipole pattern across this region at the Last Glacial Maximum (LGM, ~21 ka), with a wet southwest and dry conditions approaching the Laurentide Ice Sheet (Oster and others, 2015). Yet despite a relatively clear picture of glacial climate in western North America, the atmospheric drivers behind these patterns remain a source of debate (Lyle and others, 2012; Lora and others, 2017; Morrill and others, 2018). Early modeling studies suggested that the westerly storm track was shifted southward during LGM (COHMAP Members, 1988) while more recent work has indicated that rather than a uniform southward shift, the storm track was steered in a northwest-southeast direction across the region by high pressure situated over the Laurentide Ice Sheet (Oster and others, 2015). Other work has pointed to the importance of an influx of sub-tropically derived southwesterly winter moisture in setting up this regional pattern (Lora and others, 2017). Our understanding of glacial hydroclimate is further complicated by the pattern of hydroclimatic change across western North America following the LGM, as the majority of western pluvial lakes achieve higher levels during Heinrich Stadial 1 (18–15 ka) or later as the Laurentide Ice Sheet is decaying (for example, Munroe and Laabs, 2013; Ibarra and others, 2014).

Here, we draw upon the large body of proxy evidence and recent modeling work to provide the most up to date snapshot of glacial hydroclimatic change in the Bonneville basin and western North America broadly. We have compiled an updated network of moisture sensitive proxy records from western North America, and expanded this network to include all of North America. The present compilation builds upon our previous work (Oster and others, 2015) through the addition of recently published records that include pollen and macrofossil-based estimates of hydroclimatic change (Scheff and others, 2017; Harbert and Nixon, 2018) as well as new records and modeling local to the Bonneville basin (Quirk and others, 2018; Ibarra and others, 2019). We have expanded our proxy network, previously compiled for western North America, to include all of North America as well as northern Central America through the inclusion of pollen, macrofossil, and lake sediment records developed or compiled by Scheff and others (2017) and Shuman and Serravezza (2017).

Our proxy network includes records of soil, cave, and lake water chemistry, lake level fluctuations, and glacier mass-balance in addition to the vegetation-based records derived from lake and bog sediments and pack rat middens. For each record, we categorize the LGM (21 ± 2 ka) hydroclimatic response as "wetter," "drier," or "no change" relative to modern conditions. In categorizing proxy response, our designation is based on the original interpretation of the authors or the most recent compilations, as in the case of vegetation-based estimates (Scheff and others, 2017; Harbert and Nixon, 2018). Records for which no clear hydroclimatic designation can be made are coded as "unclear." Estimates of precipitation change from mountain glacier mass-balance modeling are only included in our compilation if they explicitly address uncertainties regarding the combined influence of temperature and precipitation change on glacier advance through independent estimates of temperature change (e.g., Laabs and others, 2006). Many glacier records are coded as unclear in our compilation due to uncertainties in the balance of temperature versus moisture variability.

We compare our network of precipitation-sensitive proxy records to the output of monthly climatologies for nine simulations of LGM (21 ka) climate conducted as part of phase 3 of the Paleoclimate Model Intercomparison Project (PMIP3) (Braconnot and others, 2012) accessed through the Earth System Grid Federation (ESGF) (Taylor and others, 2012). We use bilinear interpolation to calculate precipitation (P) and effective moisture (EM) values from annually summed precipitation and evapotranspiration of the 21-ka and Pre-Industrial (PI–0 ka) runs from the nine models in their native resolution using coordinates of the proxy record sites. For lakes we selected basin centers as representative coordinates. Additionally, we compare the proxy network to the ensemble average precipitation for the LGM and PI by averaging the P output of all models following interpolation to a 1° by 1° grid. We then calculate the annual P and EM anomalies for the LGM, expressed as percent, for each model and the ensemble using the equations:

$$P_{anom} = (P_{21ka}/P_{0ka}) \text{ x } 100 \quad (1)$$

$$EM_{anom} = (EM_{21ka}/EM_{0ka}) \text{ x } 100 \quad (2)$$

We compare the hydroclimatic changes simulated by each model and the ensemble with the change observed in each proxy record using a weighted Cohen's κ_w statistic (e.g., DiNezio and Tierney, 2013; Oster and others, 2015; Hermann and others, 2018), which measures categorical data agreement between two raters who classify items (here proxy locations) into categories (wetter, drier, no change) relative to the probability of random agreement, and weights observations according to the degree of model-proxy disagreement (Cohen, 1968). This is accomplished by multiplying a matrix of model-proxy observations by a weight matrix in which strong agreement between observers (e.g., both model and proxy suggest wetter conditions at a site) is given a weight of 0, strong disagreement (e.g., the model suggests wetter, but the proxy drier) is given a weight of one, and weak disagreement (e.g., the model suggests wetter, but the proxy suggests no change) is given a weight of 0.5. κ_w is then calculated as:

$$\kappa_w = 1 - \frac{\sum_{i=1}^{C}\sum_{j=1}^{C} w_{ij}x_{ij}}{\sum_{i=1}^{C}\sum_{j=1}^{C} w_{ij}m_{ij}} \qquad (3)$$

where:

w_{ij} and x_{ij} = elements in the weight and observed matrices, respectively
m_{ij} = elements in the matrix of scores that would arise through random chance.

To identify the maximum possible agreement between models and proxies, we varied the threshold of change in P and EM required for the model responses to fall into the wetter or drier category from 5 to 35%. Computed κ_w values can range from -1 to 1, where -1 is perfect disagreement, 0 is no agreement greater than random chance, and 1 is perfect agreement between the model and proxy records (Cohen 1968). For the EM κ_w calculations, sites falling in grid cells that contain some proportion of ocean were excluded.

RESULTS AND DISCUSSION

Our updated proxy network improves upon the spatial coverage of our previous compilation (Oster and others, 2015) by specifically increasing coverage in the Pacific Northwest and the Colorado Plateau, and also expanding the network to include records from the rest of the United States, Mexico, and northern Central America (figure 1). The updated network retains the clear wetter south–drier north dipole previously apparent in the western United States (Oster and others, 2015), but includes more records that variably suggest enhanced or reduced aridity at the LGM along the southern Colorado Plateau. Proxy records in the Midwest suggest wetter conditions, while those in the mid-south to the east coast of the United States as well as southern Mexico indicate no change in hydroclimatic conditions. Increased aridity during the LGM is suggested for Florida and parts of the deep South.

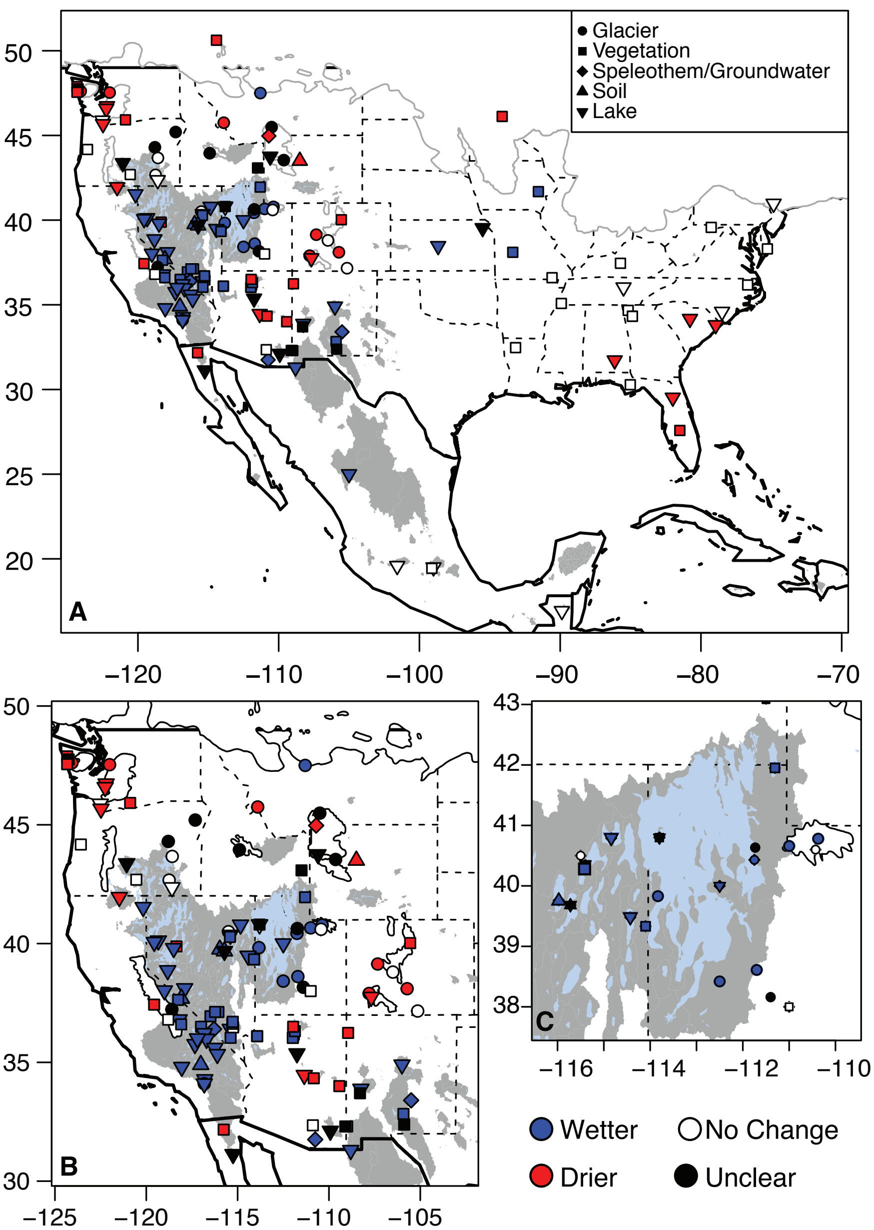

Figure 1: Proxy network for A) all of North and northern Central America, B) western United States, and C) area surrounding glacial Lake Bonneville. On all maps, proxies are denoted by type (shape) and LGM moisture conditions (color). The southern boundary of the LGM Laurentide and Cordilleran ice sheets are shown in white (Ehlers and others, 2011). Inward draining basins are shown in gray (Lehner and Grill, 2013; Ibarra and others, 2018), and the extent of pluvial lakes are shown in blue (http://www.naturalearthdata.com/downloads/10m; Soller and others, 2009).

In our previous work, we identified a suite of five models that produced high κ_w values when compared to our proxy network. These included IPSL-CM5A-LR, MPI-ESM-P, NCAR CCSM4, CNRM-CM5, and MIROC-ESM. The highest κ_w for each of these models occurred at low thresholds for precipitation change (5–10%) (Oster and others, 2015). Many of the same models perform well in comparison with our updated proxy network, still at precipitation change thresholds of 5–10%. MPI-ESM-P has the highest κ_w value, and NCAR CCSM4, IPSL-CM5A-LR, and MIROC-ESM have slightly lower κ_w values (figure 2). The model COSMO-ASO, which was not among the models showing the best agreement previously, has the third highest κ_w value in comparison with the expanded proxy network. The same five models have the highest κ_w when considering a proxy network that is spatially limited to the western United States, providing a more direct comparison to the previous proxy network. In general, the models display lower κ_w values when anomalies in EM, rather than P, are considered. However, the models MRI-CGCM3 and CNRM-CM5, which are not among those with the highest precipitation κ_w values, have the top values when considering EM anomalies (not shown). Interestingly, the ensemble average of P anomalies has a high κ_w value (0.44) (figure 2). Only MPI-ESM-P has a higher precipitation κ_w value (0.46) than the ensemble. The ensemble κ_w, however, is highest for a much larger precipitation change threshold (20%) compared to the individual models. This means that a larger proportion of the study area falls into the "no change" category, reducing the number of sites where the model and proxies strongly disagree.

The majority of the high-scoring models and the ensemble simulate increased aridity across the eastern United States and in the Pacific Northwest and wetter conditions in the southwestern United States. As with our previous study, we find that differences in model agreement with the proxy network appear to be closely related to the location and geometry in the model simulations of the transition between wet anomalies in the southwestern United States and dry anomalies in the Pacific Northwest. This transition generally occurs near the California-Oregon border at 42 °N, stretching eastward across the northern Great Basin. In many of the models with higher κ_w and in the ensemble, this transition from wet to dry precipitation anomalies trends from the northwest to the southeast across the western United States with varying degrees of undulation (figure 2). Areas of persistent disagreement between models and the proxy network may reflect a change in precipitation seasonality that is important for proxy response, but not apparent in the model annual averages used here. For instance, the aridity recorded by some proxies from the Colorado Plateau may reflect reduced monsoon rainfall during the LGM that is overshadowed in the annual model average by increased winter precipitation (e.g., Bhattacharya and others, 2018). Alternatively, apparent drying displayed by some vegetation-based proxies may primarily reflect reduced atmospheric CO_2 during the LGM rather than hydroclimatic change (Scheff and others, 2017).

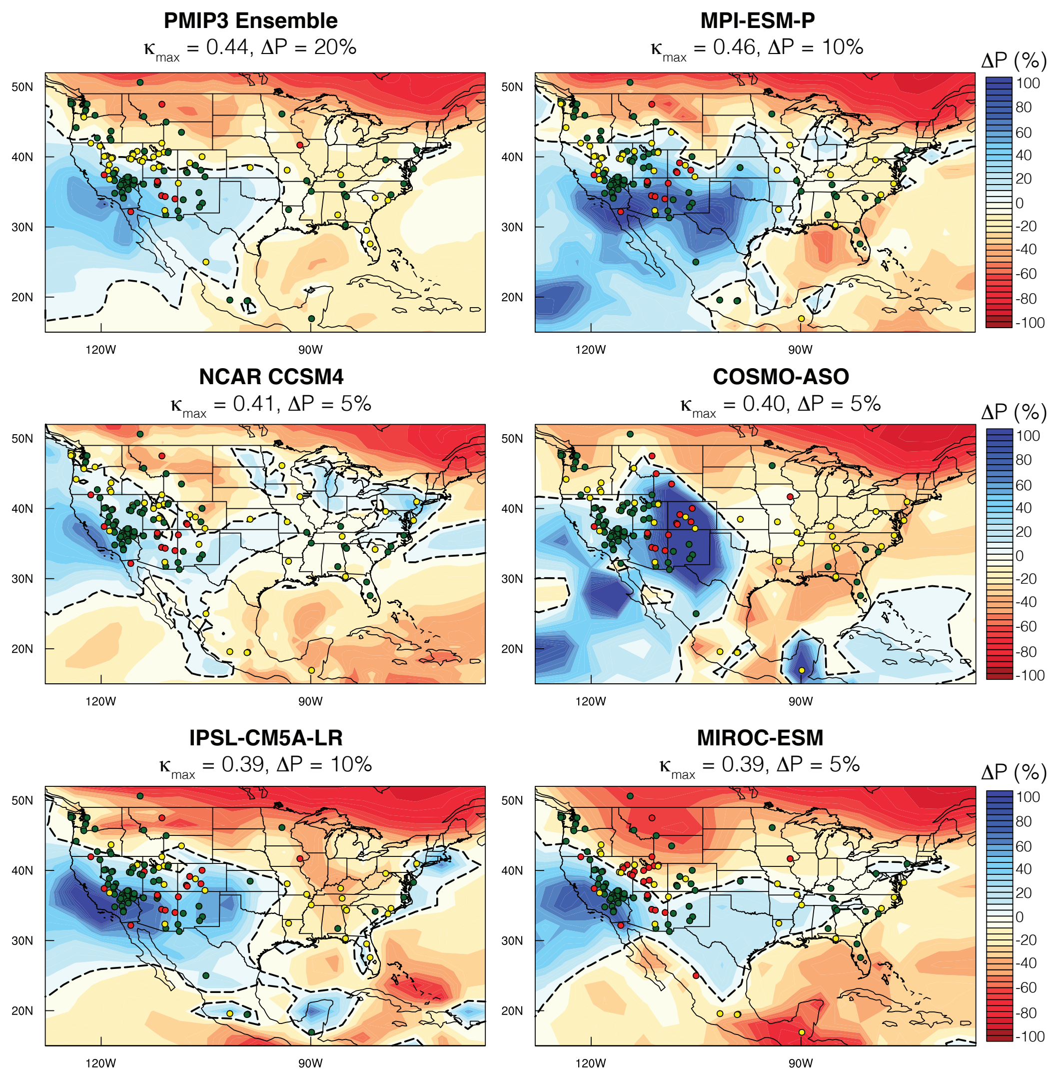

Figure 2: *Contoured percentage change in annual precipitation (% ΔP, LGM-PI) with maximum κ_w for the ensemble and the five models with the highest κ_w values. Proxies shown as agreeing (green), weakly disagreeing (yellow), or strongly disagreeing (red) with each model at maximum κ_w. Contour line of zero ΔP is dashed for each model.*

Although we do not reanalyze atmospheric dynamics of these models here, this updated proxy-model comparison is consistent with our previous assertion that squeezing and deflection of zonal winds and steering of storms along a northwest to southeast trend due to the pressure gradient caused by the permanent high-pressure system over the Laurentide Ice Sheet was an important factor in determining the spatial pattern of hydroclimatic variation across the western United States at the LGM. We do not explicitly analyze the source of increased moisture to the western United States, though our results are not inconsistent with increased southwesterly moisture intruding into the continental interior as suggested by Lora and others (2017). Further analysis of atmospheric dynamics and moisture source changes across all of North and Central America will be conducted using this expanded proxy network and the LGM simulations associated with the updated PMIP4 modeling effort, scheduled to be released in 2019 (Kageyama and others, 2017).

Lake Bonneville occupies a critical position in the context of hydroclimatic change in western North America. Situated in the northeastern Great Basin between 37.5 and 43°N, Lake Bonneville is located within the transition zone between wetter and drier precipitation anomalies noted in both the proxy records and the models. Paleoclimate proxy records from the Bonneville basin, including records from pollen, tufa deposits, and ostracodes suggest conditions that were unchanged or slightly wetter during the LGM (Oviatt and others, 1992; Davis, 2002; Kaufman, 2003; Benson and others, 2011; McGee and others, 2012). Likewise, mass balance modeling of glaciers in the Wasatch Range and Uinta Mountains to the east of Lake Bonneville also point to an LGM that was either unchanged or slightly wetter (Munroe and Mickelson, 2002; Laabs and others, 2006; Refsnider and others, 2008; Quirk and others, 2018). The climate models with the highest κ_w values place the transition from wet to dry LGM precipitation anomalies at or near the location of Lake Bonneville (figures 2 and 3), further suggesting that reduced evaporation in combination with small precipitation increases likely drove moderate to high lake levels in the northern Great Basin during the LGM (e.g., Reheis and others, 2014; Ibarra and others, 2014; 2018).

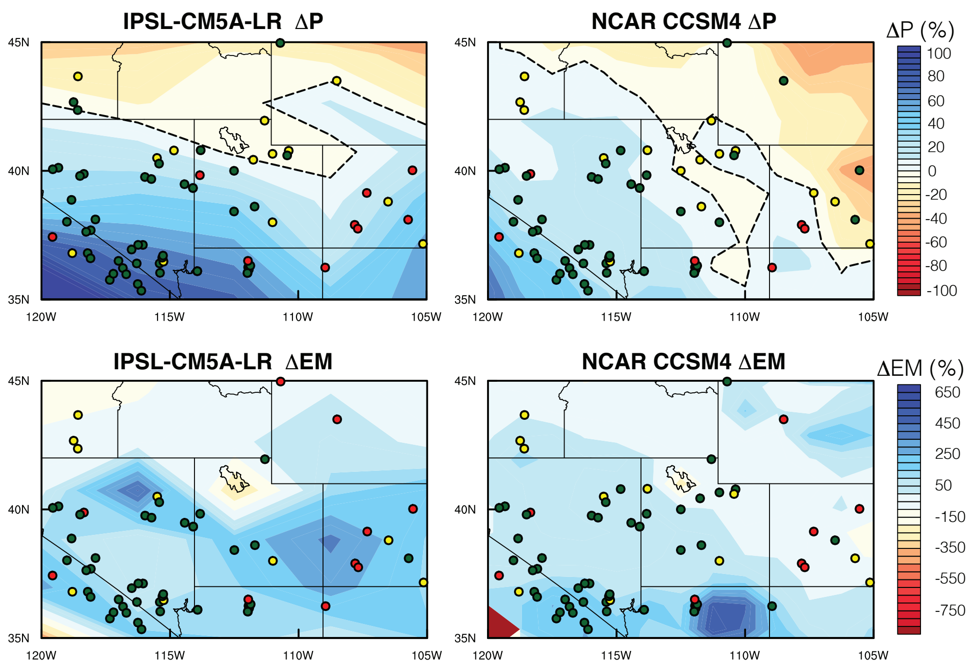

Figure 3: *Contoured percentage change in annual precipitation (% ΔP, LGM-PI) (top panels), and EM (% ΔEM, LGM-PI) (bottom panels) for the models IPSL-CM5-LR and NCAR CCSM4 for the area surrounding Lake Bonneville. Proxy sites are colored as in figure 2. The negative anomaly polygons over the location of present-day Great Salt Lake for both models suggest that the lake is included in the land surface boundary conditions. Both models show positive precipitation anomalies downwind of the lake.*

Importantly, the PMIP models do not include Lake Bonneville or other pluvial lakes in their land surface boundary conditions, omitting potentially important moisture sources for regional mountain glacier growth. However, it is apparent from the computed EM anomalies, and indicated in the model set-up variables, that the present Great Salt Lake is included in the model boundary conditions for at least two of the models with higher κ_w values, IPSL-CM5A and NCAR CCSM4 (figure 3). Interestingly, both of these models display a zone of higher LGM P anomalies just to the east of the Bonneville basin, downwind of Great Salt Lake, which is included in the model parameterization. These models display agreement to weak disagreement with the proxy records in the Bonneville basin, suggesting a narrow margin of small, positive P anomalies fueled by locally recycled vapor from Lake Bonneville is the most likely hydroclimate scenario for this region at the LGM. This observation underscores the influence that large pluvial lakes such as Bonneville and Lahontan must have had on their local hydroclimate (e.g., Hostetler and others, 1994; Galewsky, 2013), and the potential improvement to the simulation of vapor recycling effects and model-proxy agreement should these lakes be included in model boundary conditions (i.e., Pound and others, 2014) in the future.

CONCLUSIONS

We have expanded the network of hydroclimatically sensitive paleoclimate proxy records from the LGM to include all of North America and northern Central America and to provide more detailed coverage of the western United States. We compare this updated proxy network to output of precipitation and effective moisture anomalies for the LGM (21 ka) simulations associated with PMIP3, as well as with an ensemble average. We find five models that have relatively high κ_w for precipitation, all at low (5–10%) precipitation change thresholds. Only one model, MPI-ESM-P, has a higher κ_w than the model ensemble. The ensemble κ_w is highest at a larger (20%) change threshold, meaning it designates a larger part of the study area as experiencing no significant precipitation change relative to modern. Similar to our previous work, we find that proxy-model agreement is closely tied to the location and orientation of the boundary between wetter and drier conditions in the western United States. Lastly, although these models do not include pluvial lakes in their boundary conditions, EM anomalies indicate that at least two of the models that best agree with the proxy network likely do include Great Salt Lake. These two models show weak positive P anomalies downwind of the modern lake area, and are in general good agreement with Bonneville basin proxy records. This observation provides further evidence that modeling of vapor recycling and proxy-model agreement in the western United States could be improved with the inclusion of pluvial lakes in model boundary conditions for the LGM.

ACKNOWLEDGMENTS

This work was funded by National Science Foundation grant AGS-1554998 to JLO. Data associated with the proxy network compilation are available from JLO by request. We gratefully acknowledge the international climate modeling groups participating in CMIP5/PMIP3 for making their model output available for analysis. We also acknowledge Neil Kelley and Cameron de Wet for discussion and suggestions.

REFERENCES

Benson, L.V., Lund, S.P., Smoot, J.P., Rhode, D.E., Spencer, R.J., Verosub, K.L., Louderback, L.A., Johnson, C.A., Rye, R.O., and Negrini, R.M., 2011, The rise and fall of Lake Bonneville between 45 and 10.5 ka: Quaternary International, v. 235, p. 57–59.

Bhattacharya, T., Tierney, J.E., Addison, J.A., and Murray, J.W., 2018, Ice-sheet modulation of deglacial North American monsoon intensification: Nature Geoscience, v. 11, p. 848–852, doi:10.1038/s41561-018-0220-7.

Braconnot, P., Harrison, S.P., Kageyama, M., Bartlein, P.J., Masson-Delmotte, V., Abe-Ouchi, A., Otto-Bliesner, B., and Zhao, Y., 2012, Evaluation of climate models using palaeoclimatic data: Nature Climate Change, v. 2, p. 417–424, doi:10.1038/nclimate1456.

Cohen, J., 1968, Weighted kappa—nominal scale agreement with provision for scaled disagreement or partial credit: Psychological Bulletin, v. 70, p. 213–220.

COHMAP Members, 1988, Climatic changes of the last 18,000 years—observations and model simulations: Science, v. 241, p. 1043–1052.

Davis, O.K., 2002, Late Neogene environmental history of the northern Bonneville basin—a review of palynological studies, *in* Hershler, R., Curry, D., and Madsen, D., editors, Great Basin aquatic system history: Smithsonian Contributions to the Earth Sciences, v. 33, p. 295–307.

DiNezio, P.N., and Tierney, J.E., 2013, The effect of sea level on glacial Indo-Pacific climate: Nature Geoscience, v. 6, p. 485–491.

Ehlers, J., Gibbard, P.L., and Hughes, P.D., 2011, Quaternary glaciations—Extent and chronology, A Closer Look: Amsterdam, Elsevier, 1108 p.

Galewsky, J., 2013, High-resolution paleoclimate simulations of Lake Bonneville and its influence on geomorphic processes in the Uinta Mountains during the Last Glacial Maximum [abs.]: American Geophysical Union Fall Meeting, San Francisco December 9-13, abstract EP51C-04, http://abstractsearch.agu.org/meetings/2013/FM/EP51C-04.html.

Harbert, R.S., and Nixon, K.C., 2018, Quantitative late Quaternary climate reconstruction from plant macrofossil communities in Western North America: Open Quaternary, v. 4, p. 8, doi:10.5334/oq.46.

Hermann, N.W., Oster, J.L., and Ibarra, D.E., 2018, Spatial patterns and driving mechanisms of mid-Holocene hydroclimate in western North America: Journal of Quaternary Science, v. 33, p. 421–434, doi:10.1002/jqs.3023.

Hostetler, S.W., Giorgi, F., Bates, G.T., and Bartlein, P.J., 1994, Lake-atmosphere feedbacks associated with paleolakes Bonneville and Lahontan: Science, v. 263, p. 665–668.

Ibarra, D.E., Egger, A.E., Weaver, K.L., Harris, C.R., and Maher, K., 2014, Rise and fall of late Pleistocene pluvial lakes in response to reduced evaporation and precipitation—Evidence from Lake Surprise, California: Geological Society of America Bulletin, v. 126, p. 1387–1415, doi:10.1130/B31014.1.

Ibarra, D.E., Oster, J.L., Winnick, M.J., Caves Rugenstein, J.K., Byrne, M.P., and Chamberlain, C.P., 2019, Lake area constraints on past hydroclimate in the western United States—Application to Pleistocene Lake Bonneville, *in* Lund, W.R., McKean, A.P., and Bowman, S.D., editors, Proceedings volume 2018 Lake Bonneville geologic conference and short course: Utah Geological Survey Miscellaneous Publication 170.

Kageyama, M., Albani, S., Braconnot, P., Harrison, S.P., Hopcroft, P.O., Ivanovic, R.F., Lambert, F., Marti, O., Peltier, W.R., Peterschmitt, J.-Y., Roche, D.M., Tarasov, L., Zhang, X., Brady, E.C., Haywood, A.M., LeGrande, A.N., Lunt, D.J., Mahowald, N.M., Mikolajewicz, U., Nisancioglu, K.H., Otto-Bliesner, B.L., Renssen, H., Tomas, R.A., Zhang, Q., Abe-Ouchi, A., Bartlein, P.J., Cao, J., L., Q., Lohmann, G., Ohgaito, R., Shi, X., Volodin, E., Yoshida, K., Zhang, X., Zheng, W., 2017, The PMIP4 contribution to CMIP6, Part 4—Scientific objectives and experimental design of the PMIP4-CMIP6 Last Glacial Maximum experiments and PMIP4 sensitivity experiments: Geoscientific Model Development, v. 10, p. 4035–4055, doi:10.5194/gmd-10-4035-2017.

Kaufman, D.S., 2003, Amino acid paleothermometry of Quaternary ostracodes form the Bonneville basin, Utah: Quaternary Science Reviews, v. 22, p. 899–914.

Laabs, B.J.C., Plummer, M.A., and Mickelson, D.M., 2006, Climate during the last glacial maximum in the Wasatch and southern Uinta Mountains inferred from glacier modeling: Geomorphology, v. 75, p. 300–317.

Lehner, B., and Grill, G., 2013, Global river hydrography and network routing: baseline data and new approaches to study the world's largest river systems: Hydrological Processes, v. 27, p. 2171–2186.

Lora, J.M., Mitchell, J.L., Risi, C., and Tripati, A.E., 2017, North Pacific atmospheric rivers and their influence on western North America at the Last Glacial Maximum: Geophysical Research Letters, v. 44, p. 1051–1059, doi: 10.1002/2016GL071541.

Lyle, M., Heusser, L., Ravelo, C., Yamamoto, M., Barron, J., Diffenbaugh, N.S., Herbert, T., and Andreasen, D., 2012, Out of the tropics—The Pacific, Great Basin lakes, and late Pleistocene water cycle in the western United States: Science, v. 337, p. 1629–1633.

Maher, K., Ibarra, D.E., Oster, J.L., Miller, D.M., Redwine, J.L., Reheis, M.C., and Harden, J.W., 2014, Uranium isotopes in soils as a proxy for past infiltration and precipitation across the western United States: American Journal of Science, v. 314, p. 821–857.

McGee, D., Quade, J., Edwards, R.L., Broecker, W.S., Cheng, H., Reiners, P.W., and Evenson, N., 2012, Lacustrine cave carbonates—Novel archives of paleo-hydrologic change in the Bonneville basin (Utah, USA): Earth and Planetary Science Letters, v. 351, p. 182–194, doi: 10.1016/j.epsl.2012.07.019.

Morrill, C., Lowry, D.P., and Hoell, A., 2018, Thermodynamic and dynamic causes of pluvial conditions during the Last Glacial Maximum in western North America: Geophysical Research Letters, v. 45, p. 335–345.

Munroe, J.S., and Laabs, B.J.C., 2013, Temporal correspondence between pluvial lake highstands in the southwestern US and Heinrich Event 1: Journal of Quaternary Science, v.28, p. 49–58, doi:10.1002/jqs2586.

Munroe, J.S., and Mickelson, D.M., 2002, Last Glacial Maximum equilibrium-line altitudes and paleoclimate, northern Uinta Mountains, Utah, U.S.A: Journal of Glaciology, v. 48, p. 257–266.

Natural Earth pluvial lakes database: http://www.naturalearthdata.com/downloads/10m-physical-vectors/10m-lakes/.

Nowak, C.L., Nowak, R.S., Tausch, R.J., and Wigand, P.E., 1994, Tree and shrub dynamics in northwestern Great Basin woodland and shrub steppe during the late Pleistocene and Holocene: American Journal of Botany, v. 81, p. 265–277, doi:10.1002/j.1537-2197.1994.tb15443.x.

Oster, J.L., Ibarra, D.E., Winnick, M.J., and Maher, K., 2015, Steering of westerly storms over western North America at the Last Glacial Maximum: Nature Geoscience, v. 8, p. 201–205, doi: 10.1038/ngeo2365.

Oviatt, C.G., Currey, D.R., and Sack, D., 1992, Radiocarbon chronology of Lake Bonneville, eastern Great Basin, USA: Palaeogeography, Palaeoclimatology, Palaeoecology, v. 99, p. 225–241.

Pound, M.J., Tindall, J., Pickering, S.J., Haywood, A.M., Dowsett, H.J., and Salzmann, U., 2014, Late Pliocene lakes and soils–A global dataset for the analysis of climate feedbacks in a warmer world: Climate of the Past, v. 10, p. 167–180, doi:10.5194/cp-10-167-2014.

Quirk, B.J., Moore, J.R., Laabs, B.J.C., Caffee, M.W., and Plummer, M.A., 2018, Termination II, Last Glacial Maximum, and late glacial chronologies and paleoclimate from Big Cottonwood Canyon, Wasatch Mountains, Utah: Geological Society of America Bulletin, v. 130, p. 1889–1902, doi: 10.1130/B31967.1.

Refsnider, K.A., Laabs, B.J.C., Plummer, M.A., Mickelson, D.M., Singer, B.S., and Caffee, M.W., 2008, Last glacial maximum climate inferences from cosmogenic dating and glacier modeling of the western Uinta ice field, Uinta Mountains, Utah: Quaternary Research, v. 69, p. 130–144.

Reheis, M.C., Adams, K.D., Oviatt, C.G., and Bacon, S.N., 2014, Pluvial lakes of the western United States—a view from the outcrop: Quaternary Science Reviews, v. 97, p. 33–37.

Scheff, J., Seager, R., Liu, H., and Coats, S., 2017, Are glacials dry? Consequences for paleoclimatology and for greenhouse warming: Journal of Climate, v. 30, p. 6593–6609.

Shuman, B.N., and Serravezza, M., 2017, Patterns of hydroclimatic change in the Rocky Mountains and surrounding regions since the last glacial maximum: Quaternary Science Reviews, v. 173, p. 58–77.

Soller, D.R., Reheis, M.C., Garrity, C.P., and Van Sistine, D.R., 2009, Map database for surficial materials in the conterminous United States: U.S. Geological Survey Data Series 425, scale 1: 5,000,000.

Taylor, K.E., Stouffer, R.J., and Meehl, G.A., 2012, An overview of CMIP5 and the experiment design: Bulletin of the American Meteorological Society, v. 93, p. 485–498.

This content is a PDF version of the author's PowerPoint presentation.

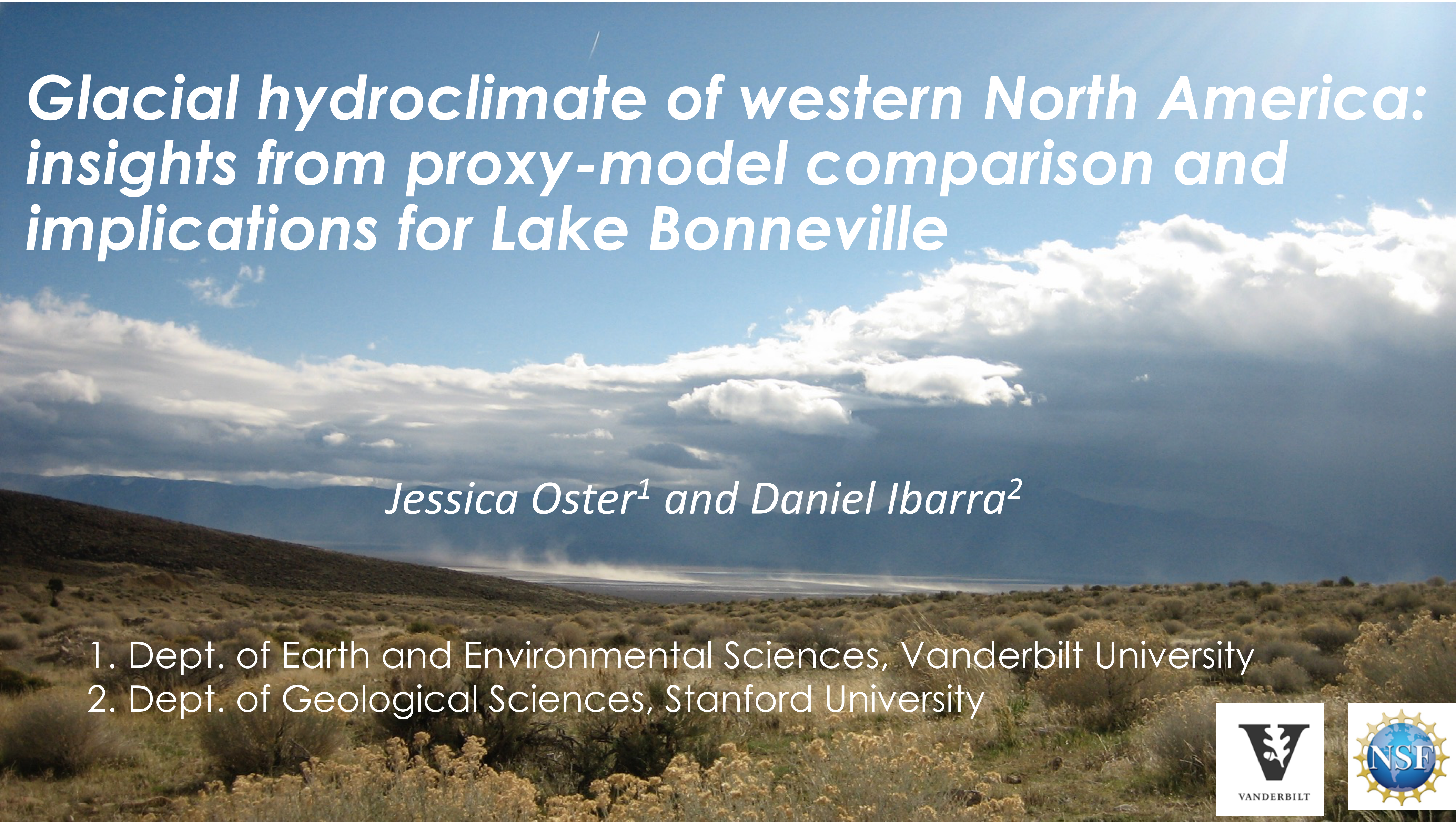

Glacial hydroclimate of western North America: insights from proxy-model comparison and implications for Lake Bonneville

Jessica Oster[1] and Daniel Ibarra[2]

1. Dept. of Earth and Environmental Sciences, Vanderbilt University
2. Dept. of Geological Sciences, Stanford University


Why Western North America?

Evidence of a Drier climate? Drowned trees in Sierra Nevada lakes

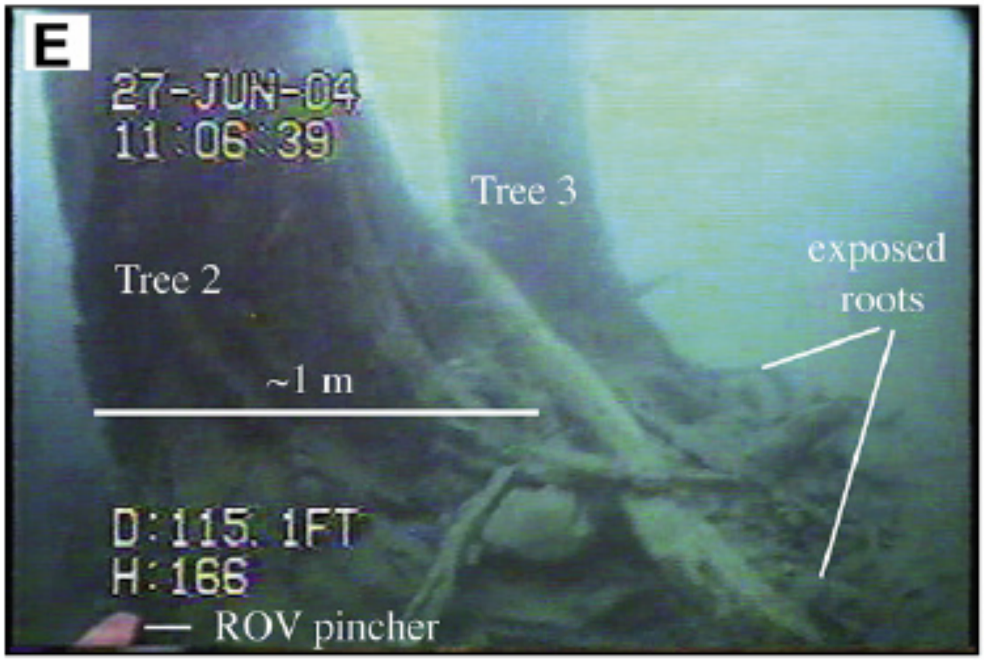

Kleppe et al., 2011

National Geographic

Evidence of a wetter climate? Fossil Shorelines of Glacial Lake Bonneville

Field sketch by G.K. Gilbert or accompanying artist - Shorelines along the Wasatch Range - USGS

HH Nichols and GK Gilbert (1884) – Bonneville Shorelines, Oquirrh Mountains, Utah
AR Orme (2008, *Geological Society, London, Special Publication*)

Why were past glacial periods wetter? And how wet were they?

COHMAP: Southward Displaced Jet Stream Hypothesis

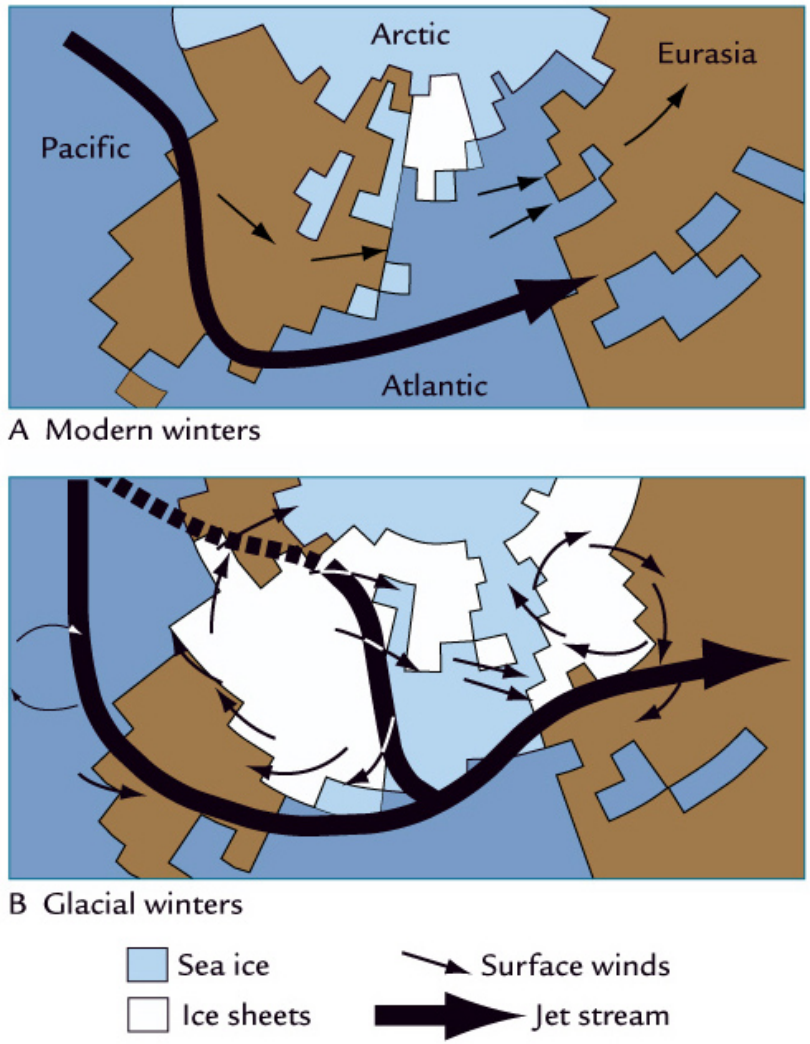

Out of the Tropics: The Pacific, Great Basin Lakes, and Late Pleistocene Water Cycle in the Western United States

Mitchell Lyle,[1*] Linda Heusser,[2] Christina Ravelo,[3] Masanobu Yamamoto,[4] John Barron,[5]
Noah S. Diffenbaugh,[6] Timothy Herbert,[7] Dyke And

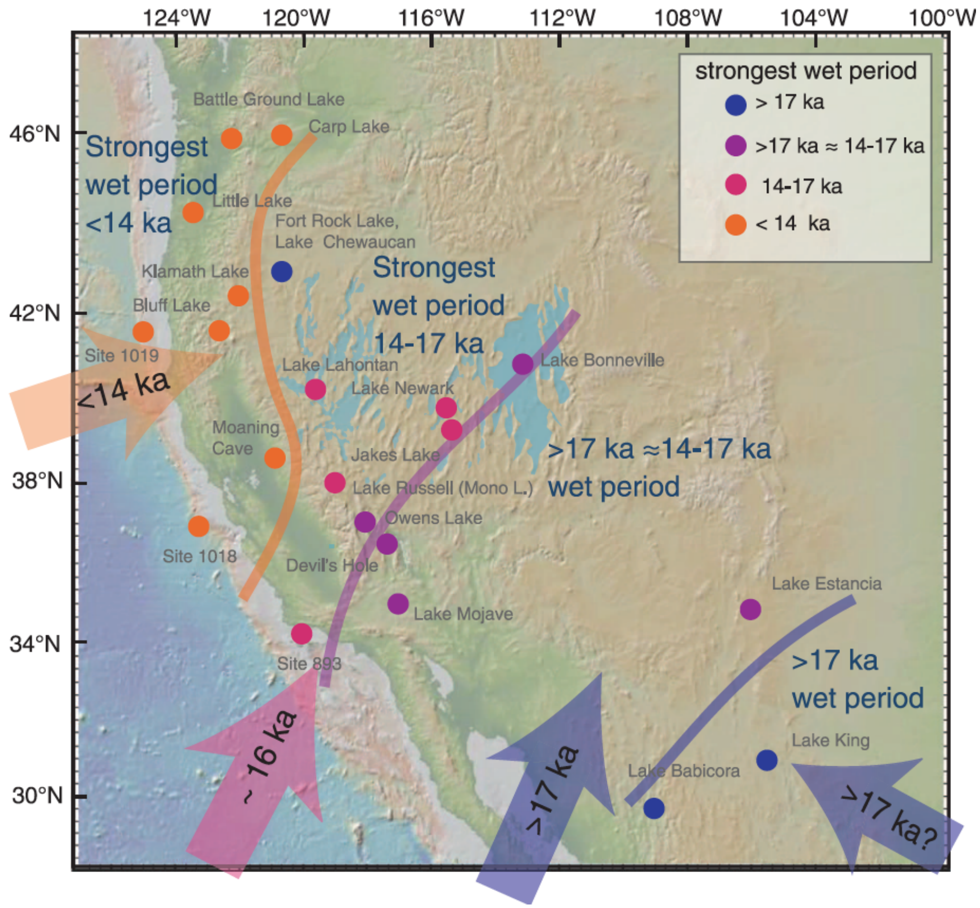

Networks of moisture-sensitive climate archives

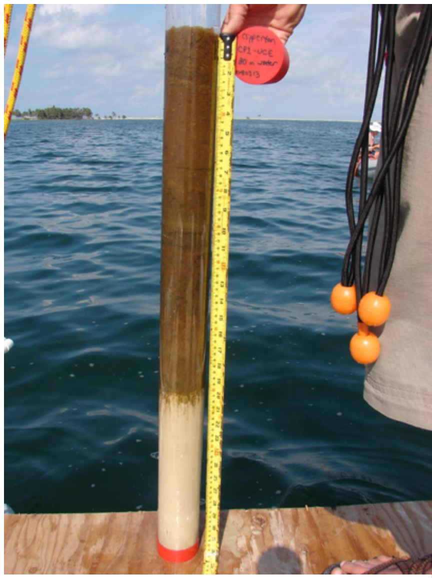

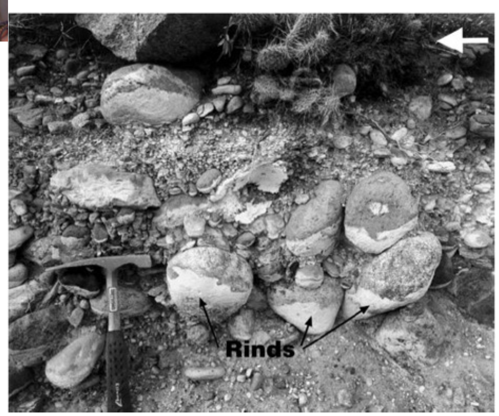

The Last Glacial Maximum

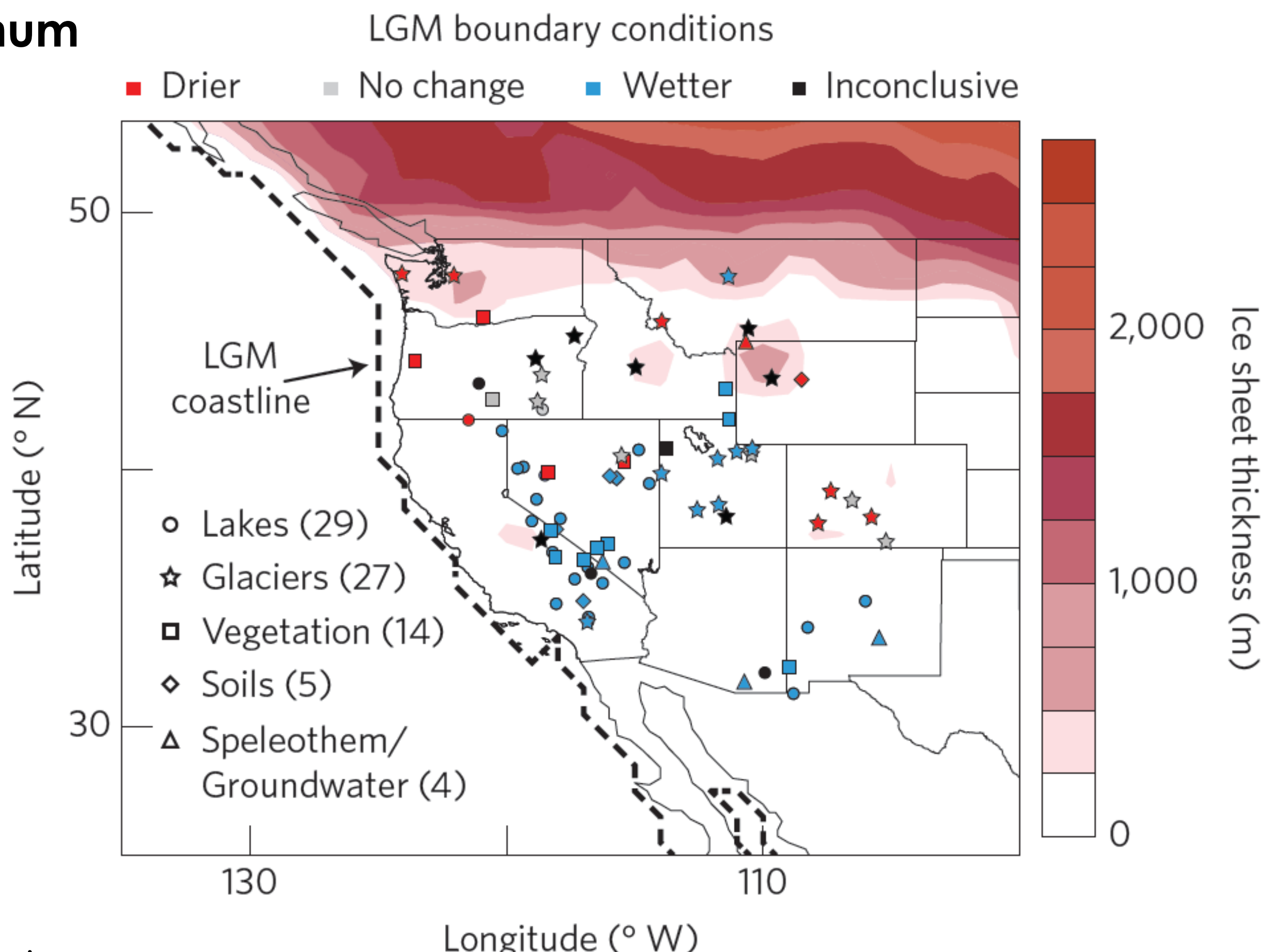

Precipitation dipole pattern separated by a NW-SE trending transition zone.

Oster et al., 2015, *Nature Geoscience*

Paleoclimate Model Intercomparison Project (PMIP)

Insolation

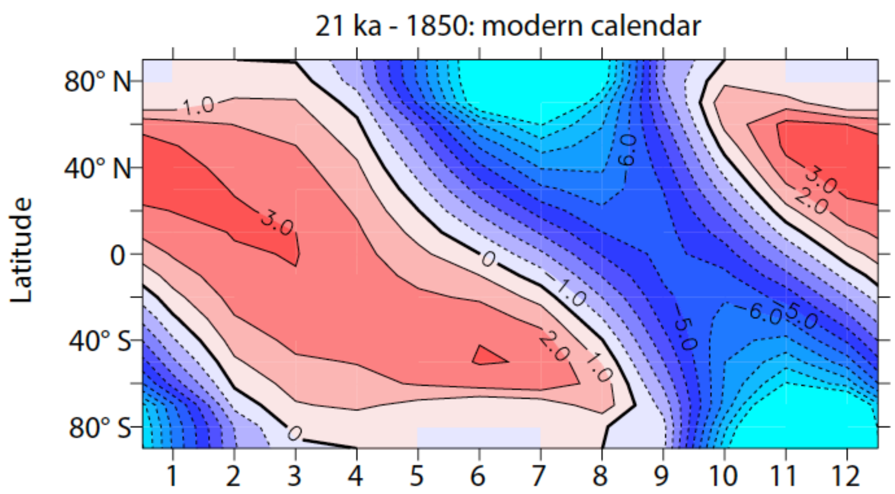

Kageyama et al., 2017

Ice Sheets, land surface

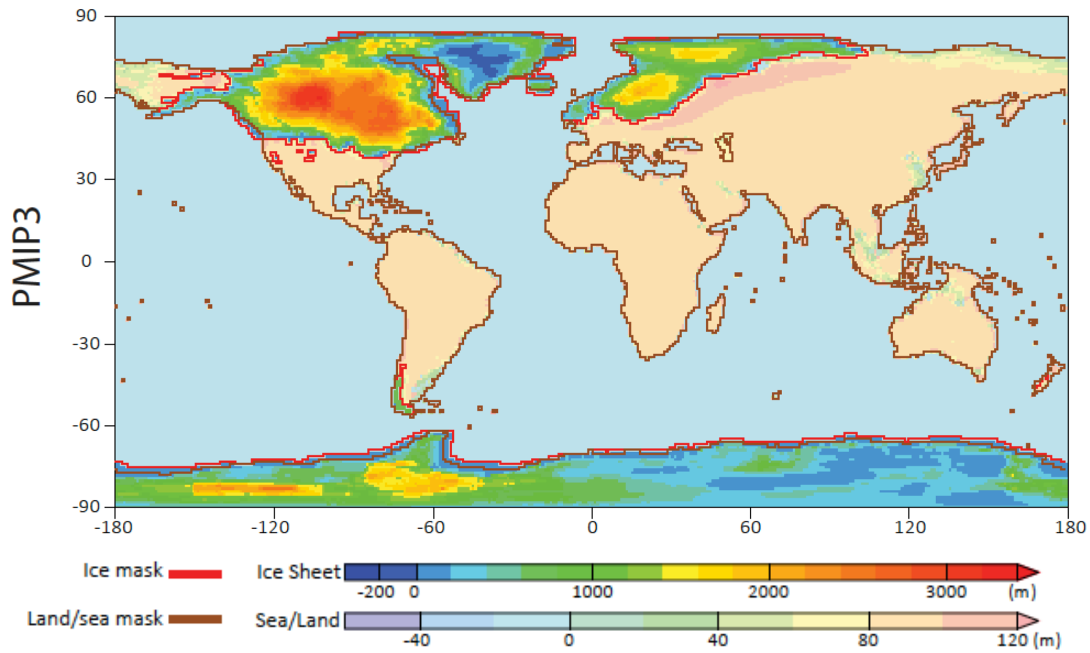

LGM Boundary Conditions

The Last Glacial Maximum

MIRO C-ESM

κ_{max} = 0.405* (ΔP = 5%)

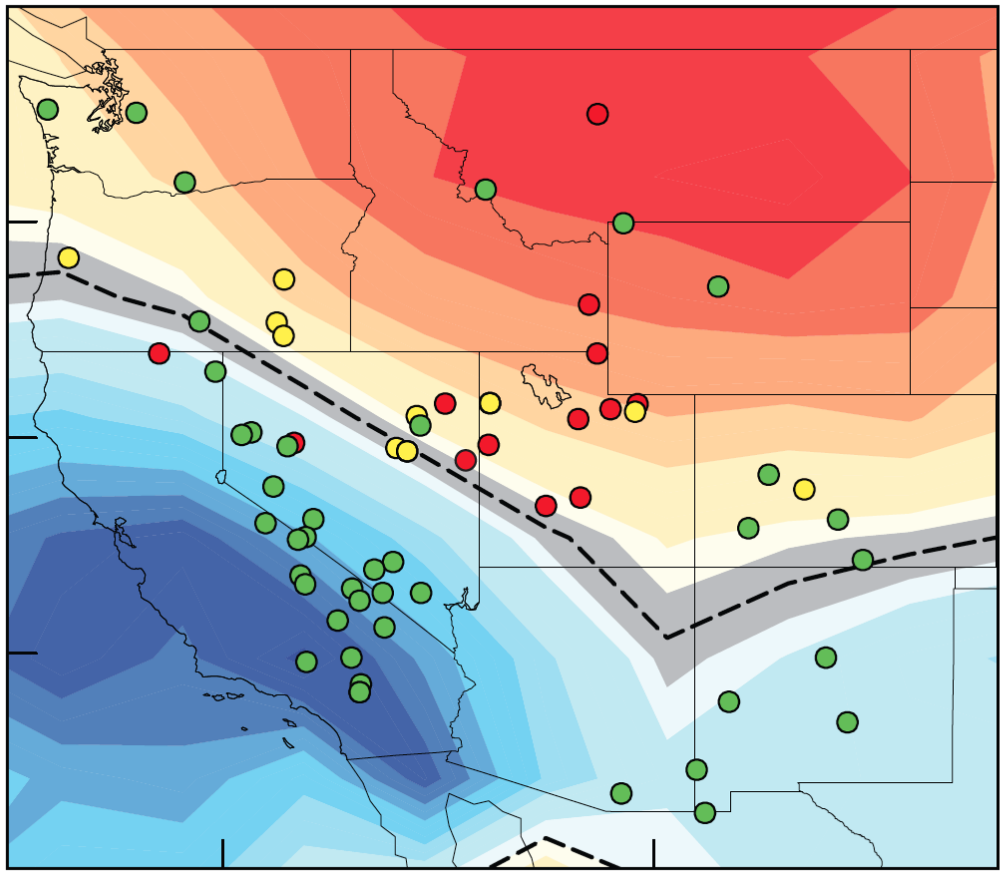

Model/proxy agree

Model/proxy weakly disagree

Model/proxy strongly disagree

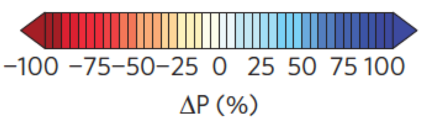

Agreement calculated using the Cohen's kappa statistic

% change in annual precip relative to pre-industrial conditions

Oster et al., 2015, *Nature Geoscience*

The Last Glacial Maximum

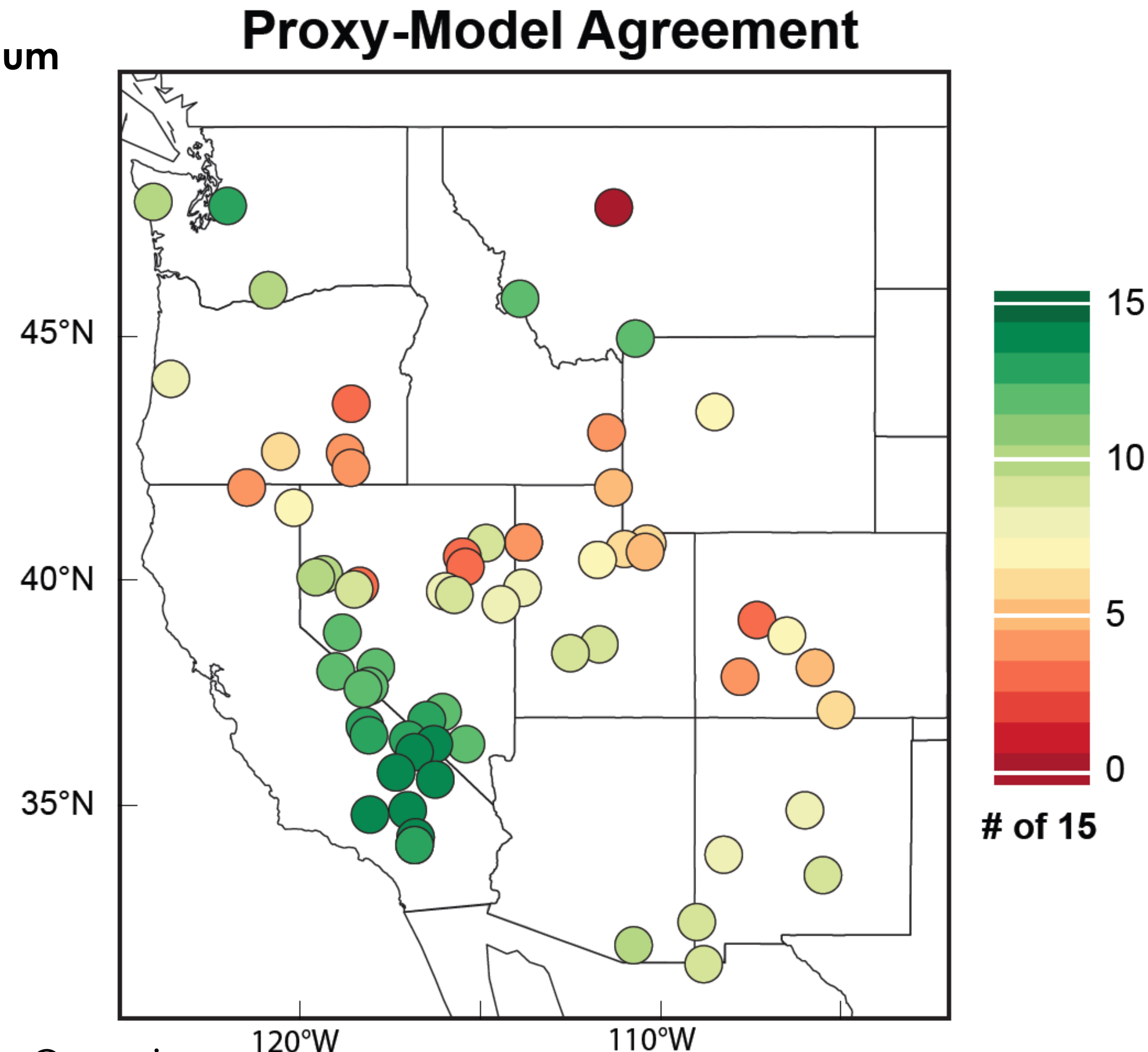

Oster et al., 2015, *Nature Geoscience*

The Last Glacial Maximum

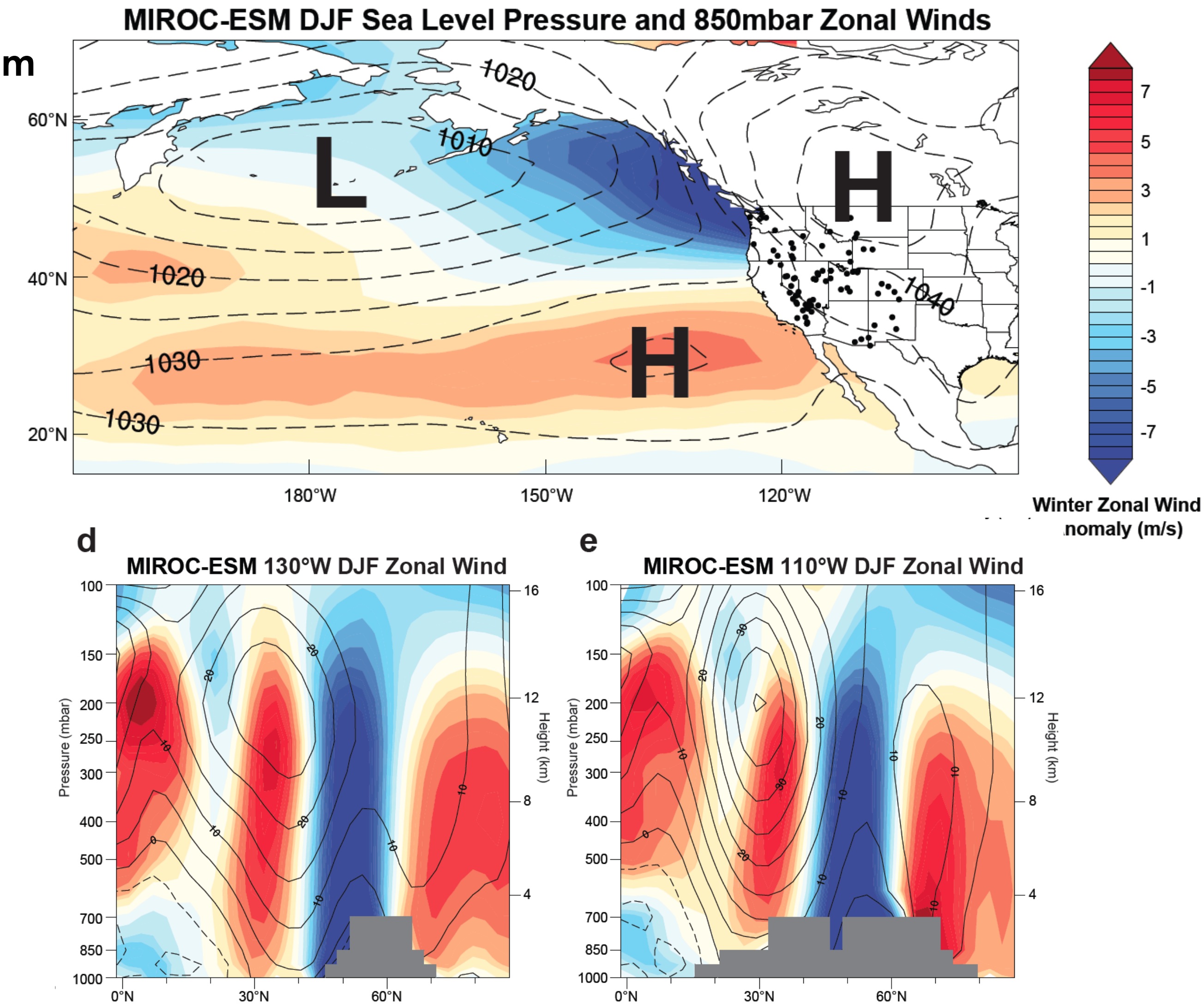

Oster et al., 2015, *Nature Geoscience*

Lora et al., 2017 - Annual Mean Precipitation anomaly (LGM-PI) for the PMIP3 ensemble compared to gridded pollen synthesis of Bartlein et al., 2011

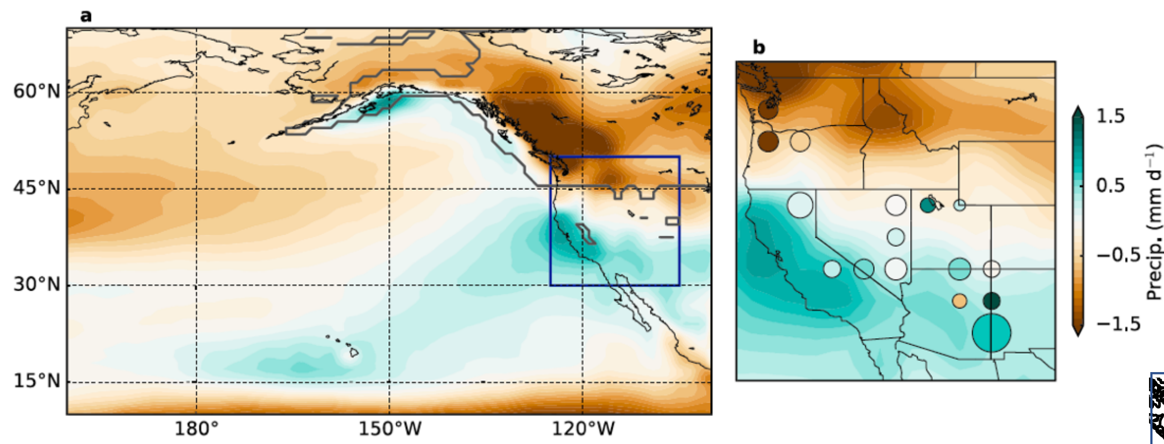

Data from Izumi and Bartlein (2016) - Inverse modeling of LGM mean annual precipitation anomalies using pollen records. Takes LGM CO_2 levels into account.

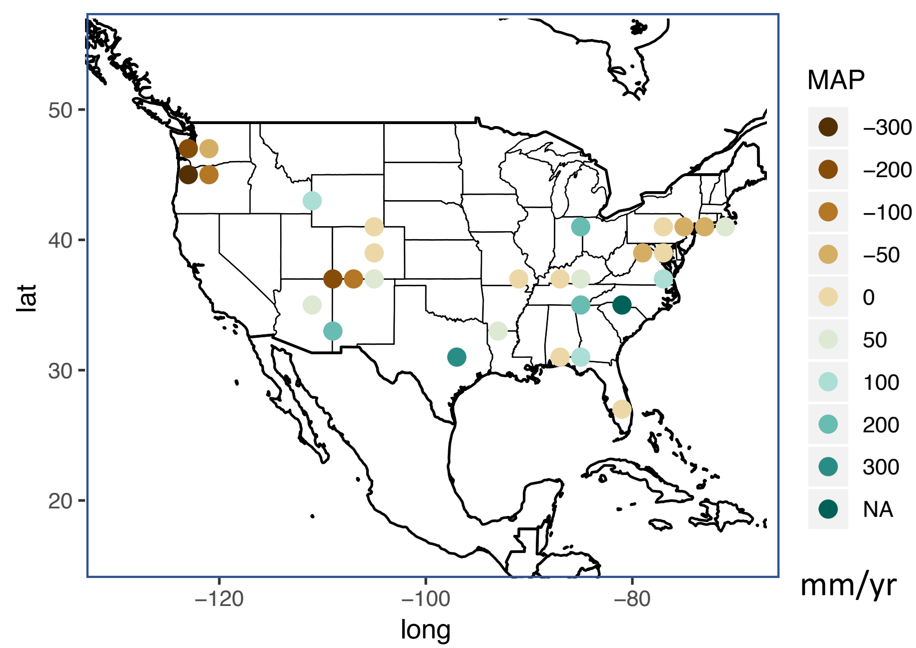

Expanding the LGM proxy network

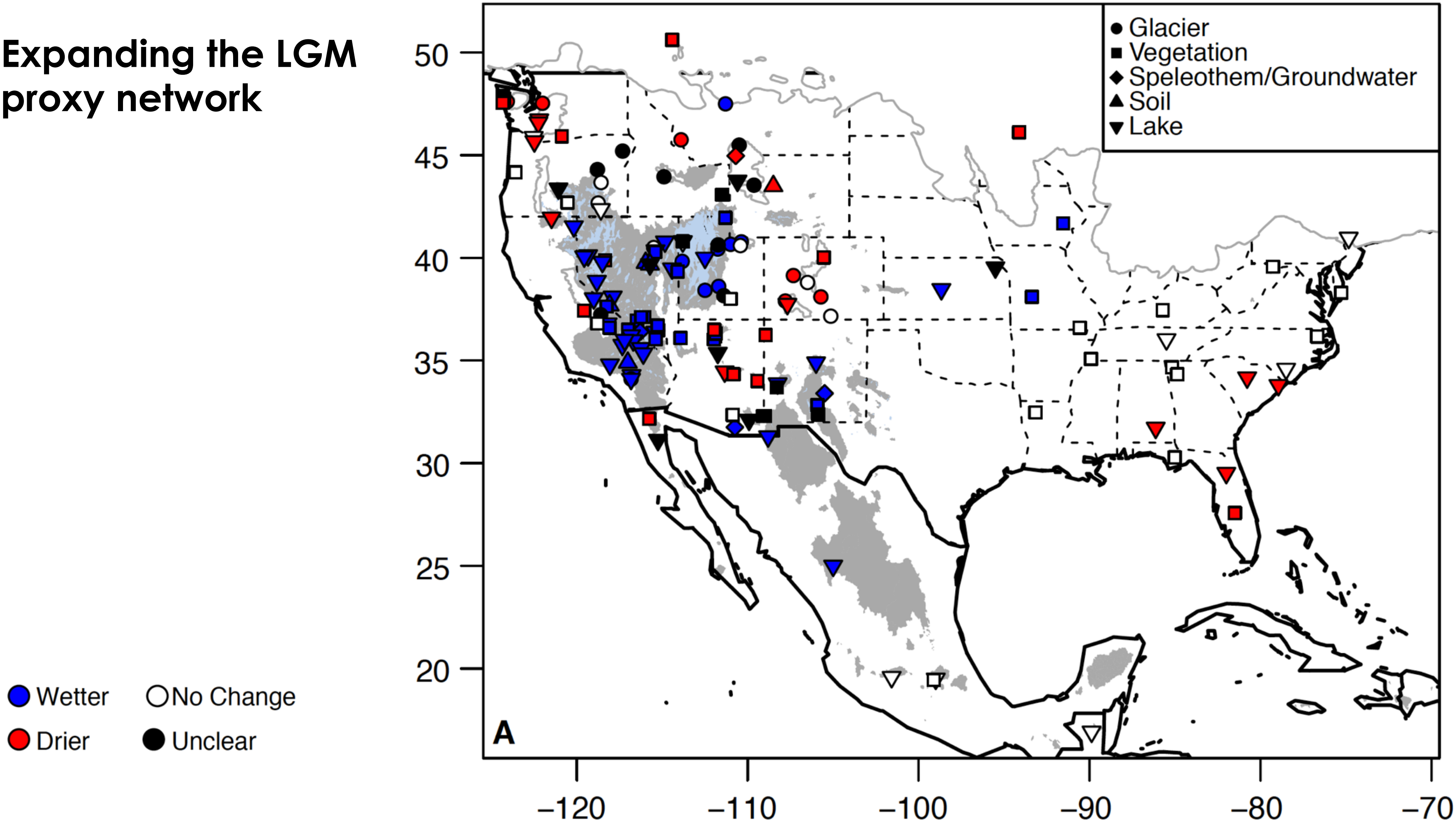

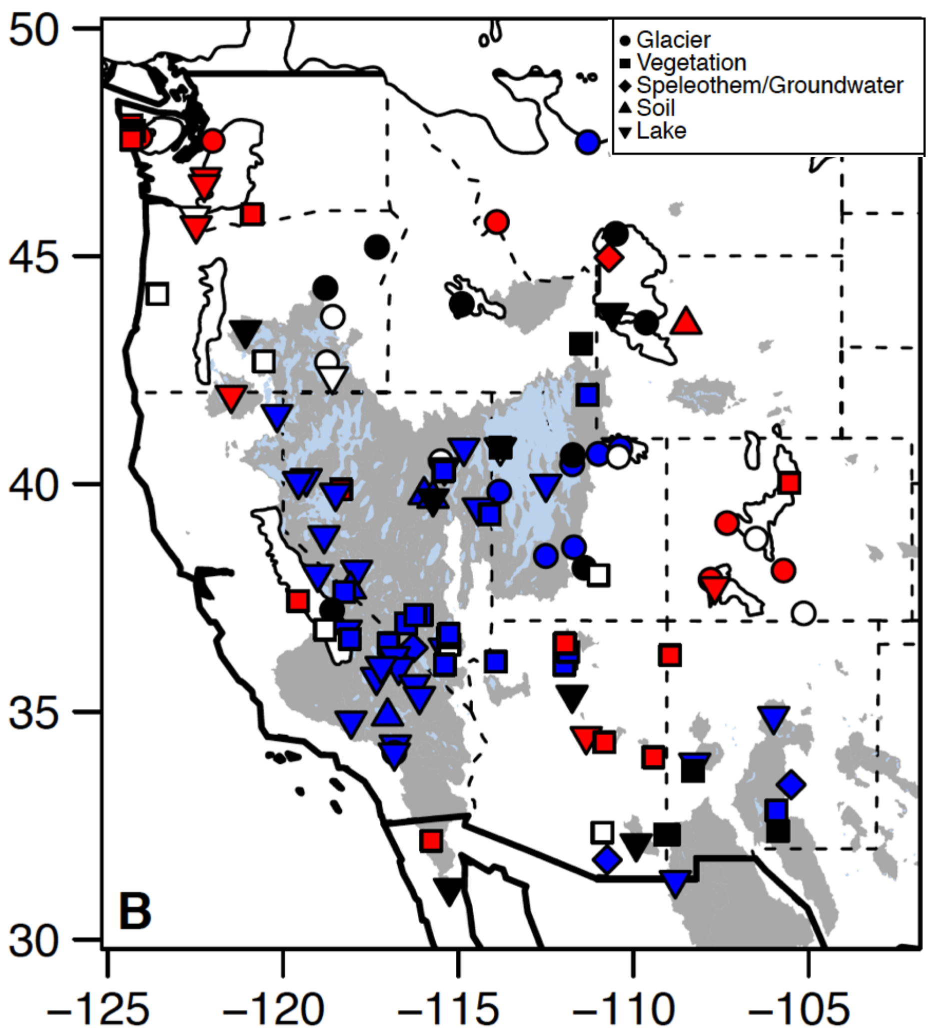

Glacier
Vegetation
Speleothem/Groundwater
Soil
Lake
B
50
45
40
35
30
−125
−120
−115
−110
−105

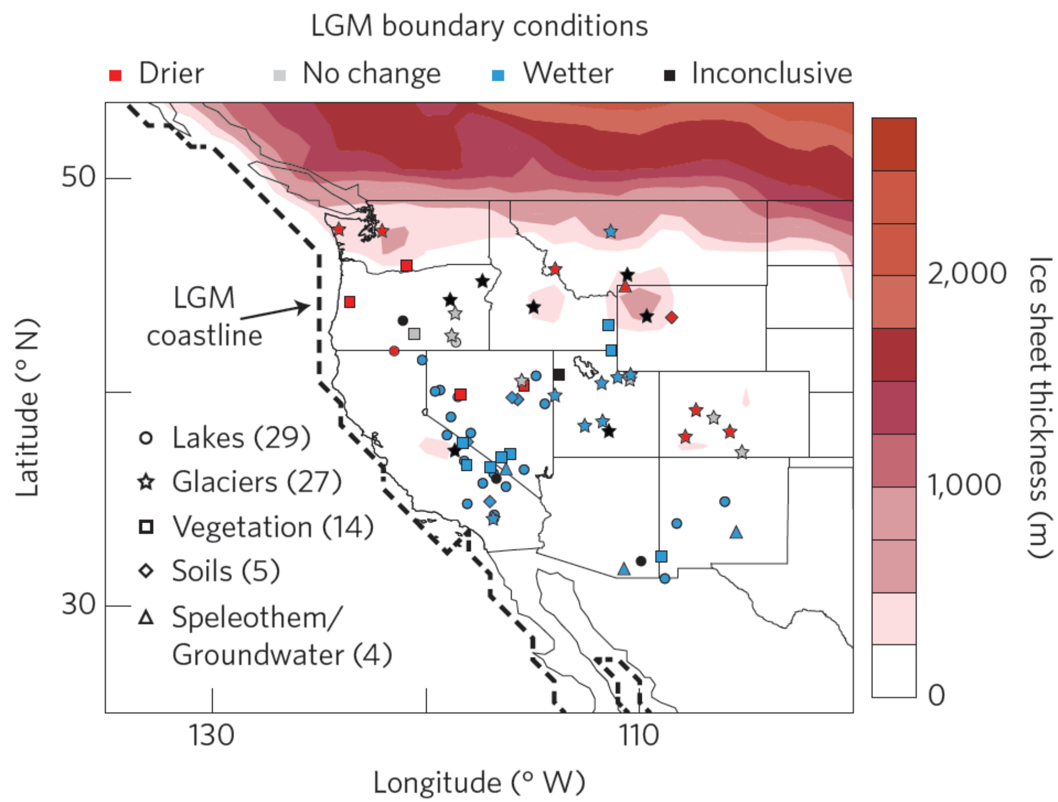

b
LGM boundary conditions
Drier
No change
Wetter
Inconclusive
LGM coastline
Lakes (29)
Glaciers (27)
Vegetation (14)
Soils (5)
Speleothem/ Groundwater (4)
Latitude (° N)
50
30
130
110
Longitude (° W)
Ice sheet thickness (m)
2,000
1,000
0

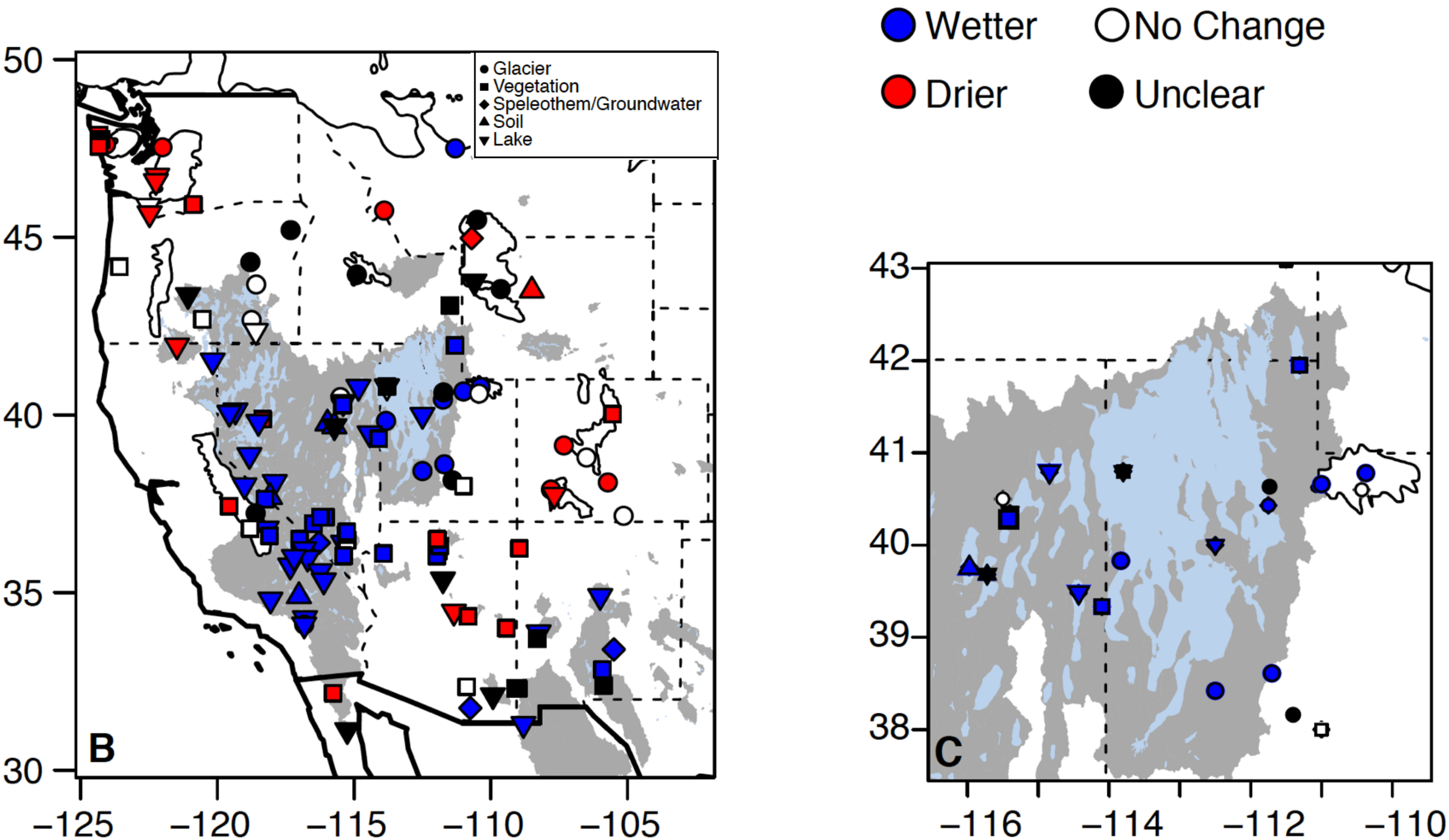

Glacier
Vegetation
Speleothem/Groundwater
Soil
Lake
Wetter
No Change
Drier
Unclear
50
45
40
35
30
−125
−120
−115
−110
−105
B
43
42
41
40
39
38
−116
−114
−112
−110
C

PMIP3 Ensemble

$\kappa_{max} = 0.44, \Delta P = 20\%$

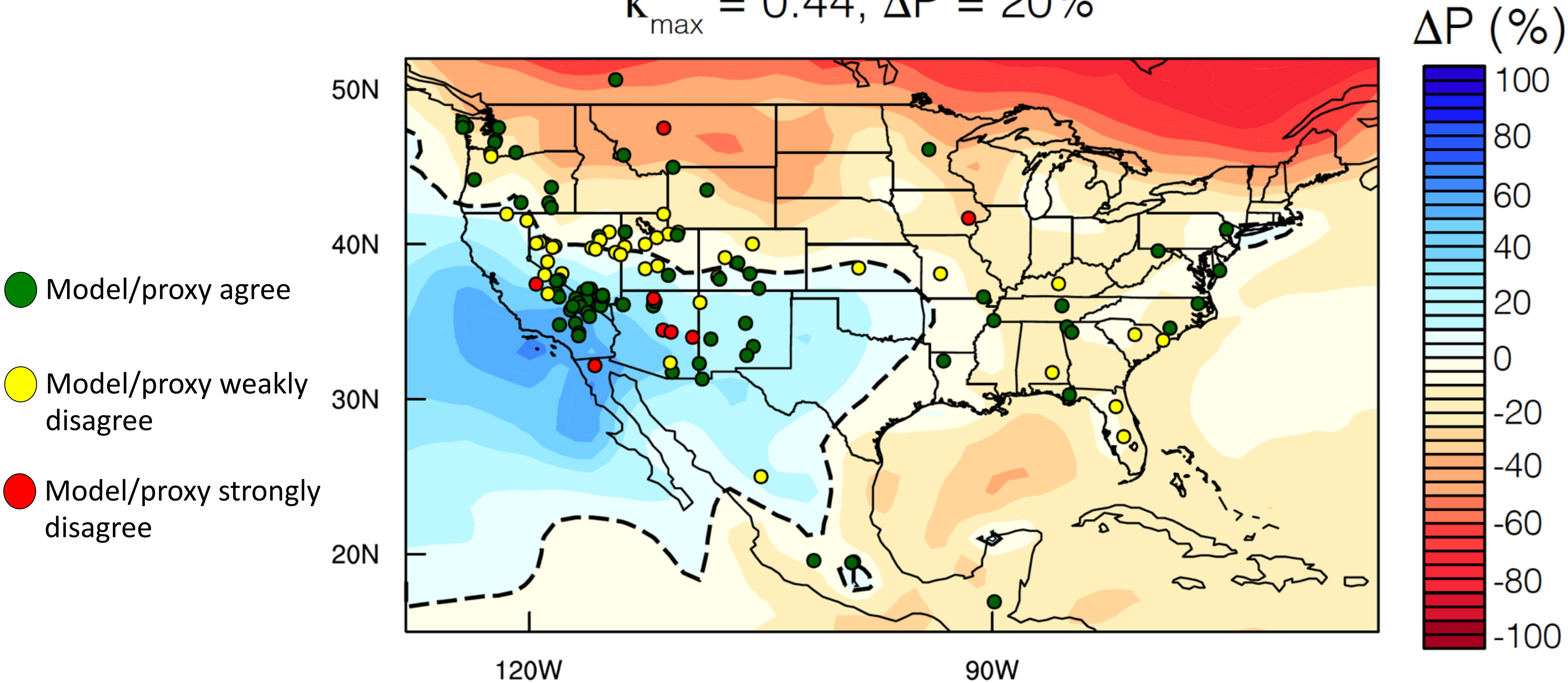

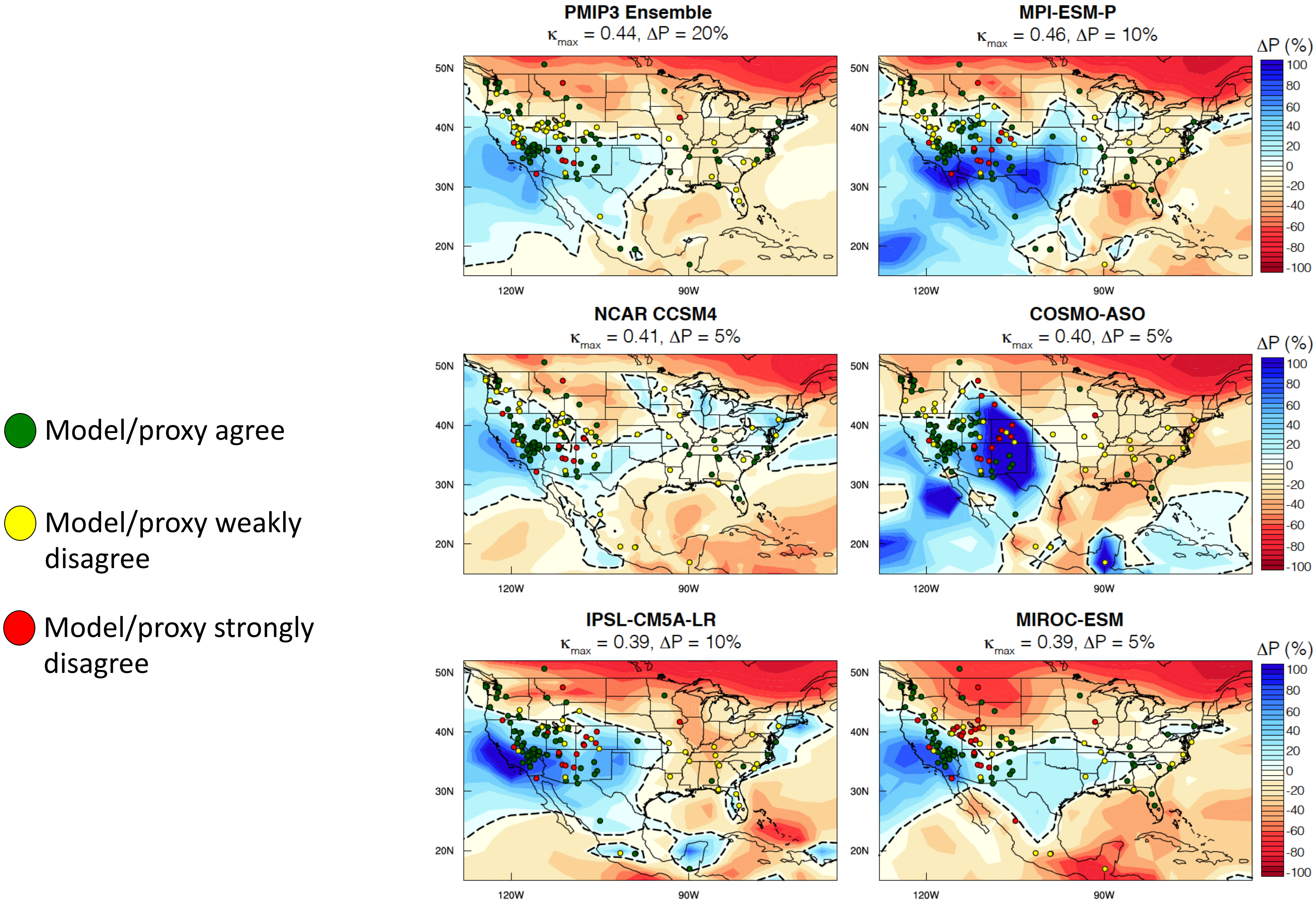

PMIP3 Ensemble
κmax = 0.44, ΔP = 20%
MPI-ESM-P
κmax = 0.46, ΔP = 10%
NCAR CCSM4
κmax = 0.41, ΔP = 5%
COSMO-ASO
κmax = 0.40, ΔP = 5%
IPSL-CM5A-LR
κmax = 0.39, ΔP = 10%
MIROC-ESM
κmax = 0.39, ΔP = 5%
ΔP (%)
100
80
60
40
20
0
-20
-40
-60
-80
-100
50N
40N
30N
20N
120W
90W
Model/proxy agree
Model/proxy weakly disagree
Model/proxy strongly disagree

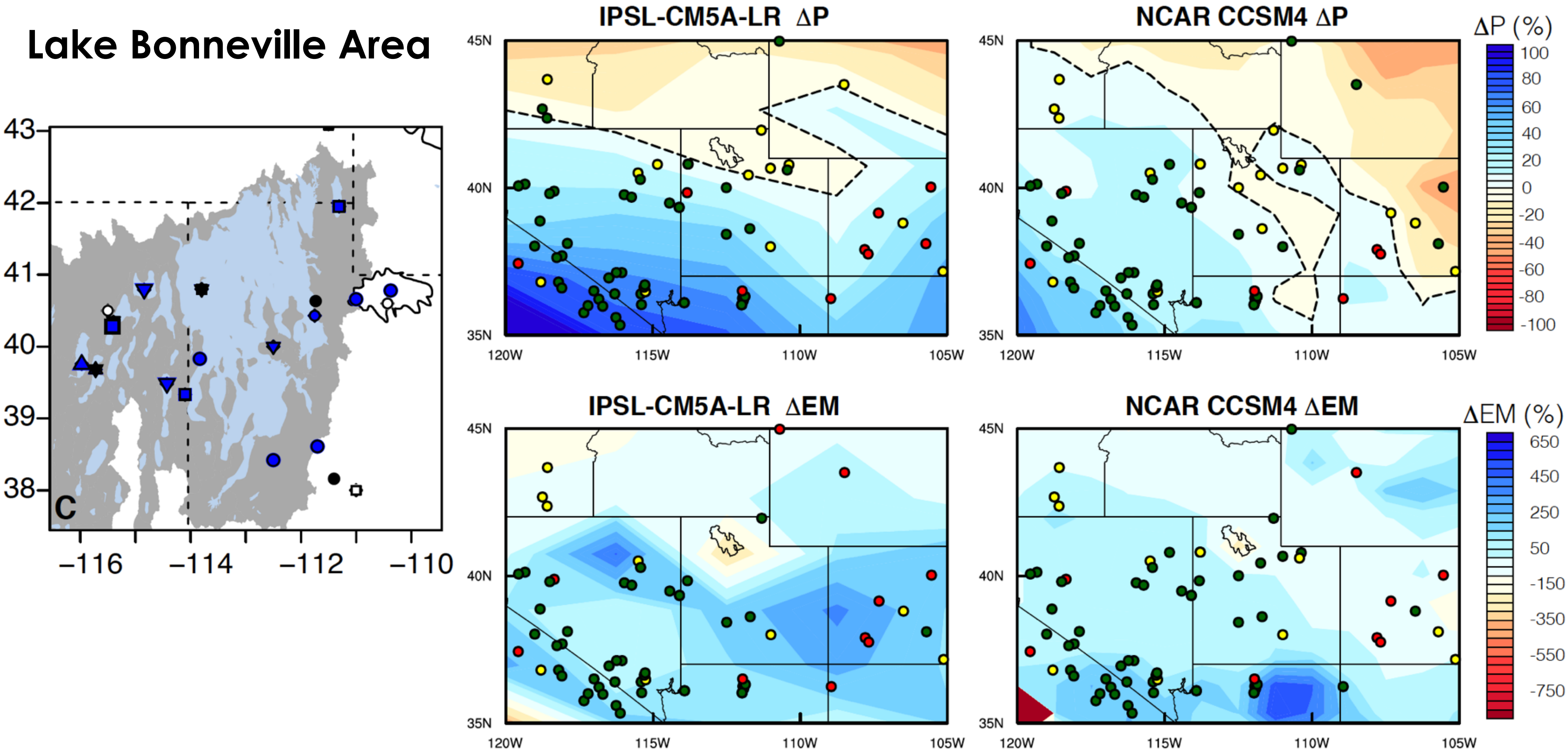

Lake Bonneville Area
43
42
41
40
39
38
C
–116
–114
–112
–110
IPSL-CM5A-LR ΔP
NCAR CCSM4 ΔP
ΔP (%)
100
80
60
40
20
0
-20
-40
-60
-80
-100
IPSL-CM5A-LR ΔEM
NCAR CCSM4 ΔEM
ΔEM (%)
650
450
250
50
-150
-350
-550
-750
45N
40N
35N
120W
115W
110W
105W

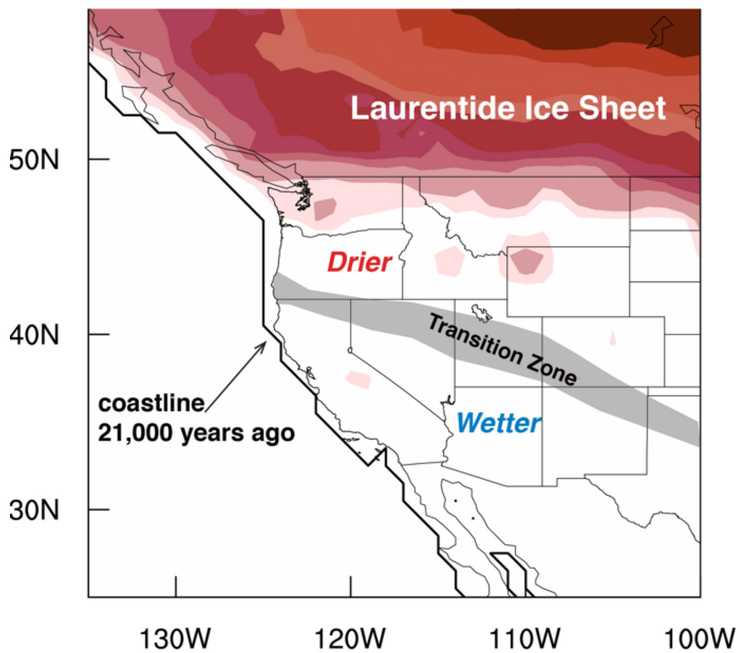

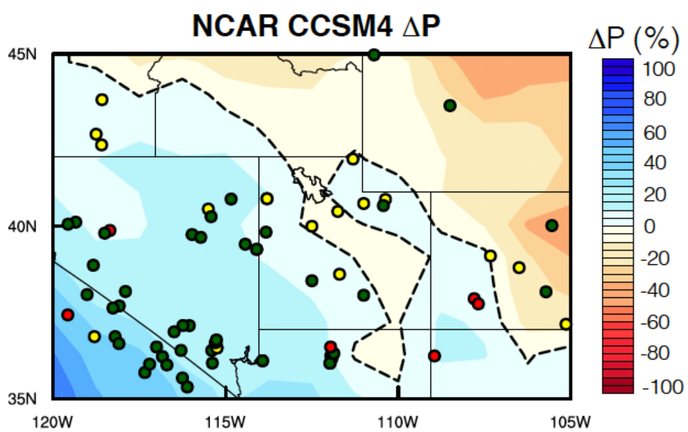

For Bonneville: Combination of small precipitation increases and reduced evaporation.

What is the downwind lake influence? Add pluvial lakes to LGM models.

Future Work: Look forward to the PMIP4 simulations
Isotope-enabled model time-slices from the LGM to the mid-Holocene to look at moisture source and transport.

Develop more and better proxy records. Gain better understanding of how they work. What are they most sensitive to? What is their seasonal bias?

The Last Glacial Maximum

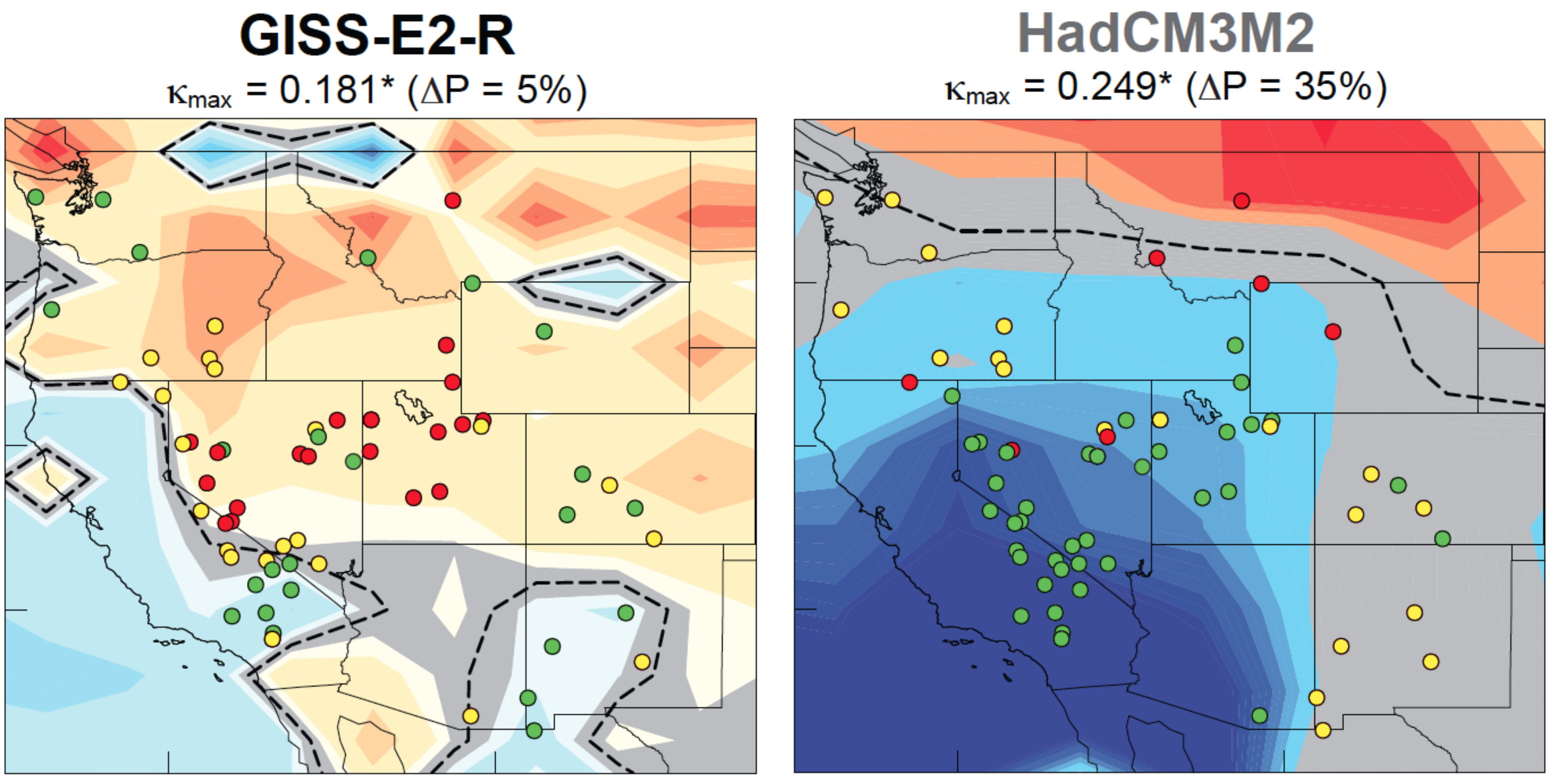

Too Dry *Too Wet*

Oster et al., 2015, *Nature Geoscience*

Wasatch Range climate during the Lateglacial and Last Glacial Maximum

Brendon J. Quirk, Jeffrey R. Moore, Benjamin J.C. Laabs, Mitchell Plummer, Marc Caffee

1. We have a better understanding of timing and extent of glaciers during the Last Glacial Maximum (LGM) and Lateglacial in the Wasatch.
2. We demonstrate the utility of combining glacier modeling and cosmogenic exposure dating to reconstruct ice position in areas lacking clear terminus features.
3. By combining our glacier-climate reconstructions and other paleoclimate records we have better constraints for Wasatch precipitation and temperature during the LGM and Lateglacial

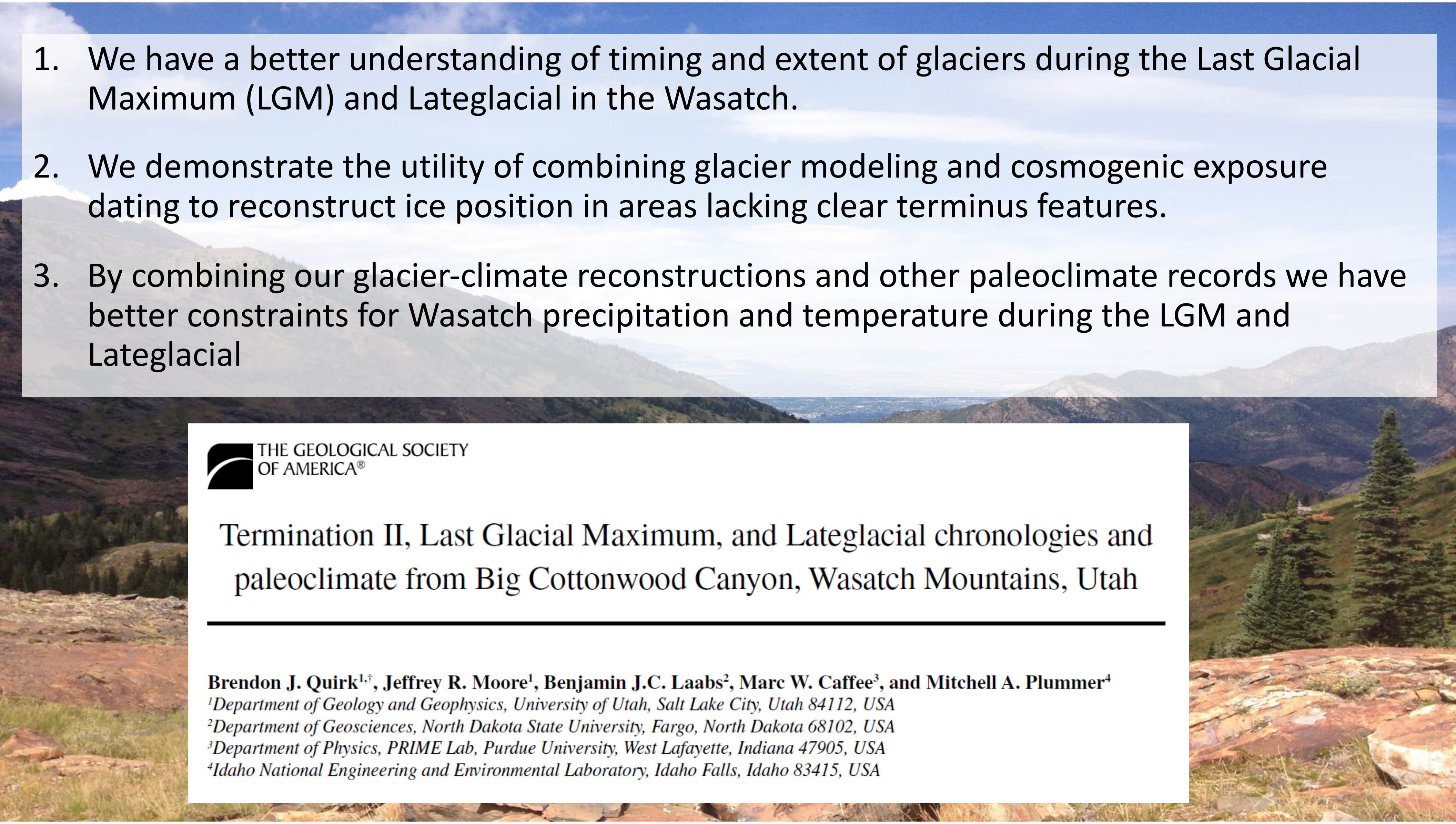

THE GEOLOGICAL SOCIETY OF AMERICA®

Termination II, Last Glacial Maximum, and Lateglacial chronologies and paleoclimate from Big Cottonwood Canyon, Wasatch Mountains, Utah

Brendon J. Quirk[1,†], Jeffrey R. Moore[1], Benjamin J.C. Laabs[2], Marc W. Caffee[3], and Mitchell A. Plummer[4]
[1]*Department of Geology and Geophysics, University of Utah, Salt Lake City, Utah 84112, USA*
[2]*Department of Geosciences, North Dakota State University, Fargo, North Dakota 68102, USA*
[3]*Department of Physics, PRIME Lab, Purdue University, West Lafayette, Indiana 47905, USA*
[4]*Idaho National Engineering and Environmental Laboratory, Idaho Falls, Idaho 83415, USA*

Overview

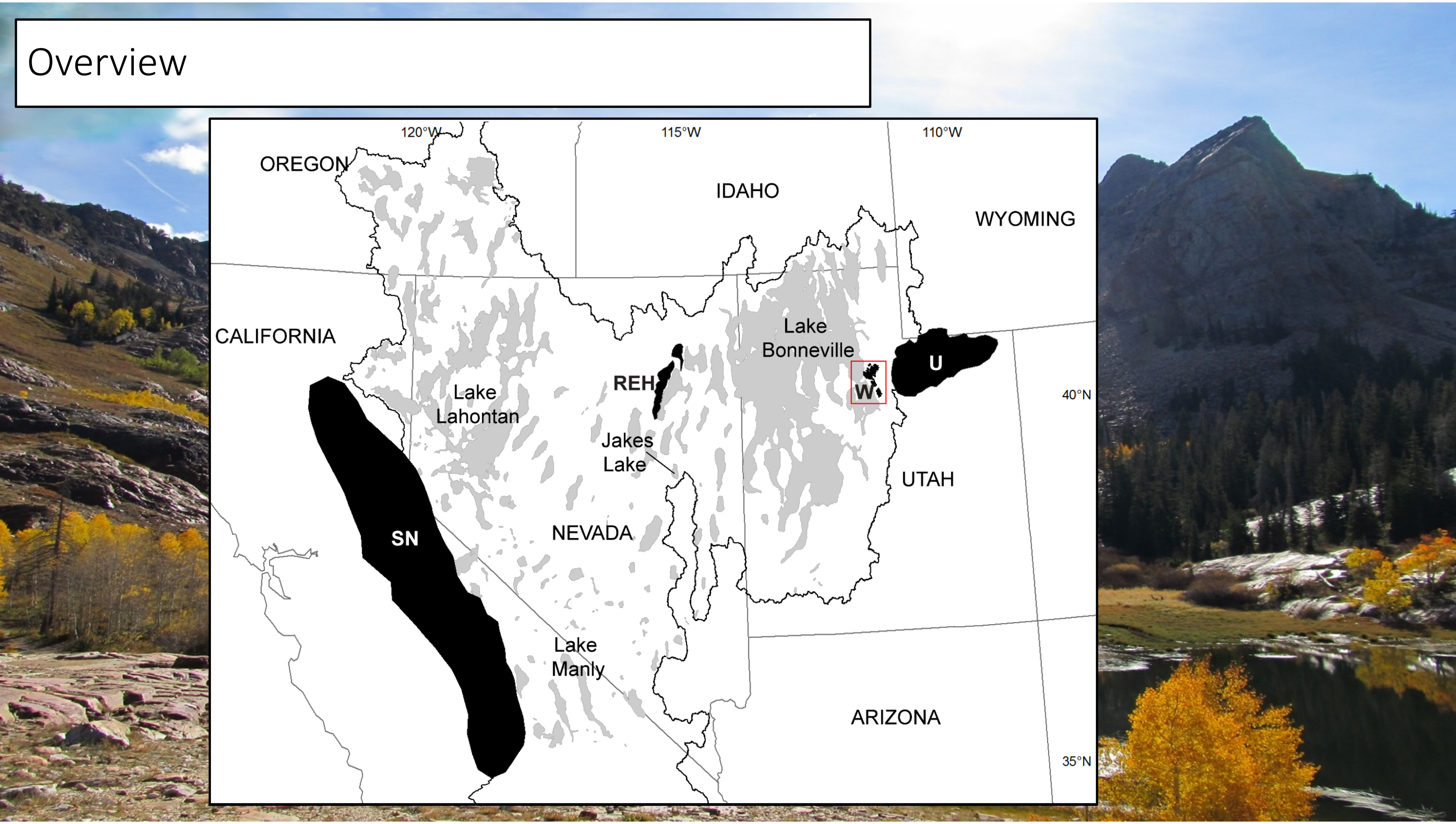
120°W
115°W
110°W
OREGON
IDAHO
WYOMING
CALIFORNIA
Lake
Bonneville
U
W
REH
Lake
Lahontan
40°N
Jakes
Lake
UTAH
SN
NEVADA
Lake
Manly
ARIZONA
35°N

Study Area & Previous Work

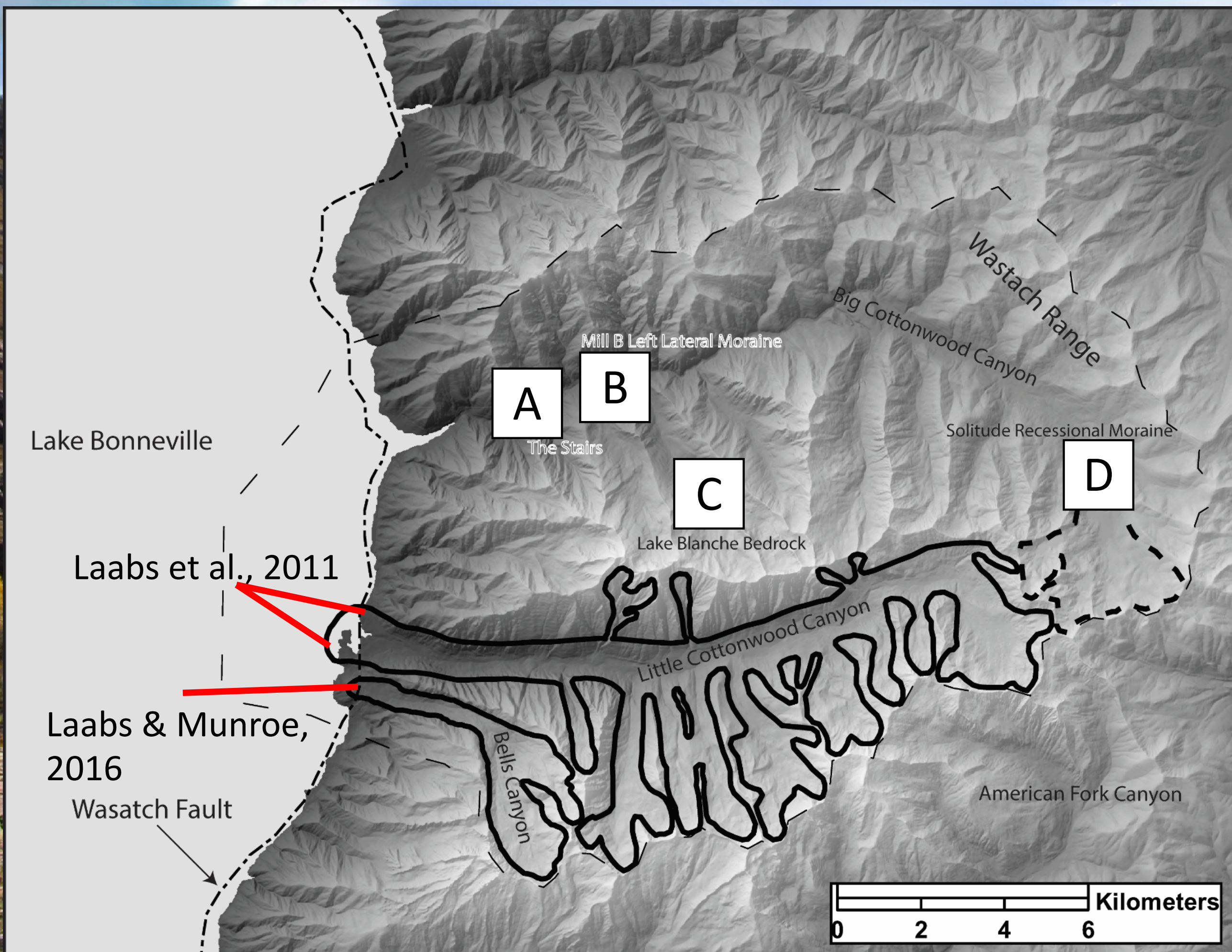

New Cosmogenic ^{10}Be Exposure Ages

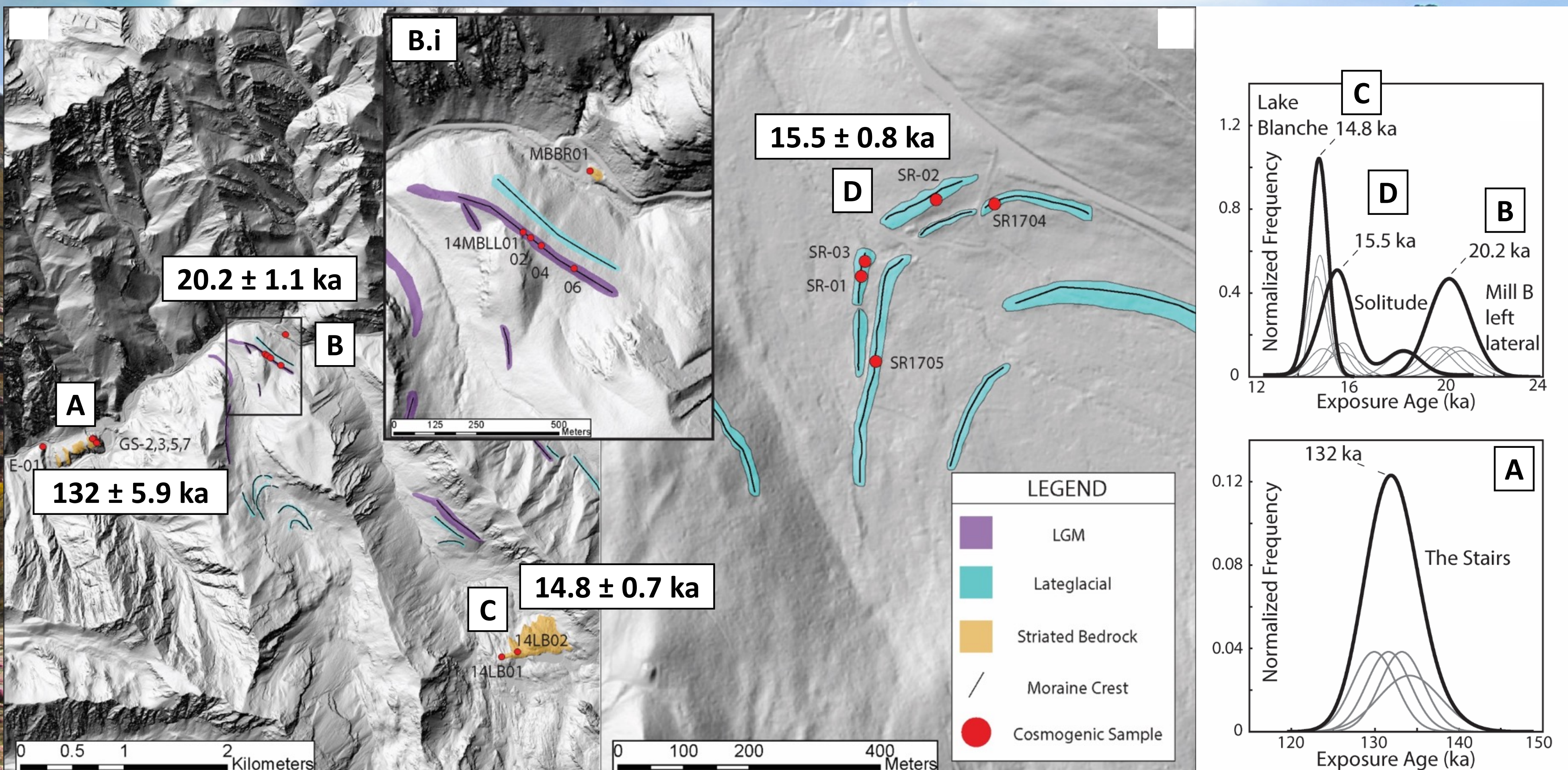

New Cosmogenic ^{10}Be Exposure Ages

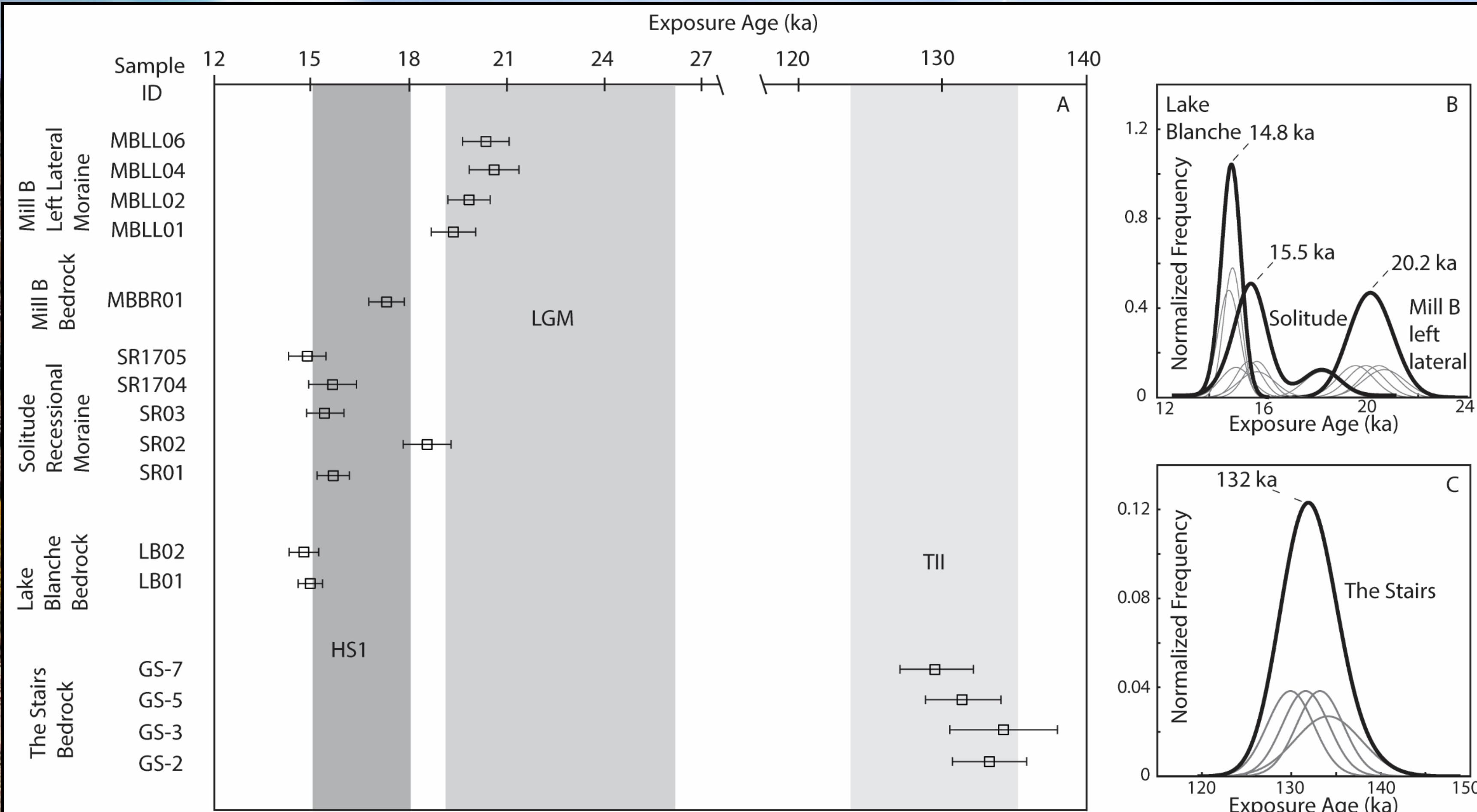

Exposure ages shown here were calculated using **version 3 of the CRONUS-Earth** online calculator (Balco et al., 2008), **Lifton-Sato-Dunai scaling** scheme (LSD; Lifton et al., 2014; Shakun et al., 2015), and **Promontory Point production rate** calibration data set (Lifton et al., 2015)

New Cosmogenic 10Be Exposure Ages

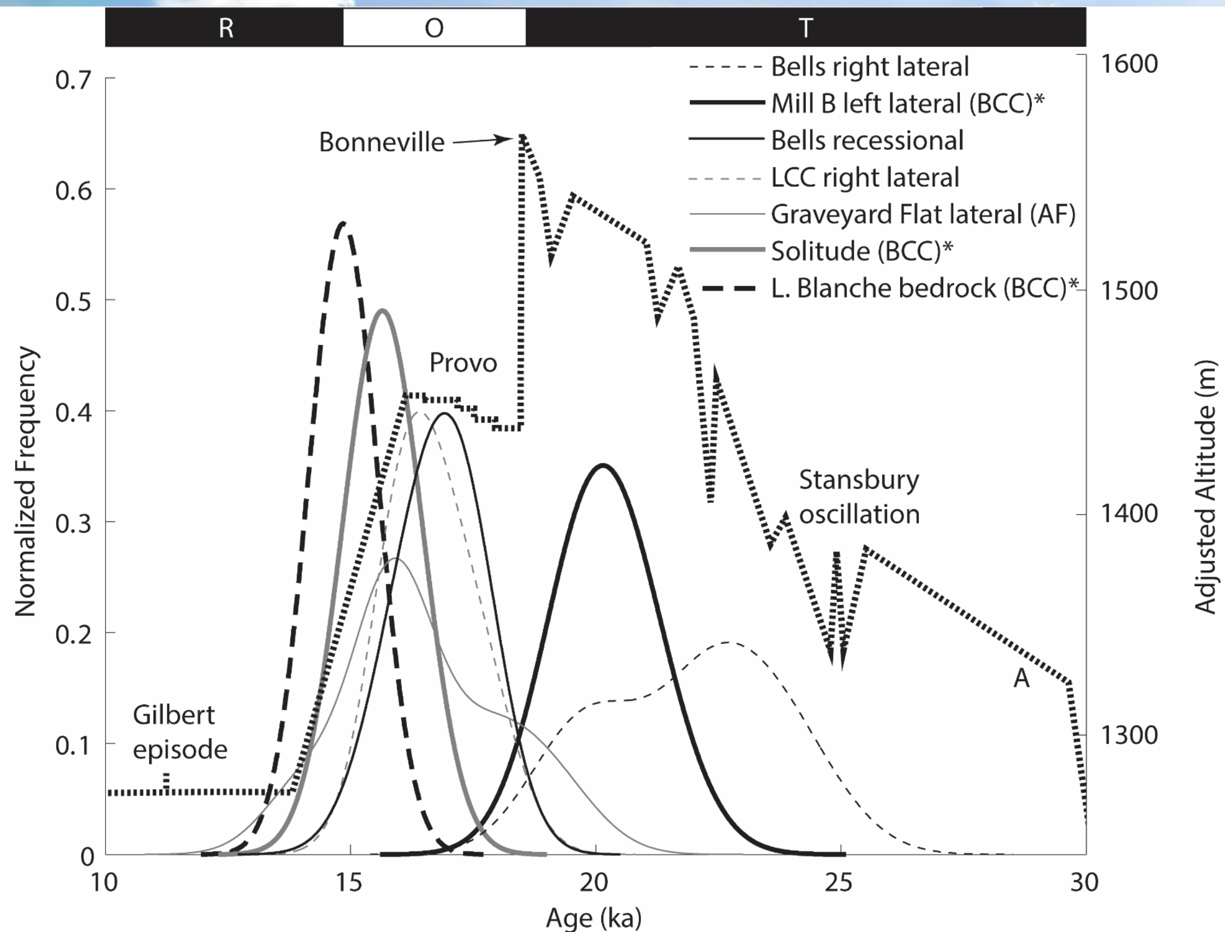

Modified from Oviatt, 2015

New and recalculated data suggest:

1. **Glacial maxima** during transgressive phase and **prior to Bonneville** high stand

2. Stadia during overflowing phase of lake

3. Rapid **deglaciation** following abandonment of **Provo** shoreline

Cosmogenic exposure ages for glacial landforms recalculated here (LSD/PP) from: Laabs & Munroe, 2016, and Laabs et al., 2011.

Plummer & Phillips (2003) Glacier Model Results

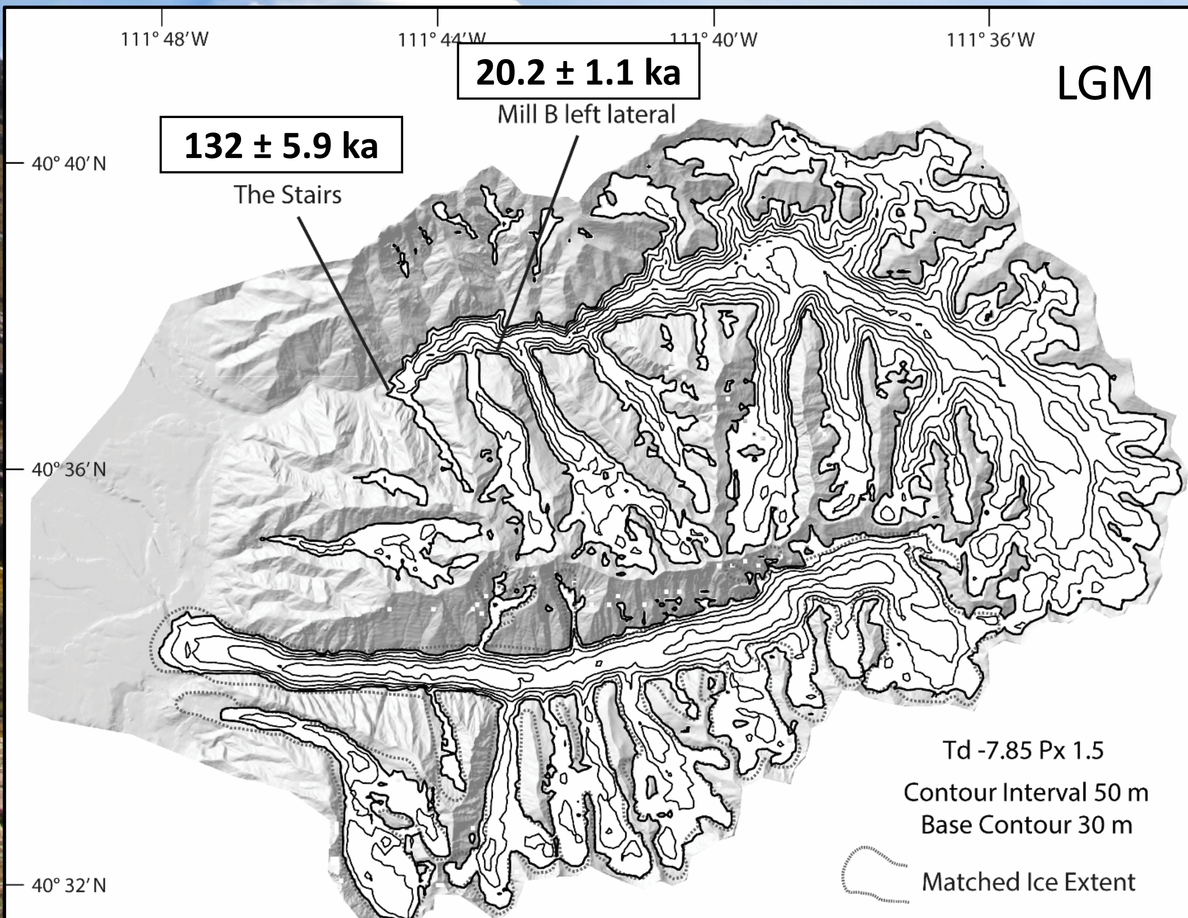

Steady-state ice extent output from Plummer & Phillips (2003) glacier model; coupled energy-mass balance and ice-flow models.

PRISM (Daly et al., 2008) mean monthly temperature and precipitation (1971-2000) models are used as direct input for the EMB model. Additional climate parameters calculated using weather station monthly data.

Ice-flow parameters are constant across entire model domain

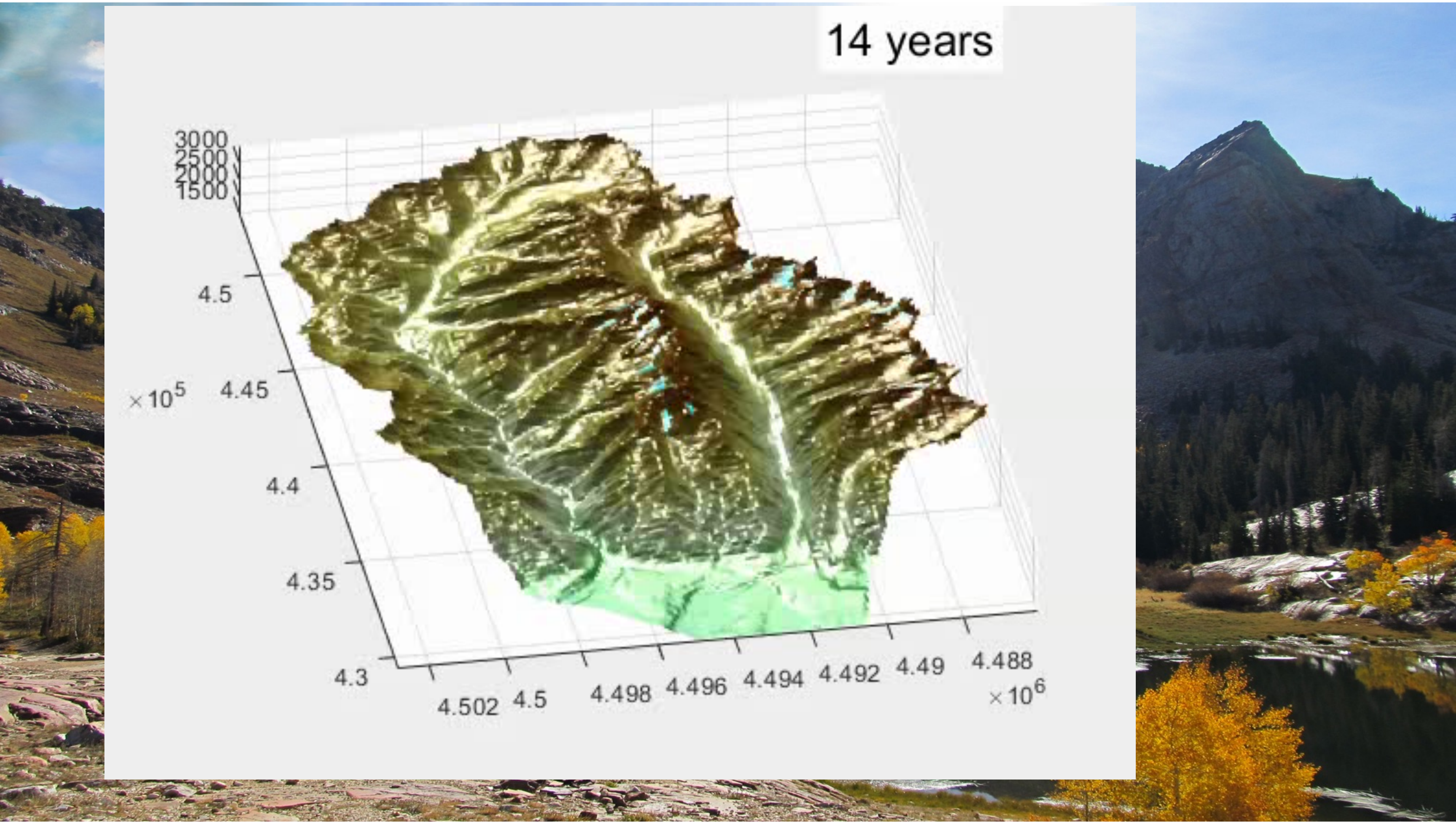
14 years
3000
2500
2000
1500
4.5
4.45
$\times 10^5$
4.4
4.35
4.3
4.502
4.5
4.498
4.496
4.494
4.492
4.49
4.488
$\times 10^6$

Plummer & Phillips (2003) Glacier Model Results

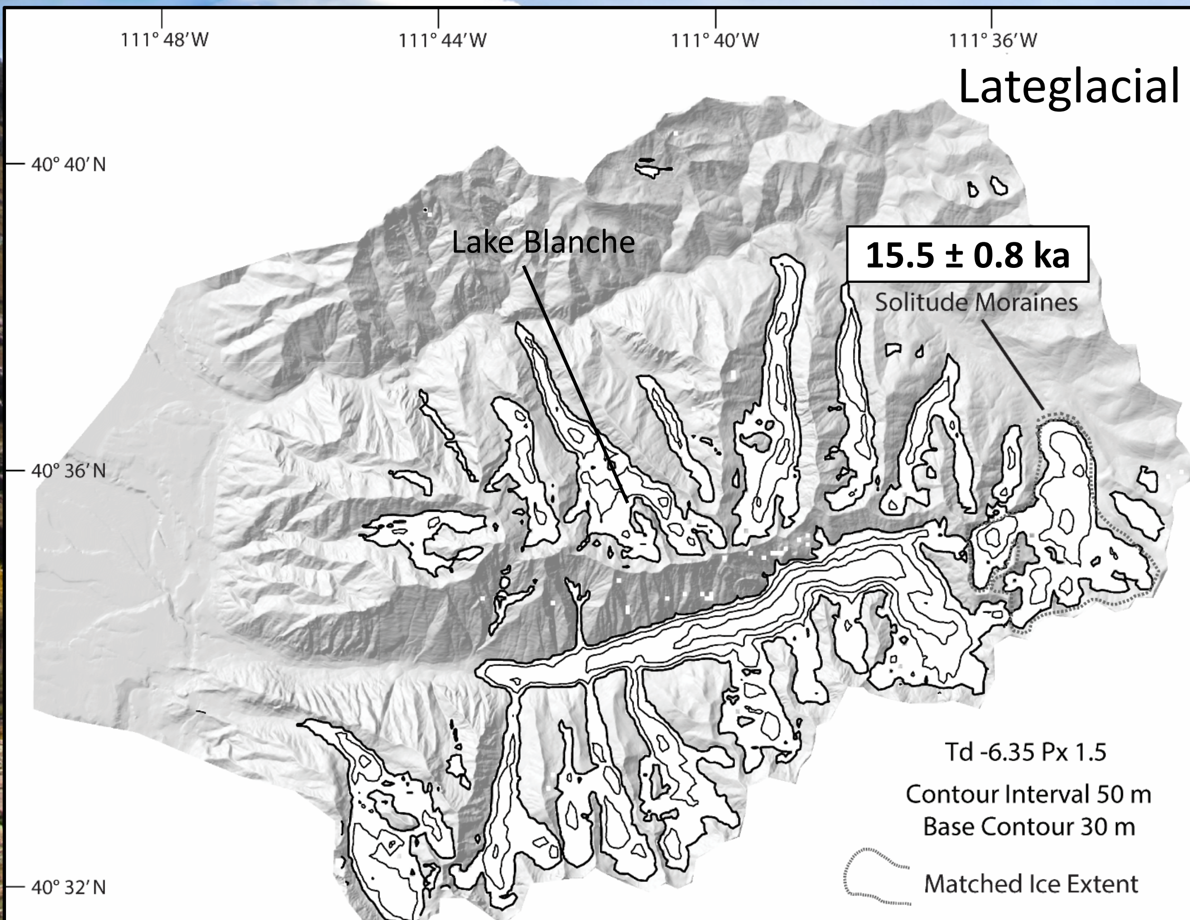

Ice extent output from Plummer & Phillips (2003) glacier model; coupled energy-mass balance and ice-flow models.

PRISM (Daly et al., 2008) mean monthly temperature and precipitation (1971-2000) models are used as direct input for the EMB model. Additional climate parameters calculated using weather station monthly data.

Ice-flow parameters are constant across entire model domain

Paleoclimate Proxy Comparisons - LGM

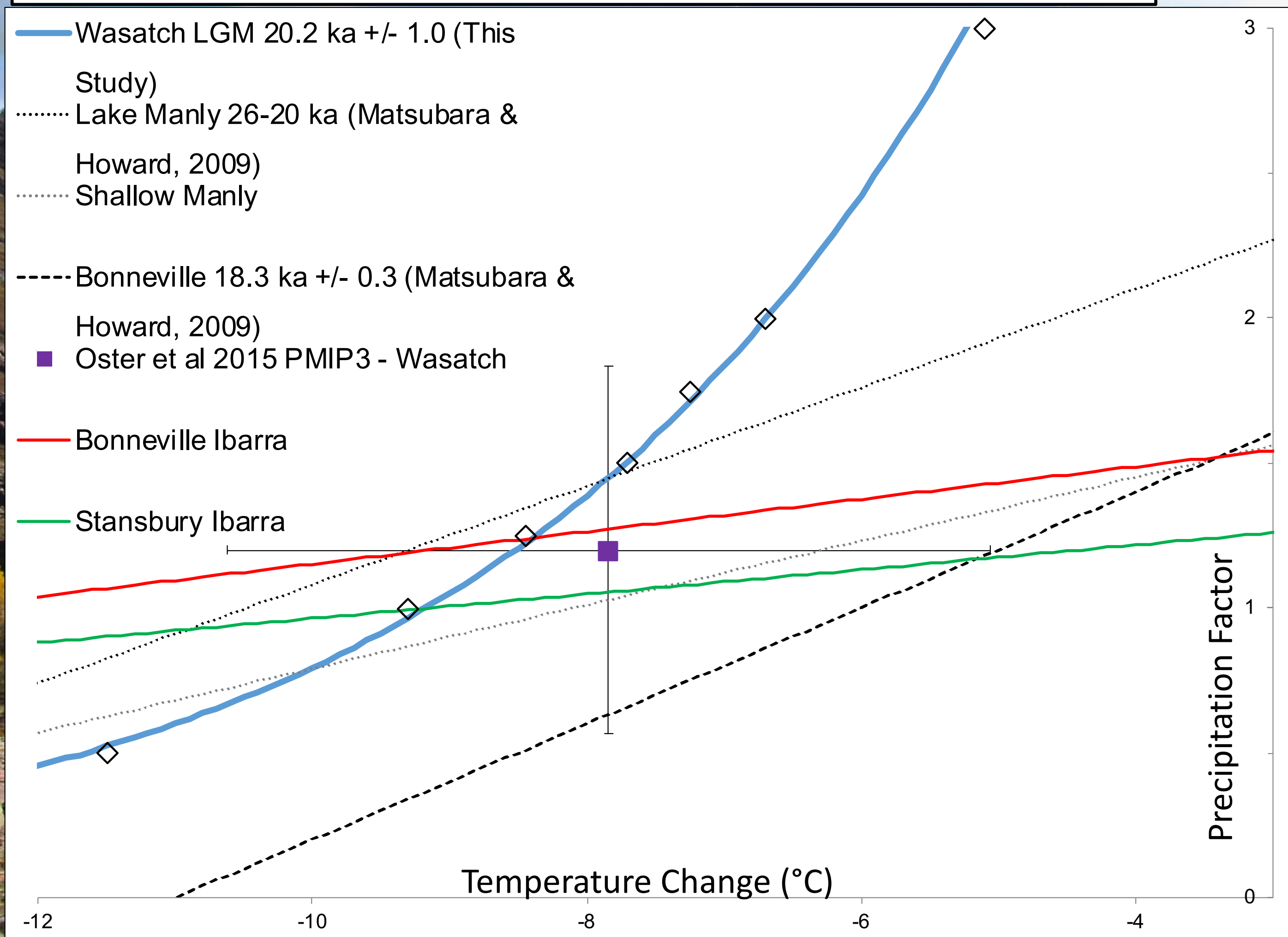

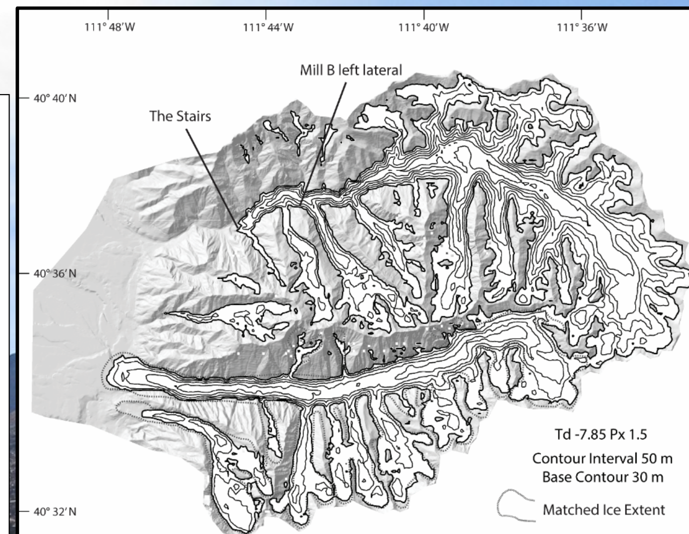

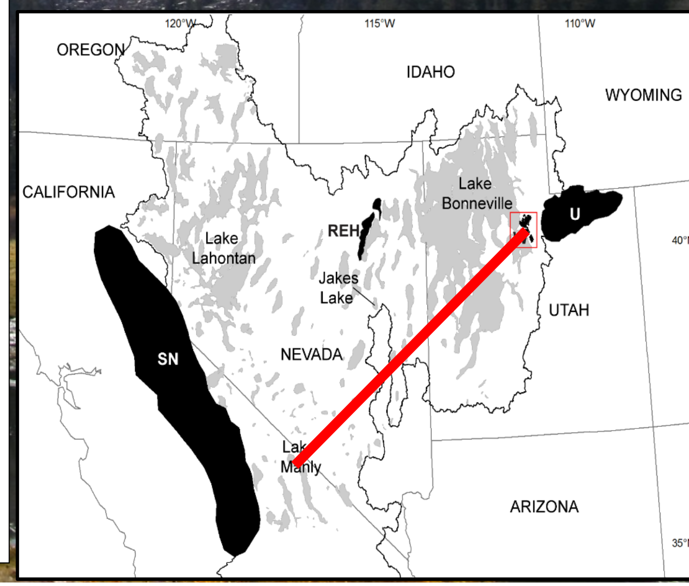

Paleoclimate Proxy Comparisons - LGM

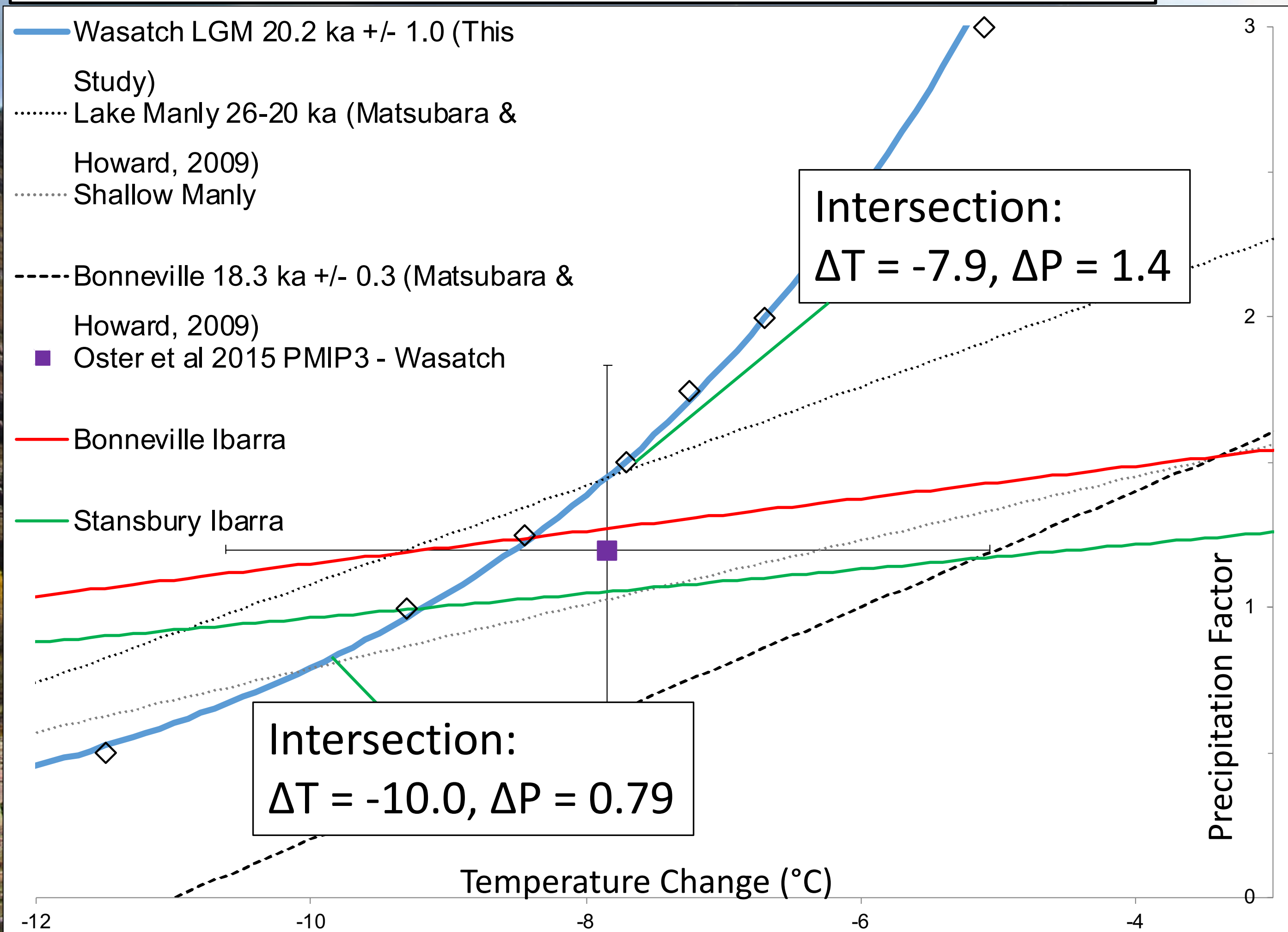

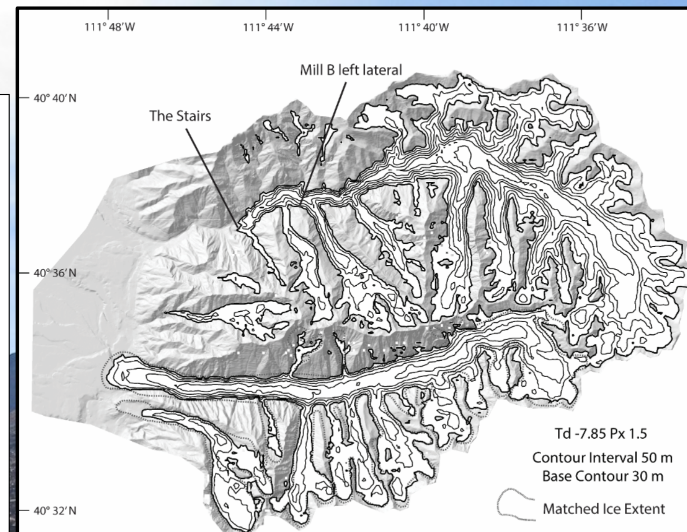

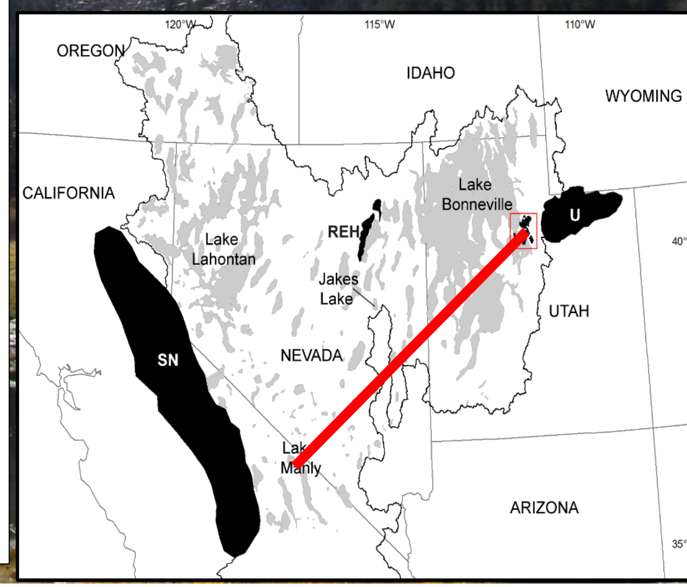

Paleoclimate Proxy Comparisons - Lateglacial

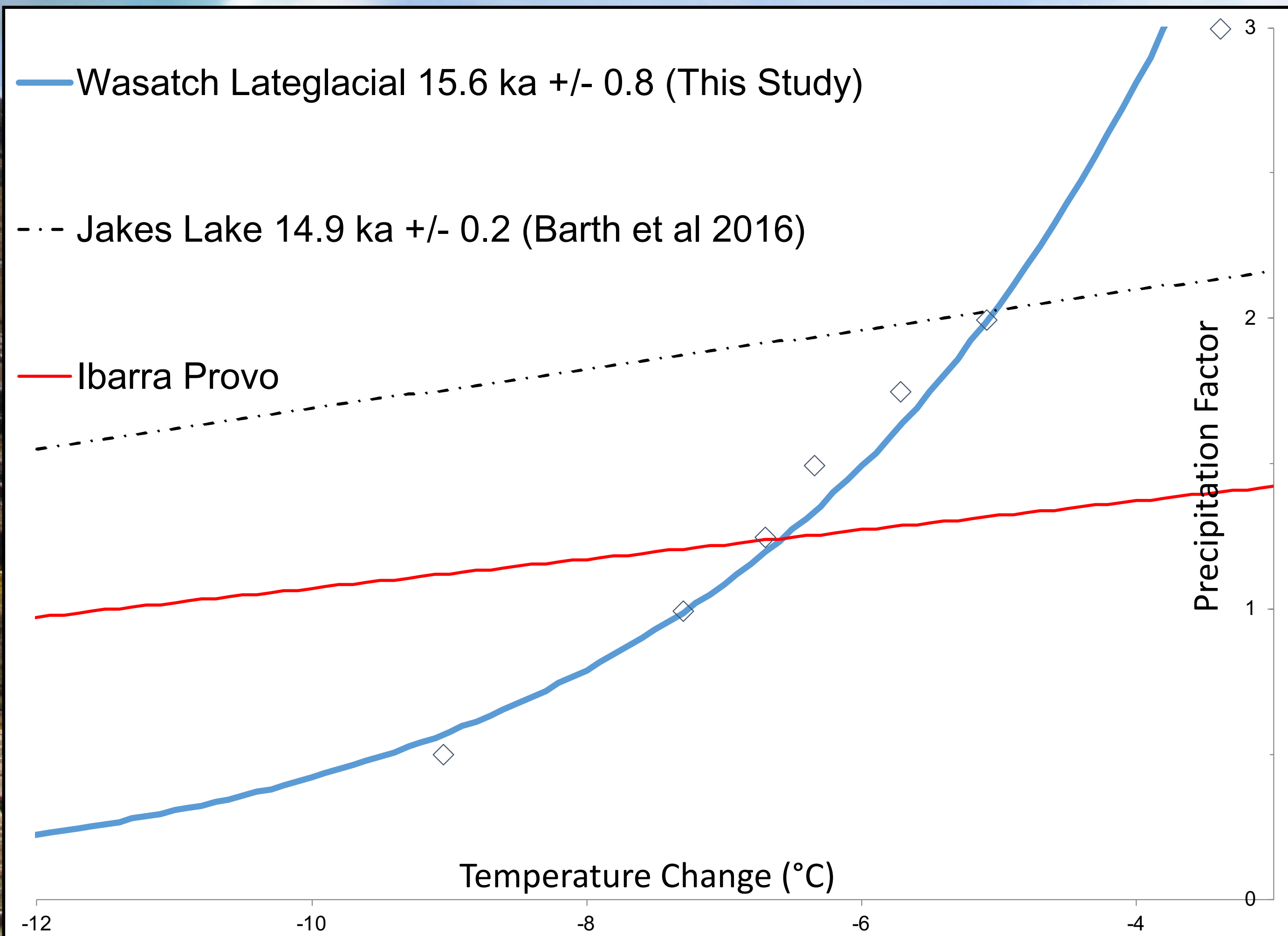

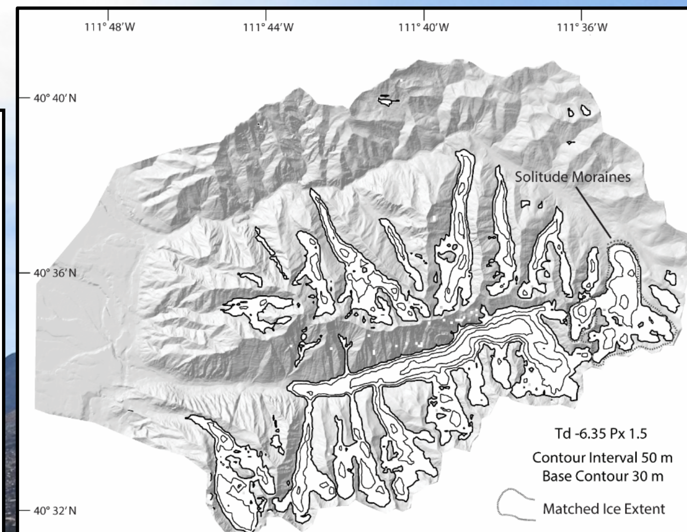

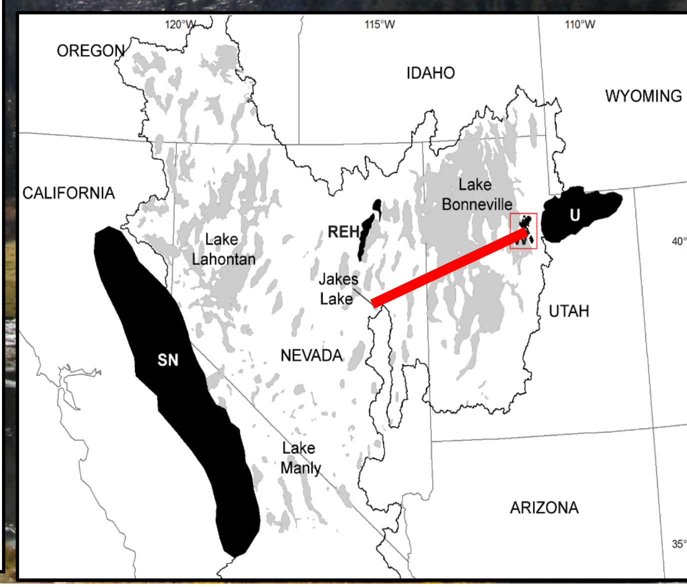

Paleoclimate Proxy Comparisons - Lateglacial

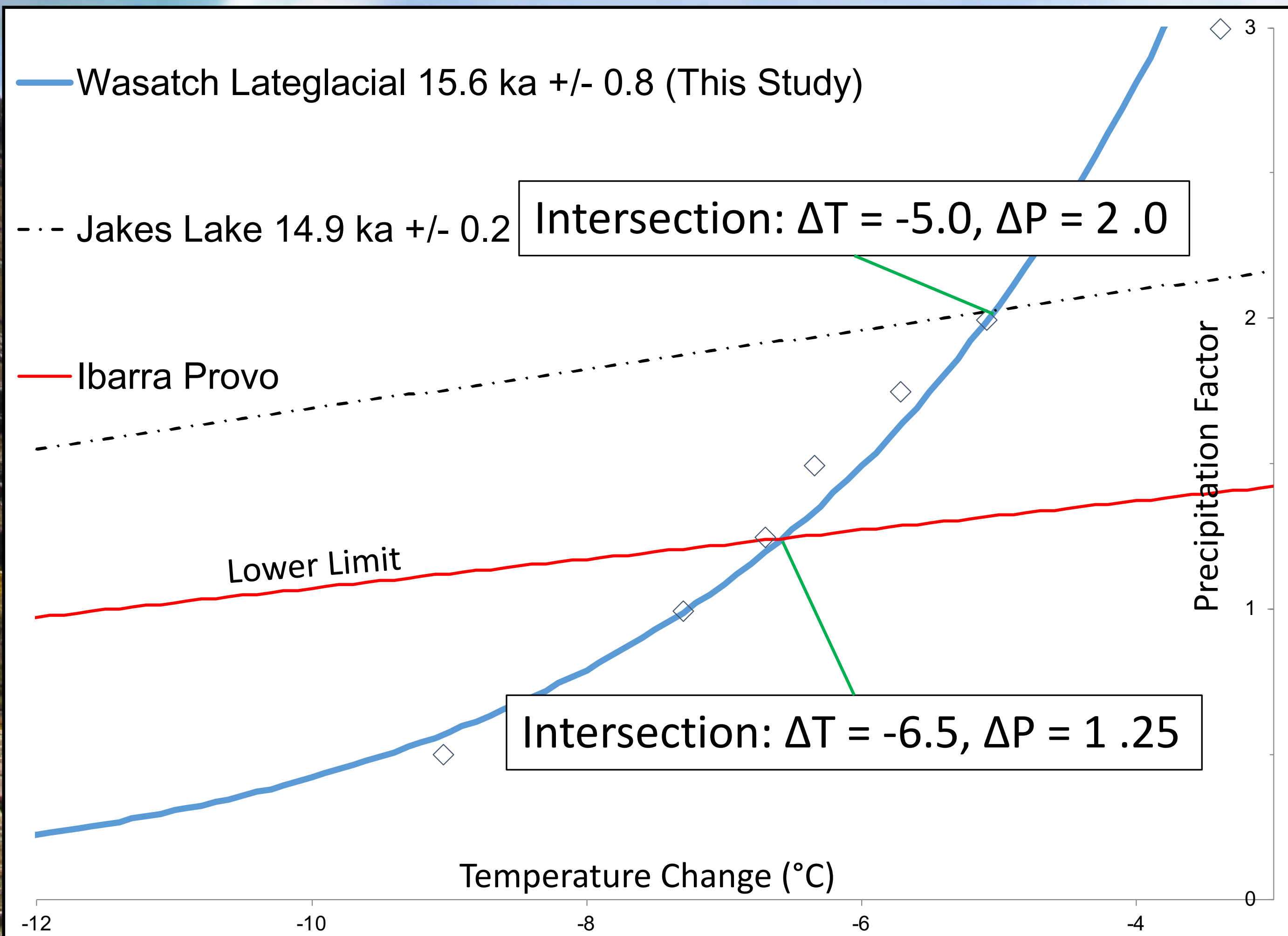

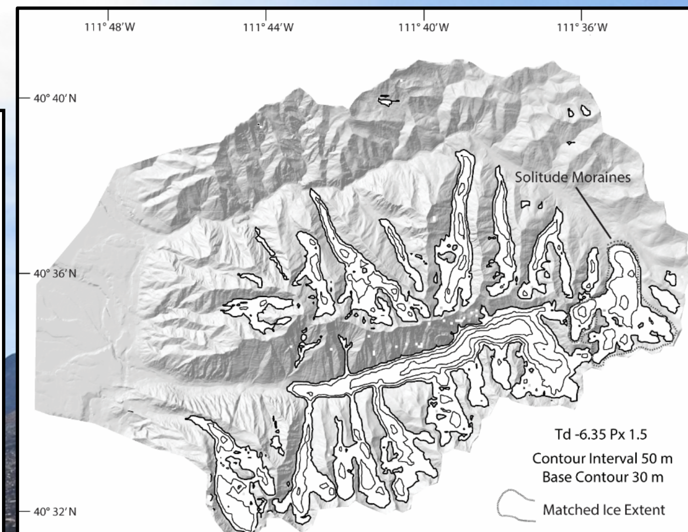

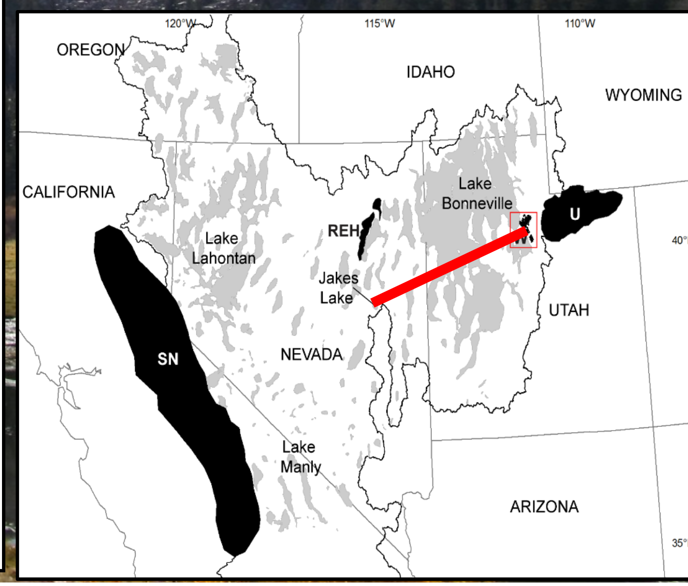

1. We have a better understanding of timing and extent of glaciers during the LGM (20.2 ± 1.0 ka)and Lateglacial (15.6 ± 0.8 ka) in the Wasatch.

2. We demonstrate the utility of combining glacier modeling and cosmogenic exposure dating to reconstruct ice position in areas lacking clear terminus features.

3. By combining our glacier-climate reconstructions and other paleoclimate records we suggest that the **LGM** in this region was characterized as cold with little change in precipitation while the **Lateglacial** was relatively warmer and wetter.

4. Much more work needs to be done to fully understand the range wide Late Pleistocene glacial chronology and paleoclimate of the Wasatch Range and Great Basin region.

Thank you and I would like to acknowledge funding from:
PRIME Lab Seed Grant Program, GSA Graduate Student Research Grant Program, The David S. and Inga M. Chapman Fund, and the The Donald R. Currey Graduate Research Scholarship

Future Work – Glacial Geochronology

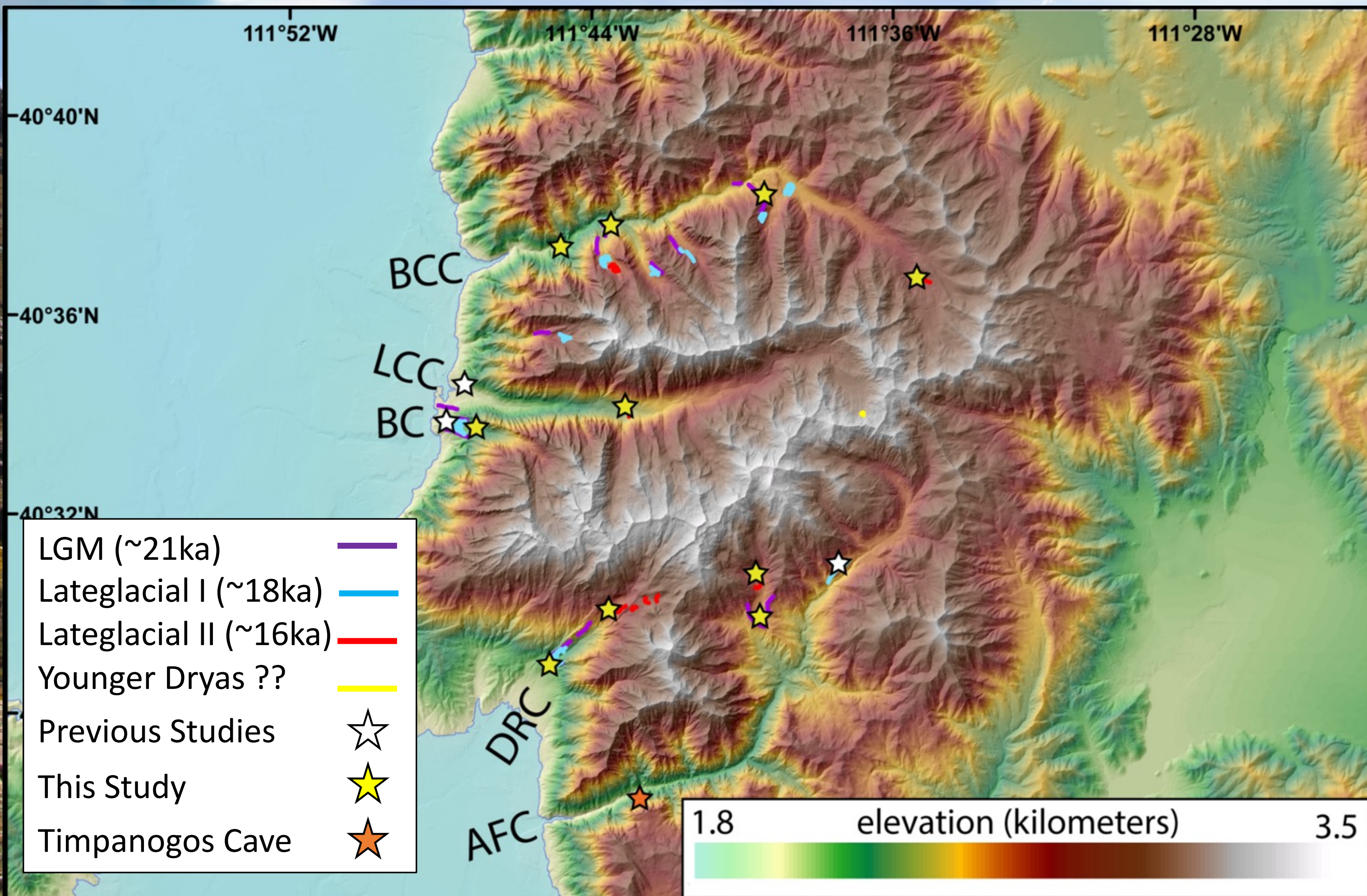

Future Work – Timpanogos Cave

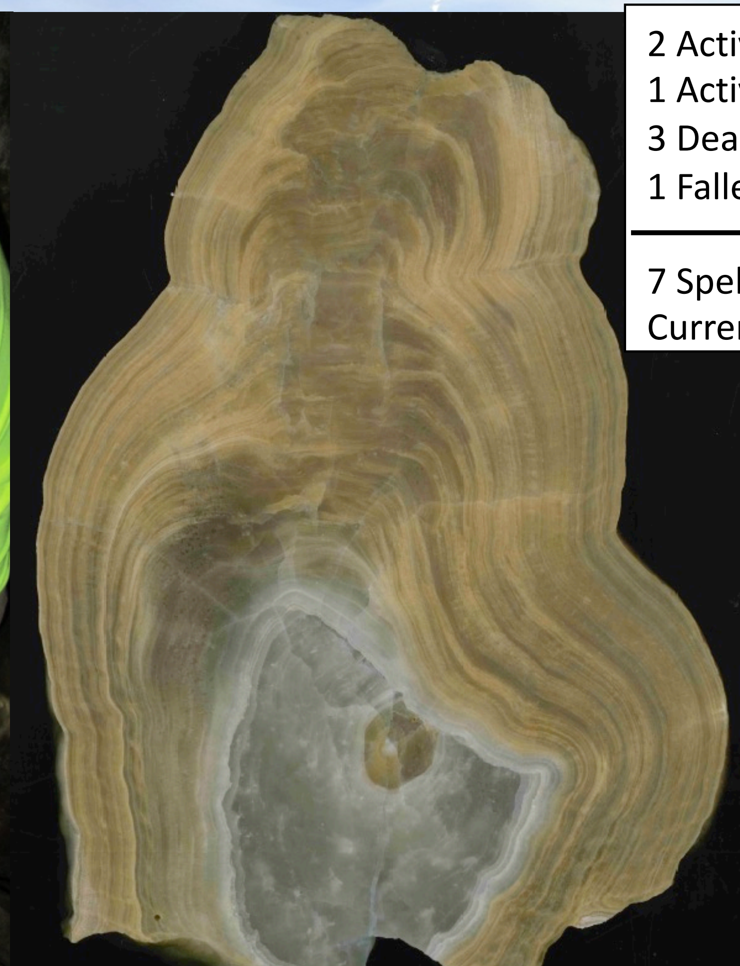

2 Active Stalagmites Cored
1 Active Flowstone Cored
3 Dead Stalagmites
1 Fallen Stalactite

7 Speleothems Total
Currently >20 230-Th ages

ICE AT THE EDGE OF THE BONNEVILLE BASIN – MOUNTAIN GLACIATION AND PALEOCLIMATE OF THE UPPER FREMONT RIVER CATCHMENT, CENTRAL UTAH

David W. Marchetti[1], Thure E. Cerling[2], Brenden T. Reilly[3], Joe S. Stoner[3], Mark B. Abbott[4], and Christopher M. Bailey[5]

[1] Natural & Environmental Sciences Department, Western Colorado University, Gunnison, CO 81231;
[2] Department of Geology and Geophysics, University of Utah, Salt Lake City, UT 84112;
[3]Paleomagnetic & Environmental Magnetic Research Laboratory, Oregon State University, Corvallis, OR 97331;
[4]Department of Geology and Environmental Science, University of Pittsburg, Pittsburg, PA 15260;
[5]College of William and Mary, Williamsburg, VA 23187

Corresponding author (Marchetti): dmarchetti@western.edu

ABSTRACT

The upper Fremont River drainage basin is in western Wayne and southeastern Sevier Counties in central Utah. The Fish Lake Hightop and Boulder Mountain within the basin hosted glacial ice during late and middle Pleistocene time. Using ^{3}He exposure age techniques, Marchetti and others (2005, 2011) and Marchetti (2006) determined exposure ages for boulders deposited on top of well-formed moraines around both Fish Lake Plateau and Boulder Mountain, and ice eroded bedrock on the Boulder Mountain summit plateau. Here, we recalculate pertinent exposure ages using the original ^{3}He data from those sources, the LSDn (Lifton and others, 2014) scaling parameters, and the original CRONUS-Earth on-line exposure age calculator (http://hess.ess.washington.edu/) v.3, which is a modified version of Balco and others (2008). We also include some recent results of a lake core taken from Fish Lake in 2014.

FISH LAKE

An eroded moraine at Jorgenson Creek in the Fish Lake area has four boulder exposure ages ranging from 77 ± 2 to 150 ± 3 ka (uncertainties are internal or analytical only) suggesting deposition during the Bull Lake glaciation or Marine Isotope Stage (MIS) 6. Fifteen boulders from sharp crested moraines at four sites around the Hightop yield a mean exposure age of 20.9 ± 1.9 ka (uncertainty is ±1 standard deviation) suggesting deposition during the Pinedale glaciation or MIS 2, and defining the local last glacial maximum (LGM) at Fish Lake. Two boulders on a recessional moraine upslope of the Pinedale moraine at Tasha Creek yielded ages of 15.1 ± 0.8 and 16.7 ± 0.8 ka (uncertainties are internal or analytical only). Paleoglacier Equilibrium Line Altitude (ELA) reconstructions in Marchetti and others (2011) indicate local LGM ELAs between 2950 and 3200 m. Comparison of climate at modern glacier ELAs to the Fish Lake paleoglacier ELAs suggest maximum LGM summer temperature depressions between -8.2 and -10.1°C.

Fish Lake is a large tectonic lake in an asymmetric graben displacing Oligocene to Miocene volcanic rocks. Although Pinedale and Bull Lake age glaciers flowed into the lake at Pelican Canyon, they occupied only part of the lake basin. Preliminary gravity surveys across the basin suggest a thick sediment package (>200 m) under modern Fish Lake, and indicate that the lake basin likely formed >1 Ma (Weinrich and others, 2014). Our research group took a ~11 m composite core of Fish Lake sediments through winter ice in 30 m of water in 2014. The full results of the core analysis are forthcoming, but Reilly and others (2018) determined an age model and measured magnetic properties to determine paleomagnetic directions via paleosecular variation stratigraphy. Magnetic susceptibility (MS) and CT# (a proxy for sediment density) variations from ca. 30–1 ka suggest the following sedimentation patterns: 1) from 30–25 ka increasing MS and CT# indicate glaciers advancing into the lake basin, 2) glacier derived sediments reach a maximum around 24–21 ka, coincident with the moraine exposure ages, and then decrease slightly and persist until about 15 ka when the MS values and CT#s drop significantly indicating a nearly complete loss of glacier-derived sediments into the lake basin, 3) the post-glacial through Holocene sections of the cores show a slight increase in mineral-rich sediments from 13–11 ka, possibly associated with Younger Dryas cooling, and 4) a subtle change in likely autochthonous lake sedimentation around 8–7 ka.

BOULDER MOUNTAIN

Boulder Mountain is a 180 km^2 upland plateau capped with the same Oligocene age volcanic rock package as the Fish Lake Plateau. There is a nearly continuous 200–300 m vertical cliff ringing the mountain 'summit' except on the western side where the relief is less pronounced. The summit plateau of Boulder Mountain had a true ice cap during the LGM and perhaps earlier glaciations. The LGM ice cap likely had one center, and ice flowed radially outward and spilled off the mountain as outlet glaciers at several reentrants. Smaller cirque constrained glaciers formed under the summit cliff in several locations, most noticeably on the NE-facing parts of the SE summit arm leading to Bown's Point. Twenty-two ^3He exposure ages from boulders on sharp crested moraines deposited by outlet glaciers in the Miller Creek/Bone Flat, Donkey Creek, and Fish Creek drainages give a mean age of 20.6 ± 1.5 ka (uncertainty is ± 1 standard deviation) suggesting deposition during the Pinedale glaciation, ~MIS 2, and defining the local LGM. Two recessional moraines considerably up-drainage from the LGM outlet glacier margins were sampled in the Fish Creek drainage of Boulder Mountain. Seven exposure ages from boulders on the Fish Creek Lake moraine yield a mean age of 16.2 ± 1.5 ka (uncertainty is ± 1 standard deviation), while five boulders from the nearby Fish Creek Point moraine yield a mean age of 15.3 ± 1.1 ka (uncertainty is ± 1 standard deviation). Both the Fish Creek Lake and Fish Creek Pont moraines have morphologies which suggest they were not deposited by an outlet glacier originating on the top of Boulder Mountain, but rather were deposited by ice constrained in the NE-facing reentrant of the Fish Creek drainage.

Eighteen ^3He exposure ages from ice-eroded and -sculpted bedrock outcrops on the summit of the mountain range from 15–119 ka. The two oldest exposure ages of 109 ± 4 and 119 ± 5 ka (uncertainties are internal or analytical only) are from near the center of the glaciated part of the mountain summit plateau and near the inferred center if the ice cap. These ages suggest mostly non-erosive ice under the ice cap near its center. Six exposure ages range from 30–90 ka, many of these samples are from near the inferred margins of the ice cap and may indicate erosive ice cover only during maximum extent of glaciations. Eight exposure ages of strongly ice-sculpted and polished bedrock near the centers of inferred outlet glacier streams on the summit range from 22–25 ka with a mean age of 23.1 ± 1.0 ka (uncertainty is ± 1 standard deviation). The discrepancy between the moraine exposure ages and the younger ice-sculpted bedrock exposure ages is interesting, and likely indicates that the ice cap outlet glacier streams may not have eroded enough bedrock (~3 m) to remove all the previous cosmogenic inheritance.

Taken together, the recessional moraine data and the ice-sculpted bedrock data suggest loss of the ice sheet on the 'summit' of the mountain sometime after 19–22 ka and before ~15–16 ka. True ice sheets are especially sensitive to ELA changes as their hypsometry can cause complete loss of accumulation zone area with even moderate ELA rise. We hypothesize that an ELA rise on the Boulder Mountain ice sheet after 19–22 ka and before ~15–16 ka shut down active ice sheet flow and loss of outlet glaciers. Subsequent cooling and ELA lowering before ~15–16 ka produced only small, well shaded glaciers on the NE-facing sides of reentrants.

REFERENCES

Balco, G., Stone, J.O., Lifton, N., and Dunai, T.J., 2008, A complete and easily accessibly means of calculating surface exposure ages or erosion rates from ^{10}Be and ^{26}Al measurements: Quaternary Geochronology, v. 3, p. 174–195.

Lifton, N., Sato, T., and Dunai, T.J., 2014, Scaling in situ cosmogenic nuclide production rates using analytical approximations to atmospheric cosmic-ray fluxes: Earth and Planetary Science Letters, v. 386, p. 149–160.

Marchetti, D.W., 2006, Quaternary geology of the Fremont River drainage basin, Utah: Salt Lake City, University of Utah, Ph.D. dissertation, 135 p.

Marchetti, D.W., Cerling, T.E., and Lips, E.W., 2005, A glacial chronology for the Fish Creek drainage of Boulder Mountain, Utah: Quaternary Research, v. 64, p. 264–271.

Marchetti, D.W., Harris, M.S., Bailey, C.M., Cerling, T.E., and Bergman, S., 2011, Timing of glaciation and last glacial maximum paleoclimate estimates from the Fish Lake Plateau, Utah: Quaternary Research, v. 75, p. 183–195.

Reilly, B.T., Stoner, J.S., Hatfield, R.G., Abbott, M.B., Marchetti, D.W., Larsen, D.J., Finkenbinder, M.S., Hillman, A.L., Kuehn, S.C., and Heil Jr., C.W., 2018, Regionally consistent western North America paleomagnetic directions from 15–35 ka—Assessing chronology and uncertainty with paleosecular variation stratigraphy (PSV): Quaternary Science Reviews, v. 201, p. 186–205.

Wenrich, E.A., Bailey, C.M., Steele, P.A., Marchetti, D.W., and Harris, M.S., 2014, Structural geology and sediment infill geometry of a high-elevation graben—the Fish lake basin, central Utah: Geological Society of America Abstracts with Programs, v. 46, no. 6, p. 560.

This content is a PDF version of the author's PowerPoint presentation.

Ice at the edge of the Bonneville Basin – mountain glaciation and paleoclimate of the upper Fremont River catchment, central Utah

David Marchetti	*Western Colorado University*
Thure Cerling	*University of Utah*
Brenden Reilly	*Oregon State University*
Joe Stoner	*Oregon State University*
Mark Abbott	*University of Pittsburg*
Christopher Bailey	*College of William and Mary*

Glaciated areas on Utah's "High Plateaus"

1. Wasatch Plateau
2. Fish Lake Plateau
3. Boulder Mountain
4. Markagunt Plateau
5. Tushar Mountains
6. N. Sevier Plateau
7. Canyon Range

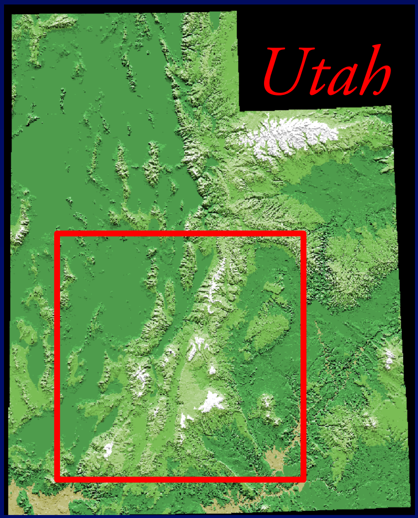

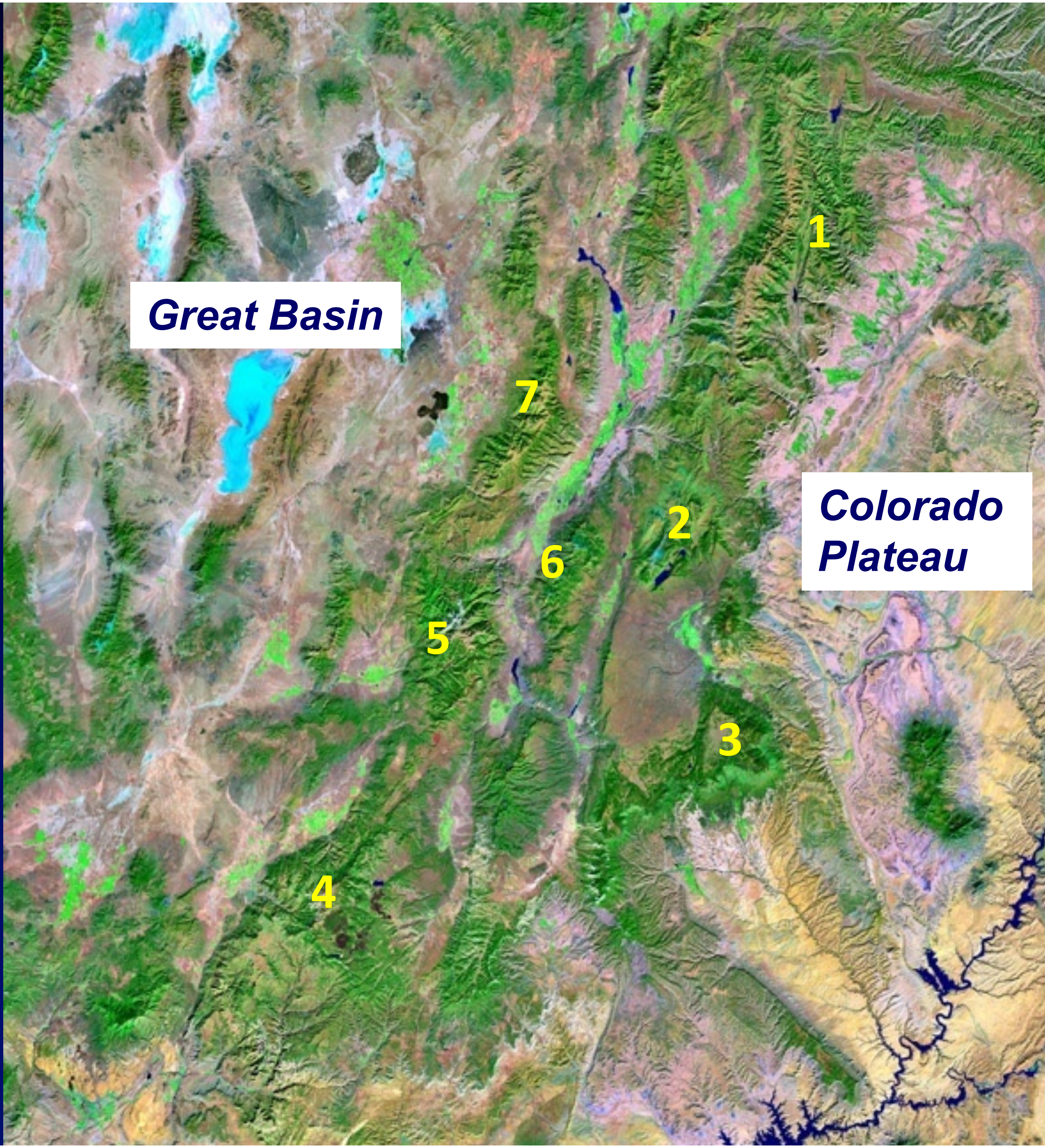

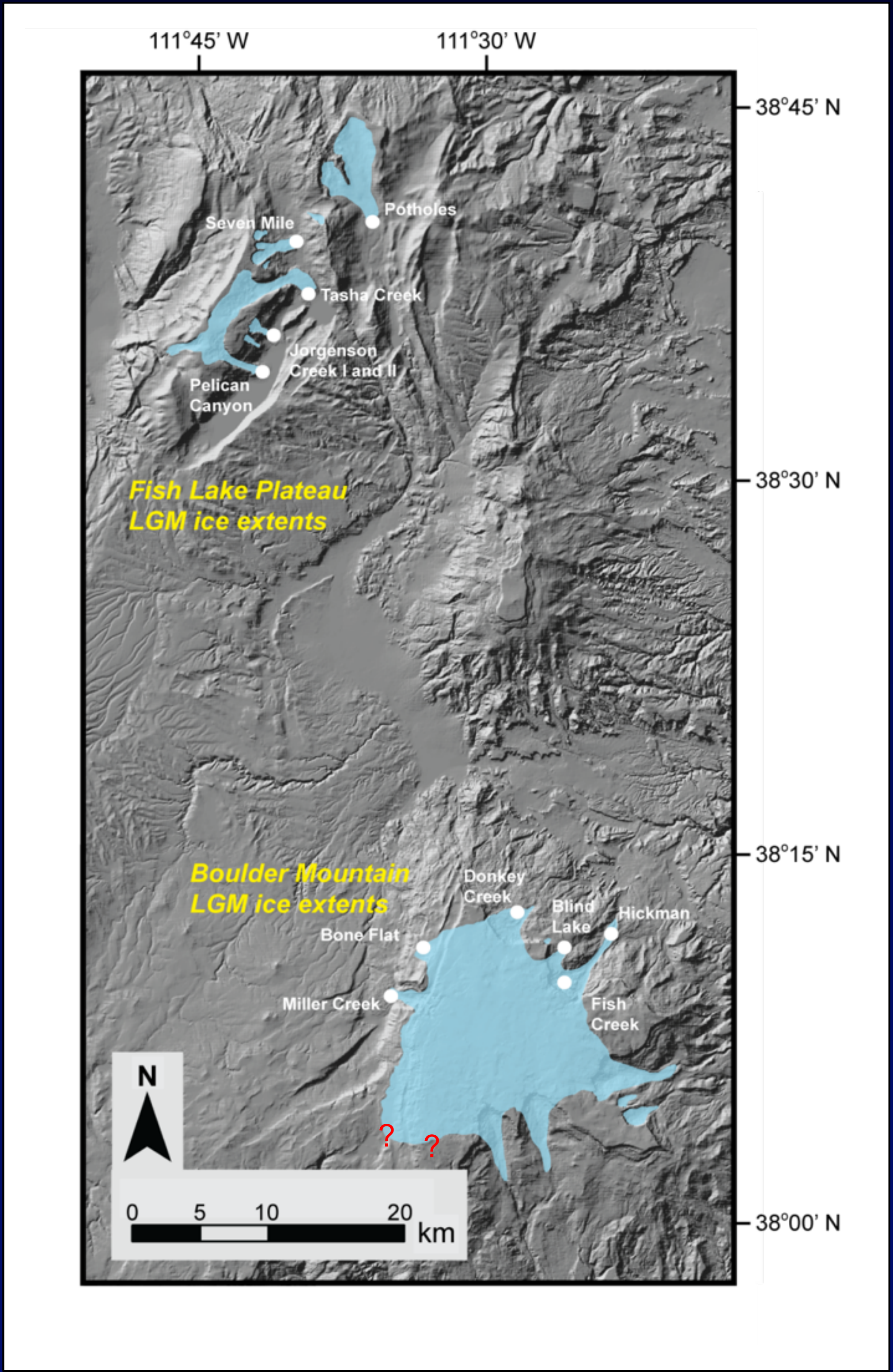

Laabs et al., in prep
QSR

Cosmogenic ^{3}He exposure age dating

pyroxenes from andesites

negligible mantle He

non-cosmogenic ^{3}He corrected for with shielded samples
(Marchetti et al., 2005 QR)

use Balco / original CRONUS calculator

scaled using LSDn
(Lifton et al., 2014 EPSL)

snow correction using modern SNOTEL site data

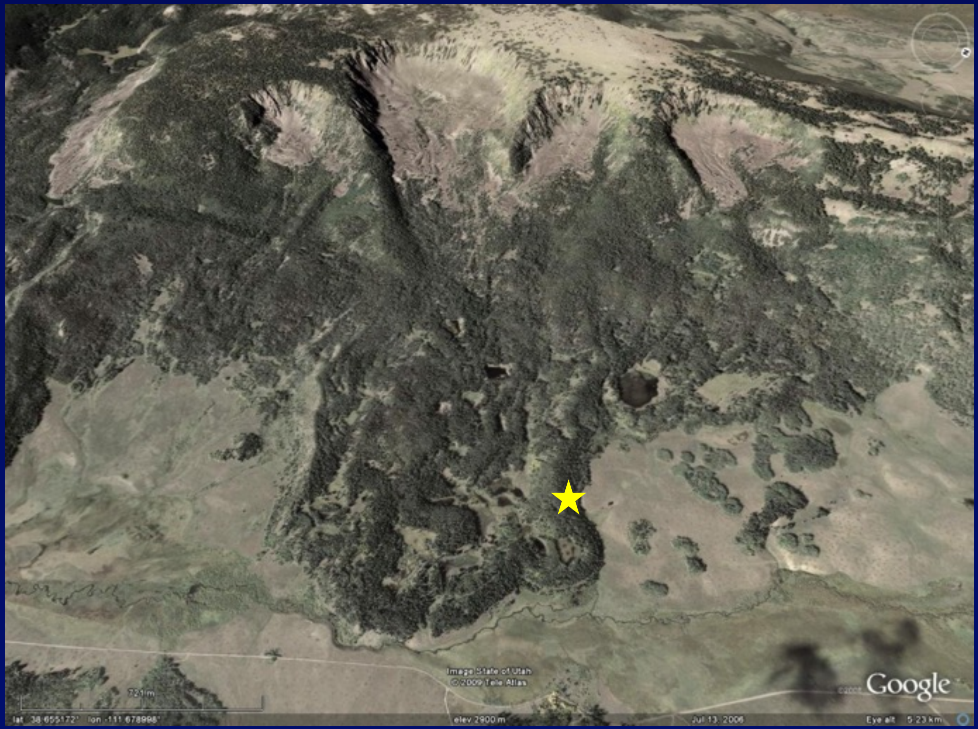

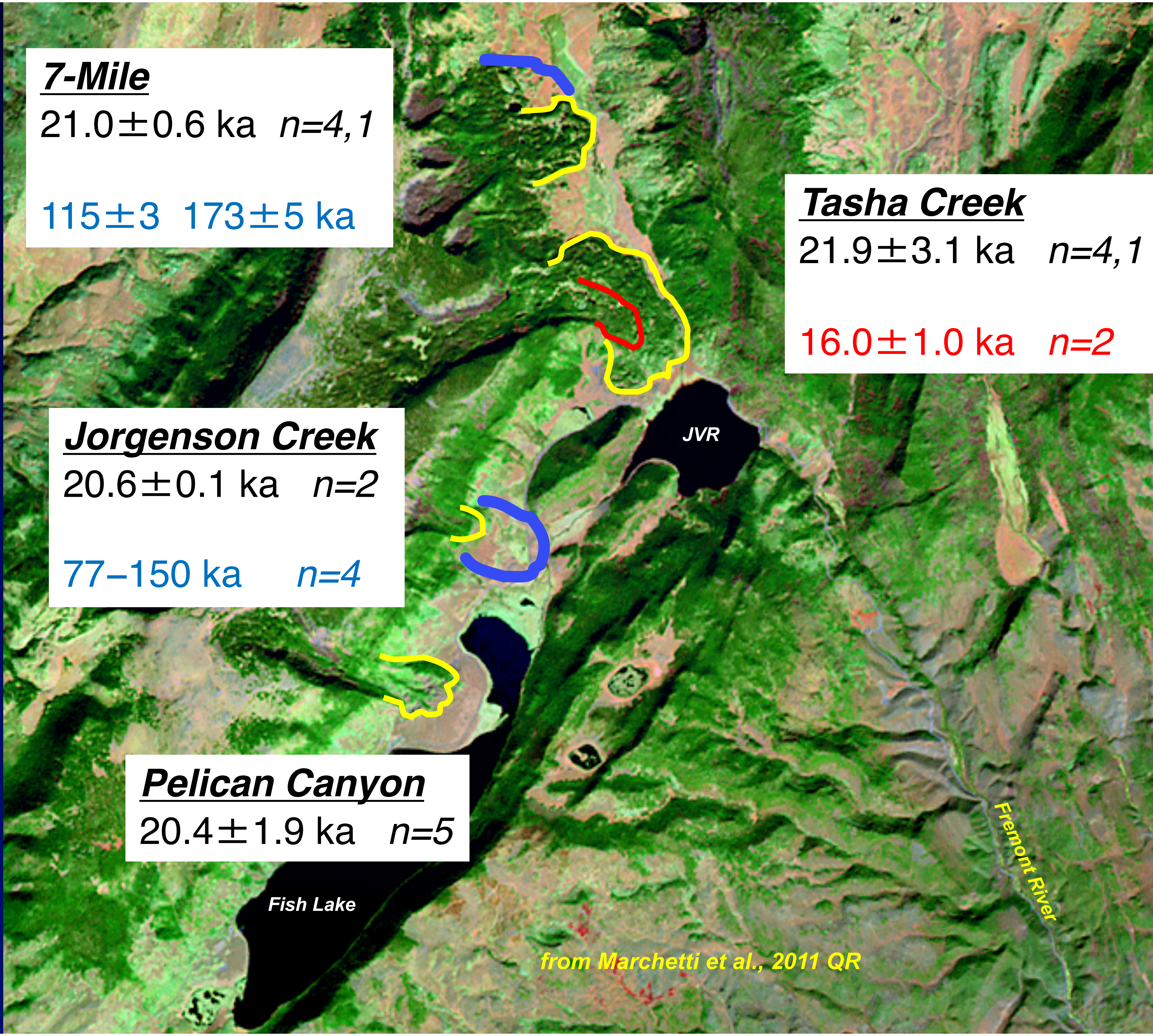
7-Mile
21.0±0.6 ka n=4,1
115±3 173±5 ka
Tasha Creek
21.9±3.1 ka n=4,1
16.0±1.0 ka n=2
JVR
Jorgenson Creek
20.6±0.1 ka n=2
77–150 ka n=4
Pelican Canyon
20.4±1.9 ka n=5
Fish Lake
Fremont River
from Marchetti et al., 2011 QR

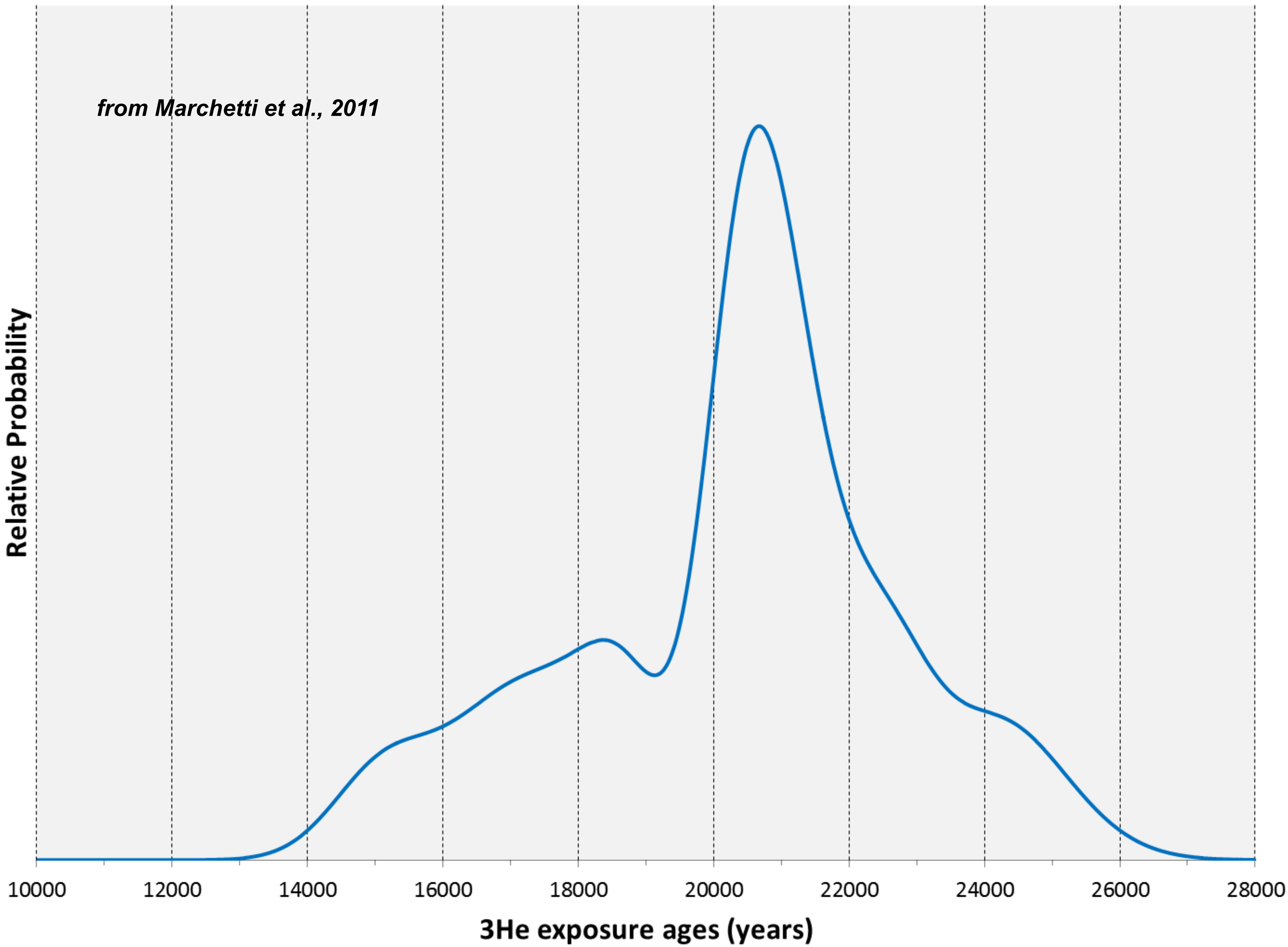
from Marchetti et al., 2011
Relative Probability
10000
12000
14000
16000
18000
20000
22000
24000
26000
28000
3He exposure ages (years)

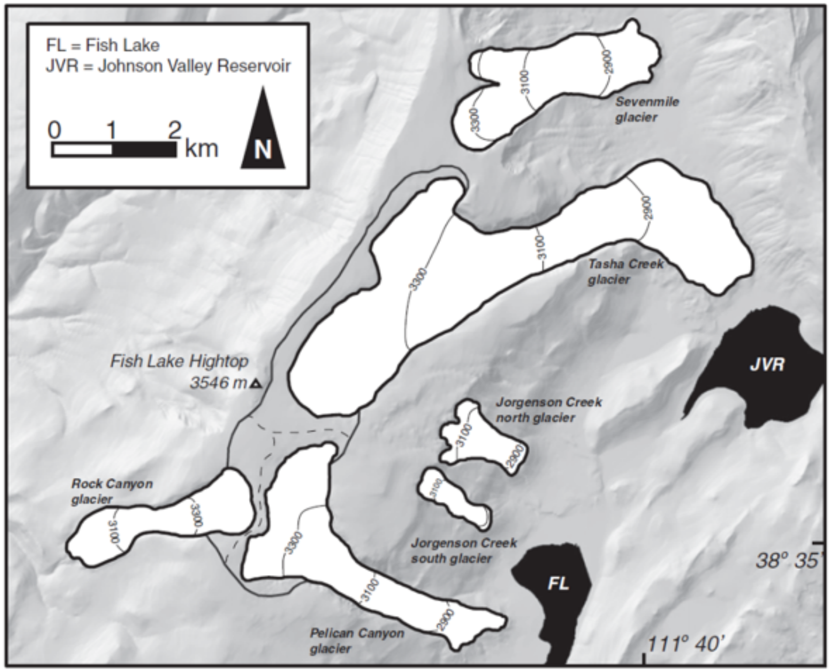

Figure 4. Reconstructions of LGM age glaciers on the Fish Lake Plateau. Contour lines are in meters and indicate reconstructed ice surface elevations.

Table 3
Paleoglacier ELA data.

Paleoglacier	Glacier area (km^2)	ELA from AAR method (m)	ELA from THAR method (m)
Cirque			
Reconstructed as individual glaciers (AAR = 0.6 ± 0.1; THAR = 0.4 ± 0.05)			
Jorgenson Creek South	0.5	3020 ± 30	3035 ± 30
Jorgenson Creek North	0.9	2980 ± 20	3020 ± 20
Seven Mile	3.5	2950 + 70/−40	3060 ± 30
Hightop			
Reconstructed as individual glaciers (AAR = 0.6 ± 0.1; THAR = 0.4 ± 0.05)			
Rock Canyon	2.1	3130 + 100/−30	3165 ± 25
Pelican Canyon	4.2	3190 + 50/−110	3030 ± 40
Tasha Creek	11.3	3130 + 90/−140	3020 ± 40
Reconstructed as part of an ice cap (AAR = 0.7 ± 0.1)			
Rock Canyon	3.1	3190 + 160/−90	n.a.
Pelican Canyon	5.1	3180 + 80/−170	n.a.
Tasha Creek	13.5	3080 + 150/−90	n.a.

Local LGM ELAs
~2950–3190 m

Summer (JJA) LGM Temp. depressions
-8.2 to -10.1 deg. C

Possible slight increase in precipitation
~1.5 x modern

from Marchetti et al., 2011 QR


Fish Lake
Preliminary coring
February 2014
Core site
1723 m
Google earth
Imagery Date: 7/26/2015 lat 38.550417° lon -111.709567° elev 2699 m eye alt 10.80 km

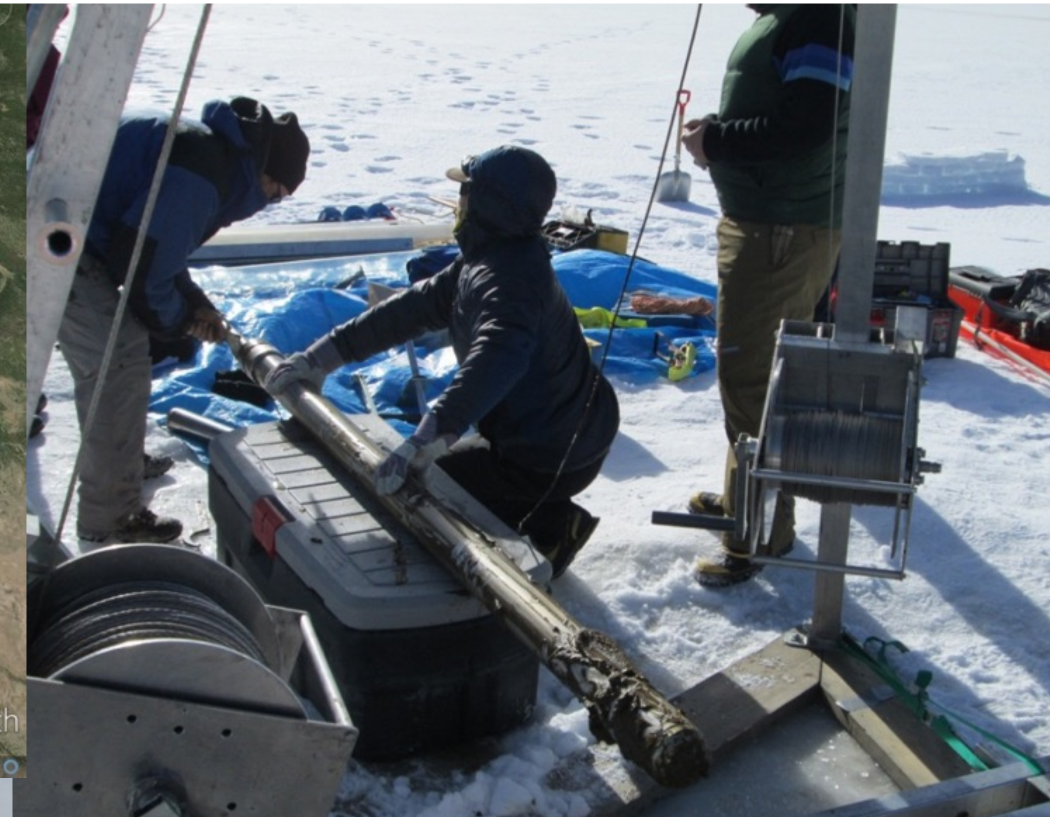

Boulder Mountain "summit"




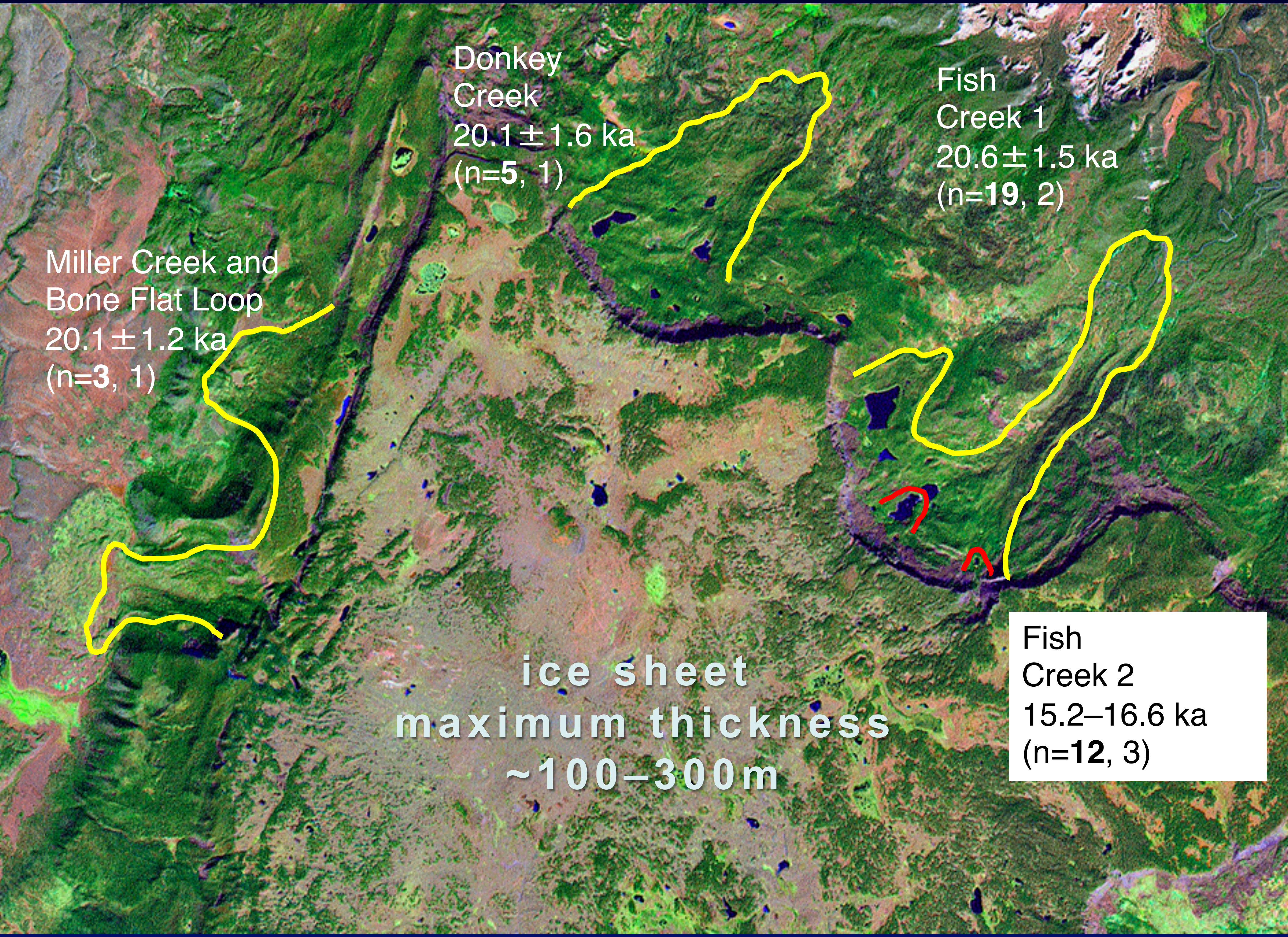
Donkey
Creek
20.1±1.6 ka
(n=**5**, 1)
Fish
Creek 1
20.6±1.5 ka
(n=**19**, 2)
Miller Creek and
Bone Flat Loop
20.1±1.2 ka
(n=**3**, 1)
ice sheet
maximum thickness
~100–300m
Fish
Creek 2
15.2–16.6 ka
(n=**12**, 3)

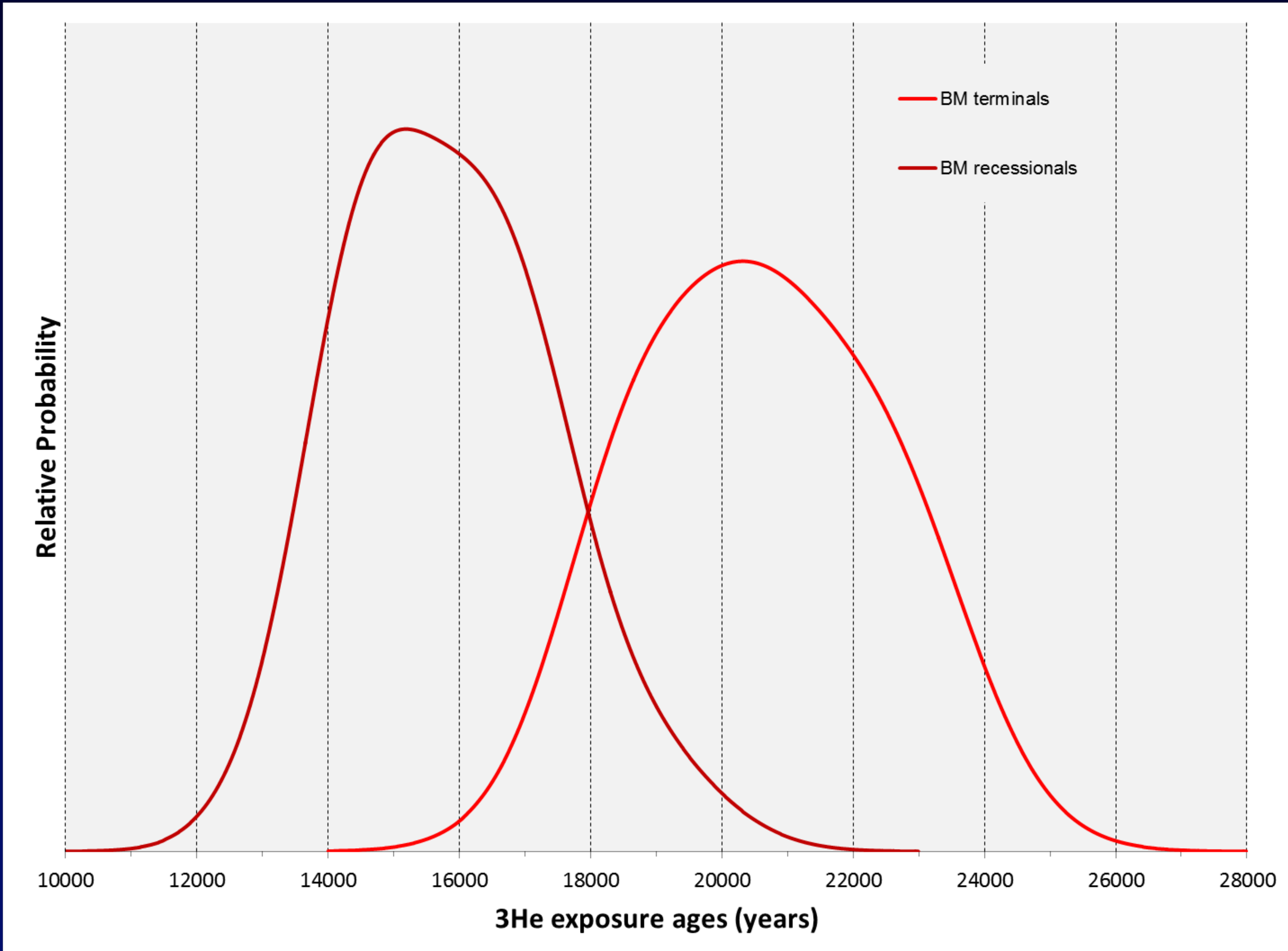
BM terminals
BM recessionals
Relative Probability
10000
12000
14000
16000
18000
20000
22000
24000
26000
28000
3He exposure ages (years)

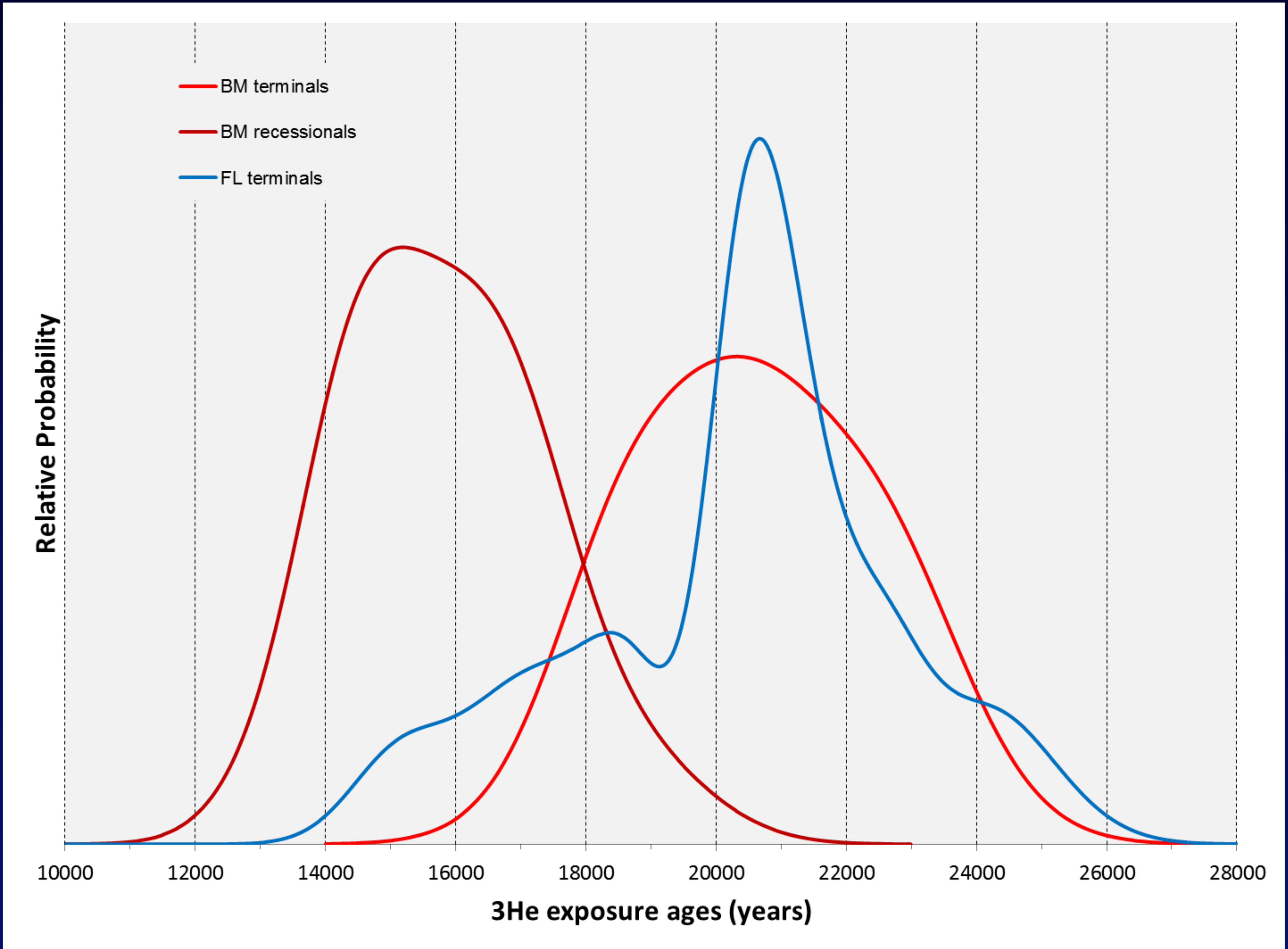
BM terminals
BM recessionals
FL terminals
Relative Probability
10000
12000
14000
16000
18000
20000
22000
24000
26000
28000
3He exposure ages (years)

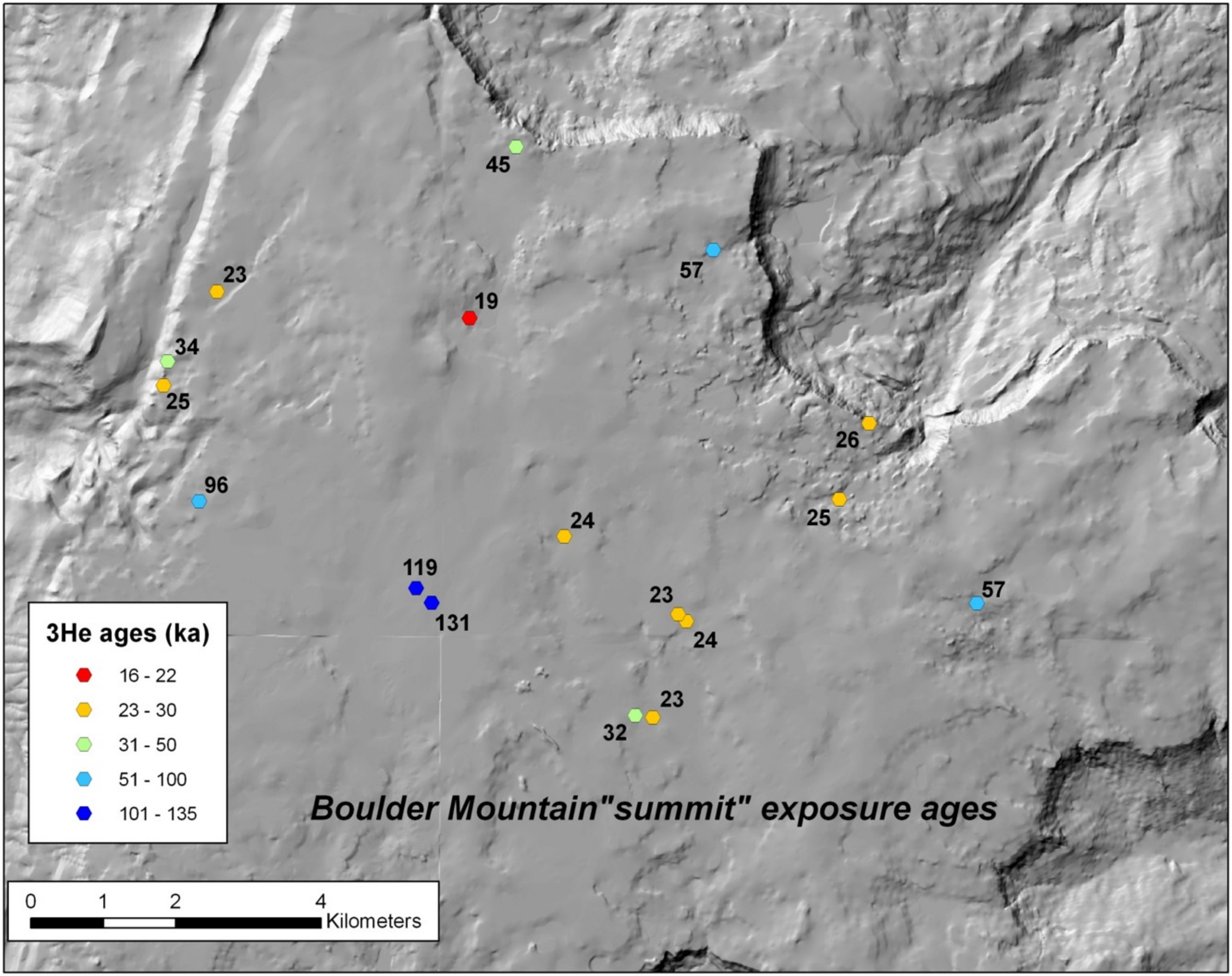

45
57
23
19
34
25
26
96
25
24
119
131
23
24
57
23
32
3He ages (ka)
16 - 22
23 - 30
31 - 50
51 - 100
101 - 135
Boulder Mountain"summit" exposure ages
0
1
2
4
Kilometers

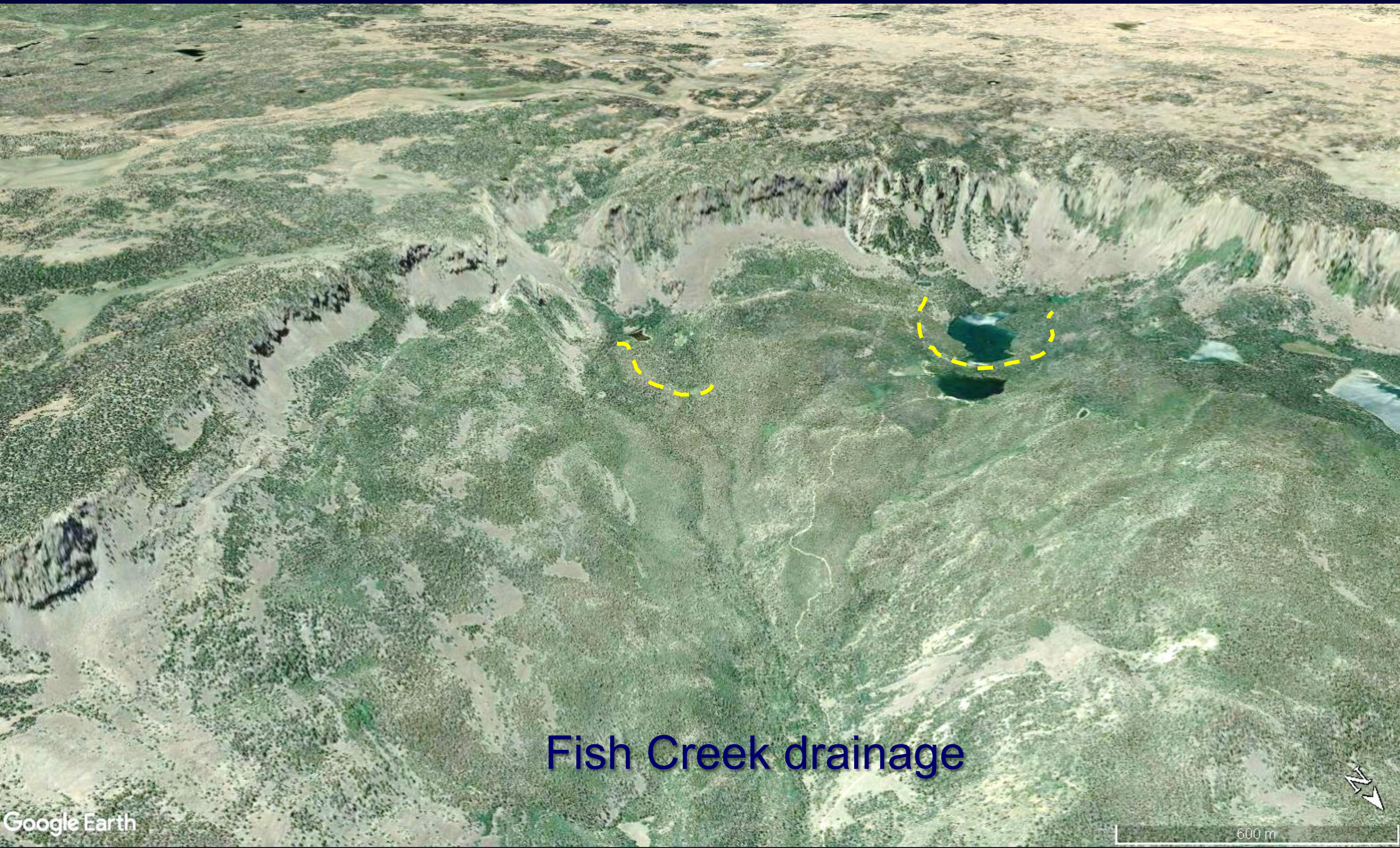
Fish Creek drainage
Google Earth
600 m
N

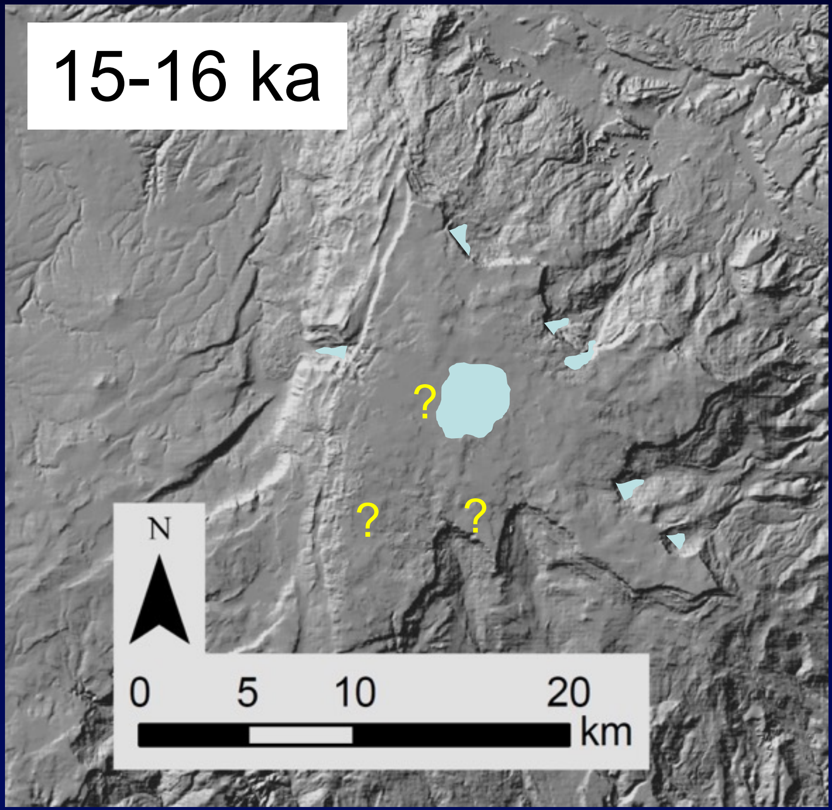

15-16 ka
?
?
?
N
0 5 10 20
km

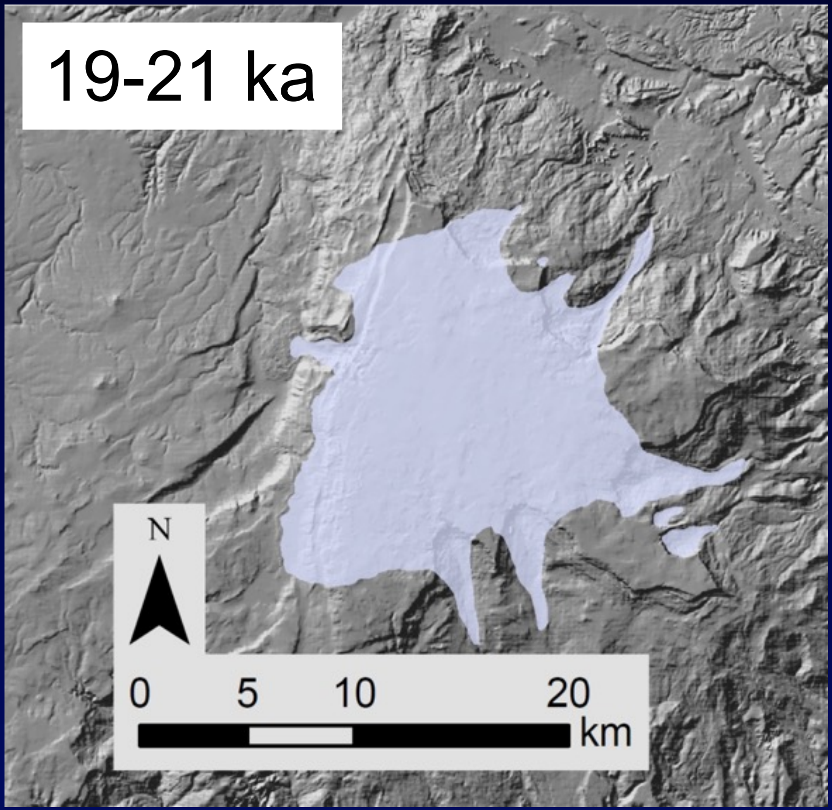

19-21 ka
N
0 5 10 20
km

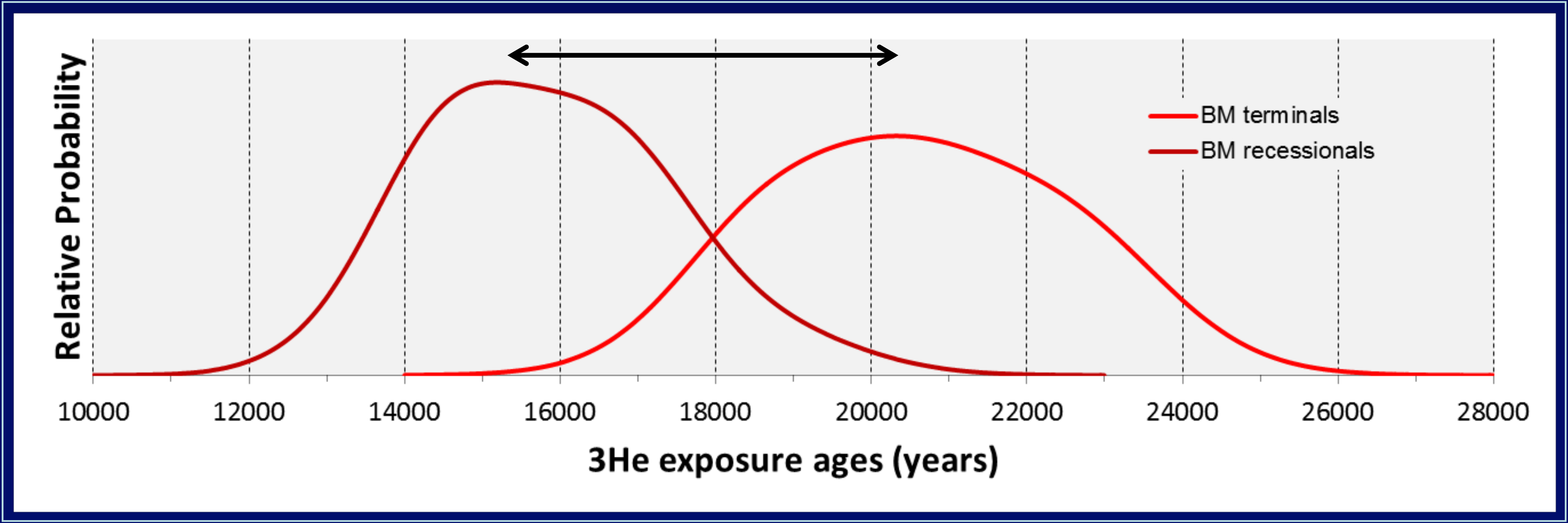

Relative Probability
BM terminals
BM recessionals
10000
12000
14000
16000
18000
20000
22000
24000
26000
28000
3He exposure ages (years)

CONCLUSIONS

- Fish Lake had Bull Lake glaciers; not found at Boulder Mountain
- Fish Lake and Boulder Mountain LGM paleo glaciers at maximum ~20-21 ka; recessional ~15-16 ka
- Fish Lake core data indicates de-glaciation by 15 ka; CT data interesting Holocene; MS data less interesting Holocene
- Possible Boulder Mtn ice sheet demise between ~20 ka and 16 ka; may hold interesting clue to post-LGM to pre B-A regional climate

Acknowledgements

A.Brunelle, C. Bailey, A. Rigby, D.K. Solomon, J. Ball, W. Weaver, D. Stoll, S. Bergman, S. Able, A. Heger, S.B. Marchetti, J. Carbaugh, T. Buckley

NSF
UGS
USGS
U.S. Forest Service and BLM

RESPONSE OF THE GREAT SALT LAKE, LAKE BONNEVILLE, AND INTERMEDIATE SHORELINES TO INTERANNUAL CLIMATE VARIABILITY

Kathleen Huybers[1], Summer Rupper[1], Gerard Roe[2]

[1]Department of Geography, University of Utah, Salt Lake City, UT 84112;
[2]Department of Earth and Space Sciences, University of Washington, Seattle, WA 98195

Corresponding author (Huybers): kat.huybers@gmail.com

ABSTRACT

Because lakes integrate year-to-year fluctuations of precipitation and evaporation, the interpretation of lake-level records is not necessarily straightforward. Even in the absence of long-term climate forcings, lake levels may exhibit fluctuations that persist on decadal, centennial, or even millennial timescales. It is important to account for this behavior when connecting paleo-lake records to paleoclimatic forcing. We demonstrate this principle for the case-study of Great Salt Lake (GSL), then extend our findings to other significant shorelines in the Bonneville basin. Employing both full water-balance and linearized lake-level methods, we model the lakes' responses to synthetic stochastic variations in precipitation, inflow, and evaporation. We show that interannual climate variability can explain much of the decadal to centennial variability in the GSL record, and infer that longer term memory would persist in larger Bonneville basin lakes. Because of this persistence, the expected range of variation for small lakes is expressed on the scale of decades to centuries. For larger lakes with a longer memory, the high-frequency variance is suppressed, but the expected magnitude of change over the course of centuries or millennia is large. On the basis of these results, we expect that interannual climate variability may play an important role in explaining the variations and transitions of the paleo-lakes in the Bonneville basin. (Portions of this abstract and work were published in: Huybers, K., Rupper, S., and Roe, G.H., 2015, Response of closed basin lakes to interannual climate variability: *Climate Dynamics*, DOI: 10.1007/s00382-015-2798-4).